CORROSION
Testing and Evaluation:
SILVER ANNIVERSARY VOLUME

Baboian/Dean, editors

STP 1000

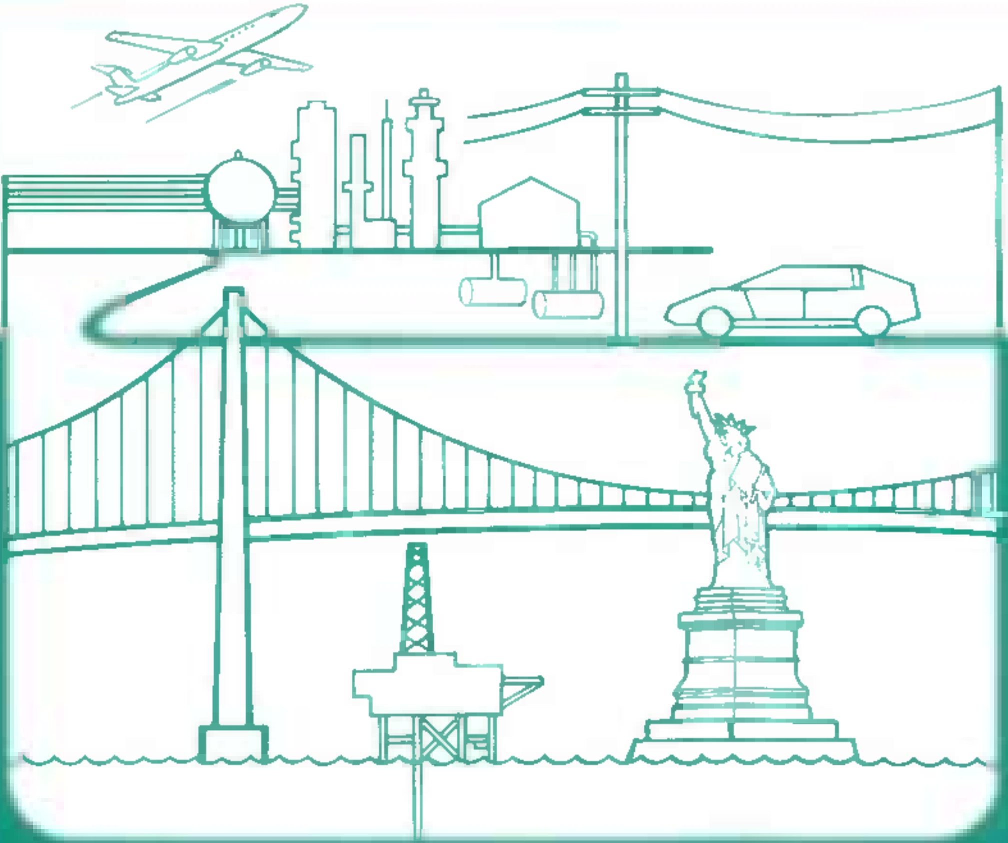

STP 1000

Corrosion Testing and Evaluation: Silver Anniversary Volume

Robert Baboian and Sheldon W. Dean, editors

ASTM
1916 Race Street
Philadelphia, PA 19103

Library of Congress Cataloging-in-Publication Data

Corrosion testing and evaluation: silver anniversary volume/Robert Baboian and Sheldon W. Dean, editors.
(STP; 1000)
Papers from the Silver Anniversary Symposium on Corrosion Testing and Evaluation sponsored by ASTM Committee G1 on Corrosion of Metals held in Orlando, FL, 6–10 Nov. 1989.
Includes bibliographical references and indexes.
"ASTM publication code number (PCN) 04-010000-27"—T.p. verso.
ISBN 0-8031-1406-0
1. Corrosion and anti-corrosives—Congresses. I. Baboian, Robert. II. Dean, S. W. III. Silver Anniversary Symposium on Corrosion Testing and Evaluation (1989: Orlando, FL). IV. American Society for Testing and Materials. Committee G1 on Corrosion of Metals. V. Series: ASTM special technical publication; 1000.
TA462.C664 1990 90-45036
620.1'1223—dc20 CIP

Peer Review Policy

Each paper published in this volume was evaluated by three peer reviewers. The authors addressed all of the reviewers' comments to the satisfaction of both the technical editor(s) and the ASTM Committee on Publications.

The quality of the papers in this publication reflects not only the obvious efforts of the authors and the technical editor(s), but also the work of these peer reviewers. The ASTM Committee on Publications acknowledges with appreciation their dedication and contribution of time and effort on behalf of ASTM.

Printed in Baltimore, MD
November 1990

Foreword

On 21 Jan. 1964, the Board of Directors approved the formation of Committee G1 on Corrosion of Metals to consolidate the various standard developing bodies concerned with corrosion testing and evaluation. An unexpected benefit of this consolidation was the attraction of a group of corrosion scientists and engineers to the committee. Their efforts provided leadership in the development of standards in areas previously neglected. These areas included electrochemical test methods, stress corrosion cracking methods, and others. In the ensuing 25 years, Committee G1 has developed more than 50 standards and has been responsible for the publication of 35 special technical publications resulting from symposia sponsored by the Committee.

In order to celebrate 25 years of exceptional productivity, Committee G1 put together a series of special events during its fall meeting in Orlando, Florida, 6–10 Nov. 1989. As part of this celebration, the Silver Anniversary Symposium on Corrosion Testing and Evaluation was held. This Symposium covered technical areas where Committee G1 has been active. A series of highlighting lectures was included to cover the state of the art in each area. In addition, research papers provided new unpublished results in these areas. As a result, 38 papers were presented at this symposium. This publication, *Corrosion Testing and Evaluation: Silver Anniversary Volume, ASTM STP 1000*, contains most of these papers.

The purpose of this STP is to summarize the state of the art in corrosion testing and evaluation in the areas where Committee G1 is active. In addition, this STP highlights areas where research has provided new information in fields related to corrosion testing and evaluation. The STP also covers areas where new standards would be desirable and where existing standards have deficiencies.

Robert Baboian, Texas Instruments, Attleboro, Massachusetts, and Sheldon W. Dean, Air Products and Chemicals, Inc., Allentown, Pennsylvania, served as symposium chairmen and were editors of this publication.

COVER: Artwork supplied by Robert L. Laverdiere, Texas Instruments, Inc.

Contents

SECTION III: ATMOSPHERIC TESTS

SECTION IV: LABORATORY TESTS

SECTION V: ELECTROCHEMICAL TESTS

Overview

This special technical publication resulted from the Silver Anniversary on Corrosion Testing and Evaluation and contains 30 papers. Six of these papers summarize the state of the art in specific areas. The introductionary paper, written by Robert Baboian, provides a global overview of the problems that corrosion damage causes with information on how these problems have become more severe in recent years. This paper also explains the rationale for corrosion testing and the value of standards in corrosion testing and evaluation.

Subject Areas

Corrosion Data and Evaluation

This section includes two papers on the newly developed computer-related technologies. Anderson highlights the field and covers the challenge of developing databases for corrosion data including the problem of incorporating data from different sources presented in different formats. The need for standards in data collection, compilation, and presentation is discussed. The possible interaction between databases and expert systems is also explored. Sturrock et al. cover the use of computers in providing advisory information. The work of the National Association of Corrosion Engineers (NACE) on the production of corrosion databases is discussed. The project sponsored by the Materials Technology Institute of the Chemical Process Industries, Inc. and carried out by NACE and the National Institute of Standards and Technology to develop material advisors for handling hazardous chemicals is covered. These new techniques for presenting comprehensive information on selecting materials is a significant new development that should be very helpful for engineers faced with handling these difficult chemicals.

The remaining papers in this section are concerned with failure analysis and corrosion evaluation. Clark and Metala discuss the value of nondestructive evaluation (NDE) in nuclear power plants. These techniques are very useful in characterizing the size and shape of defects including corrosion cracks and pits. Various NDE techniques are compared, and data analysis approaches are discussed. These approaches are essential in nuclear applications but have applications in many other industries. McCaul covers a number of failures of pump components in corrosive service and explains the techniques for analyzing these failures as well as the most common causes of pump failure. Nekoksa reviews a number of corrosion failures in water and soil environments and covers the difficult problems of stray currents and other electrochemical problems in these environments. Barton, Knotkova, and Holler present a generalized approach for selecting materials on the basis of corrosion tests and provide information for a broad range of industrial and commercial applications.

Corrosion in Environments

This section covers underground and natural water corrosion as well as environments that have an erosion component from multiphase flow. Chaker highlights the field of corrosion in soils including the development of test methods needed to identify, measure, and control corrosion in soils. This paper presents the development of various techniques for measuring corrosion in soil, especially electrochemical techniques. Escalante discusses the electrochemical basis for underground corrosion. Polarization and galvanic current measurements are discussed, and some of the problems of these measurements are covered. Induced ac increases corrosion as does the disturbance of soil through backfill. Electrochemical measurements are important techniques for detecting and quantifying underground corrosion. Palmer reviews the testing of soils for corrosivity from an engineering view point. Various parameters including soil resistivity, pH, redox potential, moisture content, chloride levels, and microbiological activity were mentioned. The question of predicting expected life of buried facilities was reviewed. Andersen and Donnellan investigated the stress corrosion cracking of manganese bronze castings in water distribution systems. Mercury, ammonia, water, and mercury clean-up chemicals were all discovered to cause cracking. Only trisodium phosphate did not cause cracking. Schorr, Weintraub, and Andrasi employed polarization resistance and mass loss measurements to separate the effects of erosion and corrosion in tests on materials for mineral processing plants. Various types of apparatus were used to simulate the service including a rotating cylinder with an impinging jet and a sliding abrasion from a rotating disk.

Atmospheric Tests

This section includes seven papers concerned with atmospheric corrosion. Dean provides an overview of the changes in the atmosphere that have occurred in the past 80 years and the challenges for the future in atmospheric exposure testing. Baker and Kirk provide a report on an exposure program for a variety of stainless steels including 200, 300, and 400 series alloys. These materials were exposed for 29 years at two ASTM sites, State College, Pennsylvania and Newark-Kearny, New Jersey. Very little corrosion was observed in these alloys aside from cosmetic discoloration, and no loss in properties or stress corrosion cracking was found. The results were compared to earlier results from marine exposures. Spence et al. discuss advanced laboratory and field testing systems for evaluating the atmospheric corrosion resistance of materials. The laboratory apparatus simulated the complex mixtures found in atmospheric exposures and included aerodynamic and chemical variables. These studies were compared to atmospheric exposure studies involving runoff collection and rain shield covering devices with deionized water sprays on galvanized steel specimens. A relationship for the corrosion of this material was derived. Spence and Haynie have formulated a model of the atmospheric corrosion of galvanized steel based on sulfur dioxide reacting with wet surfaces and acidity in the incident rain reacting with the metal surface. This model allows the separation of acid precipitation effects from gaseous sulfur dioxide effects. This type of model is termed a damage function. A follow up paper by Haynie et al. compares the corrosion rates nearest an actual structure and earlier ASTM exposure programs with the predictions based on their model. The results of these comparisons show reasonable agreement. This approach is claimed to handle real structures better than models, which do not include aerodynamic effects and the independent wet and dry deposition effects. Cramer and McDonald have developed a model based on similar wet and dry deposition to predict the atmospheric corrosion of zinc, galvanized steel, and copper. The Bureau of Mines results from the NAPAP study were used in this study. The effect of acid precipitation was found to be more important in most sites than gaseous SO_2 in affecting atmospheric corrosion of these materials based on current conditions.

Hechler et al. have studied the ASTM G-84 time of wetness sensor in a variety of atmospheric conditions. They discovered that there is significant variability in this type of sensor to dew detection. Some sensors are not sensitive to dew, and consequently they recommend to test sensors and not use any with this problem.

Laboratory Tests

This section includes six papers on a variety of subjects. Haynes highlights the subject with a review of the activities of Subcommittee G01.05 on Laboratory Corrosion Tests. The problems of revising and updating standards, especially older well-established methods, has been a major challenge in view of the need to quantify repeatability and reproducibility. New standards are being developed in the area of testing for electronic materials. Kane et al. have investigated the concept of critical pitting temperature using sodium chloride, ferric chloride, electrochemical polarization scans, and simulated service tests. They used these tests to characterize duplex stainless steel weldments. They found that pitting susceptibility could be related to ferrite content and alloy content of the weldments. Yau et al. discuss coupon testing to assess corrosion of zirconium and zirconium alloys. They noted that some of the procedures presented in ASTM Guide for Conducting Corrosion Coupon Tests in Plant Equipment (G-4) and ASTM Recommended Practice for Laboratory Immersion Corrosion Testing of Materials (G-31) were not applicable to zirconium. They presented procedures that should be used for these alloys.

Treseder highlights the development of sulfide stress corrosion tests and their importance in material selection for the petroleum production and refining industries. Five test methods used for this purpose are compared including the Shell bent beam, the uniaxial load, double cantilever beam, C-ring, and slow strain rate test. Comparisons are also provided for the environmental test variables. Everhart and Price discuss the stress corrosion cracking of nickel-copper alloys in various environments. They found that environments that caused pitting in these alloys also caused cracking. The cracking caused by stress corrosion was similar to hydrogen embrittlement and liquid metal embrittlement in that low strains produced intergranular penetration and higher strains produced a transition to transgranular cracking. Corbett covers the development of a multispecimen technique for conducting the ASTM Practices for Detecting Susceptibility to Intergranular Attack in Austenic Stainless Steels (A 262) Practice C (nitric acid) test to detect sensitization in stainless steels. This approach reduces both the cost and space requirement. This apparatus maintained the concentration of corrosion products at a low level and so improved reproducibility of the method. Comparison tests between the conventional A 262 Practice C apparatus and this multispecimen method showed good agreement.

Electrochemical Tests

This section includes five papers on a variety of new techniques. Scully highlights the section with an overview of developments in the past 30 years. The techniques of potentiodynamic and potentiostatic potential sweeps, polarization resistance, galvanostaircase, single and double loop electrochemical potentiokinetic reactivation, and electrochemical impedance are discussed. Silverman discussed the electrochemical impedance technique for predicting corrosion rates and provided more detailed information on corrosion mechanisms. He used an example from a chemical plant application where this technique was valuable in material selection and discussed sources of errors. Simpson et al. cover the use of electrochemical impedance measurements for evaluating the performance of organic coatings. They employed electrochemical impedance spectroscopy as a technique to evaluate the response of an atmospheric degradation monitor and characterized the behavior of this device. Hirozawa and Coker discuss the galvanostaircase technique for evaluating the performance of inhibitors for aluminum alloys in ethylene glycol antifreeze solutions. They focus on the interaction of surfactants with a silicate inhibitor at elevated temperatures. Berke and Hicks used both electrochemical impedance and polarization resistance to measure the corrosion rate of reinforcing steels in concrete environments. The effects of chloride migration, carbonation, and the presence of inhibitors such as calcium nitrite were investigated. The electrochemical techniques were nondestructive and produced results that correlated well with observed mass loss and visual damage assessments.

Conclusion

The papers in this STP cover both the past activities and future directions of ASTM Committee G1 on Corrosion of Metals in a comprehensive and thoughtful manner. As such, this book is a fitting milestone to mark a quarter century of progress in our battle with corrosion damage. Readers can expect to gain a broad view of the progress made and the future directions both of corrosion control and the standards that will enable the development of systems with high reliability to combat this important problem.

The authors are grateful to the officers and members of Committee G1 for their assistance and support in the planning and production of this volume and also to the publications staff of ASTM for their patience and support.

Robert Baboian
Texas Instruments, Attleboro, Massachusetts; symposium chairman and editor

Sheldon W. Dean
Air Products and Chemicals, Inc., Allentown, Pennsylvania; symposium chairman and editor

Introduction

Robert Baboian[1]

Corrosion—A Problem of International Importance

REFERENCE: Baboian, R., "**Corrosion—A Problem of International Importance,**" *Corrosion Testing and Evaluation: Silver Anniversary Volume, ASTM STP 1000,* R. Baboian and S. W. Dean, Eds., American Society for Testing and Materials, Philadelphia, 1990, pp. 7–13.

ABSTRACT: Corrosion is a problem of international importance because it affects public safety and is costly. The problem has escalated due to a number of factors including an increasing demand on the performance of materials and increasingly aggressive environments. Examples used to demonstrate the magnitude of the problem include: (1) deterioration of the infrastructure; (2) effects on transportation; (3) underground corrosion; (4) reliability of electrical and electronics equipment; and (5) concern over the fate of outdoor artistic and historic works. Corrosion testing and evaluation play an important part in solving corrosion problems. Typical concerns are listed, and the importance of planning and preparation is emphasized.

KEY WORDS: corrosion, testing, evaluation, public safety, cost, economics, materials performance, infrastructure, transportation, automobiles, aging aircraft, reinforcing steel, underground corrosion, soils, storage tanks, electrical equipment, electronics equipment, bronze statues, atmospheric corrosion

Corrosion testing and evaluation play a vital role in addressing one of the world's most important problems. The importance of corrosion in our modern, high-technology society can be measured by the magnitude of the direct and indirect problems which result from this degradation process. At one time, the National Materials Advisory Board in the United States published a list of the ten most critical issues in materials. Every single issue involved problems associated with corrosion. Frequently, corrosion has an indirect effect on materials performance, and therefore it is difficult for the general public to recognize the importance of this type of degradation. In 1975, the Congress of the United States requested a study on the economic effects of corrosion to be conducted by the National Bureau of Standards (now the National Institute of Standards and Technology). The study reported the cost in the U.S. to be approximately 4.2% of the gross national product, i.e., over 200 billion dollars in 1989 dollars [*1*]. In addition, between 15 to 25% of the corrosion cost could be avoided by making the best possible use of existing technology. Similar studies throughout the world have shown that the estimated cost of corrosion is between 2 to 5% of the gross national product for the respective country [*2*].

When one considers the economic effects of corrosion, as well as safety factors, the impact can be more fully appreciated. In fact, the effects of corrosion: (1) jeopardize human safety; (2) cause plant shutdown; (3) waste time and valuable resources; (4) cause loss or contamination of product; (5) reduce efficiency; (6) involve expensive maintenance; (7) cause overdesign; and (8) inhibit technological progress.

---

[1] Head, Electrochemical and Corrosion Laboratory, Texas Instruments, Inc., Attleboro, MA 02703.

Corrosion has become one of the world's most important problems due to a number of factors, two of the most important being: (1) increasing demands on materials; and (2) an increasingly aggressive environment. The first of these is easy to understand given the advanced technologies utilized by industries today. In many instances, materials already in place cannot perform as requirements change. Also, state-of-the-art materials cannot always meet necessary requirements. Therefore, the eight corrosion effects listed above become reality.

The environment has become more aggressive due to a number of factors. For example, Fig. 1 shows the annual use of road deicing salts in the United States to be almost nonexistent before 1950. The annual usage has increased to a peak of 12 million tons in 1979 and has leveled off at 10 million tons per year today [3]. These salts accelerate corrosion by direct splash and spray on vehicles and structures, by dissolving in streams, lakes, drinking water, etc., by leaching into our soils, and by entering our atmosphere as salt aerosols.

Figure 1 also shows annual sulfur dioxide (SO_2) and nitrogen oxide (NO_x) emissions in the United States [4]. The upward trend is similar to that for road deicing salts such that SO_2 has peaked at 30 million tons in 1970 and NO_x at 23 million tons in 1978. These pollutants are corrosive because they convert to acids. For example, acid rain and snow are the result of long-range transport of SO_2 and NO_x, which convert to sulfuric acid and nitric acid in the upper atmosphere. The synergistic effects of road deicing salts and acid precipitation on metallic corrosion have been documented so that the increase in emissions and road salt usage has produced an increasingly aggressive environment in many areas [5].

Several examples can be used to illustrate the magnitude and effect of corrosion in the world today.

Throughout the world, infrastructures are rapidly deteriorating; these include highways, bridges, parking garages, water distribution systems, waste water collection and treatment

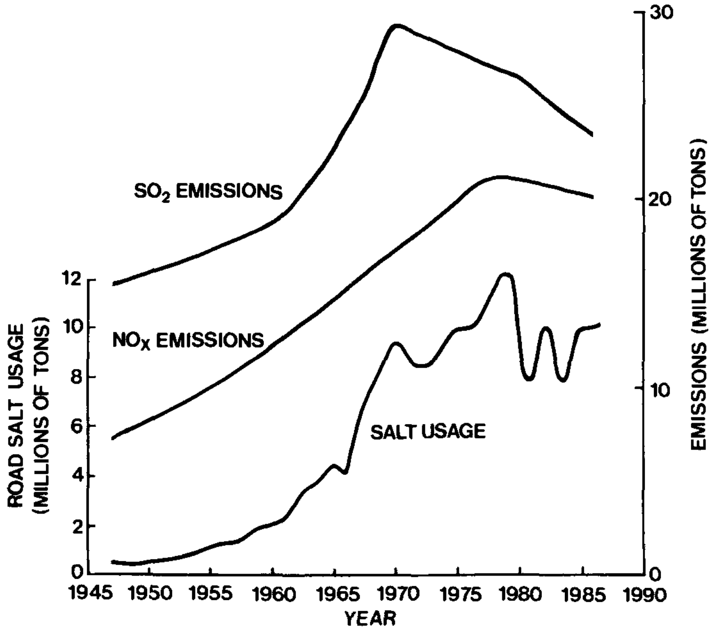

FIG. 1—*Annual deicing salt usage, SO_2 and NO_x emissions in the Unites States.*

systems, harbors, reservoirs, and railway and subway systems. In the United States, estimates range from 500 billion to 3 trillion dollars to restore the infrastructure over the next 20 to 30 years [*6*]. Of particular importance here is the problem of corrosion of reinforcing steel in concrete (rebar) not only because of the cost and safety concerns, but also because of the inconvenience that comes in making repairs. Structures affected by this problem include bridges, elevated highways, and parking garages (see example in Fig. 2). In the United States, it is estimated that of the 585 000 bridges under federal, state, and county jurisdiction, 60% are seriously affected by corrosion and 43% are structurally deficient [*7*]. The estimated cost of repair is 40 to 60 billion dollars over the next ten years.

Transportation has been affected by corrosion problems in a number of ways. The increased aggressivity of the automobile environment (Fig. 1) has produced two categories of corrosion problems: structural damage and cosmetic corrosion [*8*]. The automotive industry has successfully treated the problem of structural damage (such as corrosion perforations in Fig. 3) through the use of galvanized steel, hot waxes, and dip coatings as well as design changes to eliminate entrapment areas. However, cosmetic corrosion on automobiles still persists and is the subject of intense investigation today.

Included under transportation is the problem of aging aircraft. This public safety issue has brought intense publicity to this subject because each incident is thoroughly investigated and documented [*9*].

Underground corrosion has a far-reaching impact because it affects a wide range of industries. For example, buried electric power distribution systems can fail by concentric neutral corrosion. Telecommunications systems can be affected by corrosion of the electrical shielding in buried telephone cables leading to noise or disruption of service (Fig. 4). Buried gas distribution pipelines are cathodically protected by law as a result of public concern due to corrosion-related leaks and subsequent explosions. Corrosion problems with oil distribution pipelines, such as the 800-mile Alaska oil pipeline, have now surfaced. Leaking underground storage tanks (LUST) have become a major problem due to the resulting

FIG. 2—*Reinforcing steel corrosion causes spalling of concrete, making wood joists necessary for additional support on this elevated highway, Providence, RI.*

FIG. 3—*Perforation corrosion of auto-body panel is caused by accumulation of poultice, which traps salt and acids.*

pollution, health, and safety hazards. It is difficult to find these corrosion leaks because the tanks are buried. Estimates range up to $225,000 for a LUST site cleanup, and replacing a three-tank system of 10 000-gallon capacity costs up to $100,000 [*10*]. In 1985, the EPA introduced an interim law which stated that underground tanks and piping systems either by cathodically protected, constructed of noncorrodible materials, or be designed in a manner

FIG. 4—*Telephone cable is trenched in for field service corrosion tests on metallic shields.*

to prevent the release or threatened release of stored substances. In September 1988, the EPA announced regulations on underground storage tanks whereby new tanks must be protected from corrosion and existing tanks must be provided with leak detection. Using existing corrosion technology, the cost to protect a tank is as low as $2000, substantially less than the cost of a LUST cleanup or a tank replacement. Large above-ground storage tanks are also subject to environmentally caused corrosion damage, especially on the tank bottoms where leaks are more difficult to detect and control.

Electrical and electronics equipment have become more complex in recent years due to miniaturization. Technological advances have resulted in the development of sophisticated components with closer spacing so that extremely low levels of corrosive contaminants can cause failure (Fig. 5). Testing for this type of behavior is difficult and costly. The challenge to maintain reliability requirements in an increasingly complex system is important because significant technological advances can only occur when the corrosion issues are addressed [*11*].

International concern grows over the fate of outdoor artistic and historic works. The irreversibility of corrosion is most important when considering the deterioration of irreplaceable cultural resources such as statues, monuments, and structures of historical significance. Corrosion of outdoor bronze sculpture is one example of the seriousness of this problem. Acid deposition in the form of rain, snow, fog, dew, and dry deposits has produced a type of nonuniform corrosion which conservators refer to as "bronze plague." Throughout the world this type of bronze behavior can be observed in which the natural green patina formed in the outdoor environment is altered to include patches of black "scab" (Fig. 6). This behavior leads to accelerated corrosion of the bronze and is not aesthetically pleasing. Methods of treatment to avoid this behavior of outdoor bronzes is currently under investigation.

The above examples include corrosion problems occurring in a wide range of environments. Solutions to these problems have been and will be achieved through proper corrosion

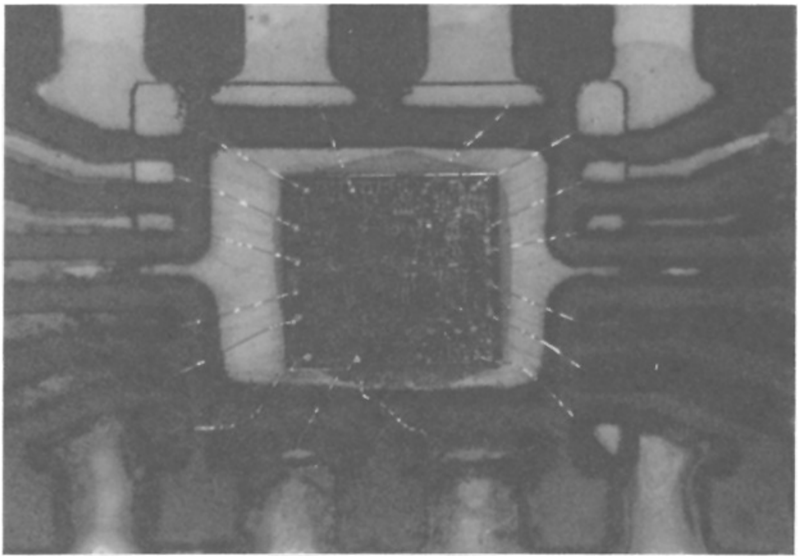

FIG. 5—*Corrosion products accumulate in integrated circuit package due to residual chemicals.*

FIG. 6—*The Hiker Statue (Providence, RI) suffers from "bronze plague," a form of degradation where the green patina is altered to include patches of black scab.*

testing and corrosion evaluation. Proper corrosion testing is essential in order to obtain meaningful results. Typical concerns include: (1) Are representative materials used in the test? (2) How does the test environment correlate with the actual service environment? (3) Are the corrosion mechanisms observed in the test the same as those in the actual service environment? and (4) What is the acceleration factor for the test? One can easily understand the basis of these concerns when considering the complexity of environments such as concrete, soils, road salt splash and runoff, acid precipitation and industrial atmospheres.

Laboratory, field, and service corrosion tests are all important in designing for corrosion resistance and solving corrosion problems. However, the difference in laboratory accelerated tests and tests in the actual environment must be understood. Accelerated tests, although shorter in duration, are not usually as reliable as field service tests. In general, accelerated tests are used for screening purposes and final decisions on materials and design are based on testing in the actual environment.

Planning and preparation are important factors in evaluation of corrosion test results and corrosion failures. Included in the test procedure must be consideration of the ease of identification of changes due to deterioration, statistical treatment of the data, and the overall reliability of the results.

In recent years, significant advancements have been made in the area of corrosion testing and evaluation. The subjects *Corrosion Data and Evaluation, Corrosion in Environments, Atmospheric Tests, Laboratory Tests,* and *Electrochemical Tests* form the sections of this book. The reader is brought up to date on these subjects in order to more adequately plan, prepare, and conduct corrosion tests and corrosion evaluations.

References

[*1*] "Economic Effects of Metallic Corrosion in the United States," NBS Special Publication 511-1, 511-2, National Bureau of Standards, Washington, DC, 1978.

[*2*] "Economic Effects of Metallic Corrosion in the United States," NBS Special Publication 511-1, p4-11, National Bureau of Standards, Washington, DC, 1978.

[*3*] Baboian, R., "Mechanisms of Automobile Corrosion and Prevention," *Proceedings*, International Corrosion Congress, Florence, Italy, April 1990, AIM, Florence, Italy.

[*4*] "Causes and Effects of Acidic Deposition," Vol. I, "Emissions and Controls," National Acid Precipitation Assessment Program, Washington, DC, 1987.

[*5*] *Materials Degradation Caused by Acid Rain*, Baboian, R., Ed., American Chemical Society, Washington, DC 1986.

[*6*] Lataision, R., "Current and Projected Impact of Corrosion Science and Engineering," *Proceedings*, 33rd Sagamore Army Materials Research, Conference, Burlington, VT, 1986, Army Materials Technology Laboratory, Watertown, MA.

[*7*] "Materials Technologies and Infrastructure Decision Making," workshop by the Federation of Materials Societies, Washington, DC, 5 Oct. 1989.

[*8*] *Automotive Corrosion By Deicing Salts*, Baboian, R., Ed., National Association of Corrosion Engineers, Houston, TX, 1981.

[*9*] Harris, R. J., *The Wall Street Journal*, 9 May 1988, p. 2.

[*10*] *Hazardous Waste Report*, Vol. 10, No. 2, Aspen Publishers, Rockville, MD, September 1988.

[*11*] Baboian, R., *ASTM Standardization News*, March 1986.

Section I: Corrosion Data and Evaluation

David B. Anderson[1]

Computerization of Corrosion Data

REFERENCE: Anderson, D. B., **"Computerization of Corrosion Data,"** *Corrosion Testing and Evaluation: Silver Anniversary Volume, ASTM STP 1000,* R. Baboian and S. W. Dean, Eds., American Society for Testing and Materials, Philadelphia, 1990, pp. 17–25.

ABSTRACT: Computerization of the wealth of available corrosion data facilitates both data access and interpretation to address specific user needs. Data collection and compilation can be enhanced by adoption of format standards which define guidelines for common terminology, documentation of performance measurement for both metals and nonmetals, data output and presentation, and for assessing data quality. Well-defined programs, using a variety of established computerization techniques, can serve as effective tools for selection of corrosion resistant materials, assessing material limitations, selection and design of corrosion control methods, and for gaining a better understanding of the significance and theoretical considerations relating to operative corrosion mechanisms.

KEY WORDS: corrosion, data, databases, artificial intelligence, computerization, data quality

Computerization of corrosion data provides important resources to aid in the utilization of existing technology for selection of corrosion-resistant materials and other methods for corrosion control and can expedite introduction and acceptance of newer materials and technologies. Computer programs provide ready access to a wide variety of numerical and text data and, perhaps more importantly, can provide interpretive guides to the captured data. These are key steps in reducing the documented costs of corrosion due to failure to utilize existing technology [*1*]. In this age of information overload, computerization can combine the time-consuming investigative steps of locating and digesting voluminous reports, publications, data compilations and other diverse, less readily available resources, consulting with peers, and analyzing the information obtained to assess relevance and significance to specific problems. There are also opportunities to provide data and interpretive tools to forge better ties between corrosion, materials science and engineering, and other related disciplines. Successful developments in any of these areas requires a clear understanding of the nature of corrosion data and the specific needs of the user audience.

The Nature of Corrosion Data

Corrosion data are dynamic representations of interactions of materials and environments and can be used to characterize both material performance and to assess the effectiveness of corrosion control technologies. This is in contrast to mechanical and physical property data for engineering materials, which are represented by results obtained under specified test conditions. The variety of corrosion data one needs to consider for any given application is indicated by the matrix shown in Fig. 1. The prospects of finding statistically valid corrosion performance data for any one specified material-environment-exposure condition-operative

---

[1] Director, NACE-NIST Corrosion Data Center, National Institute of Standards and Technology, Gaithersburg, MD 20899.

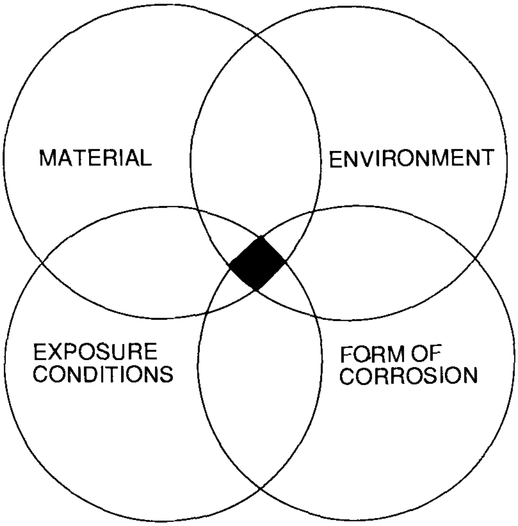

FIG. 1—*Corrosion data matrix.*

corrosion mechanism combination of interest is clearly remote. Thus we are all too often faced with the need to make educated estimations, interpretations, and interpolations with less than scientifically precise data that has not been subjected to rigorous validation and evaluation. This is the scenario for which computer representations of logic patterns used in these processes, combined with well-structured databases, have great promise.

Types of Corrosion Data

Corrosion data are available from many sources and in many forms. One common source is standardized laboratory tests, both the "dip-and-dunk" type and those based on electrochemical measurements.

Other sources include field tests, examinations of operating equipment, failure analyses, natural environment exposures, and theoretical studies. Some of the corrosion data appear in technical publications, promotional literature, textbooks, and handbooks, but even more data remain in laboratory notebooks, private inspection reports, and other sources that are not readily available and are often reported in a restricted format designed to meet an immediate need. Both numerical and textual data are involved. Quality and completeness vary, as does terminology to identify materials, environments, exposure conditions, and performance. The variability of data types and quality compound the problems in data interpretation and present added challenges to the development of useful computer programs.

A key step in addressing the terminology and data quality issues is the establishment of consensus standards for data format and quality assessment. Both of these issues are being addressed within ASTM. A corrosion data format standard guide is being developed through Committees E-49 on Computerization of Material Property Data and G-1 on Corrosion of Metals, while the data quality issue, as it relates to all material property data, is being addressed within Committee E-49.

Although a number of standard corrosion test procedures have been developed, they tend to utilize overly aggressive environments selected to accentuate specific corrosion mechanisms (for example, stress corrosion cracking, pitting, corrosion fatigue) in one class or subclass of materials, often under the guise of "accelerated tests" whose predictability of performance for longer term exposures under less stringent conditions is often suspect. Despite strict guidelines for specimen preparation, test environment, and exposure conditions, there is a general acceptance of significant variability between multiple specimens exposed under what are considered identical exposure conditions. The degree of variability appears to be dependent upon the severity of the environment relative to the inherent corrosion resistance of the material being evaluated and the dominant form of corrosion involved [*2–13*]. Perhaps this is to be expected for tests involving inhomogeneous materials exposed in equally inhomogeneous environments. Equally plausible is a realization that the critical factors for designing reproducible corrosion tests are not well defined. One could also question whether reproducibility of test results should be a primary goal of any standardized corrosion test procedure or whether we should accept the variability and study the data statistically to try to gain a better understanding of undefined factors.

Performance data for metals generally are presented in customary terms of corrosion rates, depths of attack, corrosion fatigue strengths, type and severity of cracking, etc., based on established conventions which are detailed in consensus standards. Although there are a number of standardized corrosion tests for nonmetals, conventions for presenting performance data for this class of materials are not as well established. Data presentations frequently involve establishment of somewhat arbitrary serviceability classifications such as "acceptable" or "questionable," thus substituting somewhat arbitrary data interpretations for presentations of detailed test results to allow the user to make independent judgments on material suitability for a specific application.

Some users, however, are quite happy to accept a supplier's interpretation that a given material is acceptable for a defined use rather than being faced with making a judgment based on data which one feels unqualified to interpret. Well-structured computer programs can provide the best of both worlds, providing interpretations based on consensus rules derived by corrosion experts and access to original data for personal interpretation for specific applications.

Components of Corrosion Data

Four basic components are required to describe any corrosion data:

1. *Material identification*—Unambiguous material identifiers are essential, preferably through reference to an accepted material identification numbering system such as the Unified Numbering System (UNS) developed for metals by ASTM and the Society of Automotive Engineers (SAE) or the ASTM Classification System for Specifying Plastic Materials (D 4000) for plastics. Where possible, materials should be referenced to established standards and should be categorized by class, subclass, and family using the guidelines developed by ASTM Committee E-49. Product form, manufacturing, and processing details are also important factors that can affect material performance and should be included in the material description.
2. *Environment*—It is equally important that the corrosion environments be clearly described, preferably in terms of the principal constituents using standard terminology rather than generic descriptors such as brackish water, sour gas, white liquor. All known contaminants should be included even if they are only present in trace amounts.
3. *Exposure conditions*—Details of the exposure conditions within the corrosive environment need to be clearly defined. Important examples include temperature, pH, velocity, aeration and agitation, presence of heat transfer, galvanic relationships, and applied stress.

Although velocity conditions commonly are reported in terms of the nominal fluid flow rate, more detailed descriptors should be considered to better assess hydraulic sheer forces and their effects on limiting forms of corrosion.

4. *Performance data*—Different types of performance data are required for metals and nonmetals and the specific forms of degradation under investigation. Performance data for stress corrosion cracking of metals will differ from pitting test data or property change data for nonmetals. Standards for reporting corrosion data have been developed in many of these areas and should be consulted to aid in data comparisons.

Evaluation of Data Quality

Strict guidelines have been established for evaluation and classification of physical and mechanical property data for engineering materials with classification as typical, minimum, handbook, or design data. Other qualification schemes consider categories of limited use data, qualified data, and highly qualified data [*14*]. The Committee on Data for Science and Technology (CODATA) has defined three broad classes of data [*15*].

Class A—Repeatable measurements in well-defined systems.
Class B—Observational data.
Class C—Statistical data.

Guidelines for evaluation and classification of corrosion performance properties and the elimination of user bias in selection and interpretation of related data have yet to be established. The common perception that computerized data are inherently of good quality can be destroyed if data compilations of questionable quality are promulgated. Data quality assessment is a fruitful area for future research if the promise of broader understanding of corrosion data through computerization is to be fulfilled.

Scientific evaluation of data is the estimation of the quality and reliability of the data using documented procedures. Often this requires statistical analysis and subsequent process modeling. The complexities of corrosion data tend to discourage attempts to undertake this type of rigorous data analysis. A more common approach is to develop expert consensus, often through technical society activities, and prepare summary documents addressing specific environments or applications. These documents can serve as valuable reference sources for evaluation of new data and can serve as resource documents for expert system development.

Peer review of compiled data prior to publication or distribution as an electronic database remains the most effective means of corrosion data evaluation and should be encouraged to control the promulgation of corrosion data of unknown or questionable value. The review should be done by acknowledged experts with clear guidelines for the evaluation process. This should emphasize the need for a comprehensive, judgmental appraisal to determine the quality, reliability, and adequacy for the purpose or application intended [*15*].

Corrosion Data Uses

An additional consideration in the structuring of computerized corrosion data programs is anticipation of the ways in which corrosion data are used. Table 1 provides an indication of the diversity of corrosion data users and their individual needs. Each has its own special requirements in terms of format, completeness, and quality. Identification of anticipated users and an understanding of their needs should be given highest priority in any data collection program.

TABLE 1—*Corrosion data users.*

Data User	Requirements
Corrosion experts	Planning experiments, interpreting results, providing consultation
Specification writers	Preparation and revision of specifications detailing acceptable material usage
Designers	Making material choices for new or revised designs
Purchasers	Identification of possible substitute materials
Economists	Critical material studies
Sales executives	Identification of sales opportunities and hazards
Risk assessors	Assessment of risk of corrosion for insurance purposes
Educators	Preparation and presentation of classroom materials; design and interpretation of laboratory and research experiments
Consultants	Provide basis for technical recommendations or testimony; resource information for failure analysis
Attorneys	Source of information for assessment of need for litigation
Managers	Provide background information to assist in challenging recommendations of others
Students	Provide specific information for class work, planning of research activities and reports
Maintenance engineers	Planning and improving plant maintenance procedures; material selection for repairs
Inspectors	Provide a basis for verifying compliance with specification and instructions

Corrosion Data Programs

There are a variety of computerization techniques which can be used to compile and interpret corrosion data. Some of the types currently in use are discussed below.

Databases

Databases are systematic data collections, which, when coupled with database management systems, can be electronically searched and manipulated to identify data of particular relevance to user needs. With the advent of more powerful personal computers and technology advances for operation of online and network systems, computerized databases are rapidly gaining popularity in scientific and engineering communities. They can serve as efficient tools for compiling, storing, searching, manipulating, and displaying large amounts of data, both numerical and textual. In some database designs, users can add their own data or make other modifications while in others the data and database structure are inviolate except to the original developer. In either instance, databases can function as relatively simple electronic indices to selected data compilations which the user then interprets to meet his or her needs. Often this involves data transferring to other established programs for subsequent processing, assuming there is some degree of data compatibility. Alternatively, the database can be designed with an integrated interface which guides the user to query structuring, data selection, and interpretation. Interpretation functions can be enhanced by tying the database to expert systems. These and other options are shown schematically in Fig. 2.

The complexities of corrosion data challenge database development efforts. Discrete databases can be considered which relate to: (*a*) specific forms of corrosion relative to one class of materials, for example, stress corrosion cracking of high-strength aluminum alloys, corrosion-fatigue or crevice corrosion of selected alloys classes in seawater; (*b*) specific

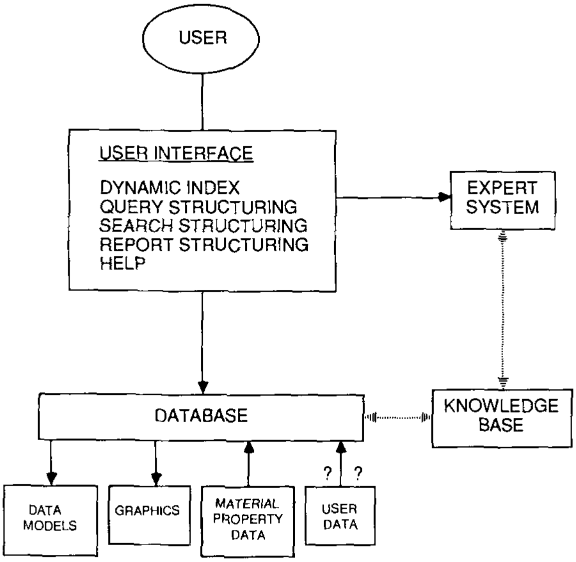

FIG. 2—*Database functions.*

environments such as acetic acid and sour gas; or (*c*) specific applications such as heat exchangers and fasteners. Alternatively, more complex structures can be developed to accommodate multiple forms of corrosion and the full range of engineering materials. An "intelligent" user interface could then be devised to guide the user to assess the limiting form of corrosion for any given application, quantify the predicted severity of corrosion damage, and provide some guidelines for life prediction.

Data can be compiled in handbook format as reference data where materials are rated A, B, C, or "acceptable," "questionable," and "unacceptable" for a broad range of environments, based on consensus opinions. Alternatively, data can be compiled as numeric results of specific tests on a specimen-by-specimen basis or can be text abstracts from the technical literature.

Expert Systems

Expert systems are specialized computer programs which can provide expert advice based on established expertise, combining documented facts with heuristics or rules of judgment. A key requirement, then, is established expertise in the areas addressed. Expert systems aid in the transformation of information to knowledge and have proven to be valuable tools for materials selection and life prediction from a corrosion resistance point of view [*16*]. Limited success has been achieved in the development of programs in evolving technology areas that require creation of expertise directly from numeric data. The programs mimic the process of consultation and reasoning used by human experts to solve specific corrosion-related problems and by their very nature find the greatest success where they are highly focused on complex problems in given application areas rather than attempting to generalize on broad areas of science and technology. Systems described in the literature cover a broad range of corrosion-related topics ranging from cathodic protection design, stress corrosion cracking of high-strength aluminum alloys, applications for stainless steels in aqueous chloride solutions to flue gas desulfurization equipment, sour oil and gas production pumps, and storage and handling of hazardous chemicals [*17–27*].

User ability to customize a program by addition of proprietary information is a particularly interesting feature that has been introduced in several programs. Programs with this feature are structured to prevent the new information from interfering with the logic patterns built into the knowledge base. However, the new information can identify supplemental conclusions or can identify proprietary fabrication or purchasing requirements.

Literature Searching

Electronic literature indexing and searching are some of the earliest uses of computers to address the information crunch in science and technology. Programs range from key word index searching which produces a bibliography and may leave the user with the task of locating specific references to optical disk programs which permit Boolean (and/and not/or) as well as proximity (context) searches of entire text which are not limited to preassigned key words. The optical disc technology permits storage and retrieval of full abstracts or extracts or possibly the full text for immediate user access.

User Interface Design

The ultimate acceptance of any computer program reflects both the competence and usefulness of the information it contains and the "user friendly" aspects of the interface that the user must master to retrieve and interpret the information being sought. The needs of query structuring and the format for data presentation are equally important. The interface can: (*a*) operate in a spreadsheet format that requires the user to be well versed in spreadsheet software manipulation; (*b*) provide a search menu that allows selection of data that satisfy specified requirements; or (*c*) provide a format for the user to describe the purpose of the query, devise an appropriate search strategy, and offer options for structuring of an interpretive data output. Typical output options are solutions to mathematical algorithms or other types of data models and graphic presentations which isolate dependent and independent variables.

It is also important that the interface present to the user a clear understanding of the options provided and the expected result from any user responses to menu selections or prompts.

Benefits of Computerization of Corrosion Data

Computerization activities can provide effective tools to process the variety of types of corrosion data to meet a variety of user needs and interests. Programs can guide users in: (*a*) selection of corrosion-resistant materials for specific corrosion limiting applications; (*b*) assessing material limitations as a function of environmental variables, economic factors, mechanical properties, or fabrication difficulties; (*c*) selection of corrosion control methods, and in some instances, designing of corrosion control systems; and (*d*) selecting data to gain a better understanding of the significance and theoretical considerations relating to selected corrosion mechanisms. The ability to utilize data from many sources—both textual and numerical—and review the data in interpretive format to provide reliable guidance for cost-effective corrosion control is a goal that is readily achievable using the many tools that are now available. It is the ability to present data in interpretive formats that ensures that maximum benefit can be derived.

Summary

Activities relating to the development of computerized corrosion data resources have provided important insights into the nature of corrosion data and their relationships to the needs of both the resource developers and the data users. Understanding of the data, the data sources, and the data users are central to any successful computerization activity. We have come a long way from simple tabular presentations of unevaluated data with little guidance for data interpretation. Continued development of unique tools that aid in the understanding of the many corrosion data resources and the transformation of information into knowledge for problem solving provide unique challenges for the future.

There are three particular areas where concentrated effects can be particularly fruitful:

1. *Development of guidelines for evaluation of corrosion data and assessment of data quality.* This requires a better understanding of the environmental and material variables that affect corrosion processes. These, in turn, should be the basis for reanalysis of standard corrosion test procedures with an aim toward defining specific data recording needs to gain better understanding of data variability and extrapolation to service life prediction.
2. *Establishment of consensus guidelines for recording corrosion data, both from the standpoint of data sources and data compilers.* Guidelines are needed for metals, nonmetals, composites, and other engineering materials which may be considered for use in corrosion applications. ASTM Committees G-1 and E-49 are making good progress in this area, but much more needs to be done to meet the needs of the variety of types of data and the needs of their users. This activity has a particularly important impact on the quality and usefulness of any efforts to compile and assimilate data from multiple sources without sufficient detail to eliminate misinterpretations.
3. *Identification of corrosion data sources and establishment of mechanisms for capture in compatible format for introduction into computerized data resources.* This will require emphasis on techniques for electronic transfer in order to eliminate the need for tedious, costly, and error-prone manual processing. These computerized corrosion data compilations can then serve as the basis for further evaluation and study to gain better insight into the nature and significance of these resources.

References

[*1*] Payer, J. H., et al., "Economic Effects of Metallic Corrosion in the United States," NBS Specific Publications 511-1 and 511-2, National Bureau of Standards, Gaithersburg, MD, May 1978.

[*2*] Tuthill, A., *Materials Performance,* Vol. 24, 1985, p. 43.

[*3*] Beetham, M., *Proceedings,* TAPPI Engineering Conference, 1986, p. 665.

[*4*] Rushton, J., et al., TAPPI press report, 1984.

[*5*] Rowe, L., in *Galvanic and Pitting Corrosion: Field and Laboratory Studies, ASTM STP 576,* American Society for Testing and Materials, Philadelphia, 1974, p. 203.

[*6*] Anderson, D., in *Galvanic and Pitting Corrosion: Field and Laboratory Studies, ASTM STP 576,* American Society for Testing and Materials, Philadelphia, 1974, p. 231.

[*7*] Crews, D., in *Galvanic and Pitting Corrosion: Field and Laboratory Studies, ASTM STP 576,* American Society for Testing and Materials, Philadelphia, 1974, p. 217.

[*8*] *Annual Book of ASTM Standards,* Vol. 03.02, "Method for Vibratory Cavitation Erosion Test, G 32-85, Section 13.

[*9*] *Annual Book of ASTM Standards,* Vol. 03.02, "Test Method for Determining Susceptibility to Stress-Corrosion Cracking of High-Strength Aluminum Alloy Products, G 47-79, Section 13.

[*10*] Rosenthal, H. and Pritchard, H., in *Stress Corrosion Testing, ASTM STP 425,* American Society for Testing and Materials, Philadelphia, 1967, p. 165.

[*11*] Sprowls, D., in *Stress Corrosion Testing, ASTM STP 425,* American Society for Testing and Materials, Philadelphia, 1967, p. 292.

[*12*] Romans, H., in *Stress Corrosion Testing, ASTM STP 425,* American Society for Testing and Materials, Philadelphia, 1967, p. 187.

[*13*] Kain, R. M., "Crevice Corrosion Testing in Natural Seawater: Significance and Use of Multiple Crevice Assemblies," *NACE Corrosion/88,* Paper No. 405, National Association of Corrosion Engineers, Houston, TX, 1988.

[*14*] Northrup, C. J. M., McCarthy, J. L., Westbrook, J. H., and Grattidge, W., "Materials Information for Science and Technology (MIST): Project Overview," *MPD–Vol. I, PVP–Vol. III,* American Society of Mechanical Engineers, New York, 1986.

[*15*] Kotani, M., Ed., *CODATA Bulletin,* No. 16, 1975.

[*16*] Brister, P. M., "Evaluation and Analysis of Computerized Material Property Databases," *CODATA Bulletin,* No. 16, 1975.

[*17*] Bogaerts, W. F., Rijckaert, M., and Bettendorf, C., "Artificial Intelligence, Expert Systems and Computer-Aided Engineering in Corrosion in Corrosion Control," *NACE Corrosion/89,* Paper No. 58, National Association of Corrosion Engineers, Houston, TX, 1989.

[*18*] Vancoille, M. J. S., Bogaerts, W. F., and Rijckaert, M. J., "Prime—The European Esprit Project on Expert Systems for Materials Selection," *NACE Corrosion/88,* Paper No. 121, National Association of Corrosion Engineers, Houston, TX, 1989.

[*19*] Rinehart, S. C. and Koch, G. H., "Corex—An Expert System for Corrosion Analysis and Treatment," presented at EPRI Seminar on Expert Systems Applications in Power Plants, Boston, MA, May 1987, EPRI, Palo Alto, CA.

[*20*] Boag, W. A., Reiser, D. B., Sprowls, D. O., and Rychener, M. D., "Cordial—A Knowledge-Based System for the Diagnosis of Stress Corrosion Behavior in High Strength Aluminum Alloys," *Proceedings,* TMS-AIME Conference on Artificial Intelligence Applications in Materials Science, October 1986.

[*21*] John, R. C., Thompson, W. T., and Karakaya, J., "Advice System of High Temperature Alloy Corrosion," *Materials Performance,* January 1989, p. 69.

[*22*] Sturrock, C. P. and Sharp, W. B. A., "An Integrated Information System Concerning Materials for Handling Hazardous Chemicals," *NACE Corrosion/89,* Paper No. 272, National Association of Corrosion Engineers, Houston, TX, 1989.

[*23*] Lichti, K. A., Karras, P., and Sturrock, C. P., "Development of a Standards Based Expert System for Selecting Materials for Oil and Gas Industry," *NACE Corrosion/89,* Paper No. 476, National Association of Corrosion Engineers, Houston, TX, 1989.

[*24*] Robinson, R. C., "Expert Computer Systems for Corrosion Control of Metallic Structures," *Materials Performance,* May 1989, p. 13.

[*25*] Sharp, W. B. A. and Sturrock, C. P., "Computer Aided Materials Selection in the Pulp and Paper Industry," *Proceedings,* 6th International Symposium on Corrosion in the Pulp and Paper Industry, Helsinki, 1989, TAPPI Press, Atlanta, GA.

[*26*] Wanklyn, J. N. and Wilkins, J. M., "Development of an Expert System for Design Consultation on Marine Corrosion," *British Corrosion Journal,* Vol. 20, No. 4, 1985.

[*27*] Westcott, C., Williams, D. E., Croall, I. F., Patel, S., and Bernie, J. A., "The Development and Application of Integrated Expert Systems and Databases for Corrosion Consultancy," NACE Corrosion/86, Paper No. 54, National Association of Corrosion Engineers, 1986.

Charles P. Sturrock,[1] *David B. Anderson,*[1] *Albert S. Krisher,*[2] *and Thaddeus S. Lee*[3]

Corrosion Evaluation Information Dissemination via Computers

REFERENCE: Sturrock, C. P., Anderson, D. B., Krisher, A. S., and Lee, T. S., "**Corrosion Evaluation Information Dissemination Via Computers,**" *Corrosion Testing and Evaluation: Silver Anniversary Volume, ASTM STP 1000,* R. Baboian and S. W. Dean, Eds., American Society for Testing and Materials, Philadelphia, 1990, pp. 26–38.

ABSTRACT: Recent advances in information processing technology have made it possible to evaluate and counter corrosion problems using computer programs as sources of reference or advisory information. Since 1982 the Corrosion Data Program of the National Association of Corrosion Engineers (NACE) and the National Institute of Standards and Technology (NIST) have produced jointly a number of corrosion databases containing useful reference information. More recently, initiatives undertaken by the Materials Technology Institute of the Chemical Process Industries, Inc. (MTI), in conjunction with the NACE-NIST Corrosion Data Program, have yielded a diverse set of materials advisory programs. The first of a series of modules providing advice on materials selection for handling hazardous chemicals has been in use by the MTI representative companies since May 1989. Distributed by NACE as CHEM•COR 1, this program suggests materials for equipment in concentrated sulfuric acid environments. A separate project involving MTI-NACE-NIST is underway to deliver an advisory program developed by corrosion experts that assesses the likely corrosion behavior of stainless alloys in a wide range of aqueous environments. Finally, MTI and NACE-NIST are separately involved in developing a number of other computer programs that disseminate corrosion information. All of these programs are discussed herein, with particular emphasis on CHEM•COR 1.

KEY WORDS: corrosion, corrosion data, material selection, expert systems, database

The dramatic increases in the rate of technological advances over the last century and in the specialization of the technical professions have created a valuable new resource. This resource is technical information. Prosperity will reward those companies and nations who produce, manage, and distribute the highest quality technical information.

Information in general is not a particularly tangible commodity and has been stored through the ages largely in people's brains and in written media. Until the Renaissance, written information was available only to the very rich, who could afford to hire scribes and to purchase printing materials. The invention of the printing press made widespread distribution of written information possible, which in turn had a major role in improving the quality of life for the nonrich. However, technical information of a practical nature did not

---

[1] NACE Engineering Software Senior Manager and Director, respectively, NACE-NIST Corrosion Data Center, NIST Building 223, Room B254, Gaithersburg, MD 20899.

[2] Executive director, Materials Technology Institute of the Chemical Process Industries, Inc., 12747 Olive Street Rd., St. Louis, MO 63141.

[3] Executive director, National Association of Corrosion Engineers, P.O. Box 218340, Houston, TX 77218.

often lend itself to distribution via written documents, and those that had technical training became much more valuable to society as a whole: witness the rise in social standing of engineers and physicians over the last century.

The digital computer is undoubtedly one of the greatest technical innovations of the twentieth century. Originally invented as a machine to do complex mathematical calculations rapidly and reliably, the computer has evolved into a more general-purpose tool for information management. The preponderance of word processing and electronic spreadsheets in virtually every office environment has made the computer virtually indispensable as an information management tool. The drop in the cost of computer memory and magnetic storage has made it possible for anyone, not just central data-processing staff, to have access to these resources, available typically within a personal computer.

Along with computers, the programs needed to run computers, known collectively as computer software, have also grown considerably in power and availability. Advances such as relational databases, expert systems, and hypertext afford tremendous opportunities to manage the ever-growing pool of technical information. Once the privilege of computer scientists in well-funded research laboratories, many of these software tools are available to users of technical information interested in developing or consulting applications based on this software.

These advances in computer technology have benefited the engineering profession, and corrosion engineers are no exception. The corrosion engineer today is confronted with an explosion of information which requires assimilation, interpretation, and proper application. New materials and methods for controlling corrosion, new methods for monitoring and evaluation system performance, and additional performance data are presented to the corrosion engineer on an almost daily basis. This information overload comes at a time when many organizations are confronted with retirement of senior personnel who carry the "corporate memory" with them on their leaving. Also, organizations frequently are operating with reduced staff levels, particularly specialized staff, such that engineers are faced with the need to perform at higher levels of productivity in order to meet the challenges presented to them. Proper application of computer technology provides one means of retaining, organizing, and retrieving the vast quantities of information confronting the corrosion engineering profession.

The NACE-NIST Corrosion Data Program

In 1982 NACE and NIST established the NACE-NIST Corrosion Data Program. The objective of the program is to collect, evaluate, and disseminate in computerized forms corrosion behavior information on engineering materials. In June of 1985 NACE and NIST jointly conducted a corrosion data workshop to determine the specific corrosion information needs of industry, academia, and government and how the Program could best meet these needs [*1*]. The workshop resulted in many recommendations, including:

1. Development of a broad-scope, computerized corrosion database that could be accessed via personal computers.
2. Design of a standard format to facilitate collection and evaluation of data.
3. Inclusion of data from industrial databases as well as published literature.
4. Development of expert systems to enhance predictive capacity when data are not available.
5. Establishment of an organization to provide necessary personnel and financial support.

With these goals, the charter of the Program was established. In addition to NACE and

NIST, the Program benefits from direct sponsorship from industry. The first industrial sponsorship of the Corrosion Data Program came from the chemical industry.

MTI-NACE-NIST Project

MTI is a cooperative research organization, representing 41 private companies, that conducts generic, nonproprietary studies of a practical nature concerning the deterioration of materials and equipment used in the process industries. In 1987 MTI initiated a project within the NACE-NIST Corrosion Data Program to develop a series of knowledge-based expert systems concerning materials for handling hazardous chemicals. MTI has received direct financial support of this initiative from the Nickel Development Institute.

Distributed by NACE as the CHEM•COR series, these modules focus on material selection and related issues for handling and storage of specific hazardous chemicals. The objectives of these modules are twofold: (1) to suggest materials for users to consider when shipping, handling, or storing a specific hazardous chemical, and (2) to provide tutorial and background information on the same subject. Two audiences for the CHEM•COR series are envisioned: (1) people who work with the specific hazardous chemicals but have little background in materials or corrosion engineering; and (2) materials and corrosion engineers who are not expert in the materials requirements of the specific hazardous chemicals, but who occasionally need reliable materials selection information. The first module in the CHEM•COR series addresses materials for the shipping, handling, and storage of concentrated sulfuric acid.

CHEM•COR 1

Development Team

Domain expertise for CHEM•COR 1 was supplied by corrosion specialists selected by MTI and subcontracted to NACE. The principal domain expert was C. P. Dillon, who has over 40 years' experience in the corrosion and materials engineering profession. He was supported in this effort by a team of four other sulfuric acid experts whose collective experience exceeds 125 years. CHEM•COR 1 was designed by Dillon and the first author and was implemented by the first author with programming assistance from Robert W. Carroll.

Description

The objectives and target audience described above indicate that a hybrid design strategy was needed for the CHEM•COR modules. Since these modules were specified to provide both advice and reference information, two software technologies were applied: expert systems and information retrieval. A technical description of expert systems with examples from CHEM•COR 1 is provided elsewhere [*2*]. Information retrieval programs enable rapid navigation through text and graphic images indexed and stored on computers. The architecture and control structure of CHEM•COR 1 are illustrated in Fig. 1. Note the hybrid design.

When CHEM•COR 1 is invoked, the user is first greeted with welcome and disclaimer screens before arriving at the Main Menu (Fig. 2). The user may consult the materials advisor (Fig. 2, Option 1) or review supplementary information (Fig. 2, Options 2–6).

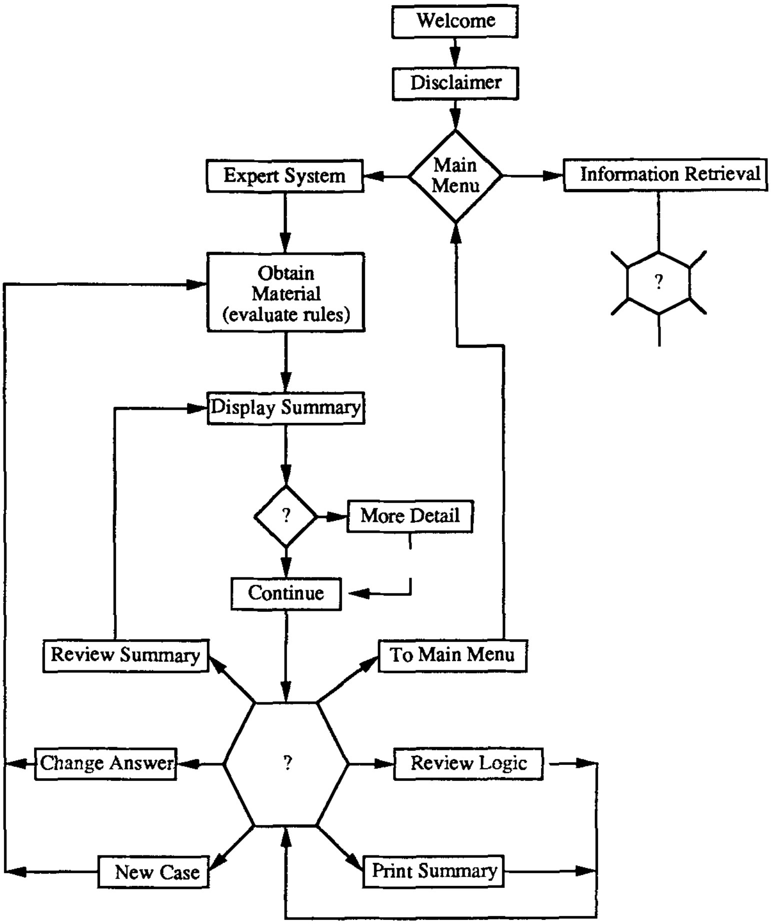

FIG. 1—*Partial architecture and control structure.*

CHEM•COR 1—Materials Advisor

When the user selects Option 1, a knowledge base of some 250 rules regarding a total of 71 materials in concentrated sulfuric acid environments is loaded into memory. The rule inferencing process is initiated, indicated by the box labeled "Obtain Material" in Fig. 1. Rule inferencing is a process in which a computer program called an inference engine evaluates the entire rulebase to determine which rules are applicable to the user's particular case. The inference engine employed for the CHEM•COR modules is KES™; the C language is used for all other programming of CHEM•COR.

To evaluate the rules, CHEM•COR 1 interviews the user. During the interview the user is asked a series of questions to determine the critical factors affecting material selection. Broadly speaking, there are three categories of factors considered: equipment, environment, and units. Equipment factors include the type, size, and mechanical constraints of common equipment used to ship, store, and handle concentrated sulfuric acid. Environmental factors include the acid concentration and temperature, the velocity of the acid and whether the flow is continuous or intermittent, and the extent or acceptance of contamination from other

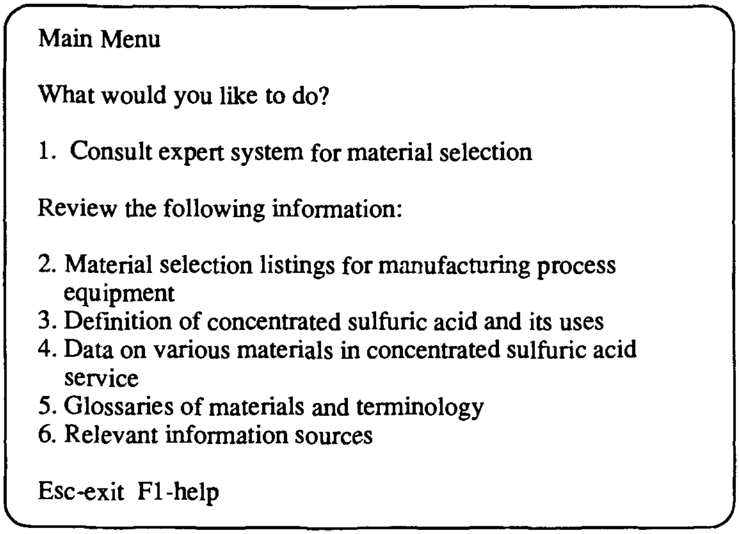

Main Menu

What would you like to do?

1. Consult expert system for material selection

Review the following information:

2. Material selection listings for manufacturing process equipment
3. Definition of concentrated sulfuric acid and its uses
4. Data on various materials in concentrated sulfuric acid service
5. Glossaries of materials and terminology
6. Relevant information sources

Esc-exit F1-help

FIG. 2.—*CHEM•COR 1 main menu.*

species such as iron, oxidizing agents, chlorides, and nitric acid. If CHEM•COR 1 needs to ask the user to input a number, the user is first asked whether inch-pound or SI units are preferred.

The interview occasionally is interrupted with short statements that provide preliminary conclusions, provisional advice, or cautionary warnings. An example of such a statement is shown in Fig. 3.

When the inferencing process is complete and CHEM•COR 1 has collected the user's case data via the interview, materials selection advice pertinent to the current case is summarized. An example summary screen is shown in Fig. 4. After reviewing the summary screen the user is given the option to see additional detail, review the summary screen, or continue. If additional detail review is chosen, the user is presented with a menu of the suggested materials from which he may choose in any combination, leading to brief statements about the composition, corrosion behavior, mechanical properties, fabrication caveats, etc. of the chosen material candidates. Examples of such statements are shown in Fig. 5.

When the user has finished reviewing the summary screens and additional detail, a menu of six options (Fig. 6) is presented. Briefly, these options are as follows:

1. Review summary—review the summary screen(s).
2. Print summary—print the summary screen(s).
3. See logic—review the rule(s) that led to the advice.

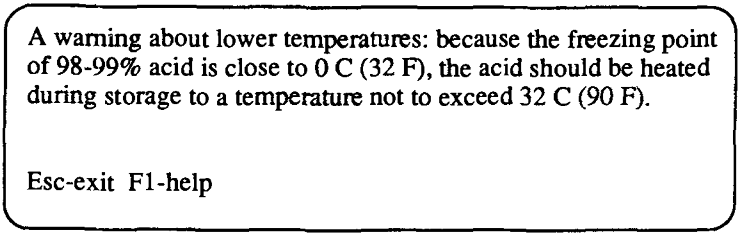

A warning about lower temperatures: because the freezing point of 98-99% acid is close to 0 C (32 F), the acid should be heated during storage to a temperature not to exceed 32 C (90 F).

Esc-exit F1-help

FIG. 3—*CHEM•COR 1 preliminary warning.*

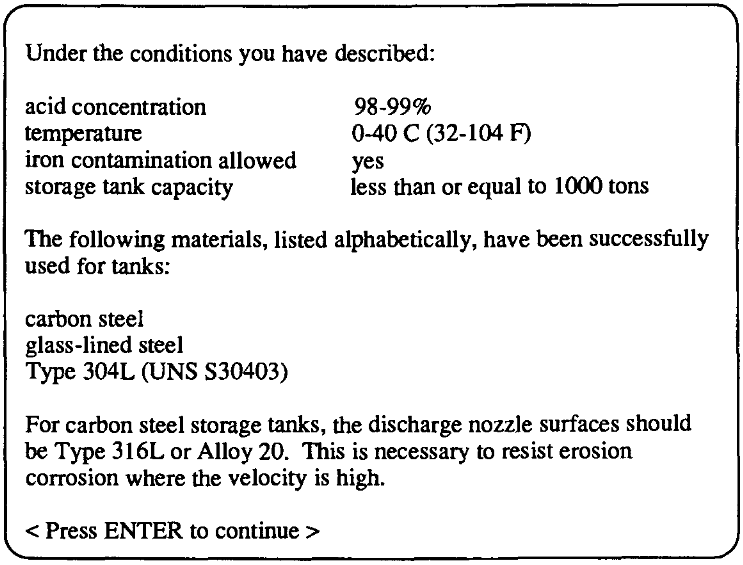

```
Under the conditions you have described:

acid concentration            98-99%
temperature                   0-40 C (32-104 F)
iron contamination allowed    yes
storage tank capacity         less than or equal to 1000 tons

The following materials, listed alphabetically, have been successfully
used for tanks:

carbon steel
glass-lined steel
Type 304L (UNS S30403)

For carbon steel storage tanks, the discharge nozzle surfaces should
be Type 316L or Alloy 20. This is necessary to resist erosion
corrosion where the velocity is high.

< Press ENTER to continue >
```

FIG. 4—*CHEM•COR summary screen.*

4. Change answer—change any combination of answers to questions during the interview and obtain updated advice.
5. New case—consider an entirely new case.
6. Return to Main Menu—return to the Main Menu.

CHEM•COR 1—Information Retrieval

The information retrieval module of CHEM•COR 1 consists of a decision tree having text files and graphs at the terminal nodes. The user navigates through the tree via a series of menus until given the option to see or print the selected information. The first and second levels of the tree are described in Fig. 7. The five classes of information available are shown as Choices 2 to 6 of the Main Menu (Fig. 2). Examples of selected text and graphic images available within CHEM•COR 1 are shown in Figs. 8 to 11. A total of 92 graph and text files

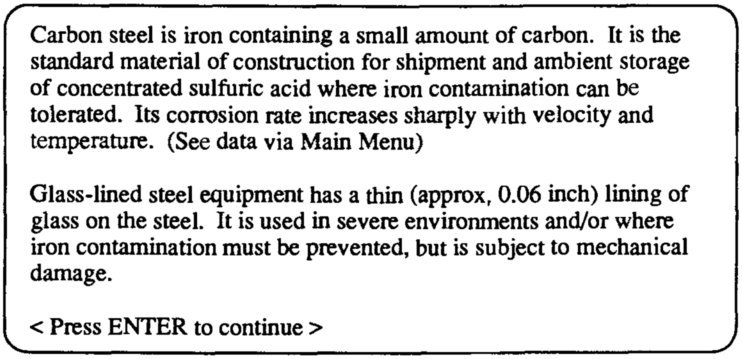

```
Carbon steel is iron containing a small amount of carbon. It is the
standard material of construction for shipment and ambient storage
of concentrated sulfuric acid where iron contamination can be
tolerated. Its corrosion rate increases sharply with velocity and
temperature. (See data via Main Menu)

Glass-lined steel equipment has a thin (approx, 0.06 inch) lining of
glass on the steel. It is used in severe environments and/or where
iron contamination must be prevented, but is subject to mechanical
damage.

< Press ENTER to continue >
```

FIG. 5—*CHEM•COR sample statements.*

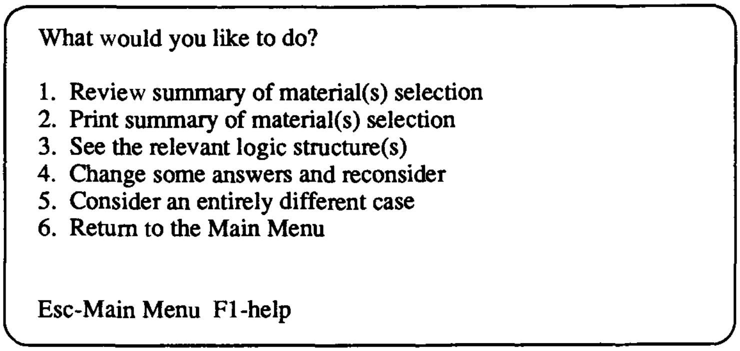

What would you like to do?

1. Review summary of material(s) selection
2. Print summary of material(s) selection
3. See the relevant logic structure(s)
4. Change some answers and reconsider
5. Consider an entirely different case
6. Return to the Main Menu

Esc-Main Menu F1-help

FIG. 6—*CHEM•COR 1 post-selection menu.*

comprising some 261 kilobytes of information (approximately 250 output screens) are available in the information retrieval module of CHEM•COR 1.

In addition to the read-only version described herein, an "open" version known as CHEM•COR 1•PLUS also is available. Users of CHEM•COR 1•PLUS may add data to the system and download their own custom versions of CHEM•COR 1 for internal distribution. However, in order to guarantee integrity of system output, there is no provision to suppress the output of CHEM•COR 1, and any custom data is clearly marked as such. The data may be added via the keyboard or retrieved directly from ASCII text files, eliminating any need to duplicate existing data. The ability to create a custom version of CHEM•COR 1 in this manner adds greatly to its value and utility, because CHEM•COR 1 can therefore be used as a vehicle to distribute proprietary information to many users within a single company, or simply for central storage of company preference and practice.

The custom options available in CHEM•COR 1•PLUS enable users to add proprietary information to CHEM•COR 1 in order to:

1. Precede a question in materials advisory mode.
2. Supplement the on-line help for such a question.
3. Respond to a user's answer to such a question.
4. Supplement the advice following the materials advisory summary.
5. Supplement the data available in information retrieval mode.

With these options, the opportunities to add custom information to CHEM•COR 1 are essentially limitless.

CHEM•COR Development Schedule

CHEM•COR 1 and CHEM•COR 1•PLUS were completed in November 1989. Future CHEM•COR modules will address such corrosives as: acetic acid, formic acid, hydrogen chloride, chlorine, sodium hydroxide, and phosphoric acid.

Related Programs

There are numerous other corrosion software projects that are in some way affiliated with MTI, NACE, and NIST. The first NACE-NIST Corrosion Data Program products were released in 1987. Derived from the NACE publication (Corrosion Data Survey),

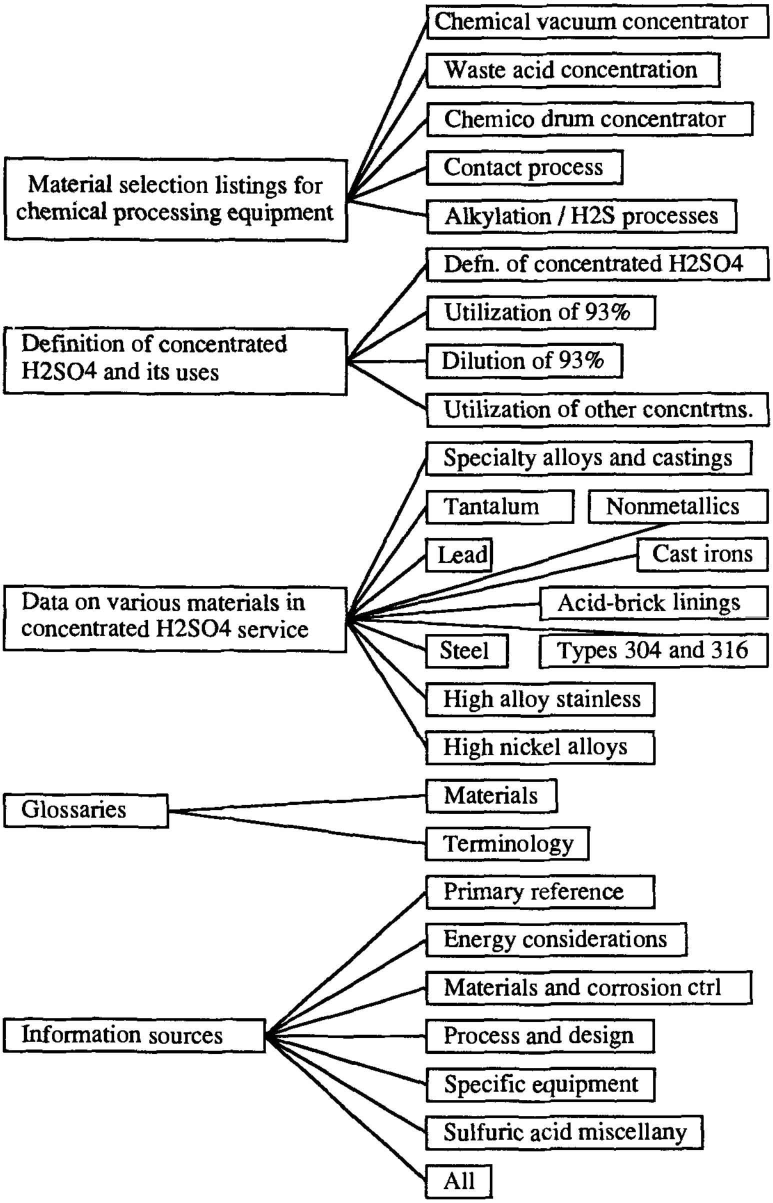

FIG. 7—*CHEM•COR 1 Levels 1 and 2 of information system.*

COR•SUR® and COR•SUR2® provide corrosion rate data on metals and nonmetals, respectively, in single corrosive environments as a function of temperature and corrosive concentration. Corrosion rate data are available in these programs for 25 common metals exposed to approximately 1000 corrosive environments and for 36 nonmetals in over 850 corrosive environments. A sample data screen from COR•SUR is shown in Fig. 12. COR•SUR and COR•SUR2 provide extremely useful reference data, but are essentially

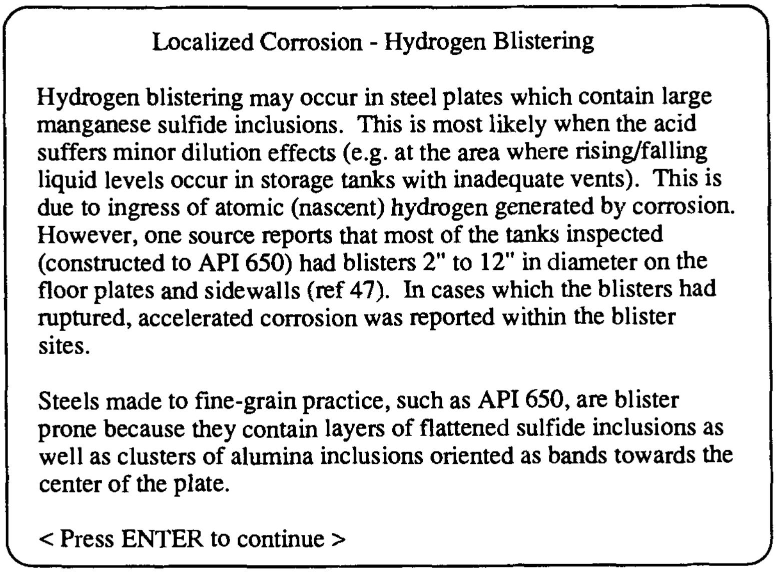

Localized Corrosion - Hydrogen Blistering

Hydrogen blistering may occur in steel plates which contain large manganese sulfide inclusions. This is most likely when the acid suffers minor dilution effects (e.g. at the area where rising/falling liquid levels occur in storage tanks with inadequate vents). This is due to ingress of atomic (nascent) hydrogen generated by corrosion. However, one source reports that most of the tanks inspected (constructed to API 650) had blisters 2" to 12" in diameter on the floor plates and sidewalls (ref 47). In cases which the blisters had ruptured, accelerated corrosion was reported within the blister sites.

Steels made to fine-grain practice, such as API 650, are blister prone because they contain layers of flattened sulfide inclusions as well as clusters of alumina inclusions oriented as bands towards the center of the plate.

< Press ENTER to continue >

FIG. 8—*CHEM•COR 1 sample text.*

"closed" systems: there is no provision for users to enter their own data or build their own corrosion databases.

For users who wish to build their own corrosion databases NACE and NIST developed and released in 1989 COR•DATA PLUS, a database package that provides a standard format for the assembly, search, and retrieval of corrosion data. COR•DATA PLUS utilizes a

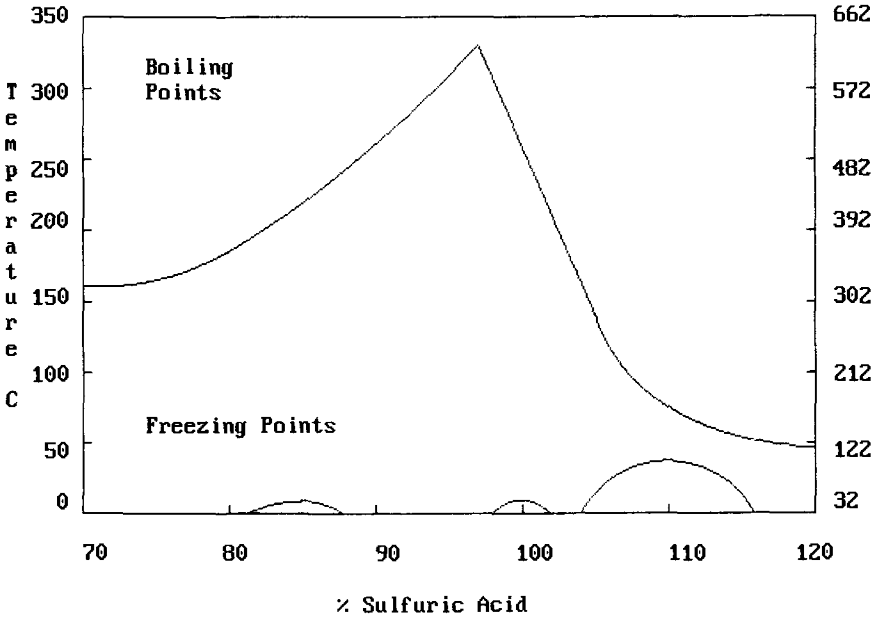

FIG. 9—*CHEM•COR 1 graph of boiling and freezing points for concentrated sulfuric acid.*

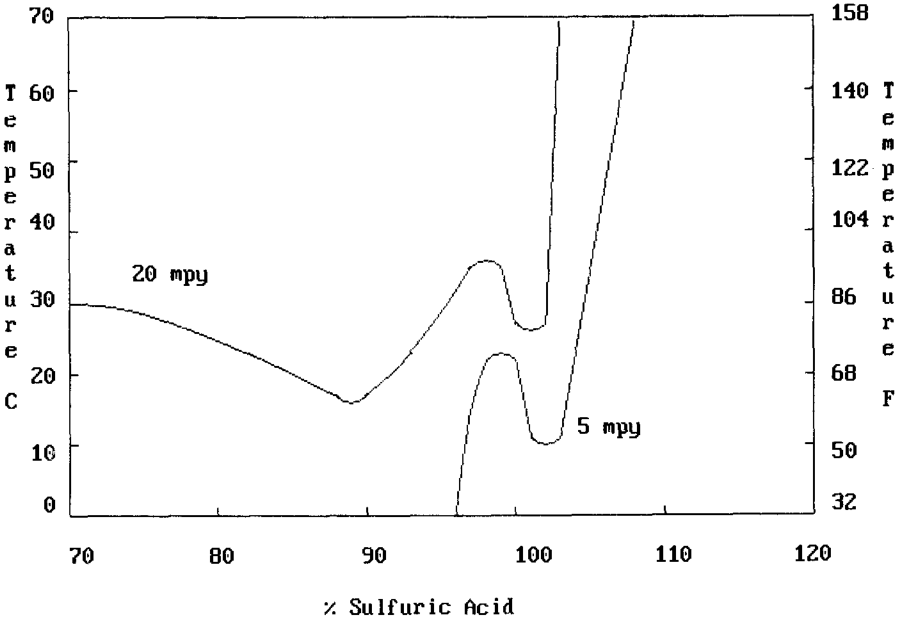

FIG. 10—*CHEM•COR 1 isocorrosion chart for carbon steel.*

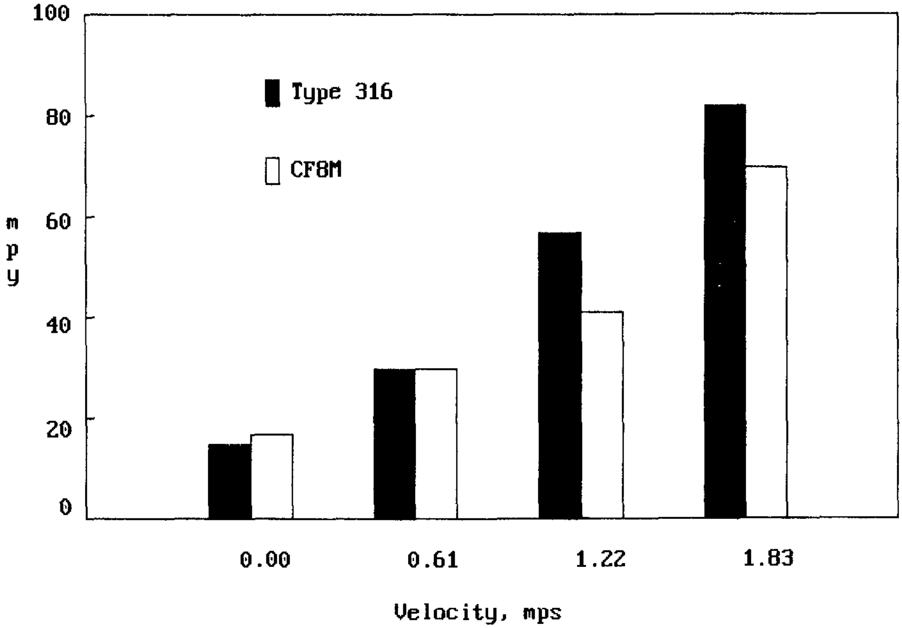

FIG. 11—*CHEM•COR 1 velocity effects in 95% sulfuric acid at 50°C (122° F).*

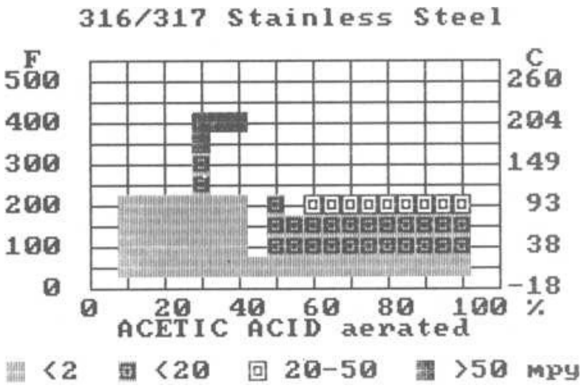

FIG. 12—*Sample data screen from COR•SUR.*

standard format for organization of corrosion data as developed by NACE Technical Committee T-3U on Computers in Corrosion Control. Use of the standard format facilitates exchange of information and consistency among users of corrosion control data.

COR•DATA PLUS Version 1.0.0 accommodates general weight loss corrosion rate data for metals and alloys plus related pitting and crevice corrosion data. Future updates will permit additions of data relating to other forms of corrosion, including stress corrosion cracking, corrosion fatigue, etc. The initial release of COR•DATA PLUS is designed for corrosion scientists and engineers to establish their own database using a series of menu-driven screens to organize the data input process. A sample dataset is included to provide the user with examples of how data are formatted and how to search and retrieve data. The sample data are derived from 300 field tests of nickel alloys in sulfuric acid process environments involving approximately 4000 specimens.

With the sponsorship of the Industrial Processing Division of the New Zealand Department of Scientific Research, NACE-NIST has developed PETRO•COR 1, an expert system for oil and gas industry applications [*3*]. PETRO•COR 1 suggests materials to consider for applications involving sucker rod pumps and is based on information in NACE and American Petroleum Institute standards and publications with enhancements that reflect current industry practice. The practices are based on advice and technical contributions from sucker rod pump manufacturers, oil and gas production companies, and individuals with expertise in specifying materials for subsurface pumps.

The Electric Power Research Institute has recently underwritten a three-year project for NACE-NIST to develop six computer modules of interest to the electric power industry [*4*]. Distributed ultimately by NACE as the POWER•COR series, these modules will address such topics as: corrosion of condenser materials, stress corrosion cracking and intergranular attack of Alloy 600 in secondary waters, cracking of structural materials in nuclear environments, corrosion in service waters, microbially induced corrosion, and corrosion in flue gas desulfurization systems. The project will involve a broad spectrum of software technology, utilizing mathematical modeling, relational databases, hypertext, and expert systems in some combination unique to each module.

One of the MTI members has developed an expert system which MTI is seeking to deliver to its entire membership. Known as AUSCOR, this program predicts the likely corrosion behavior of stainless alloys in a wide range of aqueous environments [*5*]. More specifically, AUSCOR provides an assessment of the probabilities of the modes associated with general corrosion, localized corrosion, and stress corrosion. It also provides an indication whether these probabilities are likely to be sensitive to small changes in environmental conditions.

NACE has developed corrosion-related software outside of the Corrosion Data Program. The COR•AB text retrieval package provides keyword search capabilities over a database of abstracts from NACE's journal, *Corrosion Abstracts.* Currently the database contains abstracts from the journal for the years 1982 through 1987. The final version, available in 1990, will contain abstracts from the journal for the years 1962 to 1988, inclusive.

MTI has independently developed a simple database of wrought alloys commonly used in the chemical process industries. This database consists of a total of 198 entries, covering 136 alloys. Each entry includes UNS number, trade name, generic name, supplier (for proprietary alloys), partial mechanical properties, ASTM specifications, ASME Code coverage, chemical limits, and equivalent specifications. The database is supplied as a file in Lotus 1-2-3 format, which can be used as input to most spreadsheet and database programs. Additional alloys, including cast alloys, are being added. This database has proven valuable in keeping up to date on available alloys, many of which are supplied by several suppliers under differing trade names.

Conclusion

NACE and NIST are engaged in a program to compile and organize information to assist in the cost-effective practice of corrosion engineering. The use of personal computer software modules to achieve this goal provides for cost-effective distribution of this information. These software modules are available in various forms, including numeric databases, expert systems, and text retrieval systems. Hybrid modules also are under development to allow for the integrated use of databases, expert systems, and text files. This hybrid approach provides a system that gives guidance to the inexperienced while providing more detailed technology to the experienced corrosion engineer.

References

[1] Verink, E. D., Kolts, J., Rumble, J., and Ugiansky, G. M., "Corrosion Data Program Workshop Summary," *Materials Performance,* National Association of Corrosion Engineers, Houston, TX, April 1987, pp. 55–57.

[2] Sturrock, C. P. and Sharp, W. B. A., "An Integrated Information System Concerning Materials for Handling Hazardous Chemicals," Paper No. 272, *CORROSION/89,* National Association of Corrosion Engineers, Houston, TX, 1989.

[3] Lichti, K. A., Karras, P., and Sturrock, C. P., "Development of a Standards Based Expert System for Selecting Materials for Oil and Gas Industry," Paper No. 476, *CORROSION/89,* National Association of Corrosion Engineers, Houston, TX, 1989.

[4] Anderson, D. B., Lee, T. S., and Syrett, B. C., "Computerized Corrosion Behavior Information for Electric Utility Applications," *Proceedings,* Conference on Plant Maintenance Technology, Electric Power Research Institute, Palo Alto, 1989.

[5] Basden, A. and Hines, J. G., "Implications of Relation Between Information and Knowledge in Use of Computers to Handle Corrosion Knowledge," *British Corrosion Journal,* Vol. 21, No. 3, 1986, pp. 157–162.

DISCUSSION

M. Schorr[1] (*written discussion*)—Since I work for the chemical industry, I can say that these programs are useful for solving problems in the plants. But they should include detailed data on the impurities content of sulphuric acid and the operating conditions of the system.

---

[1] IMI, Institute for Research and Development, P.O. Box 313, Haita, 31002, Israel.

C. P. Sturrock, et al. (*authors' closure*)—The corrosion data in CHEM•COR are presented as reported by the original investigator. Some data are based on laboratory tests using pure acid which does not contain contaminants, often encountered under actual operating conditions. Where field tests are reported, the original investigator may not have identified specific contaminants nor documented their influence. A determined user of CHEM•COR can review the publications cited therein for this information.

S. Garnett[1] (*written discussion*)—As already noted by others, the use of "expert systems" by nonexperts opens significant possibilities for mistakes. On the other hand, the experts will find the "expert system" inadequate. The systems being developed will cover the 10 to 15 heaviest industries, perhaps because they are the ones prepared to fund the development work. The chemical process industries, with hundreds to thousands of processes, will find the "expert systems" inappropriate for their very specific conditions and needs. Even for those 10 to 15 industries where the investment is made, the "expert systems" will require a generation before they become right and are truly useful. I believe the current need is for databases. From these the lesser and greater experts can develop their answers to the specific problems they face.

C. P. Sturrock, et al. (*author's closure*)—The use of any information resource (not only expert systems) by nonexperts opens significant possibilities for mistakes. The greater the interpretation of output required, the more mistakes will be made. Because the CHEM•COR modules are designed for use by nonspecialists, the output is very specific, e.g. "materials *x*, *y*, and *z* have been successfully used under the conditions you have specified." With such specific advice we feel there are fewer opportunities for errors through misinterpretation of output.

An expert system designed for use by experts need not be inadequate if it incorporates the expertise of many experts and can solve a wider variety of problems than any single expert. The materials advisory component of a particular CHEM•COR module is of little use to an expert on the handling and storage of the hazardous chemical in question; however, few individuals have extensive experience with all seven hazardous chemicals in the overall CHEM•COR system. Furthermore, the hybrid design of the modules includes information retrieval of corrosion rate data and references to the literature for experts who wish to probe further into the domain.

While it is true that there are thousands of processes within the chemical process industries, corrosion phenomena vary only with the choice of material and a few key environmental factors. Hot sulfuric acid corrodes carbon steel regardless of the process that brings them together. Databases of corrosion rate data (when such data are available and reliable) are useful to corrosion experts capable of interpreting the data with respect to their own needs; however, we feel uninterpreted data presented to nonspecialists invites error.

---

[1] IMI, Institute for Research and Development, P.O. Box 313, Haita, 31002, Israel.

William G. Clark, Jr.,[1] *and Michael J. Metala*[1]

The Nondestructive Characterization of Corrosion

REFERENCE: Clark, W. G., Jr. and Metala, M. J., "**The Nondestructive Characterization of Corrosion,**" *Corrosion Testing and Evaluation: Silver Anniversary Volume, ASTM STP 1000,* R. Baboian and S. W. Dean, Eds., American Society for Testing and Materials, Philadelphia, 1990, pp. 39–49.

ABSTRACT: Recent advances in nondestructive evaluation (NDE) technology have led to improved methods for quality control and in-service inspection. In addition, these same advancements have led to the development of new options for material diagnostics. No longer are NDE considerations directed only at crack detection and sizing. Detailed discontinuity characterization has become a major objective of much NDE work underway today. Specifically, this work is aimed at the creation of quantitative NDE methods which offer a rational alternative to destructive metallography for material evaluation. While this goal may be some ways off, significant progress has been made in the NDE characterization of corrosion-induced degradation. Nowhere have these developments been more evident than in the characterization of corrosion phenomena in small-diameter, heat exchanger tubing. This paper presents results from a continuing program designed to establish improved inspection methods for the assessment of corrosion degradation in nickel-alloy nuclear steam generator tubing. The major focus is directed at unique test methods and data analysis techniques which offer the potential to identify and discriminate between different kinds of corrosion degradation. While the results highlight success in the assessment of tubing, the concepts and general observations are equally applicable to other components.

KEY WORDS: tubing, degradation, eddy current, ultrasonic, corrosion, inspection, visual, nondestructive, steam, generator, diagnostics

A critical aspect of a rational corrosion control strategy is the early detection and characterization of potential degradation in the hardware-environment system of concern. The conventional approach to this problem typically involves the preparation, corrosion testing, and periodic nondestructive evaluation (NDE) of laboratory samples designed to replicate the anticipated service conditions. Results from these tests in turn are used to establish guidelines for field inspection options. In general, two major aspects of inspection capability must be considered—detection and characterization. Detection considerations relate to overall inspection sensitivity and the ability to discriminate between relevant and nonrelevant indications. Characterization, on the other hand, is the ability to define the source of the indication once detected. In the characterization arena we face the challenge of using NDE techniques to identify and discriminate between different kinds of material degradation. Where corrosion is a source of degradation, the characterization of damage is further aggravated by the number of potential mechanisms and failure modes that can be involved. Despite these complexities, the need to extract more and more information from inspection

---

[1] Materials Reliability, Westinghouse Science & Technology Center, 1310 Beulah Rd., Pittsburgh, PA 15235.

results continues to increase due to the demand for the more efficient use of materials. Early damage detection alone is not adequate. Detailed defect sizing and characterization has become the major objective of much NDE work underway today. Consequently, the technology is moving towards more sensitive tests that yield more complex data which, in turn, are more difficult to interpret. To address this challenge, the NDE community has turned to a combination of multiple mode inspections and computer-aided data analyses. Success in this activity has generated quantitative NDE capabilities which can be used as both improved quality assurance tools and new options for material diagnostics [*1*].

Nowhere have the advantages of advanced NDE been more evident than in the detection and characterization of corrosion damage in power generation applications and, in particular, high-nickel-alloy nuclear steam generator tubing.

The steam generator in a nuclear power plant serves the role of a heat exchanger where heat from water in the core is transferred to the steam system that drives the turbine-generator unit. In this application, thousands of small diameter super-alloy (Inconel) tubes are used to both expedite heat transfer and to keep the core (primary side) system separate from the steam (secondary side) system. These critical operations demand outstanding tubing performance, yet the service conditions represent perhaps the most adverse environment in the plant. High temperature and progressive concentration of even the slightest contaminant can lead to corrosion problems. Over the years, a number of corrosion-related damage mechanisms have been encountered [2]. These phenomenon include pitting, general corrosion (wastage), intergranular attack (IGA), stress corrosion cracking (SCC), corrosion fatigue, and tube denting from the growth of corrosion products at support locations. In addition, these problems have been known to occur in combination. Variations in tubing geometry (transition, bends, etc.), damage location (outside diameter versus inside diameter), and deposit growth further complicate the situation. Clearly, the accurate characterization of corrosion-related phenomena in steam generator tubing presents a formidable challenge for state-of-the-art NDE technology. This challenge, in turn, has led to the development and implementation of some of the most effective NDE capabilities in use today. While developed specifically for relatively small-diameter tubing assessment, the techniques have broad applicability to a wide range of corrosion problems in all types of components. This paper presents an overview of inspection capabilities developed for the evaluation of steam generator tubing. Particular emphasis is directed at the use of NDE techniques for the characterization of corrosion-induced material degradation. Novel inspection procedures developed for both laboratory and field use are described. Visual, radiographic, eddy current, and ultrasonic tests are included along with combined mode options and artificial intelligence-based data interpretation schemes.

Visual Inspection

Recent advancements in optical inspection equipment and, in particular, the development of charged-couple-device (CCD) video probes has kept visual methods high on the list of practical inspection options for many components, including tubing. While not widely applicable to the field inspection of steam generator tubing (because of limited access to the tubing interior), video probes are invaluable for the general assessment of laboratory samples and tubing segments removed from service. However, visual methods alone are not adequate for the quantitative characterization of corrosion damage because the test is limited to surface examination, and corrosion products (stains, deposits, etc.) can mask important damage. Enhanced visual methods involving the use of dye penetrant testing can improve the situation somewhat, but major limitations still remain.

In order to improve the value of visual inspection for the characterization of steam generator tubing, engineers at Westinghouse have developed a unique silicone rubber/dye penetrant replication technique which provides an extremely accurate panoramic view of damage on the inside surface of the tube [3]. Figure 1 illustrates the technique as applied to a corrosion test sample (tube expanded in a collar). A dye penetrant test is performed to entrap dye in any damage open to the tube surface, the excess dye is removed, and a silicone rubber mold is made of the distressed area. The rubber replica is removed when cured, and cellophane tape is applied over the replica in the area of interest. A tracing of damage is made on the tape and the tape removed and placed on a plain sheet of paper, thus creating a panoramic view of the tubing degradation as seen from a position within the tube. This view is important since it matches the perspective encountered by ultrasonic and eddy current probes used to assess tubing. A significant advantage of the replication technique is the ability to create a near-metallographic quality permanent record of tubing damage without destroying the sample. In addition, replicas can be made periodically during a corrosion test to map the extent of degradation as a function of exposure time. Figure 2 shows such results for a steam test sample. Note the intricate details of crack progression revealed by the replication technique. Such data are invaluable for the assessment of corrosion phenomena as well as for the evaluation of alternate inspection options. A major limitation of the rubber replica technique is, of course, the fact that it is applicable only to the characterization of surface degradation.

Panoramic Radiography

Another NDE technique developed at Westinghouse for the improved characterization of steam generator tubing samples is the rotating tube, single-wall X-ray technique. Figure 3 illustrates the procedure. A cylindrical film pack is placed inside the tube and the tube is rotated while being exposed to X-ray radiation passing through a narrow window. Figure 4 shows the results of a single-wall, panoramic view radiograph versus the corresponding double wall radiograph for the same tube containing extensive pitting damage. Note the improved sensitivity and resolution of the single wall test versus the more conventional double-wall technique. Such enhanced radiographic inspection capabilities permit the de-

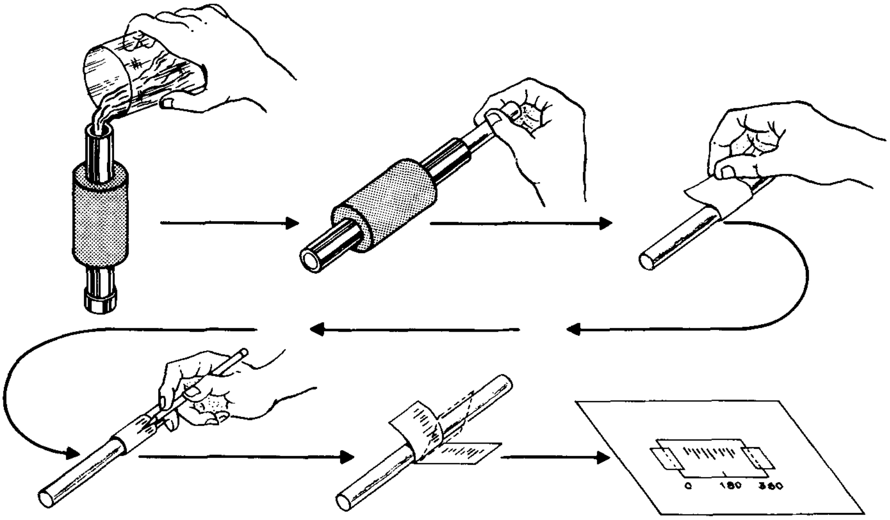

FIG. 1—*Silicone rubber/dye penetrant replication of tubing damage.*

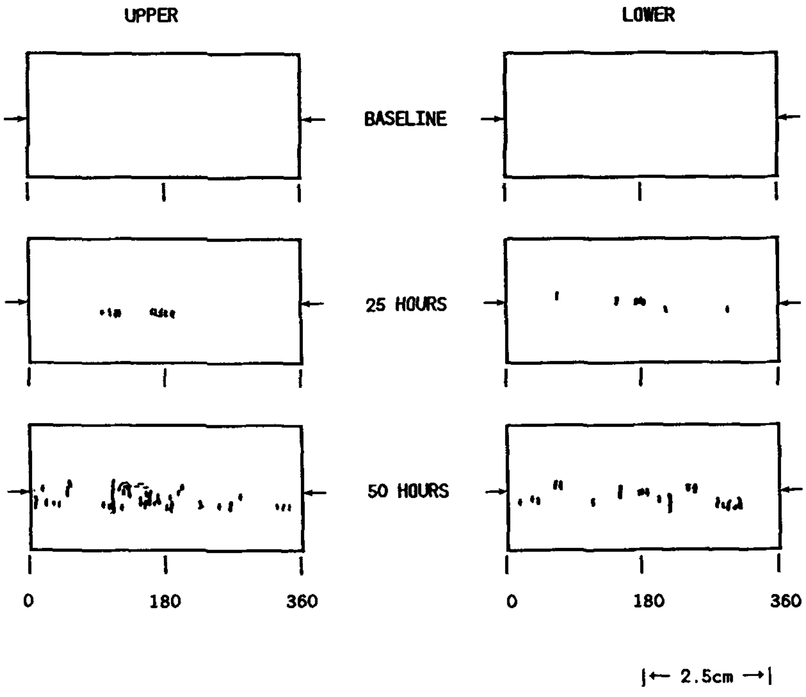

FIG. 2—*Results of periodic replication.*

tailed characterization of corrosion phenomena where through-the-tube wall characterization is important. Panoramic radiographic examination can be conducted periodically during laboratory corrosion studies, but the test cannot be applied in the field.

Eddy Current Inspection

Eddy current methods are widely used for the inspection of nonferromagnetic heat-exchanger tubing. In this test, the impact of discontinuities on the electromagnetic properties of the material provides the basis for an effective NDE method. The major advantages of eddy current testing are rapid inspection rates and outstanding detection sensitivity. However, the popular bobbin coil sensor used to scan the tubing interior surface is not very effective for defect characterization. Consequently, the bobbin coil is used primarily for the detection of corrosion damage and alternate eddy current sensors are used for improved defect characterization. Figure 5 shows two special eddy current probes designed to enhance the defect characterization capabilities of electromagnetic testing. The single-element rotating probe offers a detailed eddy current map of the tubing surface and, thus, an excellent characterization of tubing distress. Figure 6 shows a typical data display for stress corrosion cracking as detected with a single-element rotating probe. Of course, such outstanding detail is obtained at the expense of testing speed. The rotating probe test is orders of magnitude slower than the bobbin coil test.

The multiple element eddy current probe shown in Fig. 5 is an attempt to capture some of the advantages of the rotating probe with a straight pull concept. The defect characterization capabilities of the multiple element probe are much better than the bobbin coil, and data can be taken at about the same period. However, data reconstruction presents a formidable task.

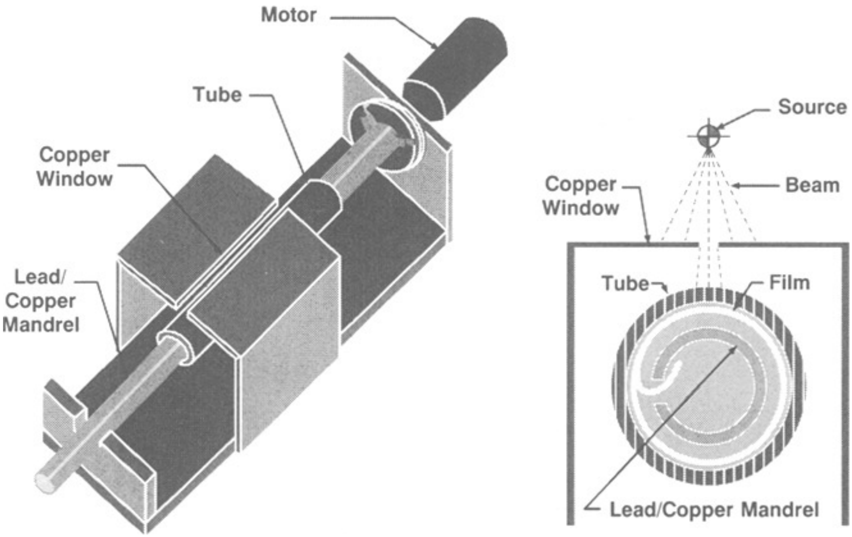

FIG. 3—*Rotating tube single-wall X-ray technique.*

An important development in eddy current testing that expands the discrimination capabilities of virtually all eddy current probes is multiple frequency testing. In this procedure, the same sensor is activated at two or more frequencies nearly simultaneously, and the frequency-induced variation in response is used to further characterize discontinuities. This technique is particularly valuable for resolving the effect of surrounding hardware, tubing geometry, and corrosion products on eddy current results. For example, a crack filled with a conducting or magnetic deposit can yield an eddy current signal much larger than that produced by the crack itself. A multifrequency eddy current assessment of the crack can

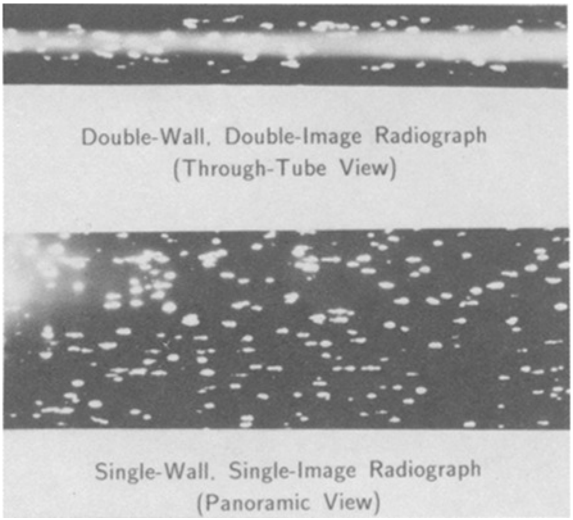

FIG. 4—*Conventional versus panoramic X-ray of tubing sample (pitting).*

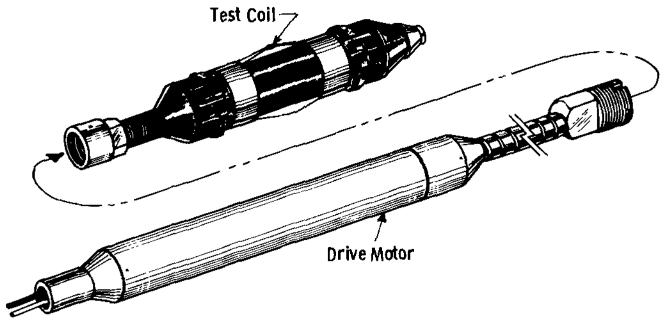

Motorized Rotating "Pancake" Coil

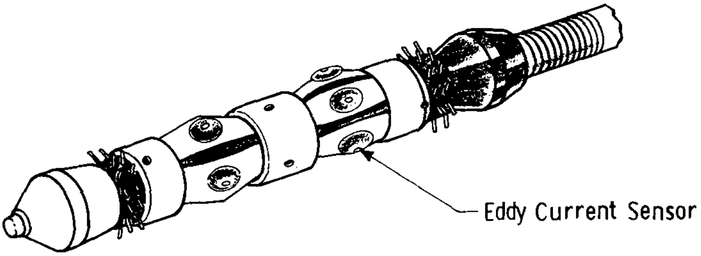

FIG. 5—*State-of-the-art eddy current probes for tubing inspection.*

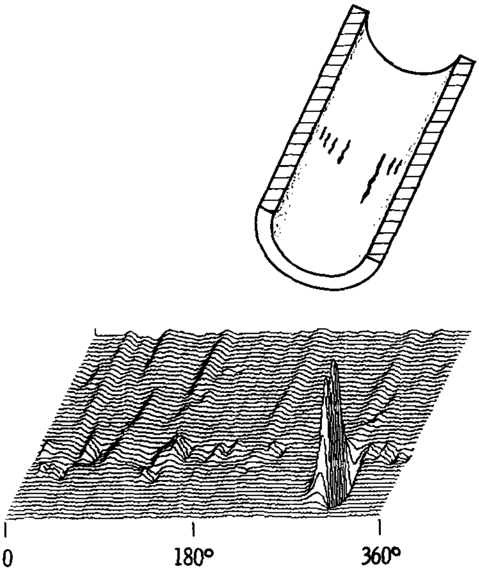

FIG. 6—*Isometric display of corrosion cracking; rotating EC probe on tube ID.*

reveal the presence of the deposit and thus provide a diagnostic capability important for the identification of corrosion mechanisms.

Despite the success of eddy current methods for the assessment of heat exchanger tubing, the test has important limitations, particularly with regard to the characterization of wall thinning and multiple-crack degradation modes. In an attempt to resolve these limitations, ultrasonic inspection techniques have been developed to supplement eddy current testing.

Ultrasonic Inspection

Ultrasonic methods are widely used as quality control tests during tubing manufacture. However, only recently has this test been considered for the routine in-service assessment of steam generator tubing. In the past, ultrasonic test methods have been used successfully to map wall thinning in steam generator tubes, but the test was considered too limited and too slow for general inspection. With the recent development of multiple-element ultrasonic inspection probes, some of the earlier concerns have been resolved and ultrasonic tests are now considered prior to pulling tubes for diagnostic purposes. Figure 7 shows two multiple-element ultrasonic probes used to assess heat exchanger tubing. The "bore-side array" (Krautkramer, Inc.) consists of eight or more ultrasonic transducers arranged in a circumferential pattern. Each sensor directs a separate angle beam sound wave along the axis of the tube. A multiplex instrumentation system is used to create an ultrasonic map of the tube cross-section as the probe is pulled through the tube. This test is particularly sensitive to circumferential cracking (major plane of the crack is perpendicular to the tube axis), but

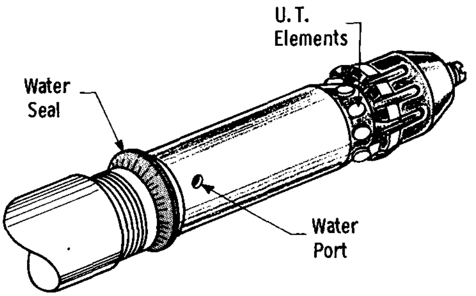

Boreside Array Probe

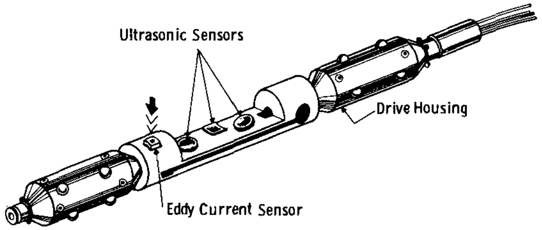

Multiple Look Angle Probe

FIG. 7—*State-of-the-art ultrasonic probes for tubing inspection.*

it cannot be used to accurately characterize axial degradation. Consequently, depending on the source of corrosion damage, the bore side array may be a rational test option.

The multiple look-angle ultrasonic probe shown in Fig. 7 is not limited to the assessment of a particular defect orientation, but, unlike the bore-side array, this probe must be rotated in the tubing. Again, outstanding defect characterization can be achieved at the expense of test speed. Figure 8 shows the results of a multiple-look angle ultrasonic assessment of a steam generator tube containing a crack in an area of wall thinning. To the best of our knowledge, no other nondestructive inspection method can match these results.

Another unique feature of the multiple-look angle ultrasonic probe is the incorporation of a spring-loaded, surface-riding eddy current sensor which permits the collection of electromagnetic data at exactly the same time as the ultrasonic test. This combined mode inspection option further expands the defect characterization capabilities of existing NDE technology. Since the ultrasonic and eddy current tests depend on completely different physical properties, the comparison of results generated at virtually the same time and at the same location permits signal discrimination beyond that possible with a single test mode. While multiple mode testing is a relatively new NDE concept, the advantages for improved discontinuity characterization make it clear that this option will become more common in the near future.

Data Interpretation

The continuing development of NDE techniques which provide ever-increasing amounts of data at faster and faster rates has created a special problem in data interpretation. In many cases the human inspector can no longer be expected to monitor results in real time and make timely decisions regarding product integrity. Again, the inspection of steam generator tubing clearly illustrates this dilemma. Combined multiple-sensor, multiple-frequency, and multiple-mode inspection techniques produce so much information that data interpretation lags far behind data collection capabilities. To address this concern, Westinghouse has pioneered the use of expert system-based artificial intelligence concepts to

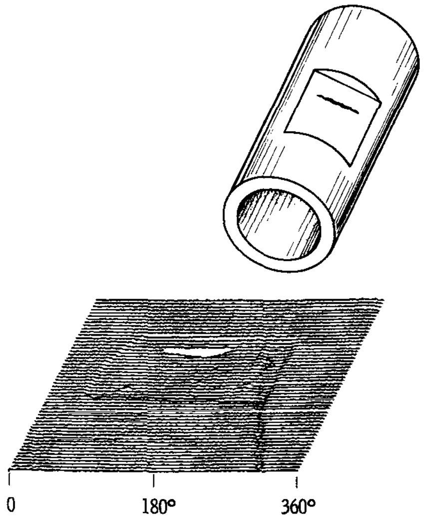

FIG. 8—*Isometric display of corrosion cracking at an area of wall thinning; rotating UT probe on tube ID.*

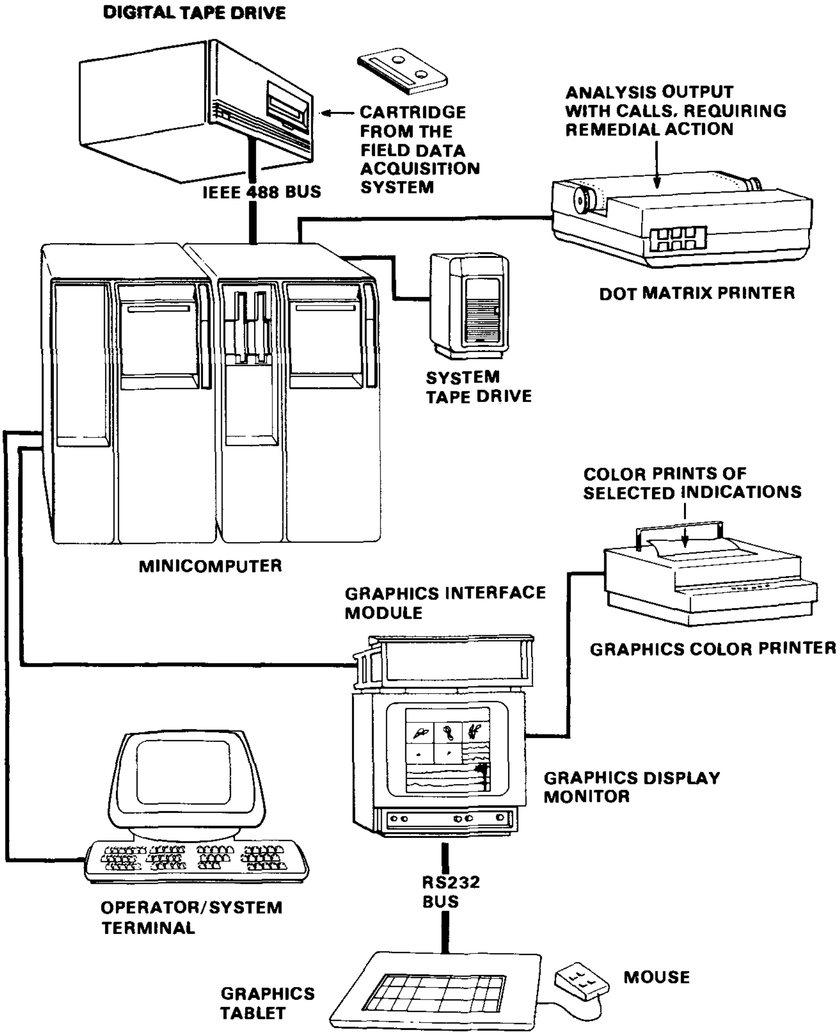

FIG. 9—*Intelligent eddy current data analysis system "IEDA."*

expedite the interpretation of multiple-element, multiple-frequency eddy current testing of SG tubing [*4*]. The Westinghouse system is called IEDA—Intelligent Eddy Current Data Analyses. Figure 9 shows a diagrammatic illustration of the IEDA system. In its present format IEDA provides a high-speed screening capability which extracts specific features from the inspection data that correspond to known discontinuities. This capability significantly reduces the amount of data that must be analyzed by human interpreters. As new rules are developed for the classification of more discontinuities (and nonrelevant indications), the appropriate pattern recognition algorithms are included in IEDA. Current plans include the expansion of intelligent data interpretation technology to ultrasonic inspection results and the pursuit of at least rudimentary self-training options where the computer can offer an opinion regarding the source of test signals. Both experimental and analytical modeling capabilities will be used to devise the smart system. Included in the goals of this program are the automatic detection, sizing, and characterization of virtually any discontinuity that can occur in steam generator tubing. To address these goals we will be pushing the discontinuity characterization capabilities of NDE methods to the limit. At the very least, we expect this activity to further enhance the ability of nondestructive test methods to define the intricate features of discontinuities such that rational material diagnostics is possible without destructive metallography.

Discussion

Significant progress has been made in the long-standing NDE problem of forward versus reverse signal interpretation. In the past it was widely accepted that NDE response could be predicted from knowledge of the defect, but the defect could not be described from NDE data alone. This situation is changing. Progress has not come easy, and even today a number of different inspection methods are required to accurately characterize discontinuities in a relatively simple component. This situation is perhaps best illustrated by the extent of the steam generator tube inspection menu used at the Westinghouse NDE Center. This chart is reproduced in Fig. 10. The options summarized in this matrix reflect some of the considerations that must be addressed to adequately characterize corrosion damage in steam generator tubing. These choices have developed as the result of extensive experience with service analyses and laboratory testing.

Despite the complexities associated with the selection and utilization of NDE methods to characterize corrosion phenomena, the advantages over indiscriminate destructive me-

WESTINGHOUSE NDE CENTER
SG TUBE INSPECTION MATRIX

☐ Radiography	☐ Double Wall ☐ Single Wall	☐ Contact Print ☐ Photo Print ☐ Radiograph
☐ CCD Video	☐ OD Surface ☐ ID Surface ☐ Forward ☐ RT Angle	☐ Thermal Print ☐ Photograph ☐ Video Tape ☐ Disc Record
☐ Eddy Current	☐ ID Bobbin ☐ OD Encircling ☐ RPC ☐ ID ☐ OD ☐ Field ☐ Needle Pt. ☐ Absolute ☐ Diff. ☐ Special ________	☐ HP-ISO Plot ☐ Compac-ISO ☐ DEC-ISO ☐ Color Topo
☐ Ultrasonic	☐ Super Probe ☐ Single Look ☐ Radial ☐ Attn. ☐ Thickness ☐ Axial ☐ Circ.	☐ Compac-ISO ☐ DEC-ISO ☐ Color Topo
☐ Replication (Silastic Mold)	☐ Dye Penetrant ☐ Profile Mold	☐ Photo ☐ 360° Photo ☐ Metrology
☐ Dye Penetrant	☐ Red Dye ☐ Fluorescent	☐ Photo ☐ Sketch

FIG. 10—*Tube inspection menu.*

tallography are tremendous. A primary advantage is the ability to conduct a thorough evaluation and yet keep the sample intact for the assessment and qualification of new and developing inspection techniques. In addition, test coupons with actual degradation as compared to notches and drilled holes provide more defensible training and calibration samples. As trends towards life cycle design options and plant life extension considerations grow, the need for the in-place nondestructive characterization of material condition grows accordingly. If the engineering community is to defend design practices that depend on the continuing recertification of hardware, the associated inspection activities will need to provide more capabilities that defect detection. To meet this challenge we must begin to expand NDE technology into the diagnostic arena. The advances in quantitative NDE related to the characterization of corrosion in steam generator tubing show what is possible with existing systems, and this work should provide the incentive for even more exciting material characterization options.

References

[*1*] Beissner, R. E. and Birring, A. S., "Nondestructive Evaluation Methods for Characterization of Corrosion," Nondestructive Testing Information Analysis Center, Report NTIAC-88-1, December, 1988.
[*2*] de la Pintiere, L., "Think Multifrequency," *Materials Evaluation*, Vol. 43, No. 2, February 1985.
[*3*] Clark, W. G. Jr., et al., "Library of PWR Steam Generator Tubing Samples," Research Report NP-5503, Electric Power Research Institute, Palo Alto, CA, January 1988.
[*4*] Attaar, M., et al., "Automated Analysis of Eddy Current Data from Inspection of PWR Steam Generator Tubing," Paper No. 85-JPGC-NE-7, *Proceedings*, ASME/IEEE Power Generation Conference, ASME, NY, October, 1985.

DISCUSSION

A. C. Van Orden[1]—Is it possible to use NDE to examine complex geometries on real-world samples such as welded or riveted joints? And what can be learned?

W. G. Clark and M. J. Metala (author's closure)—The quantitative NDE capabilities discussed in this paper, while developed specifically for tubing, are widely applicable to a range of structural components. Overall success depends upon the consistency of the component geometry and metallurgy to the extent that the NDE signature can reveal important discontinuities. Another critical factor is the availability of a sufficiently large data base which can support the diagnostic capabilities. Several of the NDE methods illustrated here are currently in use for the characterization of both welded and riveted structures.

---

[1] AS&M, NASA Langley Research Center, Hampton, VA.

Colin McCaul[1]

Evaluation of Corrosion Failures in Pumps

REFERENCE: McCaul, C., **"Evaluation of Corrosion Failures in Pumps,"** *Corrosion Testing and Evaluation: Silver Anniversary Volume, ASTM STP 1000,* R. Baboian and S. W. Dean, Eds., American Society for Testing and Materials, Philadelphia, 1990, pp. 50–65.

ABSTRACT: Pumps are subject to a wide range of corrosion problems. A considerable number of these failures can be grouped into two broad categories. In the first category, some deficiency in fabrication or processing can lead to enhanced corrosion in a normally resistant material. Intergranular attack and corrosion at casting defects are the most common problems of this type. Examples of each are discussed and remedies proposed to alleviate this problem. The second major category of corrosion failures is caused by unanticipated or unrecognized aspects of the environment which adversely affect the material. Examples are discussed wherein corrosion and subsequent cracking occurred as a result of deficiencies in water treatment which allowed the intrusion or buildup of corrodents. The examples presented in this paper illustrate the importance of metallurgical failure analysis as a tool to produce a higher quality, more reliable product.

KEY WORDS: pump, corrosion, failure, intergranular corrosion, casting defect, grain boundary film, corrosion fatigue, stress corrosion cracking, stray current corrosion

Pump manufacturers strive for enhanced reliability. This is attained through improvements in pump design and technology. Metallurgical failure analysis plays an important role in this effort as it provides insight into the factors that are critical to pump performance and longevity. While problems in pumps can be induced by a myriad of causes, frequently including misuse in operation, corrosion must rank as a leading cause of material failure.

Metallurgical evaluation of failures in pumps often is essential to an understanding of the root cause of the problem. An important aspect of this analysis is gathering information on actual service conditions. Operating personnel are frequently the best source for this information. This is followed by chemical analysis, verification of mechanical properties, and metallographic examination of the fracture surface and microstructure.

In the absence of such a rigorous examination, the role of corrosion in the initiation of cracking and other forms of deterioration often is not recognized. There is frequently a lack of appreciation by all concerned parties of the need for a detailed chemical analysis of the pumped fluid. This is particularly so in instances not involving an obvious chemical application. Data sheets frequently identify the fluid as "water," "pure water," or some other equally vague description. Actual operating conditions, in terms of fluid chemistry, may vary considerably from those specified on the data sheets. Records of operating parameters are sketchy or nonexistent, and this makes failure analysis difficult. When cracking occurs, the immediate response typically is to blame either the material or the design and to attempt to solve the problem with higher strength materials or more rigorous techniques for stress analysis. These approaches fail because they do not come to grips with the root cause of the problem. There usually is some deficiency in materials processing or fabrication which

---

[1] Manager—Materials Engineering, Dresser Pump Division, Harrison, NJ 07029.

allows corrosion to initiate in an otherwise resistant material, or an unrecognized aspect of the environment which promotes cracking.

A variety of corrosion failures in pumps are discussed in this paper. These have been selected to illustrate the more common types of failure, as well as those that occur less frequently but teach important lessons. The objective in discussing these failures is to provide information which can be utilized by both manufacturers and users of pumps. An appreciation of potential corrosion problems will enable manufacturers to optimize design and fabrication practices. It will also convey to users the importance of adequately defining and controlling the operating environment.

A report [*1*] issued by the Materials Technology Institute of the Chemical Process Industries (MTI) indicates that the leading causes of failure are intergranular corrosion and casting discontinuities, many of which have welds associated with them. Table 1, extracted from this report, indicates the scope of the problem with pump components; frequently castings of alloys CN-7M or CF-8M fail in this manner.

The frequent examples of intergranular corrosion emphasize the importance of proper heat treatment, especially when the casting will see service in an environment capable of causing intergranular attack. It might be noted that numerous environments will not induce intergranular corrosion even in deliberately sensitized material. There is less concern with sensitization induced by welding or other thermal treatments when an austenitic stainless steel pump is used in these environments, many of which are identified in a comprehensive Welding Research Council report [*2*] on this subject. In practice, the pump manufacturer

TABLE 1—*Premature failures in the chemical process industries.*[a]

Alloy Type	Part (No. of Parts)	Failure Mode	Time in Service
CN-7M	Impeller (1)	Intergranular corrosion	1 year
CN-7M	Pump (6)	Intergranular corrosion	1 to 3 months
CN-7M	Pump (1)	Intergranular corrosion	3 months
CN-7M	Valve (1)	Casting discontinuity	...
CN-7M	Backplate (1)	Casting discontinuity	...
CN-7M	Pump (6)	Leaks at weld repair	Startup
CN-7M	Valve	Casting discontinuity	...
CN-7M	Bell valve	Intergranular corrosion and casting discontinuity	...
CN-7M	Pump	Intergranular corrosion	...
CN-7M	Pump	Incorrect heat treatment	...
CF-8M	Recyclicone	Intergranular corrosion and casting discontinuity	...
CF-8M	Pump	Stress-corrosion cracking and corrosion fatigue	3 months
CF-8	Pump	Intergranular corrosion	...
CW-12M-1	Impeller (2)	Cracks at weld repair	...
CW-12M-1	Pump (1)	Intergranular corrosion	...
CW-12M-1	Pump	Intergranular and crevice corrosion	...
CD-4MCu	Pump (2)	Intergranular corrosion	...
CY-40	Pump (2)	Intergranular corrosion	3 months
Nickel 200	Sleeve (1)	Casting discontinuity	...
Illium 98	Spray nozzle	Intergranular corrosion (carbon pick-up)	...
Unknown	Pumps (several)	Poor welding (assembly)	10 months

[a] This table was extracted from Ref *1*.

often does not know the eventual service and, therefore, must take every precaution to supply material with optimum resistance to corrosion.

Examples 1 through 4 are typical of the intergranular corrosion attack identified as a leading cause of failure in the chemical industry. In each instance, chemistry of the failed component was verified to be within specification.

Example 1

A chemical pump, handling 12% sulfuric acid solution at 57°C, failed after less than one year of service. The pump was constructed of a high–alloy, austenitic stainless steel similar to CN-7M. Extensive corrosion had occurred on the shaft, which was fabricated from hot-finished bar. Metallographic examination found this corrosion to be intergranular in nature. The microstructure at the outer edge of the shaft was severely sensitized, as shown in Fig. 1, with individual grains entirely surrounded by carbide films. These films gradually disappeared toward the center of the section.

A section adjacent to that shown in Fig. 1 was subjected to solution heat treatment at 1175°C and water quenched. Figure 2 is a photomicrograph of the solution–annealed structure and illustrates that proper heat treatment will eliminate grain boundary carbides.

Dilute and intermediate concentrations of sulfuric acid are environments known to induce intergranular attack in sensitized, austenitic stainless steel. This failure, which occurred some years ago, was the direct result of failure by the bar manufacturer to quench the material at a sufficient rate. Fortunately, today there is a heightened awareness by most reputable manufacturers of the need to water–quench these materials. Purchasers of high–alloy austenitic materials should be aware that a water quench is not a mandatory requirement of

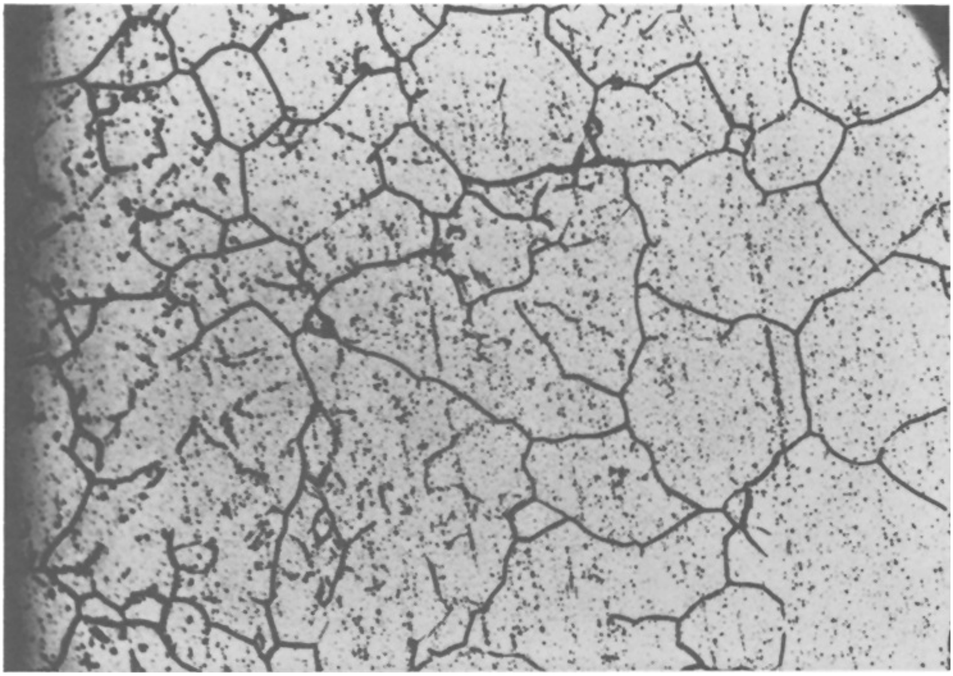

FIG. 1—*Severe intergranular carbide precipitation near outer surface of pump shaft,* ×*100.*

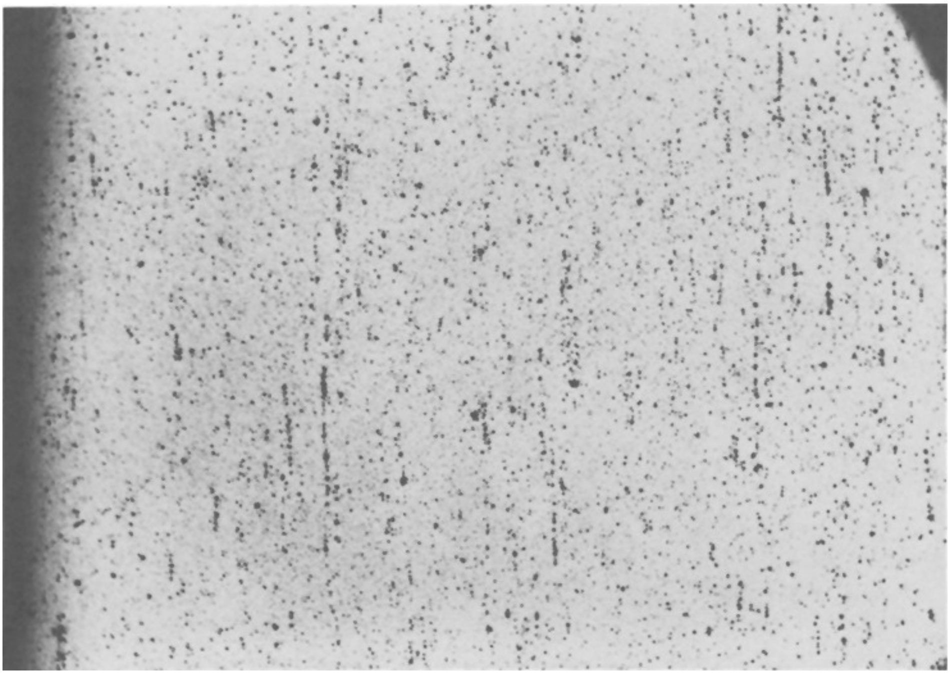

FIG. 2—*Solution anneal, at 1176°C (2150°F), followed by water quench eliminates carbides from shaft, ×100.*

many ASTM specifications covering these grades, including the ASTM Specification for Castings, Iron-Chromium, Iron-Chromium-Nickel, Corrosion-Resistant for General Application (A 743/A 743M), and the ASTM Specification for Castings, Iron-Chromium-Nickel and Nickel-Base Corrosion-Resistant for Severe Service (A 744/A 744M). For added assurance, a user can specify that material be tested in accordance with the ASTM Practices for Detecting Susceptibility to Intergranular Attack in Austenitic Stainless Steels (A 262/A 262M), a series of tests designed to detect susceptibility to intergranular attack.

Example 2

A stainless impeller in a chemical pump failed after 35 days of service in phosphoric acid containing about 1% iron and about 3% calcium sulfate fines. The failure consisted of severe intergranular attack over most of the exposed surface of the impeller. Operating temperature was about 115°C. The material was CN-7MS, a high-nickel alloy austenitic with corrosion characteristics similar to CN-7M. Owing to the high nickel, CN-7MS castings should have a fully austenitic grain structure. Figure 3 shows a typical structure for this casting, with continuous carbides in the austenite grain boundaries. In Fig. 4, corrosion is seen to be progressing along these grain boundaries into the material. It was concluded that this impeller was in the "as cast" condition and received little or no heat treatment.

Example 3

The impeller shown in Fig. 5 had been used in acid injection service. Details pertaining to the specific environment are proprietary, however impellers of the same chemistry, that

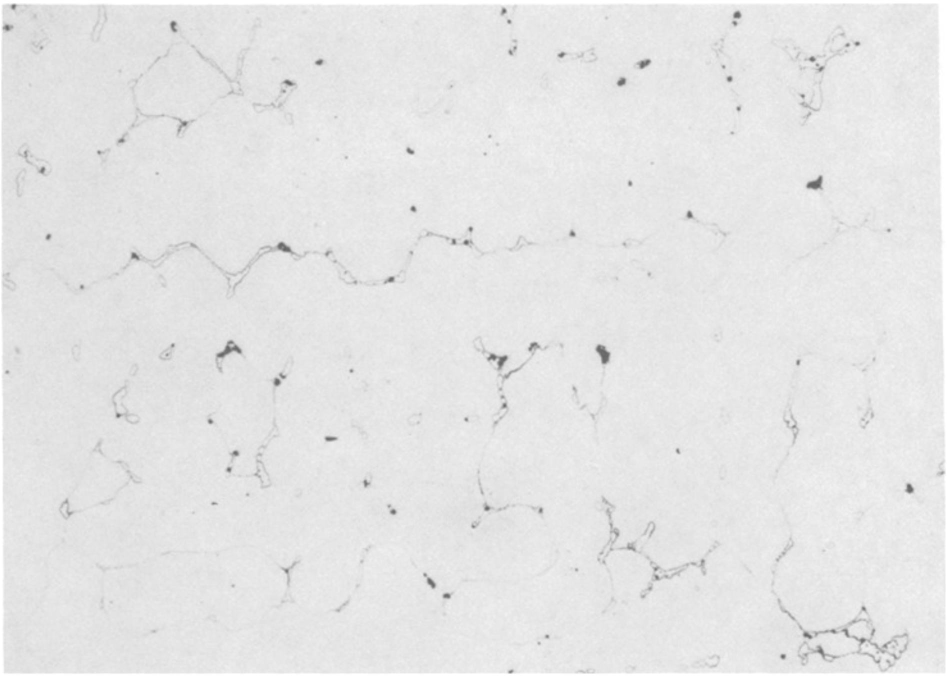

FIG. 3—*Intergranular carbides in the cast austenitic structure of a stainless pump impeller,* ×*100.*

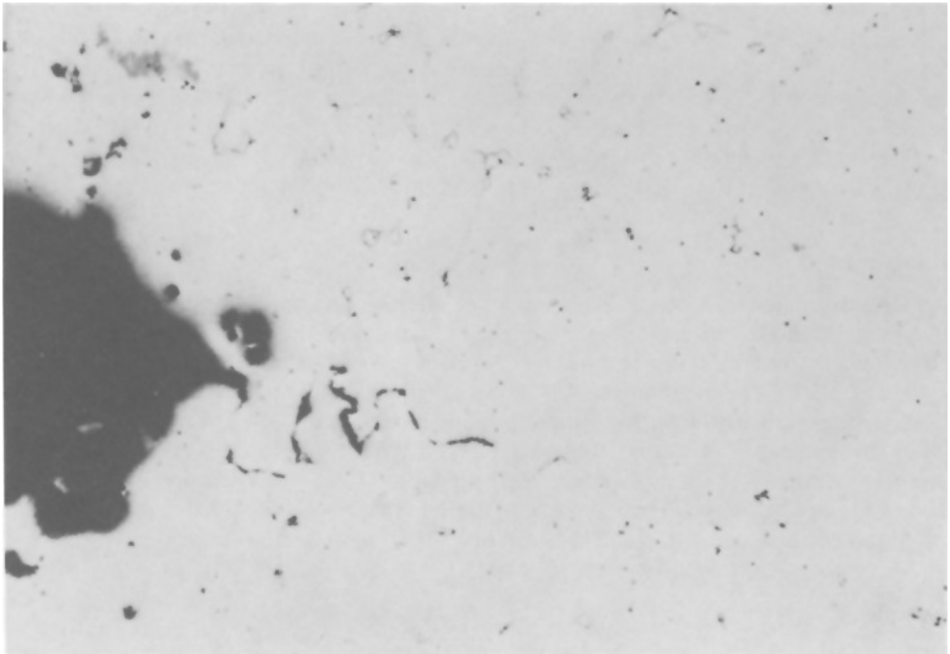

FIG. 4—*Intergranular corrosion follows the path of carbide precipitates in this pump impeller,* ×*100.*

FIG. 5—*Stainless pump impeller following acid injection service.*

being the CN-7MS composition, had been used previously with good success. Visual examination showed the attack to be intergranular in nature with widespread grain dropping. Irregularity of the attack suggests that the corrosion took place mostly while the pump was not in operation. The microstructure (Fig. 6) shows a semicontinuous network surrounded by fine, precipitated carbides. In this instance, the supplier insisted that the castings had been solution-annealed and water-quenched. Following careful examination of the vendor heat-treating practice, it was concluded that precipitation of fine carbides resulted from an appreciable delay during the heat treat operation, between the opening of the furnace doors and the quenching of the impeller.

Example 4

A CN-7MS impeller suffered severe corrosion after handling a 50% nitric acid solution containing 5 to 10 ppm chlorides at 71°C. The impeller is shown in Fig. 7. Heaviest corrosion occurred in areas where there was some shrinkage. The microstructure showed a greater than normal amount of fine carbide. This probably resulted from a slack quench which allowed precipitation of the carbide phase. A boiling nitric acid corrosion test, conducted in accordance with ASTM A 262/A 262M, Practice C, showed that the material was unsatisfactory. Corrosion rates of 0.17 and 0.22 mm/month (0.0066 and 0.0089 in./month) in 48 and 120 h, respectively, exceeded the limit of 0.15 mm/month (0.006 in./month), which experience has shown to be a reasonable upper limit for castings in CN-7MS.

Although there were no identifying marks on the impeller, it could be traced to a particular foundry by the grain-size distribution. Only two foundries produce this impeller. The practice at one is to gate in from adjacent corners, while at the other foundry, gating is from opposite corners. Figure 7 shows that this impeller was produced by the second foundry.

Example 5

A CN-7MS impeller with radical cracking was returned after service in a pump that handled black liquor at 125°C. The cracking occurred only around the hub between the vanes. The

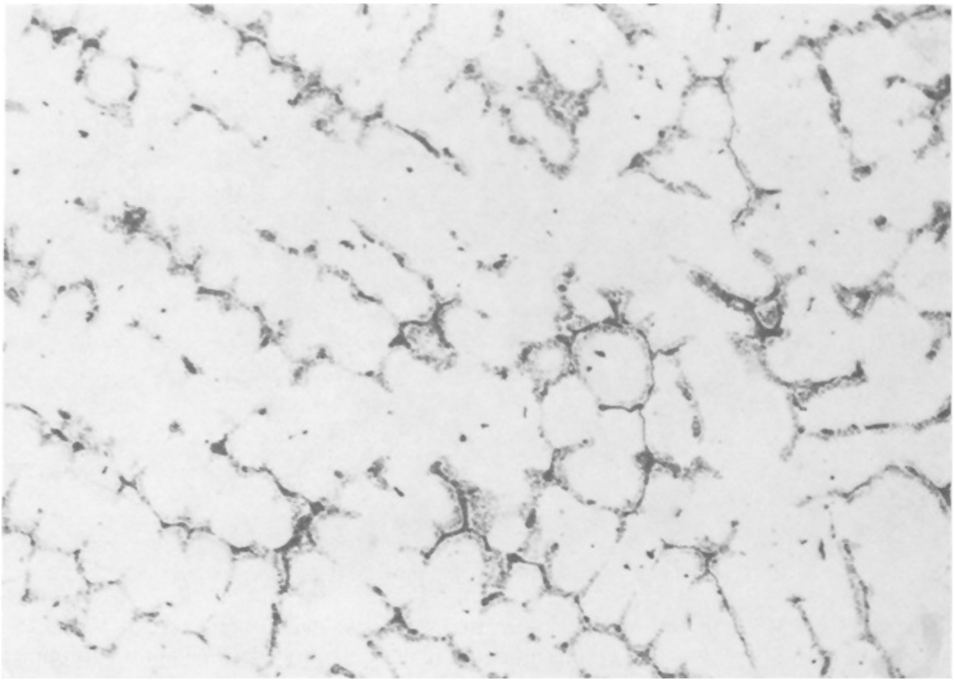

FIG. 6—*Microstructure showing semicontinuous network of fine precipitated carbides, ×100.*

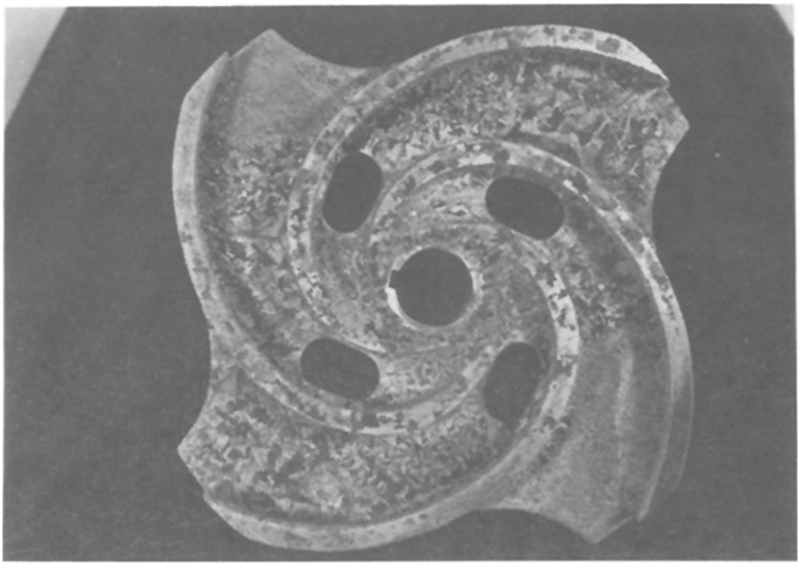

FIG. 7—*High-alloy austenitic stainless impeller, showing excessive corrosion at shrinkage in vane fillets. Grain-size distribution identified foundry.*

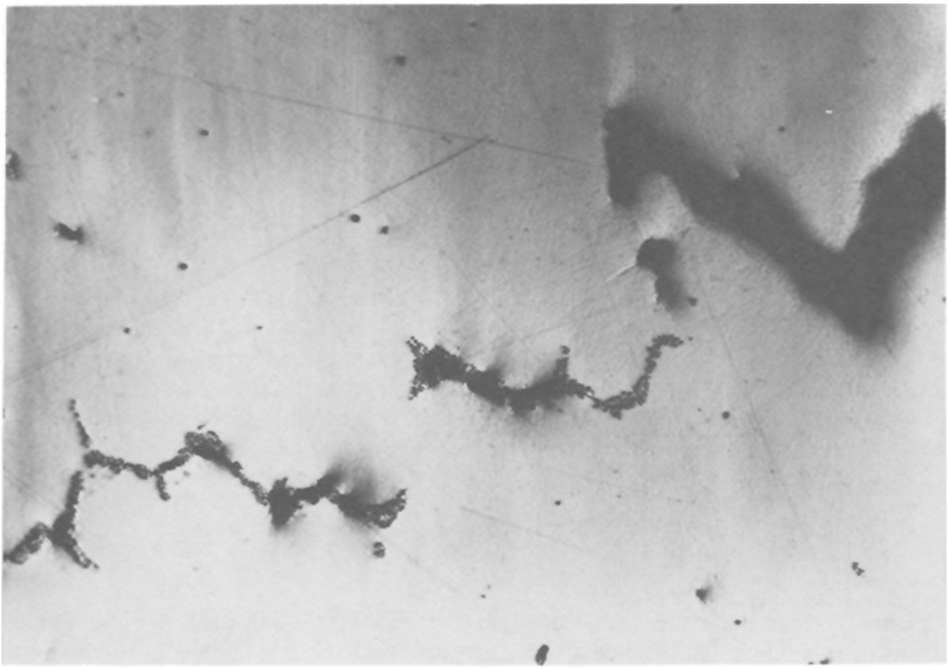

FIG. 8—*Austenitic microstructure showing progressive corrosion along grain boundary contaminant films. This condition was limited to the hub section between impeller vanes,* ×*300.*

cracking apparently was confined to this area because it is the last portion of the casting to solidify. It progressed along grain boundary films as seen in Fig. 8.

Heat treating a small section of the impeller that was afflicted with this problem did not cause the grain boundary films to dissolve or go into solution. The microstructure of the remainder of the impeller was satisfactory, and the chemistry was within specification. It was concluded that the grain boundary films are not carbides, but low melting point contaminants (phosphorus, sulfur, etc.) which have adversely affected corrosion resistance.

Recent work by J. L. Gossett [*3*] has demonstrated that the corrosion resistance of CN-7M and other higher nickel cast alloys can vary dramatically from heat to heat. These differences can be correlated with control of trace elements. The use of a secondary refining operation, argon oxygen decarburization (AOD), has been shown to be quite effective in eliminating tramp elements and thereby improving corrosion resistance. Improved weldability and less susceptibility to hot shortness are added benefits resulting from the use of AOD. While the first cost of an AOD-refined casting may be higher, fewer rejects and less weld repairs may result in a lower final cost. The higher quality inherent in an AOD-refined casting has prompted some more sophisticated users of nickel alloy pumps in critical applications to require this processing step. Clearly, this is an instance where improved foundry technology provides the means to overcome a vexing and long-term problem with the CN-7M and CN-7MS compositions.

Example 6

A CN-7MS pump casing developed leaks after six months of handling 0.2% sulfuric acid and 0.03% sulfur dioxide in a water solution at 66°C. The leaks were confined to the flange, which subsequently was sectioned and metallographically examined to reveal a badly corroded band of weld metal. Corrosion was confined to the weld. The sectioned flange is shown in Fig. 9. Drillings through the weld metal had an analysis slightly low in the key alloying elements; chromium, nickel, and molybdenum. The weld repairs apparently were made to fill in gas holes in the flange that caused leakage. Two additional gas holes are seen in the photo, slightly below the weld repair. These gas holes were located just beneath the machined surface and were not visible when the pump was assembled.

It was concluded that a rather ineffectual repair was made in the field. Cracking was detected along a considerable portion of the fusion line. Intergranular carbides in the weld heat affected zone indicated there had been no subsequent heat treatment.

Failures of this nature are not uncommon, as indicated in the MTI report. Casting defects, not uncovered by machining, may go undetected until leaks develop in service. Hydrostatic testing is not an effective means to detect this problem because the corrosion process, particularly at porosity and other defects which resemble crevices, takes some time to provide a liquid path through the metal thickness. Radiography or other forms of volumetric inspection usually are not employed due to cost considerations. Leaks discovered in the field are often repair-welded, sometimes by unqualified welders using less than adequate procedures.

Example 7

Figure 10 shows the remains of a leaded tin bronze, alloy 934, impeller after four months of service in a pump that handled a water and detergent solution at 38°C for use in a car wash operation. This was one of 300 impellers suffering to some extent from the same problem. Random check of chemical analysis showed the impellers to be the correct composition. At low magnification, it was evident that the impellers are porous at the thin section of the vanes. This porosity is common in bronze castings which solidify in a manner that

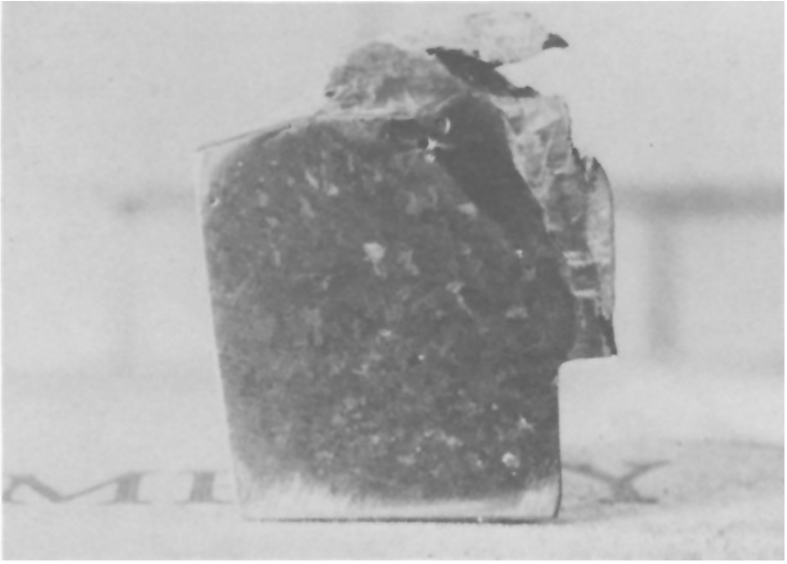

FIG. 9—*Section from pump flange showing gas pockets beneath ineffectual weld repair.*

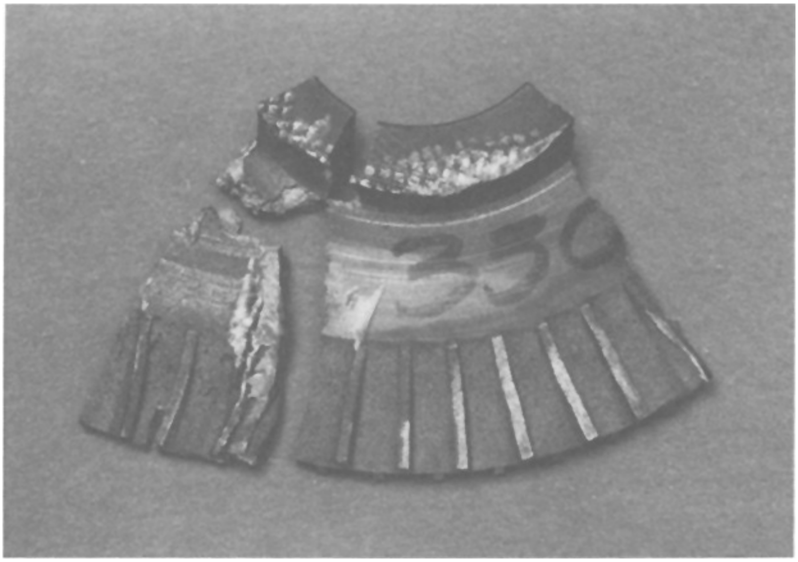

FIG. 10—*Leaded tin bronze impeller, fractured after four months handling water and detergent at 37.8°C (100°F). Porosity at machined vanes promoted failure.*

results in sound metal at the surface with maximum porosity or entrapped gas at the center. Figure 11 is a fractured section from an unmachined vane and shows the color (shading in a black and white photo) difference characteristic of this defect. It appears as thin, interconnected porosity at grain boundaries as shown in Fig. 12.

In this instance, the impeller design and method of casting resulted in sound metal being removed by machining, with porous metal remaining. There was also evidence of corrosion

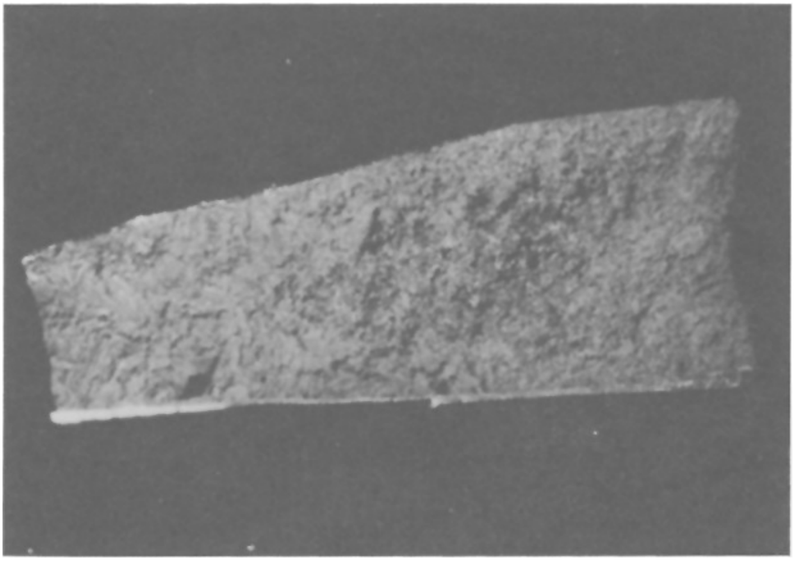

FIG. 11—*Porosity through center of unmachined impeller vane, denoted by color difference.*

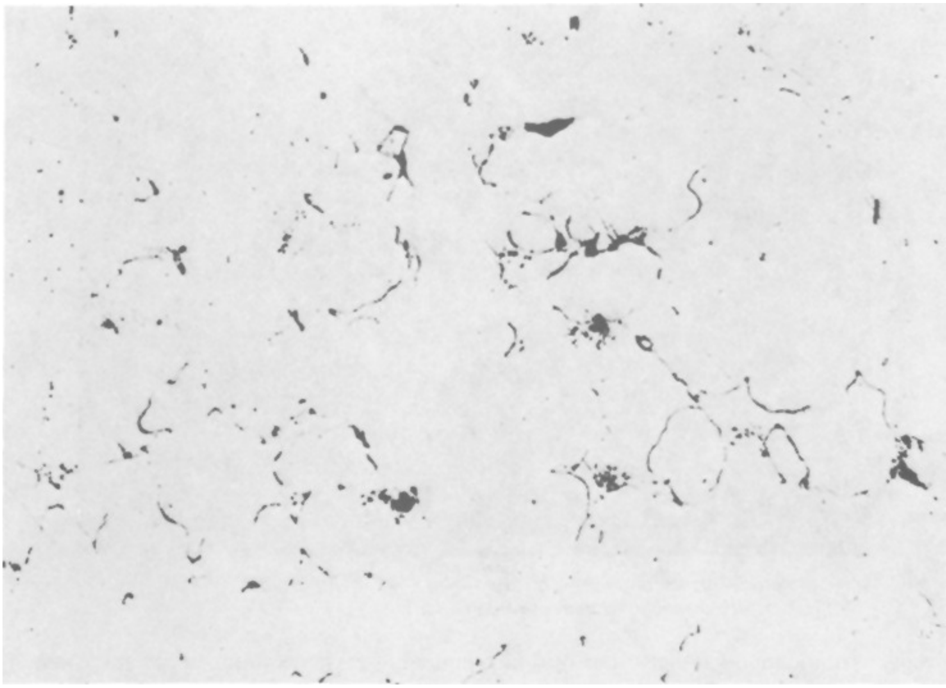

FIG. 12—*Microstructure of bronze impeller showing thin interconnected porosity at center of section.*

throughout the casting with perforation at the vane. The solution to this problem involved redesign of the impeller to reduce as-cast section thickness of the vane and the addition of chills to assure sound metal at this location. Stainless steel, recognized as being more corrosion resistant in this environment, was considered but rejected on the basis of cost.

The types of problems described in Examples 6 and 7, which go undetected during fabrication, emphasize the importance of obtaining sound, high–quality castings. It also represents a vexing problem for pump manufacturers, that being how to obtain, at low cost and without resort on a routine basis to volumetric inspection, high–quality castings. It is often difficult to reconcile this need for quality with the competing pressure to select a foundry on the basis of cost and delivery. Defects uncovered during machining are repaired where possible, but add unnecessary cost and scheduling delays. Close cooperation between the pump designer and foundry engineers can result in an optimized design which is less prone to defects, as indicated in Example 7. Improvements in foundry technology, including the use of computer-developed isothermal plots of casting solidification which identify areas of potential shrinkage, also contribute to higher quality.

Example 8

The pump shaft shown in Fig. 13 fractured after six months of service in a paper mill. Service had been specified as filtered "white water" at 66°C with a neutral pH. The water was supplied to a spray apparatus at a paper machine. The shaft material was 17-4PH-1025 stainless steel.

At first glance, this might appear as a simple fatigue failure, initiating at the keyway. In fact, another mechanism first caused metal to spall from the surface, beginning at the keyway.

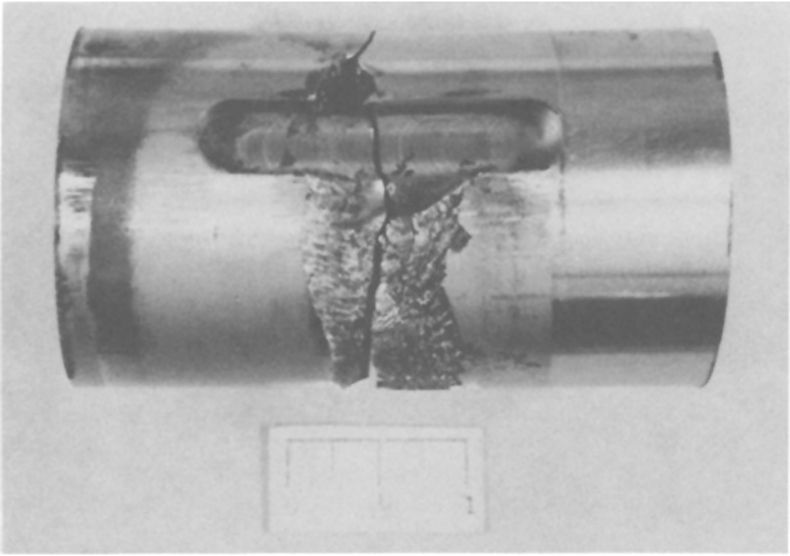

FIG. 13—*Fractured shaft, type 17-4PH stainless steel. Failure occurred after six month's handling water with pH 7 at 65.6°C (150°F) in a paper mill.*

Only then did fatigue cracks initiate. As seen in Fig. 14, a subsurface crack was propagating from a region, at the keyway, where the surface has spalled off. Fatigue striations originated from multiple origins on the spalled surface, some distance removed from the keyway. Metallographic examination indicated incipient corrosion pits and additional cracks on both spalled and intact regions of the surface near the fracture. Evidence of corrosion pits in the

FIG. 14—*Stress corrosion crack propagates from spalled region. Fatigue cracks initiate on spalled surface, some distance from keyway.*

crevice between the shaft and slip-fit, keyed impeller suggested the presence of chlorides or sulfur compounds. While no water analysis could be obtained, as is frequently the case with industrial failures, it was learned that the water handled by this pump was actually an unfiltered, general-purpose plant water. The water was used for equipment washdown and pulp mat shower spray, among other applications. The effluent is collected, clarified, pH adjusted, and then recycled. Also, makeup for this system is obtained from a major river at a point less than 30 miles from the ocean.

The river water contained some chlorides, and these could be increased significantly as a consequence of influx of salt water during seasons of minimum flow. Chlorides initially present are greatly concentrated in a partially closed system. A 10- to 20-times concentration factor is not uncommon. It is reasonable to assume further concentration in the crevice between the shaft and impeller. Thus, the necessary conditions for stress corrosion cracking were present in a susceptible material. This particular shaft had a hardness of HRC38 at the fracture, well above the minimum for this heat treat condition. High strength, or hardness, is known to enhance susceptibility to cracking. It was concluded that a stress corrosion crack initiated at the keyway, propagated as shown in Fig. 14, led to spalling and subsequent fatigue. The specific corrodent was probably chloride rather than sulfide. Corrosion pitting in this service and the highly oxidizing conditions normally found in paper mill waters support this conclusion.

There are two interesting sidelights to this failure. It seems that Type 416 stainless steel shafts had preceded 17-4PH-1025 in this service. These cracked, and, without benefit of metallographic examination or failure analysis, it was concluded that a stronger material was required. The fact that this pump is designed to operate with a carbon steel shaft having a yield strength of less than 50 000 psi was not considered. Clearly corrosion and not inadequate strength was the root cause of this problem. Substitution of a very high-strength material probably enhanced susceptibility to cracking.

Stress corrosion cracking failures of 17-4PH pump shafts in the H900 or H1025 condition have been encountered previously. Figure 15 shows a 20-year-old failure in a 17-4PH shaft.

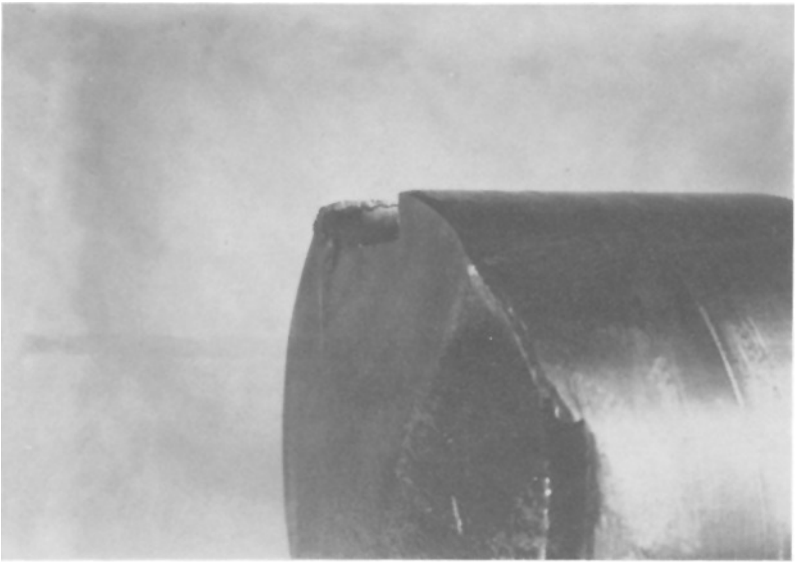

FIG. 15—*Stress corrosion cracking in a second 17-4PH stainless shaft, this taken from a steel mill descaling operation. Note the crack in the keyway, parallel to the outer surface.*

It occurred during a descaling operation at a steel mill. This also involved a closed system, handling contaminated water, and a slip-fit impeller design. The failure occurred by precisely the same mechanism, with subsurface stress corrosion cracks leading to spalling of the surface, followed by fatigue cracking through the shaft.

Reference to this older failure is made to indicate that the relatively poor resistance of 17-4PH to stress corrosion cracking has long been known. If the failed 416 shafts had been subjected to metallographic examination, it is unlikely 17-4PH-1025 would have been selected as a replacement. Failure analysis would have prevented additional failures.

Example 9

The liquid cylinder of a ductile iron plunger pump failed after three years service. This pump had been used to supply water for a steam generation application. The steam subsequently would be injected into the ground to enhance oil recovery. The data sheet for this pump indicated the fluid to be simply "water" at 30°C, although the pump manufacturer was informed that the water would be treated with an oxygen scavenger and would meet other chemistry requirements dictated by the boiler manufacturer.

As the pump was located in a remote overseas location, a local consultant was requested to determine the cause for failure. His report indicated that fatigue initiated at a pit, thought to be due to casting porosity, and located at intersecting bores, known to be the site of maximum cyclic stress. The implication was that a material defect was responsible for crack initiation. Water chemistry and its role in this failure were not considered, as it was assumed to be noncorrosive.

At this point, the pump manufacturer became involved. The failed cylinder was no longer available. A site visit was made to evaluate the condition of other ductile iron liquid cylinders in the same service. Figure 16 shows a typical cylinder immediately after it was shut down and disassembled for inspection. Active pitting corrosion is occurring, as indicated by the bright, shiny spots in the bore in the center of the photo. It was learned that the method

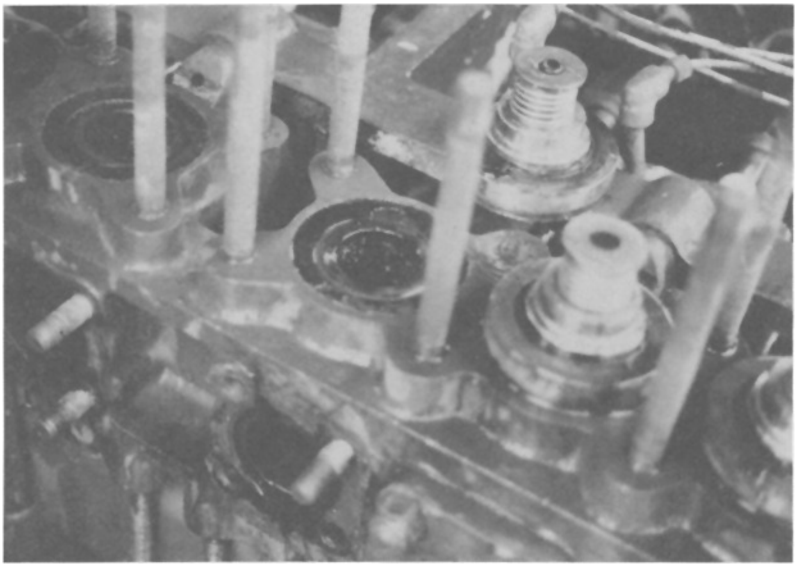

FIG. 16—*Liquid cylinder of a ductile iron plunger pump, showing active pitting in the vertical bores.*

used on site to check oxygen concentration is not capable of accurate measurement below 1 ppm. The scavenger used was sodium sulfite, widely regarded by operators and chemical suppliers as unreliable and inferior to hydrazine for this type of application [*4*]. Oxygen and sulphite can, in fact, coexist.

Obviously, inadequate water treatment allowed the intrusion of oxygen and subsequent pitting. Ductile iron, adequate for properly inhibited water, is entirely unsuitable where corrosion pitting can occur. In this instance, the use of aluminum-bronze liquid cylinders was required. Aluminum bronze, while having lower fatigue strength in air than ductile iron, is more resistant to fatigue in aggressive waters owing to its better corrosion resistance.

This example indicates the decisive role often played by water treatment, one all too frequently ignored when a component fails in a seemingly innocuous environment. It also demonstrates the frequent need to gather on-site information from operating personnel, as this is often unknown to the responsible engineer.

Example 10

One of eleven submersible pumps, in service in central Africa for only two years, lost pressure and was withdrawn from service. The pumps had been fitted with cast iron bowls, bronze impeller, and steel column pipe. It was reported that the pump failed by severe corrosion attack, which caused perforations of the bowl. Review of the water analysis indicated that it was not particularly corrosive and certainly could not have caused the extensive corrosion. Photographs of the failed pump were requested. These were provided, together with a sample taken from the casing. Figure 17 shows multiple perforations and indicates the reason for failure. The electric cable to the d-c motor which was coupled to the pump had been damaged, probably during installation of the pump into the well. While the customer recognized the defect in the cable insulation, it was not associated with corrosion failure of the bowl. Corrosion was due to stray current escaping from the damaged cable.

FIG. 17—*Multiple perforations in the cast iron casing of a submersible pump. Damaged cable insulation led to stray current corrosion.*

It apparently entered the coated casing at the undamaged and uncoated bolt heads, which provided the most convenient means of access. The current exited at the opposite end of each bolt. Corrosion was maximized at these locations, as is normally the case with stray current corrosion. Large concave-shaped pits developed rapidly on the pump bowl inner surface adjoining each bolt. Perforation soon occurred in these areas, as shown in Fig. 17.

This example was included to highlight this relatively uncommon form of corrosion and to emphasize that it should not be overlooked in instances of rapid, seemingly inexplicable corrosion.

Conclusions

Corrosion plays a role in the failure of many pump components. This often goes unrecognized, particularly in the case of cracking, which is attributed to fatigue. A superficial and incorrect diagnosis will lead to conclusions that do not eliminate the problem. In other instances, even where corrosion is recognized as being a contributing factor, the causes for this corrosion frequently are not well understood by operating personnel who must implement corrective measures.

For these reasons, a metallurgical failure analysis is often necessary to identify the role of corrosion. As shown in this report, corrosion often initiates, not because of improper material selection, but as a result of some deficiency in fabrication. In pumps supplied to the chemical industry, intergranular attack and casting defects are the primary causes for failure. Both arise from less than optimum fabrication and processing. Failure analysis enables the pump supplier, together with the foundry or heat treater, to optimize design and manufacture, thereby minimizing these problems.

Likewise, corrosion frequently results from some unanticipated aspect of the environment. Failure analysis, by pinpointing the mechanism, will usually also indicate the corrosive agent. With this knowledge, the pump user can take steps to control the corrodent or, alternatively, a better definition of the environment can be provided and more suitable materials selected.

Whether fault lies with the material or the environment, corrosion evaluation of pump failures has proven to be critical to the advance of pump technology and a key to enhanced reliability in a variety of applications.

References

[1] "Performance and Reliability of Corrosion Resistant Alloy Castings," MTI Manual No. 5, Materials Technology Institute, Columbus, OH, Feb. 1981.

[2] "Intergranular Corrosion of Chromium, Nickel Stainless Steels—Final Report," WRC Bulletin 138, Welding Research Council, New York, Feb. 1969.

[3] Gossett, J. L., *Proceedings*, NACE 1988 Annual Conference, St. Louis, MO, Paper No. 322, National Association of Corrosion Engineers, Houston, TX.

[4] Haseltine, N. G. and Beeson, C. M., *Materials Protection*, Vol. 4, No. 10, October 1965, pp. 57–61.

George Nekoksa[1]

Correlation of Failure Analysis Corrosion Testing

REFERENCE: Nekoksa, G., "**Correlation of Failure Analysis Corrosion Testing,**" *Corrosion Testing and Evaluation: Silver Anniversary Volume, ASTM STP 1000,* R. Baboian and S. W. Dean, Eds., American Society for Testing and Materials, Philadelphia, 1990, pp. 66–79.

ABSTRACT: Several test methods and procedures applicable to corrosion failure analysis of pipelines, tanks, concentric neutral (CN) cables, underground transformers, potable water pipes, cooling water systems, and plant components are examined. Correlation of different test results from the field and laboratories is shown on three case histories.

KEY WORDS: corrosion failure analysis, corrosivity of soils, corrosivity of waters, corrosion investigation, stainless steels, CN cables

An investigation of corrosion failures is often complex and requires multidisciplinary testing and analyses to determine the cause or causes of corrosion with a high degree of probability in order to understand the main corrosion processes and to select proper corrosion control methods.

Frequently the operator of a corroded structure sends metal samples for metallurgical analysis and soil or water samples for chemical analysis. The data from these analyses are very valuable, but they often do not show the whole picture. When it is found that the laboratory results are inconclusive and that more field and laboratory testing is required, it is often too late to get fresh samples and to conduct meaningful field testing on the structure.

This paper emphasizes that an investigation into the causes of corrosion should start with a comprehensive and multidisciplinary test program. This program should consider, if applicable, a review of the specifications, drawings, operational and repair records, inspections, corrosion documentation, field corrosion testing, nondestructive testing, corrosivity determination, evaluation of corrosion accelerating factors, collection of test samples, metallurgical, electrochemical, chemical, microbial, soil and other laboratory analyses, data correlation and data analysis.

Different types of corrosion cracking require specialized testing and are not discussed in this paper.

Review of Specifications, Drawings, and Records

Design and specifications of buried structures usually provide information about the materials, welding methods, heat treatment, coatings or linings, quality assurance results, type of soils and imported backfills, contacts with other structures, and grounding systems which could result in galvanic corrosion.

Design and specifications for the water cooling systems usually provide information about

---

[1] Consultant, Corrosion Failure Analysis and Control, San Ramon, CA 94583.

the materials, welding, heat treatment, coatings, water source, water quality, inhibitors, biocides, coupling different metals into galvanic cells, water temperatures, velocities, pressures, operation, maintenance, etc.

Corrosion failure histories are useful for identification of corrosive areas. A plot of cumulative failures per 100 km of buried pipes versus the average age demonstrated that the corrosion performance of ductile iron pipes has been inferior to that of cast iron [*1*]. A good correlation was found between a sharp decrease of the leak rate and the data of cathodic protection installation [*2*].

Inspection and Nondestructive Examination

If possible, a failed buried structure should be inspected immediately after excavation and completion of the emergency repairs. The inspection and examination usually provide first indications of the corrosion causes. For instance, buried coated structures with deep and rather smooth corrosion attack in coating holidays and with no attack under the disbonded edges of the coating can indicate strong stray current corrosion effects, resulting in a sharp corrosion imprint of the coating holiday on the metal. In another situation, black slimy corrosion products with a hydrogen sulfide smell can indicate corrosion by sulfate-reducing bacteria. Deep corrosion cavities at welds on buried sensitized Type 304 stainless steel pipes were indicative of microbial corrosion effects.

Corrosion attack in cooling water systems should be inspected before the corrosion products are removed by washing, brushing, or sandblasting. The shape, color, and smell of the corrosion products can provide an indication of several corrosion causes. For instance, distinctive hemispherical or conical nodules of corrosion products on the surface of carbon steel and stainless steels may indicate microbially influenced corrosion. Sulfate-reducing bacteria produce characteristic black deposits of iron sulfide, while the iron-oxidizing bacteria produce brown or reddish-brown deposits [*3,4*].

In the cooling and potable water systems, distribution of the corrosion attack can indicate galvanic effects. For instance, a copper alloy tube sheet in a condenser will galvanically corrode preferentially close to the more noble titanium tubes. Carbon steel pipe galvanically coupled with a copper pipe will preferentially corrode at the copper-steel connection. Impingement of copper tubes and pipes can be determined by characteristic horseshoe attack in locations of high velocity and turbulent flow. Cavitation caused by generating and collapsing of vapor bubbles can be recognized by a spongy-looking surface, often without any significant corrosion products. Stainless steels often corrode in crevices, under deposits, at the welds, or in areas of stagnant water where lack of oxygen and development of microorganisms could reduce passivity and cause pitting.

Good notes, photographs, and sketches of the corrosion attack are very important for determination and documentation of the corrosion causes. An inspection kit could include a measuring tape, rulers, explorer, handheld magnifier, pit-depth gage, caliper, coating thickness gage, marking pens, labels, flashlight, knife, scalpel, disposable blades, wire brush, photographic equipment for taking close-up photographs, plastic bottles for water samples, plastic bags or containers for soil samples, corrosion products and deposits, and items for cold storage or fixing of samples for microbial analysis [*4*].

Visual examination of the interior of the pipes, tubes, and machinery requires use of special tools. Borescopes, fiber optic endoscopes, TV camera crawlers, flexible solid-state endoscopes, and other visual tools with remote control are available.

Nondestructive examination can often be used to determine the extent of corrosion. For instance, radiographs of welds can show indications of large subsurface cavities before through-wall pitting occurs [*4*]. For nondestructive examination of piping systems, the ultrasonic, electromagnetic, and radiographic techniques should be considered [*5*]. Instrumented pigs can be used to monitor corrosion of pipelines.

Field Testing

Corrosion field testing often provides results that cannot be determined by any laboratory sample analyses.

Rapid failures of buried structures usually are caused by combined effects of corrosive soil and other accelerating factors. According to the results of soil testing by the National Bureau of Standards, the average maximum penetration on carbon steel samples exposed for twelve years in 44 different soils was approximately 5 mils per year (127 μm/year) and the average general corrosion rate was 0.85 mils per year (22 μm/year) [*6*]. In average soils, only long-cell, differential aeration/concentration, stray current, microbial, and galvanic corrosion or other accelerating factors can explain failures in one or few years.

Measurement of structure potentials, over-the-line and lateral potential profiles [*7,8*], potential gradient mapping, compensation for IR drops in soil [*9,10*], coating defect surveying [*10*], measurement of IR drop in the structure for current flow determination, potential measurements with cathodic protection rectifier "on" and "off" [7], corrosivity evaluation, and other field tests can determine many accelerating factors.

Structure Potential Measurement

Structure potentials or structure-to-soil potentials are measured with a high impedance voltmeter and a reference electrode. Saturated copper/copper sulfate (Cu/$CuSO_4$) electrodes are often used for measurements on buried structures, while silver/silver chloride (Ag/AgCl), zinc (Zn), or submersible Cu/$CuSO_4$ reference electrodes are preferred in waters. A saturated calomel electrode (SCE) is used mostly for electrochemical laboratory testing. A correlation between the potentials measured with different reference electrodes can be determined from the following relationship: −0.85 V (Cu/$CuSO_4$) = −0.78 V (SCE) = −0.81 V (Ag/AgCl) = +0.25 V (Zn).

The structure potentials can be used not only for cathodic protection measurements but also for evaluation of galvanic or stray current effects on buried or submerged structures without cathodic protection. Measured structure potentials can be compared with typical corrosion (open circuit) potentials of different materials, shown in Table 1. Measured struc-

TABLE 1—*Typical corrosion potentials of materials and structures in soils.*

Material	Corrosion Potential (Cu/$CuSO_4$), V
Stainless steels, Types 304, 316, 409	
In sandy soils (passive)	−0.1
In clay (active)	−0.5
Copper	−0.05 to −0.35[a]
Tin-lead alloy-coated CN copper wires	+0.2 to −0.4[a]
Carbon steel, cast iron	−0.6
Rebar in concrete (not corroding)	−0.1 to −0.3[b]
Galvanized steel pipes and conduits	−0.95
Zinc anodes	−1.1
Magnesium anodes	−1.6

[a] See Ref *13*.
[b] See Ref *14*.

ture potential, substantially more positive than the typical corrosion potential, could indicate galvanic coupling to a more noble structure or a discharge of stray currents from the tested structure. Substantially more negative potentials could indicate cathodic protection. Noble corrosion potentials of stainless steels exposed to natural waters could be an indication of microbial activity [*13*].

Potential Profiles and Gradient Mapping

Corrosion potentials taken with a moving reference electrode and potentials measured between two electrodes can be used to plot structure potential profiles and potential gradient maps [*6–11*]. Potential profiles and potential gradient maps can be very useful for evaluation of stray, galvanic, long-cell, and cathodic protection effects.

Several examples of structure potential profiling and gradient mapping are shown in Figs. 1 and 2. The importance of proper interpretation of the measured data is evident from a comparison of similar plots in Figs. 3 and 4. In Fig. 3, the high negative pipe potentials indicate corrosive area or a 'hot spot.' The corrosion rate in this 'hot spot' will be affected not only by the corrosivity of the clay but also by the long-cell corrosion caused by differential aeration between the section of the pipe in clay and in sand. In an example shown in Fig. 4, the high negative pipe potentials indicate stray current pickup and some cathodic pro-

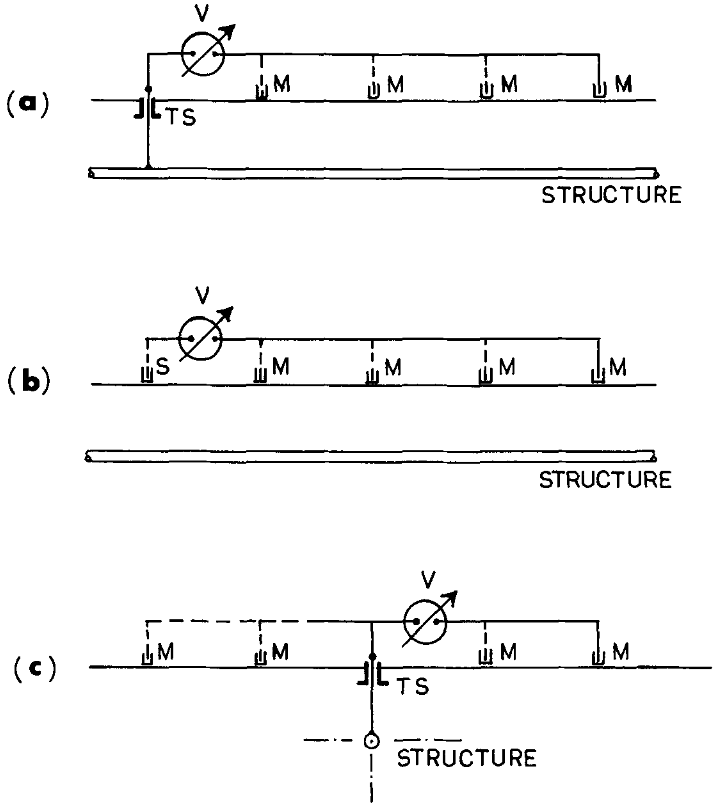

FIG. 1—*Examples of over-the-line and lateral potential profiles for a buried structure. TS = test station, V = voltmeter, M = moving Cu/CuSO$_4$ electrode, S = stationary Cu/CuSO$_4$ electrode.*

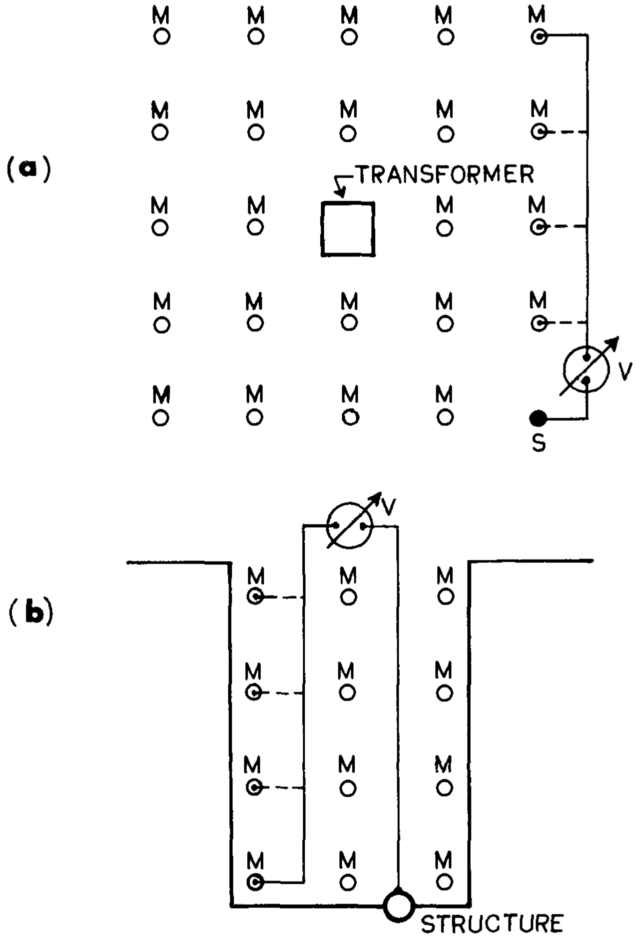

FIG. 2—*Examples of potential gradient mapping:* (a) *top view,* (b) *section of an excavation. V = voltmeter, M = moving Cu/CuSO$_4$ electrode, S = stationary Cu/CuSO$_4$ electrode.*

tection. The stray current corrosion will occur in remote areas where the pipe is polarized by the discharging stray currents in a positive direction.

Data from potential profiling are often stored and evaluated by computers and are complemented by soil resistivity and other measurements. Results of the long-cell corrosion testing should be one of the considerations for a selection of proper cathodic protection criteria.

Corrosivity Evaluation—Field and Laboratory Tests

It is often necessary to determine if the tested environment is sufficiently corrosive to explain the corrosion attack or if other accelerating conditions existed. The corrosivity evaluation can be done in a laboratory or directly in the field or by a combination of both. Because it is difficult to simulate the field conditions in a laboratory, the tests should be done, when practical, in the field.

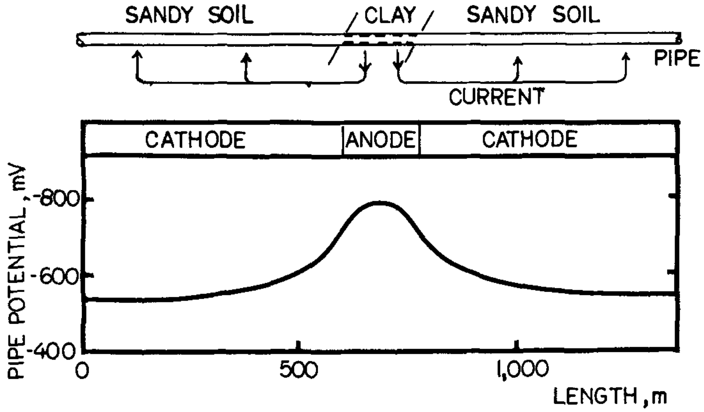

FIG. 3—*Pipe potential profile in soils with different characteristics.*

Relatively good correlation has been found between the resistivity measurement and the corrosion rate. This measurement is usually done for investigation of buried structures in the field using four pins at grade and a resistivity meter [*1,2,6,14,15*]. Follow the ASTM Method for Field Measurement of Soil Resistivity Using the Wenner Four-Electrode Method (G 57–78). Resistivity of waters and soils can be determined with a soil box. Low pH often provides an indication of increased corrosion rate [*2,6,14,15*]. Follow the ASTM Test Method for pH of soil for Use in Corrosion Testing (G 51–77).

The soil samples for chemical analyses should be taken at the corroding structure. All samples for laboratory analyses should be placed in sterilized and sealed plastic containers, kept cold, and shielded from light. Because the samples change with time, the testing on the samples should be done as soon as possible. The following characteristics could be relevant to soil corrosivity: resistivity or conductivity, moisture content, pH, total salts, calcium, magnesium, hardness as calcium carbonate, bicarbonates, chlorides, sulfates, nitrates, organic matter, hydrogen sulfide, redox potential, soil permeability, soil classification,

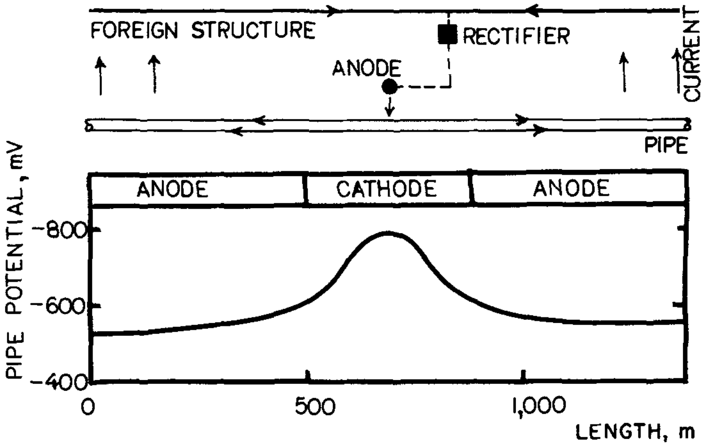

FIG. 4—*Pipe potential profile in stray current area.*

etc. The following methods have been used to rate corrosivity of soils to carbon steel by the sum of points assigned to different soil characteristics:

1. American Water Works Association Standard C105–72 [*14*] includes resistivity, pH, redox potential, concentration of sulfides, and moisture content into the soil corrosivity rating.
2. W. V. Baeckmann and W. Schwenk [*10*] have included into the soil corrosivity rating the following variables: soil type, groundwater level, resistivity, moisture content, pH, redox potential, concentration of calcium and magnesium carbonates, concentration of sulfides, presence of coal or coke, and concentration of chlorides and sulfates.
3. C. P. Dillon [*16*] has selected pH, concentration of chlorides, redox potential, soil type, and soil resistivity for rating of the soil corrosivity.
4. NACE publication TPC-7, "Prevention and Control of Water-Caused Problems in Building Potable Water Systems" (1980), includes water hardness/softness, concentration of carbon dioxide, pH, concentration of sulfates, sulfate-to-chloride ratio, and water velocity into the evaluation of water corrosivity on copper. The same publication includes hardness, alkalinity, concentration of nitrates, carbonates, bicarbonates and soluble heavy metals, temperature, and pH into the water corrosivity evaluation on galvanized steel.

The exposure tests conducted on weight loss coupons provide data for determining pitting, crevice, and general corrosion [*2,6*]. Follow the ASTM Test Methods for Corrosivity of Water in the Absence of Heat Transfer (Weight Loss Methods) (D 2688–83), the ASTM Practice for Preparing, Cleaning, and Evaluating Corrosion Test Specimens (G 1–88), the ASTM Guide for Conducting Corrosion Coupon Tests in Plant Equipment (G 4–84), the ASTM Practice for Laboratory Immersion Corrosion Testing of Metals (G 31–72), the ASTM Practice for Examination and Evaluation of Pitting Corrosion (G 46–76), the ASTM Practice for Exposing and Evaluating Metals and Alloys in Surface Seawater (G 52–88), and the ASTM Guide for Crevice Corrosion Testing of Iron Base and Nickel Base Stainless Alloys in Seawater and Other Chloride-Containing Aqueous Environments (G 78–83).

The exposure tests on electroresistance probes provide mostly general corrosion rates [*2,6,17*]. Follow the ASTM Test Methods for Corrosivity of Water in the Absence of Heat Transfer (Electrical Methods), (D 2776–79). The corrosion severity on concentric neutral (CN) wires of the primary buried CN cables can be rated by measuring the CN wire resistance between transformers and switches [*18*].

Electrochemical corrosion rate testing using linear polarization, Tafel slope extrapolation, and a-c impedance methods provide practically instantaneous readings of general corrosion rate and are often used for corrosion studies and monitoring [*2,6,17,19,20*]. Follow the ASTM Test Methods for Corrosivity of Water in the Absence of Heat Transfer (Electrical Methods) (D 2776–79). The cyclic potentiodynamic polarization tests determine the susceptibility to pitting and crevice corrosion. Follow the ASTM Test Method for Conducting Cyclic Potentiodynamic Polarization Measurements for Localized Corrosion Susceptibility of Iron-, Nickel-, or Cobalt-Based Alloys (G 61–86).

The electrochemical exposure racks have been developed for electrochemical long-term corrosion data monitoring in flowing cooling water of a power plant [*21*]. Specimens, anodes, and reference electrodes were mounted on PVC panels and wired to a test box to allow monitoring of corrosion potentials, cathodic polarization characteristics, galvanic and microbial effects on different materials versus time. General, pitting, and crevice corrosion rates, corrosion products, calcareous coating, biofilms, deposits, weld corrosion performance, and hydryzing of titanium on tension specimens can be determined in a laboratory after the exposure. The test results can be used to determine cathodic protection criteria and weld performance in a cooling system with severe microbially influenced corrosion.

Laboratory Analyses

Chemical composition of metal samples, uniformity of composition, nonmetallic inclusions, residual stress, thermal history such as welding, sensitization of stainless steels, corrosion in heat affected zone, localized and intergranular corrosion, stress corrosion cracking, erosion, and cavitation are some of the corrosion factors which should be considered for evaluation in a metallurgical laboratory [*2,6,16*].

Energy dispersive X-ray, X-ray diffraction, X-ray fluorescence, or wet chemistry analyses are often used to analyze the corrosion products. A large number of surface analytical techniques is available [*22*].

Samples of corrosion products, soil, and water should be sent to a microbial laboratory for analysis. Special sampling techniques and procedures are required to eliminate contamination and to preserve bacteria in the sample [*2,4,6,13,23*].

Possible changes of the test conditions should be considered when the testing is moved from natural environment into a laboratory. For instance, the crevice corrosion rates on Type 316 stainless steel after a few weeks of exposure were about two decades larger in natural than in sterile synthetic seawater [*24*]. Differential aeration/concentration, galvanic, water level, microbial, a-c corrosion, and other effects have been simulated and investigated in a corrosion laboratory [*2,11,18,24*].

To determine causes of coating failures, metal samples with applied organic coating should be tested for metal surface preparation, coating thickness, adhesion, electrical resistance, porosity, etc. Metallic coatings should be evaluated for composition, thickness, adhesion, porosity, corrosion potential, and galvanic performance.

Case History 1: Corrosion Failures of Spray Modules

Approximately 150 spray modules (see Fig. 5) were installed in a cooling water pond. Each spray module consisted of a Type 304 stainless steel float, suction cone, and pump. Several spray modules were found tipped over and sinking after corrosion had perforated the floats approximately eight weeks after the installation. During and immediately after the installation of the spray modules, the cooling water was brackish with resistivity of 60 Ω-cm. Several months after the spray module installation, the cooling water started to change from brackish to fresh water. All spray modules were connected to a large copper grounding grid buried in 110 Ω-cm soil.

Inspection of several spray modules showed distinct semispherical nodules of corrosion products over deep pits. The submerged parts had a slimy deposit which later changed into a thick algae growth. Pitting was concentrated at the welds, but some pits were also found on surfaces away from the welds, especially on all outside edges of the floats and suction cones. Slimy deposits, the shape of the corrosion nodules, and pits in the form of cavities indicated that the corrosion process has been affected by microbially influenced corrosion. Concentration of the pits in and at the welds indicated corrosion in the heat-affected zone and the possibility of intergranular corrosion. Concentration of the pits at the outside edges indicated possible discharge of current from the spray modules into the brackish water.

To support the preliminary findings from the inspection, a sample of the float was cut and sent for metallurgical analysis. The results of this analysis showed that the Type 304 stainless steel at the welds had been sensitized and that the float failed partly because of intergranular corrosion.

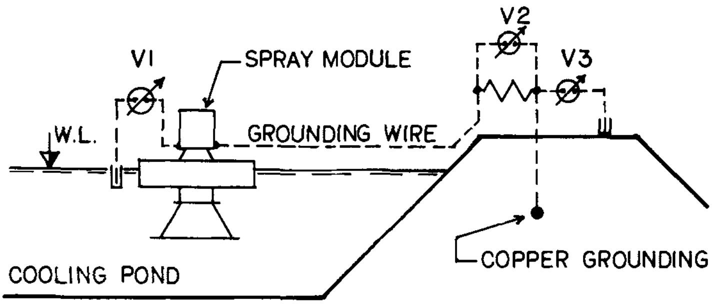

FIG. 5—*Schematic of corrosion testing on a spray module. V1 = module potential, V2 = IR drop across 0.01 or 0.001-ohm shunt, V3 = copper grounding grid potential* ($Cu/CuSO_4$).

Water, soil, and corrosion product samples were sent for a chemical and microbial analysis. Large quantities of sulfate-reducing bacteria were found in the soil (peat), cooling water, and especially under the corrosion nodules, thus supporting the microbial corrosion concept of the failure. Chemical analysis of the cooling water showed high concentration of chlorides which can cause or accelerate pitting on stainless steels.

The indication of a current discharge from the spray modules into the water was surprising, because stainless steel corrosion potential is usually more noble than potential of buried copper. The galvanic interaction between the buried copper grid and the spray modules was tested according to the schematic in Fig. 5. The spray modules were temporarily isolated from the copper grid and from each other. The test results presented in Table 2 show that the module potentials were, by approximately 50 mV, more active than the copper grid during the exposure to brackish water. This potential difference caused galvanic current to flow from the spray module into the cooling water and soil and further into the copper grid and through the grounding wire back into the spray module. In fresh water, the spray modules became noble to the copper grounding grid.

The identification of several conditions which caused rapid corrosion failures on the spray modules shows how important it is to conduct the field and laboratory testing before the corrosion conditions change and the relevant information and samples are lost.

Case History 2: Corrosion of CN Cables

An investigation into the corrosion of buried concentric neutral (CN) cables has been sponsored jointly by Pacific Gas and Electric Co. and Electric Power Research Institute [*11*]. This investigation analyzed 129 variables from 36 excavations and identified the following main corrosion causes on CN cables: differential aeration-concentration corrosion in coarse imported backfills used in native soils having resistivities lower than 12.5 kΩ-cm,

TABLE 2—*Test results measured on Type 304 stainless steel spray module.*

Cooling Water	Fresh	Brackish
Water resistivity, Ω-cm	1800	60
Soil (peat) resistivity, Ω-cm	110	110
Spray module corrosion potential ($Cu/CuSO_4$), mV	−10[a]	−290
Copper grounding grid corrosion potential ($Cu/CuSO_4$), mV	−240	−240
Galvanic current discharged from spray module, mA	...	460

[a] Measured on cleaned spray module.

galvanic corrosion of the copper wire substrate when the tin-lead alloy wire coating became more noble than the copper substrate, d-c and a-c stray currents and corrosive soils with high concentration of sulfides and cinders. The first three corrosion causes are described here in more detail:

Differential aeration—Inspection of corroded CN cables showed that grains of coarse, sandy backfill adhered to the CN wires and that pits were visible after removal of the grains. To demonstrate that differential aeration under the grains of a coarse backfill can cause or accelerate corrosion, laboratory tests were conducted in a differential aeration test box consisting of two compartments separated by a porous membrane. One compartment was filled with moist sand and the other with clay. Corrosion potentials on bare wires buried in both compartments showed that the copper wire exposed in clay was, on average, 220 mV more negative than the copper wire in sand [*11*]. Results of the field inspections, laboratory tests, and statistical analysis indicated that coarse backfill could be much more corrosive to copper than the more conductive native soil backfills. A study in Sweden reached a similarly surprising conclusion from pitting corrosion measurements on carbon steel panels buried at four different locations above the groundwater level in clay with and without sandy backfill. The corrosion-pitting rates of samples buried in native soil ranged from 50 to 190 μm/year, while the rates on samples in imported sandy backfills ranged from 140 to 430 μm/year [*15*]. The corrosion-protective effects of imported sandy backfills on buried pipelines and CN cables in most soils are questionable.

Galvanic corrosion—Deep pits were found in the CN wire copper substrate, while the tin-lead alloy coating had the original appearance. This indicated that the copper substrate corroded galvanically in the coating pinholes. To demonstrate that the coating of the wires can become cathodic to copper, samples of coated and bare copper wire were exposed in imported backfill. The measured corrosion potentials of the CN wires versus time are shown in Fig. 6. A correlation of the field and laboratory data shows that, in some imported backfills, the tin-lead alloy coating will cause galvanic corrosion attack on CN wires.

Stray currents—A crossing of CN cable and cathodically protected oil pipeline was investigated for stray current effects. The CN cable potential profiles, measured according to the schematic in Figs. 1*a* and 1*c*, showed a positive shift at the crossing indicating that the

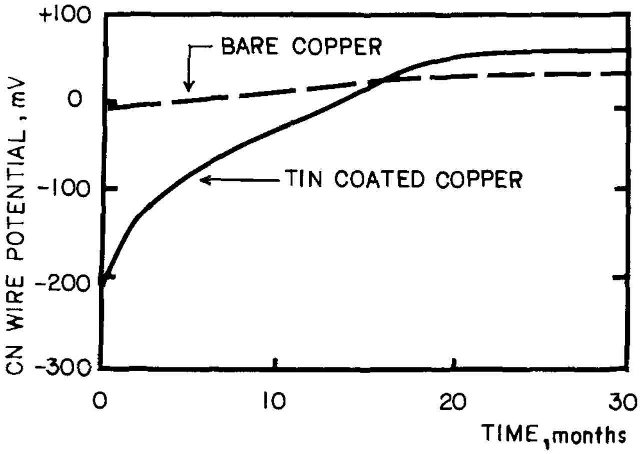

FIG. 6—*Corrosion potentials of bare and tin-alloy coated CN wires in imported backfill versus time* [11].

CN cable could be discharging current [11]. Potential gradient mapping with two reference electrodes at grade, conducted according to the schematic in Fig. 2*a*, indicated that the d-c current was flowing into the oil pipeline [11]. To determine the corrosion condition of both structures, the CN cable and the pipeline were excavated at their crossing. It was found that CN cable corrosion was most severe where the CN cable was closest to the pipeline. No corrosion was found on the pipeline. Potential gradients were measured in the excavation according to the schematic in Fig. 2*b*. Measurements, plotted in Fig. 7, show that the stray current was flowing from the CN cable through the imported backfill and native soil into the oil pipeline. As the reference electrode was moved away from the CN cable, the more positive potential readings indicated stray current discharge.

Case History 3: Corrosion of Transformers, Switches, and Pipes

Premature corrosion failures were found on coated subsurface transformers and switches manufactured from Type 409 stainless steel. Investigation into the corrosion causes and determination of the corrosive area for an early transformer and switch replacement were conducted in the field by measuring pH, resistivity, corrosion rate, structure potentials, and potential gradients.

All the failures occurred in manholes filled with groundwater. All manholes had open bottoms filled with gravel. The linear polarization tests were made at location in a beaker with a groundwater sample taken from the manhole. A probe with three previously exposed

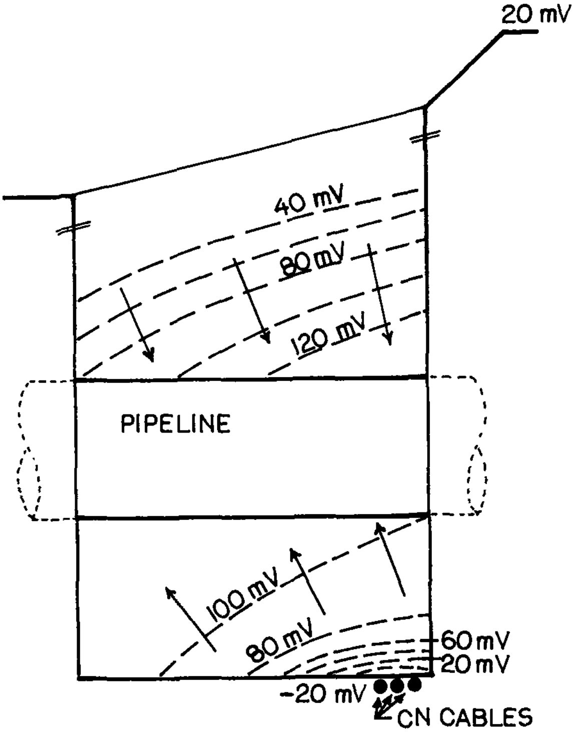

FIG. 7—*CN cable potential gradient in an excavation* [11].

and washed carbon-steel electrodes was used. After a 10-min exposure, the corrosion rate was read with a portable instrument that polarized the carbon steel electrode by ±10 mV. The carbon steel electrodes were chosen because the measured corrosion rates on stainless steels were negligible.

Tests were conducted to correlate linear polarization readings on polished and previously exposed electrodes. Observation of polished carbon steel electrodes showed localized corrosion attack in some waters after an exposure of several hours or days. With time, the corroding areas increased in size until most of the surface of the electrodes was covered with corrosion products. Correspondingly, the corrosion rates monitored on the polished carbon-steel electrodes with the linear polarization method were initially low but started to increase with time until they reached more stable and acceptable values. The short-term readings (after exposure of 10 to 30 min) on previously exposed and washed electrodes correlated reasonably well with longterm (weeks) readings on polished electrodes. The main difference was larger scatter of data from the short-term exposure test, indicating that the surface was not completely stable. It is felt that the short-term measurement on washed and previously exposed electrodes eliminates the initial low readings experienced on polished electrodes in some waters and, together with the measurement of resistivity and pH, provides a relative corrosivity rating.

Corrosion test data measured for evaluation of subsurface transformers, switches, and buried carbon steel pipes without cathodic protection, together with the time to failure and the main cause of corrosion, are presented in Table 3. The data show that Type 409 stainless steel will corrode when covered by soil or in low resistivity water with high corrosivity rating or in places affected by strong stray currents.

TABLE 3—*Corrosion data measured on transformers, switches, and pipes.*

Site Structure Material	Electrolyte				Potential Cu/CuSO$_4$, mV	Notes
	Type	pH	Resistivity, kΩ-cm	CR, µm/year		
1 Switch 409 SS	S	7.8	6.3	60	−240 B	Manhole dry, filled with soil. Failed after 15 years.
1 Switch 409 SS	S	7.8	6.3	60	−300 G	
2 Switch 409 SS	GW	6.8	1.5	300	−250 B	0.6 m of water in manhole. Failed after 10 years.
2 Switch 409 SS	GW	6.8	1.5	300	−250 WL	
2 Switch 409 SS	GW	6.8	1.5	300	−270 G	
3 Transformer 409 SS	GW	8.0	1.9	80	+1480 B	0.8 m of water in manhole. Failed after 11 weeks.
3 Transformer 409 SS					+380 WL	
3 Transformer 409 SS					−60 G	
4 Buried pipes Carbon steel	S	7.8	2.8	110	−530 G	No failure on coated pipes after 15 years.
5 Samples Carbon steel	TW	8.9	17.0	38	NA	Corrosion rate on weight-loss coupons after 1 month: 25 to 75 µm/year.

NOTE: CR = corrosion rate determined by linear polarization on carbon steel. Electrolyte type: S = soil; GW = ground water; W = tap water. Potential at: B = bottom of the manhole; WL = water level in the manhole; G = grade.

Summary and Conclusions

1. Premature corrosion failures are often caused by several different conditions. All tests necessary for determination of the main causes of corrosion failures should be considered at the beginning of the investigation when the original structure and fresh samples are available.
2. To determine the main causes of corrosion with a high degree of certainty requires correlation of results from different multidisciplinary field and laboratory tests and examinations.

References

[*1*] Jakobs, J. A. and Hewes, F. W., *Materials Performance,* May 1987, pp. 42–49.
[*2*] Van Delinder, L. S., Ed., *Corrosion Basics, An Introduction,* National Association of Corrosion Engineers, Houston, 1984.
[*3*] Licina, G. J., Paper No. 268, *Corrosion/88,* National Association of Corrosion Engineers, Houston, 1988.
[*4*] Borenstein, S. W., "Guidelines for Destructive Examination of Potential MIC-Related Failures," *Proceedings, RP 8000–26,* Microbial Corrosion-1988 Workshop, G. J. Licina, Ed., Electric Power Research Institute, Palo Alto, CA, 1989, pp. 6-1 to 6-21.
[*5*] Bell, R. J. and Reid, D. J., "Accurate Non-Destructive Testing of Corroded Service Water System Components," *Proceedings,* Service Water System Reliability Improvement Seminar, Electric Power Research Institute, Palo Alto, CA, 1988, pp. 255–272.
[*6*] Uhlig, H. H. and Revie, R. W., *Corrosion and Corrosion Control,* John Wiley & Sons, New York, 1985, pp. 181–183.
[*7*] Prinz, W. W. and Schillo, H., Paper No. 313, *Corrosion/87,* National Association of Corrosion Engineers, Houston, 1987.
[*8*] Barlo, T. J., *Materials Performance,* May 1988, pp. 49–57.
[*9*] Webster, R. D., *Materials Performance,* October 1987, pp. 38–41.
[*10*] Baeckmann, W. V. and Schwenk, W., "Handbuch des kathodischen Korrosionsschutzes," *Verlag Chemie 1971,* pp. 52–59, 83–97.
[*11*] Hanck, J. A. and Nekoksa, G., *Research to Develop Guidelines for Cathodic Protection of Concentric Neutral Cables, RP 1049–1,* Vols. 1–3, Electric Power Research Institute, Palo Alto, CA, EPRI Project Manager: T. J. Kendrew, 1981 and 1982.
[*12*] Naish, C. C. and Carney, R. F. A., *Materials Performance,* Vol. 27, April 1988, pp. 45–48.
[*13*] Licina, G. J., "Electrochemical Aspects of Microbiologically Influenced Corrosion," *Proceedings,* Microbial Corrosion-1988 Workshop, *RP 8000-26,* G. J. Licina, Ed., Electric Power Research Institute, Palo Alto, CA, 1989, pp. 2–1 to 2–33.
[*14*] Palmer, J. D., *Effects of Soil Characteristics on Corrosion, ASTM STP 1013,* V. Chacker and J. D. Palmer, Eds., American Society for Testing and Materials, Philadelphia, 1989, pp. 5–36.
[*15*] Camitz, G. and Vinka, T. G., *Effects of Soil Characteristics on Corrosion, ASTM STP 1013,* V. Chacker and J. D. Palmer, Eds., American Society for Testing and Materials, Philadelphia, 1989, pp. 37–53.
[*16*] Dillon, C. P., *Corrosion Control in the Chemical Process Industries,* McGraw-Hill, New York, 1986.
[*17*] Hanck, J. H., Nekoksa, G., and Chatre, R. M., *Materials Performance,* May 1981, pp. 9–12.
[*18*] Hanck, J. A. and Nekoksa, G., *Methods for Mitigating Corrosion of Copper Concentric Neutral Wires in Conduit, RP 1771-1,* Electric Power Research Institute, Palo Alto, CA, EPRI Project Manager: T. J. Kendrew, 1987.
[*19*] Scully, J. R. and Bundy, K. J., *Materials Performance,* April 1985, pp. 18–25.
[*20*] Rabeler, R. C., *Effects of Soil Characteristics on Corrosion, ASTM STP 1013,* V. Chacker and J. D. Palmer, Eds., American Society for Testing and Materials, Philadelphia, 1989, pp. 54–80.
[*21*] Nekoksa, G. and Gutherman, B., "Determination of Cathodic Protection Criteria to Control MIC in Power Plants," RP 2939-7 Progress Report, Electric Power Research Institute, Palo Alto, CA, Project Manager: D. Cubicciotti, 1989.

[22] Graham, M. J., Paper No. 136, *Corrosion/89*, National Association of Corrosion Engineers, Houston, 1989.

[23] Tantall, R. E., Stanton, K. M., and Ebersole, R. C., *Materials Performance*, Vol. 27, August 1988, pp. 71–83.

[24] Holthe, R., Bardal, E., and Gartland, P. O., Paper No. 393, *Corrosion/88*, National Association of Corrosion Engineers, Houston, 1988.

Karel Bartoň,[1] *Dagmar Knotková,*[1] *and Petr Holler*[1]

Choice of Testing, Evaluation Methods, and Quality Criteria in Corrosion Engineering

REFERENCE: Bartoň, K., Knotková, D., and Holler, P., "**Choice of Testing, Evaluation Methods, and Quality Criteria in Corrosion Engineering,**" *Corrosion Testing and Evaluation: Silver Anniversary Volume, ASTM STP 1000,* R. Baboian and S. W. Dean, Eds., American Society for Testing and Materials, Philadelphia, 1990, pp. 80–91.

ABSTRACT: This paper proposes a general scheme for the design of test programs to assess corrosion resistance in a meaningful way. Any metallic material or coated metal product that is to be used in a specific set of conditions may suffer corrosion. The chemical and physical factors of the service application, together with the metallic material, determine the type and extent of corrosion damage encountered. Corrosion science can be used to specify the critical environmental factors in the test method.

The test program can provide results that are important for the following: the development of new materials and coatings; the choice of protective systems for new equipment designs; the development of quality control programs and quality acceptance tests. Statistical methods are essential to determine the significance levels of results and the corresponding material specifications.

KEY WORDS: corrosion testing, corrosion resistance, coated metal, test programs, treatment of results

Corrosion resistance is a characteristic of materials. Together with the physical, mechanical, and fabrication properties, it determines the applicability of a material for a specific purpose. These properties may be measured or verified by tests. However, unlike physical and mechanical results, which can be used immediately, corrosion resistance results are often indefinite and poorly utilized.

In general, corrosion susceptibility can be defined as an undesired manifestation of a chemical interaction between the metal and its environment. Consequently, corrosion resistance is not an inherent property of a metal but rather an expression of the metal's behavior in a specific environment. There are a large number of important metal-environment systems in practice, and the number is growing steadily. As a result, it is necessary to constantly evaluate these new metal-environment systems to determine the metal's corrosion resistance in each system.

Test methods for determining corrosion resistance are specific and must be based on the conditions prevailing and the materials to be used, including coatings and other protective measures planned for the specific application. All of these details, including the specification ranges for significant variables, must be determined from individually formulated tests based on the desired service life and other goals of the application. The emphasis placed on the individual characteristics of the testing program and the evaluation methods for each metal-environment combination does not preclude the possibility of standardizing the test and

---

[1] G. V. Akimov State Research Institute for the Protection of Materials, Prague, CSFR.

evaluation methods because many applications are identical or similar and the information gathered from one system is applicable to others.

This paper proposes a general scheme for the formulation of specific test programs to characterize the corrosion resistance of metals and metal-coating systems that will produce meaningful results.

The General Scheme for Formulating a Test Program

The information necessary for this analysis is a metallic product with or without a protective coating system and the corrosive environment that will affect the product. The purpose of the analysis is to determine the corrosion resistance of the product so that the information produced is a statement of corrosion resistance. Another significant input is the nature of the testing that will produce the results required. Figure 1 shows the various components of this scheme. The connecting lines on this diagram indicate relationships that need more explanation; this is provided below.

Components of the Scheme for Formulating the Test Program

The metal in Fig. 1 is any metallic material of construction or a product, coated or otherwise, destined for use in a specific application. The conditions of the environment shown in Fig. 1 include all the factors able to affect the corrosion process, thereby causing deterioration of the metal. These include the chemical nature of the environment, that is, its composition, including the presence or absence of components with either stimulative or inhibitory effects, and the physical characteristics of the environment such as temperature, pressure, flow rates, radiation, etc.

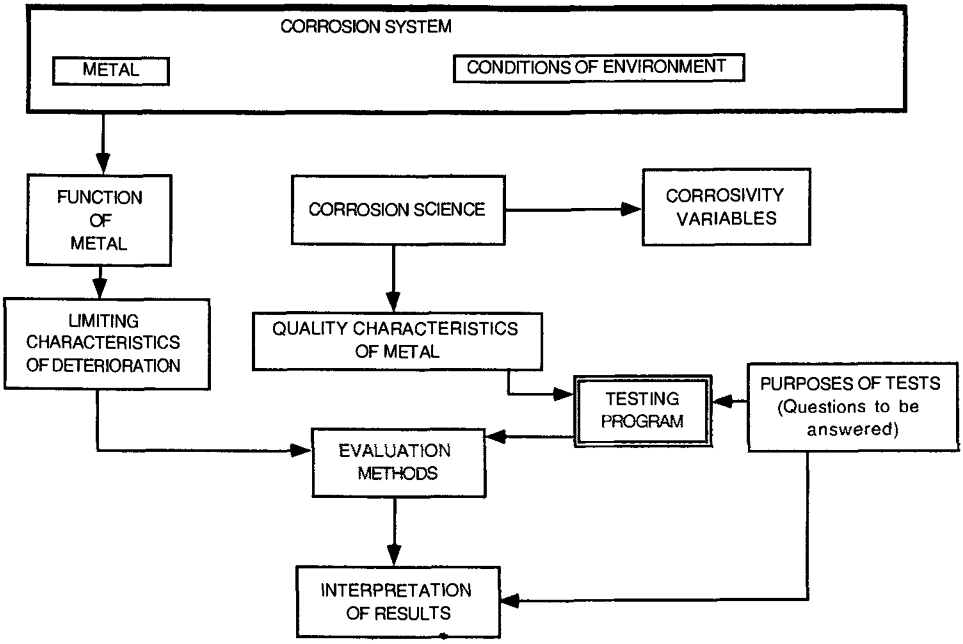

FIG. 1—*General diagram showing the approach to designing tests for assessment of corrosion resistance.*

The Testing Program

In order to arrive at a rational testing program, it is necessary to transform the input data of the system described above to both the quality characteristics of the metallic structure and the corrosivity variables of the environment such as the condensation of water or the presence of a corrosive gas, making use of data obtained from the literature of corrosion science. Unless this transformation is carried out, the formulation of the testing program and later the evaluation of the results probably will lead to naive or incorrect conclusions. Thus, the understanding resulting from the principles of corrosion science provide a basis for specifying both the quality characteristics and the corrosivity variables of the environment.

Quality Characteristics of Metal

The quality characteristics of unprotected bare metal determine their behavior in specific applications. These characteristics include: chemical composition, metallic structure, and sometimes the condition of the surface. All of these characteristics are determined by the production history of the metal, that is, the various production practices that have been used in making the metal. This also includes production practices before the final forming, machining, welding, and heat-treating steps.

Forming can affect the structure of the metal profoundly; for example, it can create internal stresses that result in some cases in such detrimental manifestations as stress corrosion cracking seen in brasses and stainless steels. In other cases, structural changes from forming can cause stress-induced intergranular corrosion in aluminum alloys. The metal surface is often contaminated during forming with aggressive substances or contamination that hinders subsequent coatings, for example, by fatty acid esters.

Machining, including grinding, grit blasting, and mechanical polishing, affects the surface structure of the metal and its profile. Machining processes can chemically change the surface of the metal by adsorption or inclusion of components from coolants, grinding compounds, and blasting media. In addition, local high temperatures often occur during machining operations, resulting in substantially changed chemical properties. The interaction of the mechanical action and the presence of coolants with these high temperatures aid in altering the surface properties of the metal during machining. For example, the contamination of stainless steel surfaces with carbon steel particles from cutting tools, grinding media, and grit blasting sometimes results in corrosion damage to the stainless steel. Residues of active anions from electrochemical machining processes, especially electrochemical deburring, can cause damage. Some heat treatment methods also produce similar results.

Welding is another processing step that changes the metal structure and can have significant effects on the corrosion behavior of the metal. Weld filler metals can vary in composition and flux residues can alter the metal surface. In addition, the heat-affected zone of the base metal receives a sometimes damaging heat treatment, and the heating and cooling causes residual stresses in the structure. A knowledge of corrosion science allows the investigator to evaluate the effects of the processing history and incorporate relevant variables into the test protocol while neglecting other effects deemed to be inconsequential.

Beyond the basic properties of the metal related to chemical composition, structure, and surface finish, the investigator needs to consider the requirements for the metal in terms of achieving a necessary level of corrosion resistance. This is true particularly for metals that generally are used in their passive state, such as the stainless steels. The passivating characteristics of these alloys may be determined by electrochemical tests, and these procedures can also reveal tendencies towards depassivation at local sites and at grain boundaries.

Electrochemical results can yield a huge quantity of information. They enable the investigators to make judgments on the applicability of the metal in situations where it is passive. These judgments are based on the assumption that the specimen was prepared properly, including all the influences of its processing history. This type of test may also be used to assess the resistance of brass to dezincification in a similar manner.

It is more complicated to determine the testing procedures for coated metal systems. A knowledge of corrosion science can be helpful here also. Coatings protect the basis metal either by forming a barrier that isolates the basis metal from exposure to the environment or by inhibiting the metal from damage by the environment. In either case the corrosion rate of the coating must be very low or zero.

Barrier coatings must have coherence and impermeability of the corrosive components from the environment. Both of these characteristics are a function of the coating thickness so that this variable is a decisive factor. All metallic coatings including zinc on steel, baked enamel, and other inorganic coatings are barrier coatings. In the case of zinc on steel, the galvanic character of the zinc layer is of secondary importance. In the case of organic coatings, both barrier and inhibition characteristics may be present, but again the thickness of the coating is a decisive factor for one or the other of these functions. In general, the inhibition function is ensurance in the case of an incomplete barrier, and incompleteness is the prevailing rule for most coating systems. In the case of thin-layer coatings such as preservation oils (for example, slushing oils), the mechanism is inhibition.

Both the cleanliness and reactivity of the basis metal are factors in determining the effectiveness of organic coatings. The status of the base metal surface is therefore an important contributor to the performance of the coating. In all organic coatings the adhesion of the coating to the metallic surface is, in fact, a partial manifestation of the capability of the coating to block the surface from contact with the environment. This adhesion results from both physical and chemical forces arising during the formation of the coating. Consequently, adhesion is lost along with the protection of the coating when the environment, especially water, is able to penetrate through the coating and contact the base metal. This is the general mechanism for deterioration of paint films. This analysis is the basis for determining the performance characteristics of a paint film. These characteristics express both the barrier and inhibitory-adhesion function. This characteristic, sometimes termed "protective efficiency," describes the resistance to undercutting of the paint in the vicinity of an area of damage (holidays) in an accelerated test.

The quality characteristics derived from corrosion science and used for coated metals have formed the basis of the Czechoslovakian system of standards. They are shown in Table 1 for selected cases. It is very important to specify in detail the function of a metallic component in an actual application. The type and degree of deterioration from exposure to environment should be evaluated, and the point at which the degradation becomes unacceptable should be determined. The following factors typically are evaluated:

1. Physical and mechanical properties of the metal, including strength hardness, toughness, and electrical conductivity.
2. Physical properties of the surface, including the frictional coefficient, electrical surface resistance, heat transfer properties and optical properties such as reflectance and absorbance of incident radiation.
3. Ability of the metal to maintain purity of the environment, for example, in food and chemical products.
4. Maintaining the aesthetic function of the metallic surfaces.

TABLE 1—*Key characteristics of metals and metal/coating systems determining their corrosion resistance.*

Metal or Metal Coating	Characteristic	Information Needed from Corrosion Science
1. Metal	Chemical Composition[a] Structure Max acceptable damage after standard test[a]	Chemical properties of metals Undesirable structural features Tendency for local corrosion damage (intergranular corrosion or corrosion cracking)
2. Zn electrodeposit on steel	Appearance Thickness	Service life of the coating, corrosion rate of coating in service
3. Cd electrodeposit on steel	See 2 above	See 2 above
4. Ni electrodeposit on steel, Cu base alloy, Al base alloy, Zn base alloy	See 2 above	See 2 above
5. Ni-Cr and Cu-Ni-Cr electrodeposit on steel, Al, base alloy Cu base alloy, Zn alloys	See 2 above Max corrosion in accelerated erosion test	See 2 above No possibility of comparing quality Resistance of defects to corrosion
6. Sn electrodeposit on steel	See 2 above	See 2 above
7. Hot-dip galvanized steel	Thickness[a]	Service life based on corrosion rate of Zn in service
8. Flame sprayed Zn or Al on steel	Thickness Adhesion	Service life based on corrosion rate
9. Anodized aluminum	Thickness[a] Seal quality[a] adhesion	Degree of protection Coating uniformity
10. Organic coating on metals	Quality of pretreatment[a] Thickness[a] Adhesion[a] Protective capacity[a]	Prerequisite for protection Minimum required for protection Minimum required for protection General requirements for protection

[a] Decisive characteristic.

In cases where metals are subjected to damage from corrosion in the above categories, specific limits can be set that will then determine when the component is no longer functional. The Czechoslovakian system of standards covers these characteristics, including the case of metals with coatings. Examples are shown in Table 2.

Corrosivity Variables

The determination of the corrosivity factors of the environment is the result of a theoretical analysis of the metal system in the specific application. The investigator can derive from a knowledge of corrosion science both qualitative and quantitative factors that will determine the course of corrosion in the system. An example of the theoretically based and generalized factors in the field of atmospheric corrosion is given in CSN 03 8203 (Czechoslovakian State Standard). The classification of corrosivity of the atmosphere begins with the uniformity of long-term exposures and the combination of two critical factors: the duration of surface wetness, and the deposition of ionizable substances on the metallic surface, such as sodium chloride (NaCl) and sulfur dioxide (SO_2). The duration of surface wetness may be calculated as the elapsed time when the relative humidity is greater than 80% and the ambient temperature is greater than 0°C. Based on these factors, five degrees of corrosivity have been set. These degrees form an important basis not only for the determination of test programs but also for the determination of protective systems. Limits can be set for other factors affecting the corrosivity of other systems.

Purpose of Tests

A very important component of the process of establishing a testing program is the purpose of the test. Primarily it depends on the phase of the development at which the necessity for testing becomes known.

Corrosion testing can be useful in the following cases:

1. In the development of new metallic materials and protective coatings. Tests can be

TABLE 2—*Selected cases of limiting characteristics for steel.*

Coating	Characteristic	Limit	Comments
Bare	Loss of thickness	Min thickness	Loss of load carrying capacity
	Localized penetration	Size tolerance of material	Loss of load carrying capacity
	Penetration of structure, e.g. intergranular	Individual choice	Danger of perforation Breaking of pressure vessel
	Reduction of chosen level of physical or mechanical properties	Individual choice	Indication of loss of strength or load carrying capacities, loss of cross section
Metallic coating	Base metal corrosion products (red rust)	5% of surface	End of protection function of coating
		0.1% of surface	End of aesthetic function of coating
	Coating corrosion products	0.1, 1, or 5% of surface	Damage to aesthetic function of coating
Organic coating	Base metal corrosion, corrosion products	1% of surface	1% = Reparable damage Loss of decorative function
		5% of surface	5% = Total loss of protection function, coating to be removed and metal recoated
	Loss of adhesion	Degrees 3,4	Loss of protective function
	Blisters	Individual determination	Protective function limited
	Change of color, loss of luster, and chalking	Individual determination	Deterioration of decorative properties

helpful in determining the basic factors controlling corrosion resistance. The results of such tests are then utilized in the setting of standards, writing of data sheets, and similar databases.

2. In choosing corrosion prevention systems for specific items of equipment to be used in well-characterized environments. The formulation of tests for this kind of assignment is especially demanding because the comparative nature of the results makes it necessary to optimize all aspects of the product, not only the basis material but also the processing steps so that the corrosion protection system becomes essential to the utility of the equipment.
3. As a quality control measure in production operation, especially in the production of corrosion protection systems.
4. As a technique for quality certification and inspection.

Table 3 shows typical cases where corrosion tests may be useful in practice.

Example of Designing Testing Program for Coated Products

The analysis of the process of applying a protective coating to a metallic component enables the development of a rational system of tests to determine the following types of information: (1) factors that determine the quality of the protective coating; (2) factors that determine the corrosivity of the test; and (3) the type of test that should be used.

The evaluation of this information together with the acceptable ranges of these factors allows an investigator to establish a valid test program. The test program consists of a series of tests that verify all the significant characteristics of the metal system. This program then establishes a level of corrosion resistance or protection efficiency for the system. The test

TABLE 3—*Typical functions of corrosion tests.*

Field of Application	General Information from Tests
Research and development of new materials or coating systems	Determination of the properties of the material or coating system that affect corrosion. Specification of properties that determine corrosion resistance.
Research and development of design and development of a new product	Verification of the choice of material for the assumed application conditions. Verification of the choice of construction and processing concept in terms of corrosion resistance. Comparison of various materials, coatings, construction and technology alternatives in terms of corrosion resistance. Comparison of specific design variations and determination of the variation with the greatest range of application in various environments. Also defines the environmental limits of applicability of the project.
Quality control in production	Determination of the key quality factors of components in the corrosion protective and the techniques for measurement. Determination of the acceptable ranges and rejection points for key variables.
Quality certification and inspection	Inspection criteria for the systems providing corrosion resistance and proper test parameters for inspection tests.

program may use tests that have accelerated or enhanced corrosivity factors. The formulation of this part of the test program is especially complicated because the number of corrosivity factors may be very large in many cases. In addition to the chemical variables and the physical characteristics of the coating, it is necessary to consider factors such as corrosion cracking, depassivation, pitting corrosion, undercutting of the coating, etc. The great diversity of factors and their degree of severity require many repetitions of variable levels in different combinations. For example, in the field of atmospheric corrosion testing or in stress corrosion cracking testing, it is necessary to have gradiations in the intensities of the various test variables and to standardize these levels of these variables. This, then, is the basis of a relatively large set of standard test methods used for the verification of corrosion resistance of materials including coated metal systems.

Standard Tests

Among the best known methods are the salt spray test, artificial seawater tests, tests with condensing water vapor, and the moist sulfur dioxide chamber test. This latter test more closely simulates the atmospheric corrosion in heavily polluted urban atmospheres. The standard tests for stainless steels include the tests for susceptibility to intergranular corrosion, pitting corrosion, and stress corrosion cracking. Also, similar tests exist for brass, including tests for stress corrosion-cracking susceptibility and the tendency toward dezincification. The problem of selecting appropriate tests from this group is further complicated by the fact that they are all much more severe in their conditions and consequently cause failures rapidly. The investigator must understand these tests in detail, in terms of both their conduct and significance in order to apply them properly and obtain meaningful results that solve practical problems. A knowledge of corrosion science is vital for this purpose. This is especially true in cases where accelerated tests are used because the process of acceleration often leads to the distortion of the mechanism of corrosion that can cause erroneous conclusions.

Service Tests

An integral part of the system of tests are service tests and those carried out under natural conditions. In particular, atmospheric tests conducted at testing sites provide results that closely approach reality. However, they are both time-consuming and expensive, and their results as difficult to apply widely. The basic requirements for carrying out atmospheric corrosion tests are given in ISO draft standard ISO/DIS 8565.

Atmospheric exposure tests are well suited to determine the basic quality requirements for metallic materials and protective systems for both technical and economic reasons. Hence, they should be incorporated in the final development stage of new materials to give guidance on corrosion characteristics. On the other hand, acceptance testing represents an independent grouping.

Special demands are required for the atmospheric exposure tests of functional elements. The selection of a test arrangement and evaluation scheme should be aimed at judging the suitability of a design or determining its performance after extended exposure and possible deterioration from corrosion. Long-term testing should be carried out in atmospheres varying in corrosivity.

A special family of tests includes those carried out in specific atmospheres. Their purpose is not to determine general features of broad validity but rather to monitor changes that occur in these specific conditions. However, it is necessary to cover a wide spectrum of atmospheric conditions in order to obtain results with broad applicability.

Interpretation of Results

In setting up test programs, the reliability level of the results must be considered. This applies especially to the type and number of specimens. The specimens should be suitable for the problem they are evaluating. The information required to plan the program comes, in part, from an analysis of the application environment and a knowledge of how metals behave in such environments. In addition to the general conclusions of this analysis, it is necessary to include the variability of the components being evaluated. This variability must be considered, both for the metal and the coating, as a result of the variations in the production process. These considerations are especially important when the purpose of the test is to choose the optimum material and processing variations of the protective system. This is also required for quality inspection.

Variation in Quality

Variation in quality is frequently found in coated items. In the case of an electroplated coating, the key quality characteristic, coating thickness, largely depends upon the shape of the part and upon the nature of the process, that is, individual or mass coating, degree of automation, and level of process control. Even when the level of process control is high, the scatter of thickness data tend to be large, with the coefficient of variation (standard deviation divided by average) averaging 30% in the case of mass-processed parts. Similar results are formed where individual metal parts have complicated shapes. Parts with paint or flame-sprayed coatings also show similar variations when complicated shapes are encountered. This is caused by the different accessibility of the surface for the coating layer. In manual coating processes the human factor causes unexpected large scatter also.

In order to prevent this scatter from being the cause of erroneous results and conclusions, it is necessary to plan the number of specimens and sampling to achieve representative results. The use of statistics and mathematical modeling is vital in these cases.

Statistical Analysis

The evaluation methods are based on the predetermined quality characteristics and the limits established for these variables. The evaluation method must determine with certainty whether the limits have been exceeded. In addition, these methods should be based on measurable physical quantities and should not cause problems. The test report of results must cover the purpose of the test (see Table 3).

In the case of determining the properties and peformance characteristics of a new material or coating system including the features that control corrosion resistance, the following information is necessary:

1. General limitations on the application environmental conditions.
2. Specification of the variables that impart quality expressed as precisely as possible, normally in the form of upper and lower tolerance limits.

The limitations on application conditions is based on a complete description of the properties of the metal and on coating systems, including chemical composition and physical and mechanical properties that may be necessary in using the new material. The description of these properties should also include information on the fields of application with any limitations of the materials in these applications. In the case of corrosion resistance, it is desirable to specify the time rate of uniform penetration in units such as micrometres per unit time.

These data, together with the corrosivity of the environment, for example, in an atmospheric exposure the corrosivity class, then form the basis for a forecast of expected service life. More information on the use of statistical methods in corrosion testing is given in the Appendix.

Statements of probable service life must be supplemented with specifications of quality-related parameters, such as the area affected by base metal corrosion. In addition, there is a random component in the behavior of many corrosive systems so that the data on service lives are stochastic in nature. Consequently, it is desirable to provide confidence intervals for projected service lines. Data on the probable service lives of some types of coatings both in term of their protective and aesthetic function are important supplements for a number of Czechoslovakian standards.

The values selected for quality-related parameters from test results must represent reasonable corrosion resistance in actual service environments. It is important that the values of the parameters selected be readily measured with sufficient accuracy to ensure adequate performance. It must be stressed that the limitations on the applications of the metal or coating are strongly related to these parameters. Therefore, the ability to utilize the metal or coating is determined by the assurance that the specifications are met.

In order to define a system with optimum corrosion resistance for a given product, the following approach should be followed. The quality-determining parameters for each alternative must be determined and the appropriate levels selected. These levels must be verified by tests for the given set of specimens and the scatter in results determined. If any convenient property is identified as a determining characteristic, for example, resistance to undercutting in a paint system, it might be advantageous to base the evaluation of alternatives solely on this property. This applies only to the protective nature of the system, not to its decorative function. This is then a decisive quality parameter.

The situation is similar in many other cases. In tests of the optimization of heat treatments in the processing of stainless steels, the key characteristic can be the resistance to intergranular corrosion or pitting corrosion or stress corrosion cracking resistance as verified by standard tests.

The key characteristic that expresses the corrosion resistance or protection efficiency can be used to determine a classification of key parameters and in the case of evaluating test programs the determination of the significance of different system components. For example, in the evaluation of various alternatives for pretreatment prior to painting, the coating thickness to achieve a given level of protection can be used. It is, however, necessary to stress the comparative nature of this statement, which generally cannot be interpreted in terms of service life, with a few exceptions. It is also necessary to point out that test results do not determine the final decision on the choice of the protective system but merely provide a basis for the final analysis.

Quality Assurance

In the case of certification and quality assurance inspection of corrosion protection systems, the statement of test results must address the basic question as to whether the corrosion protection system does or does not conform to the specifications of quality requirements. This is the reason why key quality parameters correctly measured are unavoidable in statements of results. Statistical methods are useful in comparing measured results. Methods that produce easily measured quantitative results such as coating thickness, corrosion loss in standard corrosion tests, areas of undercutting on paint films, etc., are most useful because they can be evaluated by statistical methods that can separate both production and testing variability.

Conclusion

The formulation, conduct, and evaluation of test programs to set specifications for the corrosion resistance of metals or metals protected by various coatings is a very demanding activity involving both a knowledge of the science of corrosion processes and a knowledge of the variability of the systems involved.

Because of the technical level required to handle the corrosion information and statistical analysis, this type of activity should be carried out by technically trained and competent workers.

APPENDIX

The Application of Statistical Methods in Testing

Corrosion or weathering tests are aimed at providing information in the form of a quantitative or qualitative statement that conveys the fitness for service, functional reliability, or service life of a product or component. Statistical methods usually are included in the following steps of choosing a test method: (1) performance of the test and (2) evaluation of the test.

1. In tests with no prespecified parameters such as nonstandardized tests, parameter levels should be chosen to provide as much information as possible with a minimum number of options. The analysis of variance or optimization procedure are used when parameters are selected to provide an extreme in relationships, that is, a maximum or minimum. In selecting test parameters, a range should be chosen such that changes in the mechanism of corrosion are avoided.
2. In processing test results, changes in properties or functions are dealt with by means of mathematical and statistical methods. Normal or Student-t distributions most frequently are assumed to estimate parameters such as means and standard deviations, or to calculate limiting values such as confidence intervals for selected significance levels. However, it must be noted that many laboratory tests yield other types of data distribution such as logarithmic, Weibull's, etc. In establishing a relationship between degradation and environmental factors or test parameters, inaccuracy in determining or maintaining the parameters should be considered and the uncertainty included in the calculation. It is very advantageous to make use of simple functions and as few variables as possible in these analyses. In many cases, a linear function over a limited range is more appropriate than a complex nonlinear one that generalizes the entire course of the relationship. With these functions, extrapolations should be made only in the vicinity of the experimental points.

In order to ensure that the quality of the test procedures and evaluation of test results are acceptable in contract documents, the following steps are required of testing laboratories:

1. Take proper measures to ensure correct performance of the tests, both technically and in the qualifications of the personnel. This calls for periodically verifying the testing and measuring devices and carrying out appropriate training programs.
2. Run parallel tests to analyze independent reference samples that provide documentation on whether tests and their evaluations are carried out in a proper manner.

3. Check on a regular basis the scatter of the results and whether there is any bias or systematic shift of the data to higher or lower levels. Based on this evaluation, take necessary steps that would correct such bias.

References

[1] Bartoň, K. and Kušnierik, O., *Koroze a ochrana Materiálu,* Vol. 32, 1988, p. 23.
[2] Bartoň, K. and Klimošová, Z., *Čs. standardizace,* Vol. 11, 1986, p. 169.
[3] Bartoň, K., *Čs. standardizace,* Vol. 8, 1983, p. 197.
[4] Bartoň, K. and Knotková, D., *Strojírenství,* Vol. 30, 1980, p. 598.

Section II: Corrosion in Environments

Victor Chaker[1]

Corrosion Testing in Soils—Past, Present, and Future

REFERENCE: Chaker, V., "**Corrosion Testing in Soils—Past, Present, and Future,**" *Corrosion Testing and Evaluation: Silver Anniversary Volume, ASTM STP 1000,* R. Baboian and S. W. Dean, Eds., American Society for Testing and Materials, Philadelphia, 1990, pp. 95–111.

ABSTRACT: Corrosion has become one of the major contributors to the gradual depletion of many essential materials for survival on earth. Corrosion in soils can claim the lion's share of this destruction.

This paper outlines the development of test methods needed to identify, measure, and control corrosion in soils. Recognizing the limitations of present test methods, a challenge is offered to the professional world to embark on a program to develop new techniques for testing corrosion in soils, thus leading to better control and contributing to the prosperity and continued use of the earth's resources.

KEY WORDS: soil resistivity, moisture content, soil acidity, soil corrosivity, polarization, differential aeration, pH of soil, redox potential

Soils Evaluation in the Past

History

Corrosion caused by stray current was assumed before 1900 to be responsible for all corrosion of metals buried in the soil [*1*]. The seriousness of underground corrosion was recognized by the U.S. Congress in 1910. At that time, the National Bureau of Standards was directed to study corrosion caused by stray electric currents and recommend methods for their mitigation. A ten-year extensive investigation indicated that very serious corrosion resulted from stray currents; however, equally serious corrosion occurred under circumstances that excluded stray currents.

In 1921, the American Committee on Electrolysis decided that the effect of soils on the corrosion of pipe in the absence of stray electric currents should be investigated. The National Bureau of Standards started that work in 1922. The results of those efforts began appearing in 1928 during the first Soil/Corrosion Conference followed by several others held in 1930, 1933, 1937, 1943, etc.

On the international scene, several countries had experiences similar to the U.S. and started investigation work. In 1912, the British Board of Trade issued rules and regulations to govern the installation of tramways. In 1910, Germany regulated stray-current electrolysis by limiting the potential gradient between the rails and earth, prohibiting electrical drainage to pipe systems. The Dutch Research Institute for Metals set up a Central Corrosion Com-

---

[1] Corrosion research and materials engineer, The Port Authority of New York and New Jersey, Jersey City, NJ 07310-1397.

mittee in 1931. In Australia, several organizations conducted extensive investigations of underground corrosion; the results were presented in the U.S. conferences of 1937 and 1943. In England, the Post Office Engineering Department conducted studies on corrosion of lead cable sheath, reported in 1938. In a symposium held in 1952, the British Iron and Steel Research Association reported the results of research work on underground corrosion. In Belgium, the seriousness of corrosion problems resulted in the organization of the "Centre Belge d'Etude de La Corrosion" in 1952. In Canada, severe corrosion of cast iron water mains in Winnipeg, Manitoba, led to an extended study of soil corrosion at the University of Manitoba.

Characteristics of Soils

Soil is the product of soil-forming processes acting on materials deposited or accumulated by geologic factors. The term "soil" is applied to the first few feet of finely divided, modified rock material covering the earth. Crushed rock and unmodified rock on mountain tops are not soils. Also, earth moved from its original position is not soil if it has lost its structure.

The characteristics of the soil are determined by the physical and mineralogical composition of the parent material, the climate under which it accumulated and has since existed, the plant and animal life on and in the soil, the topography of the land, and the length of time the forces of soil development have acted on the soil material. The classification of soils is based on their physical and chemical properties.

Since 1899, the U.S. Department of Agriculture has been engaged in mapping the soils of the United States. Soil reports are available for counties or larger areas. The reports do not discuss the corrosivity of the soils; nevertheless, they contain valuable information to the corrosion engineer, such as aeration, drainage, etc.

Chemical analyses of soils for corrosion purposes are usually limited to determination of the elements that are soluble in water. The base-forming elements are usually sodium, potassium, calcium, and magnesium. The acid-forming elements are carbonate, bicarbonate, chloride, nitrate, and sulfate. The nature and amount of soluble salts, together with the moisture content of the soil, generally determine the ability of the soil to conduct an electric current. The development of acidity in soils is a result of the natural processes of weathering under humid conditions.

Bacteria may affect the chemical properties of soils. Certain types of bacteria are capable of fixing atmospheric nitrogen and converting nitrogenous material in the soil to a form useful to plant life. Other bacteria convert sulfur and sulfides to sulfates, and still others accomplish the reverse reaction.

The physical properties of soils important in corrosion are mainly those that determine the permeability of the soil to oxygen or air and to water. The particle size distribution of the soil is an important factor with respect to aeration and moisture content. In coarse texture soils, such as sands and gravels, where there is free circulation of air, corrosion approaches the atmospheric type. Clayey and silty soils are characterized in general by fine-texture, high water-holding capacity and, thus, by poor aeration and poor drainage.

Factors Affecting Corrosion in Soils

Since corrosion is an electrochemical process, it requires a potential difference between two points electrically connected and immersed in an electrolyte. Electrons flow from the anodic area through the electrolyte to the cathodic area and back through the metal to complete the circuit. The anodic area is the most negative in potential and is the area that corrodes through the loss of metal ions to the electrolyte. The cathodic area is protected from corrosion because of the deposition of the hydrogen ions that carry the current.

The factors affecting corrosion in soils are aeration, electrolyte, electrical factors, and miscellaneous.

1. Aeration affects the access of oxygen and moisture to the metal, consequently affecting corrosion. Oxygen causes corrosion by combining with the metal ions to form oxides, hydroxides, or salts of metal. If these corrosion products are soluble or removed from the anodic areas, corrosion proceeds, but if the products accumulate, they may act as a protective layer to reduce corrosion or initiate localized corrosion because the corrosion products are more noble than the base metal.
2. Electrolytes affect the flow of electric current. Moisture in soils helps the current flow, thus promoting the corrosion process. The ions in the electrolyte determine the electrical conductivity as well as the acidity or alkalinity of the electrolyte, and the chemical reaction between the primary products of corrosion and the electrolyte.
3. The principal electrical factor in the corrosion of metals in soils is the variation in potential that exists at different points or areas on the surface of the metal. Potential differences involve both the metal and the electrolyte. It may be affected by local variations in either one. The amount of current that flows through the cell as a result of the potential difference is dependent upon the electrical characteristics of the electrolyte and by the polarization of the metal surfaces. The potential difference and the resulting corrosive current is not necessarily constant with time. The relative size of the anode and cathode areas is a factor in determining the amount of corrosion damage.
4. Some of the miscellaneous factors affecting corrosion in soils are the effect of different soils in contact with the same pipe, different compactness in the case of backfill in a pipe trench, foreign material or stones in contact with the pipe; bacterial action is another factor and is associated with aeration and the formation and presence of soluble salts.

Test Methods Used in the Past to Identify and Measure Corrosion in Soils

1. In 1928, the Bureau of Standards in a paper by Logan [*2*] stated, "Originally nonuniformity in the metal caused by impurities or strains was assumed to account for much of the corrosion. Then Evans and others pointed out that differences at the surface of the metal, oxygen concentration cells, etc., were factors. The soil corrosion tests indicated that the structure and chemical properties of the soils as well as the nature of the contact between the soil and the pipe must be considered."
2. In 1928, an article by Henry Hough [*3*] appeared in *Gas Age Record* where he mentioned that soil samples are normally taken at intervals of not more than one mile, by means of an auger, to the depth at which the pipe will lie when in service. The sample is placed in an air-tight container. At the laboratory it is weighed as received, air-dried, and weighed again to determine the moisture content. A solution is made by thoroughly mixing a portion of each sample with distilled water. Both the solution and the soil are then subjected to a carefully worked out series of chemical analyses to determine the amount of certain constituents known to be active factors under certain conditions in accelerating or inhibiting corrosion. In addition to the chemical analyses, each sample is subjected to determinations for hydrogen ion concentration on physical, electrolytic, and accelerated corrosion tests.
3. In 1930, *The Oil and Gas Journal* published an article by Joseph F. Putnam [*4*] entitled "Predetermination of Soil Corrosion May be Evaluated in Terms of Electrical Units. Simple Ammeter Voltmeter Test has been Devised." The article discussed theoretical considerations which included:

    a. soil corrosion in an electrolytic phenomenon.

b. Faraday's first law of electrolysis may be interpreted to state that the amount of iron lost by a buried pipe due to soil corrosion is proportional to the quantity of electricity flowing from the pipe to the soil. Thus, corrosivity (C) is proportional to current (I)

$$C \propto I$$

applying Ohm's law

$$I = E/R$$

then

$$C \propto E/R$$

4. Whenever an electrolytic reaction takes place, decomposition products are formed which set up a counter electromotive force. This value, called by physical chemists the decomposition potential (E_d), must therefore by subtracted from the causation potential (E_c) in order to obtain the value of E for the above equation

$$E = (E_c - E_d)$$

When a piece of iron is buried in the soil, a difference of potential (E_c) exists between two points A and B of the buried iron. Electrons start to flow from A through the soil to B and back through the metal to A, thereby completing the circuit. Electrically, the resistance of the metallic part of the circuit is usually so small compared with that of the soil that it may be neglected. Furthermore, the actual resistance of the soil path is difficult to determine, but it is proportional to the resistivity or specific resistivity (R_{sp}) of the soil. Thus, the relative corrosivity may be taken as

$$C = \frac{k(E_c - E_d)}{R_{sp}}$$

where k is constant, which for purposes of relative measurement is usually taken as 1000.

To determine the decomposition potential (E_d), two metal plates are immersed in an electrolyte connected through an ammeter, voltmeter, and potentiometer to a battery. A curve as shown in Fig. 1 can be drawn for various settings of the potentiometer. Beyond point P, the electrolyte obeys Ohms law. P is called the decomposition potential (E_d) of the electrolyte.

Soil Resistivity (R_{sp}):

Soil conductivity depends on many factors, such as degree of consolidation, salt content, organic matter, moisture, etc. The effect of pressure or soil packing is seen in Fig. 2.

It is probable that the rise in resistance beyond point B is due to squeezing out water under high pressures. Soils under test should be compressed to point A, beyond which the resistivity is practically constant.

Moisture is by far the most important variable in soil resistivity. In Fig. 3, it can be seen that soil resistance varies markedly with moisture content. As the moisture content is increased, the resistivity drops rapidly, becoming nearly constant until the mud point (P) is reached, beyond which the salt solution becomes diluted with an increase in moisture.

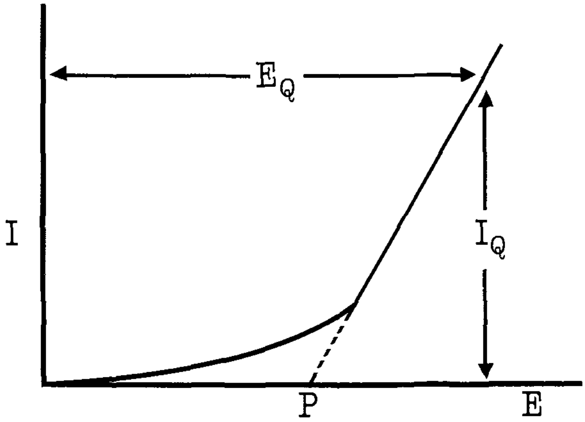

FIG. 1—*Decomposition potential—current.*

Unless the average integrated moisture content is known, no relative measurements of corrosivity will be of value. A soil sample taken with moisture content of point A when the integrated average for the year is that of point B will show the soil to be only about one fifth as corrosive as it actually is.

Many tests have been devised in which soil is saturated with distilled water with the result that fairly noncorrosive soils have often been thought corrosive, and a great deal of pipe treatment has been needlessly applied, including useless expenditures.

Electrical Tests

The soil sample is compressed in a Bakelite box between two steel end pieces which have been previously cleaned by emery cloth. Connections are made as shown in Fig. 4. The switch is first connected to position B and a resistivity measurement made on a slide wire bridge, using alternating current to eliminate polarization effects. The switch is then connected to position C; the potentiometer having been adjusted, the voltmeter (E) reads a

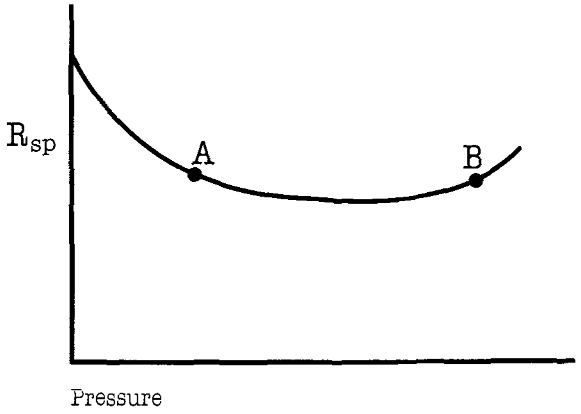

FIG. 2—*Effect of pressure on soil resistivity.*

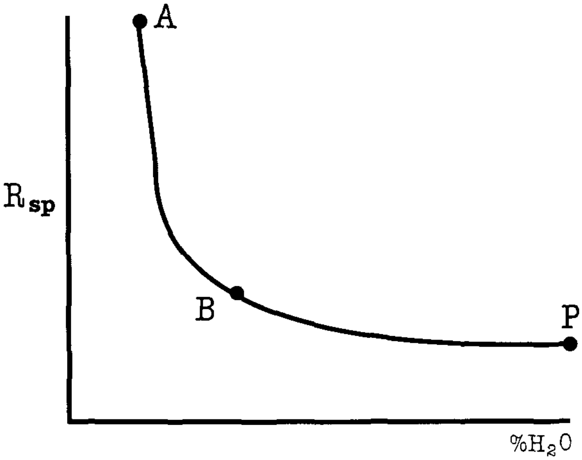

FIG. 3—*Effect of moisture on soil resistivity.*

causation potential (E_c) of 1.4 V. Figure 5 shows the relationship of current and time. When the switch is first connected to B, the full causation potential (E_c) of 1.4 V acts on the soil; being a unit cube, it has a resistance of R_{sp}. The current at zero time is

$$I_0 = \frac{E_c}{R_{sp}}$$

As the electrons start to flow, decomposition products are built up on the steel end plates, setting a counter potential which reaches the decomposition potential (E_d) in 5 to 10 min. The current value is

$$I_{10} = \frac{E_c - E_d}{R_{sp}}$$

If the ammeter reading is in milliamperes, the constant (k) is 1000. The current reading in milliamperes equals the corrosivity (C) of the soil equals causation potential (E_c) equals

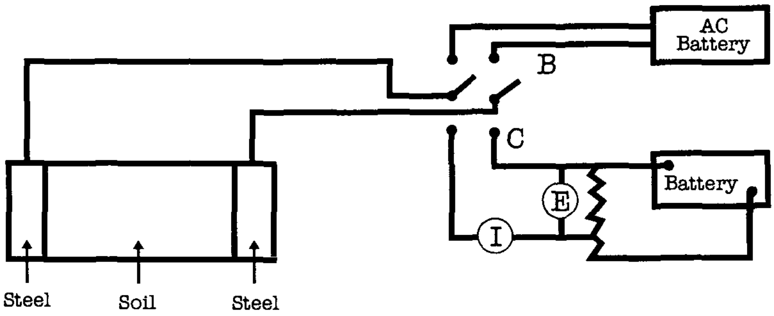

FIG. 4—*Sketch of corrosivity measuring equipment.*

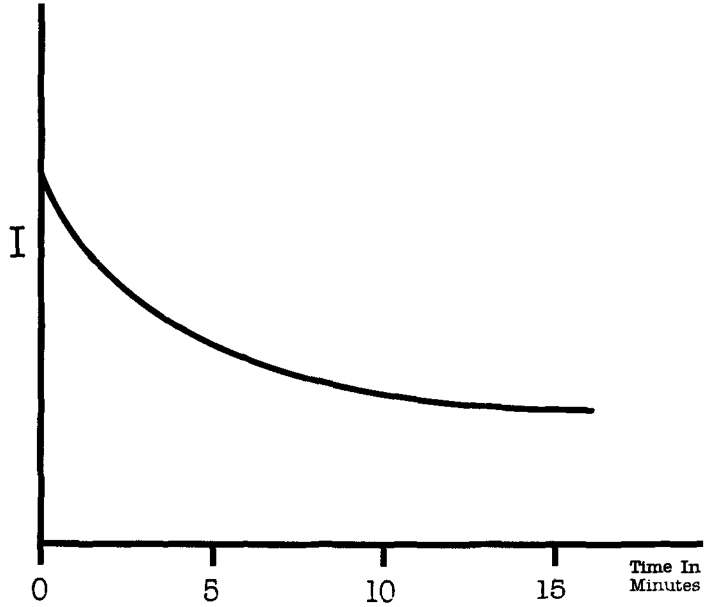

FIG. 5—*Drop in current with time.*

1.4 V. The selection of 1.4 V as a causation potential was not arbitrary but the result of an extended investigation.

Moisture and Rainfall

The fact that soil resistivity varies so sharply with moisture makes it necessary to establish an integrated average of moisture content before making a corrosivity measurement. It is necessary to know the average rainfall in the terrain under test and the time of the last rain before the sample was taken. Then the integrated average can be estimated from the knowledge of soil texture, drainage, etc.

Soil Corrosiveness Measurement Methods

The following methods were reported in *Gas Age Record* of 1932 [*6*].

Historical Methods

Use actual corrosion experienced by parallel lines in neighboring territories or lines in apparently similar soil as a guide. This does not permit satisfactory differentiation along a line as soil conditions change.

The second historical method is less precise. It depends solely upon the opinion formed after inspection of ground surface conditions.

Ground Moisture Determination

Soil corrosion is dependent upon physical condition, chemical composition, and amount of moisture. Moisture is the only variable and therefore is the controlling factor.

This method may be useful in demonstrating relative variations within any strictly limited area, but appears inherently inapplicable to comparisons between widely separated areas.

The method involves repeated field sampling, laboratory determinations of moisture content, and loss of weigh measurements on corrosion specimens.

Hydrogen Evaluation Method

A measurement of the hydrogen evolved during corrosion as reflecting the combined effect of a group of six important soil properties. This method provides for the intimate mixing of equal weights of soil and of iron filings, the immersion of the mixture in water under an inverted graduated test tube and the subsequent reading, after a definite period of time, of the quantity of gas collected.

The method, while simple, does not appear to be adequate because of the possibility of the gas volume being affected both by the generation of carbon dioxide from vegetable matter in the soil and the fineness of the soil particles. There is also the probability that the rates of corrosion in various soils will be different for iron filings and for iron or steel pipe because of differences in relative area and nature of the exposed surface.

Total Acidity Measurements

Denison found a certain measure of correlation between the total acidity of certain soils and repair records of a pipeline along which they were collected. He used chemical methods of analysis. Holler used direct electrometric titration for the same purpose. This method, like the preceding one, is limited in its applicability besides requiring a considerable degree of technical skill in laboratory manipulation. It has no usefulness in the case of alkali soils.

Loss of Weight Method

A clean, very thin, steel disk is buried in the moistened soil to be tested and maintained at constant temperature in a water saturated atmosphere for two weeks. The loss of weight of the clean dry disk is then determined.

The method eliminates measurements of the relative effect of the moisture content of the soil in situ as well as of temperature and humidity variations. The test exposes a standardized prepared metal surface, unlike the surface of commercial pipe, to corrosive action.

The Geological Method

The method is based on the fact that a particular degree of soil corrosiveness is characteristic of a definite geological soil series. This method recognizes the effect of rainfall and drainage on soil corrosiveness. Ewing [7] proposed the development of tables showing the relative corrosivity of all the various soils which may be encountered and reference to such tables after expert geological classification of the soils under investigation. It is easier to recognize a geological similarity between two soils which have caused a comparable degree of corrosion than it is to classify soils with assurance before experience has demonstrated their corrosiveness.

Electrical Methods Using an External Electromotive Force to Measure Conductivity or Resistivity

These methods are based on the electrochemical theory of corrosion and the assumption that chemical action is accompanied by the flow of electrons. Any activities facilitating such flow increases chemical action. Thus, pure dry sand has a high resistance; pure water is not a good conductor. The methods of Putnam, Williams, and Corfield all involve laboratory determinations; therefore, they are all subject to criticism that the neglect to control certain test conditions or their arbitrary definite establishment may nullify the practical value and usefulness of the results obtained.

1. Putnam proposed a test apparatus using 10 ft (3.048 m) of No. 28 iron wire wound in a 2-in. (50.8-mm)-diameter coil buried vertically in the soil to be tested. A ¼-in. (6.35-mm) iron rod connected to the bottom of the spiral provided the second connection for a 2-V battery. After four days, an inspection of the wire should show a point where the character of corrosion changed, which by measurement and proportion could be used to determine the so called "ionization potential" which Putnam claimed bore an inverse relationship to soil corrosiveness.
2. Putnam also proposed a second apparatus consisting of a unit volume box with steel end plates. The soil is packed in the box, and potential of 1.4 V is impressed across the soil for 10 min at which time the current is measured. This current is proportional to the corrosiveness of certain soils. The validity of 1.4 V was questioned, as well as the soil density, the dimensions of the box, and other variables.
3. The Williams method (and Corfield's modification) are essentially measurements of the loss of weight of pipe samples used as cathodes buried in soil samples contained in tin cans which serve as anodes. Williams uses a 2-V battery for 24 h or less. Corfield uses 6 V to increase the weight loss and availability of this size battery. The choice of a maximum 24 h is made to avoid polarization effects. The results are less accurate due to the effect of direct current on polarization, soil temperature, etc.
4. The Shepard Method [5] differs from the previous methods in its use of measurements made in the field, with minimum interference of important existing conditions such as compactness and moisture content.

Using the steel-tipped rods to make earth contacts at least 6 in. (152.4 mm) apart and a 3-V battery, instantaneous readings are made of the resulting current. These readings are indicative of relative soil resistivity, which is a measure of soil corrosiveness.

Other Electrical Methods

1. The apparatus developed by Legg used dissimilar electrodes on a single rod, and the use of external source of current is eliminated. A milliameter is used to measure the current from the primary cell set up when both electrodes are in contact with soil.
2. The Schlumberger and Leonardon methods are based on measurements of the path, direction, and magnitude of earth currents. Some attention is also paid to measurements of soil resistivity.

Methods Involving Chemical Analysis of Soil

1. Dickey never published the detailed results of his methods nor suggested any definite procedure. Thus, the only method using chemical analysis is that of Richards and Smith developed in 1927. It has since been improved.
2. The procedure includes the inspection of local climatological data, a study of any pertinent electrolysis surveys, the completion of a topographical reconnaissance, and the interpretation in the light of all such available information of chemical analyses of soil samples and of their water extracts. A survey so made recognizes the effect of all important influencing

factors and presents the nearest approach to the ideal method of determining soil corrosiveness.

Relationship of Soil Properties to Corrosion of Buried Steel

In 1938, the following conclusions appeared in *Industrial and Engineering Chemistry* in a paper by Rogers [*9*].

1. The controlling factor in soil corrosion of buried steel is the effect of variations in the soil water-air proportions. Laboratory variations of these factors allowed variations in corrosion rates of 31.1 to 1 to 56.5 to 1 to occur.
2. The electrical resistivity of a soil exerts an influence on its corrosion rate. Variations in this factor in the laboratory for Kalmia sand and over the range 12 000 to 94 ohm-cm resulted in a variation in a corrosion rate between 1.5 and 1.0 mils per year.
3. The pH of a soil exerts an influence on its corrosion rate. Laboratory tests show that varying the pH of Kalmia sand between 4.5 and 9.75 resulted in a variation in corrosion rate between 2.2 and 1.0 mils per year.
4. Comparison of soil resistivity measurements at saturation with the corresponding pipe pit depth show that there is a definite trend between resistivity and corrosion. The trend is not sufficiently accurate; but, however, is to be used as an index of soil corrosion. It can only be said that very few corrosive soils have resistivity values greater than 1800 ohm-cm. The majority of soils possess values of resistivity less than this.
5. Comparison of soil pH values with field corrosion rates indicate a complete lack of any correlation between these quantities. The method cannot be used as a field index of soil corrosion.
6. The corrosion rate of a soil in the field may be determined by following its seasonal variation in water-air volumes and checking again a laboratory index test.

A Method for Direct Determination of Soil Corrosivity in Terms of Conductivity

In the December 1937 issue of *Gas Journal* [*8*], Burton introduced a new method and an instrument for the direct laboratory determination in terms of conductivity. Accurate, reproducible, and dependable results were obtained.

The method employs an alternating current bridge using an a-c frequency of 100 cycles or more. With the use of a-c of 50 or 60 cycles, polarization effects are greatly minimized over those of d-c.

Limitations of Text Methods

In 1939, Logan [*10*] offered the following summary:

> The corrosion of pipelines depends on a number of factors which make it impossible to fully report underground corrosion phenomena in the terms commonly used for the report of corrosion data. This is especially important with respect to maximum pit depths. The maximum pit depth observed on any area will, on the average, be less than the maximum pit depth on a larger area exposed to the same conditions. Pits usually change in depth more slowly as they become older, but this change, as well as the pit depth, differs greatly for different soils. It is therefore necessary to accompany rates of penetration by data on the effects of area and time if the pit depth are to be used for an estimation of the life of pipe. Such estimates should be based on data for the particular soil conditions associated with the pipe, rather than on rates of penetration for average soil conditions. The relative depths of pits on two materials or on the same material exposed to

two soils may differ for different periods of exposure or for different exposed areas. Some of the soils which produced relatively high initial rates of corrosion were shown to be less destructive to pipelines than others with lower initial rates of corrosion.

Comparisons between experience and predictions of corrosion based on experiments are frequently unsatisfactory because the pipelines may be subjected to influences not represented in the experiment. In general, however, the observed correspondence is sufficiently good to warrant the conclusion that if local conditions are properly taken into account, the results of the soil corrosion investigation properly adjusted for the effects of area and time constitute the best available basis for decisions as to the proper wall thickness and the necessity for protection of a proposed pipeline.

Introduction of the Polarization Technique for Testing

In 1955, the *NACE Journal of Corrosion* published a paper by W. Neighbours [*11*] entitled "A New Method for Measuring Potentials of Polarized Electrodes in Soil Corrosion Cells." The method in summary included interrupting the current through a soil corrosion cell and measuring the potentials of the polarized electrodes during the period of interruption. An electronic circuit was used to interrupt the current, and the potential across the cell at interruption is balanced against a known potential; an oscilloscope was used as a null indicator. This method was developed in New Zealand; it was an improvement over a method designed by Hickling and applied by Denison and Darnielle of the Soil Bureau of the New Zealand Department of Scientific and Industrial Research. The improvements included the use of a visual method with oscilloscope presentation rather than the sound method of the Hickling meter. A circuit was developed along these lines and has proved to be satisfactory in the measurement of potentials of soil corrosion cells.

Soil Corrosivity Based on Investigation of Highway Culverts

In 1961, a paper by R. F. Stratfull [*12*] appeared in the *NACE Journal of Corrosion* entitled "A New Test for Estimating Soil Corrosivity Based on Investigation of Metal Highway Culverts." The new test method estimates relative soil corrosivity by combining the relative influences of the hydrogen ion concentration (pH) and the minimum resistivity of the soil. It establishes relative soil corrosivity by plotting these combined values on a chart showing the soil corrosivity in terms of the corrosion rate of steel buried in a similar soil as reported by the National Bureau of Standards. The results of this new test method were compared to the soil corrosivity determined by the reported weight loss of steel specimens. It was concluded that the new test is a reasonable overall indicator of relative soil corrosivity. The new test method utilized the minimum resistivity value of a soil solution that was obtained by varying the moisture content. In contrast, the NBS data are based upon a soil being saturated with moisture, with all measurements made or corrected to a temperature of 60°F (15.6°C).

A noteworthy statement was made: "Experience indicates that in a number of cases the minimum soil resistivity does not occur at the saturation point."

Differential Aeration and Its Effect on Soil Corrosion

In 1963, the *NACE Journal of Materials Protection* published a paper by Edward Schaschl and Glenn Marsh [*13*] entitled "Some New Views on Soil Corrosion." The paper stated that corrosion of steel in soil frequently has been blamed on such factors as low pH, electrolysis due to stray currents, bacterial action, or reactive chemicals in the soil. Though these factors may be important in some cases, they should be considered as exceptional rather than common causes of corrosion. A more general cause, differential aeration involving drained soil, is of primary importance. In differential aeration mechanism, oxygen and water alone are responsible for severe corrosion. The paper discussed the relationship of water saturation, resistivity, and draining characteristics with the corrosive nature of soil.

Corrosion of steel in soils can be explained in terms of long cell action arising from differential aeration. Oxygen plays the dominant role as a cathodic reactant. Cathodic activity is intense when a soil is partially drained or when it contains 50 to 95% of the water needed for saturation. In this state, the resistivity is low enough to allow extensive long cell action.

The Present Measurement Techniques of Soil Properties [*16*]

In the mid-1970s, Escalante [*15*] and Iverson [*14*] concluded that a low soil resistivity of 500 ohm-cm or below is a good indicator of a corrosive soil. At higher resistivities, above 2000 ohm-cm, the relationship is not as clearly defined. They also concluded that no correlation was found between the corrosivity of soil as measured by weight loss or galvanic current and its pH or redox potential.

Resistivity

This is the most widely used criterion for evaluating soil corrosivity. Resistivity measurements can be made in two ways. One method involves making the measurement directly at the site without disturbing the soil. Wenner's four-electrode method [*15*] is the most widely used for that technique. The second method involves removing a sample of the soil and placing it in a box with an a-c bridge and null meter to directly read the resistivity. Each method has its advantages and disadvantages leading to untrue readings. However, resistivity as a criterion, when performed properly, is probably the single best indicator of the aggressiveness of the soil.

1. The effect of temperature on soil resistivity is shown in Fig. 6. There is a gradual increase of resistivity with a decrease in temperature until the freezing point of water is reached. At temperatures below freezing, the soil resistivity increases very rapidly. The relationship between temperature and soil resistivity is controlled by the following equation

$$R_{15.5} = R_t \frac{(24.5 + t)}{40}$$

where

$R_{15.5}$ = resistance in ohms at 15.5°C,
R_t = measured resistance at t°C, and
t = temperature in °C of the soil.

2. The effect of pressure on the soil resistivity is shown in Fig. 2. It was found that the resistivity decreased with increasing pressure reading a minimum of 100 lb/in.^{2}, but above this pressure there was little change in resistivity.

3. The effect of moisture content on the resistivity of a clay soil is shown in Fig. 7. When the soil is nearly dry, its resistivity is very high. However, the resistivity decreases rapidly with increases of moisture content until the saturation point, after which further moisture has little or no affect on the resistivity.

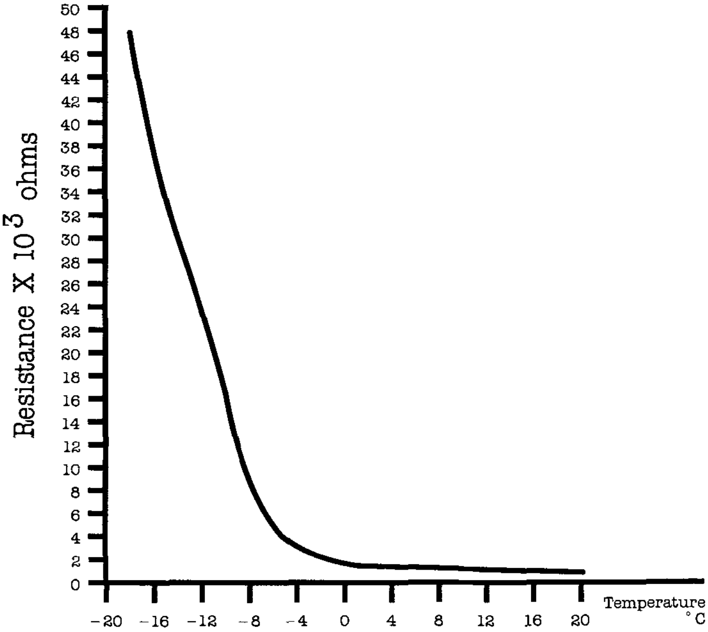

FIG. 6—*Effect of temperature on soil resistance.*

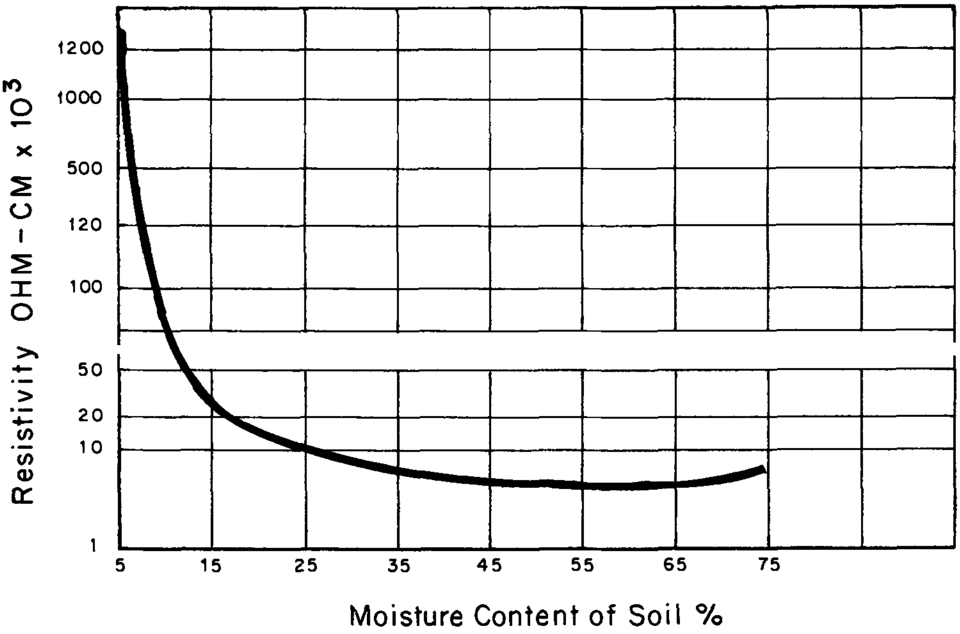

FIG. 7—*Effect of moisture content on resistivity of a clay soil.*

pH Measurement

This is the measure of acidity or alkalinity of the soil. It does not give information about the total acid content related to the corrosivity of the soil. It is recommended to measure pH of soil in its natural state, since changes after removal have been reported. pH of soil is usually measured using a portable pH meter. Calibration of the electrodes is performed just prior to the measurement using a standard buffer solution of pH of 7.

Redox Potential

Two platinum electrodes are used to measure the soil redox potential versus a saturated calomel electrode. The redox potential or oxidation-reduction potential is the potential of an inert electrode in an electrolyte developed with reference to a half cell and converted to the standard hydrogen scale.

$$E_h = \overline{E} + 0.250 + 0.06\,(\text{pH})$$

where

E_h = redox potential at pH 7 (standard hydrogen scale),
$\overline{E}$ = probe potential, the mean of two platinum electrodes, and
pH = the soil pH.

The relationship between the soil corrosivity and the redox potential (Table 1) was developed by Starkey and Wight.

Polarization Techniques

Electrochemical polarization which can provide a numerical value of the corrosion rate.

1. *Polarization Resistance Method*

The polarization resistance technique is based on the following relationship derived by Stern and Geary

$$\frac{\Delta E}{\Delta I} = \frac{i}{2.3\, I_{corr}}\, \frac{B_a B_c}{(B_a + B_c)}$$

where

ΔE = overvoltage produced by a polarizing current ΔI.
$\frac{\Delta E}{\Delta I}$ = slope of the polarization curve (polarization resistance),
B_a = slope of the anodic polarization curve in the Tafel region,
B_c = slope of the cathodic polarization curve in the Tafel region, and
I_{corr} = corrosion current.

2. *Polarization Break Method*

This technique is based on the observation that anodic and cathodic polarization curves consist of straight line segments having different slopes. The current at which the change in slope occurs is designated I_p for the cathodic and I_q for the anodic curve. The corrosion current I_c can be calculated from the following relationship derived by Pearson and confirmed by Holler

TABLE 1—*The relationship between the soil corrosivity and the redox potential was developed by Starkey and Wight.*

Range of Soil Redox Potential, mV	Classiciation of Soil Corrosion
Below 100	Severe
100 to 200	Moderate
200 to 400	Slight
Above 400	Noncorrosive

by Holler

$$I_c = \frac{I_p I_q}{I_p + I_q}$$

Challenge Offered to the Professional World

Many different soil conditions are being developed as a result of our changing world. Pollution of the underground streams by chemical contamination, abandoned deteriorated structures buried underground, nuclear waste, acid rain, leaking underground tanks, etc. will cause drastic changes in the previously known soil characteristics. Thus, we cannot depend with any degree of certainty on the physical and chemical characteristics of soils tested years ago by the Agricultural Department and other agencies. The measurements of the soil characteristics to determine its corrosivity need to be conducted just when a project is ready. Periodic monitoring of these criteria is also highly recommended to alter the needs for corrosion control.

Computers have impacted many of the measuring techniques and test procedures. However, soil corrosivity and its criteria have not benefited from that progress except in a very limited way. A challenge is offered to the professional world to develop new sensors to determine the soils corrosivity by taking into consideration the combined affect of its physical chemical criteria, and other factors. Similar sensors are needed to clearly identify, measure, and control corrosion in soils.

Summary

Corrosion by soils as an electrolyte is a serious and important subject that cannot be ignored. The cost of corrosion by soils is rising at an alarming rate. Individual characteristics have been used to indicate corrosivity without complete accuracy. The synergetic effect of all known physical and chemical characteristics of soil to determine its corrosivity is desperately needed. The protection of our current buried structures and future ones depends on this generation to develop new sensors to achieve that goal. Obviously, the market is there, but above all, the preservation of our natural resources must be our ultimate goal.

References

[1] Romanoff, M., "Underground Corrosion," National Bureau of Standards Circular 579, U.S. Government Printing Office, Washington, DC, 1957.

[2] Logan, K. H., "The Bureau of Standards Soil Corrosion Investigation," U.S. Department of Commerce, Washington, DC, 1928.

[3] Hough, H. W., "The Place of the Complete Corrosion Survey in Industry," *Gas Age Record,* 9 Feb 1929.
[4] Putnam, J. F., "Predetermination of Soil Corrosion," *The Oil and Gas Journal,* 13 Nov 1930.
[5] Allyne, A. B., "A Modern Soil Survey with Shepard Rods," *Gas Age Record,* 22 Aug 1931.
[6] Smith, W. T., "How Soil Corrosiveness Can Be Measured," *Gas Age Record,* Vol. 70, No. 6, 1932.
[7] Ewing, S., "Rough Relationship Between Corrosiveness and Resistivity for Alkali Soils," *The Oil and Gas Journal,* 21 April 1932.
[8] Ewing, S., "Engineering Principles Applied to Soil Corrosion Problems," *Gas Journal,* May 1937.
[9] Rogers, W. F., "Relationship of Soil Properties to Corrosion of Buried Steel," *Industrial and Engineering Chemistry,* Vol. 30, No. 10, 1938.
[10] Logan, K. H., "Engineering Significance of National Bureau of Standards Soil-Corrosion Data," Research Paper RP1171, National Bureau of Standards, Gaithersburg, MD, 1939.
[11] Neighbours, W., "A New Method for Measuring Potentials of Polarized Electrodes in Soil Corrosion Cells," *Corrosion—NACE,* February 1955.
[12] Stratful, R. F., "A New Test for Estimating Soil Corrosivity Based on Investigation of Metal Highway Culverts," *Corrosion—NACE,* October 1961.
[13] Schaschl, E. and Marsh, G. A., "Some New Views on Soil Corrosion," *Materials Protection,* November 1963.
[14] Iverson, W. P., "Tests in Soils," *Handbook on Corrosion Testing and Evaluation,* John Wiley & Sons, Inc., New York, 1971.
[15] *Underground Corrosion, ASTM STP 741,* E. Escalante, Ed., ASTM, Philadelphia, 1979.
[16] *Effects of Soil Characteristics on Corrosion, ASTM STP 1013,* Chaker/Palmer, Eds., ASTM, Philadelphia, 1989.

DISCUSSION

M. Schorr[1] (*written discussion*)—A pH of 1.5 may indicate the presence of about 1 mol/L of a strong acid. Neither steel nor reinforced concrete can withstand such an acidic soil. Are they planning some kind of soil treatment to neutralize the acid before starting to build the foundations?

V. Chaker (*author's closure*)—I agree that the pH of the soil is very acidic. I know that there are plans to use special concrete to withstand that environment. I am not sure that there are plans for a soil treatment.

A. VanOrden[2] (*written discussion*)—Do we have a public relations problem? If we have been studying corrosion in soils since the turn of the century, and we are reinventing the wheel, perhaps we need to provide more information to our own organizations and then to the larger technical and engineering community.

V. Chaker (*author's closure*)—I don't think we have a public relations problem. However, I believe we have a time lag between research and development and the change in the environment. In the meantime, the existing information and tools are still being used. Some of the existing information is not correct and needs to be updated. The equipment is manual and too slow. Development of sensors and equipment taking into consideration the computer age is needed. In the meantime, symposia like this one should continue to alert and challenge the technical community to evaluate each situation carefully and to work on developing advanced tools.

---

[1] IMI, Institute for Research and Development, Haifa, Israel.
[2] AS&M, NASA Langley Research Center, Hampton, VA 23665.

E. Escalante[3] (*written discussion*)—Corrosion studies at several laboratories have shown that steel piles driven into soil display negligible corrosion compared to piles in back-filled soil. These data have been collected in soil with a pH above 5.5 where the cathodic reaction is oxygen controlled. You suggest that at pHs of 1 and 2 corrosion occurs on driven steel piles. Do you believe that the cathodic reaction is hydrogen reduction in this case?

V. Chaker (*author's closure*)—Your question about the cathodic reaction in soils of pH 1 and 2 being hydrogen reduction is interesting. No tests were performed to confirm or deny that. Obviously, more tests are needed under the above-mentioned conditions before an answer can be given.

---

[3] NIST, Gaithersburg, MD.

Edward Escalante[1]

Measuring the Corrosion of Metals in Soil

REFERENCE: Escalante, E., "**Measuring the Corrosion of Metals in Soil,**" *Corrosion Testing and Evaluation: Silver Anniversary Volume, ASTM STP 1000,* R. Baboian and S. W. Dean, Eds., American Society for Testing and Materials, Philadelphia, 1990, pp. 112–124.

ABSTRACT: Polarization resistance and galvanic current measurements, used for underground corrosion studies, are described, and problems encountered in making these measurements in the field, along with solutions, are discussed. Polarization measurements, supported by physical measurements, have shown that induced alternating current increases the corrosion rate of copper concentric neutrals compared to copper neutrals without ac. These measurements also revealed that driven piles undergo less corrosion attack than similar piles in backfilled trenches. Galvanic current measurements provide valuable information on the behavior of galvanically coupled materials and can be used to compare the corrosivity of soil environments.

KEY WORDS: corrosion in soil, galvanic current, polarization resistance, underground corrosion measurements

Advances in technology allow measurements, previously considered limited to the laboratory, to be extended to field situations. These advances include improved performance of electronic components, miniaturization of equipment, and development of portable computers and high-impedance digital voltmeters, which are an important result of these advances. This paper describes equipment used in the field in the past and equipment used today with examples of data collected. These data will emphasize the difference observed in corrosion of steel between conditions of disturbed and undisturbed soils.

Measurements and Procedure

Electrochemical measurements are useful for obtaining information on corrosion of structures underground, and generally these measurements can be performed without difficulty. Corrosion rate and galvanic current are the two measurement categories that are described here. Physical measurements, for verification of electrochemical measurements, are also discussed.

Corrosion Rate Measurements

The technique of polarization resistance is useful for obtaining corrosion rate data of metals in soil. The measurement is easy to perform, and the primary complication is the necessity to eliminate or compensate for errors in the potential measurement during polarization. There are many excellent detailed descriptions of the technique [*1–3*], and only a brief review will be provided here.

---

[1] National Institute of Standards and Technology, Gaithersburg, MD 20899.

In 1957, Stern and Geary published their work mathematically describing the shape of polarization curves, showing that at values slightly removed from open circuit potential (≈ 20 mV), potential can be assumed to be a linear function of applied current [*4*]. This expression is written as

$$\left(\frac{dv}{di}\right)_{v\rightarrow 0} = -\frac{\beta_a\beta_c}{2.3\ i_{\text{corr}}(\beta_a + \beta_c)} \tag{1}$$

where

dv/di = slope of potential versus applied current,
B_a = anodic tafel slope,
B_c = cathodic tafel slope, and
i_{corr} = corrosion current.

Thus, if the tafel slopes are known, and the slope of potential versus applied current is measured, then the corrosion current can be calculated. This corrosion current, however, only represents corrosion of the working electrode (WE) during the period that the measurement is made. The mass of metal reacted during the measurement is determined using the Faraday equation [*5*]

$$\text{mass loss} = ki_{\text{corr}}t \tag{2}$$

where

k = electrochemical equivalent, and
t = time.

If several measurements are made during the exposure period of the WE, these data can be integrated over the exposure time, and an estimate of total mass loss is obtained. With information on the surface area of the WE, a corrosion rate can be calculated.

However, as is always the case, this is more easily said than done because there are several problems, especially in underground corrosion measurements, that must be considered and overcome. The difficulties encountered in corrosion measurements in soil range from very mundane problems of maintaining good electrical continuity to the structure or specimen being measured, to more technical problems of eliminating *iR* error and taking into account current distribution where necessary. Each of these problems will be addressed and discussed.

iR Error

Since the resistivity of soil is generally high ($>500\ \Omega$ cm), some means must be used to eliminate or compensate for *iR* error, the error that arises in measuring the potential of the WE in the presence of an electric current. This is often described in the following way

$$\text{WE Potential}_{\text{measured}} = \text{WE Potential}_{\text{polarized}} + (iR)_{\text{error}} \tag{3}$$

The resistive component, R, is the resistance through the soil between the WE and the reference electrode (REF). The current, i, is the current applied between the WE and the counter electrode (CE) during the polarization measurement.

One effective manner of eliminating *iR* is to use the technique of current interruption [*6*]. This takes advantage of the fact that the process of polarization, and depolarization, of the WE is a time-dependent process, whereas the *iR* component goes to zero as the applied current goes to zero. The result is that when the current to a polarized electrode is turned off, depolarization occurs relatively slowly, but *iR* is eliminated immediately. A very effective way to automatically eliminate *iR* is to use a portable computerized system that is programmed to control a data logger (voltmeter with switching capabilities) and a power supply [7]. The computer monitors the potential (Fig. 1*a*) of the WE as the applied current (Fig. 1*b*), controlled by the computer, is turned on and off. The potential of the WE is measured immediately after the current is turned off, and applied current is measured just before the current is turned off. The system is designed to reach and hold the WE at a predetermined potential (for example, −10 mV versus open circuit potential) for a length of time while data are collected and stored.

The same process can also be accomplished by manually turning off the polarizing current while the potential of the WE is monitored with a recording oscilloscope. Figure 2*a* is a plot of potential versus time, showing the instantaneous change in potential, *iR*, when the applied current is turned off (Fig. 2*b*). The *iR*-free polarized potential, V_{pol}, is discernible where the WE begins to depolarize. In some situations, when depolarization is very slow, even an analog voltmeter will allow the *iR*-free polarized potential to be identified.

A Holler bridge circuit has been used very effectively to manually eliminate *iR* during the polarization measurement [8]. This circuit is a modified Wheatstone bridge with the capability of applying polarizing current from a variable power supply. As shown in Fig. 3, the four resistances in the Wheatstone bridge are two 100 kΩ reference resistors, the soil resistance between the WE and REF, and a 100 kΩ variable resistor that is adjusted to

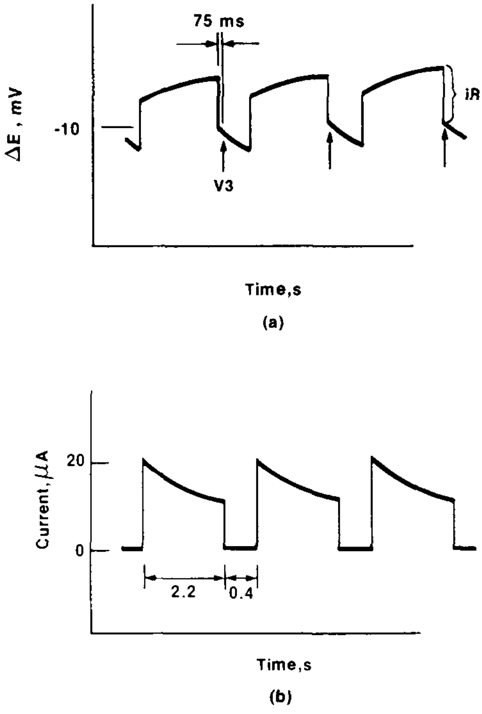

FIG. 1—*Computer-controlled trace of potential and current versus time showing* iR *component in potential.*

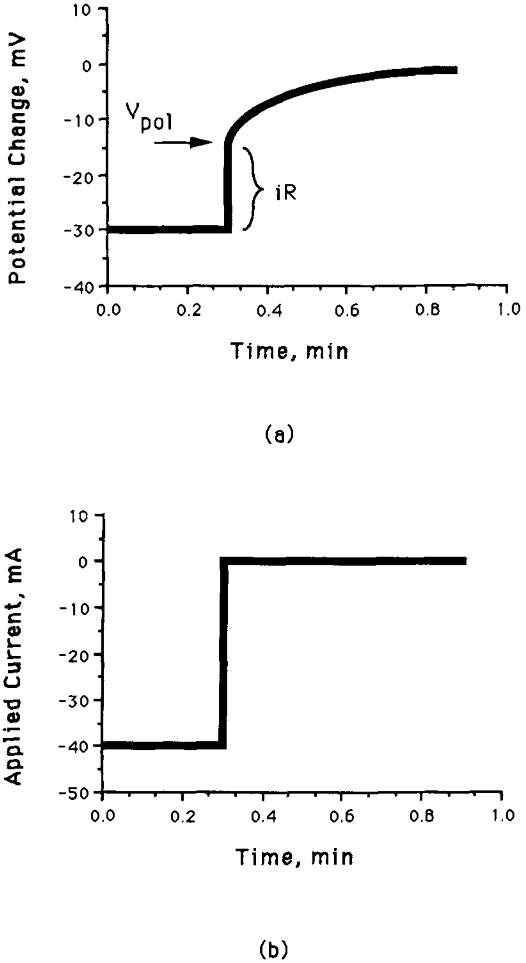

FIG. 2—*Manually controlled trace of potential and current versus time showing* iR *component in potential.*

equal the soil resistance. The circuit is balanced by applying short (≈0.5 s) pulses of current to the WE and noting the effect on potential. When the bridge is unbalanced, the *iR* component causes an instant change in the potential when the current pulse is applied. Between pulses, the variable bridge resistance is adjusted to eliminate the sudden change, due to *iR*, in potential. Once the bridge is balanced, potential measurements during subsequent current applications are *iR* free.

Finally, *iR* can also be compensated by measuring the resistance of the soil between the WE and an electrode near the REF, and after the polarization measurements are performed, using Eq 3 to correct the measured potentials.

Current Distribution

In order to calculate corrosion rate, the area of the WE must be known, and for finite structures such as piles or tanks, their area, in general, is known. Furthermore, proper

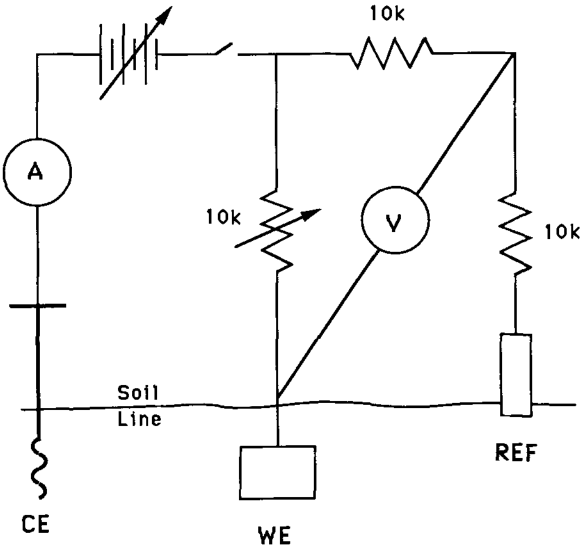

FIG. 3—*Holler bridge circuit for compensation of* iR.

placement of the CE will allow polarization of the entire surface of the structure. However, if polarization measurements are made on a structure such as an underground pipeline or cable which appear infinitely long, then the applied current can only polarize a portion of the structure at a time. In such a case, the distribution of current must be determined so that the polarized area of the structure can be identified. Once this area is known, then a corrosion rate can be calculated.

A convenient method used to determine the approximate area polarized is to measure the change in potential over the structure before and during polarization. Using an underground cable as an example, open circuit potential measurements, employing a high-impedance voltmeter, are made along the length of the cable for a distance of several meters, and the ground surface is marked at each location so each measurement can be repeated. The polarization measurement is carried out with the CE located near the midpoint of the potential measurements. The measurement is held at the point of maximum applied current, and potential measurements are repeated along the length of the cable. The difference between the open-circuit potential measurements and the potential measurements with current applied are then plotted for each measurement point as shown in Fig. 4.

This plot gives an indication of the distribution of current during the polarization measurement, and from these data the area of polarization can be approximated. The example in Fig. 4 shows the results of cathodically polarizing a concentric neutral cable located 1 m below ground level. The potential measurements were made along a line directly over the cable, and the CE was placed 1 m from the centerline of the potential measurements. These data indicate that when a current of 1.5 mA was applied, the cable was polarized from the 4-m mark to the 18-m mark, a distance of approximately 12 m. From this information, the area of the cable can be determined and a corrosion rate calculated.

Galvanic Current Measurements

It is sometimes necessary to connect unlike metals together, and in such a case it is desirable to understand the electrochemical behavior of the couple. A common technique

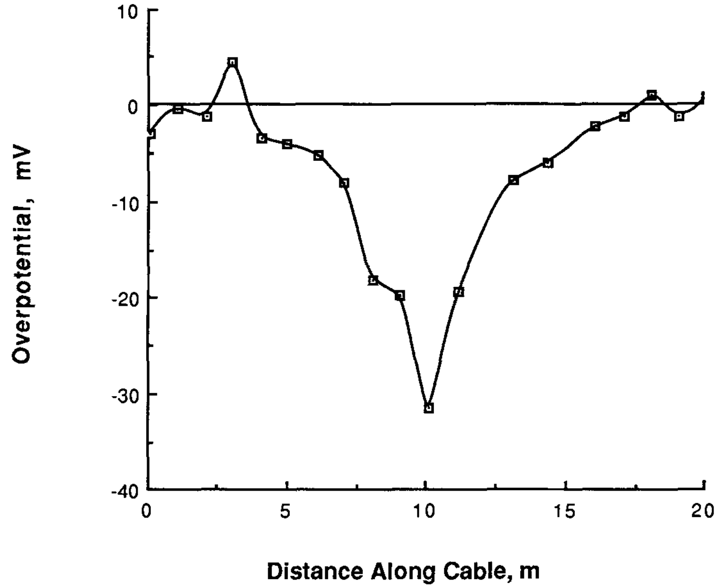

FIG. 4—*Current distribution to underground cable as indicated by plot of potential change versus position with application of 1.5 mA.*

employed is to measure the galvanic current generated between the two metals in the environment of interest. The measurement provides information on the amount of current generated and the direction of the flow of current. Since current travels from the cathode to the anode through the ammeter, the metal acting as anode is identified. With information on the area of the anode and the amount of current measured, the corrosion rate of the anode can be calculated. Excellent descriptions of this measurement technique have been published [*9,10*]. This measurement is performed on test coupons or, if possible, on the structure of interest. It is important to use an ammeter that does not introduce a resistance into the galvanic cell circuit. Such instruments, often referred to as zero-resistance ammeters, are used for this purpose and have been described [*11,12*].

Problems Encountered

Two major types of problems are encountered in making field measurements and can be categorized as (1) equipment failures and (2) electrical interference. One can attempt to avoid equipment failures by using sturdy instruments designed for field use, but often the equipment needed (such as oscilloscopes) is not designed for field use. It is not uncommon to trace equipment failures to damage during transportation, and this source of damage can be reduced through careful packing of equipment. This includes immobilizing moving components such as pen assemblies on recorders, and packing equipment in foam or other shock-absorbing material. Batteries should be removed from equipment and packed separately. If specific components are known to be prone to fail, replacement parts should be carried along.

During the process of making measurements, high-resistance contacts can be considered equipment failures. Electrical conductors must be of high quality to take the abuse of field use. Wire components should be soldered, rather than just crimped or screwed together.

Temporary electrical contact to a structure can be made with heavy duty clamps or locking pliers.

Electrical interference generally reveals its presence through erratic potential readings. It is useful to examine the signal with an oscilloscope to identify its form. Interfering signals from cathodic protection sources are a steady direct current (dc). On the other extreme are alternating current (ac) interfering signals that can range from 60 Hz from power utilities to radio station signals in the kHz range. Certainly, the worse type of interference is the erratic signal of unknown source.

Most interfering signals can be dealt with by (1) removing the interfering signal or (2) suppressing the interfering signal. The first option, turning off interfering signals, is better, especially in the case of a nearby cathodic protection system. This requires cooperation from other organizations. Suppression of d-c interference by filtering is, generally, not possible. Sometimes, if the interfering d-c signal is steady, measurements can be made in its presence, but one must be aware that the reference potential is shifted by the *iR* produced by the interference.

It is more difficult to deal with a-c interference than d-c interference. Usually the problem with ac is that of keeping it out of measuring instruments. As before, it is better to turn off the interfering signal, but with ac this usually is not possible. Filtering the input signals with bypass circuits can remove the a-c interference very successfully. However, filtering will also suppress rapidly changing signals that one may be interested in observing. Thus, filtering to remove ac and current interruption techniques for *iR* suppression may not be compatible.

Another alternative not yet mentioned is moving the equipment and reference electrode to a location where interference is reduced. If the interfering signal is intermittent, it is sometimes possible to make measurements while the interfering signal is off. This may require making measurements at night. Persistence, in the presence of interference, usually pays off with better data.

Physical Measurements

Electrochemical measurements are useful for monitoring the performance of materials during exposure. Verification of these measurements can be carried out by calculating weight loss from gravimetric measurements before and after exposure and comparing this actual weight loss with electrochemically calculated weight loss. Generally, this approach is restricted to small coupons that can be conveniently weighed. Where structures are too massive to weigh (for example, steel piling), changes in thickness measured with micrometers before and after exposure may provide sufficient information to allow calculation of corrosion rate [*13*]. Pit depth measurements are useful for evaluating the extent of localization of corrosion. Typically, the surface of interest is visually examined and the deepest pits are identified. These pits then are measured with a pit depth micrometer, and the deepest pit is recorded. It is also useful to note the total number of pits found per unit area or the percentage of the total surface area pitted.

Underground Corrosion Test Sites

Most of the data presented here has been obtained from test sites owned by the U.S. government. The exception to this is a steel piling test site in Canada owned by the Canadian National Railroad. The sites will not be described in detail here since they have been reported in the past [*12–14*]. Only a few measurements have been performed at nongovernment-owned sites.

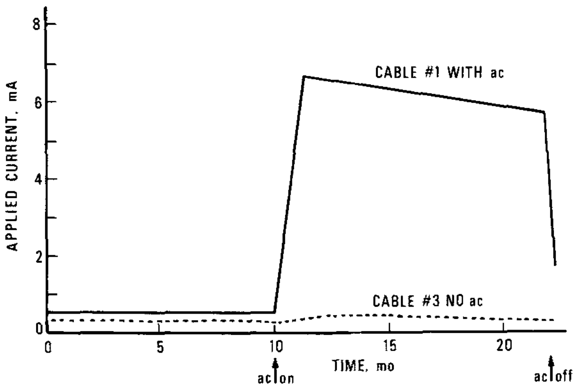

FIG. 5—*Plot of applied current versus time showing increased corrosion of underground copper neutral with applied ac.*

Results and Discussion

This section will be directed at providing examples of the type of data obtained using the techniques and approaches described. Up until the late 1970s, most polarization measurements in our laboratory were made using a Holler bridge circuit. The bridge system is rugged and of simple design, as already described, but compared to present day computerized systems it is slow and cumbersome to use.

Measurements made on underground concentric neutral cables in a simulated in-service environment indicated that ac applied between two cables, from the copper neutrals, increased their corrosion rate [*15*]. The electrochemical measurements, shown in Fig. 5, illustrate this effect when 0.7 mA/cm^2 of ac are imposed between two cables (Cable 1), and no ac is imposed on controls (Cable 3). Cable 1 shows a dramatic increase in corrosion rate with the application of ac, while the corrosion rate of the controls, without ac, remained low and constant. Physical examination of the cables after removal from the site verified the electrical measurements, and Table 1 compares the electrochemical results to the gravimetric measurements. In both cases, with and without ac, the electrochemical measurements underestimated weight loss by 20 to 30%.

Corrosion measurements made, over a 14-year period on bare steel piling supporting a bridge deck pier, indicate that the rate of corrosion of these driven piles decreased by an order of magnitude. Initial measurements were made with the Holler bridge system, but later measurements were duplicated with the portable computer system described earlier. Figure 6 shows the results obtained on 32 interconnected piles under one pier (Pier A–10). The initial corrosion rate of this pier is calculated at 0.4 mil/year (10 μm/year), which decreases to less than 0.04 mil/year (1 μm/year) after 14 years. The surface layer of soil is a fill made of cinders and clinkers on top of peat and clay with a soil resistivity ranging from 460 to 4830 Ω-cm and a pH ≈7 [*14*].

TABLE 1—*Comparison of electrochemical measurements to gravimetric mesurements.*

Cable	Gravimetric weight loss, g	Polarization weight loss, g	Error %
No. 3, no ac	26.8	17.7	34 low
No. 1, with ac	218.4	167.6	23 low

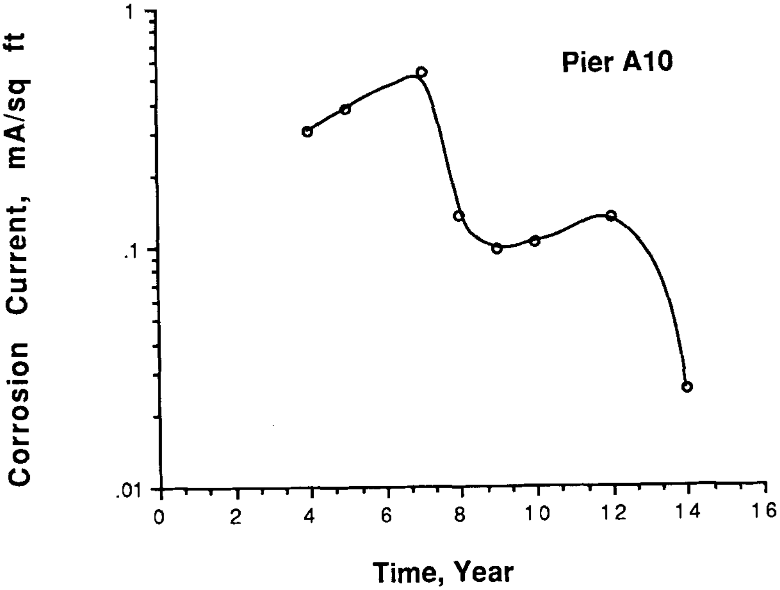

FIG. 6—*Plot of corrosion current versus time for 32 piles of Pier A2.*

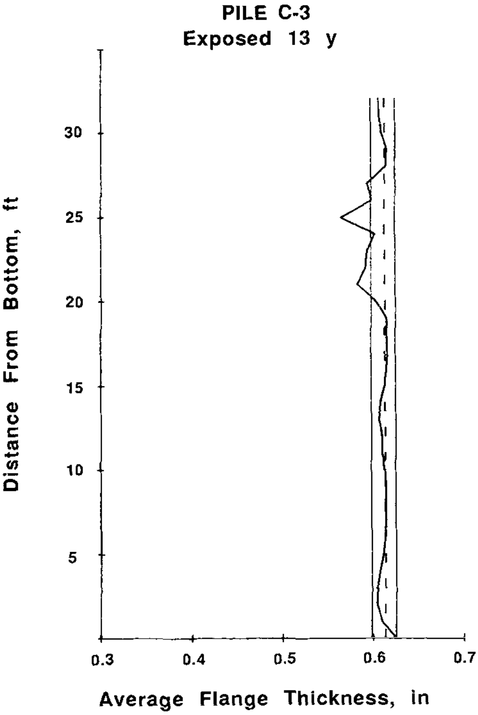

FIG. 7—*Plot of average flange thickness versus distance from bottom of vertical Pile C3.*

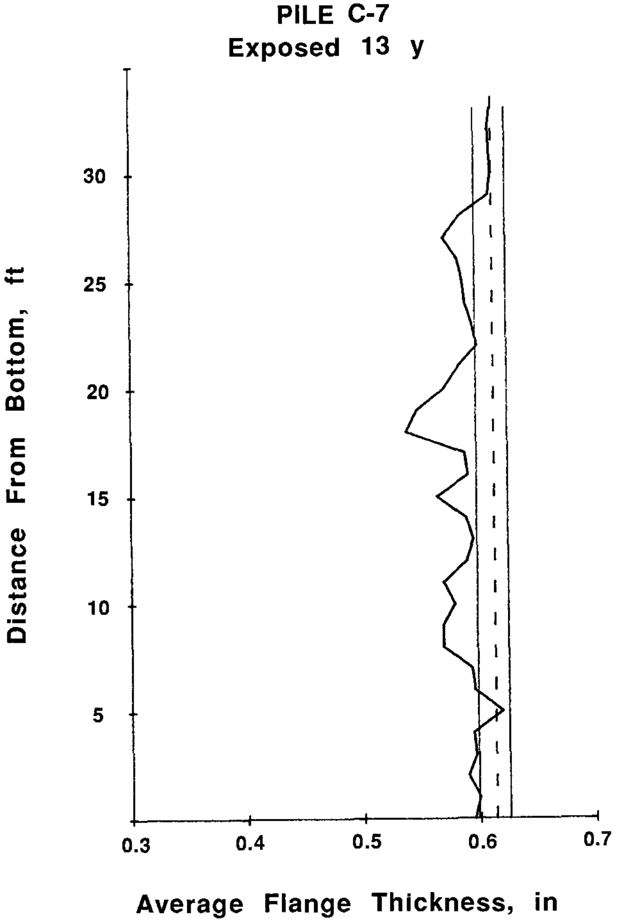

FIG. 8—*Plot of average flange thickness versus distance from bottom of horizontal Pile C7.*

Concrete-capped test piles, some driven vertically in place and others laid horizontally in trenches and backfilled with soil, were located nearby. Figure 7 is a plot of the flange profile, measured with micrometers, of Pile C3 vertically driven in place, showing its original thickness and final thickness after 13 years. Some attack is apparent near the waterline, but the remainder of the pile has undergone negligible attack. Average corrosion on Pile C3 has been calculated as 0.3 mil/year (7.5 μm/year). On the other hand, Fig. 8 shows the same type of profile for Pile C7 laid horizontally and backfilled. Note the extensive attack over the entire surface of the pile, which has developed an average corrosion rate of 1.0 mil/year (25 μm/year). The backfilled soil environment of Pile C7 is significantly more corrosive than the "undisturbed" soil environment of Pile C3.

The corrosion of several stainless steels exposed at six underground test sites has been investigated. The properties of the soils at the sites are summarized in Table 2, revealing that the average soil resistivities range from very low at Site C to high at Sites B and D. One specimen configuration used was a Type 301 stainless steel galvanically coupled to a zinc anode in such a way that the galvanic current could be measured above ground. The stainless steel and zinc electrodes were placed approximately 30 cm apart at a depth of

TABLE 2—*Properties of soils at underground test sites.*

Site	Soil	Location	Average Resistivity, Ω-cm	pH
A	Sagemoor sandy loam	Toppenish, WA	...	8.8
B	Hagerstown loam	Loch Raven, MD	32 990	5.4
C	Clay	Cape May, NJ	660	4.3
D	Lakewood sand	Wildwood, NJ	33 550	5.6
E	Coastal sand	Wildwood, NJ	23 780	7.1
G	Tidal marsh	Patuxent, MD	4 520	5.6

0.8 m. An insulated electrical wire attached to each electrode extended to the surface, where the wires were connected to complete the couple. Every three or four months, for a period of four years, the galvanic current between the electrodes was measured using a zero resistance ammeter. The galvanic current reflected the conditions of the soil environment and changes occurring at the electrode surfaces over the exposure time, and Fig. 9 illustrates the results of these measurements [*16*]. Note that the couples in the low-resistivity soils generated the highest galvanic currents, and vica versa, those in high-resistivity soil developed low galvanic currents. The specimens at Site E are unusual in that they show a decrease in galvanic current with time, indicating a change in the resistivity of the environment or changes at the metal surface.

Conclusions

Polarization and galvanic current measurements are a useful way of obtaining information on corrosion characteristics of metals and structures underground. Polarization measurements, supported by physical measurements, have shown that induced ac increases the corrosion rate of copper concentric neutrals compared to copper neutrals without ac. They

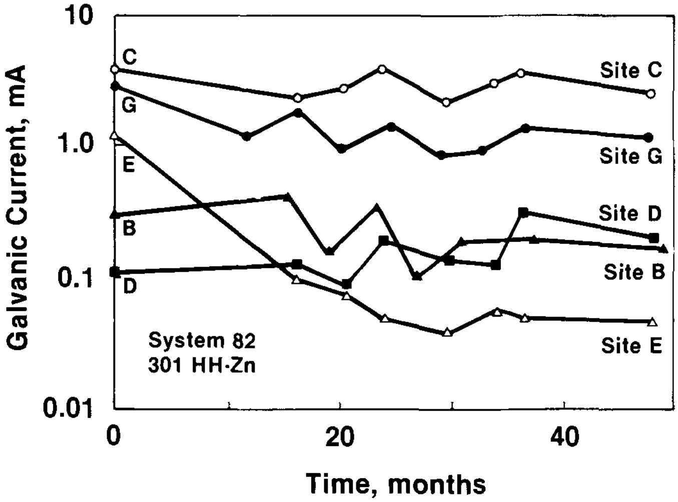

FIG. 9—*Plot of galvanic current versus time for Type 301 stainless steel coupled to zinc at six underground test sites.*

have also revealed that driven piles undergo less corrosion attack than similar piles in backfilled trenches. Galvanic current measurements provide valuable information on the behavior of galvanically coupled materials and can be used to compare the corrosivity of soil environments.

References

[*1*] Mansfeld, F., "The Polarization Resistance Technique For Measuring Corrosion Currents," *Advances in Corrosion Science and Technology*, Vol. 6, Plenum Press, New York, 1976, p. 163.

[*2*] Legault, R. A. and Walker, M. S., "Linear Polarization Measurements In the Study of Corrosion Inhibition," *Corrosion*, National Association of Corrosion Engineers, Houston, TX, June 1963, p. 222t.

[*3*] Serra, E. T. and Mannheimer, W. A., "On the Estimation of the Corrosion Rates of Metals in Soils by Electrochemical Measurements," *Underground Corrosion, ASTM STP 741*, American Society for Testing and Materials, Philadelphia, 1981, pp. 111–122.

[*4*] Stern, M. and Geary, A. L., "Electrochemical Polarization—I. A Theoretical Analysis Of The Shape Of Polarization Curves," *Journal of the Electrochemical Society*, Vol. 104, January 1957, p. 56.

[*5*] Uhlig, H. H. and Revie, R. W., *Corrosion and Corrosion Control—An Introduction to Corrosion Science and Engineering*, 3rd ed., John Wiley & Sons, New York, 1985.

[*6*] Williams, L. F. G. and Taylor, R. J., "*iR* Correction—Part I. A Computerized Interrupt Method," *Journal of Electroanalytical Chemistry*, Vol. 108, 1980, p. 293.

[*7*] Escalante, E., Whitenton, E., and Qiu, F., "Measuring the Rate Of Corrosion Of Reinforcing Steel In Concrete—Final Report," NBSIR 86-3456, National Institute of Standards and Technology, Gaithersburg, MD, October 1986.

[*8*] Holler, H. D., "Studies On Galvanic Couples—I. Measurement Of Electromotive Force And Internal Resistance Of Cells During Current Flow," *Journal of the Electrochemical Society*, Vol. 97, September 1950.

[*9*] *Galvanic Corrosion, ASTM STP 978*, H. P. Hack, Ed., American Society For Testing And Materials, Philadelphia, 1988.

[*10*] *Galvanic and Pitting Corrosion—Field and Laboratory Studies, ASTM STP 576*, R. Baboian, W. D. France, Jr., L. C. Rowe, and J. F. Rynewicz, Eds., American Society For Testing and Materials, Philadelphia, 1976.

[*11*] Lauer, G. and Mansfeld, F., "Technical Note—Measurement Of Galvanic Corrosion Current At Zero External Impedance," *Corrosion*, Vol. 26, November 1970, p. 504.

[*12*] Escalante, E. and Gerhold, W. F., "Galvanic Coupling of Some Stressed Stainless Steels to Dissimilar Metals Underground," *Galvanic and Pitting Corrosion—Field and Laboratory Studies, ASTM STP 576*, American Society for Testing and Materials, Philadelphia 1976.

[*13*] Escalante, E., "Protection of Steel Piles by Selected Coatings in a Natural Seawater Environment," *Journal of Petroleum Technology*, August 1979, p. 1035.

[*14*] Schwerdtfeger, W. J. and Romanoff, M., "Corrosion Rates on Underground Steel Test Piles at Turcot Yard, Montreal, Canada—Part 1," NBS Monograph 128, National Institute of Standards and Technology, Gaithersburg, MD, July 1972.

[*15*] Kruger, J., Bertocci, U., Escalante, E., and Mullen, J. L., "Development of In Situ Techniques for the Detection and Measurement of Corrosion of Copper Concentric Neutrals in Underground Environments," NBSIR 81-2083, U.S. Dept. of Commerce, Washington, DC, 1980.

[*16*] Escalante, E., "The Effect of Soil Resistivity and Soil Temperature on the Corrosion of Galvanically Coupled Metals in Soil," *Galvanic Corrosion, ASTM STP 978*, H. P. Hack, Ed., American Society for Testing and Materials, Philadelphia, 1989.

DISCUSSION

D. A. Jones[1] (*written discussion*)—Why did stainless steel at Sites C and G display heavy corrosion when coupled to zinc, which should act as a sacrificial anode?

---

[1] Mackay School of Mines, University of Nevada, Reno, NV 89557.

E. Escalante (*author's closure*)—Initially, we tried to visit each of the test sites once every three or four months to measure galvanic currents and protection potentials of the coupled specimens. In this way we could tell whether the anodes were still effectively protecting the stainless steel. The anodes were replaced when they were found to be ineffective. As the program progressed, it became more difficult to visit the sites in a timely manner, and during these lapses the anodes failed, leading to corrosion of the stainless steels. Sites C and G, being the two most corrosive soils, required anode replacement on a regular basis. Thus, the stainless steel at sites C and G corroded because the zinc anodes were depleted for extended periods.

P. J. Peterson[2] (*written discussion*)—(1) When using corrosion couples for measuring corrosivity of soils, should the mix potential also be measured? (2) When using linear polarization data, must we still make assumptions for the tafel slopes?

E. Escalante (*author's closure*)—(1) Yes, the mixed potential is useful in evaluating the effectiveness of the anode. When zinc is protecting steel, the mixed potential of the couple is approximately ≈ -1 V versus $Cu/CuSo_4$, and is very stable. As the zinc deteriorates, the mixed potential becomes more positive. (2) Yes, an assumption for the Tafel slope must be made, one way or another. Sophisticated systems in the laboratory can determine the Tafel slope during the polarization measurement and apply that assumption to the calculation of corrosion current. This approach requires modeling and curve-fitting capabilities. Our field approach, at that time, was less sophisticated. On the basis of gravimetric weight loss for all the specimens, we calculated a Tafel slope that gave a reasonable fit to the data.

---

[2] IBM, General Products Division, San Jose, CA.

J. David Palmer[1]

Field Soil Corrosivity Testing—Engineering Considerations

REFERENCE: Palmer, J. D., "**Field Soil Corrosivity Testing—Engineering Considerations,**" *Corrosion Testing and Evaluation: Silver Anniversary Volume, ASTM STP 1000,* R. Baboian and S. W. Dean, Eds., American Society for Testing and Materials, Philadelphia, 1990, pp. 125–138.

ABSTRACT: The state of the art in soil corrosivity testing was evaluated, with particular emphasis on field and in-situ tests that can be performed with reasonable accuracy by non-scientific personnel. Parameters reviewed include resistivity, pH, redox potential, moisture content, chloride levels, structure/soil potential, and microbiological activity. The reliability of in-situ tests versus laboratory tests is examined. Particular emphasis is placed on buried and immersed ferrous materials. A distinction is made between studies intended to determine the soil factors affecting the integrity of intended new installations and studies which examine the condition of the existing facilities and the relationship of soil parameters to structure condition and anticipated life. The latter circumstance is becoming increasingly evident as infrastructure rehabilitation studies focus on the condition and future life expectancy of buried facilities. Several approaches to expected life prediction are reviewed. Emphasis is focused on information presented in *ASTM STP 741, Underground Corrosion,* and *ASTM STP 1013, Effects of Soil Characteristics on Corrosion.* The applicability of the ASTM Method for Field Measurement of Soil Resistivity Using the Wenner Four-Electrode Method (G 57–78) and the ASTM Test Method for pH of Soil for Use in Corrosion Testing (G 51–84) is considered. The available information is consolidated into recommended practices for soil corrosivity evaluations.

KEYWORDS: soil corrosion, ferrous materials, parameters, resistivity, potential, pH, redox, moisture, sulfates, life prediction, statistical treatment

The need for soil corrosivity testing can be due to several reasons:

1. Characterization of a soil versus one or more materials.
2. Characterization of material performance (new or existing) in one or more soils.
3. Investigation of a failure.

This paper deals with pragmatic engineering considerations involved in the immersion of ferrous metals in soils that result in cost-effective considerations of service life, failure consequences, and mitigative effort. It does not deny the need for continued scientific investigation of the relative effect of environmental variables, but evaluates the currently available information from the standpoint of today's designer/specifier trying to decide what to do with a particular water main.

Fitzgerald [*1*], Bushman [*2*], and Chaker at this symposium have covered the past, present, and future activity in soil corrosion testing, but none mentions the parameter potential which is the basis for every soil, water, and concrete corrosion control standard used today.

---

[1] President, Corrosion Control Engineering Ltd., London, Ontario, Canada.

TABLE 1—*Factors affecting ferrous corrosion rates in soil.*

Soil Factors	Metal Factors
1. Moisture content.	1. Metallurgy.
2. Resistivity	2. Type and condition of coating.
3. Permeability.	3. Diameter.
4. Chloride ion content.	4. Length
5. Sulfide ion content.	5. Temperature.
6. Sulfate ion content	6. Movement or vibration.
7. Presence of corrosion-activating bacteria.	7. Stress level and stress distribution.
8. Oxygen content.	8. Presence of dissimilar metals.
9. pH.	
10. Total hardness and hardness as $CaCO_3$ of soil moisture.	
11. Stray d-c currents.	

Bushman lists the variables shown in Table 1, but assigns no relative or numerical significance. The steel pipeline industry considers only resistivity [*3*], while the cast and ductile iron industry introduces moisture, sulfides, and redox potential. Dillon [*4*] goes further by adding chlorides and soil type and admits that stainless steel will corrode underground.

Since the early focus on stray-current electrolysis as the primary cause of soil corrosion of ferrous materials, other factors have been introduced, with particular emphasis on resistivity and factors related to microbiologically induced corrosion.

Dillon's inclusion of chloride is of particular significance in the "Frozen North" with the simultaneous post–World War II introduction of deicing salt and ductile iron pipe. Subsequently, the increasing development of salt-saturated tidal lands also emphasizes the significance of this variable.

The focus of soil corrosivity interest has shifted over the years from municipal utilities to steel pipelines and back to utilities. In the oil and gas industries, coating and cathodic protection are required almost universally by code and law in the developed world. The only soil corrosion parameters of general interest to the steel pipeliners are resistivity as related to the design of groundbeds and the selection of sacrificial anodes, and potential as an indicator of relative corrosion activity.

Currently, most soil corrosivity investigations are focused on municipal water and sewage piping systems and on the remaining oil and gas systems not yet cathodically protected. The focus of the predecessor to this paper was on the former facilities [*3*], and the significant parameters will be examined primarily from this viewpoint in the following sections.

Imagine a conversation between a corrosion engineer and a new client:

Dialogue

Q. If I bury this pipe, will it corrode?

A. Yes.

Q. Why?

A. Here's a book you can read.

Q. How fast will it corrode?

A. The US NBS says that in a similar soil it would corrode at *X* mdd [milligrams/decimeter/day].

Q. Will mine corrode that fast?

A. Maybe faster or slower.

Q. How can I find out?

A. Put it in, dig it up in five years and look.

Q. What else can I do?

A. Use an inert material or coat and cathodically protect.

TABLE 2—*Summary of soil conditions at excavated test sites.*

	Soil Resistivities[a]			Soil pH			Chloride		
Site	Main	Midpoint	Building	Main	Midpoint	Building	Main	Midpoint	Building
N1	2 815	5 704	4 250	6.0-6.4	3.5-4.0	4.5	Present	ND[b]	ND
S3	26 000	37 000	25 667	5.4	5.5	5.7	Present	ND	Trace
S7A	9 555	25 333	36 000	4.3	4.1	4.4	Present	ND	Trace
S9A	17 872	14 182	17 859	5.2	5.6	5.1	ND	ND	Trace
W4	8 389	16 000	9 239	5.2	6.0	6.4	Trace	ND	ND
W5A	1 169	16 667	9 750	6.0	5.5	6.4	Present	Trace	Trace

[a] Obtained in a soil box with soil wet.
[b] Not detected.

This dialogue more or less sums up the state of our knowledge today. We feel it will be many years before we can predict soil corrosion rates to the precision that a pipeline can be designed for its first leak in 60 months in the way that a refinery engineer can design and monitor five years' pipe life in an acid unit. Considering the heterogenous nature of the average urban soil environment, the only valid parameter can be the performance of similar methods in the same environment. Once these data have been obtained, it is then practical to evaluate the relationship of soil characteristics to the material behavior and broadly predict future performance. Historically, a number of variables have been used in this process, limited by the fact that in a pressure pipe failure the soil in contact with the failure point usually is gone. The following sections will present the practical relevance of the more significant variables ranked in their deemed order of importance.

Resistivity

The reciprocal of conductivity-restivity is indicative of the ability of soil to carry the currents associated with the activity of the anode and cathode of a corrosion cell, whether local or remote. In the former case, it is the resistivity of the soil layer in contact with the pipe surface which is relevant. In the latter case, broader geological variations may prevail. In developed areas subject to industrial, atmospheric, and deicing salt pollution, and considering that many utility piping systems are not electrically continuous, the localized conditions will prevail.

Palmer [5] noted that appreciably lower resistivity of soil samples taken from the gas main ditch compared to that of undisturbed soil in the vicinity. Steinmetz and Hoxie [6] reported the curb-to-house variations shown in Table 2. The following resistivities were recently measured in sandy loam in the northeast of London, Ontario:

Open Field[2]—1.5 m (5ft), 300 000 ohm-cm
3 m (10ft), 310 000 ohm-cm
4.5 m (15ft), 213 000 ohm-cm
Edge of Road Allowance[3]—11 000 ohm-cm
61 cm (24 in.) Steel Main[3]—2 300 ohm-cm

The contaminating effect of urban pollutants in sharply lowering resistivity is quite evident. Urban soil chemical analyses regularly show chloride levels greater than the 50 ppm which Dillon apparently considers to be a threshold level. The Ford Motor Co. prepared the salt

---

[2] Four-pin Wenner at grade.
[3] Fully moistened soil box.

FIG. 1—*Automobile corrosion map of North America* (*automotive corrosion zones—Ford*).

corrosion intensity map for motor vehicles shown in Fig. 1. This map is probably quite descriptive of soil corrosion intensity. There can be little doubt that urban and highway corridor soils in the Snow Belt and the salty soils of the West are corrosive to ferrous metals.

A number of studies, including the monumental NBS program [*7*], failed to establish definitive corrosion/resistivity relationships. The rating scale commonly used [*8*] (Table 3) was originally developed by the US Department of Agriculture based on a combined assessment of resistivity, soil texture, acidity, and drainage—not on any specific field exposure data. We have found many instances of appreciable pitting of cast iron mains in soils with soil box resistivities well in excess of 10,000 ohm-cm. Schwerdtfeger [*9*], analyzing the data for wrought ferrous pipe samples exposed in the NBS study, arrived at corrosivity groupings of 500 ohm-cm, 500 to 3 000 ohm-cm, and 3 000 to 54 000 ohm-cm, predicting perforations of 8 mm (0.322 in.) wall pipe within 15 and 30 years for the first two groups, respectively. These predictions were based on empirical projections from rather widely scattered data and are contradicted by many experiences, including ours, of catastrophic failures of ductile iron piping systems after only five years' exposure in soils with resistivities greater than 1 000 ohm-cm [*10,11*].

It would appear that soil resistivity cannot be used to predict specific corrosion rates, but can be used as a guide to likely relative corrosion severity. The only resistivity values useful in this prediction are those from fully moistened samples taken from the pipe ditch at pipe level. In most urban areas, the samples needed to prepare a statistically reliable resistivity contour map can be obtained in scheduled excavations over a one-to-two year period at a very nominal cost. Contour definition can be readily provided by a computer using grid systems currently available for system inventory.

The accuracy of soil box resistivity measurements is currently being evaluated by ASTM Subcommittee G01.10. The NBS study report noted that most measurement variables can be eliminated by fully moistening the sample. This procedure would also produce the worst-

TABLE 3—*Soil corrosivity classes for uncoated steel based on total acidity, resisitivity–conductivity of the saturation extract, and drainage-texture-aeration relationships.*

Soil Corrosivity, class	Total Acidity, meq/100g	Resistivity, ohm-cm	Conductivity, mmho/cm	General Relationship	
				Drainage-Texture Relationship	Water-Air Permeability
Very low	<4	>10 000	<0.1	Somewhat excessive—excessively-drained coarse-textured soils	Rapid to very rapid
Low	4 to 8	5000 to 10 000	0.1 to 0.2	Well-drained with moderately coarse and medium-textured control section; somewhat poorly drained with coarse-textured control section	Moderate to rapid
Moderate	8 to 12	2000 to 5000	0.2 to 0.4	Well-drained with moderately fine-textured control section; moderately well-drained with medium-textured control section; somewhat poorly-drained with moderately coarse-textured control section; very poorly-drained with high, nonfluctuating water table	Moderately slow to slow
High	12 to 16	1000 to 2000	0.4 to 1.0	Well drained and moderately well-drained fine-textured soils; moderately well-drained, moderatly fine-textured soils; somewhat poorly-drained; medium and moderately fine-textured control sections; very poorly-drained soils; water table fluctuates with ft of surface.	Slow and very slow; saturated
Very high	>16	<1000	> 1.0	Somewhat poorly to very poorly-drained fine-textured soils; mucks, peats with a fluctuating water table	Very slow; saturated

case condition commonly used in municipal engineering. Statistical sampling techniques can be used easily to determine risk and error in such a sequential sampling program. A 5% risk of an error of 10% or 100 ohm-cm, whichever is greater, should be quite acceptable for engineering decision-making. This degree of accuracy has been found reasonable for soil surveys in general [*8*].

Where soil resistivity testing is carried out preliminary to new construction, it must be realistic. Where the installation will be made in a trench blasted through rock, it is obvious that the pipe will not be backfilled with rock. The corrosivity analysis must consider the likely contamination of the sand or gravel backfill by industrial, agricultural, and highway runoff.

The statistical probability technique proposed by Scott [*12*] and expanded by Husock [*13*] and Bushman [*2*] appears to be the best approach for the interpretation of resistivity data and is recommended in ASTM G 57–78.

Potential

Pipe-to-soil potential as an indicator of relative corrosion activity has long been used in the steel pipeline industry, but much less generally in the water utilities field. In the latter case, this is primarily due to the discontinuous nature of mechanically joined cast and ductile iron and reinforced concrete pipe, the lack of readily accessible electrical contacts to the pipe, and the presence of pavement. There is little argument with the understanding that the most actively corroding part of a metal structure is identifiable by the most negative potential in the absence of outside electrical effects and galvanic couples.

Close-interval potential measurement is an accepted technique in the corrosion control of bare or poorly coated structures, often followed by the installation of sacrificial anodes at the "hot-spots" so identified. The suppression of active anodic areas can result in the conversion of former cathodes into anodes, albeit corroding at a lower rate, and the process must be repeated on a regular basis until the structure is fully protected.

Potential, usually measured with reference to a saturated $Cu/CuSO_4$ reference electrode, varies appreciably as a function of the environment and pipe age, material, and condition and cannot be used accurately to predict corrosion rate. When continuously monitored, changes in potential are indicative of environmental changes. This is particularly significant when a pipe comes under the influence of stray d-c currents. Current densities not detectible on a short-term basis may be detrimental and are only indicated by a long-term positive potential shift. In a study of cast iron water main condition, the rough correlation between potential and pit depth shown in Fig. 2 was established [*14*].

Close-interval survey techniques, not requiring electrical contact with the pipe, have been used to detect currents associated with local cell activity by measuring voltage gradients at grade. These have been reported applicable to corrosion activity on reinforced concrete pipe [*15*], but are rarely used on iron pipe in urban areas because of the probability of unrelated ground currents being present.

Husock [*16*] has proposed a graphical technique (Fig. 3) for the correlation of potential and resistivity, assuming that ". . .potential peaks in high resistivity soils generate lower values of corrosion current than would be the case in low-resistivity soil." We know of no case of this approach being applied to discontinous iron piping.

Polarization resistance techniques which measure the relationship of potential to applied current are widely used to estimate corrosion rates in aqueous media and have been used in soils [*17*]. The results are specific to the metal electrode used and produce average corrosion rates rather than pitting rates. When carried out in situ on metal samples or existing structures, the technique will indicate relative corrosivity. The data could be used

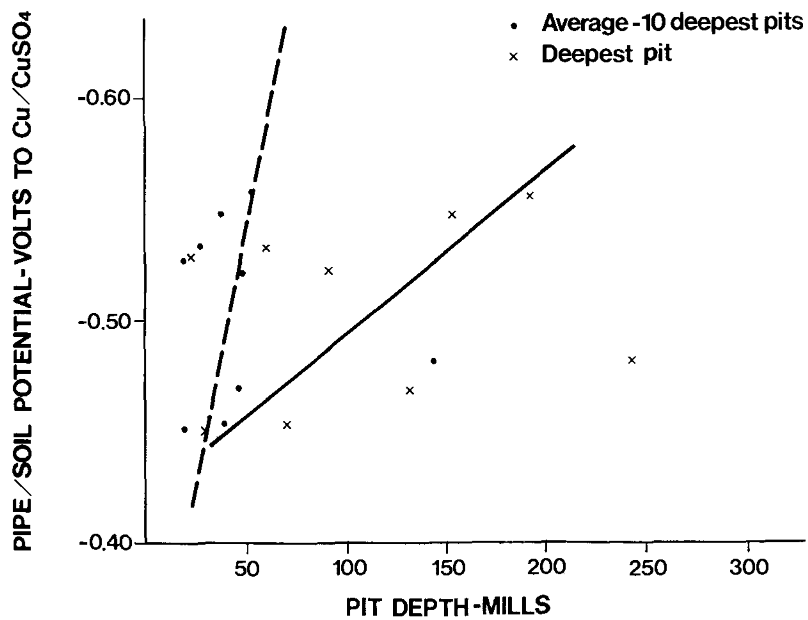

FIG. 2—*Relationship of average and maximum pit depth to potential Argentia cast iron.*

to predict the life on buried structures when information is available on the actual performance of the same material in a similar environment.

As is the case for resistivity, the measurement must be taken "in the ditch" to be representative, either using special electrodes or using actual structures. The in-the-ditch test results should represent the combined effect of all the variables herein discussed.

Moisture

A buried utility main which is not at least partially moist is difficult to imagine in the "Frozen North," where burial below frost depth is required. Where drainage is excellent and water tables are low, some pipes occasionally may be dry, but at least partial wetting must be anticipated from a corrosion standpoint. Partial immersion may produce a more aggressive wet-dry condition, commonly related to corrosion of tanks buried transiting a water table with periodic fluctuations.

NBS testing [7] showed that the effect of moisture content on soil resistivity was a rapid decrease with increased moisture content up to the saturation point and little or no effect with further moisture additions.

The pipe ditch is rarely compacted to the degree of the natural soil and remains a preferred drainage channel for surface runoff, exacerbating the previously noted pollution effects, as well as increasing the probability of a moist pipe. Where the pipe sits below a static water table with little movement of water in the ditch, the probability of anaerobic conditions will increase. This tendency would be further increased if the runoff contained components with a high biological oxygen demand.

Soil samples should be well packaged immediately on removal to preserve moisture and moistened with free water from the ditch if freely draining (sand, etc.). On-site or in-situ resistivity measurement will reduce errors due to moisture content below saturation. We have found that an ordinary domestic plant moisture meter, using a galvanic probe, gives a satisfactory moisture indication in soils that would normally be considered corrosive.

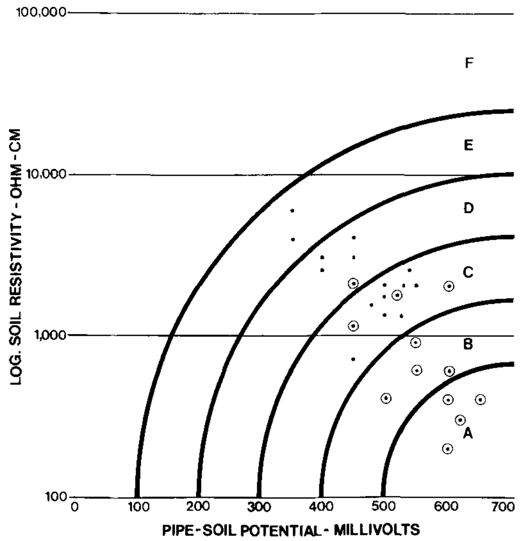

FIG. 3—*Typical plot of pipe soil potential versus soil resistivity (circled dots are leak locations).*

Chlorides

The presence of soluble chlorides in a soil will be directly reflected in its resistivity, shifting washed construction sand backfill resistivity in the direction of seawater. The resultant corrosivity may be greater than that of the natural soil in the vicinity. As well as increasing the conductivity of the environment, chlorides tend to break down naturally protective surface films and initiate pitting. Pipe repair clamps commonly feature stainless steel components, and the presence of chlorides in such a static environment may result in pitting and cracking as a function of the grade of stainless steel used.

The presence of chlorides must be anticipated in deicing salt and coastal areas and in many western soils. Chloride testing of preconstruction soil samples would be informative, but would not necessarily be descriptive of the future exposure. Unless chloride analysis is required for other reasons, testing beyond the use of indicator strips or other simple field tests is not endorsed.

A degree of accuracy sufficient to determine whether the threshold level has been exceeded normally should suffice. A 5% risk of a 10% or 10 ppm error, whichever is greater, should be acceptable.

Redox or Oxidation—Reduction Potential

This measurement is intended to identify soil conditions conducive to the activity of anaerobic bacteria, particularly sulfate reducers. The end product of the reduction of sulfates to sulfides are both depolarizing and corrosive in themselves and are often characterized by a black iron sulfide deposit.

Identification of conditions conducive to anaerobic bacterial activity can be accomplished by determining whether the soil is reducing or oxidizing by measuring the potential generated by a platinum/hydrogen or platinum/calomel probe. Negative or low positive potentials are reported to be indicative of anaerobic conditions [*18*]. The presence of sulfate reducers can be determined by culturing a soil sample in a nutritive medium.

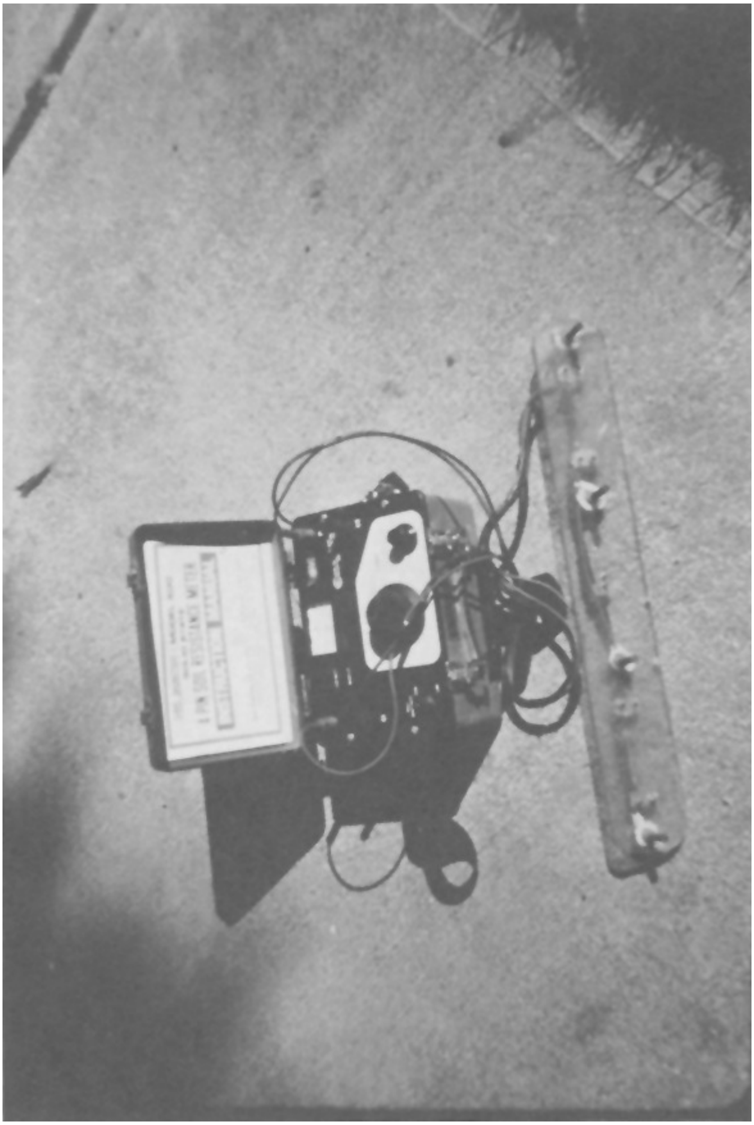

FIG. 4—*Resistivity measurement apparatus for in-the-ditch testing.*

The presence of active sulfate reducers on a pipe surface can be determined visually from deposit appearance, nasally by the evolution of hydrogen sulfide on treatment with dilute hydrochloric acid, and visually by the blackening of lead acetate paper. The identification of activity in failure or performance studies is readily accomplished, but the prediction of future activity is a difficult process.

McVey [*19*] described the considerable difficulty in obtaining reliable field data, in particular the fussy nature of platinum electrodes. As oxygen—even on the probe—can affect the reading, in-situ measurement with great care appears to be the only acceptable practice. Testing on a removed sample is unreliable and a waste of time if the sample is bagged, tossed in the trunk, and tested in the lab days later.

Correlation of redox potential with corrosion has been described as poor, and there has been little reported recent activity in this area. Iverson [*18*] noted a negative shift in redox potential with increased corrosion rates in laboratory tests of sulfate-reducing bacterial corrosion, but made no recommendations for the field application of the tests.

Mitigation of anticipated bacterial corrosion requires the application of normal industry procedures including the use of granular backfill, coating, and cathodic protection. It appears that the use of redox measurements is limited to laboratory testing, in-situ failure, and conditon examinations and should be evaluated from a yes/no standpoint rather than by the assignment of a specific rating point based on the potential value.

pH

Most rating formulas assign points to extreme pH values—below 4 and above 8.5—probably based on interpretation of simplified Pourbaix diagrams for the potential range usually associated with natural ferrous corrosion in soils. Soils with pH levels in the extremes of the above range are rarely found in the absence of outside contamination (cinders and acidic waste). Of the 125 soils included in the NBS study, only six had extreme values. Acidity was usually found in tidal marsh and peat, while alkalinity was associated with western clays and loams.

In high-chloride soils, pH relationships may be affected by the increasesd acidity resulting from autocatalytic effects in a corrosion pit [*20*]. The combination of low pH and chlorides is of particular concern where stainless steels are exposed. Natural pH levels usually can be determined from published soil surveys. There appears to be little benefit from the routine measurement of pH for new construction except in industrial areas where there is the possibility of waste acid dumping. Low pH values can be anticipated in eastern marsh and bog soils and in areas where high sulfur coal and ore are present. Mitigation involves the normal use of protective coatings and cathodic protection and the use of crushed limestone backfill as a buffering and alkalizing agent.

As indicated in ASTM G 51-77, soil pH measurements should be taken in the field, preferably in situ and least desirably in the laboratory.

Temperature

Temperature may be a significant variable when north versus south exposures are compared, particularly since northern installations tend to be deeper to avoid frost and temperatures may be steadier than in shallow southern installations. Errors in resistivity measurement can result where soil samples are removed for testing, but the reading can be corrected using a nomograph included in NBS Circular 579 [*7*]. Using this reference, if a resistivity of 500 ohm-cm is measured at 21°C (70°F) the error is about 80 ohm-cm if the natural temperature is 15.5°C (60°F). The error increases with increased temperature difference and may be greater than the previously indicated acceptable error.

Laboratory temperatures can be expected to be higher than ground temperatures, yielding lower resistivity values, with an error greater than the 10% deemed acceptable. There is considerable reason for resistivity measurements to be made in situ at pipe depth or immediately after removal of a soil sample. In-the-ditch measurements can be made using a pin arrangement shown in Fig. 4 with pin spacings of 15.9 cm (6.25 in.). This arrangement will give direct readings when used with a commercial soil resistivity meter. Where temperature correction is desired, the pertinent soil temperature can be estimated from the temperature of running local tap water.

Soil Type

The soil type can be broadly descriptive of its corrosivity if contamination effects are excluded. Poorly drained, finely textured soils will be more corrosive than well–drained, coarse soils. Peat bogs and marshes should be of concern because of low resistivity, poor aeration, and low pH. Sand backfill tends to assume the electrochemical nature of the natural soil and may be appreciably more corrosive if contaminants such as deicing salts are present.

Where "numbers" are required, a soil type shown on a soil map may be characterized by tests under a range of drainage conditions, say poor, fair, and well–drained. Some state soil maps include resistivity data. Such surveys do not usually contain urban soil data, but such descriptive information can be obtained by observing excavations carried out for other purposes.

Sulfates

Sulfate levels may be pertinent where anaerobic conditions and sulfate-reducing bacteria are present, but otherwise are more pertinent to the performance of concrete structures. The identification of sulfides may be pertinent to in-situ corrosion failure examinations, but not particularly relevant to soil corrosivity rating. It is difficult to justify the expense of routinely testing sulfate levels for ferrous installations.

Failure and Condition Inspection

Failure investigations are often complicated by the absence of the soil at the point of failure due to the nature of the failure. The corroding agent may be a small lump of clay in granular backfill. The lump is "down the block" after a major failure and may only be identified as a possible culprit in the absence of other identifiable factors. Early access to the site is often restricted by the need to return the pipe to service. The failure site may be hidden forever beneath a clamp, but a pipe section containing the failure should be cut out if at all possible. Simple soil tests may be possible, but at least a sample should be obtained at the first opportunity. Municipalities involved in resistivity mapping programs will have sealable containers on hand and will usually obtain a representative sample if the foreman remembers to do so.

The regular documentation of failure-related data can be of tremendous value in assessing a system's condition and life expectancy. Usually "break" frequency data is available, but the cause of the break is less often determined. Corrosive conditions may be identified by the description "soft pipe," but reporting this condition is a function of the workmen's experience, interest, and available time.

Where precise exterior condition data are needed for life-prediction purposes, it may be necessary to arrange a series of pipe inspections. If time permits and scheduling can be arranged, inspections may be carried out in excavations regularly required for normal operations. In one case, co-op college engineering students were provided with transportation and radio connection with a gas company maintenance dispatcher, and almost 500 inspections were completed in two three-month summer periods. Subsequent analysis showed the geographical distribution and excavation reason to be acceptably randomly distributed.

Where information is needed in a shorter time, a series of random excavations can be scheduled. An inspection frequency of no less than one mile of pipe is required for acceptable statistical accuracy according to Logan and Koenig [*21*]. The inspections should be randomly located—a process requiring a set of random numbers, and a procedure for laying out the system footage in one-mile increments and assigning numbers. Some spare locations should be designated, as some locations may be inaccessible. For less extensive systems or individual sections, sample exposure guidelines in the ASTM Recommended Practice for Conducting Atmospheric Corrosion Tests on Metals (G 50–76) can be used, requiring at least triplicate sample for each exposure period and environment. The ASTM Recommended Practice for Applying Statistics to Analysis of Corrosion Data (G 16–71) can be used where a more precise statistical basis is desired.

Where individual pipe sections are to be examined, we prefer at least three inspections, and at least ten inspections for small systems or more extended segments. At least a 1–m (3–ft) length should be examined, with good 360° access required. The character of corrosion product deposits on cast and ductile iron requires vigorous cleaning, and grit blasting is preferred. Be prepared for leaks! All significant pitting depths should be recorded, and where slab corrosion or wide pits are found, it may be necessary to determine cross-sectional area reduction and remaining hoop strength. Ultrasonic thickness measurement has not proven reliable, but some radiographic techniques are promising for minimum thickness determination. A number of procedures are available for evaluating the effects of corrosion on buried piping life. The simplest is the analysis of annual break/leak frequence, on both a historical and geographical basis. Total and local maintenance requirements can be predicted and parameters set for replacement/repair economic decisions. This and subsequent approaches are facilitated by computerized pipe inventory systems.

The NBS study report [*7*] suggests that a soil may be characterized by the following formula:

$$P = kT_n$$

where P = depth of the deepest pit,
T = time, and,
k, n = constants for the particular soil and pipe material.

Other approaches use extreme value statistics to predict maximum pit depth. Using the NBS data, Ford, Bacon, and Davis [*22*] developed tabulations based on this formula which produced a number called "percent condition." Their approach used the average of the ten deepest pits as a predictor of the deepest pit. The approach did not consider size/area effects which were considered to be negligible above 10.1 cm (4 in.) in diameter. A 1–m (3–ft) inspection length was used in pipe excavations to gather data for analysis of gas piping systems in order to develop depreciation rates for the setting of gas rate changes. We have used this approach in a number of studies, including a major study for the Consumer's Gas Co. of Toronto [*23*].

Conclusions

Resistivity appears to be the most reliable parameter in the prediction of soil corrosivity to ferrous materials, but it can only be used to predict corrosion rates with reference to actual exposure in similar soils. pH and redox potential measurements are of lesser reliability, and only then when measured in situ. Moisture generally must be presumed present from an engineering standpoint. Chloride content is of interest, particularly where stainless steel is exposed, but is reflected in resistivity measurements.

Where new construction is being considered, information obtained from the laboratory analysis of soil samples must be considered suspect, and the data should be evaluated from the standpoint of future in-the-ditch conditions, particularly deicing salt contamination.

The only reliable information concerning pipe condition and life comes from actual exposures under service conditions using statistically acceptable inspection procedures. In terms of future research directions, the polarization resistance technique appears to be promising, particularly if correlations can be established with other exposure data and parameters. For utility system operators, the best approach appears to be the methodical logging of soil and pipe performance data on a geographical basis in conjunction with a computerized inventory record including size, material, and age.

Many individuals and organizations are unaware that ASTM standards cover resistivity and pH testing, perhaps because soil testing generally comes under Committee D–18. Perhaps better promotion is required by both ASTM Committees D–18 and G–1. From a corrosion standpoint, it appears that considerable unnecessary or unreliable testing is performed.

References

[*1*] Fitzgerald, J. H. III, "The Future as a Reflection of the Past," *Effects of Soil Characteristics on Corrosion, ASTM STP 1013*, American Society for Testing and Materials, Philadelphia, 1989.

[*2*] Bushman, J. B. and Mehalick, T. E., "Statistical Analysis of Soil Characteristics to Predict Mean Times to Corrosion Failure of Underground Metallic Structures," *Effects of Soil Characteristics on Corrosion, ASTM STP 1013*, American Society for Testing and Materials, Philadelphia, 1989.

[*3*] Palmer, J. D., "Environmental Characteristics Controlling the Soil of Ferrous Piping," *Effects of Soil Characteristics on Corrosion, ASTM STP 1013,* American Society for Testing and Materials, Philadelphia, 1989.

[*4*] Dillon, C. P., *Corrosion Control in the Process Industries*, McGraw-Hill, New York, 1986.

[*5*] Palmer, J. D. "Soil Resistivity—Measurement and Analysis," *Materials Performance*, Vol. 13, No. 1, January, 1974.

[*6*] Steinmetz, G. F. and Hoxie, E. C., "A Field Test of Type 304 Stainless Steel for Gas Service," *Materials Protection and Performance*, Vol. 12, No. 9, September, 1973.

[*7*] Romanoff, M., "Underground Corrosion," National Bureau of Standards Circular 579, April, 1957.

[*8*] Miller, F. P., Foss, J. E., and Wolf, D. C., "Soil Surveys: Their Synthesis, Confidence Limits, and Utilization for Corrosion Assessment of Soil," *Underground Corrosion, ASTM STP 741*, American Society for Testing and Materials, Philadelphia, 1981.

[*9*] Schwerdtfeger, W. J., "Soil Resistivity as Related to Underground Corrosion and Cathodic Protection," *Journal of Research of the National Bureau of Standards—C, Engineering and Instrumentation*, Vol. 69C, No. 1, January-March 1965.

[*10*] Unpublished data, Ilderton, Ontario, Canada.

[*11*] Unpublished data, Belize, Central America.

[*12*] Scott, G. N., "The Distribution of Soil Conductivities and Some Consequences," *Corrosion*, August, 1958.

[*13*] Husock, B. "A Statistical Probability Method for Soil Resistivity Determination," *Underground Corrosion, ASTM STP 741*, American Society for Testing and Materials, Philadelphia, 1981.

[*14*] Unpublished report, DELCAN Corp. for Government of Newfoundland, Argentia Industrial Park, 1988.

[*15*] Rothman, P. S. and Price, R. E., "Detection and Considerations of Corrosion Problems of Prestressed Concrete Cylinder Pipe, *Corrosion of Rebars in Concrete ASTM STP 906*, American Society for Testing and Materials, Philadelphia, 1986.

[*16*] Husock, B., "A Method For Evaluating Corrosion Activity on Bare Pipelines," paper 31, *Corrosion/73*, NACE, Anaheim, CA. March, 1973.

[*17*] Jones, D. A., "Principles of Measurement and Prevention of Buried Metal Corrosion by Electrochemical Polarization,"*Underground Corrosion, ASTM STP 741*, American Society for Testing and Materials, Philadelphia, 1981.
[*18*] Iverson, W. P., "An Overview of the Anaerobic Corrosion of Underground Metallic Structures, Evidence of a New Mechanism," *Underground Corrosion, ASTM STP 741*, American Society for Testing and Materials, Philadlephia, 1981.
[*19*] McVey, R. E., "Soil Oxidation-Reduction Potential and its Determination as Related to Anaerobic Corrosion of Buried Steel," *A Collection of Papers on Underground Pipeline Corrosion*, Vol. IV, G. B. McComb, Ed., 1960.
[*20*] *Corrosion Basics-An Introduction*, National Association of Corrosion Engineers, Houston, TX, 1984.
[*21*] Logan, K. H. and Koenig, A. E., "Methods of Inspection of Pipelines," *Journal of the American Water Works Association*, Vol. 31, No. 1451, 1939.
[*22*] East Ohio Gas Co., testimony submitted to the Ohio Public Utilities Commission.
[*23*] Palmer, J. D., "An Investigation of the Life of Buried Gas Mains," Ontario Research Foundation, Toronto, November, 1967.

George A. Andersen[1] *and Paul B. Donnellan*[1]

Stress-Corrosion Cracking of Mn-Bronze Castings and Test Specimens in New York City Water Distribution Shafts

---

REFERENCE: Andersen, G. A. and Donnellan, P. B., **"Stress-Corrosion Cracking of Mn-Bronze Castings and Test Specimens in New York City Water Distribution Shafts,"** *Corrosion Testing and Evaluation: Silver Anniversary Volume, ASTM STP 1000*, R. Baboian and S. W. Dean, Eds., American Society for Testing and Materials, Philadelphia, 1990, pp. 139–150.

ABSTRACT: Stress-corrosion cracking (SCC) has been found to be the cause of failure of 48-in. (1219.2-mm) and 30-in. (762-mm) diameter manganese bronze gate valve bodies, a 48-in.-diameter shaft cap, and 1½-in. (38-mm)-diameter nuts. All of these in-service failures occurred in New York City distribution shafts for Water Tunnels Nos. 1 and 2. The valves and shaft cap, which were made of Copper Development Association (CDA) Alloy C86500, failed in predominantly transgranular mode with some intergranular cracking. The nuts, made of CDA Alloy C86300, cracked in an intergranular mode only.

With numerous manganese bronze castings presently in service in all 37 water distribution shafts in New York City, a stress-corrosion cracking test program has recently been initiated. The specimens used were of the modified compact wedge-loaded type made of CDA Alloy C86500. The purpose of the test was not only to find which distribution shafts contained an aggressive SCC environment, but to identify any corrosive agents in the shafts. All 37 shaft environments produced cracking in one or more of the specimens tested in 15 to 63 days. Most of the cracking occurred with the pH in the range from 7.5 to 9.5.

The spillage of elemental mercury from flowmeters in the shafts plus the introduction of chemicals used for mercury cleanup accelerated the SCC investigation. Mn-bronze specimens were tested in jars containing ammonia, mercury, water, trisodium phosphate, and commercial mercury cleaning solutions. All chemical induced cracking in the specimens in a range from 1 to over 300 days, except mercury and trisodium phosphate.

Scanning electron microscopy was used to characterize the crack pattern of several in-service failures and SCC test specimens. Energy-dispersive analysis was used to identify the corrosion products on the crack surfaces.

KEY WORDS: stress-corrosion cracking, high-strength manganese bronze castings, gate valves, shaft caps, intergranular cracking, transgranular cracking, mercury, scanning electron microscope fractograph

The City of New York supplies 1.5 billion gallons of water per day, gravity fed from three upland surface supplies. Two water tunnels are presently in operation while a third one is under construction. There are 37 distribution shafts throughout the city operated by the Maintenance Division of Field Operations for the Bureau of Water Supply and Wastewater Collection.

The Quality Assurance and Corrosion Control Section of the Bureau has performed failure analysis of waterworks equipment for the last five years. Stress-corrosion cracking (SCC) has recently been found to be the cause of failure of a number of shaft components, including

---

[1] Administrative engineers, City of New York Bureau of Water Supply and Wastewater Collection Department of Environmental Protection, New York, NY 10004.

a shaft cap, a pitot connection located below a shaft cap, three gate guard valves at two shafts, and many critical fasteners. The failed components have been exposed to both water and air. They have mainly been of two grades of cast high-strength manganese bronze, Alloys C86300 and C86500. Other SCC environments that may have contributed to these failures include ammonia (from nearby sewage backup or rodent waste), mercury (from flowmeter spillage), and other chemicals considered for use in the mercury cleanup. It has long been known that water and water vapor may cause SCC of copper alloys [*1*]. Recently, alpha-beta brass tested in tension and in distilled water was found to fail in a transgranular cleavage mode [*2*].

High-strength manganese bronze stems, 200 ft (60.9 m) long and 6 in. (152.4 mm) in diameter used to hold section valves in the open position at two shafts may now be susceptible to SCC due to an environmental change. These stems, which are under considerable tensile stress, are now in an environment that contains mercury cleanup chemicals. If either stem fails, the section gate would fall and suddenly stop flow in one of the water tunnels. After failure, there would be no direct way to open the section valve. The consequence of such an event or similar occurrence has prompted the Bureau to initiate a program to investigate the SCC of cast manganese bronze.

Recently, specimens of Alloy C86500 manganese bronze were machined and tested in the actual shaft environment and in laboratory simulated environments. This paper presents case histories of several SCC failures in cast manganese bronze and reviews results of stress-corrosion cracking failures of the following cast Mn-bronze components and specimens:

1. In-service failures of valves, shaft caps, and nuts in New York City water distribution shafts.
2. Constant strain SCC specimens made of Alloy C86500 placed in all 37 water distribution shafts.
3. Laboratory tests of modified compact wedge-loaded SCC specimens made of Alloy C86500 exposed in various chemicals considered for use in a mercury cleanup program.

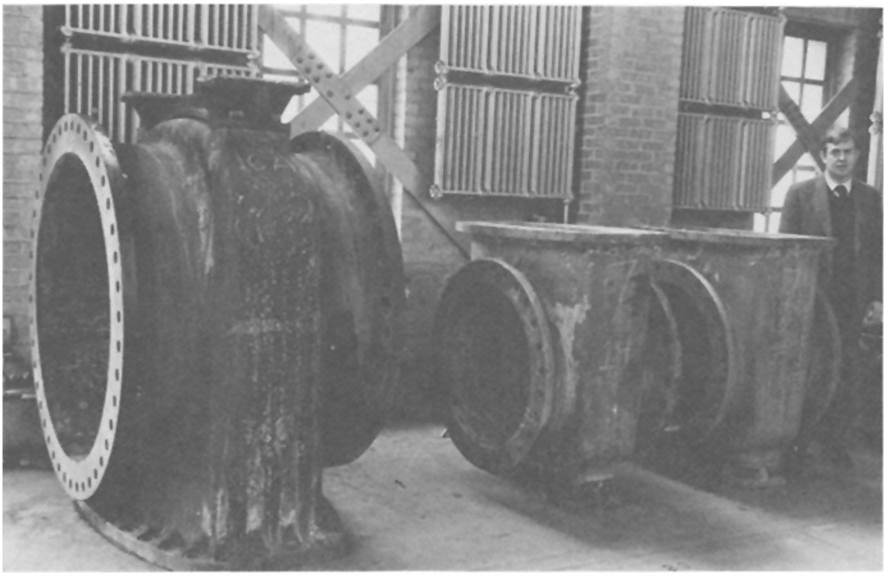

FIG. 1—*One 48-in. gate valve body and two 30-in. gate valve bodies of Alloy C86500.*

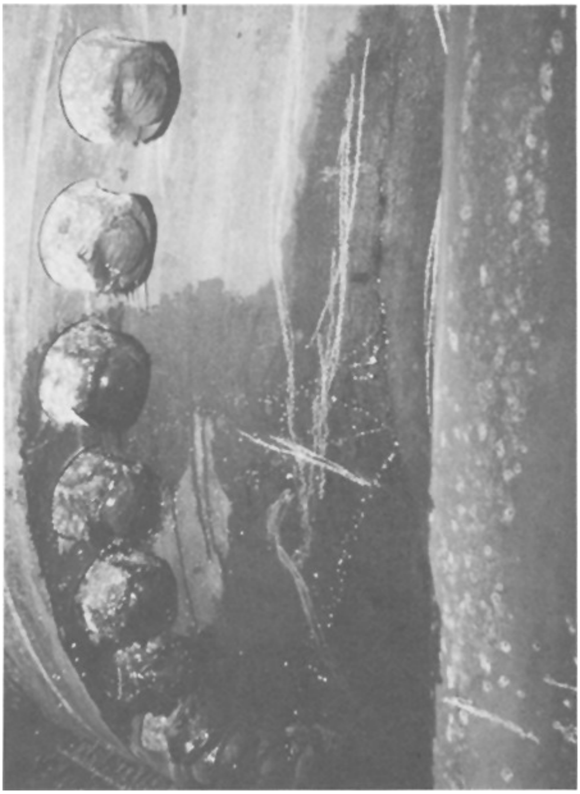

FIG. 2—*48-in. valve body leaking from a crack at shaft chamber.*

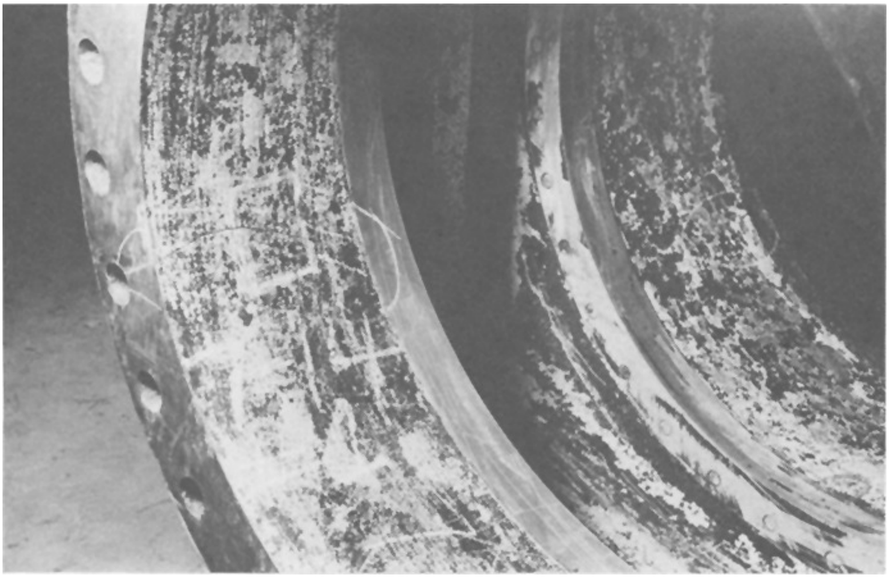

FIG. 3—*Crack propagated to the interior surface on a 30-in. valve.*

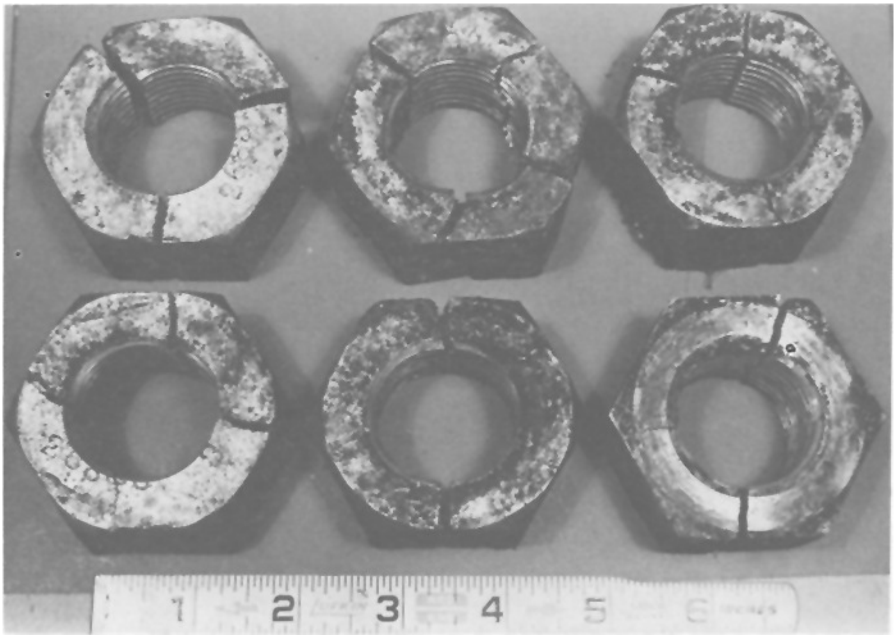

FIG. 4—*Alloy C86300 manganese bronze nuts failed on flange of 48-in. valve.*

Service Failures

The 48-in. (1219.1-mm)-diameter and 30-in. (762-mm)-diameter Alloy C86500 Mn-bronze valve bodies which cracked after being in service for 50 and 70 years, respectively, are shown in Fig. 1. The 48-in valve is also shown in Fig. 2 at the point of failure. Figure 3 shows a crack propagating the entire wall thickness of the 30-in. valve body. Figure 4 shows six Alloy C86300 1½-in. (38-mm) diam Mn-bronze nuts, which cracked at multiple locations. These nuts, selected from 44 which failed, were in service for about 50 years in moist atmospheric exposure; they were used on the flanges of the same 48-in.-diameter gate valve body which failed. It should be noted that mercury cleanup chemicals were not used in the valve chambers until all of the aforementioned failures occurred.

Results and Discussion

Metallographic examination of failed sections of all three valve bodies reveal transgranular cracking as shown in Fig. 5; the microstructure consists of alpha phase needles in a beta phase matrix. Small amounts of iron produced the numerous black dots dispersed throughout the microstructure. The crack generally progressed around the alpha phase. Figure 6 shows the multiple branched cracking that is characteristic of SCC in high-zinc copper alloys. Visual examination combined with metallography indicates that all stress corrosion cracks in the valve bodies initiated on the exterior surfaces. This was evidenced by the varying degree of corrosion on the fracture surfaces.

Typical chemical composition of the service failures examined is shown in Table 1. The nuts, made of Alloy C86300, failed almost exclusively in an intergranular mode as shown

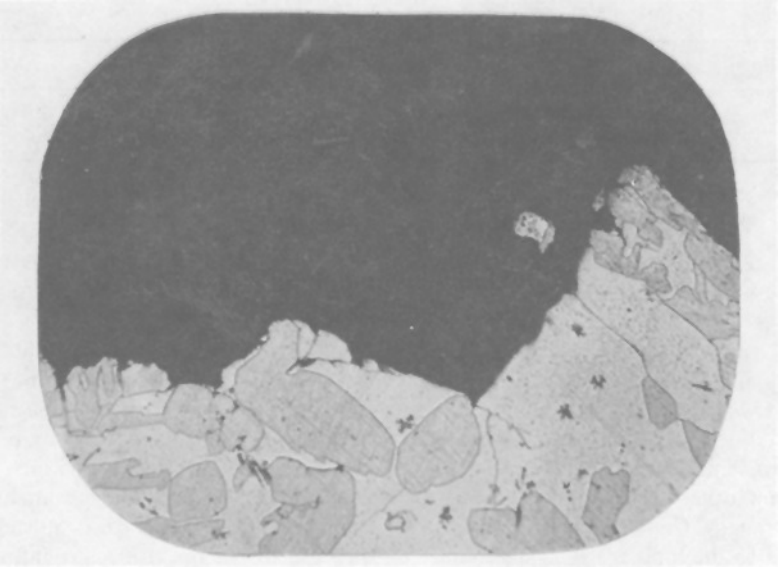

FIG. 5—*Transgranular crack in beta phase of Alloy C68500. Crack propagates around alpha needles* (×*100*).

in Fig. 7. Alloy C86300 differs from Alloy C86500 in that the alpha needles are much larger in Alloy C86500. Iron-rich particles are present in both alloys.

Intergranular cracking of these alloys near room temperature is characteristic of SCC. This is also shown in Fig. 8, which is a scanning electron microscope fractograph showing the smooth intergranular facets or rock-candy structure. Assembly stresses contributed to the SCC of the nuts as well as the valve body.

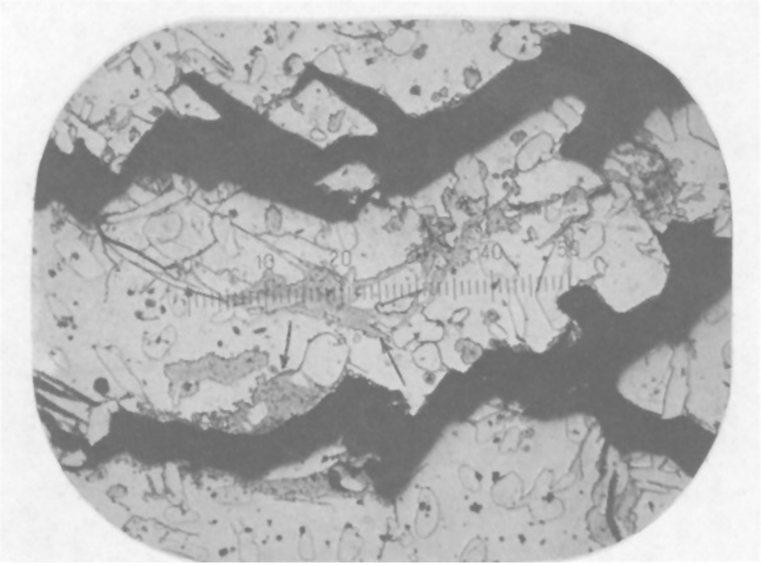

FIG. 6—*Branched transgranular cracking characteristic of SCC failures* (×*100*).

TABLE 1—*Chemical composition of service failures.*

CDA Alloy	Service Part	Cu	Sn	Zn	Fe	Al	Mn
C86500	Valve body	57.67	0.39	39.11	1.36	1.48	0.12
C86300	Nut	64.85	0.19	23.39	2.04	6.14	3.00

SCC of Specimens in Shafts

Replacement of all manganese bronze castings will not be feasible for at least 15 years. The stress-corrosion cracking test program was conducted at all shaft locations to determine the areas which are the most conducive SCC environments. All specimens tested were 1/2 in. (12.7 mm) thick, made of Alloy C86500, and of the type that is a modified compact wedge loaded with a bolt. A speciment is shown in Fig. 9. This complies with MC(Wb) of the ASTM Standard Terminology Relating to Fracture Testing (E 616). The specimens were machined from a sound section of one of the valve bodies. Specimens were not precracked. Strain was introduced by a stainless steel bolt torqued to approximately 65 in. · lb. It was determined that this amount of torque brought the wedge front of the specimens near the yield strength. Control specimens were loaded and left on an office desk. Specimens were exposed to the ambient shaft air by placing them on top of the riser caps and immersing them in water in the sump pits. Note that the shaft tests were performed after chemicals were used in the shaft during the mercury cleanup. The chemicals tested for SCC are described in the next section.

Results and Discussion

All 37 shaft environments produced cracking in one or more of the specimens tested. The time to failure ranged from 15 to 63 days. None of the control specimens have cracked after one year in a dry office. The majority of the cracks occurred in specimens placed on the

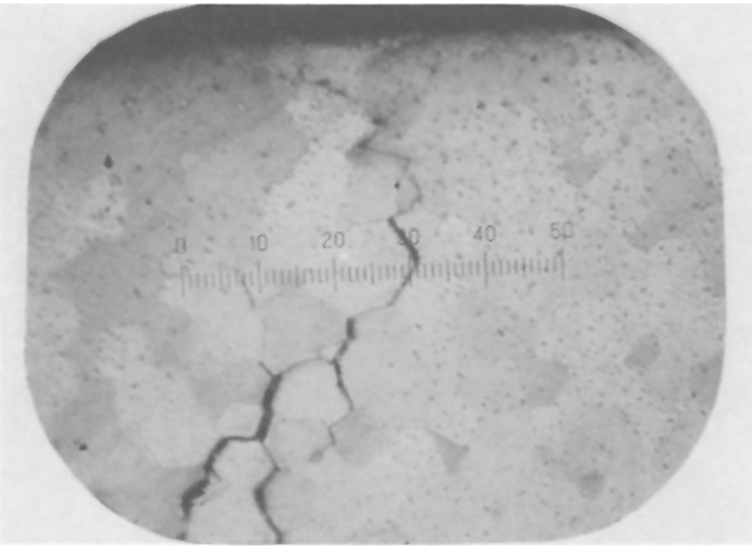

FIG. 7—*Intergranular crack in Alloy C86300 nut, predominantly beta phase* (×*100*).

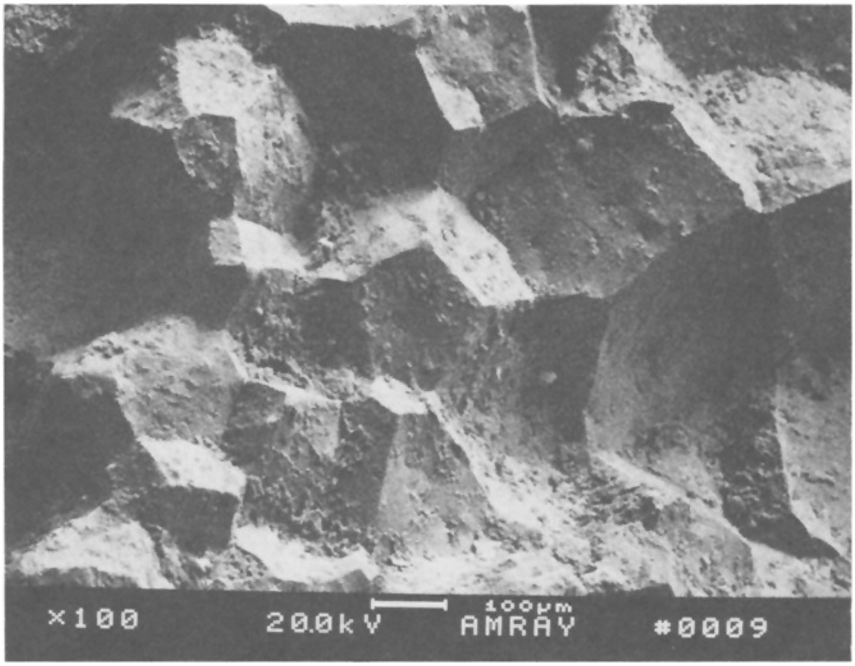

FIG. 8—*SEM fractograph with a "rock candy" appearance on Alloy C86300 nut.*

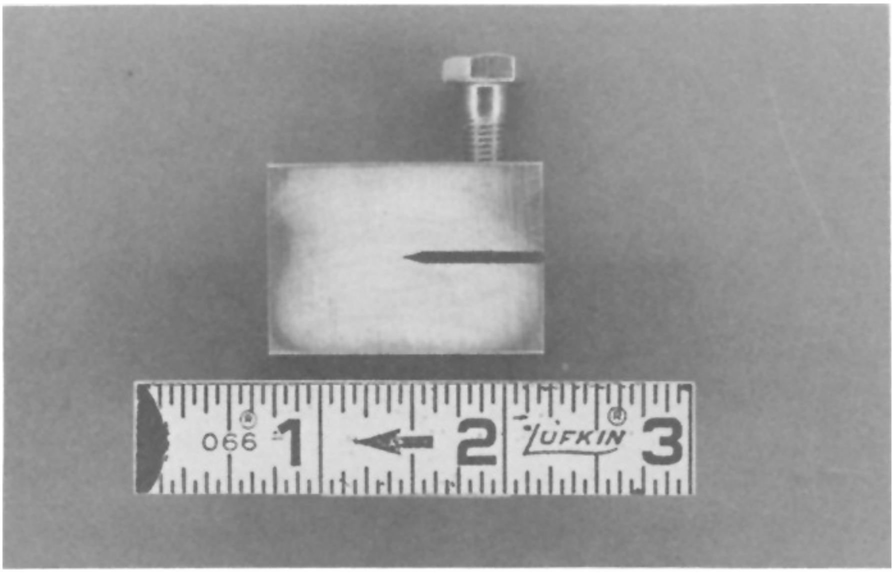

FIG. 9—*Modified wedge open-loading SCC specimen (1/2 in. thick), made of Alloy C86500.*

riser caps. The pH of the water in each shaft chamber was found to range from an average of 7.0 to an average of 11.5 in the sump pits. In the test locations where the pH was high (greater than 11), there was only one cracked sample. Most of the cracking occurred with the pH in the range from 7.5 to 9.5.

SCC of Specimens in Laboratory Tests

The spillage of elemental mercury from flowmeters in the shafts and the subsequent introduction of chemicals used for mercury cleanup expanded the SCC investigation to include laboratory tests. Also necessitating these tests were the aforementioned shaft situations where Mn-bronze stems were possibly prone to SCC catastrophic failure. Alloy C86500 test specimens identical to the one used in the shafts were tested in glass jars containing ammonia, mercury, water, trisodium phosphate, and commercial cleaning solutions. Tests were also conducted in mixtures of the aforementioned liquids. Specimens were immersed in the partially filled jars, and additional specimens were suspended above the liquids to expose them to vapors of the liquid.

Results and Discussion

The results of the laboratory tests are shown in Table 2. The specimens cracked in concentrated ammonia in one day, in dilute ammonia in four days, in distilled water in eleven days, and did not crack in trisodium phosphate or mercury vapor. A cleaning solution of 85% sodium thiosulfate and 15% ethylene diamine tetraacetic acid mixed with water caused cracking in 95 days. Another concentrated cleaning solution of an activated carbon-iodine mixture brought on cracking in 28 days.

Trisodium phosphate concentrated appears to be an effective inhibitor and has been recommended for future mercury cleanup, if necessary.

It should be noted that there are records of earlier failures in Mn-bronze castings in the distribution shafts; however, no metallurgical analysis is available. While failure analysis was not performed and SCC of the Mn-bronze valves, nuts, and other components presumably was not realized until after 50 years of service, the initiation of the cracking occurred much earlier; this can be exhibited by the dealloying of cracked regions shown in Fig. 6.

TABLE 2—*Results of laboratory SCC tests.*

	Time to Cracking, days	
Test Environment	Liquid	Vapor
Aqua ammonia (concentrated, approximately 10% NH_3)	Not tested	1
Aqua ammonia (dilute, approximately 2% NH_3)	Not tested	4
Distilled water	11	12
Mercury (no water)	Not tested	No cracking[a]
A[b] + water (saturated)	No cracking[a]	95
B[c] + water (saturated)	28	28
A + B (equal volumes of saturated solutions)	29	29
Na_3PO_4 (1% aqueous solution)	No cracking[a]	No cracking[a]
A + Na_3PO_4 (saturated)	No cracking[a]	Between 300 and 550

[a] After 550 days.

[b] Commercial mercury cleanup solution of 85% sodium thiosulfate and 15% ethylene diamine tetraacetic acid.

[c] Mercury cleanup solution; an activated carbon-iodine mixture.

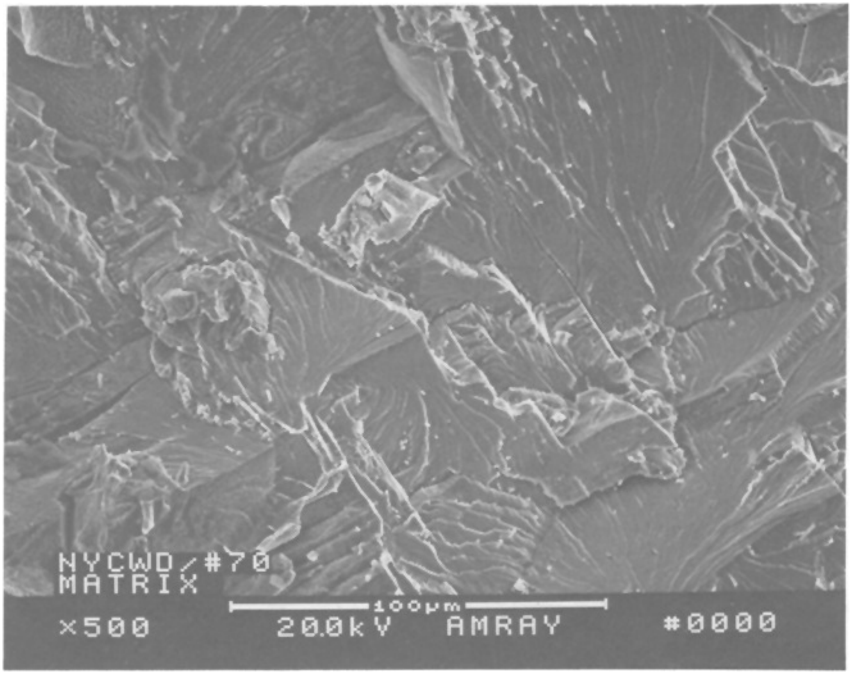

FIG. 10—*SEM fractograph of Alloy C86500 SCC specimen that failed in cleavage mode.*

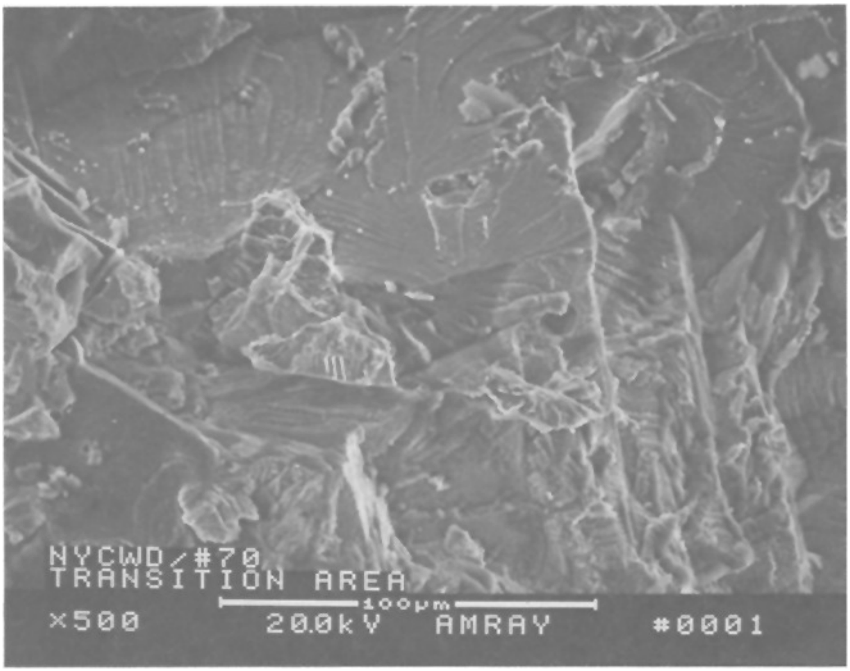

FIG. 11—*SEM of transition fractograph of SCC specimen: cleavage mode on left, ductile rupture on lower right.*

Since all of the Mn-bronze components were cast alloys, locked-in stresses as well as service stresses in tension contributed to the failures.

After the tests were completed, specimens were selected at random and their fracture surfaces examined by scanning electron microscopy. All specimens failed in a predominantly transgranular cleavage mode of cracking as illustrated in Fig. 10. To determine the location of the SCC crack front, several specimens were overloaded to complete fracture and examined in a scanning electron microscope. The fracture transition from SCC to overload failure is exhibited in fractographs shown in Figs. 11 through 13. The SCC crack front is at the point of transition from cleavage mode to microvoid coalescence, which is characteristic of Mn-bronze overload. Traces of any known SCC-causing corrodent were not found on any of the fracture surfaces examined to date.

Energy-dispersive X-ray analysis was used to examine specimens which failed both in areas of SCC fracture surfaces and torque overload fractures for comparison. An energy dispersive X-ray spectrum of the ductile overload region is shown in Fig. 14. Note that the copper-zinc ratio is approximately 60 to 40%. Figure 15 shows the X-ray spectrum of the stress-corrosion cracked surface after being immersed in a shaft sump pit; note that the copper-zinc ratio has almost reversed due to corrosion which occurred after cleavage cracking had opened the sample. This is a manifestation of a dezincification reaction with a zinc-rich corrosion product at the cracked surface.

Conclusions

Stress-corrosion cracking has been found to be the mechanism of failure of various manganese-bronze valve bodies and other components in New York City water distribution shaft chambers.

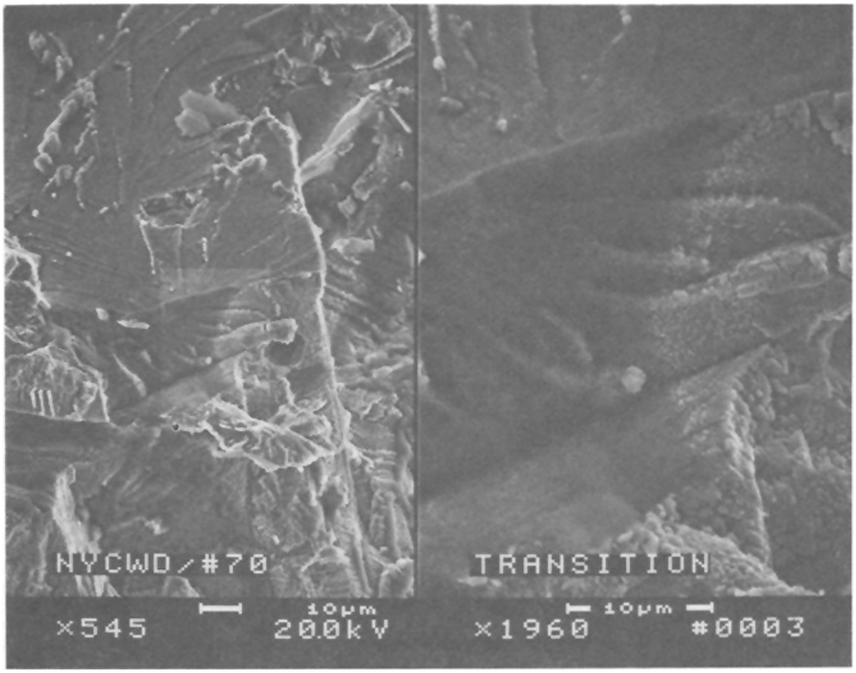

FIG. 12—*Transition fractograph of SCC specimen with dual mag/split screen SEM.*

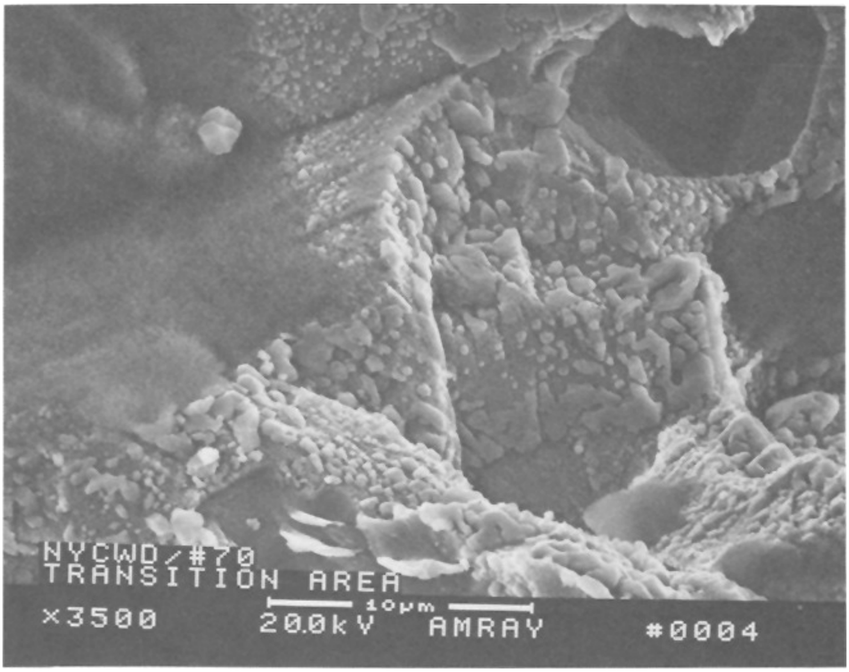

FIG. 13—*SEM of transition area of Fig. 12 at ×3500 showing ductile rupture pattern of Alloy C86500.*

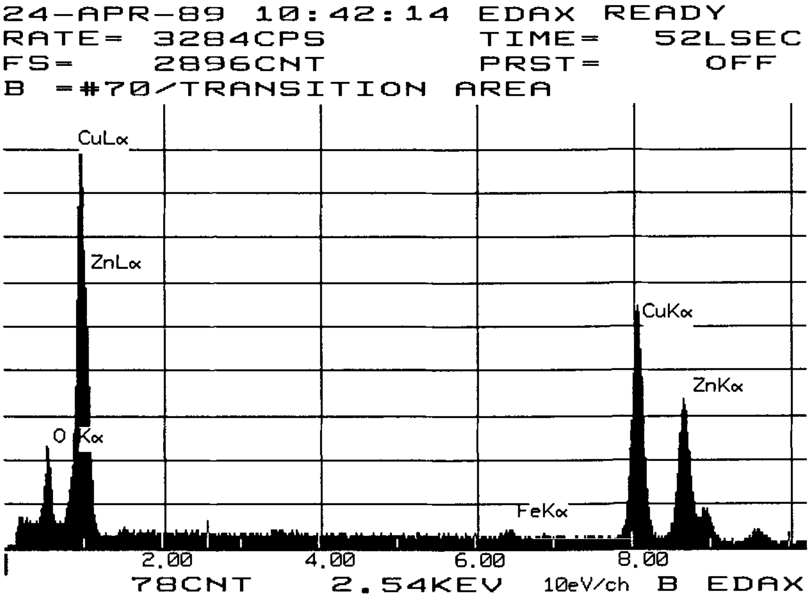

FIG. 14—*Energy dispersive X-ray spectrum of fracture surface caused by overload.*

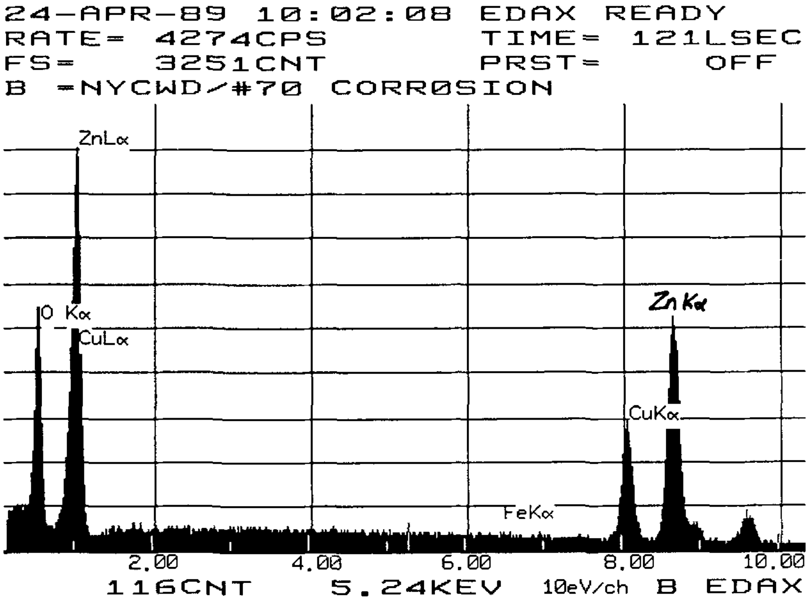

FIG. 15—*Energy dispersive X-ray spectrum of fracture surface caused by SCC.*

Placing specimens in various locations within 37 New York City water distribution shafts has revealed environments which induce SCC in all shafts. Most cracking was found to occur in chambers where the water tested had a pH in the range from 7.5 and 9.5. Above pH 9.5 there was little or no cracking.

Mercury and mercury cleanup chemicals considered for use in the distribution shaft chambers all were tested for the potential of causing SCC in specimens. The testing provided direction in the selection of cleanup chemicals.

Fractography of failed specimens using scanning electron microscopy proves SCC in a cleavage mode for Alloy C86500. Normal overload failure of this alloy results in a dimpled rupture pattern. Fractography of failed nuts made of alloy C86300 reveals SCC in an intergranular mode.

In critical areas in New York City water distribution shafts, where Mn-bronze components are in a condition prone to SCC, precautionary measures can be taken, including dehumidification and avoidance of deleterious chemicals.

Acknowledgments

The authors wish to thank W. Leong for assisting in the failure analysis. Thanks also go to S. Heslowitz for supervising the test program. Thanks are in order to A. Ragucci, R. Gainer, E. Scheader, and J. Conway for their continued encouragement in this work. We are also grateful to E. Griffin of AMRAY, Inc., Bedford, MA, for providing the SEM fractographs and energy dispersive X-ray spectrums.

References

[*1*] Fontana, M. G. and Greene, N. D., *Corrosion Engineering*, 2nd ed., New York, NY, 1978, p. 100.

[2] Hintz, M. B., Nettleton, L. J., and Heldt, L. A., *Metallurgical Transactions*, Vol. 16A, 1985, p. 971.

Michael Schorr,[1] Erica Weintraub,[1] and David Andrasi[1]

Erosion-Corrosion Measuring Devices

REFERENCE: Schorr, M., Weintraub, E., and Andrasi, D., "**Erosion-Corrosion Measuring Devices,**" *Corrosion Testing and Evaluation: Silver Anniversary Volume, ASTM STP 1000,* R. Baboian and S. W. Dean, Eds., American Society for Testing and Materials, Philadelphia, 1990, pp. 151–159.

ABSTRACT: Two instruments for the study and measurement of erosion-corrosion (EC) were developed and built: the erosion-corrosion unit (ECU) and the erosion-corrosion tester (ECT). These instruments simulate the shear and impact forces acting on industrial equipment to evaluate the corrosive wear effects of the fluid on the equipment and their interaction. The specimen in the ECU consists of a cylinder rotated about a vertical axis while a jet of slurry impinges continuously onto its curved surface through an interchangeable nozzle. The ECT applies rotational sliding abrasion by the slurry on a static disk specimen. In both devices, a three-electrode system (working, reference, and counter electrodes) is used to evaluate the electrochemical corrosion component by the polarization resistance technique. The contribution of mechanical erosion to the synergetic EC process is measured by weight loss on long-term exposures.

The instruments were applied as follows: in industrial plants to monitor the influence of corrosion parameters during production, in pilot plants and in the laboratory to evaluate and select corrosion-resistant alloys, to assess the corrosivity of the ores and slurries handled, and for analysis of EC failures.

The instruments are described and their characteristics compared. The results obtained in several environments are presented and their significance discussed.

KEY WORDS: corrosion, erosion-corrosion monitoring, electrochemical techniques, slurries, laboratory tests, plant tests, instruments, stainless steels, Ni-base alloys

Erosion-corrosion (EC) is a complex phenomenon in which chemical, electrochemical, hydrodynamic, mechanical, and metallurgical aspects are intimately connected. Its form and magnitude depends on several factors: the nature and composition of the fluid, including aggressive ions such as Cl^- and F^-; flow regime; velocity; angle of impingement; energy of impact; and the solid particle properties: size, shape, density, hardness, and friability.

EC is characterized in appearance by deep gullies, grooves, waves, rounded holes, and valleys, exhibiting a directional pattern usually related to the direction of the fluid flow. These EC effects impair the protective film present on passive alloys such as stainless steels, causing breakdown of passivity. On active alloys such as carbon steel, an active surface is maintained. In this way, the corrosion process is accelerated by mechanical removal of asperities, proturbances, and corrosion products such as oxides or phosphates which otherwise might form a protective layer. A continuously renewed surface is generated, enhancing corrosion activity.

Corrosion, erosion, and abrasion are frequent problems in chemical and mineral processing plants, leading to failures of equipment operating under severe hydrodynamic conditions

---

[1] Head, corrosion engineer, and senior technician, respectively, Corrosion and Materials Section, IMI (TAMI)—Institute for Research and Development Ltd., P.O.B. 313, Haifa, Israel 31002.

such as pumps, turbines, centrifuges, agitators, ball mills, etc. The combined and simultaneous action of these deterioration processes results in various types of surface wear of the equipment, which are defined in accordance with the following guides: the ASTM Definitions of Terms Relating to Corrosion and Corrosion Testing (G15–85a) and the ASTM Terminology Relating to Erosion and Wear (G 40–83).

In equipment handling, in particular in moving corrosive fluids containing suspended solid particles such as in slurries, the main phenomenon is EC, a particular type of localized corrosion caused by the synergetic action of mechanical erosion and electrochemical corrosion. Several environments and equipment are affected by EC in local plants: handling and processing slurries, for example phosphate ore washing; wet process phosphoric acid (WPA) production; periclase hydration; and carnallite and sylvinite slurries, used in potash production.

In order to understand the causes and mechanisms of EC phenomena and to measure its magnitude, the chemical and mineral industries apply different laboratory and plant devices which simulate service conditions and sometimes increase the severity of the chemical, mechanical, and hydrodynamic factors involved in EC.

Many EC-measuring devices have been designed and constructed in the last years and frequently are reported in the literature [*1–5*]. They are based, in principle, on simulation of the mechanical forces acting on the plant equipment surface and a measurement of the mechano-chemical effect on a static or dynamic metallic specimen exposed to a moving fluid. The EC effect is assessed by physical changes (weight, length, volume, roughness), by an electrochemical measurement, or by applying both techniques simultaneously or successively.

IMI Erosion-Corrosion Measuring Devices

During the past years the Corrosion Laboratory of IMI (TAMI)—Institute for Research and Development was engaged in the study of corrosion in several industrial plants handling aggressive slurries and in the selection of EC-resistant alloys to be used in these plants. Since EC is the main type of corrosion encountered in these systems, it was necessary to develop devices to study and measure EC phenomena in these slurries. Accordingly, two instruments were developed, built, and applied in several plants.

Erosion-Corrosion Unit (ECU)

This instrument simulates EC phenomena occurring in equipment handling flowing fluids, enhanced by suspended solids in slurries or entrained solids in brines. A jet of slurry or brine is impinged continuously on the curved surface of the submerged rotating specimen, through a nozzle. The instrument measures corrosion potential and instantaneous corrosion current by the polarization resistance technique in accordance with the ASTM Practice for Conducting Potentiodynamic Polarization Resistance Measurements [G 59–78 (1984)].

Figure 1 presents a schematic diagram of the apparatus, which consists of three parts: the cell, the agitated vessel, and the electrochemical measuring instrument.

The cell (*a*)—In a polypropylene vessel (1) (diameter 12 cm, height 18 cm) the alloy under test in the form of a cylinder (2) (diameter 20 mm, height 6 mm) is rotated about a vertical axis (3) while a jet of fluid is impinged continuously onto its curved surface through an interchangeable nozzle (4). The specimen and its mercury contact (5) are kept in place by means of a hollow rod holder. Immediately adjacent to the cylinder are an auxiliary platinum electrode (6) and a reference electrode (7).

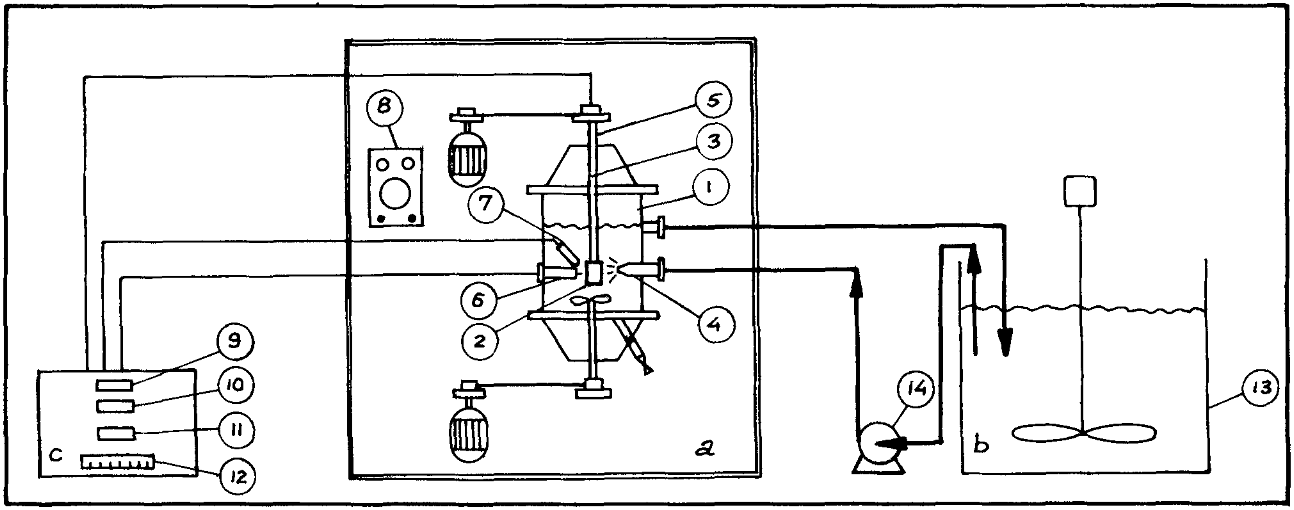

FIG. 1—*Schematic diagram of the IMI erosion-corrosion unit (ECU).*

The effects due to rotation, impingement, and simultaneous rotation and impingement are determined by varying the specimen's rotational velocity and the jet's impact energy.

Agitated vessel (*b*)—The cell is connected to an agitated vessel (13) which supplies the solids-containing fluid via a pump (14).

The electrochemical measuring instrument (*c*)—This instrument measures the potential (9) of the specimen and the corrosion current (10) which flows between the specimen (2) and the auxiliary electrode (6) when a fixed, 20-mV polarization potential (12) is applied to the specimen. The potential is set with respect to an Ag/AgCl or a SCE reference electrode (6) with a polypropylene body. The instrument also measures the oxidation-reduction potential E_{ORP} of the fluid. The electronic instrument was designed by Ch. Yarnitzky, Technion—Israel Institute of Technology, and built by Opal Co., Israel [*6*].

Erosion-Corrosion Tester (*ECT*)

The instrument applies rotational sliding abrasion on a static metallic specimen to simulate the corrosive wear effects of the solids-containing fluid on the surface of the equipment. The abrader material and its shape vary according to the solids type, the plant equipment, and their interactions. The magnitude of the effect on electrochemical corrosion is measured by the polarization resistance technique to determine the instantaneous corrosion rate and by weight loss to assess the contribution of mechanical erosion.

The tester described in Fig. 2 consists of two parts:

The EC cell (*a*)—The cell (3) is a polypropylene cylinder, 40 cm high and 10 cm in diameter. It contains three electrodes; the working electrode (5) in the form of a disk, made from the alloy under the test and the Ag/AgCl reference electrode (8) and auxiliary platinum electrode (9), both immediately adjacent to the disk (5). The cell is immersed into the vessel (1) containing the agitated fluid (2). A cross-shaped, rigid polypropylene abrader (6) or a soft rubber wiper (6a) is attached to the base of the rotating shaft (7). The solids are swept outwards and their particles are ground on the specimen surface. The shape of the abrader

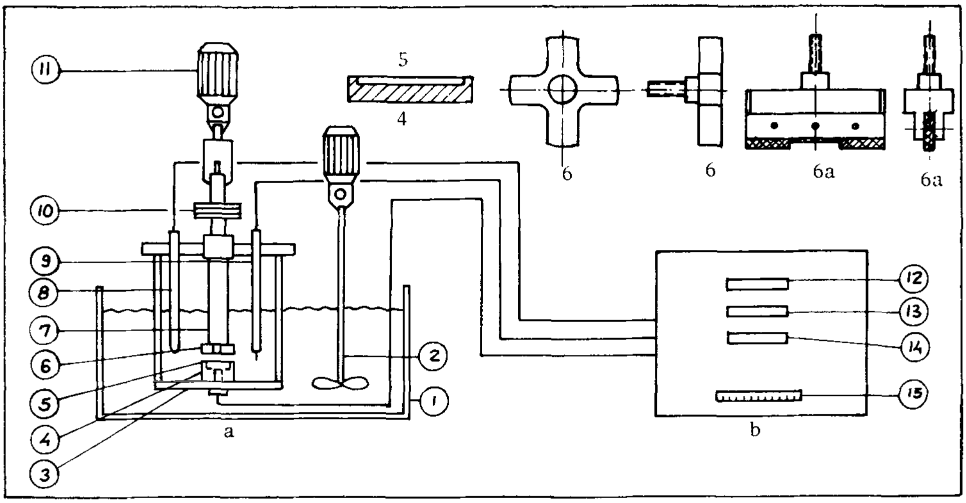

FIG. 2.—*Schematic diagram of the IMI erosion-corrosion tester* (*ECT*).

TABLE 1—*Comparative evaluation of the IMI erosion-corrosion measuring instruments.*[a]

Instrument Characteristics	EC Unit	EC Tester
Instrument-Slurry interaction	Slurry from the WPA reactor is pumped through a nozzle into the instrument	Direct immersion in the agitated WPA slurry
Corrosion Specimen:		
Shape and dimensions	Cylinder: diameter 20 mm, height 6 mm	Disk: diameter 35.6 mm, height 3 mm
Exposed surface, area	Curved, 3.8 cm^2	Flat, 10.0 cm^2
Mechanical forces:	Slurry jet impinging on rotating specimen	Weighed rotating abrader (or wiper) bearing on specimen
Mechanical parameters	Specimen rotational velocity; slurry jet velocity and impact	Abrader (wiper) rotational velocity; pressure on specimen
Specimen motion	Rotating or static	Static
Slurry motion	Linear jet	Sliding on flat specimen
Specimen-slurry interaction	Homogeneous mass of slurry impinges on rotating or static specimen	Discrete ore particles abrade static specimen
Effect on specimens	Erosion by a moving slurry	Circular scratching abrasion
Specimen appearance (after test)	Uniformly polished surface which may be shiny or matt according to degree of erosion-corrosion	Fine, circular concentric scratches
Electrochemical parameters:		
Potential	Uniform shift from the passive to the active state	Fluctuating shift from the passive to the active state
Current	Regular values, proportional to the intensity of the mechanical forces applied	Fluctuating values, proportional to the intensity of the mechanical forces applied and increased by scratching of discrete solid particles
Instantaneous corrosion rate	Acceptable values	Acceptable values

[a] The measurements were conducted in the same WPA slurry.

(and wiper) permits the particles to be swept onto the specimen surface. The severity of the mechanical action is controlled by weights (10) mounted on the rotating shaft and by increasing the rotational velocity of the shaft.

Electrochemical measuring instrument (*b*)—This instrument measures the open-circuit potential (12) of the specimen and the corrosion current (13) which flows between the specimen (5) and the auxiliary electrode (9) when a fixed, small polarization potential (15) is applied to the specimen, set with respect to the reference electrode (8).

Comparative Evaluation of the IMI EC Devices

A comparison of the characteristics and the performance of the ECU and the ECT is shown in Table 1. Although the interaction between the equipment surface and the moving slurry is expressed in different modes, by regulating the operating conditions and the intensity of the mechanical forces, similar corrosion rates are obtained in the same alloy/environment system.

TABLE 2—*Erosion-corrosion measurements in WPA slurry.*

		Corrosion Rate,[a] $\mu A/cm^2$ (mm/year)			
Alloy Tested	Corrosion Potential, SCE, V	Static	Rotation Speed	Impingement Velocity	Rotation Plus Impingement
AISI 316 SS	0.27 to − 0.13	58 (0.60)	161 (1.7)	384 (4.0)	845 (8.9)
Fe-20Cr-25Ni	0.28 to 0.26	6.1 (0.06)	10.6 (0.11)	47 (0.50)	103 (1.1)
Nickel-base	0.35 to 0.25	1.1 (0.01)	1.9 (0.02)	6.4 (0.08)	13.8 (0.46)

[a] The measured corrosion current density, i_{corr}, in $\mu A/cm^2$ is converted into a weight loss and expressed as loss in wall thickness in mm/year. Hydrodynamic parameters: Rotation speed, 1200 rpm; jet impingement velocity, 5.1 m/s.

Applications in Chemical and Mineral Industries

The EC devices were applied in several industrial plants to control corrosion during production. The devices were also applied in pilot plants, and in the laboratory to evaluate and select EC-resistant alloys and to assess the corrosivity of the fluids handled.

Phosphoric Acid Production [7,8]

Wet process phosphoric acid (WPA) is produced by attack of phosphate ore by concentrated sulphuric acid. Impurities such as Cl^- and F^- increase the corrosivity of the medium. EC appears mainly in the reaction stage, where an aggressive slurry, containing 42% phosphoric acid (H_3PO_4), 2% sulfuric acid (H_2SO_4), and 30% solid particles (gypsum, sand, quartz, and undissolved rock) is processed at 75°C (167°F). The main equipment undergoing EC are the reactor agitators and pump impellers, made of an austenitic stainless steel (Fe-20Cr-25Ni-4.5Mo-1.5Cu), in short, Fe-20Cr-25Ni.

Typical results obtained with the ECU connected to an industrial WPA plant reactor are shown in Table 2. The duration of the test for each alloy is 1 h. The temperature in a slurry supply vessel is controlled electronically and measured in the cell to 75 +/− 1°C. The trial included a Ni-base alloy (Ni-15Cr-16Mo-5Fe-2.5Co-4W). The results show that the rate of corrosion increases significantly as the hydrodynamic conditions increase in severity. The rates observed under conditions of simultaneous rotation and impingement are 15 to 50 times greater than those under static conditions.

The EC instruments were employed in WPA pilot plants to evaluate the corrosivity of various phosphate ores [*9,10*] and for selection of EC-resistant alloys to be used for the fabrication of industrial plant equipment [*11*].

In an industrial plant trial [*12*], the ECT was applied to assess the effect of the addition of siliceous clays to the WPA reaction system, to complex the free hydrofluoric acid and minimize its corrosivity. AISI 316 SS high-alloyed austenitic stainless steels (Steel A, Fe-20Cr-25Ni-4.5Mo-1.5Cu, and Steel B, Fe-27Cr-31Ni-3.5Mo-1.5Cu) and a Ni-base alloy (Ni-15Cr-16Mo-5Fe-2.5Co-4W) were tested. The results of several runs with and without addition of clay, shown in Fig. 3, indicate clearly the significant reduction of EC rates in the presence of clay. The ECT was set at a rotation speed of 100 rpm and the load on the abrader was 1.1 kg/cm². The EC rate was measured by the linear polarization resistance technique.

Figure 4 presents anodic polarization plots (at a scan rate of 60 mV/min) of a Fe-20Cr-25Ni alloy, obtained both on a static specimen and on a specimen being abraded by the ECT. The current fluctuations, Plot b, indicate a rapid sequence of breakdown of the passive film by the mechanical action of the hard, sharp particles in the slurry, followed up by the

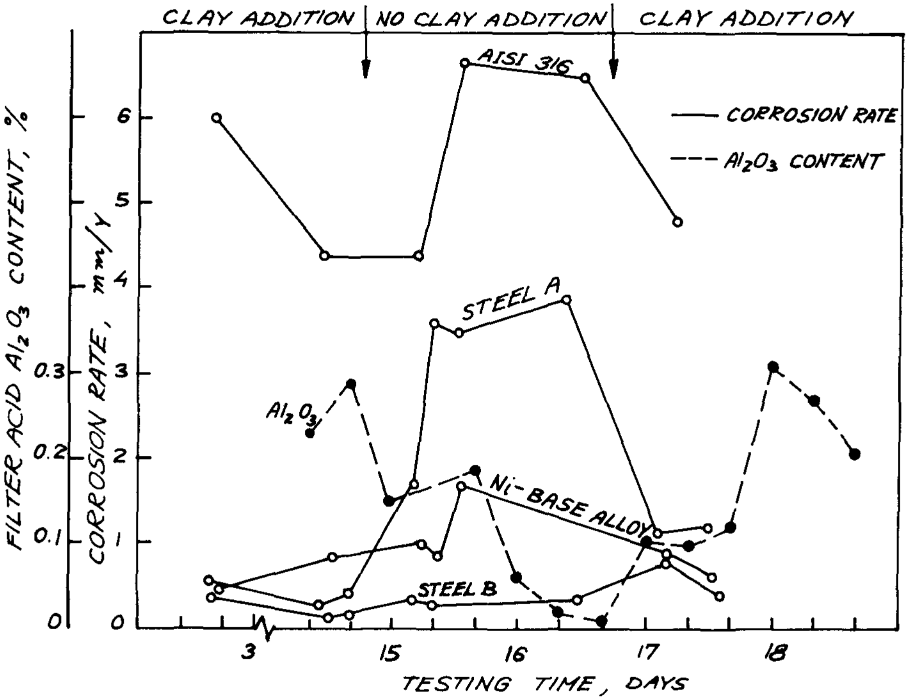

FIG. 3.—*Influence of clay addition in WPA production on EC rate.*

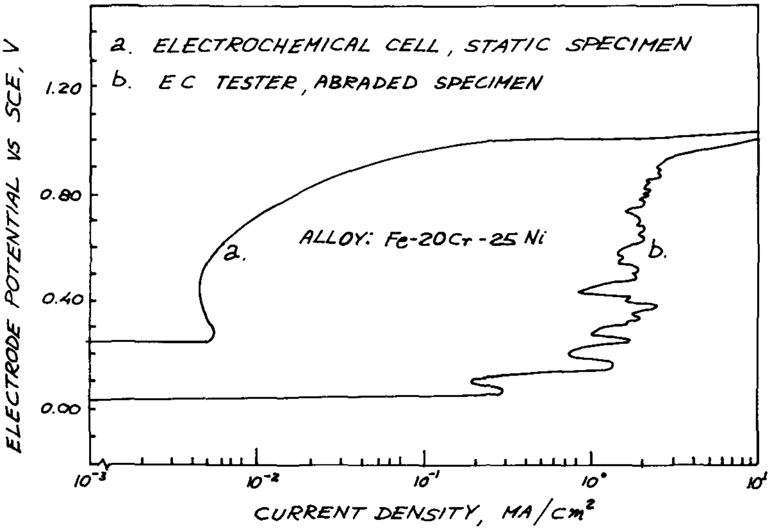

FIG. 4.—*Potentiodynamic anodic polarization plots in WPA slurry at 80°C (176°C).*

formation of a protective oxide film. On the other hand, Plot a shows stable and smaller currents. Both plots reach the same value in the transpassive region. A similar behavior was reported by M. Matsumura et al. during erosion-corrosion measurements [3].

Copper Ore Grinding

Wet grinding plants for communition of ores which operate by the application of compression and shear forces between the equipment's hard metallic surfaces and the ore particles suffer from mechanical wear. The problem is sometimes aggravated by electrochemical corrosion when brackish water and/or electrolyte solutions are involved.

In a wet-grinding plant processing a siliceous copper mineral, the main plant equpiment, which includes rotating ball mills, spiral classifiers and mixing tanks, is made of hard carbon steel, austenitic manganese steel, and cast irons.

The EC tester was used to assess the degree of corrosive wear that might occur on the plant equipment. Two types of corrosion tests were carried out: plant tests under operating conditions by exposing specimens prepared from the alloys used in the plant, and laboratory tests by immersing the ECT cell in the agitated slurry. The ECT was operated at a shaft rotation speed of 100 rpm with a load on the abrader of 1.1 kg/cm^2.

The rates of electrochemical corrosion, mechanical erosion, and conjoint corrosion and erosion were measured. The results, summarized in Table 3, show that damage to the plant equipment is due mainly to the mechanical actions of erosion, abrasion, and impact.

The contribution of corrosion to the overall wear process in these slurries is up to 10%, depending on the slurry pH, the characteristics of the mineral particles, and mainly on the severity of the mechanical operating conditions.

Conclusions

Based on the knowledge and experience accumulated during the application of the EC instruments and a continuing survey of the literature, the following conclusions have been drawn:

1. The EC devices have been developed to a stage that ensures a reliable and useful performance in several types of solids-containing fluids.
2. The EC devices evaluate mechanically accelerated corrosion by application of mechanical forces that simulate the interaction between a moving fluid and the surface of industrial plant equipment.

TABLE 3—*Corrosive wear in copper ore slurries*

Test Location	Test Device	Test Specimen	Wear Process	Medium	Measurement	Loss Rate, mm/year
Laboratory	EC tester	Disk	Electrochemical corrosion	Water, slurries	Corrosion current	0.2–2
Laboratory	EC tester	Disk	Mechanical corrosion	Slurries (coarse and fine)	Weight loss, thickness loss	25–90
Wet grinding plant	Spiral classifier	Shoe	Mechano-chemical erosion-corrosion (corrosive wear)	Slurries (coarse and fine)	Weight loss, thickness loss	2–15
Wet grinding plant	Ball mill	Liners and balls	Mechano-chemical erosion-corrosion (corrosive wear)	Slurries (coarse and fine)	Weight loss, thickness loss	20–110

3. The EC measurements allow one to distinguish between the quantitative contribution of mechanical erosion (or abrasion) and electrochemical corrosion to the total synergetic corrosive wear process.

4. The EC tester provides a convenient tool for in situ determination of instantaneous EC, mainly in industrial plants, since it is easy to install and operate and gives reliable results.

References

[*1*] Heil, K., Heitz, E., and Weber, J., "Apparatus for Testing Materials at High Flow Speeds," *Sonder-druck aus Material—prufung 23*, No. 5, 1981, S. 166/170 (German).
[*2*] Postlethwaite, J. et al., *Corrosion*, Vol. 30, No. 8, 1974, p. 285.
[*3*] Matsumura, M. et al. in *Laboratory Corrosion Tests and Standards, ASTM STP 866,* G. S. Haynes and R. Baboian, Eds., American Society for Testing and Materials, Philadelphia, 1985, pp. 358–372.
[*4*] Ogino, K. et al., *Corrosion*, Vol. 44, No. 2, 1988, p. 97.
[*5*] Jang, J. W. et al., *Corrosion,* Vol. 44, No. 11, 1988, p. 836.
[*6*] Yarnitzky, C. and Schorr, M., *Proceedings,* 48th Meeting of the Israel Chemical Society, 1981, abstract.
[*7*] Becker, P., "Chapter 10: Corrosion," *Phosphates and Phosphoric Acid*, 2nd ed., Marcel Dekker, New York, 1987.
[*8*] Schorr, M., *Corrosion Manual, Part 1, WPA,* International Fertilizer Development Center, 1981.
[*9*] Schorr, M., Weintraub, E., Andrasi, D., and Finkelstein, N. P., *Proceedings,* 8th Inernational Congress on Metallic Corrosion, Mainz/M, 1981, pp. 1384–9.
[*10*] Rabinovitz, J. A. et al., "The Production of Phosphoric Acid from Phosphate Slimes with High Chloride Content," *Proceedings,* IFA Technical Conference, TA/82/10, Greece, 1982.
[*11*] Cogan, E., "Development, Testing and Use of a New Erosion-Corrosion Resistant, Austenitic Stainless Steel," *Corrosion Reviews,* Vol. 7, No. 4, 1987, p. 311.
[*12*] Schorr, M. et al., "Use of Clays for Corrosion Control in WPA Production" *Proceedings,* 8th Israel Minerals Engineering Conference, 1986, (Hebrew).

Section III: Atmospheric Tests

Sheldon W. Dean[1]

Corrosion Testing of Metals Under Natural Atmospheric Conditions

---

REFERENCE: Dean, S. W., "**Corrosion Testing of Metals Under Natural Atmospheric Conditions,**" *Corrosion Testing and Evaluation: Silver Anniversary Volume, ASTM STP 1000*, R. Baboian and S. W. Dean, Eds., American Society for Testing and Materials, Philadelphia, 1990, pp. 163–176.

ABSTRACT: Atmospheric corrosion has been a significant cause of metal degradation ever since metals have been used. The testing of metals for their performance in the atmosphere has been carried out for about 80 years. The early tests focused on the performance of materials in various atmospheric conditions so that accurate estimates of useful lives could be obtained. This work showed that sulfur dioxide from fuel combustion and chlorides from marine sources were the main accelerants of atmospheric corrosion. More recently, the focus of testing has changed to determine how variations in atmospheric constituents affect corrosion of metals. Standardization has become more important in carrying out tests and evaluation of results as well as evaluating the corrosivity of the atmosphere. The concept of standard classification of the atmospheres is discussed along with some outstanding issues in atmospheric corrosion testing.

KEY WORDS: atmospheric corrosion, time of wetness, sulfation plate, classification of atmospheres, weathering steel, acid precipitation, site monitoring, chloride candle, particulates, kinetics

It has been known for centuries that most metals, when exposed to natural atmospheric conditions, will corrode and the degradation that this corrosion causes is a significant fact limiting the useful life of the metal object. Some recent examples of atmospheric corrosion causing significant damage include: the cables supporting the Williamsburg Bridge over the East River in New York City have become significantly corroded and consequently their load-bearing capacity has been degraded [*1*]; the cast iron components of the dome on the tower of the Philadelphia City Hall had to have major repair and in some cases replacement because of atmospheric corrosion [*2*]. Many other examples of atmospheric corrosion damage can be cited.

Atmospheric corrosion generally is considered to be corrosion that occurs from exposure of metals to atmospheric conditions, including natural environmental conditions with precipitation and dew. Atmospheric corrosion damage includes general attack, cracking, and localized corrosion, although this paper will be concerned mainly with general attack. Atmospheric corrosion does affect buildings and other structures such as bridges, towers, monuments, fences, barriers, and signs. It also affects automobiles, trucks, railcars, aircraft, ships, and other means of transportation. This paper will cover the development of atmospheric corrosion testing methods that have evolved with special emphasis on ASTM Committee G–1 activities and ISO/TC156 efforts. The role of standards in atmospheric exposure testing is highlighted together with a discussion of unresolved issues.

---

[1] Chief engineer—Materials, Air Products and Chemicals, Allentown, PA 18195-1501.

Although atmospheric corrosion has been recognized as a major cause of metal degradation for many years, it has been an ongoing challenge to make accurate predictions of the rate of atmospheric corrosion and the effectiveness of preventive measures. Shortly after the American Society for Testing and Materials was founded, the need for having reliable information on the performance of metals in the atmosphere was recognized [*3*]. It was further discovered that laboratory tests to simulate atmospheric corrosion were singularly unsuccessful. Consequently, it was decided to initiate atmospheric corrosion tests to determine the type of damage that occurred as well as the rate that damage was occurring. In this way ASTM has been a leader in recognizing atmospheric corrosion and attempting to measure it. Initial work that was done in this field showed that atmospheres vary greatly in their corrosivity, that urban and industrial areas have substantially higher corrosion rates for most engineering materials than rural areas, and furthermore, that marine environments and locations within a mile or two of the ocean surf also suffer higher corrosion rates than other inland areas [*4*].

Consequently, an informal classification system evolved for atmospheric exposures consisting of industrial, marine, and rural environments. It was determined that sulfur dioxide from combustion of fossil fuels was the primary corrodent that differentiated industrial areas and that chlorides from sea salt accelerated the corrosion in marine environments. In general, the acceleration of corrosion that occurred in marine atmospheres is different from that which occurred in industrial atmospheres in that it tends to cause localized corrosion in many alloys. This system of classifying atmospheric exposures gained wide acceptance in the field of atmospheric corrosion testing until about 1960 [*5*].

The role of ASTM in atmospheric corrosion testing up to this point had been divided among many different committees concerned with different metals and metal products, and the major emphasis had been to understand the performance of these metals and products in various atmospheres. With the formation of ASTM Committee G-1, Subcommittee 4 (G01.04) was given the responsibility for atmospheric corrosion testing. This responsibility now included testing to determine the performance of materials, standardization of test methods for atmospheric corrosion, the standardization of monitoring methods for exposure sites, and the promotion of knowledge concerning atmospheric corrosion [*6*].

Atmospheric Corrosion Testing in a Changing Environment

The decade of the 1960s was marked by a growing awareness that industrial activity was a major contributor to the pollution of the atmosphere. This pollution was causing a variety of problems deemed unacceptable. Consequently, restrictions were placed on environmental discharges. As a result of these new regulations, the sulfur dioxide concentrations in urban and industrial areas have decreased substantially in the United States. This has been accomplished by the construction of tall stacks mainly for coal-burning power plants that transport the sulfur-containing flue gases into the upper atmosphere where they become oxidized to sulfur trioxide and sulfuric acid. Nitrogen oxides are also present in these flue gases and become oxidized to nitric acid. As a result, the pH of precipitation hundreds of miles downwind from these stacks has been reduced substantially. This effect has been especially troublesome in rural areas that previously had been free of industrial pollutants. The problems of acid precipitation or acid rain have been noted both in the United States and in Europe [*7*].

An early concern with the discovery of acid precipitation was how it would affect atmospheric corrosion. Since the levels of gaseous pollutants have been reduced, the cost of achieving further reductions is higher, and so there has been a growing need and desire to determine a cost/benefit relationship between the levels of pollutants in the atmosphere and the damage that these pollutants cause. Accordingly, the Environmental Protection Agency along with other government agencies has been attempting to develop damage functions expressing the relationship between corrosion rates and the concentration of pollutants both in the gaseous atmosphere and precipitation [*8*].

It is very important in terms of pollution control laws to differentiate between damage caused by gases in the environment and substances present in precipitation because, as a general rule, only gases originating from sources that are nearby cause damage, while substances in precipitation may originate from sources hundreds or even thousands of miles away. The damage function concept then provides a way to assess the economic impact of the pollution so that a cost/benefit analysis can be carried out. Atmospheric cleanup has caused the average sulfur dioxide concentration at the industrial ASTM Newark/Kearny atmospheric exposure site to be lower than the rural ASTM State College site. [*9*]. Consequently, there is concern as to what the results from these sites will mean in ongoing and future ASTM exposure programs.

The Role of Standardization in Corrosion Testing

In ASTM prior to the formation of ASTM Committee G–1, atmospheric exposure tests were carried out by several committees to generate the data they needed for writing standards [*6*]. In many cases, rather carefully thought-out techniques were used to carry out these exposures but the procedures were not formalized as standards. With the formation of Committee G–1 and Subcommittee G01.04 on Atmospheric Testing, it was recognized that a standard on carrying out atmospheric exposures of metallic panels would be desirable. The ASTM Practice for Conducting Atmospheric Corrosion Tests on Metals (G 50–76) was written for this purpose. Subcommittee G01.04 was involved in several other projects, including initiation of exposure programs and review of the progress of exposure programs already under way.

As time progressed, the writing of standards has become a more important activity in Subcommittee G01.04. A variety of ASTM standards are now in place that are relevant to atmospheric corrosion testing. These are shown in Table 1 and include both the cleaning and evaluation of specimens and the visual evaluation of coated specimens. Monitoring of exposure sites has been another area of interest and activity. Techniques for using panels to monitor sites corrosivity are discussed in the ASTM Practice for Characteristics of Atmospheric Test Sites (G 92–86).

Galvanic corrosion in the atmosphere is another concern, and two standards have been written on this subject. One has completed the standardization process, The ASTM Test Method for Assessing Galvanic Corrosion Caused by the Atmosphere (G 104), and the other is in progress. ASTM G 104 was based on ISO 7441 developed by the International Organization for Standardization Technical Committee 156. Techniques for monitoring sulfur dioxide through sulfation plates and chloride deposition using wet candle techniques have been developed. The ASTM Practice for Monitoring Atmospheric SO_2 Using the Sulfation Plate Technique (G 91–86); describes the use of the sulfation plate technique to monitor SO_2 both at exposure sites and other locations. The chloride candle method is still under development.

The prediction of the performance of weathering steels has been a difficult challenge. Initial work showed that low levels of copper improved the performance of steels in the atmosphere, and consequently copper-bearing steels became popular for exterior applications. Subsequent work demonstrated that low-alloy steels performed even better than the copper-bearing steels. The development of weathering steel was based on this principle. Initially, limited short-term exposures of weathering steels indicated that those steels would

TABLE 1—*ASTM standards relevant to atmospheric exposure testing.*

Purpose	Designation	Notes
Specimen preparation	G 50	Flat panels
Specimen preparation	G 104	Galvanic specimen
Specimen cleaning	G 1	General mass loss
Specimen evaluation	G 33	Metal-coated steel
Specimen evaluation	G 46	Pitted samples
Specimen evaluation	B 537	Electroplated samples, pitting
Specimen evaluation	G 104	Galvanic panels
Specimen evaluation	New[a]	Galvanic wire on bolt
Exposure method	G 50	Flat panels
Exposure method	G 104	Galvanic panels
Site monitoring	G 84	Time of wetness
Site monitoring	G 91	Sulfation plate
Site characterization	G 92	Standard panel tests
Site monitoring	New[a]	Chloride candle
Alloy Resistance	G 101	Weathering steels

[a] Standards currently under development.

lose about half as much metal as copper-bearing steels, which in turn lost about half as much metal as plain carbon steels. Consequently, the specifications for weathering steels were written in this way. However, it was soon observed that steels generally show corrosion rates that decrease with exposure time and weathering steels show a greater decrease than other steels. Furthermore, the extent to which these decreases occurred was a strong function of the atmospheric conditions that prevailed during the test period. Consequently, there was a need to have a method for estimating what the performance of a low-alloy steel would be to determine its suitability as a weathering steel.

A study of the performance of steel alloys in the atmosphere as a function of composition was carried out and reported by Larrabee and Coburn [*10*]. The results of this study were analyzed by Legault and Leckie [*11*]; this analysis provided a quantitative evaluation of the effects of alloy element on atmospheric corrosion in a controlled exposure. This analysis was used by Subcommittee G01.04 to define an arbitrary corrosion resistance index based on steel composition. The composition range of weathering steel was used to set limits for this corrosion resistance index. The new ASTM Guide for Estimating the Atmospheric Corrosion Resistance of Low Alloy Steels (G 101–89) was developed using this corrosion resistance index to determine if a low-alloy steel of known composition will perform as a weathering steel in environmental exposures. The previous approach of requiring that weathering steel be twice as resistant as copper-bearing steels would require that no steel could be used as a weathering steel until corrosion tests have been performed to establish its performance [*12*]. There are no tests except atmospheric exposure that would be suitable, and any reasonable atmospheric exposure would require several years to achieve reliable results. In addition, the variability of atmospheric exposure results, especially in a short-term test, makes any evaluation of corrosion resistance questionable. The ASTM G 101 approach provides an absolute basis for the evaluation that does not require exposures or the delays that such testing would require.

ISO

The International Organization for Standardization (ISO) has formed Technical Committee TC156 for the purpose of writing corrosion testing standards. At its first meeting in

TABLE 2—*ISO standards on atmospheric corrosion and atmospheric corrosion testing.*

Designation	Title
ISO7441	Determination of Bimetallic Corrosion in Outdoor Exposure
DIS8565	Atmospheric Corrosion Testing–General Requirements for Field Tests
DP9223	Classification of Corrosivity Categories of Atmospheres
DP9224	Guiding Values for the Corrosivity Categories of Atmospheres
DP9225	Aggressivity of Atmosphere—Method of Measurement of Pollution Data.
DP9226	Method of Determination of Corrosion Rate of Standard Specimen for the Evaluation/Corrosivity

Riga, USSR in 1976, ISO/TC156 identified atmospheric corrosion testing as a priority area for standards development. Subsequently, Working Group 3 was organized for the purpose of writing standards on atmospheric corrosion testing. Working Group 4 was organized for the purpose of developing a classified method to classify the corrosivity of the atmosphere. Working Group 3 has produced two ISO standards: one on galvanic corrosion testing in the atmosphere and the other on a general method of corrosion testing. Working Group 4 has produced four draft standards on the subject on classifying the atmosphere and using the classification techniques to predict long-term atmospheric corrosion performance of materials of construction. These standards are listed in Table 2.

Working Group 4 has also undertaken a major worldwide atmospheric exposure program to attempt to develop a basis for using the proposed procedure for evaluating atmospheric corrosivity [*13*]. This program is known as ISO-CORRAG. The United States is participating in this program through ASTM Committee G–1. Eleven other countries throughout the world are also participating in this program. They are listed in Table 3.

Classification of Atmospheres

The traditional approach of classification of atmospheres has been to make a determination based on the surroundings, e.g., industrial, urban, or rural. One problem with this approach is that there are different degrees of industrial activity and differences with regard to urban density, types of fuel in use, and proximity to surf. To account for these variations, compound classes such as mild industrial-marine have been used. This approach has not provided a quantitative classification approach that would allow a prediction of site corrosivity. This

TABLE 3—*Exposure sites in ISO CORRAG program.*

Country	Number of Sites	Climate	Type of Atmosphere
Canada	1	Moderate	Industrial
Czechoslovakia	3	Moderate	Urban, industrial, rural
FGR	1	Moderate	Industrial
Finland	3	Moderate	Urban, rural
France	9	Moderate	Marine, rural, industrial, urban
Japan	1[a]	Moderate	Urban
Norway	6	Moderate, cold	Urban, industrial, marine
Spain	4	Moderate	Urban, rural, industrial, marine
Sweden	3	Moderate	Urban, marine
UK	4	Moderate	Urban, marine, rural, industrial
USA	6	Moderate, tropical	Rural, urban, marine, industrial
USSR	4	Moderate, cold	Marine, urban, rural

[a] Two more sites may be included.

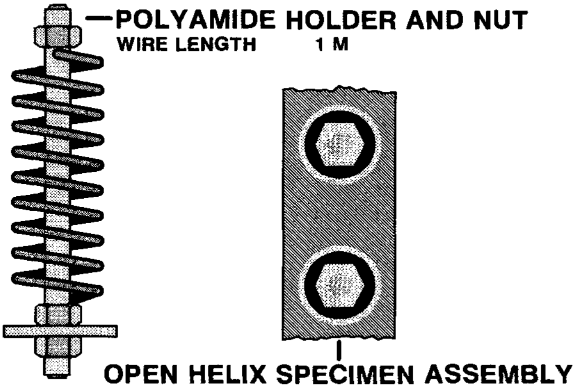

FIG. 1—*Open helix specimen assembly.*

problem has now been compounded by the pollution control regulations that make even heavy industrial areas low in sulfur dioxide. Therefore, tests done previously in these areas are no longer representative of the site corrosivity of these areas. Fortunately, in many cases, the most severely corrosive areas have improved substantially, but rural areas are somewhat more severe than previously measured because of increased acidity in the precipitation. Consequently, there is a real need for a quantitative system of classifying atmospheric corrosivity.

The ISO/TC156 activity to develop a quantitative system of classifying atmospheric corrosivity hopefully will address this need [*14*]. There are two approaches for assessing site corrosivity. One approach requires that standard specimens of relatively pure aluminum, steel, copper, and zinc be exposed for a one-year period. Flat panels, 100 by 150 mm in size, or wire helices, Fig. 1, may be used. The corrosion mass loss is measured and the site corrosivity is determined from these mass loss values. Because different metals respond to compounds in the atmosphere differently, it is possible that the corrosivity class for different metals could be different at the same location. Table 4 shows the corrosivity classes based on one-year corrosion mass loss values for the four specimen metals.

The other approach is to obtain measurements or estimates of the sulfur dioxide concentration, chloride deposition, and time of wetness at the location in question. A variety of techniques are available for measuring or estimating these quantities. For example, the time of wetness may be measured using a sensor such as is described in the ASTM Practice for Measurement of Time of Wetness on Surfaces Exposed Wetting Conditions as in Atmospheric Corrosion Testing (G 84–84). Alternatively, the time of wetness may be estimated by measurements of the relative humidity and calculation of the fraction of the time that the relative humidity is greater than 80% and the temperature is above freezing. After the

TABLE 4—*ISO/TC156 corrosivity classes for metals based on one-year exposure results, mass losses.*

Steel, g/m^2	Copper, g/m^2	Aluminum, g/m^2	Zinc, g/m^2	Corrosion Category
<10	<0.9	~0	<0.7	1
10–200	0.9–5	<0.6	0.7–5	2
201–400	5–12	0.6–2	5–15	3
401–650	12–25	2–5	15–30	4
>650	>25	>5	>30	5

TABLE 5—*Wetness class based on time of wetness.*

Wetness Class	Time Wet, %	Hours Wet per Year	Examples of Occurrence
T1	<0.1	<10	Indoor
T2	0.1–3	10–250	Indoor, unheated
T3	3–30	250–2600	Shed storage or cold climate
T4	30–60	2600–5200	Outdoor temperate climate
T5	>60	>5200	Tropical outdoor or surf

time of wetness is known, a wetness class, T, is determined from Table 5. Sulfur dioxide, P, and chloride, S, classes are determined in a similar manner from Table 6. The corrosivity class is then determined from Table 7 using all three of the input classes. This procedure is shown schematically in Fig. 2.

After the corrosivity class is obtained by either method the extent of corrosion damage can be estimated for either short- or long-term exposures using Table 8. The values in Table 8 show ranges of performance one might expect, and for practical purposes this is probably adequate.

One important drawback to this approach is that it does not take into account the acid precipitation effect. It also does not give information on sheltering effects or on microclimate effects that occur from situations such as puddles, cool spots, splash, dirt accumulation, etc. These local situations can cause substantially accelerated corrosion in some cases.

Current Issues in Corrosion Testing

Site Monitoring

With the rather substantial changes in environmental conditions at ASTM sites, it is apparent that the qualitative definitions of what a site is are no longer descriptive of the corrosion performance that can be expected. For example, industrial sites in the United States are no longer locations with high sulfur dioxide contents, and consequently the atmosphere may not be as corrosive as it has been previously [*9*]. On the other hand, rural sites are now experiencing acid precipitation, and thus more damage may be appearing in these locations than previously experienced. The initial results of the ISO-CORRAG exposure test programs have shown little difference between rural and industrial sites [*23*]. In future exposure tests at ASTM sites and others, it will be more important to obtain environmental data or at least exposure of control test materials so that there can be a measurement of the site corrosivity. A measurement of other site characteristics, such as the sulfur dioxide concentration, may also be helpful in terms of estimating the importance of

TABLE 6—*Sulfur dioxide and chloride classes.*

SO_2			Chloride	
SO_2 Class	Deposition Rate, $mg/m^2/day$	Concentration, mg/m^3	Cl Class	Deposit Rate, $mg/m^2/day$
P0	<10	<12	S0	<3
P1	10–35	12–40	S1	3–60
P2	36–80	41–90	S2	61–300
P3	81–200	91–250	S3	>300

TABLE 7—*Corrosion classes for environmental classes.*

SO_2 Class	T2			T3			T4			T5		
	S0–S1	S2	S3	S0–1	S2	S3	S0–S1	S2	S3	S0–S1	S2	S3
Unalloyed Steels												
P0–P1	1	2	3–4	2–3	3–4	4	3	4	5	4	5	5
P2	1–2	3–4	3–4	3–4	3–4	4–5	4	4	5	5	5	5
P3	2	3	4	4	4–5	5	5	5	5	5	5	5
Zinc and Copper												
P0–P1	1	1–2	3	3	3	3–4	3	4	5	4	5	5
P2	1–2	2	3	3	3–4	4	3–4	4	5	5	5	5
P3	2	3	3–4	3	3–4	4	4–5	5	5	5	5	5
Aluminum												
P0–P1	1	2–3	4	3	3–4	4	3–4	3–4	5	4–5	5	5
P2	1–2	3–4	4	3	4	4–5	3–4	4	5	4–5	5	5
P3	2–4	4	4	3–4	4–5	5	4–5	5	5	5	5	5

Note: T = Wetness class; P = SO_2 class; S = Chloride class.

the site variables on the corrosion process. This can then allow the investigator to predict how material will perform in other atmospheric environments.

Top Side-Bottom Side

A major concern of any exposure program is the interpretation of the data that is obtained. A 100 by 150 mm panel exposed at an angle of 30° horizontal facing south is a very convenient test configuration. The issue, however, is how to take this information and apply it to other exposures, even in the same location. Many investigators have noted differences between the top and the bottom side of the panel [*15*]. The top side of the panel tends to have more

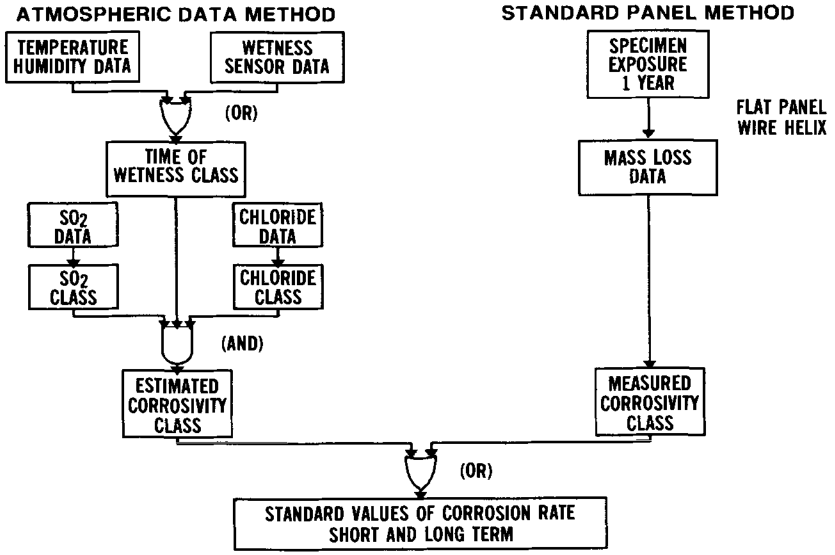

FIG. 2—*Schematic information flow diagram of the alternative approaches to atmospheric corrosivity classification.*

TABLE 8—*Atmospheric corrosion rates for corrosion class, μm/year.*

Corrosion Class	Steel		Copper		Zinc		Aluminum		Weathering Steel	
	ST	LT	ST	LT	ST	LT	ST	LT	ST	LT
1	<0.5	<0.1	<0.01	<0.01	<0.1	<0.01	<0.01	<0.01	<0.1	<0.1
2	0.5–2	0.1–1.5	0.01–0.1	0.1–0.1	0.1–0.5	0.01–0.5	0.01–0.025	0.01–0.02	0.1–2	0.1–1
3	2–10	1.5–6	0.1–2	0.1–1.5	0.5–2	0.5–2	0.025–0.2	0.02–0.2	2–8	1–4
4	10–35	6–20	2–3	1.5–3	2–4	2–3.5	0.2–1.0	0.2–1	8–15	4–10
5	>35	>20	>3	>3	>4	3.5–8	>1.0	>1.0	>15	>10

NOTE: ST = Average corrosion rate during the first ten years of exposure; LT = Steady state corrosion rate for long-term exposures.

exposure to rain and particulates. However, the rain exposure tends to wash off the particulates that accumulate. Unfortunately, there is no general rule on the relative behavior of the top side of the panel versus the bottom side. The ISO CORRAG program has employed both flat panels and wire helices. Wire helices do not have a top side-bottom side configuration but exposure occurs at all angles. It has been rather widely observed that the helices tend to corrode at a higher rate than the flat panels, but the reason for this difference in behavior has not been apparent [*16*].

Time of Wetness

Many investigators have noticed that panels exposed to the atmosphere go through periods of being wet and then drying out. The wet periods seem to be the time when corrosion occurs, and so it has been of interest to measure the time of wetness and use this time as the basis for calculating corrosion damage. Wetness can occur from either dew or precipitation. In general, dew formation appears to be more damaging than precipitation because the time of wetness from dew is longer and dew equilibrates with the acid gases in the atmosphere rapidly. On the other hand, dew formation seldom yields sufficient moisture to cleanse the surface to any significant degree.

A variety of techniques have been proposed for measuring time of wetness. Initially, this was done by means of a zinc panel with platinum strips and an electronic device that switched on a timer when a potential developed between the zinc and platinum [*17*]. This device was rather unwieldly, and its results appeared to be dependent on the method of attaching the platinum strips to the zinc electrode. More sophisticated devices have been developed that can be used not only for time of wetness in atmospheric exposures but also are applicable for use inside building walls and other places with difficult access. The detection principle is based on a galvanic couple between either gold and zinc or gold and copper. A standard based on this type of device was developed by ASTM Committee G-1 (ASTM G 84).

Another approach to the time of wetness concept came out of the Kucera-Mattsson atmospheric corrosion monitor [*18*]. This technique was studied in some detail by Mansfeld who showed that it could be used to measure time of wetness [*19*]. Two variations of this approach have been used. One employs a steel-copper couple and a zero-resistance ammeter to monitor current flow between these electrodes. The other approach employs two steel electrodes and a polarization resistance approach to detect wetness.

Another approach to time of wetness is to measure the relative humidity as a function of time and assume that wetness occurs when the relative humidity exceeds 80% [*20*]. This is the basis of the ISO TC156 WG4 temperature humidity complex. It has been widely recognized that these different techniques for measuring time of wetness give different results; however, the more surprising consequence is that the variations in time of wetness are relatively small when measured by different techniques. For practical purposes, these differences have little effect on estimates of corrosion damage.

Sheltering

Another concern is the question of sheltering. It has been observed that corrosion in sheltered areas is often quite different from that which occurs in bold exposures. Weathering steels, for example, are less able to develop protective patinas in sheltered areas, especially in areas where loose corrosion products and dirt can accumulate. It is therefore important to be able to run tests in the atmosphere that will anticipate the problems of sheltered areas. A variety of techniques have been used in the past, including louvered boxes and roofs over exposure sites. However, more work needs to be done to understand the behavior of materials in these types of exposures.

Other Pollutants

There is no question that chlorides from marine sources and elsewhere are a major factor in contributing corrosive components to atmospheric exposures. However, with the reduction in local sulfur dioxide concentrations, other gases in the atmosphere may begin to have important roles. It is known, for example, that aluminum alloys at West Coast locations experience higher corrosion rates than other locations. This has been attributed to the presence of nitrogen oxides in the atmosphere, perhaps in the absence of sulfur dioxide [*21*]. It is not clear, however, why nitrogen oxides should affect the corrosion rate of aluminum and not other metals such as copper alloys. It is also not clear how one should measure the nitrogen oxide concentrations in the atmosphere or in precipitation.

Sulfation Plates

The sulfation plate technique for monitoring sulfur dioxide in the atmosphere was developed as an inexpensive monitoring technique that would integrate the exposure of sulfur dioxide over a reasonably long period of time, for example, 30 days. Another approach to monitoring sulfur dioxide exposure is to take atmospheric samples and measure the sulfur dioxide contents at regular intervals, such as every few minutes or every hour. Of course this approach is substantially more expensive and requires rather sophisticated equipment at the exposure sites in order to obtain the samples and carry out the analysis technique and record the results. It also requires that electric power be available at each exposure site where the monitoring is carried out.

Another approach is to use a wet candle for sulfur dioxide absorption. However, wet candles require even more attention than the sulfation plate because the wet candle needs to be changed once a week. It also occupies more space and is more subject to problems such as freezing. Neither the sulfation plate, nor the volumetric sampling, nor the wet candle techniques are useful for measuring sulfur content in precipitation. The sulfation plate will pick up sulfuric acid aerosols where these would tend to be lost in a volumetric sample.

One unanswered question regarding sulfation plates is whether the sulfation plate is more effective when the lead peroxide is wet from dew than when the plate is dry. It seems likely that the wet peroxide would be more effective and in this way would simulate corrosion product-covered surfaces better than the volumetric sampling process. Also, the mass transfer to a horizontal surface such as a sulfation plate is affected by the local wind currents in a similar manner to a flat panel. Consequently, a sulfation plate should give a somewhat weighted average of sulfur flux to the surface rather than a measure of the bulk concentration of sulfur dioxide. It should be noted that sulfation plates are normally exposed in an inverted orientation to exclude sulfates from precipitation. This should not affect the kinetics of mass transfer of sulfur dioxide from the air to the reactive surface, but it should be noted that the technique is not truly similar to flat panel or other geometries, and so the results must be viewed as approximations of service conditions.

In the case of the wet candle technique, for both chloride and sulfur dioxide the exposed area is in question. In the case of the conventional wet candle, the area should probably be the surface of the tube used to construct the wet candle; however, the extrapolation of a vertical cylinder to a flat panel or some other orientation does raise some questions. All of these questions leave some room for doubt on how to interpret the results of the measurements.

Particulates

Many investigators have noted that the particulates are a source of concern in atmospheric corrosion. Pitting on the skyward side of panels exposed in industrial locations has been associated with the deposition of fly ash [*22*]. Loose rust deposits on weathering steels have created conditions that have lead to the formation of nonprotective rust layers. It is likely that particulates cause other corrosion problems; for example, particulates are known to aggravate the corrosion of auto body steels, especially in occluded areas. It is not apparent how one can determine the effect of particulates in simple tests, and furthermore, it is not obvious that all particulates behave in the same way. More work is necessary to characterize this problem. In particular, it would be desirable to use standard procedures to measure the quantity and types of particulate matter that deposit on corrosion specimens.

Evaluation

Another area of importance in atmospheric corrosion testing of metals is the question of evaluation results. Normal procedure has been to clean the corrosion products from the specimens' surfaces at the end of the exposure and to obtain mass loss and pit depth and possibly change in tensile properties of the exposed panel. More recently, investigators have looked at the crystal structure and morphology of the corrosion product films that develop on atmospheric specimens [*23*]. Also, microanalysis techniques such as electron microprobe surveys reveal interesting results and sometimes have been able to explain the behavior of materials.

Atmospheric corrosion testing generally leads to nonlinear kinetics. This is especially true in relatively short-term exposures and is probably a result of the development of a semi-protective corrosion product film on the specimen surface. As time goes on this film tends to thicken and becomes more protective. Consequently, mass loss versus time curves can usually be best correlated by using an expression of the type

$$M = Kt^n \tag{1}$$

where:

m = the total mass loss caused by corrosion per unit of the exposed area, with typical units of g/m^2,
t = the exposure time, typically years,
K = a proportionality constant, and
n = the mass loss exponent.

This expression of kinetics has been generally observed for steels, especially weathering steels and aluminum alloys. In these cases, the mass loss exponent generally varies between 0.5 and 1. Generally, the smaller the mass loss exponent, the more protective the coating and the better the long-term performance of the alloy. Zinc alloys generally show mass loss exponents very close to 1. Copper alloys, on the other hand, do not generally follow these kinetics. The power law function has been criticized as an approach for extrapolating long-term corrosion behavior on the grounds that ultimately linear kinetics should prevail and, if the power law relationship is used beyond its range of applicability, it will seriously underestimate the resulting corrosion damage. Unfortunately, the transition time from power law to linear kinetics has not been well established. Further work to develop good reliable models for the kinetic behavior of metals in atmospheric exposures would be very helpful, both in interpreting results and in making long-term predictions.

Conclusions

1. The environment in the United States has become significantly less corrosive in urban and industrial areas, particularly to ferrous metals such as zinc and zinc alloys.
2. The emphasis of atmospheric corrosion testing in recent years has changed from the measurement of how materials behave in various atmospheric conditions to how environment variables affect the kinetics of degradation of various materials.
3. Because the atmosphere has changed rather substantially in recent years, it has become much more important to characterize atmospheres where tests are carried out and develop techniques for predicting how materials will behave under different atmospheric conditions.
4. Standards for atmospheric testing, site monitoring, and specimen evaluation have played an important role in technology development and increasingly there will be a need for better and more sophisticated standards in this area.
5. More work has been done on the development of models for atmospheric corrosion including more sophisticated kinetic expressions. There will continue to be a need to refine these models.

Acknowledgments

The author is grateful to Air Products and Chemicals, Inc. for permission to publish this paper.

References

[1] Eiselstein, L. E. and Caligiuri, R. D., "Atmospheric Corrosion of the Suspension Cable on the Williamsburg Bridge," *Degradation Metals in the Atmosphere, ASTM STP 965*, S. W. Dean and T. S. Lee, Eds., American Society for Testing and Materials, Philadelphia, 1988, pp. 78–95.

[2] "Coating System to Help a Landmark Last Another 100 Years," *Plating and Surface Finishing*, Vol. 76., No. 7, 1989, pp. 20–23.

[3] Coburn, S. K., "Introduction," *Atmospheric Factors Affecting the Corrosion of Engineering Metals, ASTM STP 646*, S. K. Coburn, Ed., American Society for Testing and Materials, Philadelphia, 1978, pp. 1–4.

[4] Swandby, R. K., "Corrosives," *Corrosion Resistance of Metals and Alloys, Second Edition*, F. L. La Que and H. R. Copson, Eds., Reinhold Publishing Co., New York, 1963, p. 47.

[5] Mattsson, E. and Lindgren, S., "Hard-Rolled Aluminum Alloys," *Metal Corrosion in the Atmosphere, ASTM STP 435*, American Society for Testing and Materials, Philadelphia, 1968, pp. 240–256.

[6] Ailor, W. H., "ASTM Atmospheric Corrosion Testing: 1906 to 1976," *Atmospheric Factors Affecting the Corrosion of Engineering Metals, ASTM STP 646*, S. K. Coburn, Ed., American Society for Testing and Materials, Philadelphia, 1978, pp. 129–151.

[7] "Acidification Today and Tomorrow," a Swedish study prepared for the 1982 Stockholm Conference on the Acidification of the Environment, translated from the Swedish by Simon Harper, Swedish Ministry of Agriculture, 1982, pp. 102–110.

[8] Haynie, F. H., "Environmental Factors Affecting the Corrosion of Galvanized Steel," *Degradation of Metals in the Atmosphere, ASTM STP 965*, S. W. Dean and T. S. Lee, Eds., American Society for Testing and Materials, Philadelphia, 1988, pp. 282–289.

[9] Lipfert, F. W., "Effects of Acidic Deposition on the Atmospheric Materials," *Materials Performance*, Vol. 26, No. 7, July 1987, pp. 12–19.

[10] Larrabee, C. P. and Coburn, S. K., *Proceedings, First International Congress on Metallic Corrosion*, Butterworth, London, 1962, p. 276.

[11] Legault, R. A. and Leckie, H. P., "Effect of Alloy Composition on the Atmospheric Corrosion Behavior of Steels Based on a Statistical Analyses of the Larabee-Coburn Data Set," *Corrosion in Natural Environments, ASTM STP 558*, American Society for Testing and Materials, Philadelphia, 1974, pp. 334–347.

[12] Komp, M. E., "Atmospheric Corrosion Ratings of Weathering Steel—Calculation and Significance," *Materials Performance*, Vol 26, No. 7, July 1987, pp. 42–44.

[13] Dean, S. W., "ISO CORRAG Collaborative Atmospheric Exposure Program: A Preliminary Report," *Degradation of Metals in the Atmosphere, ASTM STP 965*, S. W. Dean and T. S. Lee, Eds., American Society for Testing and Materials, Philadelphia, 1988, pp. 385–431.

[14] Dean, S. W., "A New Quantitative Approach to Classifying Atmospheric Corrosion—ISO Breaks New Ground," *Standardization News*, Vol. 15, No. 5, May 1987, pp. 36–39.

[15] Legault, R. A. and Pearson, V. P., "Kinetics of the Atmospheric Corrosion of Galvanized Steel," *Atmospheric Factors Affecting the Corrosion of Engineering Metals, ASTM STP 644*, S. K. Coburn, Ed., American Society for Testing and Materials, Philadelphia, 1978, pp. 83–96.

[16] Dean, S. W., "ISO CORRAG Collaborative Atmospheric Exposure Program—First Exposure Report on United States Program," Report to ASTM Committee G-1, January 1989.

[17] Grossman, P. R., "Investigation of Atmospheric Exposure Factors that Determine Time-of-Wetness of Outdoor Structures," *Atmospheric Factors Affecting the Corrosion of Engineering Metals, ASTM STP 646*, S. K. Coburn, Ed., American Society for Testing and Materials, Philadelphia, pp. 5–16, 1978.

[18] Kucera, V. and Mattsson, E., "Electrochemical Techniques for Determination of the Instantaneous Rate of Atmospheric Corrosion," *Corrosion in Natural Environments, ASTM STP 558*, American Society for Testing and Materials, Philadelphia, 1974, pp. 239–260.

[19] Mansfeld, F., "Evaluation of Electrochemical Techniques for Monitoring of Atmospheric Corrosion Phenomena," *Electrochemical Corrosion Testing, ASTM STP 727*, F. Mansfeld and V. Bertocci, Eds., American Society for Testing and Materials, Philadelphia, 1981, pp. 215–237.

[20] Knotkova-Cermakova, D. and Barton, K., "Corrosion Agressivity of Atmospheres (Derivation and Classification)," *Atmospheric Corrosion of Metals, ASTM STP 767*, S. W. Dean and E. C. Rhea, Eds., American Society for Testing and Material, Philadelphia, 1982, pp. 225–249.

[21] Byrne, S. C. and Miller, A. C., "Effect of Atmospheric Pollutant Gases on the Formation of Corrosive Condensate on Aluminum," *Atmospheric Corrosion of Metals, ASTM STP 767*, S. W. Dean and E. C. Rhea, Eds., American Society for Testing and Material, Philadelphia, 1982, pp. 359–373.

[22] Dean, S. W. and Anthony, W. H., "Atmospheric Corrosion of Wrought Aluminum Alloys During a Ten-Year Period," *Degradation of Metals in the Atmosphere, ASTM STP 965*, S. W. Dean and T. S. Lee, Eds., American Society for Testing and Materials, Philadelphia, 1988, pp. 191–205.

[23] Kihira, H., Ito, S., and Murata, T., "Quantitative Classification of Patina Conditions for Weathering Steel Using a Recently Developed Instrument," *Corrosion*, Vol. 45, No. 4, April 1989, pp. 347–352.

DISCUSSION

W. W. Kirk[2] (*written discussion*)—In response to Mr. Kinstler's question regarding time-of-wetness sensing, Subcommittee G01.04 is currently reviewing ASTM Standard Practice

---

[2] Chairman, ASTM Subcommittee G01.04, La Que Center for Corrosion Technology, Wrightsville Beach, NC 28480.

for Measurement of Time-of-Wetness on Surfaces Exposed to Wetting Conditions as in Atmospheric Corrosion Testing (G 84). A notation is included in that standard stating that the Sereda sensor is available commercially from Epitek Electronics, Ltd., Kanata, Ontario, Canada. A recent telephone check confirmed that the sensor is being manufactured and is, indeed, available.

S. W. Dean (*author's closure*)—I appreciate Mr. Kirk's discussion on the availability of G 84 sensors. Having these devices readily available should make the use of the time-of-wetness measurement a desirable component of atmospheric exposure studies as well as in other applications where moisture condensation may occur.

Earl A. Baker[1] *and W. W. Kirk*[1]

Long-Term Atmospheric Corrosion Behavior of Various Grades of Stainless Steel in Rural, Industrial, and Marine Environments

REFERENCE: Baker, E. A. and Kirk, W. W., **"Long-Term Atmospheric Corrosion Behavior of Various Grades of Stainless Steel in Rural, Industrial, and Marine Environments,"** *Corrosion Testing and Evaluation: Silver Anniversary Volume, ASTM STP 1000,* R. Baboian and S. W. Dean, Eds., American Society for Testing and Materials, Philadelphia, 1990, pp. 177–190.

ABSTRACT: Stainless Steels have been used in outdoor applications for many years. The classic example is the roof of the Chrysler Building in New York City that was constructed in 1926; it has been cleaned only once (in 1961) to remove surface deposits and restore its original gleam. Architecture, industry, and transportation (land, air, water, and space) all utilize stainless steels, and the list of components in each is endless.

Eleven grades of stainless steel were evaluated after 29 years of exposure at two ASTM test sites: the rural atmosphere at State College, PA and the industrial atmosphere at Newark/Kearny, NJ. Previous evaluation of these same materials from the Kure Beach, NC 25- and 250-m marine sites have been reported and are referenced in this paper. The alloys evaluated include 200, 300, and 400 series stainless steels. This paper dwells on results from the rural and industrial sites, but summarizes alloy corrosion behavior from the mildest rural atmosphere to the most severe marine environment.

All materials at each site had the same general appearance, and no significant corrosion was evident. In the rural atmosphere, all stainless steel surfaces remained virtually unchanged after 29 years of exposure. In the industrial atmosphere, all alloy surfaces were dark brown to black in color, resulting from the deposit of industrial airborne particles. These deposits could be removed by brisk rubbing with a wet cloth and nonabrasive cleanser, nearly returning the surfaces to their original appearance.

No evidence of stress corrosion cracking was found around any welds or Erichsen cups. Mechanical properties of all alloys were unaffected by these long exposures.

KEY WORDS: stainless steels, atmospheres, rural, industrial, marine, long-term corrosion, reflectivity, pitting, mechanical properties, welds, Erichsen cups

Stainless steels have been used successfully for many years in various environments for architectural applications, sculptures, transportation vehicles, and other components. Historically, the austenitic grades of stainless steel have been chosen for these applications. *The Book of Stainless Steels* [*1*], published in 1933, describes the use of stainless steel in the Chrysler Building in New York City, and the architect predicted a wonderful future for stainless steels in architecture. The Chrysler Building was first cleaned in 1961 [*2*], 32 years after its construction, to remove dirt deposited on the surface from the atmosphere.

In 1958, former ASTM Committee A–10 on Iron-Chromium, Iron-Chromium-Nickel, and Related Alloys established a test program to determine the long-term atmospheric corrosion

[1] Senior research technologist and president, respectively, LaQue Center for Corrosion Technology, Inc., P. O. Box 656, Wrightsville Beach, NC 28480.

behavior of various grades of stainless steel in rural, industrial, and marine environments. Guidelines were established that specified the types of materials, types of test panels, test panel preparation, and exposure test locations. These guidelines were distributed throughout industry to obtain the needed test panels for test exposure.

Removals of selected materials were conducted after three, five, and seven years from all sites as indicated in the ASTM annual proceedings of Committee A–10, Subcommittee IV from 1961 through 1969 [*3*].

Upon the merger of Committee A–10 with Committee A–1 on Steel, Stainless Steel, and Related Alloys in 1972, the program was continued with no further documented action until 1984. At that time, the LaQue Center for Corrosion Technology, Inc. (LaQue Center) initiated an evaluation of the test panels on exposure at its marine atmospheric test sites in Kure Beach (KB), NC. With the approval of Committee A–1 and Committee G–1 on Corrosion of Metals, test panels were removed from the Kure Beach 25- and 250-m sites and evaluated under the sponsorship of Inco Europe and the Nickel Development Institute (NiDI). Results from these evaluations have been published [*5*]. NiDI currently is sponsoring the evaluation of companion stainless alloys exposed at the ASTM test sites in State College (SC), PA, classified as a rural site, and Newark/Kearny (NK), NJ, historically classified as an industrial site. However, relatively recent results have been reported [*4*] which show the NK site to be only slightly more corrosive than a rural atmosphere during a 1976 to 1979 study.

The objective of this paper is to focus on the results gathered from the evaluation of stainless steels exposed in rural and industrial environments, introduce a new method to assess material performance, and present additional data gathered from marine atmospheric exposures.

Experimental Procedure

The following guidelines for the preparation of test panels, as identified in Tables 1 and 2, were established.

1. Flat Panels
   a. Each test panel was nominally 100 by 356 by 0.94 mm (+1.27, −0.79).
   b. Rolling direction was perpendicular to the 356–mm length.
   c. Panels of any given material were fabricated from the same heat (Tables 1, 2).
2. Spot Welded Panels
   a. Materials were supplied as 100 by 100 by 0.94 mm (+0.25, −0.00) and 100 by 200 by 0.94 mm (+0.25, −0.00) specimens for spot welding into panels 100 by 356 mm. The identification code was along one side, parallel to the direction of rolling.
3. *Arc Welded Panels*
   a. Materials were welded and sheared into panels 100 by 356 by 3.2 mm (+0.25, −0.13).
   b. Panels of any given material were fabricated from the same heat.
4. *Erichsen Cup Panels* [*ASTM Test Method for Ball Punch Deformation of Metallic Sheet Material* (*E 643–84*)]
   a. Material was supplied as 76 by 356 by 0.94 mm (±0.25) specimens.
   b. Panels were supplied with three Erichsen cups (two to 80% and one to 50% maximum depth of expected value for failure), equally spaced along the center line with the small cup in the center. The small cup and one large cup were drilled with a 6.35-mm drill.
5. *All Panels*
   a. Passed the boiling nitric acid test as outlined in ASTM Standard Practices for Determining Susceptibility to Intergranular Attack in Austenitic Stainless Steels (A 262/A 262M).

TABLE 1—*Materials used for corrosion evaluations.*

	Type of Panel						
AISI Type	Temper	Finish	Flat	Spot Welded	Arc Welded	Erichsen Cup	Supplier
201	Soft	Cold rolled	X	X	...	X	US Steel
201	1/4 hard	Cold rolled	X	...	...	...	US Steel
201	1/2 hard	Cold rolled	X	...	...	...	US Steel
201	3/4 hard	Cold rolled	X	X	...	...	US Steel
201	Soft	2B	...	...	X	...	US Steel
202	Soft	Cold rolled	X	X	...	X	Allegheny Ludlum
16-16-1	Soft	Cold rolled	X	...	...	X	Allegheny Ludlum
16-16-1	1/2 hard	Cold rolled	X	X	...	...	Allegheny Ludlum
301	Soft	Cold rolled	X	...	...	X	Allegheny Ludlum
301	1/4 hard	Cold rolled	X	X	...	...	Allegheny Ludlum
301	1/2 hard	Cold rolled	X	...	...	...	Allegheny Ludlum
301	3/4 hard	Cold rolled	X	X	...	...	Allegheny Ludlum
302	Soft	Cold rolled	X	X	...	X	Republic[a]
302	1/4 hard	Cold rolled	X	...	...	...	Republic
302	Soft	2B	...	...	X	...	Republic
302	Quenched	No. 4	X	...	...	...	Republic
302	Quenched	No. 7	X	...	...	...	Republic
304	Soft	Cold rolled	X	X	...	X	Republic
304	Soft	2B	...	...	X	...	Republic
304L	Soft	2B	...	...	X	...	Armco
316	Soft	Cold rolled	X	X	...	X	US Steel
316	Soft	2B	...	...	X	...	US Steel
316L	Soft	2B	...	...	X	...	Armco
321	Soft	2B	...	...	X	...	Eastern Rolling[b]
347	Soft	2B	...	...	X	...	Eastern Rolling
410	Annealed	No. 2	X	X	...	X	Crucible[c]
430	Soft	Cold rolled	X	X	...	X	Sharon

[a] Republic is now LTV Steel.
[b] Eastern Rolling is now Eastern Stainless Steel.
[c] Crucible is now Colt Industries.

TABLE 2—*Nominal Composition for Materials (principle elements), percent.*

Stainless Steel Type	Cr	Ni	C, max	Mo	Mn	N, max	Fe	Other
201	17	4.5	0.15	...	6.5	0.25	Balance	...
202	18	5	0.15	...	8	0.25	Balance	...
16-16-1	16	1	...	...	16	...	Balance	...
301	17	7	0.15	...	...	...	Balance	...
302	18	9	0.15	...	...	...	Balance	...
304	18.5	9.5	0.08	...	...	...	Balance	...
304L	18.5	10.0	0.03	...	...	...	Balance	...
316	17	12	0.08	2.25	...	...	Balance	...
316L	17	13	0.03	2.25	...	...	Balance	...
321	18	11	0.08	...	...	...	Balance	Ti = 5× C level min
347	18	11	0.08	...	...	...	...	Ti = 5× C level min Cb + Ta = 10× C level min
410	12	...	0.15	...	...	...	Balance	...
430	17	...	0.15	...	...	...	Balance	...

All test panels were sent to the LaQue Center, where they were sorted and distributed to the following six atmospheric test sites for exposure:

1. State College (SC), Pennsylvania (rural).
2. Newark/Kearny (NK), New Jersey (industrial).
3. Brazos River, Texas (industrial/marine).
4. Battelle, Columbus, Ohio (urban).
5. Kure Beach (KB), North Carolina (marine 25-m).
6. Kure Beach (KB), North Carolina (marine 250-m).

Test panels were exposed at the State College, PA, Newark/Kearny, NJ, and Kure Beach, NC test sites during May to October, 1958. Scheduled removals were made after three, five, and seven years, and the panels were distributed to different participating companies (Table 1) for evaluation. Unfortunately, no results have been found from those removals that relate to corrosion behavior or appearance. The only results available are mechanical properties measured after three years' exposure at the SC, NK, and KB sites. Duplicate test panels were removed from Kure Beach in 1984 after 26 years of exposure and at the State College, PA and Newark/Kearny, NJ test sites in 1987 after 29 years of exposure with the permission of ASTM Committees A-1 and G-1.

Over the years, several methods have been used to assess the performance of stainless steels in the atmosphere. The MDL Method (Manufacturing Development Laboratory of Ford Motor Co.) uses charts to convert the percent defective area (pits or corroded area) to a rating number [*5*]. This system is a part of the ASTM Practice for Rating of Electroplated Panels Subjected to Atmospheric Exposure (B 537). In an earlier paper [*6*], this system was used to rate the pit density on the surface of stainless steels exposed at Kure Beach, NC for 26 years. Also reported was the percent of the surface area that was covered by rust stain or visible rust, $Fe(OH)_3$.

Another paper [*7*] describes a photometric technique to analyze visible light reflectivity from the surface of stainless steels. A colorimeter (color difference meter) was used to analyze visible light reflectivity from the surface of stainless steel panels.

Being confronted with the fact that all the various grades of stainless steel at one test site can have the same appearance and no corrosion may be evident, some other objective method was needed to evaluate performance. It was necessary to compare some surface property with corresponding companion controls of the same heat that had not been exposed. This was done by measuring the reflectivity with a D&S Alphatometer Model A1, a miniaturized thermopile-type pyranometer that measures solar reflectivity, absorptivity, and transmissivity. To obtain reflectivity of a surface, the alphatometer is aimed at the sun, and the RD1 scaling digital voltmeter is adjusted to read 1.00 (100% reflectivity); then the alphatometer is aimed at the surface of interest, and the RD1 indicates reflectivity directly as a percentage of the maximum.

Reflectivity measurements were made on the various grades of stainless steel from the SC, NK, and KB test sites and were compared with measurements taken on companion unexposed controls from the original stock. These results now have documented the performance of eleven types of stainless steels, some with different cold-rolled tempers, in rural, industrial, and marine environments.

Chemical Analyses

Two materials, Types 304 and 316 stainless steel, were selected for chemical analysis as given in Table 3 to determine that the compositions were within established limits.

TABLE 3—*Chemical analysis of austenitic stainless steels exposed in the marine atmosphere for 26 years.*

	Weight %, Balance Fe								
	C	Mn	Si	Ni	Cr	Mo	P	S	N_2
Type 304 stainless steel, 25-m lot									
Nominal	0.08	2.00	1.00	8.0	18.0	...	0.045	0.030	...
composition[a]	max	max	max	10.5	20.0	...	max	max	...
Spectrographic, combustion, and wet chemical analysis	0.05	1.0	0.50	8.2	17.8[b]	0.40	0.01	0.021	0.05
Type 316 stainless steel, 25-m lot									
Nominal	0.08	2.00	1.00	10.0	16.0	2.0	0.045	0.030	...
composition[a]	max	max	max	14.0	18.0	3.0	max	max	...
Spectrographic, combustion, and wet chemical analysis	0.05	1.30	0.35	13.3	18.0	2.5	0.013	0.015	0.02

[a] Nominal composition, reference: *Metals Handbook,* Vol. 3, 9th ed., 1980.

[b] Slightly low but within the tolerance allowed on a check chemical analysis as noted in the ASTM Specification for General Requirements for Flat-Rolled Stainless and Heat Resisting Steel Plate, Sheet, and Strip (A 480/A 480M).

Mechanical Properties

Five materials (Types 201-1/2h, 301-1/2h, 302-1/4h, 304 ann, and 316 ann) were selected for mechanical properties evaluation. Samples tested were taken from storage (26 years), SC (29 years), NK (29 years), and KB 25- and 250-m lots (26 years). Since more rust staining was noted in the marine environments, five additional material conditions (Types 201 ann, 201-1/4 h, 301 ann, 301-1/4 h, 302 ann) were selected from the latter two sites for tension tests.

Corrosion Evaluation

All materials were evaluated for evidence of corrosion attack in the form of rust, rust stain, pitting, crevice attack, and cracking or weld failure. Panel surfaces were examined with a modified Unitron microscope with attached ONO Sokki digital linear gage.

Results

Rural Atmosphere

The various grades of stainless steel exposed in a rural test site at State College (SC), PA, as illustrated in Fig. 1, displayed the same general overall appearance. In 1987, after 29 years, panels of each type of stainless steel were removed from the test.

Since no difference in appearance among the alloys and no corrosion was evident, the reflectivity of each material (not cleaned) was measured and compared with the reflectivity of an unexposed control of the same material. The measurements taken are given in Table 4. The mechanical properties of Types 201, 301, 302, 304, and 316 were tested, and the results are given in Table 5.

The few particles or stain spots found on the side facing skyward appear to be related to deposits from birds, insects, vegetation, or simply water stains. The particles and stain spots could be removed easily with a damp cloth and mild soap. It is evident that the spots and

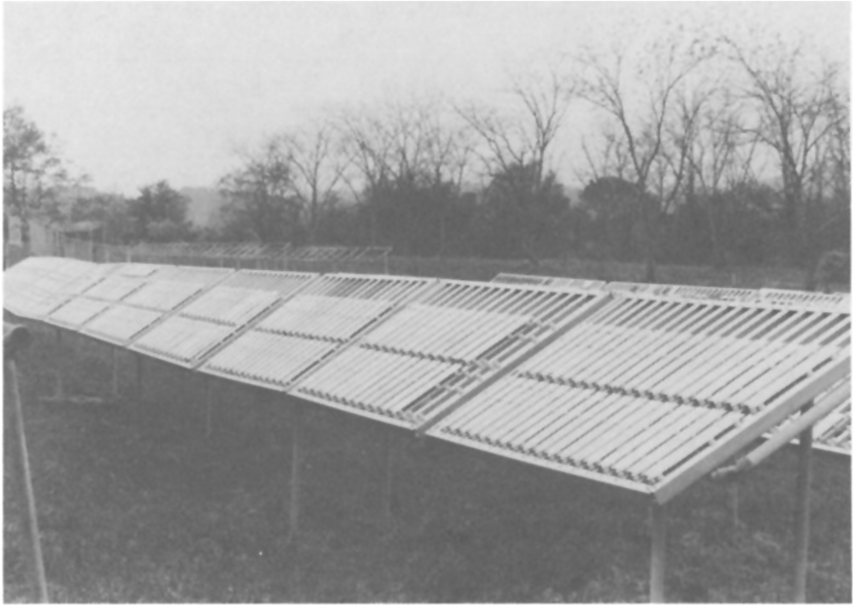

FIG. 1—*View of rural test site at State College, PA, where various grades of stainless steel have been on exposure for 29 years (1958 to 1987). The test panels are positioned at 30° to the horizontal facing south.*

stain cycle appear and disappear frequently due to weather conditions (rain or snow) and as seasonal changes occurred (pollen, insects, leaves, grass clippings, etc.).

All the stainless steels exposed in this rural environment exhibited the following qualities:

1. Original appearance retained.
2. Corrosion resistant.
3. Sound spot welds.
4. Sound arc welds.
5. No evidence of corrosion or cracking on either the surfaces in tension or in compression at the Erichsen cups.
6. No loss of mechanical properties.

Industrial Atmosphere

The various grades of stainless steel exposed in the industrial test site at Newark/Kearny (NK), NJ, as illustrated in Fig. 2, displayed the same general, overall appearance. A dark brown stain covered the skyward surface with scattered small, dark spots. These dark nodular spots (1 mm in diameter) are soft and have a consistency of tar or paint. An energy-dispersive X-ray (EDAX) analysis identified the presence of several elements in these deposits: aluminum, 1.1%; calcium, 3.6%; silicon, 4.2%; titanium, 3.8%; sulfur, 1.7%; chromium, 1.7%; potassium, 1.2%; and iron, 82.7%.

The relatively high levels of iron, titanium, silicon, and calcium suggest that the deposits are indeed paint. This same surface coverage was visible on all other specimens exposed at this site. Overspray from coating a nearby bridge or an industrial plant site are likely sources.

TABLE 4—*Reflectivity*[a] *of stainless steels after long term exposure in rural, industrial, and marine environments.*

		Rural State College, PA		Industrial Newark/ Kearny, NJ		Marine 250-m Lot Kure Beach, NC		Marine 25-m Lot Kure Beach, NC	
Material	Control	Sky	%[b]	Sky	%[b]	Sky	%[b]	Sky	%[b]
201 soft	58	58	100	27	46.6	47	81.0	28	48.3
201 1/4	63	63	100	32	58.8	59	93.7	29	46.0
201 1/2	68	68	100	33	48.5	58	85.3	31	45.6
201 3/4	68	67	98.5	33	48.5	57	83.8	32	47.1
201 2B	42	42	100	23	54.8	31	73.8	22	52.4
202 CR	58	58	100	31	53.4	51	87.9	26	44.8
16-16-1 soft	62	55	88.7	29	46.6	34	54.8	25	40.3
16-16-1 1/2	69	69	100	37	53.6	45	65.2	32	46.4
301 soft	57	57	100	28	49.1	34	59.6	24	42.1
301 1/4	63	63	100	30	47.6	58	85.7	32	50.8
301 1/2	63	63	100	31	49.2	57	90.5	30	47.6
301 3/4	66	66	100	31	47.0	61	92.4	34	51.5
302 soft	57	57	100	27	47.4	35	61.4	28	49.1
302 1/4	63	63	100	30	47.6	49	77.8	29	46.0
302 soft 2B	58	57	100	31	54.4	44	77.2	28	49.1
302 No. 4	64	64	100	33	51.6	57	89.1	31	48.4
302 No. 7	65	62	95.4	34	52.3	63	96.9	31	47.7
304 soft	61	61	100	28	49.5	45	73.8	29	47.5
304 soft 2B	54	54	100	29	53.7	37	68.5	24	44.4
316 soft	61	61	100	27	44.3	61	100	31	50.8
316 soft 2B	54	54	100	29	53.7	53	98.1	29	53.7
316L soft 2B	60	60	100	30	50.0	48	80.0	29	48.3
321 soft 2B	49	49	100	26	53.1	33	67.3	24	50.0
347 soft 2B	44	44	100	26	59.1	32	72.7	23	52.3
410 annealed No. 2	61	56	91.8	26	42.6	21	34.4	10	16.4
430 soft CR	64	62	96.9	33	51.6	29	45.3	22	34.4

[a] Measurements made with a D&S Alphatometer Model A1 on one panel of each material from each test.

[b] Percent reflectivity retained equals % reflectivity exposed panel skyward side divided by the reflectivity of control panel of same material from storage.

In general, these small deposits had nothing to do with any corrosion of the alloys but did contribute to the dark color.

In addition to the dark deposits, a few microscopic bright orange nodules were found on all alloys and were identified to contain approximately: 92% iron, 3% chromium, 1% silicon, 2.5% sulfur, and 1% calcium. These appear to be minute corrosion product stains, not even visible to the naked eye. Under some of these nodules, a microscopic area was found to be very slightly etched.

Since all the materials had essentially the same general appearance and the extent of corrosion was not considered significant, the reflectivity of each test panel was measured, as described in the procedure, and compared with an unexposed control. Results are given in Table 4. The mechanical properties of Types 201, 301, 302, 304, and 316 stainless steel are given in Table 5.

The surface dirt on the skyward side was easily removed from all grades of stainless steels with a damp cloth and mild (nonabrasive) household cleanser. The groundward side of all alloys had a soot-like film that was also easily removed.

TABLE 5—*Mechanical properties of stainless steels exposed in different environments.*

Material Properties	Control, 26 years[a]	Rural, 29 years	Industrial, 29 years	Marine 250-m Lot, 26 years	Marine 25-m Lot, 26 years
201 1/2:					
YS, psi	142 000	120 000	123 000	137 000	136 500
UTS, psi	155 000	156 000	159 000	157 000	155 500
elongation, %	21.5	20.0	21.0	21.0	23.0
301 1/2:					
YS, psi	139 000	142 000	135 000	135 000	142 500
UTS, psi	177 500	186 000	181 000	180 500	184 500
elongation, %	21.5	23.0	22.0	24.3	23.3
302 1/4:					
YS, psi	110 000	108 000	107 000	112 000	110 000
UTS, psi	130 500	130 000	127 000	127 000	130 000
elongation, %	19.5	19.0	21.0	21.5	22.5
304 annealed:					
YS, psi	41 250	41 300	40 600	41 000	39 950
UTS, psi	82 250	82 300	86 000	89 750	89 750
elongation, %	56.5	56.0	56.0	59.8	59.8
316 annealed:					
YS, psi	46 850	49 500	45 100	43 450	43 750
UTS, psi	91 250	90 500	88 100	92 500	92 000
elongation, %	48.0	47.0	46.0	49.0	51.0

[a] Stored for 26 years.

A few isolated pits of 0.05-mm maximum depth were found on the martensitic (Type 410) and ferritic (Type 430) stainless steels. The crevice of the spot-welded panels of these two alloys was very slightly etched at the edge of the overlap.

It was concluded that all the different grades of stainless steel had generally the same aesthetic appearance. The austenitic stainless steels displayed a few microscopic etched spots on the side facing skyward. No crevice attack was evident in the crevice of the spot-welded panel. The martensitic and ferritic stainless steels did suffer microscopic pitting attack on the side facing skyward, and very slight attack (surface appears etched) was found in the crevice of the spot-welded panels.

All the stainless steels exposed in this industrial environment exhibited the following characteristics:

1. Alloys exhibited some microscopic pitting and staining.
2. Spot welds were sound, no evidence of intergranular attack was found, and no crevice attack was found in the overlapped area.
3. Arc welds were sound, with no evidence of cracks.
4. No corrosion or cracking was evident on either the surface in tension or in compression at the Erichsen cups.
5. No loss of mechanical properties.

Marine Atmosphere

The stainless steels exposed for 26 years in the 25- and 250-m lots at Kure Beach, NC (Fig. 3) were evaluated, and the results were reported previously [*6*]. It was determined that further investigations were warranted to provide more definitive data on chemical

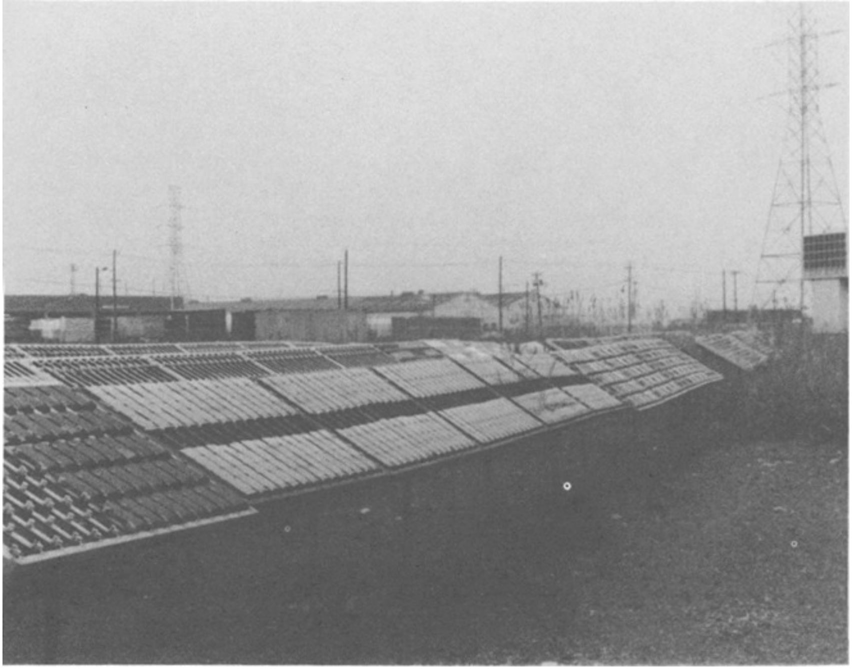

FIG. 2—*View of industrial test site at Newark/Kearny, NJ, where various grades of stainless steel have been on exposure for 29 years (1958 to 1987). The test panels are positioned at 30° to the horizontal facing south.*

composition, pitting, reflectivity, and mechanical properties of these materials. Reflectivity was measured after 26 years of exposure, and these data are compared with the rural and industrial data in Table 4.

The mechanical properties of ten materials were examined to document yield stress, ultimate stress, and percent elongation after 26 years to compare with values for unexposed controls (held in storage) and data from three years of exposure, as given in Tables 6 through 8. The 26-year data for five materials are compared with data from the same five materials exposed at the rural and industrial sites in Table 5. The results confirmed that these stainless steels exposed in the most severe environment for stainless steel, the marine atmosphere [*5*], did not lose any of their mechanical properties after 26 years.

A focusing-depth microscopic examination of the skyward side of all materials revealed the pitting attack was greater than previously reported (0.01-mm evaluation by mechanical dial depth gage) [*4*]. The results are given in Table 9.

Stainless steels exposed in marine environments exhibited the following characteristics:

1. Rust and rust staining that was dependent on alloy content and distance from the ocean.
2. Shallow pitting and crevice attack.
3. Sound arc welds with no cracks evident.
4. Spot weld failures on Type 430 stainless steel.
5. No loss of mechanical properties.

FIG. 3—*Views of the atmospheric lots at Kure Beach, NC, where various grades of stainless steel have been exposed for 26 years (1958 to 1984).* Top: *view of 25-m lot panels facing east.* Bottom: *view of 250-m lot panels facing south.*

TABLE 6—*Mechanical properties*[a] *of stainless steels exposed in the 25-meter lot.*

	3 Years' Exposure			26 Years' Exposure		
Alloy	Yield Stress, psi	Ultimate Stress, psi	Elongation, % in 2 in.	Yield Stress, psi	Ultimate Stress, psi	Elongation, % in 2 in.
201 annealed	60 200	110 850	58.2	58 300	111 000	54.8
201 1/4 hard	106 920	136 920	37.0	102 000	131 000	35.3
201 1/2 hard	128 680	162 050	22.5	136 500	155 500	23.0
301 annealed	39 900	102 100	58.9	36 850	106 500	63.0
301 1/4 hard	110 350	179 700	27.5	117 000	177 000	30.3
301 1/2 hard	131 200	190 700	22.6	142 500	184 500	23.3
302 annealed	36 030	87 530	56.5	35 750	88 500	59.0
302 1/4 hard	107 100	134 950	19.8	110 000	130 000	22.5
304 annealed	38 200	85 610	54.0	39 950	89 750	59.8
316 annealed	46 550	91 820	51.0	43 750	92 000	51.0

[a] The mechanical properties are averages of two samples tested from a given test or control panel.

Discussion

Rural Atmosphere

In the rural atmosphere at State College, PA it was found that all austenitic, martensitic, and ferritic types of stainless steel retained their original texture and appearance after 29 years of exposure. Some particles or organic matter were observed to have deposited on the panels clinging to the surfaces for some period of time, but eventually would be washed naturally or could be removed with a damp cloth. The stainless steel surfaces remained unchanged, retaining virtually 100% of their original reflectivity. No corrosion was found on any of these materials, and there was no change in the mechanical properties.

Industrial Atmosphere

In the industrial atmosphere at Newark/Kearny, NJ it was found that changes to the stainless steels after 29 years of exposure were minimal. All were covered by the same type and quantity of airborne particles which attached to the panel surfaces. The adherence of some of these particles was such that they would not wash off naturally and reduced the aesthetic quality of the stainless steel. It was found that, after 29 years of buildup, all the types of stainless steel retained 40 to 50% of their reflectivity. Also, the attached particles could be removed easily with a wet cloth and mild nonabrasive cleanser, returning the metal surface to its original appearance. It was found that the austenitic stainless steels did have a few microscopic spots where the metal surface was very slightly etched. The martensitic and ferritic stainless steels displayed more microscopic pits and etched spots. Overall, corrosion on all types was considered insignificant. There was no change in the mechanical properties.

Marine Atmosphere

In the marine atmosphere at Kure Beach, NC, all types of stainless steel exhibited a good resistance to corrosion over 26 years of exposure. Microscopic pitting was measured on the boldly exposed surfaces of all materials. At the 250-m site, the average pit depth ranged between 0.02 and 0.08 mm on the flat surface. At the 25-m lot, the average pit depth ranged between 0.03 and 0.12 mm on the flat surface.

TABLE 7—*Mechanical properties*[a] *of stainless steels exposed in the 250-m lot.*

Alloy	3 Years' Exposure Yield Stress, psi	Ultimate Stress, psi	Elongation, % in 2 in.	26 Years' Exposure Yield Stress, psi	Ultimate Stress, psi	Elongation, % in 2 in.
201 annealed	60 160	113 270	58.2	58 250	112 000	55.8
201 1/4 hard	107 880	137 020	37.0	101 500	132 000	35.3
201 1/2 hard	139 950	159 440	23.2	137 000	157 000	21.0
301 annealed	40 550	101 300	58.6	40 800	103 500	59.8
301 1/4 hard	103 900	178 050	25.5	113 500	172 500	27.5
301 1/2 hard	134 700	190 200	23.8	135 500	180 500	24.3
302 annealed	35 010	86 280	57.5	36 350	89 750	61.3
302 1/4 hard	109 600	134 350	20.0	112 000	127 000	21.5
304 annealed	41 140	86 000	56.0	41 000	89 750	59.8
316 annealed	47 800	91 880	52.8	43 450	92 500	49.0

[a] The mechanical properties are averages of two samples tested from a given test or control panel.

All of the stainless steels exhibited rust staining and rust coverage to varying degrees. In the 250-m marine atmospheric site, considered a moderate marine site, the 200 and 300 series stainless steels showed less than 50% rust stain coverage and the percent reflectivity retained was between 60 and 100%. Reflectivity retained on Types 410 and 430 stainless steel was 34.4 and 45.3%, respectively. In the 25-m marine atmospheric site, considered a severe marine site, the 200 and 300 series stainless steels showed 100% rust and rust stain coverage, and the percent reflectivity retained was between 40 and 50%. The reflectivity retained on Types 410 and 430 stainless steel was 16.4 and 34.4%, respectively. Rust staining on all stainless steels exposed in the marine atmosphere could be removed but only by a scrub brush and abrasive cleanser, by commercial cleaning solutions, or by 30% nitric acid.

The spot-welded stainless steels displayed some crevice corrosion between the overlapped plates. In this crevice area, significant pitting and intergranular corrosion was observed. In the 250-m lot, the average attack on the eleven stainless alloys ranged from 0.01 to 0.10

TABLE 8—*Mechanical properties*[a] *of stainless steel controls held in storage 3 and 26 years.*

Alloy	3 Years Yield Stress, psi	Ultimate Stress, psi	Elongation, % in 2 in.	26 Years Yield Stress, psi	Ultimate Stress, psi	Elongation, % in 2 in.
201 annealed	62 880	113 390	57.2	56 500	110 000	52.8
201 1/4 hard	104 880	136 480	36.8	103 000	131 000	33.3
201 1/2 hard	138 700	164 540	23.5	142 000	155 000	21.5
301 annealed	40 400	100 500	58.5	39 900	102 800	62.0
301 1/4 hard	108 100	180 900	27.5	110 000	174 500	29.0
301 1/2 hard	133 750	192 000	22.2	139 000	177 500	21.5
302 annealed	35 570	86 680	58.0	35 400	87 500	59.0
302 1/4 hard	108 900	134 300	21.0	110 000	130 500	19.5
304 annealed	40 420	87 120	58.2	41 250	85 250	56.5
316 annealed	47 950	91 600	50.8	46 850	91 250	48.0

[a] The mechanical properties are averages of two samples tested from a given test or control panel.

TABLE 9—*Average pitting attack*[a] *on stainless steels after 26 years' exposure in marine atmospheric lots.*

Material	250-m Lot		25-m Lot	
	Panel Surface, mm	Crevice, mm	Panel Surface, mm	Crevice, mm
201 soft CR	0.05	0.05	0.08	0.10
201 1/4 CR	0.03	...	0.10	...
201 1/2 CR	0.03	...	0.09	...
201 3/4 CR	0.04	0.09	0.09	0.13
201 soft 2B	0.06	...	0.05	...
202 soft CR	0.07	0.09	0.04	0.09
16-16-1 soft CR	0.06	...	0.07	...
16-16-1 1/2 CR	0.06	0.12	0.08	0.23
301 soft CR	0.04	...	0.08	...
301 1/4 CR	0.03	0.05	0.10	0.19
301 1/2 CR	0.04	...	0.12	...
301 3/4 CR	0.04	0.05	0.04	0.12
302 soft CR	0.05	0.08	0.06	0.12
302 1/4 CR	0.04	...	0.05	...
302 soft 2B	0.04	...	0.04	...
302 No. 4 Q	0.05	...	0.06	...
302 No. 7 Q	0.05	...	0.07	...
304 soft CR	0.05	0.06	0.07	0.11
304 soft 2B	0.04	...	0.03	...
304L soft 2B	0.05	...	0.10	...
316 soft CR	0.04	0.05	0.06	0.14
316 soft 2B	0.02	...	0.03	...
316L soft 2B	0.03	...	0.05	...
321 soft 2B	0.04	...	0.05	...
347 soft 2B	0.05	...	0.06	...
410 annealed No. 2	0.08	0.07	0.12	0.15
430 soft CR	0.05	0.05	0.11	0.21

[a] Pit depths measured by a modified Unitron microscope with a digital linear gage attachment at ×210 magnification.

mm. Type 430 stainless steel did suffer failures at spot welds in both the 250- and 25-m lots because of corrosion of the weld.

All the arc-welded stainless steels exposed showed no evidence of weld failure.

All stainless steels with Erichsen cups exposed showed no evidence of stress corrosion failure in the stressed areas. There were a great many more pits visible on the side of the Erichsen cup than were found on the flat surface of the test panels exposed in the 25-m lot. Even in light of the corrosion noted in the marine environments, no changes in mechanical properties were evident.

Conclusions

The aesthetic qualities of various grades of stainless steel will vary in different environments, as observed after 26 to 29 years of exposure.

1. In a rural or relatively clean environment, nature usually will provide sufficient cleaning, and the surface will retain its original appearance indefinitely.
2. In an industrial environment, some airborne particles can adhere to the surface which,

after many years, may require cleaning. This can be accomplished with a slight scrubbing with a brush or cloth, mild soap, and water. The metal surface can be restored almost to its original appearance. Austenitic stainless steels can suffer microscopic etched spots. Martensitic and ferritic stainless steels can suffer microscopic pitting and etched spots.

3. In the rural and industrial environments, the minor amounts of corrosion can be considered insignificant. No effects of intrinsic material properties, for example, composition, surface finish, temper, or metallurgical structure could be observed.

4. In the very corrosive marine atmosphere, because of the constant presence of chlorides, stainless steels will develop various degrees of rust staining associated with microscopic pitting and etching on the surface, depending on the alloy content (chromium, nickel, and molybdenum) and distance from the ocean. The degree of rust staining will usually be established within two to five years and will cycle slightly thereafter for many years. The surface can be cleaned with a scrub brush and abrasive cleanser, metal cleaning solutions, or 30% nitric acid. The surface will return to a bright finish, although the surface texture may change slightly.

References

[*1*] Krivobok, V. N., *The Book of Stainless Steels,* E. E. Thum, Ed., The American Society for Steel Treatment, Cleveland, 1933.

[*2*] LaQue, F. L., "Stainless Steel—What It Is and What Will It Do," *Stainless Steel for Architecture Use, ASTM STP 454,* American Society for Testing and Materials, Philadelphia, 1969, pp. 3–13.

[*3*] *Proceedings,* Report on ASTM Committee A-10 on Iron Chromium, Iron-Chromium-Nickel and Related Alloys, Subcommittee IV, American Society for Testing and Materials, Philadelphia, Vol. 58, 1958 through Vol. 72, 1972.

[*4*] Baker, E. A. and Lee, T. S., "Calibration of Atmospheric Test Sites," *Atmospheric Corrosion of Metals, ASTM STP 767,* American Society for Testing and Materials, Philadelphia, 1980, p. 261.

[*5*] Black, H. L. and Lherbier, L. W., "A Statistical Evaluation of Atmospheric, In Service and Accelerated Corrosion of Stainless Steel Automotive Trim," *Metal Corrosion in the Atmosphere, ASTM STP 435,* American Society for Testing and Materials, Philadelphia, 1968, pp. 3–32.

[*6*] Baker, E. A. and Lee, T. S., "Long-Term Atmospheric Corrosion Behavior of Various Grades of Stainless Steel," *Degradation of Metals in the Atmosphere, ASTM STP 965,* American Society for Testing and Materials, Philadelphia, 1987, pp. 52–67.

[*7*] Kearnes, J. R., Johnson, M. J., and Pavik, P. J., "Corrosion of Stainless Steels in the Atmosphere," *Degradation of Metals in the Atmosphere, ASTM STP 965,* American Society for Testing and Materials, Philadelphia, 1987, pp. 35–50.

John W. Spence,[1] Edward O. Edney,[1] Fred H. Haynie,[1]
David C. Stiles,[2] Eric W. Corse,[2] Mike S. Wheeler,[2] and Susan F. Cheek[2]

Advanced Laboratory and Field Exposure Systems for Testing Materials

---

REFERENCE: Spence, J. W., Edney, E. O., Haynie, F. H., Stiles, D. C., Corse, E. W., Wheeler, M. S., and Cheek, S. F., **"Advanced Laboratory and Field Exposure Systems for Testing Materials,"** *Corrosion Testing and Evaluation: Silver Anniversary Volume, ASTM STP 1000,* R. Baboian and S. W. Dean, Eds., American Society for Testing and Materials, Philadelphia, 1990, pp. 191–207.

ABSTRACT: A unique laboratory exposure system for exposing materials to complex air mixtures that simulate atmospheric conditions has been developed for studying the aerodynamic and chemical processes controlling atmospheric degradation of materials. Runoff studies using covering-spray devices were also developed to provide insight into the effects of atmospheric acidity on materials in the early stage of field exposure. Using these facilities, exposure studies of galvanized steel panels have shown that the deposition of sulfur dioxide (SO_2) is controlled by the gas phase resistance of the atmosphere during periods of surface wetness. The delivery of SO_2 to the galvanized steel surface is controlled by the atmosphere. Each molecule of SO_2 that deposits to the wet surface will react with one zinc (Zn) atom to form zinc sulfate ($ZnSO_4$). During periods of surface dryness, the surface density of SO_2 corresponds to the formation of a saturated monolayer of SO_2. The deposition of nitrogen dioxide (NO_2) is an order of magnitude less than SO_2 during periods of surface wetness and appears to be controlled by the surface resistance of galvanized steel. The delivery of NO_2 is limited to its solubility within the aqueous surface film. Of the atmospheric gases, nitric acid (HNO_3) readily deposits during periods of surface wetness and dryness. Rain acidity contributes to the corrosion of zinc according to the stoichiometric relationship $2(H^+) = Zn^{2+}$. The corrosion film that forms on zinc is soluble in rain due to dissolved atmospheric carbon dioxide (CO_2). The dissolution of the corrosion film depends on the residence time of rainwater on the surface of the galvanized steel panel.

KEY WORDS: laboratory exposure system, field covering spray device, galvanized steel, atmospheric corrosion, atmospheric wet and dry deposition, sulfur dioxide, nitrogen dioxide, nitric acid, rain acidity

In 1980 Congress passed the Acid Precipitation Act, which established an interagency task force to plan and implement a ten-year national research program. The task force implemented the National Acid Precipitation Assessment Program (NAPAP) by forming task groups composed of federal agencies to investigate the various aspects of acidic deposition. Task Group VII, Effects on Materials and Cultural Resources, was formed to investigate the effect of acidic deposition on materials.

The primary mission of Task Group VII is to provide NAPAP with cause and effect

---

[1] U.S. Environmental Protection Agency, Research Triangle Park, NC 27711.
[2] NSI Environmental Sciences, Research Triangle Park, NC 27709.

relationships for the incremental effects of acidic deposition on materials-at-risk. A listing of the materials that Task Group VII considers to be at risk to acidic deposition is shown in Table 1. The U.S. Environmental Protection Agency (EPA) and the Bureau of Mines (BOM) are responsible for planning and conducting effects research on materials of construction, whereas the National Park Service and the U.S. Geological Survey have been funded to study cultural materials. A general description of the Materials Effects Research Program and procedures that have been adopted by Task Group VII has been reported previously [*1*]. Information from this exposure program will be used by NAPAP to prepare State of Science and Assessment Reports to Congress in 1990.

Prior material exposure studies that EPA [*2–5*] and other researchers [*6–8*] have conducted indicate that atmospheric pollutants such as sulfur dioxide (SO_2), relative humidity, or time of surface wetness can accelerate the degradation of many of the materials shown in Table 1. The cause-and-effect relationships that the task group was charged with developing had to show the incremental effects of atmospheric species associated with dry deposition and wet deposition on the materials at risk. Dry deposition involves atmospheric gases that are delivered to materials when the surface is dry and when it is wet with dew. Wet deposition concerns those atmospheric species delivered to materials in rain, snow, etc. To distinguish the damage to materials by dry deposition from that by wet deposition, the task group had to develop unique chamber and field exposure systems for the research program.

This paper describes exposure systems and techniques that were developed during NAPAP for determining the key chemical and physical parameters associated with dry deposition and wet deposition of atmospheric species to material surfaces. Major findings that were obtained for acidic deposition damage to galvanized steel are presented in this paper.

Experimental

Laboratory Exposure System

For studying deposition under controlled environmental conditions, a laboratory exposure system was developed by NSI-Environmental Sciences, under contract to EPA, for exposing

TABLE 1—*Materials being tested for acidic deposition damage.*

Materials-At-Risk	Agency
Construction materials	Bureau of Mines and US Environmental Protection Agency
1010 carbon steel Cor-Ten A steel 110 copper 3003 H14 aluminum 191 zinc G-90 galvanized steel Galvalume	
Exterior coatings on metal Exterior coatings on wood	
Cultural materials	National Park Service and US Geological Survey
Salem limestone Vermont marble	
Bronze	

materials in the presence of simulated urban environments and other complex air mixtures. This chamber has some characteristics of earlier chambers that were developed for EPA [*9,10*]. Earlier studies have shown that laboratory environmental exposures provide considerable insight into the effects of pollutants on materials degradation [*10–12*].

A diagram of the exposure system, which consists of a material exposure chamber coupled to an 11.3-m^3 chamber for generating photochemical smog, is shown in Fig. 1. The system operates as a continuous, stirred-tank reactor in which the large chamber serves as a pollutant reservoir for exposing materials within the flow chamber. The procedures for charging the chamber with individual pollutants and reactants for generating smog within the chamber have been reported previously [*13*]. Banks of black lights and sun lamps, which are not shown in Fig. 1, are located on both sides of the 11.3-m^3 chamber to initiate the photochemical reaction for smog. The composition of the photochemical smog mixture is continuously recorded by air-monitoring instrumentation [*13*]. The formation of smog at desired levels of concentration can be maintained by adjusting the flow rate of the reactants and the residence time in the 11.3-m^3 chamber. Materials within the exposure chamber are exposed to photochemical smog of known steady-state, chemical composition. As shown in Fig. 1, the material exposure chamber is connected to the photochemical chamber, and blowers are used to maintain turbulent flow conditions in the chamber.

A cross-sectional drawing of a materials exposure chamber is shown in Fig. 2. The exposure chambers are equipped with lamps, thereby permitting the simulation of sunlight during the exposure cycle. Test panels are mounted to a chill plate which permits the temperature of the panels to be lowered below the dew point temperature of the chamber, thus forming condensation on the test panels.

Exposure systems are operational at the U.S. EPA in the Research Triangle Park, NC and on the campus of the North Carolina State University (NCSU) in Raleigh, NC. The EPA chamber has two materials exposure chambers for exposing a total of 14 panels, whereas the NCSU chamber has four chambers for exposing up to 48 panels. Figure 3 shows the NCSU four chambers with bottles for collecting condensation from the panels.

The condensation is analyzed by ion chromatography and atomic absorption spectroscopy to identify the gaseous species within the smog mixture that deposit and the soluble products that form through reactions with the material test panel. Details on the instrumentation and procedures for analyzing for the cations and anions within the condensation have been reported previously [*14,15*]. In addition, the volume and pH of each sample are recorded.

Field Exposure Devices

When Task Group VII began the Materials Effects Research Program, five field sites were located in the eastern, northeastern, and midwestern United States for boldly exposing the materials shown in Table 1. Air quality, meteorological parameters, rain chemistry, and airborne particles were monitored continuously at these sites. Techniques that were used to measure the rate of environmental damage to the materials have previously been reported [*1*].

In a prior EPA material exposure field study, statistical regression techniques showed that the effects of pollutants were masked by strong covariances with other environmental parameters [*5*]. At the five material exposure sites that Task Group VII established, the range of rain acidity (pH) was not large. To enhance the study of the effects of wet and dry acidic deposition on boldly exposed materials, automatic covering-spray devices were installed at the Research Triangle Park, NC and Steubenville, OH sites. The NC site is a rural environment, whereas the OH site is a highly industrial site. The annual average SO_2 loading at the OH site is approximately eleven times that for the NC site.

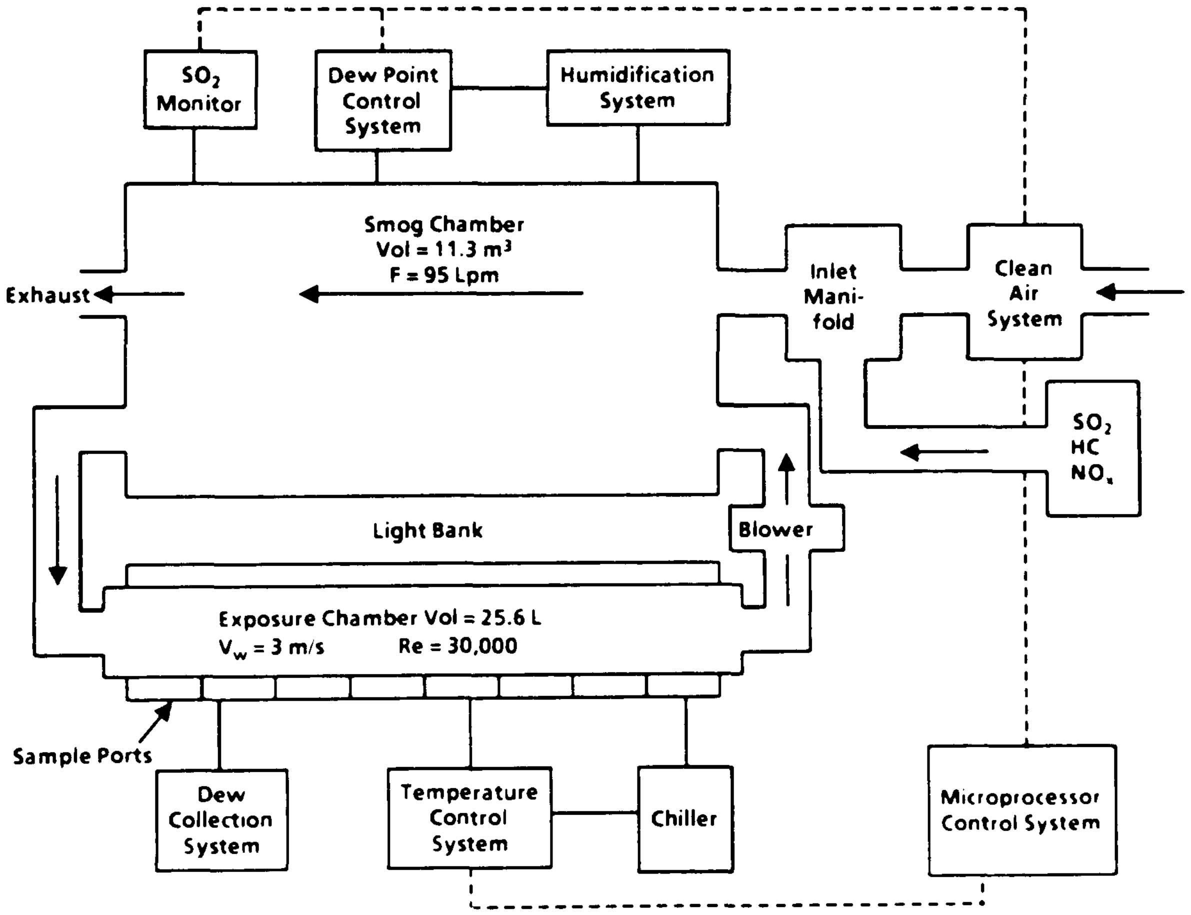

FIG. 1—*Diagram of environmental exposure system at U.S. Environmental Protection Agency.*

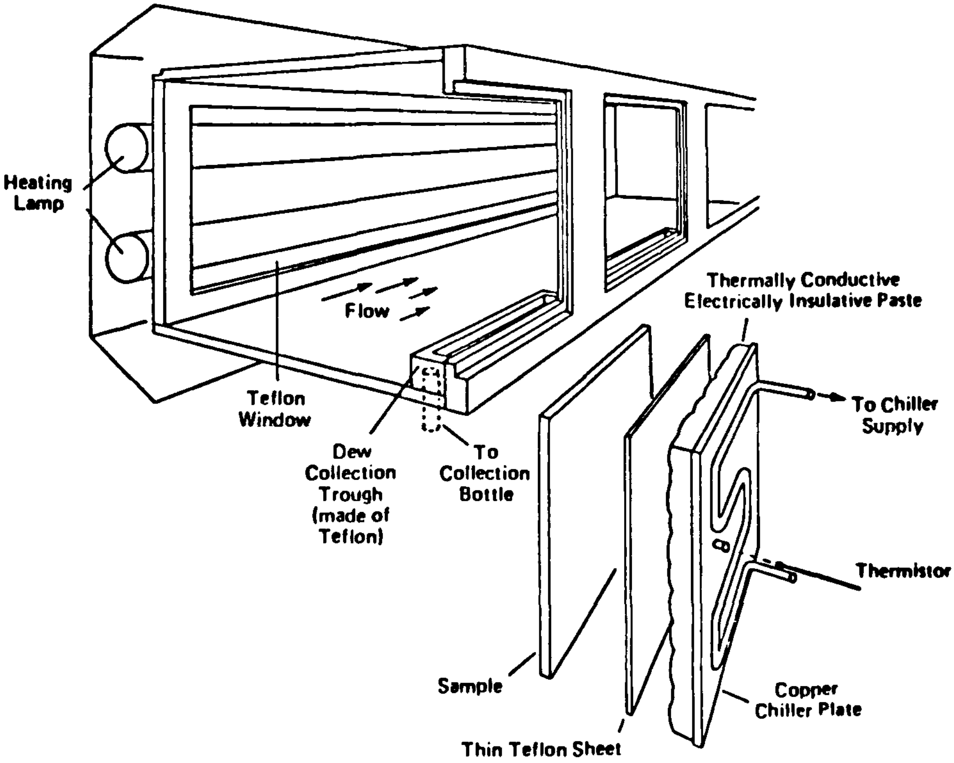

FIG. 2—*Cross-sectional diagram of material exposure chamber.*

The covering-spray device, as diagrammed in Fig. 4 and as shown at the NC site in Fig. 5, separates the effects of wet acidic deposition and those of dry acidic deposition on materials [*16*]. This device covers one set of test panels and sprays an identical set with deionized water of pH 5.6 during each rain event. The covering device sprays approximately the same volume of water that falls for each rain event. However, the spray does not simulate rain intensity nor direction of rainfall. After each rain event, the moveable racks are returned automatically to the boldly exposed position.

As shown in Fig. 4, collection bottles are mounted to the exposed material panels to collect rain and spray runoff for each rain event. The runoff collections are analyzed in a manner similar to that used for the condensation samples that are obtained from panels exposed in the laboratory exposure system. The analysis of the spray collections provides information on the effects of the dry deposition process, that is, the reaction of gases during periods of surface wetness (dew) and dryness. The analysis of rain runoff collections from the boldly exposed test panels provides information on the effects of both dry and wet deposition. Since the analyses of the runoff collections provide information of the soluble reaction products of the corrosion film, it complements the weight loss measurements of galvanized steel panels that BOM is conducting [*1*].

Preparation of Test Panels

For the laboratory and field exposure experiments, galvanized steel panels were prepared from sheet stock of 20-gage zinc-coated (hot-dipped) steel. The average thickness of the

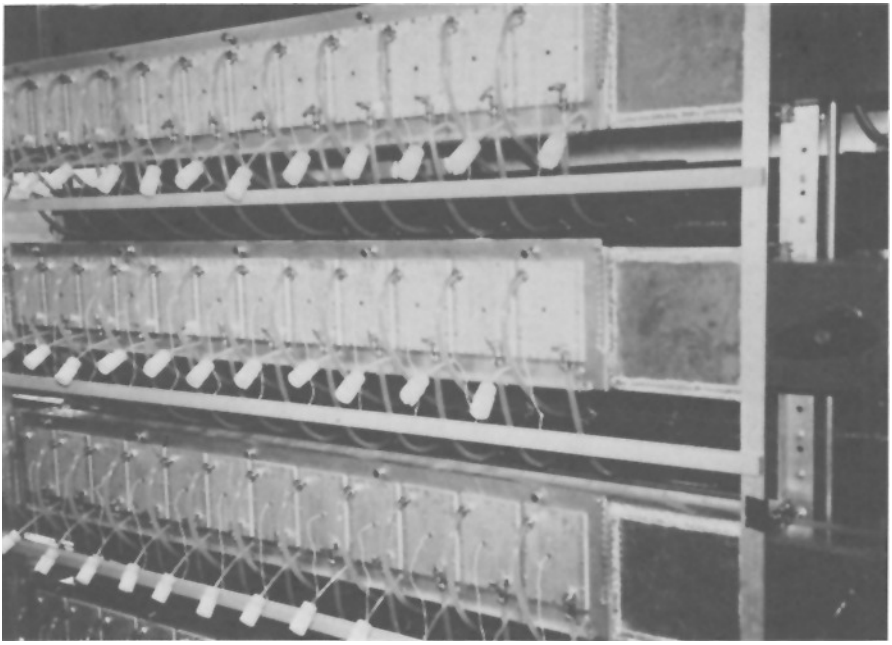

FIG. 3—*Material exposure chambers for the exposure system at North Carolina State University.*

zinc coating was 20 μm. Test panels were sheared to enhance smearing of the edges with the zinc coating. This procedure tends to minimize edge effects during exposure [*1*]. For the chamber exposures, test panels were 8 by 13 cm, whereas the standard 10 by 15-cm panels were used for the field exposures. All panels were cleaned prior to exposure by immersion in 10% by weight of ammonium chloride (NH_4Cl) at 60 to 80°C for 2 min. The panels were next rinsed with deionized water, then with anhydrous methanol, and allowed to dry. During field exposures, the panels were mounted at 30° facing south. For the chamber exposure experiments, both clean panels and panels that had been field exposed for several months at the NC site were exposed.

Results

Controlled exposures using a laboratory exposure system were conducted to study the transport of gaseous compounds to panels of galvanized steel. The transport of a gaseous compound to a surface is expressed as a deposition velocity (V_d, cm/s), which is defined as the flux to a surface divided by the ambient concentration. These experiments involved the analysis of condensate (simulated dew) collections from panels during exposures to single pollutants and to mixtures of photochemical smog with and without SO_2. The velocity at which gaseous compounds deposited on galvanized steel panels was determined two ways: (1) from the concentration of chemical species in the condensate and its volume; and (2) from the difference in the gas phase concentrations during periods of surface dryness and wetness [*13*].

The results of the chamber deposition studies, as shown in Table 2, indicate that SO_2, nitric acid (HNO_3), and formaldehyde (HCHO) readily deposit onto the panels of galvanized steel in the presence of condensation. Of these gases, HNO_3 was found to deposit during periods of wetness and dryness [13]. The deposition of nitrogen dioxide (NO_2) is lower than that of the other gases and is limited by its solubility and reactivity in the condensation on the panels. This finding is consistent with investigations of the rate of uptake of NO_2 by surface waters [17]. The deposition of SO_2, HNO_3, and HCHO can be viewed as being controlled by the gas phase resistance of the atmosphere, since these gases are readily soluble in the aqueous film on the galvanized steel panel, whereas, NO_2 deposition is controlled by the surface resistance of the aqueous film on the galvanized steel panels. In these studies, it was not possible to determine the deposition velocity of other gaseous species such as ozone (O_3), peroxyacetyl nitrate (CH_3COONO_2), acetaldehyde (CH_3CHO), or hydrogen peroxide (H_2O_2). However, concentrations of these species were observed to remain relatively constant during wet and dry exposure periods of the panels [13].

As indicated in Table 2, the anion of hydroxymethane sulfonic acid, $HCHOHSO_3^-$, was present in the condensate. This anion probably formed as the adduct of HCHO and bisulfite (HSO_3^-) and prevented the formation of sulfate (SO_4^{2-}) from the sulfite (SO_3^{2-}) or its HSO_3^- precursor. Because the adduct was observed in the presence of high concentrations

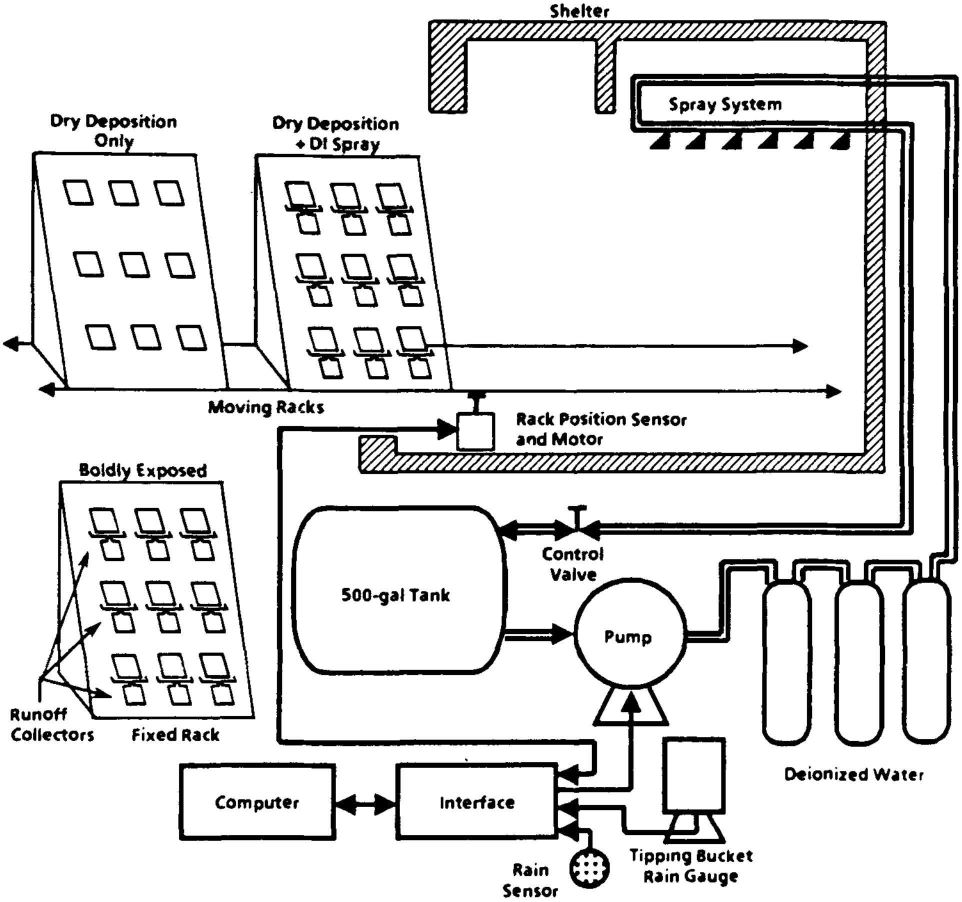

FIG. 4—*Diagram of automatic materials covering-spray device.*

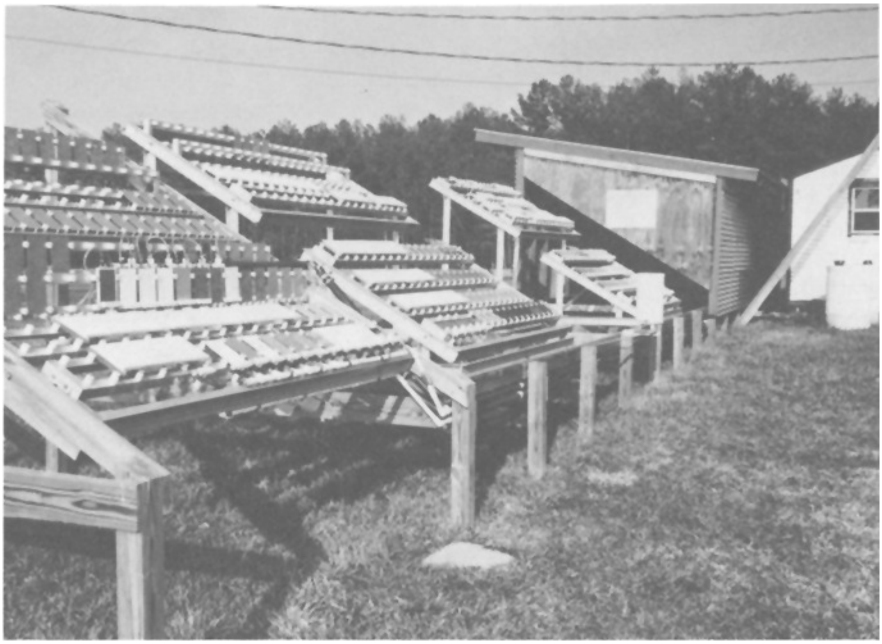

FIG. 5—*Automatic materials covering-spray device at the NC exposure site.*

of HCHO, it is questionable whether this reaction occurs on galvanized steel in the ambient environment. However, the adduct has been identified in Los Angeles fog [*18*].

Exposure experiments were conducted in which the SO_2 concentration was increased incrementally over a range of 3.0 to 650 ppb [*14*]. At each level of SO_2 concentration, the concentration of zinc ion (Zn^{2+}) in the condensate collections was determined and plotted as the flux of Zn^{+2} (Fig. 6) against the flux of SO_4^{2-}. Linear least square fits of the data provided a value of 1.06 for the slope and a correlation coefficient of 0.995. If it is assumed that all of the deposited SO_2 appears as SO_4^{2-} in the condensate, the slope (1.06) gives the effective stoichiometry for the reaction of SO_2 and the corrosion product film. This indicates that, for every SO_2 molecule that deposits on galvanized steel during periods of surface wetness, an equal number of Zn atoms react to form zinc sulfate ($ZnSO_4$).

For these studies, most of the deposition of gaseous compounds, except for HNO_3 (Table

TABLE 2—*Gas phase deposition velocity of atmospheric species.*

Gases	Anion Measured in Condensate	Deposition Velocity, V_d (cm/s)
SO_2	SO_4^-	0.8
NO_2	NO_2^-	0.03
HNO_3	NO_3^-	2.0 (0.7)[a]
HCHO	$CHOO^-$	0.6
HCHO + SO_2	$HCHOHSO_3^-$	...

[a] The value in parentheses is based on the deposition obtained after subtracting the HNO_3 surface density from the deposition obtained by dew analysis.

2), occurred during periods of surface wetness of the panels. However, SO_2, NO_2, and HCHO were found to deposit on dry panels until saturation occurred. In the case of SO_2, the saturation surface density on dry panels was found to correspond to a monolayer of adsorbed SO_2 [*13*].

During chamber exposure experiments, panels were removed and sprayed with solutions of ammonium bisulfate (NH_4HSO_4) of varying pH levels to investigate simulated rain acidity. The dependence of the Zn^{2+} measured in the spray runoff collections on incident pH for panels exposed to 30-ppb SO_2 is shown in Fig. 7. The zinc flux represents the number of nmol of zinc dissolved into the sprayed solution per cm^2 of panel per cm of spray (cm_R). The flux is numerically equal to zinc concentration expressed as nmol per mL. The zinc concentration is observed to increase by less than a factor of 2 as the pH of the incident spray drops from 5.6 to 4.0, whereas an increase of nearly an order of magnitude is observed between pH 4.0 and 3.0. Panels that were exposed to 3, 30, and 45-ppb SO_2 were also sprayed with NH_4HSO_4 solutions of various pH values. Statistical differences were observed

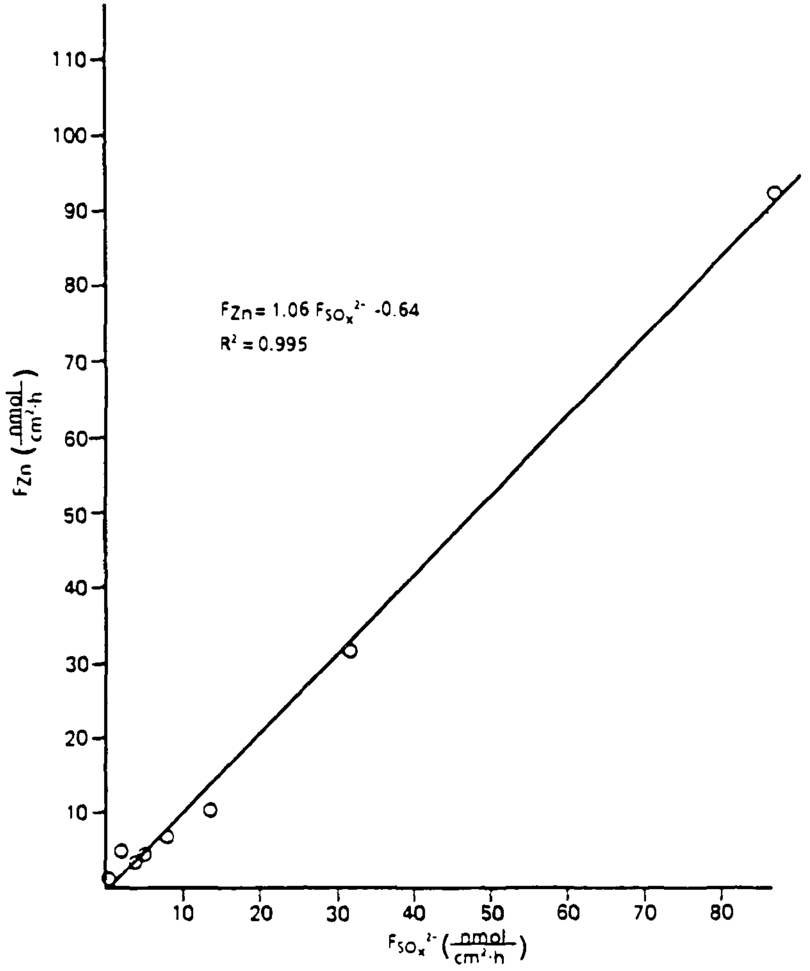

FIG. 6—*Plot of zinc flux as a function of sulfate flux in the condensation.*

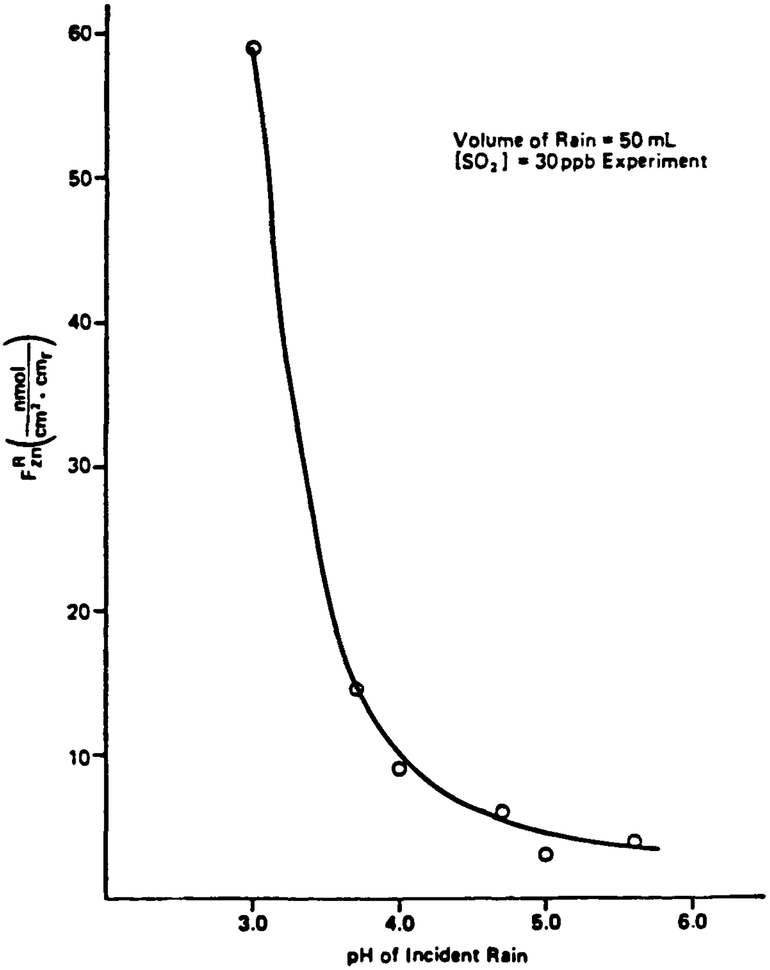

FIG. 7—*Plot of zinc flux as a function of incident pH.*

(Fig. 8) for the slopes and intercepts of data from exposing panels at the three concentrations. The slope and intercept were observed to decrease as the SO_2 exposure of the panels increased.

In order to enhance the study of the dry and wet deposition, runoff samples were collected from galvanized steel panels that were exposed to ambient conditions and sprayed with deionized water by using the covering device at the NC site. Runoff collections for eleven rain and spray events that occurred between April 25 and July 12, 1987, were analyzed for major anion and cation species [*15*]. Average measurements of cations and anions (expressed as nmol/cm^2/day) are shown in Table 3 for the 78-day collection period for galvanized steel and for Teflon panels. Teflon was exposed, as it represents a relatively inert surface to atmospheric reactions. Chemical species found in the deionized water spray represent those that deposit during periods of dry deposition and are soluble in dilute solutions of carbonic acid. The deionized water spray was found to equilibrate readily with atmospheric carbon dioxide (CO_2) to produce a pH of approximately 5.6. The ambient rain runoff collections contain those species that deposit during periods of dry deposition and are soluble in the

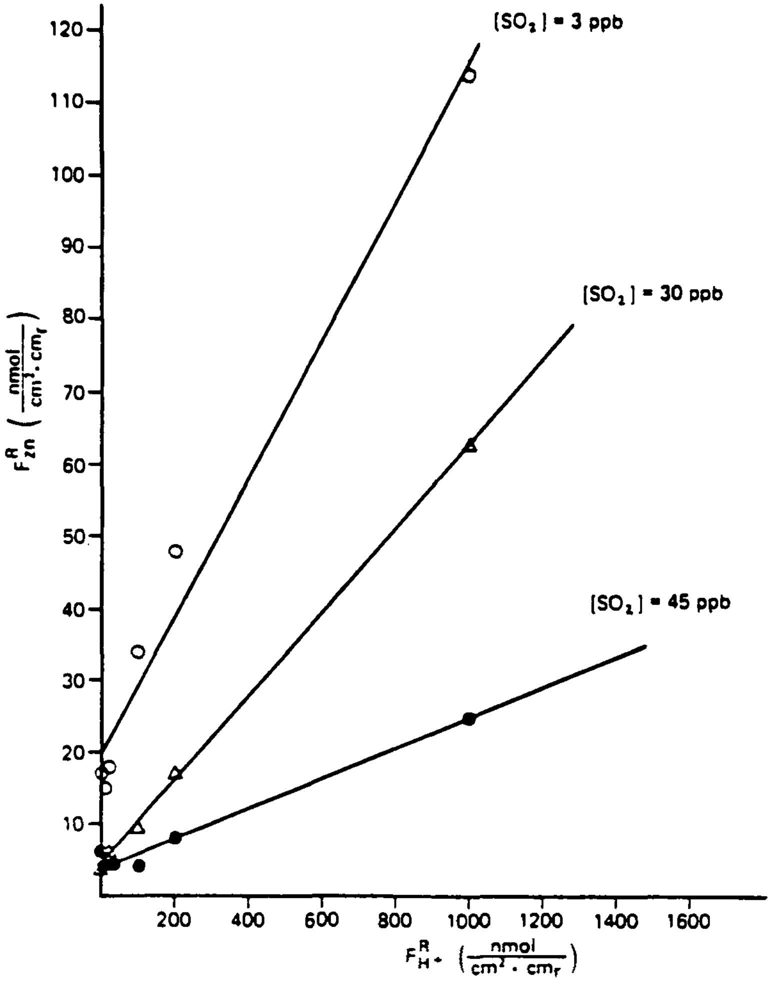

FIG. 8—*Zinc flux as a function of incident hydrogen ion flux for SO_2 exposures at 3, 30, and 45 ppb.*

rain, as well as unreacted chemical species in the incident precipitation. For the eleven rain events, the rain pH had a range of 3.7 to 4.4.

The presence of sodium (Na^+), potassium (K^+), and calcium (Ca^{2+}) in the spray and rain collections, as shown in Table 3, is likely due to coarse dry particles that deposited to the surface of the panel or simply washed out of the atmosphere during rainfall. These cations were found in the runoff collections from the galvanized steel and Teflon panels. The Zn^{2+} was present only in collections from the galvanized steel panel, was not measured within the rain or spray from the Teflon panel, and, in comparison to the other cations within the spray and rain runoff samples, was present in substantial amounts. Thus, ambient precipitation clearly contributes to the formation of soluble zinc corrosion products.

The contribution of the ammonium ion (NH_4^+) in the rain dominated the amount due to dry deposition within the spray runoff for both the galvanized steel and Teflon panels. These values likely represent lower limits, as the NH_4^+ measurements were made weeks after the samples were collected.

Since the pH of the ambient rain was below 4.4, the low hydrogen ion (H^+) measurement

TABLE 3—*Average spray and rain runoff results for NC site.*

	Ionic Concentration, nmol/cm^2 day											
	Vol[a]	H^+	Na^+	NH_4^+	K^+	Ca^{++}	Zn^{++}	$HCOO^-$	CH_3COO^-	Cl^-	NO_3^-	SO_4^-
						GALVANIZED STEEL						
Spray	1437	0.05	0.26	0.04	0.31	0.44	4.65	0.54	0.36	1.04	0.60	2.41
Rain	951	0.03	0.73	0.68	0.59	0.87	12.95	1.58	0.49	3.11	4.13	7.93
						TEFLON						
Spray	461	0.08	0.38	0.09	0.69	0.73	...[b]	0.10	0.03	0.42	0.90	0.68
Rain	764	3.34	0.51	0.65	0.44	1.04	...[b]	0.37	0.18	0.65	2.94	2.42

[a] Total runoff volume, mL.

[b] Not measurable.

in the rain and spray runoff samples for the galvanized steel indicates reaction of the H^+. The H^+ within the ambient rain samples from the Teflon surface had the highest value for the cations measured in the runoff, whereas the H^+ within the spray was lower than expected for an inert surface.

Both the formic ion ($HCOO^-$) and the acetic ion (CH_3COO^-) were measured from the spray and ambient collections from the galvanized steel and Teflon panels; however, these measurements are suspect because of short-term stability of these anions. Lower measurements were obtained for these anions for the spray and rain samples from the Teflon panel.

Of the anions measured in the runoff collection, substantial amounts of nitrate (NO_3^-) and SO_4^{2-} as well as chloride (Cl^-) were present in the rain samples from the galvanized steel panels. Considerably more NO_3^-, SO_4^{2-}, and Cl^- were measured in the rain runoff samples than for the spray collections from the galvanized steel and Teflon panels. For the spray, the NO_3^- is most likely due to uptake of gaseous HNO_3 and particulate NO_3^-. The SO_4^{2-} within the spray may also come from particles containing SO_4^{2-} and from the absorption of SO_2 in the films of surface moisture and its subsequent oxidation to SO_4^{2-}. The presence of the Cl^- is likely attributed to the dry deposition of particles.

The average charge balance for the cations and anions with the spray and rain and their ratios for the galvanized steel and Teflon panels are shown in Table 4. Within the limits of the measurements, the ratios of cations to anions for the Teflon spray and rain samples were close to unity, whereas there appears to be an excess of cations over anions for both runoff samples from the galvanized steel. This suggests the presence of undetected ions.

Discussion

The experimental results obtained from the environmental chamber system and from the runoff experiments using the covering-spray device at the NC site provide considerable

TABLE 4—*Charge balance results.*

	Spray, nmol/cm^2/day			Rain, nmol/cm^2/day		
Material	F(+)	F(−)	F(+)/F(−)	F(+)	F(−)	F(+)/F(−)
Galvanized steel	10.84	7.36	1.47	29.67	24.09	1.23
Teflon	2.70	2.81	0.96	7.02	8.98	0.78

insight into parameterizing dry and wet deposition effects on the corrosion of galvanized steel panels. In these experiments, chemical species found in either the condensation during the chamber experiments or the runoff in the field experiments represent the soluble corrosion products that form because of wet and dry deposition of atmospheric species. Results of these experiments have been used to propose a damage function model for the effects of dry and wet deposition on the corrosion of galvanized steel [*19*]. Characterization of the corrosion film that forms on galvanized steel during ambient exposures was not pursued in these experiments but is being conducted during field weight loss experiments by the Bureau of Mines [*1*]. Results from this field study will be used to test and evaluate the galvanized steel model.

In the environmental exposure chambers, the uptake of SO_2 on galvanized steel was enhanced by the presence of a surface moisture film. In the presence of moisture, SO_2 will undergo a series of reversible ionizations that result in the acidification of the film [*20*]

$$SO_2 + H_2O = SO_2 \cdot H_2O \tag{1}$$

$$SO_2 \cdot H_2O = HSO_3^- + H^+ \tag{2}$$

$$HSO_3^- = H^+ + SO_3^- \tag{3}$$

A chemical equilibrium will be established whereby the SO_2 uptake will decrease in the acidified moisture. In the presence of alkaline compounds, such as basic zinc carbonate, $2ZnCO_33Zn(OH)_2$, that form on galvanized steel during exposure [*21,22*], the H^+ (Eq 3) will be consumed. This reaction shifts the equilibrium and permits more uptake of SO_2 into the surface moisture film. The corrosion of galvanized steel is coupled to the atmospheric deposition of SO_2. Regression analysis of field corrosion of galvanized steel in the St. Louis area indicated stoichiometry for the reaction of absorbed SO_2 [*3*]. This is in excellent agreement with the results of exposing galvanized steel to SO_2 (Fig. 6) during the environmental chamber experiments. The presence of SO_4^{2-} in the chamber condensation film and in the field spray runoff indicates that some form of sulfite ($SO_2 \cdot H_2O$, HSO_3^-, or SO_3^{2-}) has been oxidized. The formation of SO_4^{2-} will shift the equilibrium of Eqs 1, 2, and 3 to the right. Upon evaporation of the surface moisture film, $ZnSO_4$ will remain within the corrosion product film of the galvanized steel.

Acids that deposit through wet deposition can react with galvanized steel by anodic dissolution of the zinc coating and by dissolution of the basic zinc carbonate coating [*21,22*]. The low H^+ concentration that is shown in Table 3 for the rain runoff samples for galvanized steel clearly indicates that practically all of the acidity within the rain has reacted within the galvanized steel panels. Laboratory experiments in which preweathered galvanized steel panels were sprayed with various pH levels of sulfuric and nitric acid show that two H^+ ions react with one Zn^{2+} ion in solution [*23*]. This stoichiometric relationship ($2H^+ = Zn^{+2}$) is in reasonable agreement with runoff results from the Bureau of Mines exposure study in Washington, DC [*24*]. As shown in Fig. 8, the corrosion of galvanized steel by acidity may depend on its exposure history and likely involves a mechanism of competing formation and dissolution of the basic zinc carbonate film.

The charge balance as shown in Table 4 suggests that a substantial amount of anions is not detected in the spray or the ambient runoff collections. Zinc carbonate ($ZnCO_3$) is a major constituent of the corrosion product film of galvanized steel [*22,23*] and is slightly soluble in water. The missing anion could be HCO_3^- since it is one of the major ionic constituents of an aqueous mixture of $ZnCO_3$ [*25*]. The difference in the positive and negative charge concentrations and the spray volume in Table 3 provided an estimated value that is well below 80 nmol/L for Zn^{2+} concentration in a saturated aqueous solution in the presence of 320 ppm CO_2 [*26*]. Considering the residence time of the spray on the galvanized steel panels, it seems likely that $ZnCO_3$ is being dissolved by the presence of atmospheric CO_2. A surface residence time effect has been observed during laboratory spray experiments of deionized water [*23*]. Dissolution of the zinc corrosion film appears likely, even in the absence of anthropogenic acidity in rain.

Other anions including $HCOO^-$, CH_3OO^-, NO_3^-, and Cl^- were present in both the spray and rain runoff collections. For the spray, the NO_3^- most likely arose from the dry deposition of gaseous HNO_3 and particulate NO_3^-. NO_2 is a major constituent of photochemical smog, but chamber exposure experiments show it does not play a significant role in acidifying the surface moisture film on galvanized steel. A synergistic reaction of NO_2 with SO_2 has been reported to produce sulfuric acid [*27*]. This reaction has not been observed within the environment exposure chamber experiments; however, design of specific experiments to study the synergistic reaction have not been undertaken. Except for the rain runoff collections, $CHOO^-$ and CH_3OO^- are very low. If these anions result from the corresponding acids, they could contribute to the corrosion of galvanized steel. The Cl^- that appears in the runoff collections likely resulted from sea salts and crustal particles. No measurements of gaseous hydrochloric acid (HCl) were made at the site; however, its ambient concentrations are expected to be extremely low (<1 ppb). The presence of Cl^- likely contributes to the corrosion of galvanized steel by increasing the time of surface wetness. Most Cl^--containing salts are deliquescent.

Particulate Na^+, K^+, and Ca^{2+} are not major constituents of the spray and rain runoff collections and do not appear to enhance the corrosion of the galvanized steel at the NC site. High-volume particulate concentrations averaged 32 $\mu g/m^3$ for the NC site. In a recent analysis of spray runoff from galvanized steel at the OH site, the average Zn^{2+} was 1.9 times the NC value, even though the average atmospheric SO_2 for the OH site is eleven times that for the NC site [*28*]. The Ca^{2+} at the OH site was found to be 19 times the value for the NC site for the deionized spray runoff. Preliminary analysis suggests that the dry deposition of alkaline particles, such as $CaCO_3$, may neutralize the atmospheric deposition of acidic species at the OH site. Further analysis of runoff data and the ambient concentrations at the OH and NC sites is required.

Conclusion

A unique laboratory exposure system has been developed at EPA for exposing materials to simulated atmospheric conditions. Results from short-term exposure experiments can be used to acquire insight into the aerodynamic and chemical processes that control the atmospheric corrosion of galvanized steel. A second laboratory exposure system was recently built on the campus of the North Carolina State University. This system can expose 48 test panels to different aerodynamic conditions. Much information has been gained regarding atmospheric deposition from the analyses of condensation and spray rinses of test panels. Field covering-spray devices provide an effective means for studying the impacts of dry and wet deposition damage to galvanized steel and other materials. By conducting runoff studies, large amounts of corrosion data for galvanized steel can be obtained over short exposure periods. Major findings that have been obtained from experiments with the environmental exposure system and field covering-spray device regarding the atmospheric corrosion of galvanized steel are summarized as follows:

1. During periods of surface wetness, the deposition of SO_2 and HCHO is controlled by

the gas phase resistance of the atmosphere. For every molecule of SO_2 that deposits, one Zn atom reacts to form $ZnSO_4$. The saturation surface density of SO_2 on dry panels was found to correspond to a monolayer of absorbed SO_2.

2. The deposition velocity of NO_2 in the presence of surface condensation is an order of magnitude less than that of SO_2. NO_2 deposition is controlled by the surface resistance.
3. Gaseous HNO_3 will readily deposit during periods of surface wetness and dryness.
4. Rain acidity contributes to the corrosion. Laboratory and field exposures suggest that $2H^+$ ions react with one Zn^{2+} ion in solution.
5. The corrosion film is soluble in rain as the results of dissolved atmospheric CO_2. The dissolution appears to depend on the residence time of rain water on the surface.

With NAPAP ending in 1990, these unique facilities will be available for environmental testing and development of materials. By passing the Technology Transfer Act of 1986, Congress expressed a desire to make technology developed by the government available to private industry and other organizations through cooperative research and development agreements.

Acknowledgment

The information in this document has been funded wholly or in part by the U.S. Environmental Protection Agency under Contract 68-02-4443. It has been subjected to Agency review and approved for publication. Mention of trade names or commercial products does not constitute endorsement or recommendation for use.

References

[1] Flinn, D. R., Cramer, S. D., Carter, J. P., and Spence, J. W., *Durability of Building Materials,* Vol. 3, 1985, p. 147.
[2] Haynie, F. H. and Upham, J. B., *Materials Protection and Performance,* Vol. 10, 1971, p. 18.
[3] Haynie, F. H., *Durability of Building Materials and Components, ASTM STP 691,* American Society for Testing and Materials, Philadelphia, 1980, p. 157.
[4] Haynie, F. H., *Degradation of Metals in the Atmosphere, ASTM STP 965,* American Society for Testing and Materials, Philadelphia, 1986, p. 282.
[5] Haynie, F. H. and Spence, J. W., *Journal of Pollution Control Association,* Vol. 34, 1984, p. 941.
[6] Guttman, H., *Metal Corrosion in the Atmosphere, ASTM STP 435,* American Society for Testing and Materials, Philadelphia, 1968, p. 223.
[7] Atterass, L. and Haagenrud, S., in *Atmospheric Corrosion,* W. H. Ailor, Ed., John Wiley, New York, 1982, p. 873.
[8] Kucera, K., Haagenrud, S., Atteraas, L., and Gullman, J., *Degradation of Metals in the Atmosphere, ASTM STP 965,* American Society for Testing and Materials, Philadelphia, 1986, p. 264.
[9] Spence, J. W., Stump, F. D., Haynie, F. H., and Upham, J. B., EPA Report 650/3-75-001, U.S. Environmental Protection Agency, Research Traingle Park, NC, 1975.
[10] Harker, A. B., Haynie, F., Mansfield, F., Strauss, D. R., and Landis, D. A., *Atmospheric Environment,* Vol. 16, No. 11, 1982, p. 2691.
[11] Haynie, F. H., Spence, J. W., and Upham, J. B., EPA Report 600/3-76-015, US Environmental Protection Agency, Research Triangle Park, NC, 1976.
[12] Campbell, G. G., Schurr, G. G., Slaevirkowski, G. C., and Spence, J. W., *Journal of Paint Technology,* Vol. 46, 1974, p. 59.
[13] Edney, E. O., Stiles, D. C., Spence, J. W., Haynie, F. H., and Wilson, W. E., "Materials Degradation Caused by Acid Rain," ACS Symposium Series 318, American Chemical Society, Washington, DC, 1986, p. 172.
[14] Edney, E. O., Stiles, D. C., Spence, J. W., Haynie, F. H., and Wilson, W. E., *Atmospheric Environment,* Vol. 20, No. 3, 1986, p. 541.
[15] Edney, E. O., Cheek, S. F., Stiles, D. C., Corse, E. W., Wheeler, M. L., Spence, J. W., Haynie, F. H., and Wilson, W. E., *Atmospheric Environment,* Vol. 22, No. 10, 1988, p. 2263.

[16] Spence, J. W., Haynie, F. H., Edney, E. O., and Stiles, D. C., "Materials Degradation Caused by Acid Rain," ACS Symposium Series 318, American Chemical Society, Washington, DC, 1986, p. 194.
[17] Lee, Y. N. and Schwartz, S. E., *Journal of Geophysical Research*, Vol. 86, 1981, p. 11971.
[18] Munger, J. W., Jacob, D. J., and Hoffman, M. R., *Journal of Atmospheric Chemistry*, Vol. 1, 1984, p. 335.
[19] Spence, J. W. and Haynie, F. H., EPA Project Report No. EPA600/3-88-027, US Environmental Protection Agency, Research Triangle Park, NC, 1988.
[20] Hoffman, M. R. and Jacob, D. J., *SO_2, NO and NO_2 Oxidation Mechanisms: Atmospheric Considerations*, Ann Arbor Science, Ann Arbor, MI, 1984, p. 101.
[21] Barton, K. and Baranek, K., *Werkst Corros*, 1959, p. 377.
[22] Flinn, D. R., Cramer, S. D., Carter, J. P., Hurwitz, D. M., and Linstrom, P. J., "Materials Degradation Caused by Acid Rain," ACS Symposium Series 318, American Chemical Society, Washington, DC, 1986, p. 119.
[23] Stiles, D. C. and Edney, E. O., *Corrosion*, Vol. 45, No. 11, 1989, p. 896.
[24] Cramer, S. D., Carter, J. P., Linstrom, P. J., and Flinn, D. R., *Degradation of Metals in the Atmosphere, ASTM STP 965*, American Society for Testing and Materials, Philadelphia, 1986, p. 239.
[25] Stumm, W. and Morgan, J. J., *Aquatic Chemistry: An Introduction Emphasizing Chemical Equilibria in Natural Waters*, Wiley-Interscience, New York, 1970, p. 182.
[26] Weast, R. C., *Handbook of Chemistry and Physics*, The Chemical Rubber Co., Cleveland, OH, 1965, p. B-239.
[27] Kucera, V., "Materials Degradation Caused by Acid Rain," ACS Symposium Series 318, American Chemical Society, Washington, DC, 1986, p. 119.
[28] Edney, E. O., Cheek, S. F., Corse, E. W., Spence, J. W., and Haynie, F. H., *Journal of Environmental Science and Health*, Vol. A24, No. 5, 1989, p. 439.

DISCUSSION

G. Downs[1] (*written discussion*)—Your paper addresses gaseous and liquid contaminants. Have you considered particulate contaminants, salt crystals, dust organic particulates, etc.?

J. W. Spence et al. (*author's closure*)—Material specimens are exposed to gaseous pollutants and aerosols that form within the photochemical chamber of the laboratory exposure system. Particulate contaminants, etc. are not introduced into the laboratory exposure system. Material specimens that have been exposed in the field for various lengths of time can be tested in the laboratory exposure system. This permits the study of gaseous pollutants and aerosols on the corrosion film of metals as it forms during different ambient field exposures. Of course, material specimens are exposed to particulates, gaseous pollutants, etc., using the covering-spray systems that were designed to study wet and dry deposition during field exposure.

D. A. Jones[2] (*written discussion*)—You described various atmospheric parameters: particle deposition, pollutant fluxes, acidity, and dissolved constituents of drain water from exposed panels. Have you made any progress in direct measurements of surface reaction or degradation by electron microscopy, analytical electron spectroscopy, or other methods?

J. W. Spence et al. (*author's closure*)—The results I have described using the laboratory exposure system and field covering-spray devices pertain to only the soluble corrosion

---

[1] U.S. Army DPG Tropic Test Site, APO Miami 34024.
[2] Mackay School of Mines, University of Nevada, Reno, NV 89559.

reaction products of galvanized steel panels. Scanning electron microscopy, X-ray photoelectron spectroscopy, etc. are being used by Steve Cramer with the Bureau of Mines to characterize the corrosion product film of various metallic materials as part of the NAPAP project. Results of this work were presented by Steve during the symposium.

P. J. Peterson[3] (*written discussion*)—1. NO_2 is a very good oxidizer. $NO_2 + e^- \gg NO_2^{-1} +$ NO_2 and HNO_2 are very hard to distinguish by analytical instruments, therefore the lack of loss of NO_2 by analysis does not mean that it was not consumed by the corrosion reactions.

2. On galvanized steel, $Cl \gg Na$; on Teflon, $Cl = Na$, and Na on Teflon $\approx$ Na on galvanized steel, therefore NaCl is not the only source of Cl on galvanized steel. HCl? This would be collected on galvanized steel but not on Teflon.

J. W. Spence et al. (*author's closure*)—Our investigation, which involved only the soluble corrosion products of galvanized steel, indicates that NO_2 and HNO_2 are not major contributors to the corrosion of galvanized steel, especially when SO_2 is present. I don't believe NO_2 has been identified as a major component of the corrosion film that is being conducted by Steve Cramer with the Bureau of Mines.

The Cl^- that was detected in our runoff collections during the field exposure of galvanized steel may indeed be from the dry deposition of gaseous HCl and particulate Cl^-. There are times during the summer months that high Cl^- concentrations are observed in rain and runoff collections at the NC site. These concentrations are likely associated with sea salt in the rain that results from a Bermuda high in the Atlantic.

---

[3] IBM, General Products Division, San Jose, CA.

John. W. Spence[1] *and Fred H. Haynie*[1]

Derivation of a Damage Function for Galvanized Steel Structures: Corrosion Kinetics and Thermodynamic Considerations

REFERENCE: Spence, J. W. and Haynie, F. H., **"Derivation of a Damage Function for Galvanized Steel Structures: Corrosion Kinetics and Thermodynamic Considerations,"** *Corrosion Testing and Evaluation: Silver Anniversary Volume, ASTM STP 1000,* R. Baboian and S. W. Dean, Eds., American Society for Testing and Materials, Philadelphia, 1990, pp. 208–224.

ABSTRACT: A damage function for predicting the corrosion of galvanized steel structures by wet and dry deposition has been developed from the thermodynamics and kinetics of atmospheric corrosion chemistry. The function mathematically expresses the competing reactions for the buildup and dissolution of the basic zinc-carbonate corrosion film with exposure time. Major findings as expressed by the theoretical function are as follows:

1. During periods of surface wetness, SO_2 reaching the surface reacts stoichiometrically with the zinc.
2. Rain acidity reacts stoichiometrically with the zinc.
3. The corrosion film of basic zinc carbonate is soluble in clean rain. The dissolution depends on the residence time of rain on the galvanized steel surface.
4. Deposition velocity controls the rate of corrosion of galvanized steel structures by gaseous SO_2 during periods of wetness.

This paper recommends testing the applicability of the proposed damage function with field corrosion data that is being acquired by the Bureau of Mines and the U.S. Environmental Protection Agency and with corrosion data from prior field exposure studies. In this manner a validated damage function should be developed for conducting an assessment of acid deposition to galvanized steel structures.

KEY WORDS: galvanized steel, damage function model, sulfur dioxide, rain acidity, nitric acid, carbon dioxide particles

For the National Acid Precipitation Assessment Program (NAPAP), Task Group VII has been conducting a materials effects program to develop damage functions for manmade and cultural materials at risk because of atmospheric wet and dry deposition. An overview of the research program, including the materials-at-risk, exposure sites, site atmospheric measurements, testing methodology, etc., has been previously reported [*1*]. A damage function is a mathematical expression that relates the rate of degradation of a material to the various contributing environmental factors associated with dry and wet deposition. Dry deposition involves atmospheric gases and particles that deposit during periods of surface dryness and wetness with condensation. Wet deposition involves those chemical species associated with rain, fog, or snow. The functions that Task Group VII develops will be used by NAPAP

---

[1] Atmospheric Research and Exposure Assessment Laboratory, U.S. Environmental Protection Agency, Research Triangle Park, NC 27711.

along with other information such as distribution of materials to prepare state of science and assessment reports to Congress in 1990.

The Bureau of Mines (BOM) and the U.S. Environmental Protection Agency (EPA) are conducting exposure studies of galvanized steel because it is fabricated into many products that are boldly exposed to wet and dry deposition. Coating steel with zinc is one of the least expensive and more durable methods for protecting steel structions. The service life of galvanized steel structures such as roofing and fencing depends on maintaining the zinc coating during exposure.

As shown in Table 1, different galvanized steel products corrode at different rates even when exposed at the same location over the same period of time. Even the relative placement of specimens on an exposure rack can make a difference in corrosion rates. The American Society for Testing and Materials (ASTM) has established standard procedures for atmospheric testing so that corrosion data from different sites may be compared. Using these procedures and simultaneously measuring environmental parameters, a corrosion-environmental data set can be produced from which an empirical damage function can be derived using multiple regression techniques. The resulting empirical coefficients and their calculated standard errors of the damage function have limited applicability. Within the limits of the standard errors of the function, the empirical damage function can predict the corrosion rate of similar specimens at other sites provided that environmental data with the same accuracy and precision used to derive the function are available for the other sites.

The use of an empirically derived damage function to predict corrosion rates of galvanized steel structures with environmental data of unknown accuracy and precision raises considerable concern. Galvanized steel structures are not standard specimens. Moreover, it is not possible to determine the environmental parameters surrounding each structure with the same accuracy and precision. Not only would biased errors be produced by such a damage function, but also the calculated confidence limits would be misleading.

To address this concern, the following steps are being taken to develop a damage function for galvanized steel that can be used to assess damage to real structures:

1. Use of fundamental principles of thermodynamics and kinetics to derive a damage function.

TABLE 1—*Corrosion rates of zinc on galvanized steel products exposed to different environments prior to 1954* [7].

	Mean Corrosion Rates and Estimated Standard Deviation, μm/year	
Site	Sheet	Wire and Fencing
Altoona, PA	7.57 ± 0.54	
Pittsburgh, PA	5.63 ± 0.34	10.86 ± 1.02
Sandy Hook, NJ	2.74 ± 0.30	4.37 ± 0.45
Bridgeport, CT		4.25 ± 0.44
Lafayette, IN		2.94 ± 0.34
Ithaca, NY		2.68 ± 0.42
State College, PA	1.27 ± 0.29	2.48 ± 0.24
Ames, IA		1.68 ± 0.19
College Station, TN		1.22 ± 0.43
Santa Cruz, CA		0.83 ± 0.26
Manhattan, KS		0.79 ± 0.27
Davis, CA		0.76 ± 0.42

2. Establishment of the applicability and consistency of the function by using laboratory and field experiments.
3. Confirmation of applicability to changing real-world environments by using standardized exposure procedures at test sites where the accuracy and precision of environmental parameters are known.
4. Checks on how well the function can predict corrosion rates on real structures with environmental parameters of unknown accuracy and precision.

This paper describes the development of a damage function for the effects of wet and dry deposition on galvanized steel structures by applying fundamental principles of thermodynamics and atmospheric corrosion kinetics. Confirming the applicability and consistency as well as environmental testing of the damage function is the subject of a separate paper. By following the steps as outlined above, a damage function for galvanized steel structures should emerge that is suitable for use by NAPAP in preparing reports to Congress and by EPA in developing control strategies for acidic deposition.

Atmospheric Exposure

Atmospheric corrosion of galvanized steel products involves electrochemical reactions that are initiated when the zinc surface becomes wet with rain, mist, or dew [*2,3,4*]. Chemical analysis of the corrosion film that forms during exposure of galvanized steel products indicates the formation of basic zinc carbonate, $2ZnCO_3Zn(OH)_2$ [*4,5*]. The film likely forms by the reaction of atmospheric carbon dioxide (CO_2) with electrochemical reaction products.

The basic zinc carbonate film will tend to inhibit the corrosion of the zinc provided the film is not removed or chemically altered. Under these conditions, the rate of zinc corrosion would be controlled by diffusion through the film and would be inversely proportional to the thickness of the film. The corrosion time function would exhibit a parabolic shape. In the presence of acidity, the basic zinc carbonate film may be dissolved or chemically changed, the thickness of the film would be reduced, and the corrosion would be less inhibited.

During atmospheric exposure of galvanized steel products, there are environmental conditions in which the mechanism of formation and removal of the basic zinc carbonate film are competing. Haynie previously derived the following relationship for corrosion of zinc [*6,7*]:

$$C = Bt + A[1 - \exp(-BC/A)]/B \qquad (1)$$

where C = corrosion, (μm)
t = time, year,
B = solution rate of the film, μm/year, and
A = diffusivity of corrosive species through the film, μm^2/year.

After long exposures, the term $-BC/A$ of Eq 1 is large; therefore, $\exp(-BC/A)$ approaches zero and Eq 1 becomes a linear function.

$$C = A/B + Bt \qquad (2)$$

The net zinc corroded (C) after steady state is reached is the sum of the zinc in the film (A/B) and the zinc dissolved from the film (Bt).

In polluted, acidic environments, the corrosion of zinc would be expected to be linear early in the exposure. The A/B term of Eq 2 would be the intercept, and the B term represents the slope with a constant corrosion rate. The intercept would be proportional to the steady thickness of the film when the rate of film dissolution is equal to the rate of its formation. Diffusivity (A) through the film can be affected by pollutant species incorporated in the film. The solution rate (B) of the film is expected to be a function of the rate of delivery of acidic pollutants to the film. The B term may be separated into environmental terms involving wet and dry deposition. The wet and dry delivery mechanisms provide a means of describing the corrosion rate-controlling factors. In the next section, we attempt to apply fundamental principles of atmospheric corrosion kinetics and thermodynamics to derive a damage function for the corrosion of galvanized steel structures.

Dry Deposition

During exposure of galvanized steel structures, both gaseous and particulate pollutants are deposited to the zinc surface; however, the machanisms of deposition differ. The rate of delivery of gases to a surface is determined by airflow, whereas particulate matter is deposited by gravitational settlement and wind-blown impaction.

Deposition Velocity of Gases—The ambient concentration of gaseous pollutants is related to pollutant flux to a surface by defining deposition velocity (V_d) as the ratio of the flux to the ambient concentration measured at some point away from the surface. Deposition velocity is simply a coefficient that relates flux of a pollutant to its ambient concentration. For gaseous pollutants, deposition velocities are usually around 1 cm/s [*8*].

Transport phenomena for various shapes and orientations with respect to fluid flow have been compiled [*9–11*]. Considerable engineering data exist on momentum, heat, and mass transfer as a function of the Reynolds number, which is defined as length times the velocity of air divided by the kinematic viscosity of air. The length term in the Reynolds number varies with the shape and orientation of the surface over which air flows. When only surface friction is considered, the following relationship is applicable for air at normal temperatures and pressures.

$$f/2 = J_m = J_h \tag{3}$$

where f = friction factor for momentum transfer,
J_m = factor for mass transfer, and
J_h = factor for heat transfer.

The factors are dimensionless terms. From analogy with momentum transport, the deposition velocity of gases that readily absorb on surfaces and that have a Schmidt number of approximately one can be expressed as follows

$$V_d = V^{*2}/V = Vf/2 \tag{4}$$

where V^* = friction velocity, and
V = average wind speed.

The friction velocity, V^*, is equal to $V(f/2)^{1/2}$. The deposition velocity to a particular shape can be estimated provided the J factors or the friction factor, f, are known as a function of the Reynolds number.

Most corrosion data, particularly for galvanized steel or zinc, are determined by using standard 102 by 152-mm flat panels. Thus, the effect of wind flowing over these specimens is important when attempting to extrapolate to structures of different shapes and sizes. Figure 1 is a sketch of the boundary layer of fluid flowing over a flat panel. The relationships between the friction factor and Reynolds number (length) for different flow regions are shown. The edge of the boundary layer is where the fluid velocity approximates the free-stream velocity. For the standard panels at normal wind speeds, the flow is expected to be laminar, whereas for most roofing and siding on real structures the flow is likely to be turbulent.

Fencing constitutes a major portion of all boldly exposed galvanized steel. Fortunately, the relationship for flow perpendicular to cylinders has been studied in some detail for momentum, heat, and mass transfer. Sherwood and Pigford [*12*] have demonstrated remarkable agreement between $f/2$, J_h, and J_m as a function of Reynolds number with cylinder diameter as the length term. The data are closely approximated by the relationship:

$$f/2 = J_h = J_m = 0.63\sqrt{RE_D} \tag{5}$$

where RE_D = Reynolds number = DV/ν,
D = cylinder diameter over which air flows, cm,
ν = kinematic viscosity of air, 0.15 cm^2/s at 20°C, and
V = wind velocity, cm/s.

From Eqs 4 and 5 it can be seen that wind velocity and the shape and size of a surface affect the deposition velocity. It is informative to compare deposition velocities calculated for standard plates with those for a large sheet 5 m long and for 9-gage, 3.76-mm-diameter, galvanized fence wire. With kinematic viscosity at 0.15 cm^2/s and wind velocity (V) in metres per second, the following deposition velocities in centimetres per second were calculated

Corrosion panels: $V_d = 0.73\sqrt{V}$ (6)
Large sheet: $V_d = 0.25V^{6/7}$ (7)
Fencing: $V_d = 4\sqrt{V}$ (8)

For an average wind speed approaching each surface of 3 m/s, the respective deposition velocities are 1.3, 0.64, and 6.9 cm/s. Based on these values, fencing is expected to corrode faster than roofing or siding when exposed to the same polluted environment. These relationships for determining the deposition velocities to different surfaces are essential in estimating the corrosion of galvanized steel structures. A dry-deposition study of different galvanized steel structures is being conducted by EPA for NAPAP. This study should provide an evaluation of Eqs 6 through 8.

Although gases may be delivered to different surfaces at calculated deposition velocities, the net flux of a gas to a surface is not necessarily proportional to the deposition velocity. The depositon of a gas to a dry surface will likely proceed until saturation occurs. The net flux of the gas would then be zero, because the amount of gas delivered to the surface is equal to that removed. As previously discussed, zinc corrodes by an electrochemical process when the surface is wet. Therefore, it is important to have a means of estimating time of surface wetness of galvanized steel structures. This permits the flux of a gas that is soluble and reacts to be determined during periods of surface wetness.

Time of Surface Wetness—Atmospheric corrosion of zinc will occur when the surface is wet by rain or dew. Dew will form if the surface temperature is below an effective dew point. The presence of hygroscopic salts such as sodium chloride (NaCl) or calcium sulfate ($CaSO_4$) tends to increase the effective dew point or equivalently lowers the critical relative

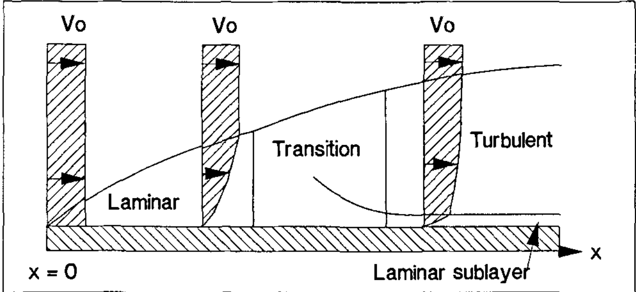

REGION	f/2
LAMINAR	$0.664/\sqrt{REx}$
TRANSITION	$0.015/(REx)^{1/7} - 1700/REx$
TURBULENT	$0.015/(REx)^{1/7}$

$REx = xVo/\nu$ = length Reynolds No.

FIG. 1—*Boundary layer on a flat plate.*

humidity (RH_c) at the zinc surface. Tables of relative humidities in equilibrium with saturated salt solutions at different temperatures are readily available [*13*]. The RH_c for NaCl is about 75% and is relatively constant with temperature. In contrast, the data for zinc sulfate ($ZnSO_4$), which has been identified on galvanized steel panels during exposure studies, fit the relationship

$$RH_c = 96.03 - 0.313DP \tag{9}$$

where DP = ambient dew point temperature, °C.

When the surface of zinc is wet depends not only on the surface temperature and ambient relative humidity, but also on the accumulated corrosion products. Thus, the time of surface wetness (t_w) of zinc can best be defined as the amount of time it is raining plus when the relative humidity exceeds a critical relative humidity (Eq 9) and when the dew point is greater than 0°C or not freezing. Significant corrosion is not expected to occur when the surface is frozen.

In practice, the time of surface wetness (t_w) is most often estimated from the amount of time some selected RH_c is exceeded. Different researchers have used different values, with the most common value of 85%. The use of 85% is probably a good approximation where polluant levels, particularly SO_2, exceed 30 $\mu g/m^3$. In areas where levels are less than that, Eq 9 is probably a better approximation. In marine locations or in areas where deicing salts are used, 75% may be a better estimate of RH_c.

Deposition of Gases—The solubility of atmospheric gases in liquid water has been determined as the coefficient of Henry's law. The solubility of nitrogen dioxide (NO_2) in liquid water has a value of 1×10^{-12} mol/L atm at 25°C [*14*]. Therefore, very little NO_2 is expected to deposit on the zinc surface during periods of surface wetness. Sulfur dioxide (SO_2) that has a solubility of 1.24 mol/L atm in liquid water at 25°C [*15*] will readily deposit during periods of surface wetness and will react with the zinc [*16,17*]. SO_2 has been observed to deposit on a dry surface of galvanized steel panels until a monolayer of SO_2 formed [*17*]. This should enhance the corrosion of the panels during periods of surface wetness with dew. Other atmospheric gases such as nitric acid (HNO_3) and formaldehyde (HCOH) are quite soluble.in liquid water. HNO_3 is the only atmospheric gas that readily deposits to zinc surfaces during periods of surface wetness and dryness [*18*]. Unless the HCOH that deposits undergoes chemical reaction, it will likely be reemitted to the atmosphere upon evaporation of the surface moisture on the zinc. In summary, the deposition of SO_2, HNO_3, and HCHO appears to be controlled by the gas-phase resistance of the atmosphere, whereas NO_2 deposition is controlled by surface resistance of the galvanized steel structures.

Of the atmospheric pollutant gases, SO_2 and HNO_3 can react with the zinc and basic zinc carbonate film. Table 2 presents reactons of interest and the equilibrium constants for each at 25°C. The equilibrium constants for these reactions were calculated from thermodynamic data that was obtained from the National Bureau of Standards Table of Chemical Thermodynamic Properties [*19*] as tabulated in the Appendix. The calculated equilibrium constants for the first four reactions in Table 2 for SO_2 and HNO_3 with zinc and basic zinc carbonate are observed to be rather large. This suggests stoichiometric reactions of these gases with the zinc surface when conditions favor the kinetics. For every SO_2 molecule or every two HNO_3 molecules that deposit to the wet surface of galvanized steel, a zinc ion (Zn^{2+}) will be consumed. Reactions 5 and 6 of Table 2 indicate that when both SO_2 and HNO_3 deposit, the formation of sulfates (SO_4^{2-}) is favored on wet zinc surfaces. As suggested by these equations, a minimum amount of zinc nitrate [$Zn(NO_3)_2$] would be expected within the zinc corrosion film as HNO_3 is emitted back into the atmosphere as a gas. The calculated equilibrium constants for these reactions strongly suggest that, in polluted environments, SO_2 will play a major role in the corrosion of galvanized steel structures, even when HNO_3 is present.

The zinc corrosion (C_d) due to the deposition of gaseous SO_2 during periods of surface wetness and dryness may be expressed as follows

$$C_d = 0.045V_d(SO_2)t_w + 1.29 \times 10^{-4}A_rN \tag{10}$$

where C_d = zinc corrosion due to the deposition of SO_2, μm,
V_d = deposition velocity, cm/s,
SO_2 = ambient SO_2 concentration, μg/m^3,
t_w = time of surface wetness, years,
A_r = ratio of actual to apparent surface, and
N = number of periods between surface wetness.

The first term of Eq 10, $0.045V_d(SO_2)t_w$, represents the deposition of SO_2 during periods of surface wetness due to condensation (dew). The coefficient, 0.045, represents the stoichiometric reaction of SO_2 with the wet zinc surface to form $ZnSO_4$. The V_d component, as shown in Eqs 6 through 8 for different galvanized steel structures, determines the flux of SO_2 to the zinc surface from atmospheric measurements of SO_2 concentrations (μg/m^3). The time of surface wetness, t_w, accounts for the deposition or flux of atmospheric SO_2 during periods of wetness to galvanized steel structures. In polluted environments, the t_w may best be estimated from Eq 9, which permits the determination of the RH_c for the surface wetness of galvanized steel structures from ambient dew point measurements.

The last term within Eq 10, $1.29 \times 10^{-4}A_rN$, represents the corrosion of zinc that is associated with the formation of a monolayer of SO_2 during periods of surface dryness. This

TABLE 2—*Equilibrium constants for selected acidic gas reactions* (*see the Appendix*).

Reaction	ln(*k*)
1. $Zn_{(cr)} + SO_{2(g)} + O_{2(g)} \Rightarrow Zn^{2+} + SO_4{}^{=}{}_{(ao)}$	238.56
2. $Zn_{(cr)} + 2HNO_{3(g)} \Rightarrow Zn^{2+}{}_{(ao)} + 2NO_3{}^{-}{}_{(ao)} + H_{2(g)}$	86.76
3. $Zn(OH)_{1\,2}(CO_3)_{0\,4(cr)} + SO_{2(g)} + 0.50_{2(g)} \Rightarrow Zn^{2+}{}_{(ao)} + SO_4{}^{=}{}_{(ao)} + 0.4CO_{2(g)} + 1.6H_2O_{(l)}$	106.44
4. $Zn(OH)_{1\,2}(CO_3)_{0\,4(cr)} + 2HNO_{3(g)} \Rightarrow Zn^{2+}{}_{(ao)} + 2NO_3{}^{-}{}_{(ao)} + 0.4CO_{2(g)} + 1.6H_2O_{(l)}$	50.3
5. $H_2O_{(1)} + 2NO_3{}^{-}{}_{(ai)} + SO_{2(g)} + 0.50_{2(g)n} \Rightarrow SO_4{}^{2-}{}_{(ao)} + 2HNO_{3(g)}$	56.14
6. $Zn(NO_3)_2\ 6H_2O_{(cr)} + H_2SO_{4(l)} \Rightarrow ZnSO_4 \cdot 6H_2O_{(cr)} + 2HNO_{3(g)}$	4.5

NOTE: g = gaseous; cr = crystalline solid; l = liquid; ai = aqueous solution, ionized substance standard, and ao = aqueous solution, anionized substance or anionized for which no further ionization is considered.

corrosion is shown as a function of the exposed surface area and the number of periods between surface wetness. The coefficient, 1.29×10^{-4}, represents the micrometres of zinc loss of a clean zinc surface due to the absorption of a monolayer of SO_2.

Deposition of Particles and Aerosols—The deposition velocity for particles to surfaces is more difficult to determine than the deposition for atmospheric gases. Particle size, shape, and density as well as surface orientation are factors that affect the deposition velocity of particles [*20*]. Atmospheric monitoring of particles involves determining fine-mode (submicrometre diameter) and coarse-mode fractions. Deposition velocities for fine-mode particles are low with averages $7.4 \times 10^{-4} \pm 4.8 \times 10^{-4}$ cm/s for both horizontal and vertical surfaces. By contrast, average deposition velocities for coarse-mode particles to horizontal and vertical surfaces are reported as 1.55 ± 0.08 cm/s and 0.34 ± 0.12 cm/s, respectively [*21*]. Acid aerosols that would react with zinc surfaces are most often found in the fine-mode fraction of total suspended particulate (TSP). Because of the low deposition velocities of fine particles, acidic aerosols are not likely to contribute significantly to the corrosion of galvanized steel structures. On the other hand, constituents found in coarse-mode particles are likely to affect the corrosion, particularly horizontal galvanized steel structures. Coarse-mode particles that deposit will increase the surface area upon which atmospheric gas may absorb and subsequently react during periods of wetness. If constitutents of these particles are hygroscopic, the RH_c would be lower, thereby facilitating the deposition of gaseous pollutants to the wet surface. Coarse-mode particles that contain cation species with electrode potential more negative than zinc may react preferentially with gaseous pollutants that deposit during periods of surface wetness.

Wet Deposition

Rain not only contributes to the time of surface wetness of galvanized steel structures but also delivers reactive species to the surface. The rate of delivery of a reactive species is the amount of rain per unit time multiplied by its ion concentration.

Rain Acidity Due to Hydrogen Ions (H^+)—The acidity of rain, which is due to H^+, is expected to increase the corrosion rate of galvanized steel structures by reaction with the basic zinc carbonate film or the zinc metal. The H^+ within the rain would be consumed according to the following stoichiometric relationship: $2H^+ = Zn^{2+}$. The upper limit of H^+-induced corrosion of zinc would simply be a function of the amount of rainfall and its H^+ concentration or pH. The H^+ concentration, equivalents per litre, is 10^{-pH}. Hence, hydrogen ion equivalents delivered per square centimetre of horizontal surface is the amount of rain times $10^{-3-\text{pH}}$. One equivalent of H^+ per square centimetre of zinc will consume 4.6 cm of zinc (that is, the ratio of equivalent weight to density). The relationship for zinc corrosion of galvanized steel structures caused by rain acidity (C_{RA}) may be expressed as follows

$$C_{RA} = 46R10^{-\text{pH}} \tag{11}$$

where C_{RA} = zinc corrosion due to H^+, μm, and
R = total rainfall during exposure, cm.

For standard test panels exposed at 30° from the horizontal, the average corrosion on both sides would be less by a factor of 0.5 cos 30°.

Rain Acidity Due to Carbon Dioxide (*CO_2*)—Rain acidity is also caused by dissolved CO_2 within the atmosphere. This produces bicarbonate ions (HCO_3^-) that likely contribute to the solubility of the basic zinc carbonate on galvanized steel structures. If it is assumed that rainwater equilibrates with both atmospheric CO_2 and the galvanized steel surface, then the zinc corrosion can be estimated from the solubility of the basic zinc carbonate film. A description of the derivation of the zinc corrosion estimate using principles of thermodynamics is shown in the Appendix.

Figure 2 depicts a plot of Zn^{2+} concentration as a function of atmospheric carbon dioxide at 298.16 K for the three solid phases: $ZnCO_3$, $Zn(OH)_2$, and $3Zn(OH)_2 \cdot 2ZnCO_3$. Within the range of normal atmospheric CO_2 concentrations, the basic zinc carbonate appears to be the least soluble and would likely precipitate from a saturated solution of Zn^{2+}. The concentration of Zn^{2+} for reaction of CO_2 and H_2O with basic zinc carbonate as the solid

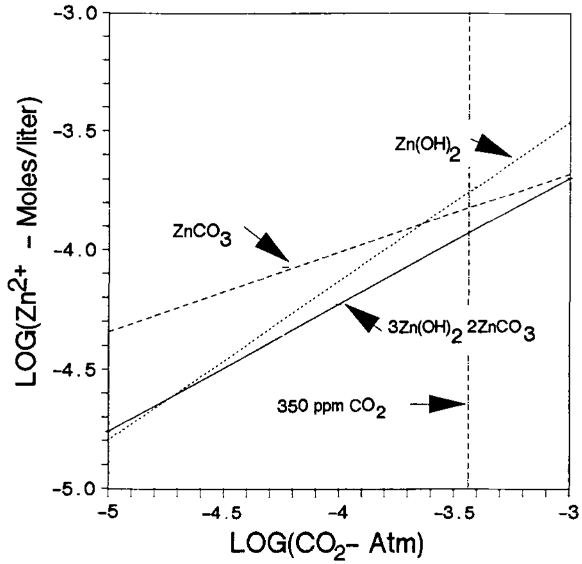

FIG. 2—*Solubility of films as a function of CO_2 at 298.16 K.*

phase can be determined by the following relationship

$$Zn^{2+} = [k(CO_2)^{1.6}/4]^{1/3} \tag{12}$$

where Zn^{2+} = concentration, mol/L,
k = equilibrium constant, mol/L, and
CO_2 = atmospheric concentration, atm.

Atmospheric concentrations of CO_2 have been observed to vary at an urban location within a range between 300 and 550 ppm [*22*]. The average in the United States is assumed to be 345 ppm. Figure 3 is a plot of the estimated solubility of basic zinc carbonate as a function of temperature at 345 and 500 ppm atmospheric CO_2. This plot was derived from thermodynamic functions in the Appendix and Eq 12. Temperature has a greater effect on solubility than does CO_2 concentration. Solubility in winter is expected to be about double what it is in summer. Within the range of 0 to 20°C, the curve for solubility of basic zinc carbonate exposed to 345 ppm CO_2 is closely approximated by the relationship

$$Zn^{2+} = \exp(-21.343 + 3651/T) \tag{13}$$

where Zn^{2+} = solubility of basic zinc carbonate, mol/L, and
T = temperature, K.

Using this relationship, the amount of zinc corrosion due to CO_2 dissolved in rain may be expressed as a function of the amount of rainfall and residence time factor

$$C_{RC} = 91.56 \exp(-21.34 + 3651/T)rR \tag{14}$$

where C_{RC} = zinc corrosion due CO_2 in rain, μm,
r = residence time factor, and
R = rainfall, cm.

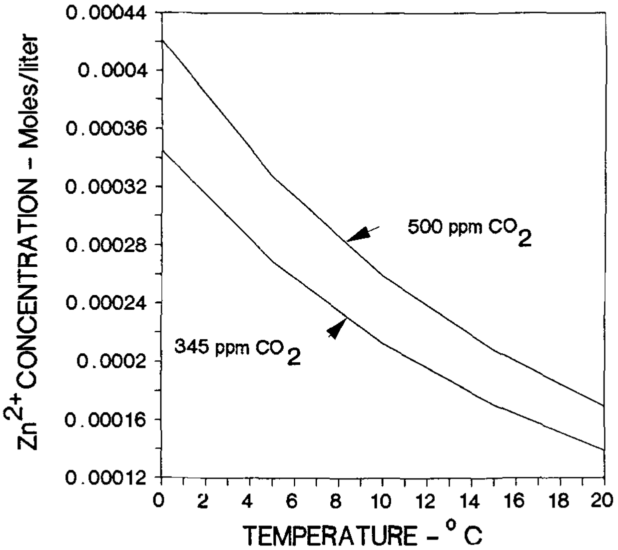

FIG. 3—*Solubility of basic zinc carbonate as a function of temperature.*

Since rainwater may not remain in contact long enough with the zinc surface of various galvanized steel structures to reach equilibrium [*23*], a residence time factor is included in Eq 14. The residence time should vary with rain intensity and should be proportional to the length of surface over which the rain flows and the angle of exposure. This suggests that equilibrium may be reached for large sheets such as roofing. On the other hand, it may be more appropriate to assume that there will be little effect on fence wire. As previously mentioned, for standard test panels mounted at 30° to the horizontal, this effect would be less by a factor of 0.5 cos 30°.

Results

By combining the dry and wet deposition terms that were derived for the corrosion of zinc surfaces, the following linear damage function for predicting the long-term corrosion (μm) of galvanized steel structures is proposed

$$C = F + C_d + C_{RA} + C_{RC} \tag{15}$$

For this function, the F term represents the zinc remaining in the corrosion film and is expressed according to Eq 2 as A/B for steady-state corrosion of zinc. The diffusivity (A) and solution (B) rates of the corrosion film can best be evaluated from long-term field corrosion data that are being acquired by the BOM at five field exposure studies for NAPAP [*1*]. The other terms for zinc corrosion of the function are for the deposition of SO_2 during periods of surface wetness and dryness (C_d, Eq 10) for the rain acidity (C_{RA}, Eq 11) and for the dissolution of the basic zinc carbonate film due to atmospheric CO_2 (CR_c, Eq 14) that is dissolved in rain. These terms can best be evaluated from field and laboratory runoff studies of galvanized steel that the BOM and EPA have conducted for NAPAP.

A term for the deposition of coarse-mode particles has not been included in the proposed damage function. As previously discussed, coarse particles that likely deposit on zinc surfaces may increase the surface area as well as the time of surface wetness. The incorporation of terms for the effects of particles, as well as other atmospheric gases into Eq 15, must await the evaluation of NAPAP field monitoring and corrosion data by the BOM and EPA.

Discussion

During long exposure periods, the zinc remaining in the basic zinc carbonate corrosion film (F) that forms on galvanized steel structures should be relatively constant. For long exposure periods, the contributions to zinc corrosion that are due to the dry deposition of SO_2, C_d, the acidity in rain, C_{RA}, and the CO_2 dissolved in rain, C_{RC}, may be determined by assuming certain environmental conditions. As an example, for the following environmental parameters

Wind speed	3 m/s
Time of surface wetness	0.30 years
Rainfall	100 cm
Temperature	23°C

Table 3 indicates the zinc corrosion (μm) of standard panels due to C_d, C_{RA}, and C_{RC} at 10 and 80 μg/m^3 SO_2 and at rain pH of 4.2 and 5.0. The sum of C_d, C_{RA}, and C_{RC} (Table 3) does not represent total zinc corrosion because the zinc remaining in the corrosion film is not known but assumed to be constant for these calculations.

TABLE 3—*Predictions of zinc corrosion* (C) *by dry deposition of SO_2* (C_d), *rain acidity* (C_{RA}), *and dissolved CO_2 in rain* (C_{RC}) *for standard test panels.*

		Corrosion, μm			
SO_2, μg/m^3	pH	C_d	C_{RA}	C_{RC}	C
10	4.2	0.223	0.290	0.558	1.071
80	4.2	1.451	0.290	0.588	2.282
10	5.0	0.223	0.046	0.588	0.857
80	5.0	1.451	0.046	0.588	2.085

For environments with an SO_2 concentration of 10 μg/m^3 and rain acidity of 4.2, the zinc corrosion of the panel is 1.071 μm, and the CO_2 in rain (C_{RC}) contributes about 52% of the corrosion. The dry deposition of SO_2 contribution is about 20% of the zinc corrosion. However, the SO_2 deposition during periods of panel dryness represents about 27% of the 0.223 μm of zinc corrosion due to dry SO_2 deposition (C_d). In order to make this determination, the ratio of actual-to-apparent surface (A_r) was assumed to be 3.0, and the number of periods (N) between surface wetness was 250 for the SO_2 deposition term of Eq 10. When the SO_2 concentration is increased to 80 μg/m^3 with the rain pH remaining at 4.2, the zinc corrosion due to the dry deposition of SO_2 (C_d) is 1.45 μm. At this level of SO_2 concentration, the SO_2 deposition to a dry panel would contribute about 3% to the zinc corrosion. For these conditions, the dry deposition of SO_2 during periods of surface wetness with condensation would contribute about 64% of the zinc corrosion of 2.282 μm. If the SO_2 level is lowered from 80 to 10 μg/m^3, the corrosion model predicts a 53% reduction in zinc corrosion of standard panels for rainfall of 4.2 pH and for the environmental parameters as shown above.

When the acidity of rain is decreased to a pH of 5.0 and the SO_2 level is 10 μg/m^3, the contribution of rain acidity on the zinc corrosion is about 5%, whereas pH 4.2 rain contributes about 27% at the same level of SO_2. The model predicts about 20% less zinc corrosion when rain acidity is reduced from 4.2 to 5.0 pH. At 80 μg/m^3 of SO_2, a rain acidity of 5.0 pH contributes about 2.0% to the zinc corrosion, which is considered to be negligible.

As observed in Table 3, the contribution of CO_2 dissolved in rain (C_{RC}) on zinc corrosion remains constant for the various conditions. The C_{RC} term of the corrosion model was derived, as indicated by Eq 14, as a function of temperature, which was assumed to be 23°C. The residence time factor (r) was assumed to be 0.5 for standard test panels. EPA and BOM field studies involving rain runoff and simulated rain of pH 5.6 should provide a determination of r values for test panels and sheets of galvanized steel. As shown in Fig. 3, the solubility of basic zinc carbonate is a function of temperature as well as ambient CO_2 concentration. A CO_2 concentration of 345 ppm was assumed for calculating the C_{RC} shown in Table 3. However, CO_2 concentrations should be determined for the geographic area for which zinc corrosion of galvanized steel structures is to be estimated.

For galvanized steel fencing that is exposed to 80 μg/m^3 of SO_2 and rain acidity of 4.2 pH, the proposed model would predict zinc corrosion to be 8.30 μm for the three terms. The dry deposition of SO_2 would represent more than 90% of the zinc corrosion, while the rain acidity would contribute only 3.5% of the corrosion of the fencing. The proposed model predicts higher zinc corrosion for galvanized steel fencing than for standard panels that are exposed to the same environment.

The above scenario is intended to illustrate the capability of the proposed model for partitioning the contributions of wet and dry acidic deposition on galvanized steel structures.

Before further application of the proposed function, it should be tested with field corrosion and environmental data that have been acquired by the BOM and EPA for NAPAP.

Conclusions

A linear damage function for estimating the corrosion of galvanized steel structures by wet and dry acidic deposition has been developed from thermodynamics and kinetics of atmospheric corrosion chemistry. The function was derived in terms of the competing reactions for the buildup and dissolution of the basic zinc carbonate film that forms on galvanized steel structures during exposure. The contributions to zinc corrosion by the dry deposition of SO_2, by H^+ in rain, and by dissolved CO_2 in rain can be estimated for various galvanized steel structures by the proposed model. A second paper involves the evaluation and testing of the function with field exposure data that were obtained by BOM and EPA for Task Group VII during NAPAP. The damage function should also be checked using historical corrosion data for standard test exposure panels as well as different structures. By using this approach, a validated damage function for estimating the effects of acidic deposition on galvanized steel structures should be developed.

Acknowledgment

The information in this document has been funded wholly or in part by the U.S. Environmental Protection Agency. It has been subjected to Agency review and approved for publication. Mention of trade names or commercial products does not constitute endorsement or recommendation for use.

APPENDIX

Thermodynamic Data

Thermodynamic data that was used to calculate equilibrium constants for reactions involving the solubility of zinc corrosion film is presented in Table 4. It comes from Ref. *27*, Appendix B, except for those footnoted values that were estimated from solubility data.

Derivation of the Zinc Corrosion Estimate

Grauer and Feitknecht have used solution thermodynamics and X-ray analysis to determine the stability of basic zinc carbonate with respect to H^+ and CO_2 concentrations [*24*]. Their investigations of the basic zinc carbonate/water/carbon dioxide system resulted in determination of the equilibrium constant (k) for the overall reaction

$$Zn(OH)_{(2-2x)}(CO_3)_x + 2H^+ = Zn^{2+} + xCO_2 + (2 - x)H_2O \qquad (16)$$

However, Kelley and Anderson [*25*] and Hougen et al. [*26*] have also shown that the overall reaction, based on electrical charge balance, may be expressed as follows

$$Zn(OH)_{(2-2x)}(CO_3)_x + xH_2O + (2 - x)CO_2 = Zn^{2+} + 2HCO_3^- \qquad (17)$$

Within a pH range of 5 to 9, the concentrations of H^+, OH^-, CO_3^{2-} ions were found to be negligible with respect to the Zn^{2+} and HCO_3^- ions. The effective difference between

TABLE 4—*Standard thermodynamic properties of formation at 25°C.*

Substance	State	ΔH°, kcal/mol	ΔF°, kcal/mol	S°, cal/mol	C_p, K
CO_2	g	−94.051	−94.254	51.085	8.87
CO_2	ao	−98.901	−92.251	28.107	(47.04)[a]
$CO_3^{=}$	ao	−161.84	−126.15	13.599	...
HCO_3^-	ao	−165.39	−140.241	21.797	(81.1)[a]
H_2CO_3	ao	−167.22	−148.92	44.79	(65.039)[a]
Ca^{++}	ao	−129.739	132.309	12.691	...
$CaCO_3$	cr	−288.461	−269.787	22.204	19.57
H^+	ao	0.0	0.0	0.0	0.0
H_2O	l	−68.315	−56.675	16.709	17.995
Mg^{++}	ao	−111.58	−108.7	−33.007	...
$MgCO_3$	cr	−261.902	−241.898	15.703	18.05
NO_3^-	ao	−48.996	−25.989	34.99	−20.698
HNO_3	l	−41.611	−19.29	37.198	26.26
HNO_3	g	−32.28	−17.859	63.666	12.751
HNO_3	ai	−49.56	−26.589	34.99	−20.698
O_2	g	0.0	0.0	49.029	7.016
O_2	ao	−2.796	3.92	26.506	...
SO_2	g	−70.994	−71.748	59.326	9.529
SO_2	ao	−77.194	−71.863	38.695	...
$SO_3^{=}$	ao	−151.9	−116.276	−6.931	...
$SO_4^{=}$	ao	−217.321	−177.948	4.804	−70.029
H_2SO_3	ao	−149.67	−126.13	33.389	...
H_2SO_4	ao	−217.079	−180.667	31.501	−20.076
H_2SO_4	l	−194.548	−164.915	−37.501	33.2
H_2SO_4	ai	−217.321	−177.948	4.804	−70.029
Zn	cr	0.0	0.0	9.95	6.07
Zn^{++}	ao	−36.781	−35.148	−26.793	10.994
$Zn(OH)_2$	cr	−153.42	−132.294	19.40	17.304
$ZnCO_3$	cr	−194.259	−174.837	19.69	19.051
$3Zn(OH)_2 \cdot 2ZnCO_3$	cr	(−850.21)[a]	(−749.935)[a]	(102.42)[a]	(90.015)[a]
$Zn(NO_3)_2$	ai	−135.901	−88.329	43.188	−30.114
$Zn(NO_3)_2 \cdot 6H_2O$	cr	−551.3	−423.688	109.202	77.2
$ZnSO_4$	cr	−234.895	−208.294	26.41	23.709
$ZnSO_4$	ai	−254.099	−213.095	−21.989	−59.034
$ZnSO_4 \cdot 6H_2O$	cr	−663.829	−555.554	86.902	85.49

NOTE: g = gaseous; cr = crystalline solid; l = liquid; ai = aqueous solution, ionized substance standard, and ao = aqueous solution, anionized substance or anionized for which no further ionization is considered.

[a] Estimated from solubility data.

Reactions 1 and 2 and may be expressed as follows

$$2(H_2O + CO_2 = H^+ + HCO_3^-) \qquad (18)$$

Thus, the equilibrium constant for Reaction 2, ln k_2, may be expressed as the equilibrium constant for Reaction 1, ln k_1, plus twice the equilibrium constant for Reaction 3, 2 ln k_3.

The equilibrium constants that were calculated by Grauer and Feitknecht [*24*] are compared in Table 5 with values calculated from thermodynamic data that were recently tabulated by Wagman et al [*27*]. No values for the free energy of formation are reported for basic zinc carbonate. The difference for the equilibrium constants (ln k) shown in Table 5 for Ref *24*, for the reaction of zinc hydroxide and zinc carbonate, provided a value of −1.0004. This value was used with data from Wagman [27] to calculate the values of ln k shown in

TABLE 5—*Comparison of equilibrium constants for film dissolution, ln*(K)[a].

	Reaction 1		Reaction 2	
Solid Phase	Ref *1*	Ref *4*	Ref *1*	Ref *4*
Beta Zn(OH)	27.078	27.349	−8.916	−8.728
$ZnCO_3$	18.306	18.971	−17.688	−17.106
$Zn(OH)_{1.2}(CO_3)_{0.4}$	22.565	(22.994)[b]	−13.429	(−13.083)[b]

[a] At 298.16 K.

[b] Data from Wagman [*27*] used to calculate ln K values shown in parentheses.

parentheses in Table 5. These values are in reasonable agreement with those provided in Ref *24*. The value for the energy of formation of basic zinc carbonate, $3Zn(OH)_2 2ZnCO_3$, was now calculated as −749.532 kcal/mol/K.

Since a strong temperature inverse relationship of CO_2 solubility in water exists, the solubility of zinc carbonate is likely to be greater at 18°C than at 25°C [*28*]. With thermodynamic relationships, this temperature dependence may be expressed as follows

$$\Delta F = \Delta H - T\Delta S \tag{19a}$$

$$\Delta H = I_H + \Delta CpT \tag{19b}$$

$$\Delta S = I_S + \Delta C_p \ln T \tag{19c}$$

$$\ln k = I_s/R - I_H/RT + \Delta C_p(1 - \ln T)/R \tag{19d}$$

where R = gas constant,
T = absolute temperature,
ΔC_p = change in heat capacity,
I_s, I_H = constants,
ΔF = change in free energy,
ΔH = change in enthalpy, and
ΔS = change in entropy.

If thermodynamic parameters for reactants and products for Eq 17 were known, the equilibrium constant could be calculated as a function of temperature by Eq 19*d*. However, heat capacity data for the bicarbonate ion (HCO_3^-) is not available. In addition, the equilibrium constants at three or more temperatures would be needed to empirically determine the constants I_s and I_H for Eq 19*d*.

Fortunately, temperature and CO_2-dependent solubility data [*28*] exist for magnesium carbonate ($MgCO_3$) and calcium carbonate ($CaCO_3$). These data were evaluated with respect to the equilibrium constant for the overall reaction scheme

$$MeCO_3 + H_2O + CO_2 = Me^{2+} + 2HCO_3^- \tag{20}$$

By using a least-square fit of Eq 19*d*, values for the I_s, I_H, and ΔC_p for $MgCO_3$ and $CaCO_3$ were derived as shown in Table 6. The ΔC_p are not significantly different for the solubilities of the two carbonates. Thus, a variance-weighted average of 127.3 ± 36.7 cal/mol · K may be a reasonable estimate for the solubility of zinc carbonate. With this value and C_p values

TABLE 6—*Regression coefficients and standard deviations.*

Carbonate	I_s, cal/mol · K	I_H, cal/mol	ΔC_p, cal/mol · K
Magnesium	−763.657 ± 0.424	−51036 ± 9136	124.725 ± 62.981
Calcium	−784.455 ± 0.123	−47303 ± 8501	127.791 ± 28.496

for $ZnCO_3$, H_2O, CO_2, and Zn^{2+} [27], the C_p for HCO_3^- was determined to be 81.1 ± 18.8 cal/mol · K.

By using this value for the C_p for the HCO_3^-, it is possible to calculate the following coefficients for Eq 20 for the solubility of basic zinc carbonate

$$Zn(OH)_{1.2}(CO_3)_{0.4} + 0.4H_2O + 1.6CO_2 = Zn^{2+} + 2HCO_3^- \tag{21}$$

The C_p for the basic zinc carbonate is calculated as 0.6 times the C_p of zinc hydroxide plus 0.4 times the C_p of zinc carbonate. The C_p difference for the reaction is calculated to be 134.8 ± 36.7 cal/mol · K from Table 5. The free energy change (ΔF) for the reaction is 7.753 kcal/mol. The enthalpy and entropy of formation of basic zinc carbonate are not known but should not be very different from the sums of the values of the reactants $Zn(OH)_2$ and $ZnCO_3$ of which it is composed. The enthalpy change (ΔH) and entropy change (ΔS) for Reaction 6 are thus calculated to be −19.997 kcal/mol and −91.143 cal/mol · K, respectively. With Eq 19*a* and these values, the free energy change for the reaction is 7.178 kcal/mol, which is ~0.575 kcal/mol less than the value calculated from the reported equilibrium constant. Splitting the difference between the two values yields −19.7 kcal/mol for ΔH and −92.109 cal/mol·K for ΔS. By using Eqs 19*b* and 19*c*, I_H and I_s are calculated to be −59902 ± 10943 cal/mol and −860.2 ± 209.1 cal/mol · K, respectively. Because the coefficients are related through the thermodynamic equations, values within the ranges of the standard deviations have little effect on the overall solubility-temperature relationship. A thermodynamic function error of 1 cal/mol·K, however, can cause an error on the solubility of about 18%.

References

[*1*] Flinn, D. R., Cramer, S. D., Carter, J. P., and Spence, J. W., *Durability of Building Materials,* Vol. 3, 1985, p. 147.

[*2*] Nrigau, S. O., *Sulfur in the Environment. Part II: Ecological Effects,* John Wiley & Sons, New York, 1978, p. 1.

[*3*] Anderson, F. A., in *Symposium on Atmospheric Testing of Non-Ferrous Metals, ASTM STP 175,* American Society for Testing and Materials, Philadelphia, 1955, p. 132.

[*4*] Barton, K., *Protection Against Atmospheric Corrosion,* John Wiley, New York, 1972, p. 194.

[*5*] Flinn, D. R., Cramer, S. D., Carter, J. P., Hurwitz, D. M., and Linstrom, P. J., *Materials Degradation Caused by Acid Rain,* American Chemical Society, Washington DC, 1986, p. 119.

[*6*] Haynie, F. H., in *Degradation of Metals in the Atmosphere, ASTM STP 965,* American Society for Testing and Materials, Philadelphia, 1988, p. 282.

[*7*] Haynie, F. H., in *Durability of Building Materials and Components, ASTM STP 691,* American Society for Testing and Materials, Philadelphia, 1980, p. 157.

[*8*] Owers, M. J. and Powell, A. W., *Atmospheric Environment,* Vol. 8, 1974, p. 63.

[*9*] Bennett, C. O. and Myers, J. E., *Momentum, Heat, and Mass Transfer,* McGraw-Hill, New York, 1982.

[*10*] Bird, R. B., Stewart, W. E., and Lightfoot, E. N., *Transport Phenomena,* John Wiley & Sons, New York, 1962.

[*11*] Knudson, J. G. and Katz, D. L., *Fluid Dynamics and Heat Transfer,* University of Michigan, Ann Arbor, 1953.

[*12*] Sherwood, T. K. and Pigford, R. L., *Absorption and Extraction,* McGraw-Hill, New York, 1952.

[*13*] Lange, N. A., *Handbook of Chemistry,* McGraw-Hill Book Co., New York, 1956, p. 1092.

[*14*] Spence, J. W. and Haynie, F. H., *Galvanic and Pitting Corrosion—Field and Laboratory Studies, ASTM STP 576,* American Society for Testing and Materials, Philadelphia, 1976, p. 132.

[*15*] Edney, E. O., Stiles, D. C., Spence, J. W., Haynie, F. H., and Wilson, W. E., *Atmospheric Environment,* Vol. 20, No. 3, 1986, p. 541.

[*16*] Schwartz, S. E. and White, W. H., *Advances in Environmental Science and Technology,* Vol. 12, 1983, p. 1.

[*17*] Maah, H. G., *American Geophysical Union,* Washington, DC, 1982, p. 187.

[*18*] Edney, E. O., Stiles, D. C., Spence, J. W., Haynie, F. H., and Wilson, W. E., *Materials Degradation by Acid Rain,* American Chemical Society, Washington, DC, 1986, p. 172.

[*19*] Wagmar, D. D., Evans, W. H., Parker, V. B., Schumm, R. H., Halow, I., Bailey, S. M., Churney, K. L., and Nuttall, R. L., *Journal of Physical and Chemical Data,* Vol. 1, No. 2, 1982.

[*20*] Haynie, F. H., *Aerosols,* Lewis Publishers, Chelsea, MI, 1986, p. 2104.

[*21*] Haynie, F. H., 1988, accepted for publication in *Aerosol Science and Technology,* 1990.

[*22*] Reagan, J. A., *Investigation Study of Anomalous Data in the RAPS Data Base,* EPA Contract 68-02-3012 Report, Rockwell International Corp., Creve Coeur, MO, 1980.

[*23*] Stiles, D. C. and Edney, E. O., *Corrosion,* Vol. 45, No. 11, 1989, p. 896.

[*24*] Grauer, R. and Falknecht, W., *Corrosion Science,* Vol. 7, 1967, p. 629.

[*25*] Kelley, K. K. and Anderson, C. T., *Bulletin 384,* US Department of the Interior, Bureau of Mines, US Government Printing Office, Washington, DC, 1935.

[*26*] Hougen, O. A., Watson, K. M., and Ragatz, R. A., *Chemical Process Principles—Part II. Thermodynamics,* John Wiley & Sons, New York, 1959, p. 1063.

[*27*] Wagman, D. D., Evans, W. H., Parker, V. B., Schumm, R. H., Halow, I., Bailey, S. M., Churney, K. L., and Nuttall, R. L., *Journal of Physical and Chemical Data,* Vol. 11, No. 2, reference data published in the NBS tables of chemical thermodynamic properties, American Chemical Society and American Institute of Physics, 1982.

[*28*] Linke, W. F., *Solubilities—Inorganic and Metal—Organic Compounds,* Vol. II., American Chemical Society, Washington, DC, 1965.

Fred H. Haynie,[1] *John W. Spence,*[1] *Fred W. Lipfert,*[2]
Stephen D. Cramer,[3] *and L. Garner McDonald*[3]

Evaluation of an Atmospheric Damage Function for Galvanized Steel

---

REFERENCE: Haynie, F. H., Spence, J. W., Lipfert, F. W., Cramer, S. D., and McDonald, L. G., **"Evaluation of an Atmospheric Damage Function for Galvanized Steel,"** *Corrosion Testing and Evaluation: Silver Anniversary Volume, ASTM STP 1000,* R. Baboian and S. W. Dean, Eds., American Society for Testing and Materials, Philadelphia, 1990, pp. 225–240.

ABSTRACT: A model for corrosion of zinc based on competing mechanisms of the formation and dissolution of a protective film of basic zinc carbonate was evaluated. The model consists of a diffusivity term (ions through the film) which controls the buildup of a protective film and a solubilization term which controls the rate of dissolution of the film. The model was evaluated by using comprehensive data collected from field experiments designed to separate the effects of wet and dry acid deposition from normal weathering effects such as clean rain, temperature, wind speed, and relative humidity. These data were used primarily to evaluate the theoretically calculated components of the dissolution rate term because after about three years it becomes the rate upon which long-term corrosion behavior may be predicted. The model was also evaluated with respect to historical long-term data for different shapes and sizes of galvanized products.

The field data used in this evaluation were found to be consistent with values predicted by the model. Thus, the model can be used with reasonable confidence to predict long-term corrosion behavior of different structures in real environments if those environments are properly described.

KEY WORDS: zinc corrosion, acid rain, sulfur dioxide, deposition velocity, corrosion products

A damage function for galvanized steel was developed for the National Acid Precipitation Assessment Program (NAPAP) to use in assessments for Congress. A damage function is a mathematical expression that relates the rate of degradation of a material to various contributing environmental factors. The model function was developed for galvanized steel on the basis of theoretical considerations [*1*] and laboratory experiments [*2–5*]. The simplest expression of the model is that the rate of corrosion is inversely proportional to the thickness of a protective basic zinc carbonate film and that after a few years of exposure a steady state is reached in which film growth equals film dissolution and the corrosion rate becomes constant. This dissolution rate, upon which long-term corrosion behavior can be predicted, is controlled by the rate of delivery of reacting species to the zinc (Zn) surface rather than activation energies for reactions. The mathematical expression contains term A with units of diffusivity and term B, which is a dissolution rate.

The Bureau of Mines and the US Environmental Protection Agency (EPA) have conducted

---

[1] Environmental engineer and chemist, respectively, U.S. Environmental Protection Agency, Research Triangle Park, NC 27711.

[2] Environmental engineer, Brookhaven National Laboratory, Upton, NY 11973.

[3] Metallurgist, Bureau of Mines, Albany, OR 97321.

comprehensive field exposure studies of galvanized steel and zinc as well as other metals. Standard mass loss and mass gain data were collected, and rain runoff was collected and analyzed for ionic species. The mass loss–mass gain data are well suited for analyzing the diffusivity term, *A*, which controls most of the short exposure variations in corrosion behavior. These data are the subject of another paper. The runoff data are the result of analyses of soluble species and thus are well suited for determining the effects of various components on the dissolution term, *B*.

The EPA conducted runoff experiments on three types of exposures of 10.2 by 15.2-cm specimens at Research Triangle Park, NC (RTP) and Steubenville, OH (STU) on a rain event basis. The Bureau of Mines conducted a separate experiment on 30.5 by 61-cm specimens at Washington, DC (DC), collecting runoff samples monthly. In this paper the data from these two studies are analyzed separately in a similar manner and the results compared.

To test the universal applicability of the model, long-term ASTM data on colocated galvanized sheet, fencing, and standard specimens were analyzed with respect to best estimates of environmental conditions that existed during their exposures at different sites.

Evidence for Dissolution Mechanism

There are three main components of the theoretical model associated with dissolution of zinc on galvanized steel: (1) zinc replacing hydrogen ions (H^+) in solution; (2) solubilization of basic zinc carbonate by dissolved carbon dioxide (CO_2); and (3) the formation of soluble zinc sulfate from the deposition of sulfur dioxide (SO_2) gas. The reactions with hydrogen and sulfur dioxide are essentially stoichiometric and relatively fast; thus, the overall rates are controlled by the rates of delivery of those species to the zinc surface. The dissolution of basic zinc carbonate by carbonic acid is a slower process; thus, equilibrium is not likely to be reached within the time water remains on a surface that is not horizontal. Although some coefficients in the model can be calculated from first principles, others such as the residence time factor must be determined empirically from experimental data.

The best evidence for these processes is obtained through determining input-output material balances of different soluble species. These determinations have been made by using environmental data and runoff data for specimens exposed under conditions designed to separate the different effects. Such an experiment was performed by EPA. A different but similar experiment was performed by the Bureau of Mines.

EPA Experiment

Details of the experiment performed by EPA have been reported [*6–8*]. The essential parameters are that runoff from galvanized steel and relatively inert painted specimens, exposed at two well-monitored sites under different conditions, were collected and analyzed for each rain event. The RTP site is a relatively "clean" site with low ambient levels of both sulfur dioxide and particulate matter. The STU site is relatively "dirty" with high levels of both pollutants. Specimens were exposed at 30 and 90° from horizontal to ambient rain. Another set of specimens exposed at 30° was protected from ambient rain by using a covering device and sprayed with deionized water (DI) each time it rained.

Previous papers have reported subsets of results [*6–8*]. This paper presents results of analyses of all of the data collected at each site. Exposures at RTP were from February 1986 through May 1988, and exposures at STU were from November 1986 through May

1988. There were 135 different rain events at RTP during 28 months and 61 events at STU during 19 months. Collections from each specimen were analyzed for pH, cations (by atomic absorption), and anions (by ion chromatography).

Rain volume and chemistry were measured on a monthly basis as a part of acid precipitation network [*9*]. Particulate matter concentrations and chemistry were measured weekly [*10*]. Meteorological parameters and gaseous pollutants were monitored continuously, with the data reduced to hourly averages or accumulations [*11*].

To do an input-output analysis, the measured parameters must cover the same exposure periods. Thus, the minimum period is set by the rain chemistry measurements. With the magnitude of measurement variability fairly constant, the relative error for small samples such as a rain event is greater than it is for longer accumulations. Most of the data were analyzed as quarterly accumulations. Because July through September 1986 at RTP was relatively dry, October rains were added to that quarter, leaving November and December as a two-month period. The beginning and ending periods at both RTP and STU were only two months.

The runoff results of interest for galvanized steel specimens are given in Table 1. These data were obtained from single specimens exposed at one of the three sets of conditions.

An estimate of within-sample variability is needed to determine if observed differences among conditions are statistically significant or if they are the result of experimental variability. Data were collected also on relatively inert painted specimens and Teflon. These surfaces respond similarly to the various environmental conditions and serve as multiple specimen samples that can be subjected to analysis of variance. These data also indicate what accumulates on nonreactive surfaces.

The results of analysis of variance on the inert surfaces are given in Table 2. These results are based on data for five quarterly periods and four paints that were common to both sites.

TABLE 1—*Quarterly runoff accumulations from galvanized steel.*

	Accumulation, nmol/cm^2								
	DI Spray, 30°			Ambient Rain, 30°			Ambient rain, 90°		
Site	Volume, mL	Zn^{++}	SO$_4^{=}$	Volume, mL	Zn^{++}	SO$_4^{=}$	Volume, mL	Zn^{++}	SO$_4^{=}$
STU	2180	848	1003	1780	1657	2085	295	...	1613
	696	478	524	806	1228	843	235	408	1204
	2617	927	990	2927	1994	2585	1136	1061	1571
	2266	600	788	4547	3109	3585	2145	2626	2263
	1539	1317	1523	2559	3701	4669	738	2584	2292
	1560	1312	1485	2710	3721	3510	1209	3596	2417
	788	798	820	969	1806	1823	383	1496	1406
RTP	1026	612	488	622	563	515	405	...	1361
	701	309	275	497	453	429	511	545	713
	1672	373	187	1556	719	555	1266	948	678
	799	386	268	743	1065	741	241	656	601
	2243	845	651	1610	1828	1188	345	547	480
	2550	631	404	1284	1213	702	534	328	219
	2157	487	253	2391	2108	1085	882	687	412
	1937	502	251	925	1066	593	105	266	199
	1085	731	544	847	1939	1481	75	294	246
	1129	404	269	730	1109	649	...	...	...

TABLE 2—*Analysis of variance of sulfate on inert paints.*

Variable	Degrees of Freedom	Concentration		Volume		Accumulation	
		Mean Square	*f*	Mean Square	*f*	Mean Square	*f*
Site	1	105 457	111.2[a]	17 510 994	47.4[a]	16 901 912	243.2[a]
Period	4	12 295	13.0[a]	6 040 562	16.4[a]	745 521	10.7[a]
Paint	3	2 199	2.3	241 082	0.7	127 174	1.8
Exposure	2	76 382	80.6[a]	11 870 755	32.1[a]	2 128 916	3.1
Residual	109	948	...	369 564	...	69 495	...

[a] Statistically significant at the 1% level.

The dependent measurements of runoff volume, sulfate concentration, and sulfate accumulation (volume times concentration) were each analyzed with respect to the variables of exposure site, exposure period, paint type, and type of exposure (rain or DI spray and angle). With the residual variability consisting of all the possible interactions between these variables taken as error, the type of paint is not a statistically significant factor for differences among the measured parameters. In other words, the within-sample variability for paints is the same as the residual variability for the analysis of variance. With the exception of type of exposure on sulfate accumulation, all of the other variables produce highly significant effects. No effect of paint type was expected; therefore, the residual variability is believed to be a good estimate of error associated with the measured quarterly parameters. The standard error for runoff volume on 155-cm^2 specimens is 609 mL per quarter. The standard error for sulfate accumulations is 264 nmol/cm^2. Measurement precision is more than an order of magnitude better than these errors based on data dispersion. These standard errors can be used to analyze differences between exposures and to test models for lack of fit.

Ion balances show that sulfate is the major negative charge contributor and, depending on the exposure, either hydrogen or calcium is the major positive ion contributor in runoff from inert surfaces. The sulfate generally is balanced by hydrogen and calcium.

Calcium was measured in the runoff from the inert surfaces. (Some paints containing calcium carbonate were exposed at the same time but were not included in the analysis of the inert samples.) Most of the calcium comes from the deposition of coarse mode particles (diameters >2.5 μm) with a small amount contributed by ambient rain. Average deposition velocities for coarse-mode particles to 30 and 90° specimens were determined by (1) subtracting the rain contribution of calcium from the average runoff accumulations on inert surfaces for each period and exposure and (2) regressing that data on average particulate matter calcium concentrations in air for the same periods at each site. The results are 1.15 ± 0.13 and 0.63 ± 0.12 cm/s for the 30 and 90° specimens, respectively. These values are consistent with values of 1.55 ± 0.08 and 0.34 ± 0.12 cm/s calculated from particle size distribution data using scanning electron microscopy in a soiling study of ambient particle deposition on horizontal and vertical surfaces done at the RTP site [*12*]. The greater deposition velocity to horizontal surfaces is due to the additional effects of gravitational settling.

The sulfate accumulation on inert surfaces comes from particles, rain, absorption of sulfur dioxide on the sample surface, and the neutralization of calcium from particles. If absorption on the surface is negligible, the sulfate accumulation should equal the calcium from particles plus the sulfate from rain. Calcium from particles was calculated by using particulate matter concentrations and the above deposition velocities. These values were added to the amounts of sulfate contributed by rain, and sulfate accumulations were regressed on the combined values. The 50 sets of data give an excellent fit of the model, producing a coefficient of

1.02 ± 0.05 (model value is 1) and a standard error of 180 nmol/cm^2/period which is less than 264 nmol/cm^2/period estimated above as standard error. This gives an *f* statistic for lack of fit of only 0.68, which indicates that lack of fit is insignificant.

Not all of the sulfate measured in the runoff from galvanized steel is available to react with the basic zinc carbonate film. Some sulfur dioxide preferentially absorbs on and reacts with the calcium which also is deposited on the galvanized steel. The amount is indicated by what is deposited to the inert surfaces. Some sulfate in rain is balanced by calcium and cations other than hydrogen, and this sulfate is not available to react with zinc. In any case, the theoretical model considers the hydrogen ion concentration in rain; therefore, to avoid doubling the effect with both hydrogen and sulfate ions, sulfate in rain should be excluded from the sulfate available to react with zinc. With these amounts subtracted from the sulfate accumulations on galvanized steel, what is left is sulfur dioxide deposition available to react with the basic zinc carbonate.

Hydrogen ions from rain and sulfur dioxide deposition are two of the three theoretical components in the dissolution model. The third component is the solubility associated with dissolved carbon dioxide (bicarbonate ions). The equilibrium solubility of basic zinc carbonate with 345 ppm carbon dioxide in the atmosphere is believed to follow the temperature relationship [*1*]

$$Zn^{2+} = \exp(-21.343 + 3651/T) \tag{1}$$

where,

Zn^{2+} = zinc ion, mol/L, and
T = temperature, Kelvin units.

The average temperature of the DI spray that was stored indoors is assumed to have been 20°C. The average temperature of the ambient rain is assumed to have been equal to the average dew point for the fraction of time in each period that the relative humidity exceeded 75%. The maximum possible effect of dissolved carbon dioxide then is obtained by using the temperatures in Eq 1 and multiplying them by the water volumes collected from each specimen. Table 3 presents the resulting three calculated components and the measured accumulations of zinc dissolution.

Estimation of Model Coefficients

Multiple linear regression of the measured zinc dissolution against the three theoretical components produces a fit with a standard error of 370 nmol/cm^2, which is not significantly different from the previously calculated standard error of 264 nmol/cm^2. The resulting coefficients for SO_2, H^+, and HCO_3^- effects, respectively, are 1.002 ± 0.108, 0.686 ± 0.289, and 0.201 ± 0.065. They all are significantly different from zero, and the SO_2 and H^+ coefficients are not significantly different from theoretical coefficients of one. The bicarbonate ion coefficient is significantly less than one, indicating that rain does not remain on the specimens long enough to reach equilibrium (residence time factor). If the effects of SO_2 and H^+ are assumed to be stoichiometric (coefficients equal one), the residence time factor for the bicarbonate ion becomes 0.162 ± 0.028 and the standard error for the regression is reduced slightly to 366 nmol/cm^2. This model can account for 85% of the variability. If 8% is associated with experimental error, the 7% not accounted for does not constitute a significant lack of fit.

These results provide evidence that once the components reach the surface they behave according to model expectations. For SO_2 and H^+, the rates of deposition on the basic zinc

TABLE 3—*Calculated components of zinc dissolution.*

		Accumulations, nmol/cm^2			
Exposure	Site	SO_2 deposition	$H^+/2$	HCO_3^-	Zn^{2+}
DI 30°	STU	682	0	1936	848
		20	0	618	478
		621	0	2324	927
		−211	0	2012	600
		959	0	1367	1317
		1274	0	1385	1312
		330	0	700	798
	RTP	420	0	911	612
		193	0	623	309
		128	0	1485	373
		219	0	710	386
		596	0	1992	845
		331	0	2264	631
		203	0	1915	487
		201	0	1720	502
		499	0	964	731
		224	0	1003	404
Rain 30°	STU	1327	457	3243	1657
		144	191	1526	1228
		1151	1144	3604	1994
		1239	1074	4456	3109
		3259	401	4511	3701
		2593	639	4578	3721
		1037	272	1294	1806
	RTP	374	62	935	563
		224	115	543	453
		326	199	1505	719
		618	84	1097	1065
		1013	139	2772	1828
		463	181	1397	1213
		703	429	2088	2108
		451	94	1359	1066
		1329	120	1316	1939
		467	155	957	1109
Rain 90°	STU	871	56	445	408
		956	444	1399	1061
		1080	507	2102	2626
		1739	116	1301	2584
		1987	285	2043	3596
		1021	108	511	1496
	RTP	542	118	558	545
		507	162	1225	948
		550	27	356	656
		424	30	594	547
		110	76	581	328
		262	158	770	687
		161	11	154	266
		212	11	117	294

carbonate surface control the dissolution rates. The model for the H^+ delivery is the concentration of the ion in rain times the volumetric rate of rain striking a unit of surface. Ambient concentration times deposition velocity during periods of wetness plus approximate monolayer adsorption during periods of dryness is the model for delivery of SO_2.

If rain is assumed to fall vertically and the amount of rainfall is measured, the amount striking a particular size specimen exposed at a particular angle can be calculated. Unfortunately, rain is blown by wind and does not fall vertically as evidenced by the significant amount of runoff collected from specimens exposed at 90° to the horizontal. Also, losses can occur when drops bounce or splatter on these relatively small specimens. In Table 4, measured averages and standard deviations of volume accumulations are compared with calculated volumes from rain measurements falling vertically on 155-cm^2 specimens exposed at 30° to the horizontal. These results indicate that from 23 to 58% of the calculated volumes could be lost from these small specimens. From 18 to 29% of what is calculated for 30° specimens runs off of 90° specimens.

Both volume losses and specimen-to-specimen variability are important factors to consider when analyzing data from small specimens. These effects should be inversely proportional to the area of exposed surface; thus, application of the theoretical model to large areas of roofing and siding should be less sensitive to volume losses. Because of wind, siding probably is exposed to about 20% of the volume that may be calculated for roofing. Cylindrical shapes, such as fence wiring, are less likely to have splash losses than small flat specimens because most of the drops will strike at a low angle. Application of the model to the diameter and length of fence wiring is not expected to introduce significant error.

Data in Table 3 are fluxes of SO_2 to galvanized steel specimens exposed under various conditions. The SO_2 accumulation data (based on runoff) are measures of SO_2 flux, and if

TABLE 4—*Comparison of calculated and measured runoff accumulation volumes.*

Site	Calculated Volume, mL	Measured Runoff Accumulation Volumes[a], Mean and Standard Deviation—mL					
		DI 30°		Rain 30°		Rain 90°	
STU	2210	2564	700	1194	513	293	72
	1741	765	276	701	90	218	47
	4130	2917	883	2603	223	1036	128
	2683	2850	969	3529	561	1556	315
	2389	1773	540	1953	385	697	53
	2102	1637	119	2388	200	874	182
	2088	1027	284	986	92	402	25
RTP	2125	1548	433	647	54	402	156
	2081	1247	500	623	129	519	39
	5785	3587	1909	2018	327	1187	185
	2174	1499	1155	858	134	238	14
	2019	1625	813	1164	427	405	102
	3139	1301	815	1292	595	700	168
	4670	1579	701	2259	918	1152	194
	2109	1183	658	1199	498	170	76
	2432	604	311	851	477	115	52
	1790	733	358	1010	690	......	

[a] Based on volumes from 155 cm^2 specimens.

the regression coefficients for H^+ and HCO_3^- are used to subtract their effects, the zinc accumulation data provide another measure of the same fluxes. These combined data can be compared with environmental data to determine the applicability of the gaseous flux components of the theoretical model (deposition during different definitions of periods of wetness and monolayer deposition during periods of dryness).

Materials Balance with Ambient Conditions

The collected ambient data used in the model were hourly averages of SO_2 in parts per billion, wind speed, temperature, dew point, and relative humidity. Hourly accumulated rainfall was also used. The SO_2 values were converted to concentrations per unit volume considering the effect of temperature on gas volume. Deposition velocities, V_d, in centimeters per second were calculated from wind speed using the theoretically determined relationship for standard specimens

$$V_d = 0.73\sqrt{v} \tag{2}$$

where v is wind speed in meters per second. Possible hourly accumulations of SO_2 then were calculated by multiplying the specimen surface area by the volume concentration times the deposition velocity. Accumulations for each period were determined by summing the hourly accumulations when criteria for different definitions of wetness were met. The criteria were that a critical relative humidity was exceeded, and that the dew point was greater than 0°C or it was raining. Different critical relative humidities were selected at intervals of 5% from 75 to 95%. The number of periods of dryness for each exposure period and selected criteria were counted.

From the data in Table 3 it is evident that significantly more SO_2 is deposited on galvanized steel specimens exposed to ambient rain than those exposed to the DI spray. This behavior is consistent with model expectations. Because of the hydrogen ion effect, the ambient rain specimens corrode faster than the DI spray specimens. This effect is more pronounced in the first stages of corrosion when the basic zinc carbonate film has not built up because zinc directly replaces hydrogen ions in solution. More corrosion can increase SO_2 deposition in two ways: (1) by the buildup of hygroscopic corrosion products increasing the fraction of time the surface is wet, and (2) the corrosion increases the actual surface area upon which a monolayer may deposit during periods of dryness. Thus H^+ has both direct and synergistic effects with SO_2.

The SO_2 accumulation data in Table 3 were lumped with calculated accumulations by using the regression equation to adjust the zinc runoff data for the effects of H^+ and HCO_3^-. These data were divided into two sets, DI spray and ambient rain. Each set then was regressed for each assumed level of critical relative humidity (from 75 to 95%) on two sets of environmental parameters: (1) periods of dryness; (2) theoretically calculated accumulations of SO_2.

Because the rate-controlling factor during periods of wetness is gas phase resistance, the SO_2 accumulation coefficients for DI spray and ambient rain should be the same, but the critical relative humidity for the ambient rain should be less than that for the DI spray because of the expected greater accumulation of hygroscopic corrosion products. For the DI spray, the regression that produces a coefficient closest to the theoretical value of one is the criterion that includes 90% as the critical relative humidity. For the ambient rain, the critical relative humidity that gives a coefficient nearest to one is 75%. The results for these two regressions are given in Table 5.

TABLE 5—*Regression results for rates of deposition of SO_2.*

Exposure	Coefficients		Standard Error, nmol/cm^2	Lack of Fit, f[a]
	Dry	Wet		
DI spray	1.96 ± 0.86	1.05 ± 0.19	292	1.11
Rain	4.48 ± 1.54	1.14 ± 0.17	667	2.53

[a] Experimental error assumed to be 264 nmol/cm^2. (Both values indicate no significant lack of fit.)

All of the coefficients are significantly different from zero, and both regressions show no significant lack of fit. Based on laboratory experiments, saturation of a clean, flat surface during a period of dryness is expected to produce a coefficient of 1.4 nmol/cm^2 [*4*]. The comparable regression coefficient for the DI spray is not significantly different from this value, indicating an actual-to-apparent surface area ratio of only 1.4. The coefficient for the ambient rain is significantly different, and the resulting actual-to-apparent surface area ratio is calculated to be 3.2. The fraction of time that 75% relative humidity is exceeded is about twice the fraction of time that 90% relative humidity is exceeded. Based on these results, the contribution of SO_2 to the corrosion of zinc is about twice what it would be if there were no acidity in rain. This is an interaction effect of H^+ and SO_2.

Bureau of Mines Experiment

The experimental procedure has been described by Cramer et al. [*13*] and essentially consists of the analysis of monthly rain collections from 30.5 by 61-cm specimens of zinc and stainless steel exposed at 30° to horizontal, facing south. Similar specimens of copper and weathering steel were also exposed. Unlike the volumes for the small specimens at RTP and STU, the volumes collected on the larger specimens were in very close agreement with each other and, except during a few months, agreed very well with rain bucket collections. This suggests there was little, if any, loss due to splash, which was not the case for the smaller specimens. Collection and analysis of environmental data were similar to that at RTP and STU except that weather data were taken at nearby Washington National Airport.

The data were aggregated into quarterly accumulations with exposures started in June 1985. They were treated in the same manner as the RTP and STU data with generally the same results. Stainless steel was used as an inert surface in calculating deposition velocity for coarse mode particles, and calcium was used as the indicator element. The regression deposition velocity was 1.09 ± 0.21 cm/s, which is consistent with the values obtained in the EPA studies. The sulfate, hydrogen ion, and carbonic acid coefficients for the DC data were not statistically different from the coefficients obtained from the RTP and STU data.

The environmental data were treated in the same manner as the RTP and STU data, including calculating accumulations of sulfur dioxide based on deposition velocities to standard 10.2 by 15.2-cm specimens. Deposition velocities to 30.5 by 61-cm specimens are believed to be less than those for standard specimens, since length Reynolds numbers (*Re*'s) are high enough that some turbulence is expected.

The effects of bicarbonate and hydrogen ions in rain are both covariant with rain volume. Therefore, the stoichiometric hydrogen ion effect was subtracted from the zinc runoff accumulations and the results regressed on the critical relative humidity criteria for SO_2 deposition, periods of dryness, and calculated solubility based on bicarbonate. As with the RTP and STU data, the critical relative humidity criterion giving a SO_2 effect coefficient closest to one was 75%. The resulting coefficients and their standard errors were 0.964 ± 0.554, 2.428 ± 4.044, and 0.258 ± 0.057 for deposition during periods of wetness, for that during periods of dryness, and the bicarbonate in rain (clean rain) effects, respectively.

Although the coefficient for deposition of SO_2 during periods of wetness is not significantly different from zero, it also is not different from that obtained from the RTP and STU data. It is lower as the effect of the difference in specimen size predicts. The coefficient for deposition during dryness is statistically different neither from zero nor for the coefficient from the RTP-STU regression results. The magnitude indicates an actual to apparent surface area ratio of 1.73. The coefficient for the effect of bicarbonate ion (residence time factor) is statistically different from zero and is higher than the similar coefficient obtained on smaller specimens.

The relative contributions of the different model components to the corrosion of zinc at the DC site are illustrated in Fig. 1. The theoretical and empirical coefficients are combined and the data converted to equivalent losses of thickness that are accumulated with time. The results are corrosion-time curves. At Washington, the major contributor to corrosion of this zinc specimen is the bicarbonate or "clean rain" effect. The effects of hydrogen ion in rain and the deposition of SO_2 during periods of wetness are about the same. Deposition of SO_2 during period of dryness has a relatively minor, almost constant-with-time effect.

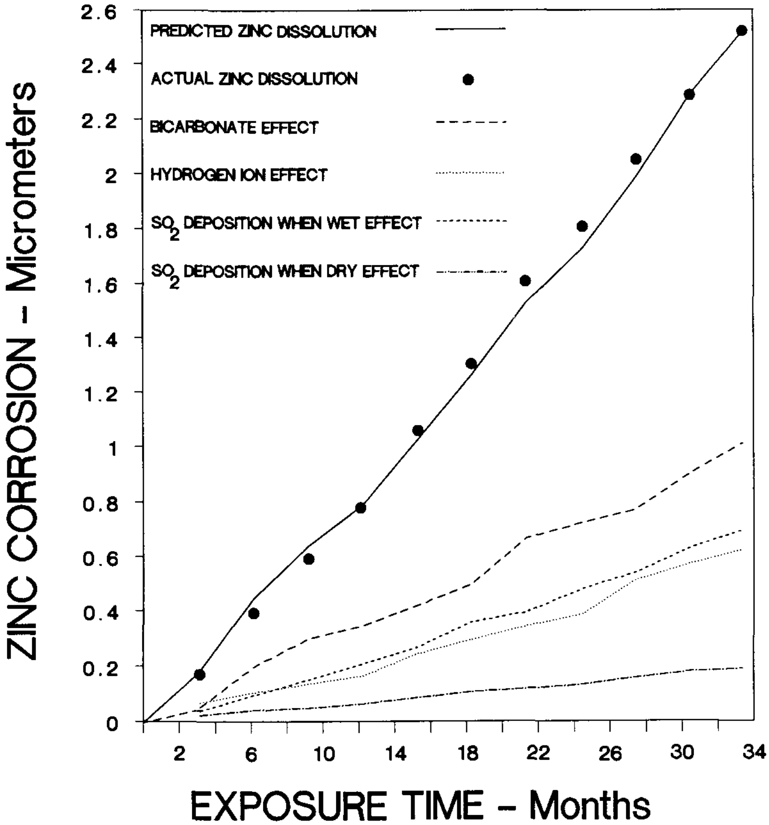

FIG. 1—*Contributions to zinc corrosion at Washington, DC.*

Comparison of Results from EPA and Bureau of Mines Experiments

The predicted and actual corrosion time curves for the three sites are shown in Fig. 2. Although STU has higher ambient levels of SO_2 than DC, the corrosion rates are about the same. Higher wind speeds and longer rain residence times on the larger specimens at DC have compensated for the higher concentration of SO_2 at STU. Although the corrosion rate at the relatively clean RTP site is small, it is still about half of what it is at the STU site with much higher levels of SO_2. This is because the "clean rain" and hydrogen ion effects are about the same at the two sites.

Application of Model to Historical Data for Different Shapes

Zinc on galvanized structures of different shapes and sizes corrodes at different rates, even when exposed to the same environment. This difference is believed to be due to differences in deposition velocities to different structures such as sheet and fencing [*14*]. Differences in corrosion rates of 10.2 by 20.4-cm specimens and 71 by 91-cm sheet can be seen when the results of two long-term studies done at approximately the same time in the sixties and seventies at the same ASTM sites are compared [*15,16*]. Corrosion on the smaller specimens of rolled zinc was determined by mass loss. Corrosion of the galvanized sheet was determined visually as percent rust. The latter was converted to thickness loss by assuming normal distribution of thickness with a standard deviation of 20%. Additional data on corrosion rates of chainlink fencing in four cities has been obtained by measuring the remaining thickness of galvanizing on highway fencing exposed for different lengths of time

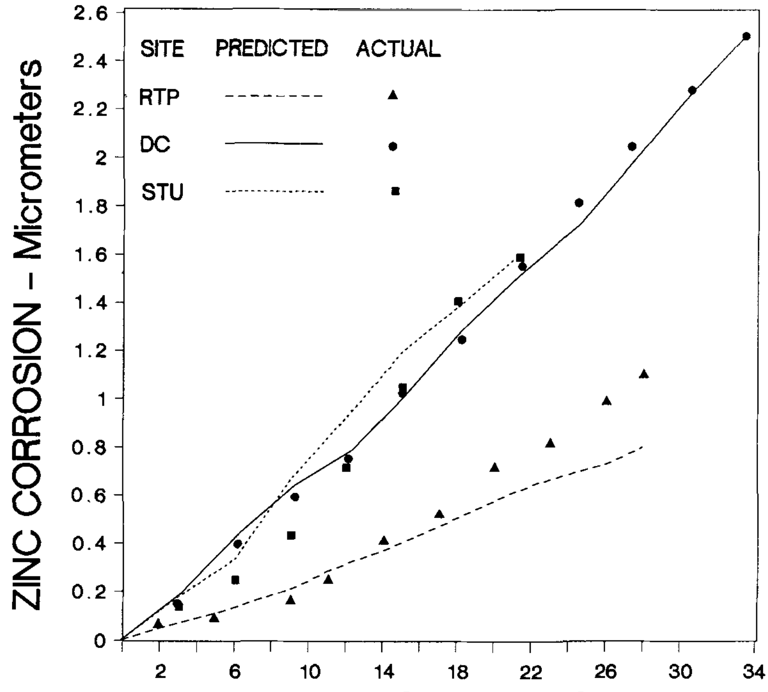

FIG. 2—*Actual corrosion rates compared with predictions at three sites.*

[17]. These data provide long-term corrosion rates (from 7 to 30 years) for different shapes and sizes with which the dissolution model predictions may be compared.

Estimating Environmental Conditions

The climatic parameters at each location were obtained from long-term averages at weather service stations. The fraction of time when a surface was wet was estimated by using an empirical relationship among times when 75% relative humidity is exceeded as well as the average temperature and dew point, based on data at RTP. The pH of rain is assumed to be 4.2 in the eastern states and 5 on the West Coast. Average SO_2 levels were estimated from available EPA data at monitoring sites and times closest to the exposure sites and periods. All of these data are subject to considerable error, which affects the predictability of the model. The results are given in Table 6.

Application of Model to Environmental Data

The model consists of four components, as follows

$$\text{Corrosion Rate} = a_o\, H^+ + a_1\, HCO_3^- + a_2\, SO_2\text{dry} + a_3\, SO_2\text{wet} \qquad (3)$$

with the terms calculated from environmental conditions and with the a_i coefficients for the model components differing with application to specific structures. The rain component coefficients, a_0 and a_1, vary because the amount of rain striking the surface varies with structure and orientation. For flat surfaces exposed at 30°, the amount of rain striking the upper surface when falling vertically is cos30° times the measured amount of rainfall. Although mass-loss measurements are based on both upper and lower surfaces, the rain effect only applies to the upper half. Splash losses occur on small specimens but not on larger specimens (approximately one half). For wire or fencing, one diameter of rain is spread over the perimeter or 3.14 diameters of surface.

The residence time factor, r, for small specimens empirically determined in the EPA experiment is around 0.16. Surface tension on small-diameter wire should increase the residence time of rain drops, and it takes longer for rain to run off larger sheet materials. A factor of 0.3 was assumed for both structures. For all except Denver (dry climate with longer but fewer dry periods) the effect of deposition of SO_2 during periods of dryness

TABLE 6—*Estimates of environmental conditions at different sites.*

Site	Temperature, °C	Dew Point, °C	RH, %	Wind Speed, m/s	Rain, cm	$f > 75\%$	SO_2, $\mu g/m^3$	pH
Newark	12.5	5.1	65.5	4.2	112	0.34	245	4.2
Kearny	12.5	5.1	65.5	4.2	112	0.34	55	4.2
Pt. Reyes	13.7	8.4	74.0	4.7	49	0.47	6	5.0
Brazos River	21.0	15.2	72.0	4.0	94	0.45	4	4.2
State College	10.2	3.3	67.5	4.2	99	0.35	14	4.2
State College	10.2	3.3	67.5	4.2	99	0.35	25	4.2
Pittsburgh	10.2	4.1	70.5	4.0	92	0.39	300	4.2
Denver	11.0	0.1	53.5	3.9	39	0.20	25	4.2
Philadelphia	12.6	5.1	65.5	4.3	105	0.34	125	4.2
Hartford	9.5	1.7	64.0	3.8	113	0.30	56	4.2
Houston	20.5	15.2	74.1	3.5	114	0.48	9	4.2

($a_2SO_2$dry) is assumed to be constant at 0.07 μm/year (the empirical value obtained from the DC data). Denver was assumed to be half of that.

The hydrogen ion term is

$$H^+ = R \times 10^{-pH} \tag{4}$$

where R is annual rainfall in centimeters.

The bicarbonate term is

$$HCO_3^- = r \times R \times Zn^{2+} \tag{5}$$

where,

r = the residence time factor, and,
Zn^{2+} = zinc solubility calculated using Eq 1.

The term for the effect of sulfur dioxide deposition during periods of wetness is

$$SO_2wet = 0.045 \times V_d \times f_{75} \times SO_2 \tag{6}$$

where

V_d = deposition velocity, cm/s,
f_{75} = the fraction of time when the relative humidity exceeds 75%, and
SO_2 = the average sulfur dioxide concentration, μg/m^3.

Deposition velocity depends on wind speed and on shape and size. The basic relationship is

$$V_d = 100 \times v \times f/2 \tag{7}$$

where

v = wind speed, m/s, and
f = the friction factor which is shape-, size-, and wind speed-dependent.

Coefficients needed to calculate zinc corrosion rates in micrometers per year for the three different shapes and sizes are given in Table 7. The *Re* is length times wind speed divided by kinematic viscosity of air. The square root of the length times width is used for the length term for the flat surfaces. A diameter of 3.72 mm is used for the fencing. Flow over flat plates will be mostly parallel to the surface. Flow over fence wire can range from parallel to perpendicular to the wire axis. Parallel is used in this application, which gives a constant deposition velocity of 3.19 cm/s.

TABLE 7—*Dissolution model coefficients for different structures.*

Structure	a_0	a_1	$a_3 = f/2$
Large sheet	39.7	23.8	$0.015/(Re)^{1/7}$
Weight loss, specimens	19.8	6.4	$0.664/(Re)^{1/2}$
Wire:			
Parallel	14.6	13.1	$8/(Re)$
Perpendicular	14.6	13.1	$0.63\ /(Re)^{1/2}$

In Figure 3 the calculated results are compared with the actual corrosion rates. Even with these rough estimates of environmental conditions, the model can account for 33% of the variability in corrosion rates. If the Pittsburgh and Philadelphia fencing data are excluded, the model can account for 73% of the variability. The model overestimates the corrosion rate of fencing at high SO_2 levels by about 60%. Overestimation for sheet materials exposed to the same conditions is only about 17%. This suggests that the estimated deposition velocity used for fencing was too high and that the estimate of the SO_2 level at Pittsburgh during the fifties was probably too high.

Summary and Conclusions

Two different studies at three sites provided evidence confirming a model for dissolution of zinc and the corrosion product film that tends to protect a galvanized steel surface. One zinc ion replaces two hydrogen ions in rain that reaches the surface. Equilibrium with bicarbonate ions from dissolved carbon dioxide is not reached because the residence time for rain on the surface is not long enough. Sulfur dioxide gas adsorbing on the surface reacts stoichiometrically when water is present. Regression analysis of the runoff data produced coefficients consistent with the model and indicated no significant lack of fit.

Although particulate matter calcium compounds cause more adsorption of sulfur dioxide

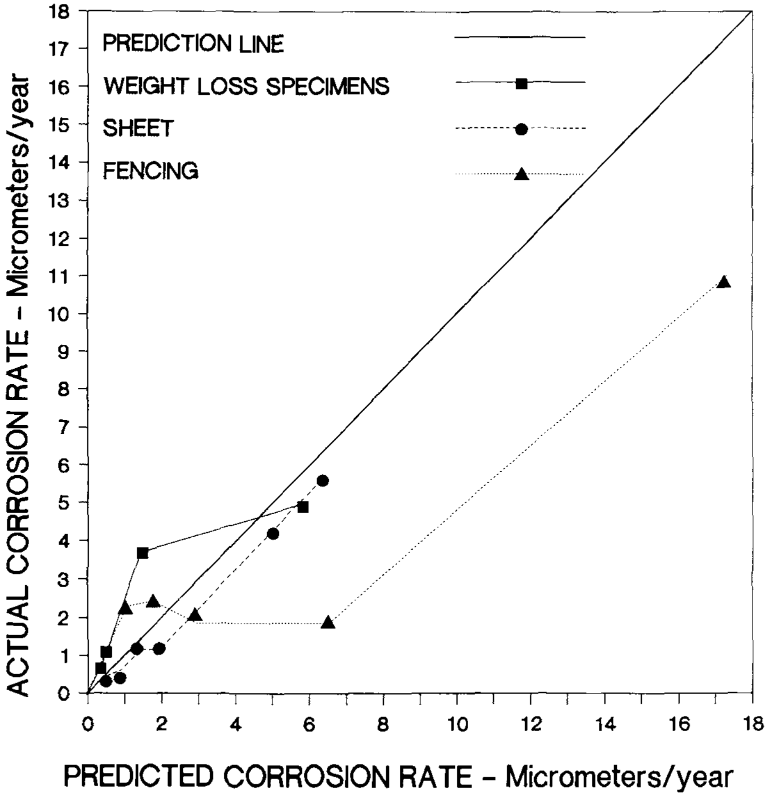

FIG. 3.—*Comparison of actual with predicted corrosion rates for different shapes and sizes.*

on the surface, the additional amount does not react with zinc or the protective corrosion product film because it preferentially reacts with the more active calcium compounds. Therefore, calcium has no direct effect to either accelerate or protect zinc corrosion.

Analysis of the data indicates that nearly twice as much sulfur dioxide is adsorbed on surfaces exposed to acidic rain than simulated clean rain. This is believed to be the result of the formation of corrosion products that are more hygroscopic in acidic rain exposures than in clean rain exposures. This, in effect lowers the critical relative humidity used in the application of the model from 90 to 75% and increases the area for adsorption during periods of dryness. There is not enough variation in the levels of pH in the data to determine the functional relationship of this interaction.

The model provides estimates of corrosion of galvanizing on different structures that are in reasonable agreement with measured corrosion rates. Predictability suffers from inaccuracy of estimates of environmental data as much as or more than it does from possible errors in the model. One model parameter, however, that appears to lead to an overestimation is the calculation of deposition velocity to wire or fencing. The effect of this overestimation is significant at estimated high levels of sulfur dioxide which, fortunately, do not exist in the United States at present. The relative error is much smaller at existing pollution levels.

With reasonably good environmental data, the model can be expected to partition the effects of pollutants from clean conditions for use in assessing economic effects on the corrosion of galvanized steel products.

Disclaimer

The information in this paper has been funded by the United States Environmental Protection Agency and has been subjected to Agency review and approved for publication. Mention of trade names or commercial products does not constitute endorsement or recommendation for use.

References

[1] Spence, J. W. and Haynie, F. H., "Derivation of a Damage Function for Galvanized Steel Structures: Corrosion Kinetics and Thermodynamic Considerations," this STP, American Society for Testing and Materials, Philadelphia, 1990.

[2] Haynie, F. H., *Materials Degradation Caused by Acid Rain,* American Chemical Society, Washington, DC, 1986, p. 162.

[3] Edney, E. O., Stiles, D. C., Spence, J. W., Haynie, F. H., and Wilson, W. E., *Materials Degradation Caused by Acid Rain,* American Chemical Society, Washington, DC, 1986, p. 172.

[4] Edney, E. O., Stiles, D. C., Spence, J. W., Haynie, F. H., and Wilson, W. E., *Atmospheric Environment,* Vol. 20, 1986, p. 541.

[5] Haynie, F. H., *Degradation of Metals in the Atmosphere, ASTM STP 965,* American Society for Testing and Materials, Philadelphia, 1987, p. 282.

[6] Edney, E. O., Stiles, D. C., Corse, E. W., Wheeler, M. L., Spence, J. W., Haynie, F. H., and Wilson, W. E., *Materials Performance,* Vol. 28, 1988, p. 47.

[7] Edney, E. O., Cheek, S. F., Stiles, D. C., Corse, E. W., Wheeler, M. L., Spence, J. W., Haynie, F. H., and Wilson, W. E., *Atmospheric Environment,* Vol. 22, 1988, p. 2263.

[8] Edney, E. O., Cheek, S. F., Corse, E. W., Spence, J. W., and Haynie, F. H., *Journal of Environmental Science and Health,* Vol. A24, 1989, p. 439.

[9] *NAPAP Annual Report, 1986,* National Acid Precipitation Assessment Program, Washington, DC, 1986, p. 75.

[10] McElhoe, B., *Journal of the Air Pollution Control Association,* Vol. 23, 1988, p. 1171.

[11] Tang, R-T., Barlow, P. M., and Waldruff, P., "Material Aerometric Database for use in Developing Materials Damage Functions," EPA Project Report 600/3-89/031, Atmospheric Research and

Exposure Assessment Laboratory, US EPA, Research Triangle Park, NC, 1989.

[12] Haynie, F. H. and Lemmons, T. J., *Aerosol Science and Technology* Vol. 13, August 1990.

[13] Cramer, S. D., Carter, J. P., Linstrom, P. J., and Flinn, D. R., *Degradation of Metals in the Atmosphere, ASTM STP 965,* American Society for Testing and Materials, Philadelphia, 1987, p. 229.

[14] Haynie, F. H., *Durability of Building Materials and Components, ASTM STP 691,* American Society for Testing and Materials, Philadelphia, 1980, p. 157.

[15] Showak, W. and Dunbar, S. R., *Atmospheric Corrosion of Metals, ASTM STP 767,* American Society for Testing and Materials, Philadelphia, 1982, p. 135.

[16] Tonini, D. E., *Atmospheric Corrosion of Metals, ASTM STP 767,* American Society for Testing and Materials, Philadelphia, 1982, p. 163.

[17] Cunningham, S. B., Chico, T., and Haynie, F. H., "Corrosion Rates of Galvanized Chain-link Fence: A Field Study," APCA Preprint 85-8.9, Air Pollution Control Association, Pittsburgh, 1985.

Stephen D. Cramer[1] *and L. Garner McDonald*[1]

Atmospheric Factors Affecting the Corrosion of Zinc, Galvanized Steel, and Copper

REFERENCE: Cramer, S. D. and McDonald, L. G., "**Atmospheric Factors Affecting the Corrosion of Zinc, Galvanized Steel, and Copper,**" *Corrosion Testing and Evaluation: Silver Anniversary Volume, ASTM STP 1000,* R. Baboian and S. W. Dean, Eds., American Society for Testing and Materials, Philadelphia, 1990, pp. 241-259.

ABSTRACT: The Bureau of Mines, as part of the National Acid Precipitation Assessment Program, studied the atmospheric corrosion of zinc, galvanized steel, and copper at five sites in the eastern United States for periods up to five years. Air quality, meteorology, precipitation chemistry, and particulate chemistry were monitored at each site. Long-term (steady-state) corrosion rates were measured by mass loss and by determining the rate that corrosion products were removed in precipitation runoff. A three-term runoff flux model fit long-term field corrosion data well, giving R^2 values greater than 0.95. The model was based on the fluxes of precipitation volume, wet-deposited hydrogen ion, and dry-deposited sulfur dioxide that are available from regional environmental monitoring activities. The parameter values obtained from this model agreed with values obtained by direct measurement, indicating they are physically significant. These parameters are the dry deposition velocity of sulfur dioxide to the metal, the number of hydrogen ions needed to release a metal ion from the corrosion product, and a product of residence time and the solubility of the corrosion product in precipitation. Experimental evidence suggests the model needs a fourth term for the dry deposition of particulates that deposit on the metal and neutralize a fraction of the acidic species subsequently deposited. Damage to zinc, galvanized steel, and copper from wet and dry acidic deposition was estimated to be 50% or more of the total damage at each of the five sites. Damage to zinc at the Ohio site by acid deposition was more than 80% of the total damage. For copper, damage from the wet deposition of hydrogen ions was greater than that from the dry deposition of sulfur dioxide at four of the five sites.

KEY WORDS: corrosion, atmospheric corrosion, metals, copper, zinc, air quality, rain chemistry, acid rain, acid deposition, sulfur dioxide, dry deposition, deposition velocity, damage function, corrosion products

Zinc, primarily as galvanized steel, and copper are commonly used in outdoor construction because of their favorable resistance to atmospheric corrosion. Degradation of these materials in outdoor applications is the result of weathering processes involving the chemistry and meteorology of the environment and surface chemical and electrochemical processes. Anthropogenic species can alter the corrosion process by favoring specific reaction paths and by providing new reaction paths [*1–11*].

Damage functions can simplify the description of the corrosion process by quantitatively relating the response of a property of interest, such as corrosion rate, to the chemistry and meteorology of the environment [*2,5,6,12–16*]. This approach sacrifices, to some degree, specificity in describing the mechanism and kinetics for a quantitative characterization of

---

[1] Chemical engineer and metallurgist, respectively, Albany Research Center, U.S. Bureau of Mines, Department of the Interior, Albany, OR 97321.

the major effects of the environment on the property. On the other hand, the value of the approach can be greatly enhanced by the application of sound chemical and physical principles to model the functional relationship.

Early efforts at modeling the atmospheric corrosion performance of zinc and copper produced empirical relationships with limited applicability to other atmospheric environments [*2*,*17*]. Nevertheless, the strong effect of sulfur dioxide was identified in a number of studies [*2–4,10,17*]. Recent studies of atmospheric corrosion involving a more complete characterization of the environment have been conducted under the National Acid Precipitation Assessment Program to measure the differential impact of acid deposition on metals damage. As part of this work, Lipfert et al. [*12,15*] developed damage functions for copper and zinc using available historical corrosion and environmental data and addressing the effects of sulfur dioxide and precipitation. Spence [*8*], Flinn [*18*], Edney [*6*], Haynie [*13*], and Cramer [*9*] have conducted detailed studies of environmental effects on galvanized steel corrosion.

Zinc and copper form a number of corrosion products during the initial atmospheric exposure and the weathering processes that follow [*7,10,11*]. The response of these corrosion products to the environment, that is, reactions with environmental constituents resulting in film dissolution, is one important factor in determining the protection provided by the corrosion film. A second factor is the intrinsic film-forming properties of the corrosion products. Atmospheric corrosion is the result of these two processes, film formation and film dissolution. The total mass loss from a corroding metal surface, $m(t)$, at time, t, is the sum of the mass incorporated in the corrosion film, $m_f(t)$, and that dissolved in precipitation and washed from the surface in runoff, $m_r(t)$, as follows

$$m(t) = m_f(t) + m_r(t) \tag{1}$$

Metal ions in the corrosion film can be mobilized in runoff by reactions with environmental species [for example, hydrogen ion (H) and sulfur dioxide (SO_2)] that form readily soluble compounds and by the inherent solubility of the corrosion products in precipitation without these environmental species. The runoff term is the sum of these processes over the exposure period

$$m_r(t) = \int_0^t \beta(t)dt \tag{2}$$

where β is the runoff flux and defines the rate that the corrosion product is dissolved in and removed from the surface by precipitation. Haynie [*19*] has used the time derivative of Eq 1 to develop a two-parameter film growth rate law

$$\frac{dm_f}{dt} = \frac{dm}{dt} - \beta \tag{3a}$$

$$= \frac{\alpha}{m_f} - \beta \tag{3b}$$

where the corrosion rate is the reaction rate at the metal/film interface and is assumed to be inversely proportional to film mass (or thickness), m_f, and α is a characteristic of the film.

The relative importance of film growth and runoff varies widely early in the exposure and is strongly dependent on the initial exposure conditions. Cramer et al. [*9*] have shown that zinc corrosion films continue to grow well beyond one year of exposure and copper corrosion films grow for much longer times. Nevertheless, once the steady-state film thickness has been achieved and $dm_f/dt = 0$, further corrosion is controlled by the runoff losses

$$\frac{dm}{dt} = \beta \tag{4}$$

This paper presents a model relating the runoff flux from zinc, galvanized steel, and copper to environmental factors. The parameters of this model will be computed from runoff data obtained at a site in Washington, DC. The model will be tested by computing these same parameters using long-term corrosion data obtained at five sites in the eastern United States. The contributions of environmental factors, namely dry deposition of sulfur dioxide and wet deposition of excess hydrogen ions, to the annual average runoff losses at these sites will be reported.

Experimental Procedure

Runoff Experiment

Single, large panels of rolled zinc (UNS-Z44330) and electrolytic tough-pitch (ETP) copper (UNS-C11000) were exposed for 33 months in Washington, DC, so that a total mass balance could be made on all environmental and metal species deposited or reacting on the panel surface. This was done by collecting and analyzing the precipitation incident on the panel (wet deposition), the precipitation runoff that drained from the skyward side of the panel, and by periodic analysis of the skyward-side corrosion film chemistry.

The zinc was hot rolled and contained (in weight percent) 0.81 copper (Cu), 0.003 lead (Pb), and 0.003 iron (Fe). The copper was hot rolled and annealed. It contained 0.03 max nickel (Ni), 0.003 max silicon (Si), and 0.03 max Pb. The panels measured 0.3 by 0.6 m (1 by 2 ft) and were 1.6 mm (1⁄16 in.) thick. The groundward side was masked with electroplating-grade vinyl tape to prevent corrosion. Prior to exposure, the skyward side was cleaned to remove organics and "as-received" corrosion product according to the ASTM Recommended Practice for Preparing, Cleaning, and Evaluating Corrosion Test Specimens (G1–72).

The panels were mounted with nylon screws in a rigid polypropylene tray designed to capture all precipitation runoff from the panel. The ratio of the tray area to panel area was 1.03. The trays were mounted at an angle of 30° with the horizon and faced south. The trays drained through a vertical 0.9-m Teflon tube (1.9 cm inside diameter) into a 20-L container. Evaporation losses from the collected runoff and direct absorption of acidic gases were minimized by the long, small-diameter diffusion path between the container and the tray. Runoff from the panels was collected at monthly intervals for analysis.

The effects of particulate deposition on runoff chemistry were determined at the same time by collecting runoff from an inert surface. A panel of Type 304 stainless steel (UNS-S30400) was chosen for this purpose. Panel configuration, mounting, and runoff collection and analysis were identical to that for the zinc and copper panels.

Wet deposition to the panels was collected using a wet/dry precipitation collector. Monthly wet-only precipitation samples were collected concurrently with the runoff samples for analysis.

All runoff and wet deposition samples were analyzed for the following ions: H, Na, K, Ca, Mg, NH_4, SO_4, NO_3, PO_4, and Cl [*20*]. Hydrogen ion concentration was determined by direct measurement of pH. The ammonium ion and the anions were determined by ion chromatography. The remaining cations were determined by atomic absorption (AA). In addition, the runoff samples from zinc were analyzed for Zn, from copper for Cu, and from stainless steel for Zn, Cu, Fe, and Cr, all by AA. Volume and collection time were also recorded.

A separate set of one-sided 10 by 15 cm (4 by 6 in.) zinc and copper panels were exposed concurrently with the larger runoff panels for mass loss and corrosion film chemistry determinations. The groundward side of each panel was masked with the vinyl tape to prevent corrosion. They were prepared identically to the runoff panels and exposed to the atmosphere in accordance with the ASTM Recommended Practice for Conducting Atmospheric Corrosion Tests on Metals (G50–76) at an angle of 30° facing south. Sets of three panels each were removed after exposures of 1, 3, 12, and 33 months. Corrosion products were quantitatively removed from zinc panels with 15 vol % ammonium hydroxide and from copper panels with 33 vol % hydrochloric acid (ASTM G1–72). The solutions containing the dissolved corrosion products were analyzed by wet chemical techniques to determine the composition of the corrosion film. All panel weights were recorded to 0.1 mg.

Field Corrosion Experiment

Mass loss panels were exposed at five eastern sites (North Carolina, Washington, DC, New Jersey, New York, and Ohio) which represent differing combinations of the environmental parameters considered important in determining the effects of acid deposition on materials damage [*21*]. Specific information on the sites is given in Table 1. Air quality, precipitation chemistry, and meteorology were monitored continuously at each of the sites from 1982 through May 1988. The facilities at the Washington, DC, site, shown in Fig. 1, are typical of those at each site.

In addition to zinc and copper, galvanized steel was exposed at the five sites. The chromate-treated 28-gage galvanized steel strip was continuous hot-dipped and had a coating weight (for two sides) of 0.27 kg/m^2 (0.90 oz/ft^2). The coating thickness was 19 μm. The mass loss panels measured 10 by 15 cm. They were treated in the same way as the one-sided mass loss panels used in the runoff experiment except that they were not masked on one side. Galvanized-steel corrosion product was stripped and subsequently analyzed by the same procedure used for zinc. Panels were exposed in triplicate for periods of 12, 36, and 60 months. All panel weights were recorded to 0.1 mg.

Experimental Results

An array of mass transfer, chemical, and electrochemical processes that can occur on copper and zinc surfaces in an atmosphere where sulfur dioxide is the primary gaseous pollutant is shown in Fig. 2. The mass balance for species i in the corrosion film showing the relationship between the input fluxes and the output flux can be written as follows

$$m_{f,i}(t) = \int_0^t [F_{w,i}(t) + F_{d,i}(t) + F_{c,i}(t) - F_{r,i}(t)]dt \tag{5}$$

where

$m_{f,i}(t)$ = mass per unit area of species i accumulated in the corrosion film,
$F_{w,i}$ = wet deposition flux,
$F_{d,i}$ = dry deposition flux,
$F_{c,i}$ = corrosion reaction flux, and
$F_{r,i}$ = runoff flux.

TABLE 1—*Materials exposure sites.*

	NC	DC	NJ	NY	OH
Location	Research Triangle Institute Research Triangle Park, NC 27709	West End Library 24th and L St., NW Washington, DC 20037	Bell Communications Research Chester, NJ 07930	Adirondack Ecological Center Huntington Wildlife Forest Newcomb, NY 12852	Jefferson County Services Building 814 Adams St. Steubenville, OH 43952
Operator	Research Triangle Institute	Department of Environmental Services, District of Columbia	DOE Environmental Measurements Laboratory	College of Environmental Science and Forestry, State University of New York	North Ohio Valley Air Authority
Coordinates	78°52′ 9″ W 35°54′12″ N	77°03′ 5″ W 38°54′13″ N	74°40′ 7″ W 40°49′42″ N	74°13′25° W 43°58′25″ N	80°37′20″ W 40°21′35″ N
Elevation[a]	97.5	27.5	265	500	250
Mean[b] Temperature, °C	14.9	14.3	8.1	5.3	11.7

[a] Meters above mean sea level.

[b] Averaged over period January 1982 to May 1988, except OH, which was May 1985 to May 1988.

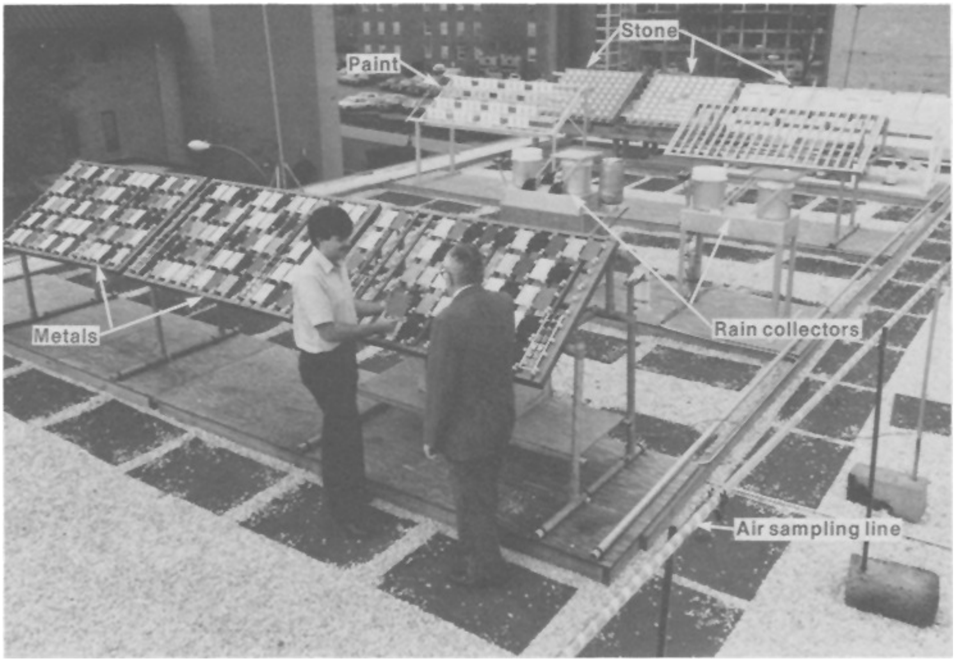

FIG. 1—*Washington, DC, materials exposure site on the roof of the West End Library including metals, stone, and paint samples, collector for precipitation chemistry sample, and sampling line for continuous air quality measurements.*

Each term in Eq 5 except dry deposition flux is known from experimental measurements. One can take the time derivative of Eq 5 and rearrange terms to solve for $F_{d,i}$

$$F_{d,i}(t) = \frac{dm_{f,i}}{dt}(t) + F_{r,i}(t) - F_{w,i}(t) - F_{c,i}(t) \tag{6}$$

Each term on the right side of Eq 6 was replaced by the average flux and accumulation rate for the monthly measurement cycle of the runoff experiment to obtain the dry deposition flux of sulfur to the surface of the runoff panels, $F_{d,s}$.

A small sulfur dry deposition flux was measured for the stainless steel panel. Since no chromium or iron was detected in the runoff that could be attributed to corrosion of the stainless steel panel, the sulfur most likely come from dry deposition of sulfate-containing particulates and from reactions of sulfur dioxide with basic particulates, for example (Ca,Mg)O and $CaCO_3$, on the panel surface under humid conditions. The assumption was made that these two sources contribute the same amount of dry-deposited sulfur to the copper and zinc panels. The net sulfur available to react with the corrosion product, $F^*_{d,s}(t)$, is the sulfur flux to the zinc and copper panels corrected for the sulfur associated with particulates.

$$(t) = F_{d,s}(t) - F_{d,SS}(t) \tag{7}$$

where

$F_{d,SS}$ = the stainless steel sulfur dry deposition flux.

With particle deposition excluded, the net sulfur flux to copper and zinc is attributed to dry deposition of sulfur dioxide. It is related to the ambient atmospheric concentration of sulfur dioxide by the mass transfer coefficient, v_d, commonly called the dry deposition velocity since it has the units of velocity, centimetres per second [6,22]

$$v_d(t) = F^*_{d,s}(t)/[\mathrm{SO_2}(t)] \tag{8}$$

where $[\mathrm{SO_2}(t)]$ is the ambient atmospheric concentration of sulfur dioxide. Monthly dry deposition velocities for sulfur dioxide, computed from the runoff experiment using Eqs 6–8, are plotted in Figs. 3 and 4 for zinc and copper, respectively. The mean values of the dry deposition velocities are: zinc, 0.44 ± 0.15 cm/s, and copper, 0.16 ± 0.09 cm/s.

Multiple layers of water have been shown to adsorb on zinc surfaces [23], and presumably copper surfaces, at ambient temperatures and a relative humidity of 93%. Moisture is more readily available on corroded zinc and copper surfaces from capillary condensation and from the hydrophilic nature of their corrosion products. Sulfur dioxide dissolves in this water to form the bisulfite ion, which in turn is readily converted to sulfate by ozone, hydrogen peroxide, and transition metal ions [24]. Transition metal ions such as iron are available in

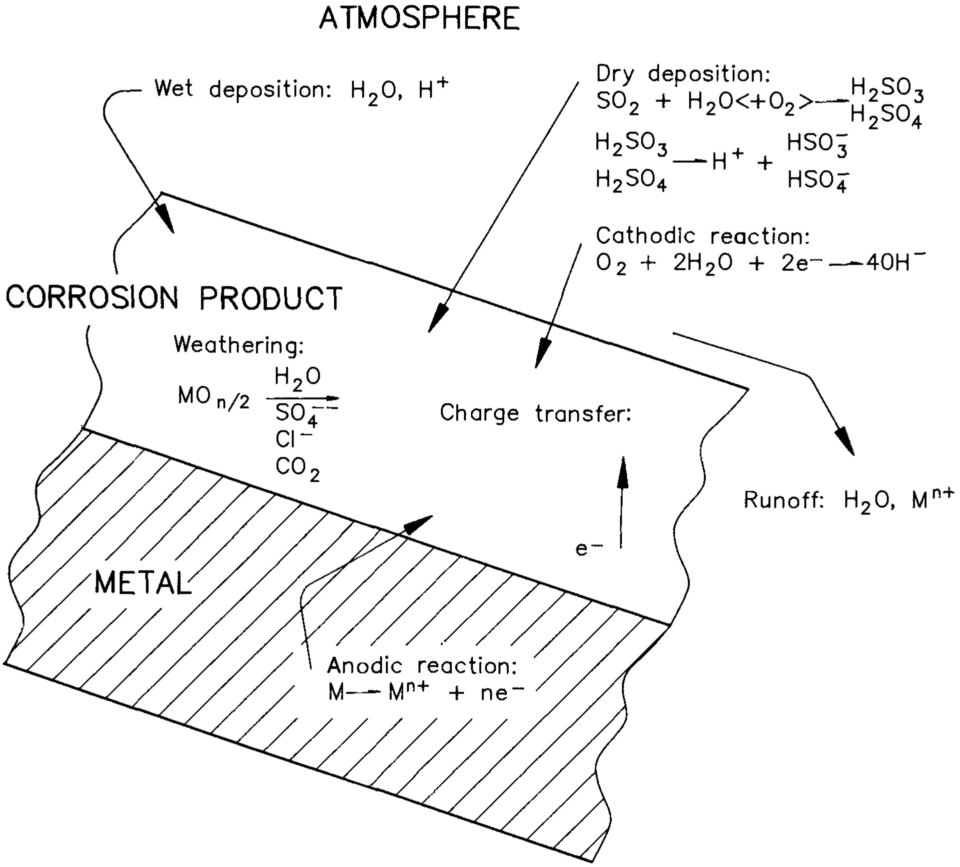

FIG. 2—*Chemical, electrochemical, and mass transfer processes that can occur during corrosion in atmospheres containing sulfur dioxide as the primary gaseous pollutant.*

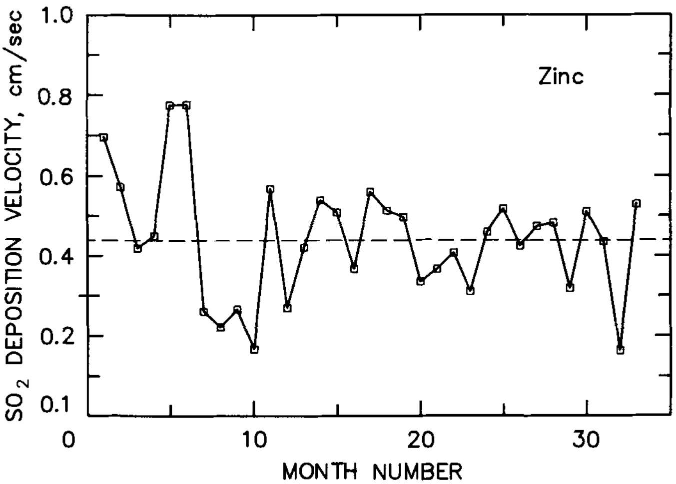

FIG. 3—*Monthly dry deposition velocities for sulfur dioxide to zinc measured at Washington, DC, beginning June 1985. Broken line is the average value of 0.44 cm/s.*

deposited particulates [25]. Two hydrogen ions are released for every sulfur dioxide molecule deposited on the surface in this process. These hydrogen ions then react with corrosion products to form soluble compounds which can be flushed from the surface by precipitation. The amount of corrosion product in this dry deposition contribution to the runoff flux should be stoichiometrically related to the dry-deposited sulfur dioxide. The associated runoff flux term, written in terms of equivalents of metal dissolved, is

$$S(\text{dry}) = a_1 v_d[\text{SO}_2] \tag{9}$$

The coefficient a_1 is a conversion factor to give S(dry) the correct units.

The dry deposition contribution to the runoff flux, S(dry), is subtracted from the runoff

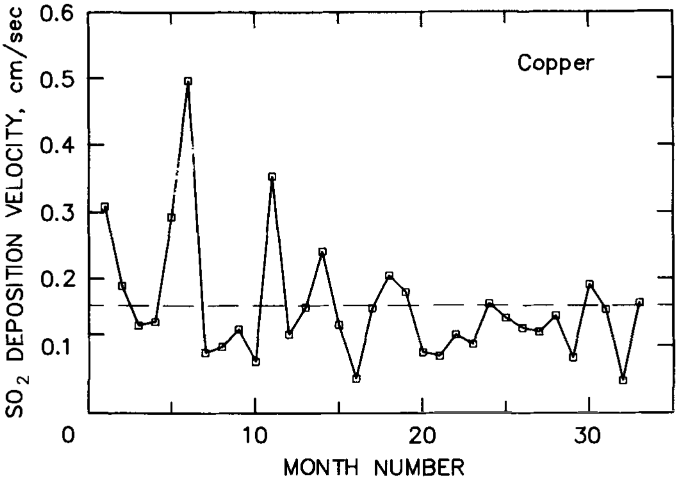

FIG. 4—*Monthly dry deposition velocities for sulfur dioxide to copper measured at Washington, DC, beginning June 1985. Broken line is the average value of 0.16 cm/s.*

flux, β, and divided by the precipitation volume flux, V', to give the concentration of metal ions in the runoff attributed to wet deposition, $[\beta - S(\text{dry})]/V'$. This concentration has been plotted in Figs. 5 and 6 versus the net change in the concentration of the wet-deposited hydrogen ions that occurs as the precipitation washes the panel surface. Zinc carbonate and zinc hydroxycarbonates are among the principal compounds formed in the atmospheric corrosion of zinc [*9–11*]. The two dashed lines in Fig. 5 correspond to the 1:1 and 2:1 stoichiometric ratios for hydrogen ion required to release zinc from the corrosion film in the following reactions

$$ZnCO_3 + H^+ \longrightarrow Zn^{2+} + HCO_3^- \qquad (10a)$$

and

$$ZnCO_3 + 2H^+ \longrightarrow Zn^{2+} + H_2O + CO_2 \qquad (10b)$$

The solid curve is the least squares fit of the data. It corresponds to a value for the stoichiometric ration of 3.2 and an intercept of 46.5 μmols Zn/L. The intercept is the solubility of the corrosion product adjusted for the residence time of precipitation on the panel surface. Two similar curves are shown in Fig. 6 for copper corresponding to the following reactions

$$Cu_2O + 2H^+ \longrightarrow 2\,Cu^+ + H_2O \qquad (11a)$$

and

$$CuO + 2H^+ \longrightarrow Cu^{2+} + H_2O \qquad (11b)$$

The solid curve is the least square fit of the data. It corresponds to an n of 2.6 and an intercept of 18.9 μmols Cu/L.

The results presented in Figs. 3 to 6 indicate that much of the dispersion in the runoff

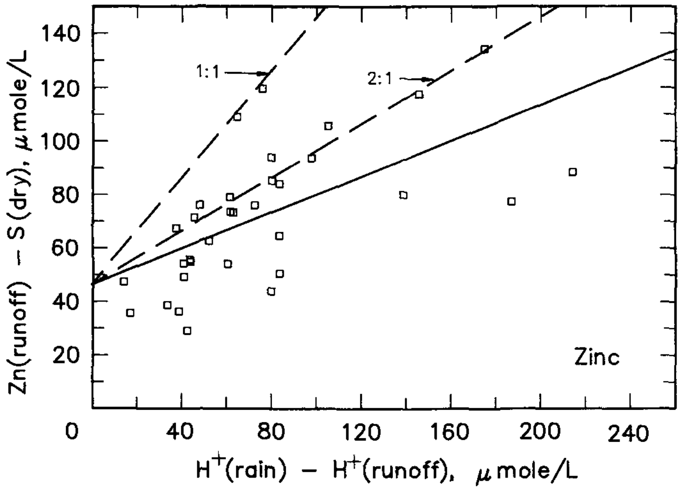

FIG. 5—*Effect of wet deposition on zinc runoff. Solid line is least squares fit of data. Broken lines correspond to 1:1 and 2:1 stoichiometric ratios for the moles of hydrogen ion required to release one mole of zinc from the corrosion product.*

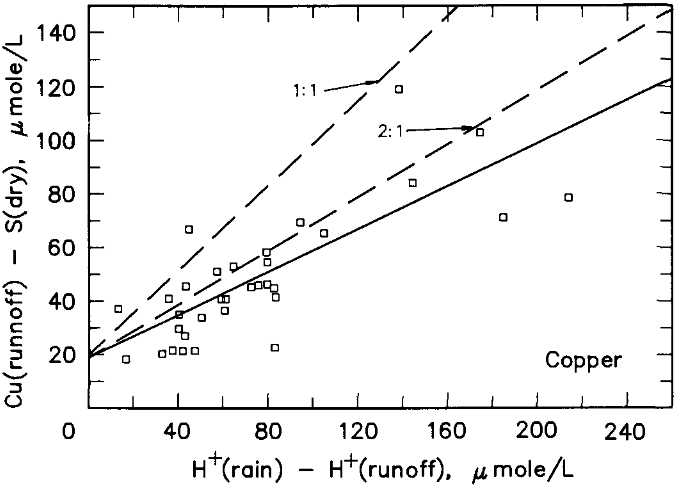

FIG. 6—*Effect of wet deposition on copper runoff. Solid line is least squares fit of data. Broken lines correspond to 1:1 and 2:1 stoichiometric ratios for the moles of hydrogen ion required to release 1 mol of copper from the corrosion product.*

flux data can be accounted for by a three-term model

$$\beta = rSV' + H_L'/\mathrm{n} + a_1 v_d\,[\mathrm{SO_2}] \tag{12}$$

where

V' = the precipitation volume flux,
H_L' = the wet-deposition hydrogen ion flux,
r = a residence time factor (valued from 0 to 1),
S = the solubility of the corrosion product in precipitation at pH 5.6 (the pH of water in equilibrium with the ambient carbon dioxide concentration), and
n = the stoichiometric coefficient for the reaction of hydrogen ion with the corrosion product.

Runoff flux data obtained from the field corrosion experiment were used to determine how well Eq 12 represented the runoff data using the aerometric and precipitation chemistry data that typically are available from regional monitoring activities. Average runoff flux values were computed for this purpose from the mass loss and corrosion film chemistry data for every exposure at each of the five sites. Average values of V', H_L', and $[\mathrm{SO_2}]$ were also computed for each exposure. A least squares fit of Eq 12 was performed for zinc, galvanized steel, and copper using the data for exposures of 12 to 60 months at the five sites. The regression was not weighted. The regression for each metal included data from seventy 12-month, four 36-month, and four 60-month exposures. Each exposure was the result of triplicate corrosion measurements.

One of the two reactions given in Eq 10 is the dominant dissolution reaction (or proxy for an equivalent dissolution reaction) for zinc. Similarly, one of the two reactions in Eq 11 is the dominant dissolution reaction for copper. The value of the stoichiometric coefficient in Eq 12 is either 1 or 2. The results in Figs. 5 and 6 indicate that a value of 2 is the correct choice for both zinc and copper. With this value fixed, Table 2 gives the estimates of the other parameters obtained from Eq 12 obtained by a least squares fit. The R^2 values are computed relative to $\beta = 0$. The predicted values of β are shown as a function of the observed values for galvanized steel exposed at the five sites in Fig. 7. The R^2 for this case is 0.98.

Discussion

The deposition velocity is dependent upon factors characteristic of the environment and of the receiving surface. Environmental factors most important to the dry deposition of sulfur dioxide are wind speed, temperature, and the orientation, size, and shape of the surface. Important surface factors are roughness, area, wetness, temperature, and composition. The variation in the monthly deposition values in Figs. 3 and 4 are a reflection of these factors, particularly wind speed and surface wetness. The measured values represent an average of these effects over the measurement period.

The inverse of the deposition velocity can be regarded as proportional to the sum of an aerodynamic resistance, r_a, and a surface resistance, r_s, [22]

$$v_d \propto \frac{1}{r_a + r_s} \tag{13}$$

The aerodynamic resistance is dependent on the environmental factors noted above, and the surface resistance depends on the surface factors. As a simple example, an increase in wind speed decreases the aerodynamic resistance; an increase in surface wetness decreases the surface resistance. Both effects increase the deposition velocity. These kinds of effects lead to the results in Figs. 3 and 4. More commonly, however, complex and interacting atmospheric and surface processes occur, some of short duration, which significantly affect the dry deposition rate.

Because of this, the fit of Eq 12 to field corrosion data seeks to find an effective deposition velocity that represents the dry deposition of sulfur dioxide in a broad geographic region having similar climatological characteristics. The deposition velocities reported in Table 2 are statistically highly significant. Furthermore, they were not site dependent, indicating that the deposition rate at each of the five sites was effectively represented by the values given in Table 2. While these values depend upon the statistical inference of a relationship between the corrosion and the environmental data, the values measured in the runoff experiment at Washington, DC do not. The quantities needed to define those values were measured directly. The sulfur dioxide dry-deposition velocities obtained for copper by the two methods agreed identically. The values for zinc differed by only 15% and were not statistically different. This agreement would suggest that the dry-deposition velocities in Table 2 are not only statistically significant but are also physically significant. They should

TABLE 2—*Parameter values for runoff flux model based upon 12- to 60-month exposures in field corrosion experiment, 1982 to 1988.*

		Flux Term Parameters		
Metal	R^2	Precipitation rS, μM/L	Hydrogen Ion, mol H/mol Zn	Sulfur Dioxide v_d, cm/s
Zinc	0.96	26.8 ± 13.8	2	0.385 ± 0.046
Galvanized steel	0.98	26.2 ± 6.4	2	0.298 ± 0.023
Copper	0.98	18.4 ± 7.9	2	0.167 ± 0.028

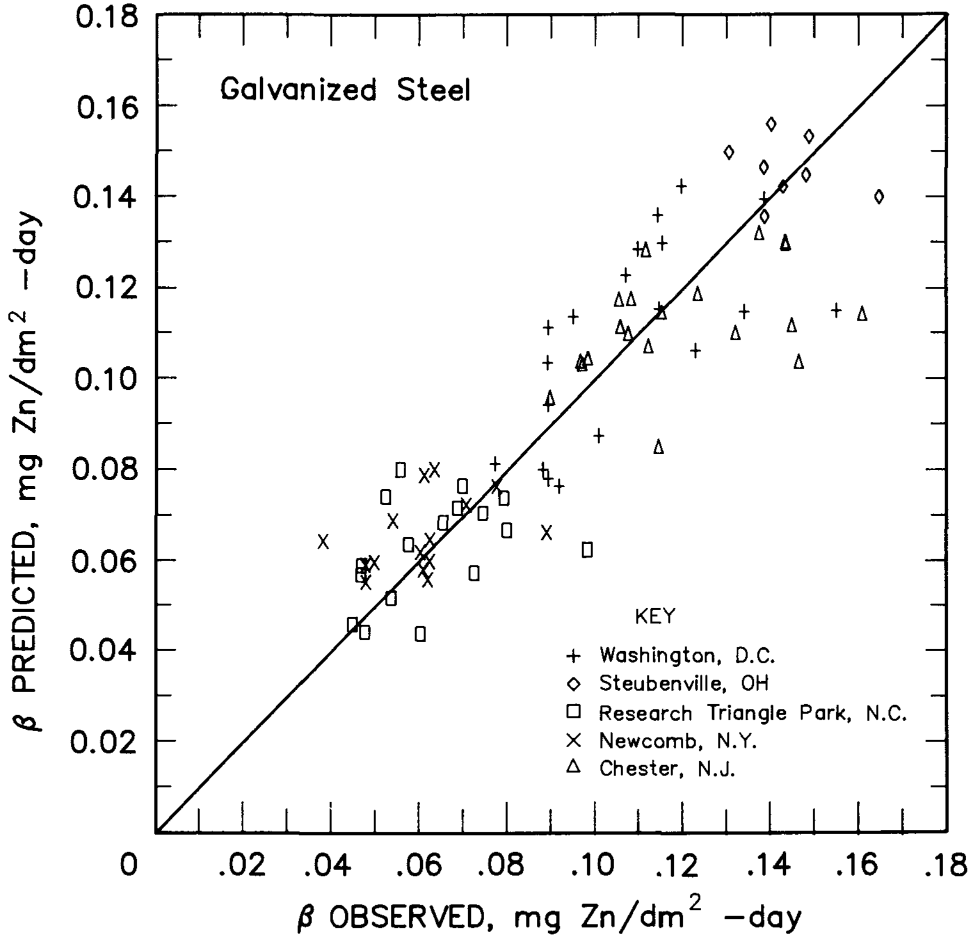

FIG. 7—*Predicted precipitation runoff flux for galvanized steel exposed 12 to 60 months at five sites; obtained using the parameters in Table 2.*

apply to at least a broad part of the eastern United States encompassing the Middle Atlantic states and New England. On the other hand, it is unlikely that they would apply to the more arid parts of the country.

Barring differences in the roughness of the developing corrosion product, the aerodynamic resistance of copper, zinc, and galvanized steel panels exposed under identical conditions would be the same. Differences in the deposition velocity for these metals would, therefore, occur because of differences in the surface resistance. The higher deposition velocity for zinc than for copper indicates that the copper corrosion product has a substantially lower affinity for sulfur dioxide than the zinc corrosion product. The higher deposition velocity for zinc than for galvanized steel indicates a higher surface resistance for galvanized steel. This is the effect expected from the chromate treatment applied to galvanized steel to inhibit "white rusting" and to reduce the reactivity of the surface.

Predicted runoff losses were obtained from the runoff experiment by integrating Eq 12 over the 33-month period of the experiment. The mean dry deposition velocities and the slopes and intercepts from Figs. 5 and 6 were used to compute the predicted values. The values for zinc and copper are plotted in Figs. 8 and 9, respectively, along with the measured runoff losses, as a function of the accumulated precipitation volume. The contributions of the individual runoff terms are given by the curves for: (1) the dry deposition of sulfur dioxide; (2) sulfur dioxide and the wet deposition of excess hydrogen ion; and (3) sulfur dioxide plus hydrogen ion and dissolution in pH 5.6 water. All three terms make significant contributions to the dissolution of the corrosion product in runoff. Dry deposition of sulfur dioxide has the greatest effect on the zinc corrosion products. Wet deposition of hydrogen ions has the greatest effect on the copper corrosion products.

The sum of the three terms overestimates the measured runoff for both copper and zinc, particularly in long exposures. This difference is small, representing only 15% of the runoff loss for zinc and 10% of the runoff loss for copper. This systematic and not insignificant deviation for both metals in long exposures suggests that other important processes may be involved. One source of this deviation could be the effect of temperature on the corrosion product solubility. Also, high precipitation fluxes could reduce residence times and conceivably reduce the mass of corrosion product dissolving in the runoff.

The most likely source of the deviation between predicted and measured runoff is the reaction of hydrogen ions with basic particulates dry deposited on the panel surface. This would be in addition to any such reaction that occurred on the stainless steel panel and was corrected for in Eq 7. The basic particulates would include $CaCO_3$ and (Ca,Mg)O. Not all calcium particulates are basic or would contribute to this process. The fraction of basic particulates reacting would depend upon the composition of the corrosion product surface

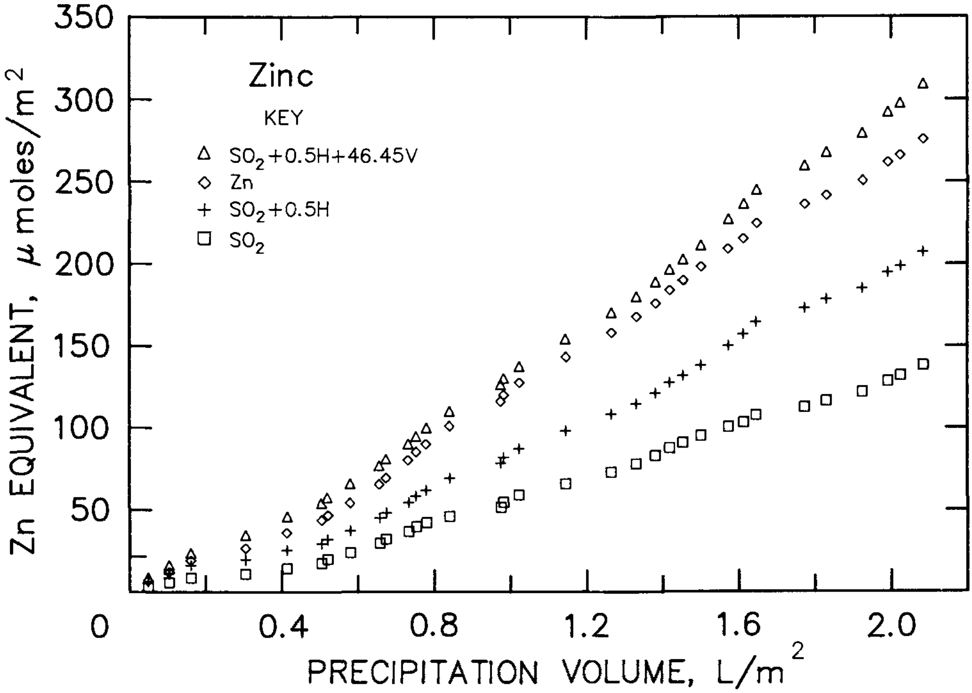

FIG. 8—*Accumulated zinc in precipitation runoff and contributions of wet and dry deposition to corrosion product dissolution for Washington, DC, runoff experiment.*

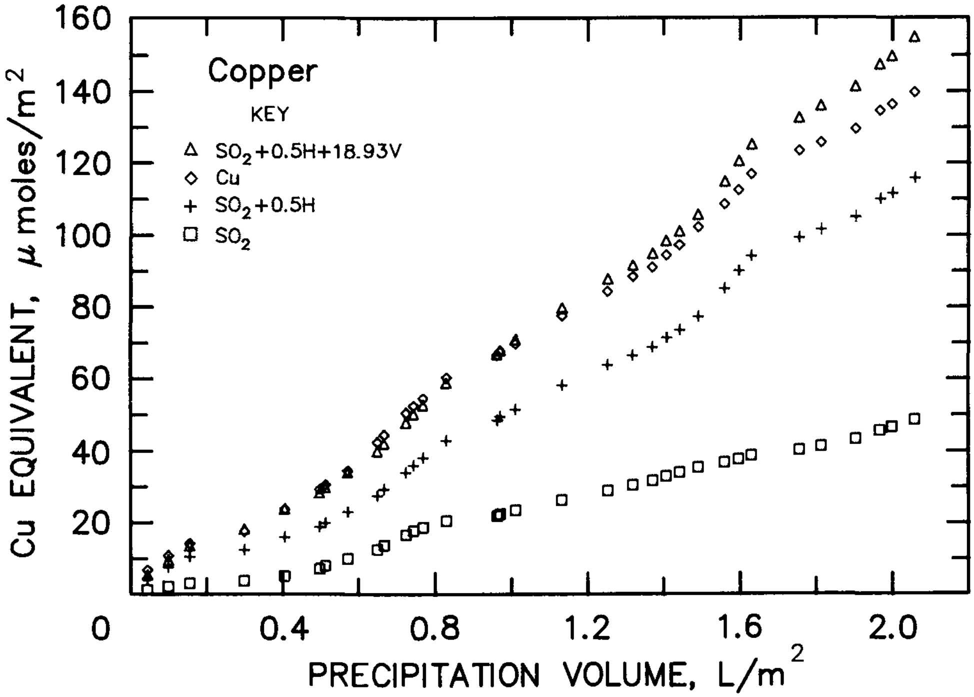

FIG. 9—*Accumulated copper in precipitation runoff and contributions of wet and dry deposition to corrosion product dissolution for Washington, DC, runoff experiment.*

at any time and the relative reaction rates of hydrogen ion with the corrosion products and with the particulates. The dry deposition flux for calcium could serve as an indicator for this process. One would also need to know the fraction of the particulates that are basic and the relative rates of the neutralization reactions occurring on the panel in long-term exposures. As the corrosion products on zinc and copper weather and form more stable mineral compounds, it is possible that reactions of the available hydrogen ions with basic particulates accounts for an increasing fraction of the acidic species consumed on the panel surface. This would require modifying Eq 12 to include a term proportional to the calcium dry deposition flux, $F_{d.Ca}$, that would reduce the amount of corrosion product dissolved by acid deposition, as follows

$$\beta = rS(T)V' + H_L'/n + a_1 v_d [SO_2] - a_2 F_{d.Ca} \tag{14}$$

The calcium dry-deposition flux can be estimated from the ambient particulate concentrations and chemistry [25]. The term a_2 includes the fraction of basic calcium particulates in the total dry deposition flux. It also includes a factor for weighting the kinetics of the different neutralization reactions. The factor $S(T)$ in the first term of Eq 14 is the solubility of the corrosion product at temperature T. While Eq 14 has not been validated, the results in Figs. 8 and 9 indicate that the addition of a term for basic particulates would improve the model. Such a term would also help explain the slopes in Figs. 5 and 6, which gave stoichiometric coefficients greater than 2. By the very construction of Figs. 5 and 6, all of the effect of the neutralizing particles was assigned to the wet deposition flux. Because of this, substantially more hydrogen ions would appear to be needed to release a zinc or copper ion than required by the stoichiometric equations.

The limit to which zinc can react with acid deposition is defined by the solubility curves given in Fig. 10. The carbonate ion equilibria are given in this figure for water saturated with carbon dioxide at ambient conditions (CO_2 partial pressure = 3×10^{-4} atm). The solubility of zinc carbonate in water saturated with carbon dioxide at partial pressures from 10^{-5} to 10^{-1} atm is also shown in this figure along with the solubility of β-$Zn(OH)_2$, one of the zinc hydroxides more likely to form under atmospheric corrosion conditions [*26*]. The two solubility curves intersect at about pH 7.5. At lower pH values zinc carbonate is more stable; at higher pH values zinc hydroxide is more stable. The conditions at the outer surface of the zinc corrosion product, where the pH would be lowest and the carbon dioxide concentration highest, favors the formation of zinc carbonate under ambient conditions. Those near the metal/film interface favor the formation of zinc hydroxide.

The cross-hatched area contains the pH-concentration data for the 33 monthly runoff samples. All of the measured zinc concentrations lie below or on the solubility curves. A substantial part of the zinc collected in the runoff is due to the highly soluble zinc sulfate formed by dry deposition sulfur dioxide that readily washes from the panel surface early in each precipitation event. After this has occurred, a mass balance shows that the zinc concentration in the runoff during the remainder of the precipitation event is well below the values in the cross-hatched area. One estimate of this concentration is given by the data in Fig. 5, where the concentration on average is 46.5 μmol Zn/L plus that which is dissolved

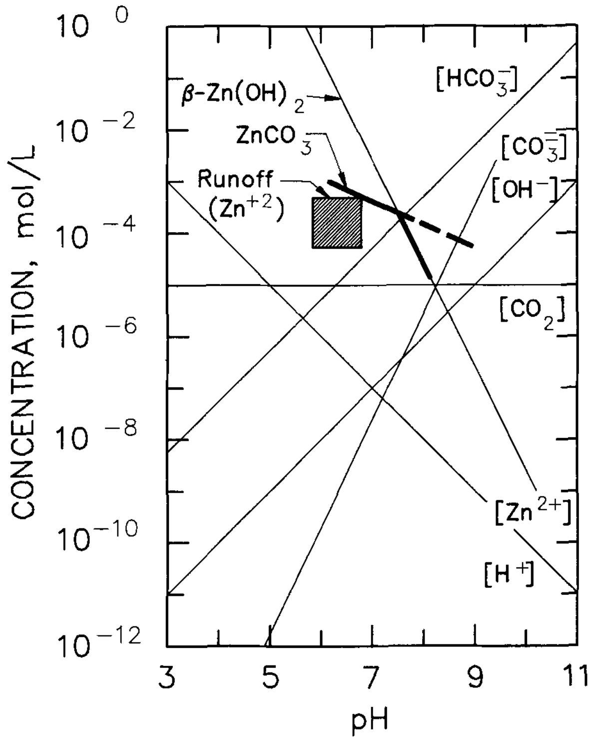

FIG. 10—*Solubility of* $ZnCO_3$ *and* β-$Zn(OH)_2$ *as a function of solution pH. Cross-hatched area defines zinc concentrations in the monthly precipitation runoff collected at Washington, DC, over 33 months.*

TABLE 3—*Annual average environmental parameters for runoff flux model, 1982 to 1987.*

Site	Precipitation Volume Flux, L/m² - day	Hydrogen Ion Flux, mmol H⁺ / m² - day	Sulfur Dioxide Concentration, ppb
North Carolina	2.74	107.1	2.3
Washington, DC	2.66	109.6	10.1
New Jersey	3.58	211.3	6.3
New York	2.89	120.1	1.6
Ohio[a]	2.32	201.9	20.7

[a] Averages for 1985 to 1987.

by the excess hydrogen ions. This is at least an order of magnitude lower than the solubility given by the curves in Fig. 10 and suggests a value for the residence time factor of less than 0.1. The lower value of the solubility obtained from the field corrosion data, Table 2, compared to the value from the Washington, DC, runoff data may reflect the influence of the lower temperatures observed at the New Jersey, New York, and Ohio sites in Table 1.

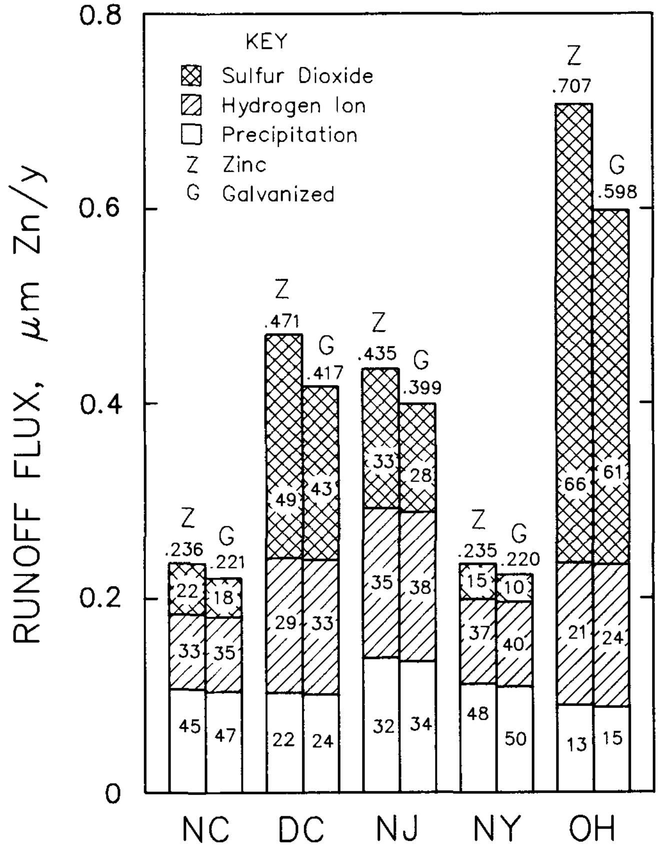

FIG. 11—*Annual average contribution of wet and dry deposition to corrosion damage resulting from precipitation runoff for zinc (Z) and galvanized steel (G). The numbers at top of bars are total damage rates in μm/year. The numbers in shaded segments are corresponding percentages of the total.*

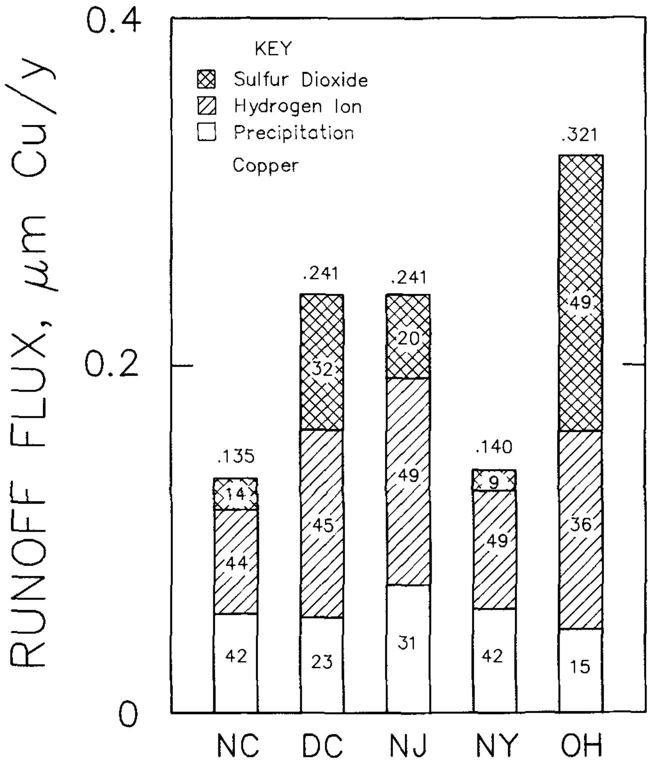

FIG. 12—*Annual average contribution of wet and dry deposition to corrosion damage resulting from precipitation runoff for copper. The numbers at top of bars are total damage rates in μm/year. The numbers in shaded segments are corresponding percentages of the total.*

The parameter values given in Table 2 were used in Eq 12 to estimate the annual average corrosion damage resulting from runoff losses at each of the sites. Average values of the precipitation volume flux, hydrogen ion flux, and sulfur dioxide concentration were computed from the precipitation chemistry and air quality data for the years 1982 to 1987 (1985 to 1987 for the Ohio site) (Table 3). These values gave the results in Fig. 11 for zinc and galvanized steel and in Fig. 12 for copper, expressed as a uniform corrosion penetration rate in micrometres per year.

The dominant feature in Fig. 11 is that acid deposition (wet and dry) accounts for 50% or more of the total damage to zinc and galvanized steel at all sites. At the Ohio site it accounts for more than 80% of the damage because of the large contribution of the sulfur dioxide term. Even at the two sites where sulfur dioxide concentrations are low, total damage is doubled by acid deposition because of the strong contribution of the hydrogen ion term. The reason that total damage varies by a factor of 3 when sulfur dioxide concentrations vary by a factor of more than 10 is that other terms also make significant contributions to the total damage.

The dominant feature in Fig. 12 is that acid deposition accounts for more than 50% of the total damage to copper. The hydrogen ion term is the principal contributor to the total damage at four of the five sites. Dry deposition is not as important to copper damage as is wet deposition except when sulfur dioxide concentrations are high.

Conclusions

Atmospheric corrosion rates for zinc and copper in long-term (steady-state) exposures are equivalent to the loss rates for corrosion product dissolved in precipitation runoff. A three-term runoff flux model, involving the precipitation volume, the hydrogen ion wet deposition, and sulfur dioxide dry-deposition fluxes, describes the runoff flux from field corrosion measurements on zinc, galvanized steel, and copper at five sites in the eastern United States with R^2 values greater than 0.95. Systematic deviations in the runoff results indicate the model would be improved by adding a term for the dry deposition of particulates that neutralizes a fraction of the acid deposition subsequently deposited and, hence, reduces the runoff flux.

The parameters in the three-term model obtained by a least squares fit of field corrosion data agreed well with values obtained by direct measurement of dry deposition and runoff fluxes. Because of this, the parameters are not only statistically significant but also physically significant. The stoichiometric coefficient for the neutralization of corrosion product by hydrogen ions was 2 for both zinc and copper. The average dry deposition velocity for sulfur dioxide to zinc was 0.44 cm/s and for copper was 0.16 cm/s. The higher value for zinc indicates the zinc corrosion product has a higher affinity for sulfur dioxide than the copper corrosion product. The value for galvanized steel was less than for zinc as a result of the chromate treatment given the steel. The product of residence time and solubility for the zinc corrosion product in precipitation was 46.5 μmol Zn/L; for the copper corrosion product it was 18.9 μmol Cu/L. The zinc value was more than an order of magnitude below the solubility values for likely zinc corrosion products and yields a residence time factor of about 0.1. The lower solubilities computed for the field corrosion experiment compared to the runoff experiment suggests that the solubility term in the three-term model should include a temperature dependence. Curves of pH versus solubility indicate that zinc carbonate formation is favored in the outer portion of the corrosion product and zinc hydroxide near the metal/film interface.

Damage to zinc, galvanized steel, and copper from wet and dry acidic deposition is estimated to be 50% or more of the total damage at each of the five sites. Damage from acid deposition was more than 80% of the total at the Ohio site. For copper, damage from the wet deposition of hydrogen ions was greater than that from the dry deposition of sulfur dioxide at four of the five sites.

Acknowledgment

This research was funded by the Bureau of Mines and the National Acid Precipitation Assessment Program through a cost-sharing interagency agreement between the Bureau and the Environmental Protection Agency.

References

[*1*] Dunbar, S. R. and Showak, W., *Atmospheric Corrosion,* W. H. Ailor, Ed., Wiley-Interscience, New York, 1982, pp. 524–552.

[*2*] Guttman, H. and Sereda, P. J., *Metal Corrosion in the Atmosphere, ASTM STP 435,* American Society for Testing and Materials, Philadelphia, 1968, pp. 326–359.

[*3*] Walton, J. R., Johnson, J. B., and Wood, G. C., *British Corrosion Journal,* Vol. 17, No. 2, 1982, pp. 65–70.

[*4*] Hudson, J. C. and Stanners, J. F., *Journal of Applied Chemistry,* Vol. 3, February 1953, pp. 86–96.

[*5*] Kucera, V., *Metals Degradation Caused by Acid Rain,* R. Baboian, Ed., American Chemical Society, Washington, DC, 1986, pp. 104–118.

[6] Edney, E. O., Stiles, D. C., Spence, J. W., Haynie, F. H., and Wilson, W. E., *Metals Degradation Caused by Acid Rain,* R. Baboian, Ed., American Chemical Society, Washington, DC, 1986, pp. 172–193.
[7] Mattsson, E., *Materials Performance,* Vol. 21, No. 7, 1982, pp. 9–19.
[8] Spence, J. W., Haynie, F. H., Stiles, D. C., and Edney, E. O., *Degradation of Metals in the Atmosphere, ASTM STP 965,* S. W. Dean and T. S. Lee, Eds., American Society for Testing and Materials, Philadelphia, 1988, pp. 339–353.
[9] Cramer, S., Carter, J. P., Linstrom, P. J., and Flinn, D. R., *Degradation of Metals in the Atmosphere, ASTM STP 965,* S. W. Dean and T. S. Lee, Eds., American Society for Testing and Materials, Philadelphia, 1988, pp. 229–247.
[10] Barton, K., *Protection Against Atmospheric Corrosion,* Wiley, New York, 1973, pp. 15–73.
[11] Graedel, T. E., *Journal of the Electrochemical Society,* Vol. 136, No. 4, 1989, pp. 193C–203C.
[12] Lipfert, F. W., Benarie, M., and Daum, M. L., *Corrosion Effects of Acid Deposition,* Electrochemical Society, Pennington, NJ, Proceedings, Vol. 86-6, 1986, pp. 108–154.
[13] Haynie, F. H., Spence, J. W., Lipfert, F. W., Cramer, S. D., and McDonald, L. G., this volume.
[14] Haynie, F. H., *Durability of Building Materials, ASTM STP 691,* American Society for Testing and Materials, Philadelphia, 1980, pp. 157–175.
[15] Lipfert, F. W., *Materials Performance,* Vol. 26, No. 7, 1987, pp. 12–19.
[16] Haagenrud, S. E., Henriksen, J. F., and Gram, F., *Corrosion Effects of Acid Deposition,* Electrochemical Society, Pennington, NJ, Proceedings, Vol. 86-6, 1986, pp. 78–97.
[17] Guttman, J., *Metal Corrosion in the Atmosphere, ASTM STP 435,* American Society for Testing and Materials, Philadelphia, 1968, pp. 223–239.
[18] Flinn, D. R., Cramer, S. D., Carter, J. P., Hurwitz, D. M., and Linstrom, P. J., *Materials Degradation Caused by Acid Rain,* R. Baboian, Ed., American Chemical Society, Washington, DC, 1986, pp. 119–151.
[19] Haynie, F. H., *Degradation of Metals in the Atmosphere, ASTM STP 965,* S. W. Dean and T. S. Lee, editors, American Society for Testing and Materials, Philadelphia, 1980, pp. 282–289.
[20] "Analysis of EPA Regional Acid Deposition Samples," Quality Assurance Plan, EPA Contract No. 68-02-3496, RTI No. 4311-2186, Research Triangle Institute, Research Triangle Park, NC, October 1982.
[21] Flinn, D. R., Cramer, S. D., Carter, J. P., and Spence, J. W., *Durability of Building Materials,* Vol. 3, 1985, pp. 147–175.
[22] Sehmel, G. A., "Dry Deposition Velocities," PNL-SA-12156, Pacific Northwest Laboratory, Richland, WA, March 1984.
[23] Strekalov, P. V., Agafonov, V. V., and Mikhailovski, Y. N., *Protection of Metals,* Vol. 8, 1972, p. 521.
[24] Graedel, T. E., Mandich, M. L., and Weschler, C. J., *Journal of Geophysical Research,* Vol. 91, 1986, p. 5205.
[25] McElhoe, B., Kellog, R., Karasek, N., and Barlow, M., "Particulate Matter Measurements at Materials Exposure Sites for September 1986 to October 1987," available from J. Spence, Atmospheric Research and Exposure Assessment Laboratory, US Environmental Protection Agency, Research Triangle Park, NC, 1988.
[26] Pourbaix, M., *Atlas of Electrochemical Equilibria in Aqueous Solutions,* National Association of Corrosion Engineers, Houston, 1974, pp. 406–413.

Jean Jacques Hechler,[1] Jean Boulanger,[1] Denis Noël,[1]
Robert Dufresne,[2] and Christian Pinon[2]

A Study of Large Sets of ASTM G 84 Time-of-Wetness Sensors

REFERENCE: Hechler, J. J., Boulanger, J., Noël, D., Dufresne, R., and Pinon, C., "**A Study of Large Sets of ASTM G 84 Time-of-Wetness Sensors,**" *Corrosion Testing and Evaluation: Silver Anniversary Volume, ASTM STP 1000,* R. Baboian and S. W. Dean, Eds., American Society for Testing and Materials, Philadelphia, 1990, pp. 260–278.

ABSTRACT: Three sets of 32 to 39 ASTM time-of-wetness G 84–84 sensors were exposed during summer and winter in Montreal. For the summer periods, all sensors responded well to rain but had a very different sensitivity to dew, with some sensors never responding to dew. For the winter period all sensors responded well to condensation below the freezing point. The ASTM sensor selection criteria are sound for atmospheres having a small dew time-of-wetness compared to the rain time-of-wetness. For atmospheres having a large dew time-of-wetness, the sensors should be tested in order to discard those which are not very sensitive to the dew. A sensitivity factor for each sensor within a given set can be determined experimentally in order to increase the precision of the time-of-wetness values.

KEY WORDS: time-of-wetness, TOW, moisture sensor, corrosion, metals, atmosphere, humidity, measurement, calibration

One of the most important parameters responsible for the degradation of materials exposed to the atmosphere is moisture, which can be present as rain, dew, snow, hoarfrost, etc. In order to quantify the influence of this parameter, various techniques have been developed to measure what is now called "time-of-wetness" (TOW), that is, the time during which the surface of a material is wet. It is well known that metallic materials corrode essentially when wet and that their corrosion obeys electrochemical laws. It was therefore obvious to look to electrochemical sensors to determine the TOW [*1–6*]. One is the sensor developed by P. J. Sereda upon which the ASTM Standard Practice for Measurement of Time-of-Wetness on Surfaces Exposed to Wetting Conditions as in Atmospheric Corrosion Testing (G 84–84) is based. This sensor has proven to be very useful in the past [*7–9*] even though it has been more or less ignored in recent extensive atmospheric corrosion studies in the western world. This is in contrast with studies performed in the communist countries members of COMECON (Council of Mutual Economic Aid), where similar sensors are used on a regular basis [*6*], and with the recent extensive efforts to establish atmospheric damage functions for materials where the notion of TOW is always present [*10,11*].

Basically, this sensor consists of a system of two different electrodes insulated electrically, which develop a galvanic potential when moisture covers both electrodes. Different sizes,

---

[1] Institut de Génie des Matériaux, Conseil National de Recherches du Canada 75, Boulevard de Mortagne, Boucherville, Quebec, Canada J4B 6Y4.

[2] Départment de Génie Electrique, Ecole Polytechnique, Université de Montréal, Case Postale 6079, Succ. A, Montreal, Quebec, Canada H3C 3A4.

configurations, and electrodes were studied during the course of its development [*2–4*]. Currently, a second generation of these sensors is available commercially [*12*]. This sensor (Fig. 1) has a gold and a copper electrode on an insulated plastic base. It is very small (1.8 by 1.1 by 0.1 cm) in order to follow closely the thermal history of the material on which it is located. The TOW is defined as the time for which the voltage is higher than a predetermined threshold which, according to ASTM G 84–84, can be 10 or 20 mV. Except for a study of three of these sensors exposed simultaneously at the same location as mentioned in ASTM G 84–84, no study of a large number of these sensors has yet been undertaken. Such a study appeared necessary to the authors, who obtained very different values of TOW with two sensors exposed for the same period at the same location [*13*]. The objectives of the project were: (1) to better understand the functioning of the sensor; (2) to quantify the possible errors when using one isolated sensor; (3) to reveal eventual differences of quality during production; (4) to define the procedures necessary to select a set of sensors capable of being used to adequately show differences in TOW at different locations during the same period; and (5) to understand better the meaning of the measured TOW.

Experimental

Sensors Selection

The sensors used all came from a set of 150 made during production runs E 8603 and E 8537. When tested as received and in a dry state they all had an impedance greater than 100 MΩ. They were then all tested according to the ASTM procedures as follows. After immersion in a salt solution (10 mg/L sodium chloride, 1% ethanol) for 1 h, their voltage, V_1, was measured; it varied from 30 to 160 mV. After one week at ambient temperature and at 100% relative humidity, 124 sensors produced voltages, V_2, between 10 and 105 mV. The remaining 26 showed voltages between −20 and 10 mV. The 110 sensors used for the

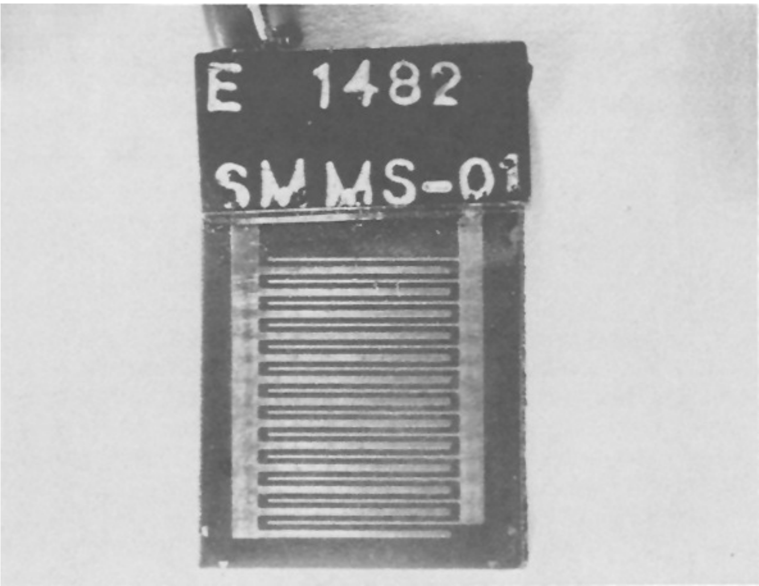

FIG. 1—*The ASTM G 84 sensor. The electrode on the right is the gold electrode.*

study were chosen at random from among the set of 124. Examples of values of V_1 and V_2 are given in Table 1 for the first set of sensors used. They represent well the kind of values which can be obtained after the selection.

Exposure of the Sensors and Site of the Study

Two sets of 39 sensors were studied at temperatures above the freezing point during two periods in summer: Period 1 (41 days), when humidity was mostly due to rain, and Period 2 (16 days), which had little rain but much dew. A third set of 32 sensors was studied at subzero temperatures in winter: Period 3 (42 days). These periods, considerably shorter than the 17 months of ASTM G 84-84, were partly imposed by the date the authors wanted to study the microclimates around a building using these sensors [*14*]. These three periods have nevertheless demonstrated the basic behavior of these sensors at all useful temperatures.

Each individual sensor was glued with epoxy resin on a 4 by 4 by 1/16-in. aluminum plate. This plate was screwed on the plastic waterproof box which contains the measuring circuit. For each period, 39 (32 for Period 3) such assemblies were placed on an ASTM G 50-type rack on the roof of the Ecole Polytechnique of the Université de Montréal along with four similar assemblies having a temperature sensor to measure the temperature of the aluminum plate (Fig. 2). The sensors were exposed to the south 30° above the horizontal facing the sky.

The Ecole Polytechnique building is located on the western slope of Mount Royal and overlooks the neighboring residential areas of Montreal some 100 m below. The pollution from the immediate surroundings is due mainly to the automobile exhaust gases coming from nearby parking lots and to occasional fumes coming from the chemistry laboratory

TABLE 1—*Characteristics of selected sensors used during Period 1. The TOW is the measured value for the 20-mV threshold obtained by continuously scanning the sensors.*

Sensor Number	Measured TOW, h	Voltage After Immersion in Salt Solution (V_1), mV	Voltage After 1 Week at 100% RH (V_2), mV	Maximum Voltage During Period 1 (V_{max}), mV	Sensor Type
33	191.2	114	35	158	2
31	183.8	79	28	138	2
34	177.8	77	38	152	2
43	175.4	70	11	147	1
32	169.1	110	46	173	1
8	163.7	112	50	158	2
44	163.0	92	82	176	2
18	160.2	114	29	159	1
12	159.1	103	20	131	2
37	158.8	61	23	133	2
36	157.2	111	35	172	1
27	156.5	70	48	135	2
23	151.2	68	26	159	3
16	145.9	92	22	119	3
46	143.0	100	60	137	3
6	136.9	83	10	155	3
11	123.2	122	20	134	3

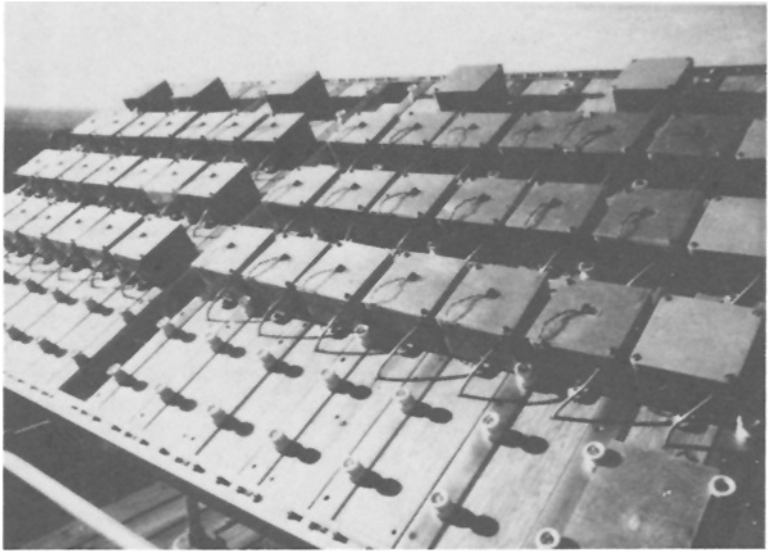

FIG. 2—*The 39 sensors exposed on an ASTM G 50 standard rack.*

and the cafeteria. With each sensor having the same environment, it was assumed that their respective location on the rack had no influence on their response.

Data Acquisition System

A special measuring system designed to measure the TOW over large buildings using a minimum of wires was used. Basically, the system consists of a central microcomputer (Apple II+) which, through optocouplers, controls an interface circuit which in turn drives a communication line consisting of a pair of single wires. This line is used to power the measuring circuits on which the sensors are connected and also to carry the measured voltages back to the computer. Each measuring circuit consists of a digital address decoder which, on recognizing its own address inscribed on the circuit, activates an analog measuring circuit. A voltage-to-frequency converter then is used to send an a-c signal through the line to be detected and interpreted by the computer. Other details of this system are given in Refs *15* and *16*. The calibration of the whole system showed an error of around 1 mV at the 20 mV level (5%) for temperatures between −40 and +60°C. Although it has been remarked previously that sometimes the voltage becomes negative (the copper electrode being the cathode), this phenomenon could not be analyzed here since the measuring system used could not measure negative potentials, which were thus replaced by zero. The sensors were scanned continuously, each individual voltage being measured about every minute in order to get the total TOW, which was determined for a threshold of 20 mV. Every 30 min, the voltages, the temperatures, and the total TOWs were printed and stored on floppy disks. Measurements of relative humidity were added for Period 3. Around 200 000 measurements were made on the sensors during the 99 days of testing reported here. This huge amount of data was transferred to a VAX 3500 (Digital Equipment Co.) and analyzed by a specially developed software.

Results

Qualitative Study of the Voltage Changes with Time during the Summer Periods

Figure 3 shows the typical curves which can be obtained during a summer day: one period of night and morning dew (4:00 to 8:00 h) and two periods of rain (16:00 to 21:00 h and 22:00 to 24:00 h). These curves have been fully described in earlier papers [2–4]. The dew period appears at the same time as a decrease in temperature, which causes a slow increase of the voltage of the sensors. These voltages decrease slowly again as the sensors start to dry when the temperature increases with the appearance of the sun. The beginning of the rainfall causes a rapid fall in temperature, which is associated with a sudden rise of the voltages. At the end of the rainfall, the temperature rises slowly, causing a slow drying of the sensors and a slow decrease in their voltages. Thus, by recording the temperatures and the voltage of the sensors, it is easy to see how many rain periods and dew periods occurred just by looking at the shape of the voltage curves. Period 1 thus had 18 periods of dew and 38 rainfalls. Period 2 had 13 periods of dew and only two rainfalls. Common voltage values were about 60 to 150 mV for rain periods and 5 to 40 mV for dew periods.

At the beginning of a rainfall after several dry days, the curves displayed a particular shape. The voltages increased rapidly, then decreased after about half an hour before staying relatively constant for the remainder of the rain. This behavior has already been mentioned by Sereda [2] and is similar to the observation made by Kucera and Mattson [5]. They attributed it to the absorption of gaseous pollutants during the dry periods, which are responsible for a large corrosion current when in contact with water. This clearly shows that

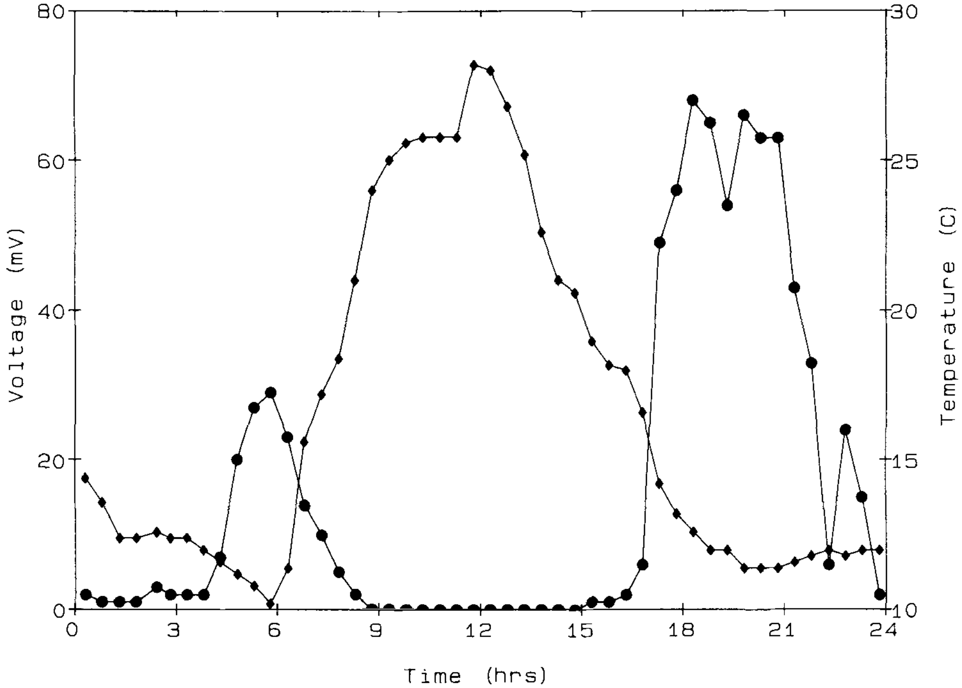

FIG. 3—*Voltage (—●—) of Sensor #15 and temperature (—◆—) changes during periods of dew and rain.*

within a given period of wetness the corrosion intensity can be very different and that dry deposition between two wetness periods is partly responsible for it.

A careful study of the complete set of curves shows that, in a general manner, the sensors:

1. See the beginning of a period of rain at the same time.
2. Take different times to dry completely after a period of wetness, except when the temperature is high.
3. Do not all see the dew.
4. Give very different potentials for the same humidity but show identical variations.

As a result, the TOW determined from these voltages will be different, and these differences have as their origin:

1. A different sensitivity for each sensor (dew periods more or less detected, voltages more or less high, etc.).
2. Climatic conditions (temperature, size of the last drops of rain leading to different times of drying, etc.).

It nevertheless appears at this point of the study that the dispersion of the time of wetness values mainly is caused by the dew periods more than the rain periods.

Quantitative Study of the Results for the Summer Periods.

As mentioned, two sets of data were recorded. The first set was the measured TOW for the 20-mV threshold. With each voltage being measured about every minute, the error of the measured total TOW was therefore small (minutes compared to hours). The second set was the voltage values printed and recorded every 30 min. These values will be used to compute the TOW corresponding to thresholds different from 20 mV. Having only one value every 30 min, the maximum error of the TOW was 30 min each time the voltage crosses the chosen threshold. This may cause a nonnegligible error. In computing these TOWs, the experimental curve, consisting of straight lines between two consecutive recorded points, has been used instead of the complete real curves, which are unknown. In order to estimate the error made in using this experimental curve, the measured and computed values corresponding to the 20-mV threshold were determined for all sensors for Period 1. The minimum and maximum errors were 1.7 and 8.3%, respectively, with a mean value of 5.3%. This error remained small. Therefore, in the following, the experimental curves were considered as a good representation of the unknown real curves.

Response curves—ASTM G 84-84 suggests 10 or 20 mV as thresholds for the definition of the TOW. Except that these two values lead to very similar values of the TOW, no study has yet been made to justify the use of these particular values. By drawing a response curve of these sensors (TOW versus threshold) some information might come out. Using the experimental curve and computing the TOW for the threshold values from 5 to 100 mV for Period 1, three types of curves are obtained (Fig. 4). Type 1 can be characterized by a curve having a more or less apparent flat portion around 30 mV. The longer this flat portion is, the more independent of the threshold is the value of the TOW. This type of curve, having a flat portion where the TOW is less dependent on the threshold values, might allow a better definition of the TOW; a fixed and empirical value for a threshold in this case is not necessary, and eventually this flat portion may be related to some specific corrosion conditions on the surface of the sensors leading to a more physical definition of the TOW. Table 1 gives the measured TOW for the 20-mV threshold for some sensors of Type 1 as well as for the other

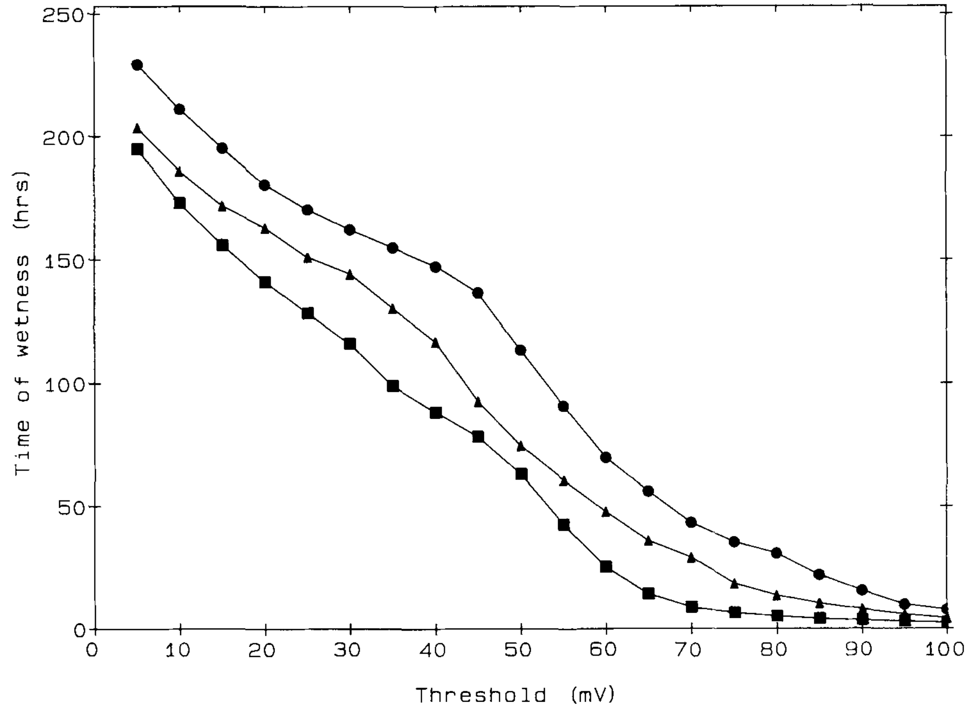

FIG. 4—*Typical response curves for the three types of sensors used during Period 1. Type 1: Sensor 43 (—●—); Type 2: Sensor 27 (—▲—); Type 3: Sensor 6 (—■—).*

types. The Type 2 sensor has a curve which has no flat portion but nevertheless presents more or less an inflection point. This type of sensor can give TOW values higher than those of Type 1 with a larger dispersion. Type 3 sensor has a curve which decreases continuously without even an inflection point. It is very difficult to try to define a TOW using this type of curve since there is really no distinct point on it. Type 3 curves can differ greatly from one sensor to another. This type of sensor gives TOW values considerably lower than the two other types.

The Type 1 and Type 2 curves have, generally speaking, a slight hump around 80 mV. This characteristic feature is related to the phenomenon described earlier where the voltages of the sensors have higher values at the beginning of a rainfall after a dry period. Such a feature was completely absent for the Type 3 sensor. This denotes a certain inactivity of this type of sensor.

Qualitatively, it has been shown that the response of the sensor to dew can be quite different, and therefore the response curves for rain and dew have also been drawn. These curves were obtained by carefully analyzing the whole Period 1 in order to delimit in time the periods corresponding to each type of humidity. All rain and dew periods then were regrouped and analyzed separately. Figures 5 and 6 give these curves for the same sensors as in Fig. 4. The rain response curves have almost all the same shape where the flat portion is again apparent. The rain TOW values are relatively close for thresholds up to around 20 mV. The dew response curves are quite different even at the 10 to 20-mV level. It is also important to note that the dew TOW values for the 5-mV threshold are almost double those

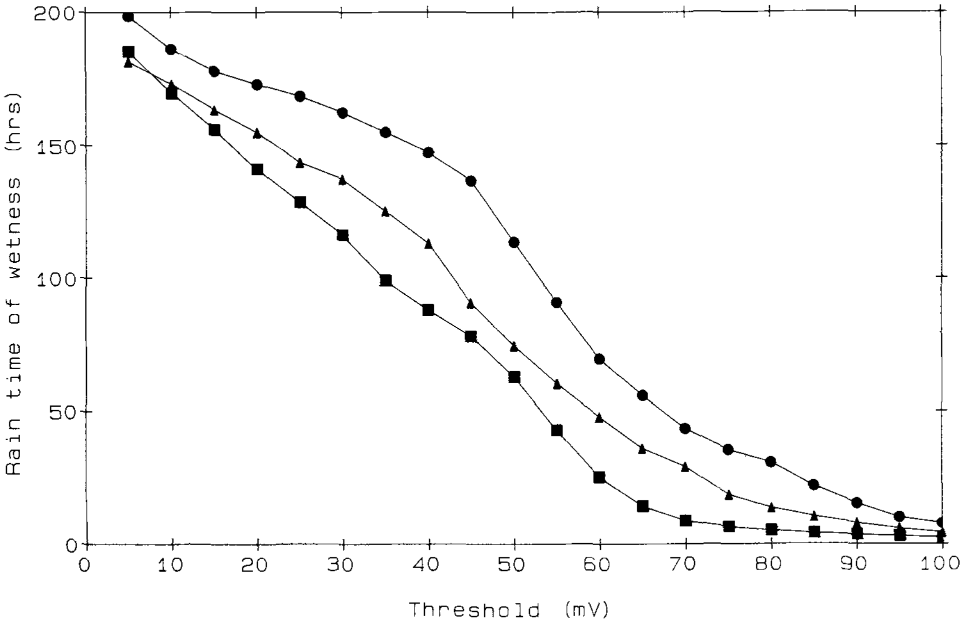

FIG. 5—*Rain response curves for the three sensors of Fig. 4.*

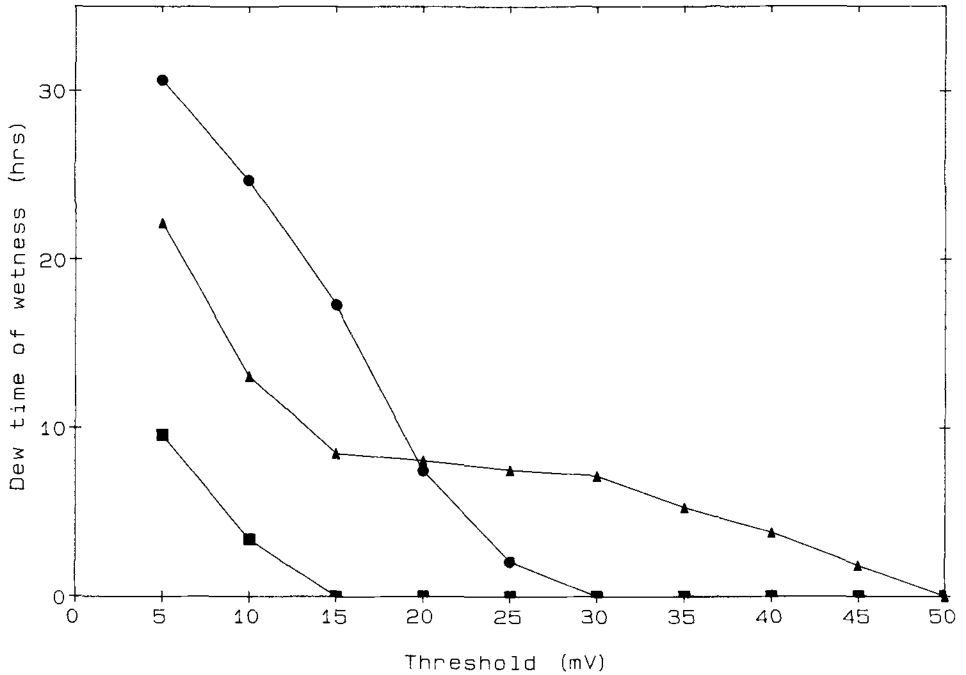

FIG. 6—*Dew response curves for the three sensors of Fig. 4.*

for the 10-mV threshold. The ASTM G 84–84 thresholds therefore appear somewhat high to give a good total length of the dew periods.

From all these curves, it is obvious that no special threshold stands out. The 10 or 20-mV values have no special significance. The only justification that can be given here is that they are around a certain inflection point on the response curves, showing that the TOW change with the threshold value is minimal.

Statistical studies—This analysis was performed in order to get information on the TOW standard deviation. Tables 2 and 3 show the results of the analysis performed on the total, rain and dew TOW for Periods 1 and 2 and the separate contribution of the two types of humidity. For Period 1 in Table 2 it can be seen that, for a threshold of 10 mV corresponding here to the smallest TOW standard deviation, the rain TOW is 185.3 h and the dew TOW 10.3 h, which represents 5% of the total TOW. The standard deviation of the values for the dew periods (56%) is much larger than the standard deviation for the rain periods (7.1%), a difference of almost one order of magnitude. The dew TOW is small compared to the rain TOW, and the standard deviation due to the dew does not have any effect on the standard deviation of the total TOW (7.3%). This will not be the case for periods where the dew is significant compared to the rain, as it is the case for Period 2 where the dew TOW for the 10-mV threshold is 26% of the total TOW. Although the rain TOWs are very different for Periods 1 and 2, their standard deviations are almost identical (7 and 9%) for the 10-mV threshold. This shows that all 78 sensors studied have a similar response when exposed to the rain. Since they all see the beginning of the rain at the same moment, the standard deviation of the TOW comes in part from the difference in time they take to dry. These values are slightly higher than the 4% value as given in ASTM G 84–84.

The standard deviation of the dew TOW is again very high for Period 2 and much higher than for Period 1, but seems to decrease substantially with the lengths of the dew periods. This result confirms that the standard deviation of the TOW here is mainly due to the dew. The influence of the dew is predominant for the thresholds from 5 to 25 mV. In Table 3 it can be seen that the standard deviation (Column 4) decreases from 5 to 25 mV, then increases after 30 mV. The minimum standard deviation corresponds here not to 10 mV, as for Period 1, but to 30 mV. Again the result is that no special threshold value stands out since the best threshold depends on the type of humidity, the length of these humid periods, and so on.

Evolution of the TOW with time—It has been seen that some of the sensors are less sensitive to humidity. If a homogeneous set of sensors is needed (for instance to measure small TOW changes from one location to another), these sensors have to be tested before use. The evolution of the TOW and its standard deviation with time can show how long they should be tested and if, in some way, a sensitivity factor can, again experimentally, be established. This has been done for Period 1.

Figure 7 represents the evolution of the calculated TOW (10-mV threshold) for the sensors having the highest and the lowest final TOW. The horizontal portions represent dry periods, and the remaining portions represent wet periods. The TOW change with time was studied using specific times on the horizontal portions when all sensors were dry. The mean TOW standard deviation for the 10-mV threshold stayed fairly constant (7.3 to 8.9%) with time and therefore close to the value obtained at the end of Period 1. It thus seems possible to test the sensors over a short period of time since the results are the same for longer periods.

Curves like those in Fig. 7 for sensors having high and close final TOW are almost identical. On the contrary, the curves for sensors having low and close final TOW diverge to some extent, especially during the periods of dew. In Fig. 7, it can be seen that the distance between the two curves increases continuously with time. This could mean that the sensors have a simple behavior compared to the mean TOW value. Table 4 gives the evolution with time of the TOW of individual sensors divided by the mean value of the TOW for typical

TABLE 2—*Contribution of rain and dew to the total TOW for Period 1.*

	Total Period			Rain Periods			Dew Periods		
Threshold, mV	Mean TOW, h	Standard Deviation, h	Standard Deviation, %	Mean TOW, h	Standard Deviation, h	Standard Deviation, %	Mean TOW, h	Standard Deviation, h	Standard Deviation, %
5	218.3	17.2	7.9	199.1	12.4	6.2	17.9	7.3	41
10	196.0	14.3	7.3	185.3	13.1	7.1	10.3	5.8	56
15	180.2	15.2	8.4	174.1	15.5	8.9	5.9	4.6	78
20	166.0	18.3	11.0	162.8	18.6	11.4	3.2	3.5	110
25	152.0	23.6	15.0	150.2	23.7	15.8	1.9	2.6	140
30	136.6	28.3	20.7	135.3	28.2	20.8	1.3	2.1	160
35	118.9	37.6	27.4	117.9	32.5	27.6	1.0	1.7	170
40	100.5	35.6	35.6	100.0	35.6	35.6	0.5	1.2	240

TABLE 3—*Contribution of rain and dew to the total TOW for Period 2.*

	Total Period			Rain Periods			Dew Periods		
Threshold, mV	Mean TOW, h	Standard Deviation, h	Standard Deviation, %	Mean TOW, h	Standard Deviation, h	Standard Deviation, %	Mean TOW, h	Standard Deviation h	Standard Deviation, %
5	33.9	19.9	60	19.1	1.5	8	14.3	19.2	134
10	24.1	13.4	56	17.9	1.6	9	6.2	12.5	200
15	19.8	8.5	43	16.8	1.9	11	3.0	7.6	250
20	17.2	5.3	31	15.9	2.1	13	1.3	4.2	320
25	15.6	4.5	29	14.8	2.5	17	0.8	3.0	380
30	14.1	4.0	28	13.6	3.0	22	0.5	1.9	380
35	12.5	4.4	35	12.2	3.7	30	0.3	1.6	640
40	10.7	4.5	44	10.5	4.0	38	0.2	1.5	730
45	9.0	4.7	52	8.8	4.2	48	0.2	1.4	700
50	7.1	4.3	61	7.0	4.2	60	0.1	0.9	900

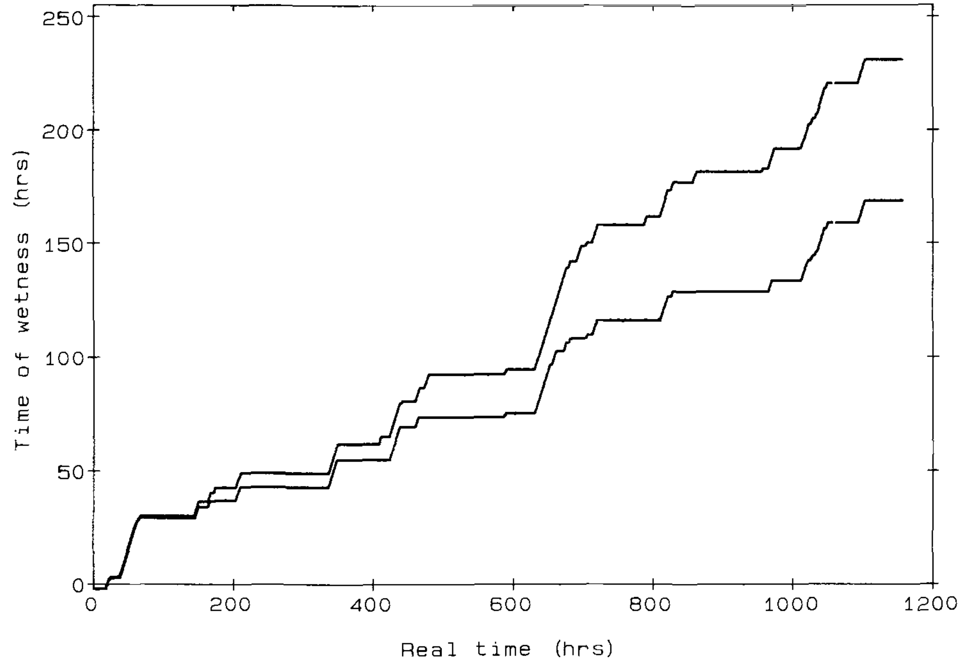

FIG. 7—*TOW evolution with time for the sensors having the highest and the lowest TOW during Period 1.*

sensors for the 10-mV threshold. It appears that, in a general manner, this ratio varies slightly in this experiment during the first 500 h and then for the majority of the sensors it changes less than 2% during the remaining testing time. For a threshold of 20 mV there are 16 sensors out of 39 presenting a variation higher than 2% but only 9 for a threshold of 10 mV. Here again 10 mV seems better. Sensors of Type 3 show larger variations than Types 1 and 2 and at the same time give lower values of this ratio.

Finally, it seems that, for sufficiently long times, the TOW given by any sensor is related to the mean TOW, which could be taken as the real TOW, by a factor which can be determined experimentally as done here and which can be quite different from unity. This factor represents the physical differences between the sensors arising from manufacture, conditioning, etc. It is different from the sensitivity factor related directly to humidity parameters (such as relative humidity) as discussed in Refs *3* and *4*, which is difficult to assess. This experimental factor should increase considerably the precision of the TOW measurements.

Qualitative Study of the Voltage Change with Time for the Winter Period

Period 3 had around 40 wetness periods, all corresponding to condensed humidity except for three periods of wet snow or freezing rain. Common voltage values were between 40 and 200 mV for this period.

Figure 8 shows typical curves obtained at subzero temperatures. As already mentioned [*4*], a voltage develops down to −30°C, proof of some electrochemical reactions and therefore of corrosion. This happens in an almost general way when the relative humidity is higher than 40 to 45% at all subzero temperatures, including periods of nonwet snow. The voltage curve follows very closely the variations of the relative humidity with values always different from zero when the relative humidity is higher than 40 to 45%. Some of these voltages are surprisingly high, up to 500 mV, and are usually associated with a rapid rise in temperature, causing melting of the snow lying or falling on the sensors, and with freezing rain. These high voltages might indicate some important corrosion reactions caused by species contained in the snow or in the freezing rain. This is in accordance with results showing that, on the same building, the corrosion rates of clean copper surfaces are around twice as high in winter as in autumn [*14*].

When the response of all sensors for the whole period is carefully analyzed, it appears that they respond better to condensation at subfreezing temperatures than at temperatures higher than 0°C. If in summer some sensors never responded to dew, during the winter, with only a few exceptions, all humidity periods were seen by all sensors.

TABLE 4—*Evolution with time of the ratio TOW/mean TOW for selected sensors used in Period 1. The TOW values are those calculated for the 10-mV threshold.*

Sensor	Time, h	$\frac{\text{TOW}}{\text{mean TOW}}$
Sensor giving highest TOW:		
33	107	1.023
	248	1.089
	534	1.173
	742	1.210
	911	1.201
	1156	1.189
Sensor giving lowest TOW:		
46	107	0.992
	248	0.963
	534	0.938
	742	0.895
	911	0.870
	1156	0.873
Sensor giving a TOW close to the mean TOW		
39	107	0.918
	248	1.025
	534	0.989
	742	1.020
	911	0.999
	1156	1.009
Sensor giving a TOW close to the mean TOW		
13	107	1.092
	248	0.928
	534	0.915
	742	0.990
	911	0.986
	1156	1.001
Sensor giving a TOW higher than mean TOW:		
43	107	0.983
	248	1.184
	534	1.323
	742	1.155
	911	1.105
	1156	1.077

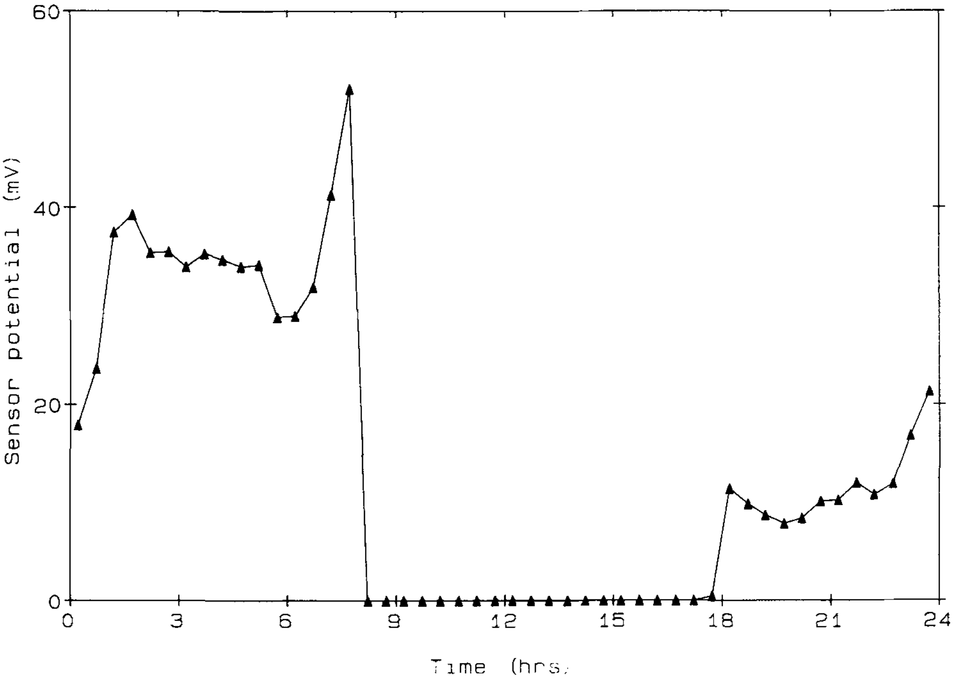

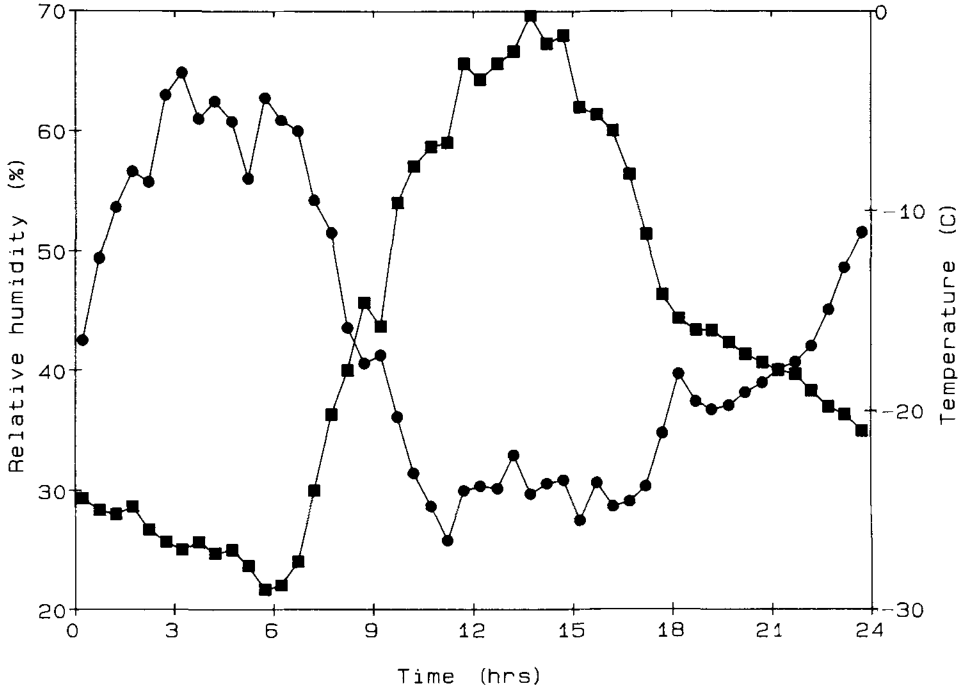

FIG. 8—*Typical voltage* (—▲—), *temperature* (—■—), *and relative humidity* (—●—) *curves during a wetness period at subfreezing temperatures.*

Quantitative Study of the Voltage Change with Time for the Winter Period

Period 3 voluntarily was limited to 42 consecutive days where temperature was always below 0°C, except for three short periods of wet snow or freezing rain, although the testing extended well into spring. Therefore no attempt has been made to study separately the contribution of the different types of humidity as for Period 1.

Response curves—Figure 9 shows typical response curves obtained during the winter. The shape of the curves is similar to the shape of Sensors 3 during the summer periods. Again no special threshold appears, even less so than for the summer periods since no inflection point appears around the 10 to 30-mV thresholds.

Statistical analysis—Figure 10 shows how the mean TOW changes with the threshold values. Its standard deviation increass continuously with the threshold value and is around 11% for the 10 to 20 mV values. This value appears to be better than the 20% value given in ASTM G 84–84. This analysis has been extended to study the influence of temperature. Figure 11 shows the distribution of the TOW at subfreezing temperatures. This distribution shows that, for the whole Period 3, half of the TOW appears at temperatures lower than −6°C. Since corrosion decreases with the TOW, it can be seen that corrosion is likely to be small below −15°C and nonexistant below −20°C, explaining earlier results. The standard deviation of the TOW, around 11% for periods having temperatures lower than −5°C, increases to around 55% for periods with temperatures lower than −20°C.

Evolution of the TOW with time—This evolution is given in Table 5. The standard deviation for subzero temperatures stays around 11% for the whole period. Curves like those given in Fig. 7, giving the TOW evolution with time, show that they follow a similar progression, which suggests a simple relation with the mean TOW. For the three sensors giving the highest, the lowest, and the mean TOW, Table 5 gives also the ratio TOW/mean TOW and its change with time. The values of these ratios, which can be quite different from unity,

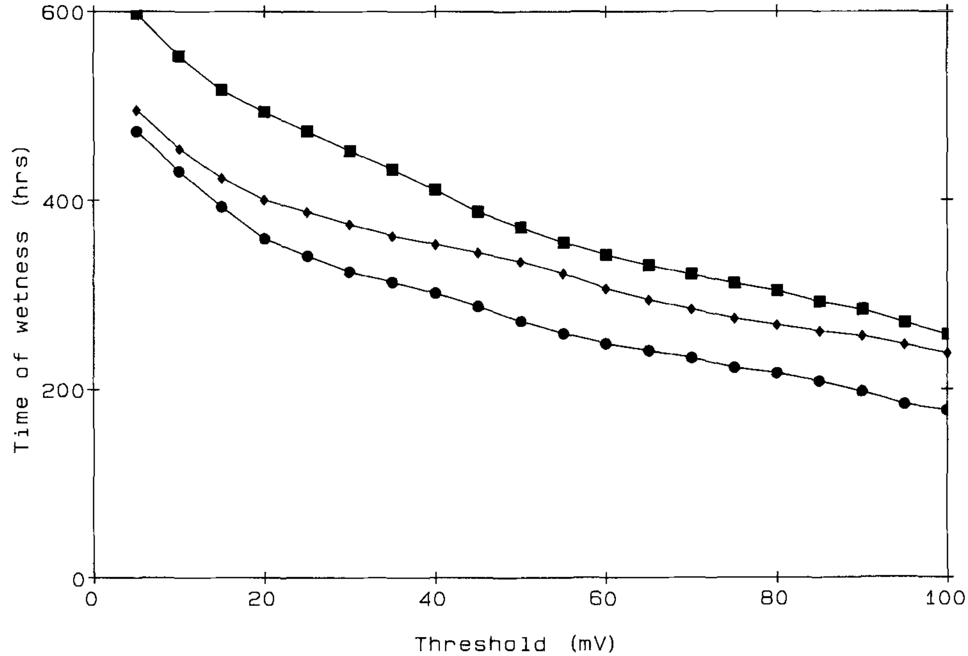

FIG. 9—*Response curves for several sensors at subfreezing temperatures.*

remain fairly constant during the whole period. So again, if small changes of TOW have to be detected simultaneously on different locations, a sensitivity factor can be determined by calibration. For both winter and summer periods it was verified that no relationship existed between these factors and the locations on the rack, especially for the sensors at the edge of the rack.

Comparison Between the Characteristics of the Sensors Before Exposure and their Behavior During the Tests

Before exposing the sensors, they were selected on the basis of their V_1 and V_2 values. During the tests the maximum value, V_{max}, displayed by each sensor was noted. These three values are given in Table 1 for Period 1. It can be seen that there is no obvious relationship between these values. For instance, Sensor 31, which gives one of the highest TOW, has V_1 = 79 mV whereas Sensor 46, which gives one of the lowest TOW, has V_1 = 100 mV. The contrary was expected. The same goes for V_2. If the TOW is represented as a function of V_{max}, there is no clear relation except for a very slight tendency of sensors having a higher V_{max} to give a higher TOW. The voltage values, which are easy to measure in the laboratory, are not able to predict their behavior in service. An observation with an optical microscope showed the good quality of all these sensors. No difference could be detected. The only thing that was noticeable was, that for certain sensors, the glue used at the base of the electrical connections covered one or two fingers of the electrodes. The difference in behavior of the sensors, in the absence of any other obvious physical differences, could be due to a

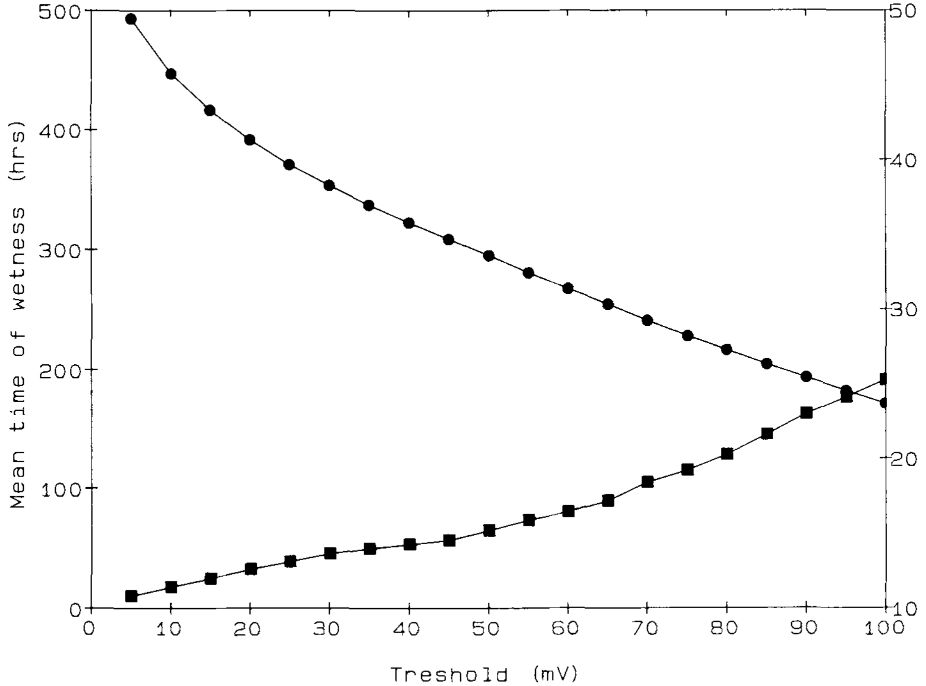

FIG. 10—*Variation of TOW* (—●—) *and its standard deviation* (—■—) *with the threshold value at subfreezing temperatures.*

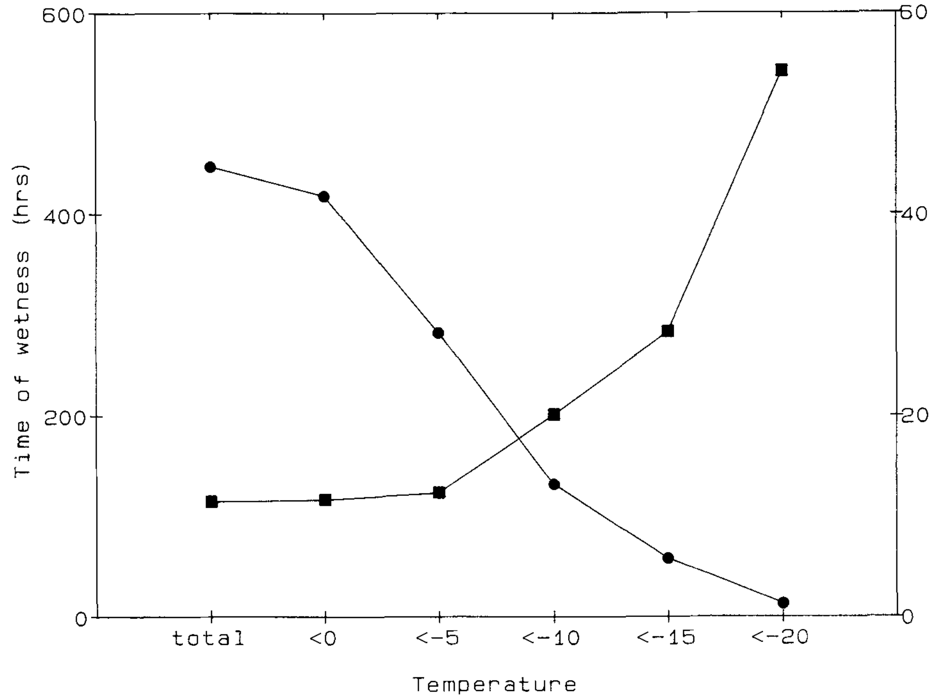

FIG. 11—*Variation of TOW* (—●—) *and its standard deviation* (—■—) *with temperature at subfreezing temperatures.*

certain solubilization of this glue by humidity which, after drying, could stay on the electrode and modify its surface properties, especially its moistening properties.

After Period 1, a study by infrared spectroscopy (FTIR reflectance) was undertaken on several sensors, especially on those not very sensitive to the dew. No trace of organic products were detected on the electrodes. The only difference observed in the spectra is a slightly higher absorption due to OH groups on the copper electrode for the less sensitive sensors. On the same electrode the absorption due to Cu_2O also seems smaller for the less sensitive sensors. This last observation could mean that a certain thickness of the corrosion products is necessary to retain the dew and initiate corrosion reaction on the copper electrode.

TABLE 5—*Evolution with time of the mean TOW and of the ratio TOW/mean TOW for three sensors during Period 3. The TOW values are those calculated for the 10-mV threshold.*

Time, h	Mean TOW, h	TOW Standard Deviation, %	$\frac{\text{TOW}}{\text{mean TOW}}$		
			Sensor 90	Sensor 100	Sensor 117
159	83.4	10.4	1.157	1.061	0.815
353	166.9	9.6	1.150	1.010	0.839
659	293.9	11.6	1.179	0.988	0.846
905	390.7	12.0	1.244	1.016	0.828
1008	449.5	11.4	1.228	1.019	0.828

Enlarged photographs of selected sensors were also taken in order to check accurately the distances between the two electrodes. These distances do not differ very much, having values between 160 and 185 μm. Except for a slight tendency of the total TOW to decrease with the electrode distances within each type, there is no evident apparent correlation between these distances and the TOW when all types of sensors are considered. No correlation appears either with V_{max} for dew nor rain.

Since the TOW has a large dispersion for the few periods, the wettability of the sensing element substrate might therefore be the important factor; depending on its surface-moisturing properties, it requires more or less deposited dew to form a continuous film of humidity to bridge the separation between the electrodes. The first generation of the sensors, having only 50 μm (2 mils) between the electrodes [2], could thus have been more sensitive to dew. Further development of these sensors will have to concentrate on these two parameters: the wettability of the substrate and the distance between the electrodes.

Discussion

Choice of a Threshold Value for the Definition of the TOW

Although a certain number of electrochemical studies have been done in the field of atmospheric corrosion, it has not yet been possible electrochemically to measure convincingly the instantaneous corrosion rate. These determinations are difficult since the electrolyte in this case is a very thin film of dew, rain, or even only the adsorbed humidity on the surface of the metal [*17*]. Trying to correlate the instantaneous corrosion rate of copper with the voltages measured here also appears very difficult since the same corrosion conditions do not lead to a unique voltage value for all sensors. It should nevertheless be mentioned that some relations exist if one considers the special behavior of the sensors at the start of the rain following a dry period and the high voltages which can be associated with the high corrosion in winter. It is therefore impossible to define theoretically a certain threshold which would correspond, for example, to a known negligible corrosion rate, the corresponding TOW giving the time during which corrosion happens.

It has been seen that it is possible to determine a range of voltage for the sensors of Type 1 (10 to 30 mV) where the TOW varies slowly with the threshold. According to the study of the influence of the dew, the flat portion of the response curves associated with this domain can only be explained by a poor sensitivity to dew. Dew generally caused voltages on these sensors that do not exceed 10 to 15 mV. Rain caused voltages in excess of 40 mV. There is thus a range from 15 to 40-mV voltage values very seldom shown by this type of sensor. This threshold, which appears experimentally, thus has no theoretical foundation.

From Tables 2 and 3, the importance of the different thresholds can be discussed. According to ASTM G 84–84, the ratio TOW(20 mV)/TOW(10 mV) is 0.875. This is exactly the value found here for Period 3 and for the rain TOW of Periods 1 and 2 (not the total TOW). When the total TOW is considered, the values for Periods 1 and 2 are 0.847 and 0.714, respectively, indicating a larger difference between the two TOWs than given in the norm. If only the dew TOW is considered, then the values are 0.311 and 0.210, respectively, meaning that the change of threshold from 20 to 10 mV multiplies the dew TOW by a factor of about 3 and 5, respectively. And if the threshold is changed from 20 to 5 mV, then the dew TOW changes by a factor of about 6 and 11, respectively. This raises the importance of knowing the corrosion rates and their respective values for different humidities. If the corrosion rates during the dew periods are small compared to the corrosion rates during the rain period, then the dew TOW is unimportant and a high threshold can be taken. If this is not the case, then a low threshold must be taken.

Since no such information is available at this time, it follows from this study that the only criteria for selecting a threshold value could be those of precision, that is, the value giving the best standard deviation. The statistical treatment shows that the best TOW threshold can vary depending on the respective importance of the periods of rain and dew. Therefore this best value might change with time at a given location and will be different at the same time at different locations. Considering that this best TOW threshold was always around the 10 to 20 mV specified by ASTM G 84–84 and that the standard deviation changes little around these values, these values therefore appear to be acceptable until further information is gained on the atmospheric corrosion rates.

Selection Criteria for the Sensors

According to the present study, two cases have to be considered. If the sites to be studied have little or no dew, the criteria mentioned in ASTM G 84–84 are sufficient. A TOW standard deviation of around 7% can be used as an error estimate even if the TOW contains up to around 5% of dew TOW. If the sites to be studied have a nonnegligible dew, the ASTM criteria in this case are strongly insufficient since, as it has been shown, these criteria can apply to a sensor completely insensitive to the dew. The reason for this behavior could not be explained here even with a surface study. Recent, more careful preparation of other sensors, such as washing with good organic solvents, seems to enhance the sensitivity of the sensor to light humidity. The only way to select a set of similar sensors is to test a larger number of sensors than needed before using them in an experiment. The testing period must have a good quantity of rain and dew in order to compare their behavior for both types of humidity. The testing period will then provide the TOW standard deviation. In both cases, the precision of the TOW determination can be increased by determining the sensitivity factor for each sensor.

Conclusion

This study has shown the behavior of a large number of currently commercially TOW sensors exposed simultaneously at the same location. It apears that these sensors give precise values of the rain TOW. Their response to condensed humidity is less good, but reliable values of the TOW can nevertheless be obtained by adding to the ASTM G 84–84 selection criteria a period of testing in a real atmosphere before use. The low cost, the ease of use, and the better knowledge of their functioning as presented here should continue to make them a useful tool in studies of atmospheric degradation.

Acknowledgment

The authors thank Dr. K. Cole for the surface infrared study of the sensors and B. Harvey for technical assistance. Special thanks are due to Dr. P. J. Sereda for his comments during the writing of the manuscript.

References

[*1*] Tomashow, N. D. in *Theory of Corrosion and Protection of Metals*, Chapt. 14, MacMillan, New York, 1966.
[*2*] Sereda, P. J., "Measurement of Surface Moisture, A Progress Report," Bulletin No. 228, American Society for Testing and Materials, February 1958, pp. 53–55.
[*3*] Sereda, P. J., "Measurement of Surface Moisture, Second Progress Report," Bulletin, No. 258, American Society for Testing and Materials, May 1959, pp. 61–63.

[4] Sereda, P. J., Croll, S. G., and Slade, H. F., "Measurements of the Time-of-Wetness by Moisture Sensors and Their Calibration," *Atmospheric Corrosion of Metals, ASTM STP 767,* American Society for Testing and Materials, Philadelphia, 1982, pp. 267–283.

[5] Kucera, V. and Mattson, E., "Electrochemical Technique for the Determination of the Instantaneous Rate of Atmospheric Corrosion," *Corrosion in Natural Environments, ASTM STP 558,* American Society for Testing and Materials, Philadelphia, 1974, pp. 239–260.

[6] Strekalov, P. V., Mikhailovkii, Y. N., Dzincharadze, G. K., Knotkova, D., and Vlachova, Y., "Monitoring the Time of Retention of a Phase Moisture Film on Metals During Atmospheric Corrosion," *Protection of Metals,* Vol. 22, 1987, pp. 397–404.

[7] Yamasaki, R. S., Slade, H. F., and Sereda, P. J., "Determination of Time-of-Wetness Due to Condensed Moisture," *Durability of Building Materials,* Vol. 1, 1983, pp. 353–361.

[8] Yamasaki, R. S., "Characterization of Wet and Dry Periods of Plastic Surfaces during Outdoor Exposures," *Durability of Building Materials,* Vol. 2, 1984, pp. 155–169.

[9] Sereda, P. J., "Weather Factors Affecting Corrosion of Metals," *Corrosion in Natural Environments, ASTM STP 558,* American Society for Testing and Materials, Philadelphia, 1974, pp. 7–22.

[10] Haynie, F. H., "Environmental Factors Affecting the Corrosion of Galvanized Steel," *Degradation of Metals in the Atmosphere, ASTM 965,* American Society for Testing and Materials, Philadelphia, 1987, pp. 282–289.

[11] Benarie, M. and Lipfert, F., "A General Corrosion Function in Terms of Atmospheric Pollution Concentrations and Rain pH," *Atmospheric Environment,* Vol. 20, 1986, pp. 1947–1958.

[12] The Sereda Miniature Moisture Sensor, Model SMMS-01, manufactured by Epitek Electronics, 100 Schneider Road, Kanata, Ontario, Canada K2K 1V2 or Commerce Park, Ogdenburg, NY 13669, USA.

[13] Hechler, J. J., Boulanger, J., and Noël, D., "Experimental Lakes Area Corrosion Program: Report for the period December 1984-November 1985," Technical Report IGM 87RT-202-557-6, NRCC 27569, National Research Council of Canada, Ottawa, 1987.

[14] Hechler, J. J., Boulanger, J., Noël, D., Dufresne, R., and Pinon, C., "Variation in Metallic Atmospheric Corrosion and its Parameters on a Building," Paper 032, *Proceedings,* Vol. 2, 9th European Congress on Corrosion, Utrecht, The Netherlands, October 1989, published by The Netherlands Corrosion Centre, proceedings available from the Jaabeurs Congress Bureau, P.O. Box 8500, 3503 RM Utrecht.

[15] April, G. E., Pinon, C., Dufresne, R., and Hechler, J. J., "Atmospheric Corrosion Studies with Microcomputer Monitoring," *Proceedings,* Software and Hardware Applications of Microcomputer, Beverly Hills, CA, International Society for Mini and Microcomputer (ISMM), Anaheim, CA, 1986, pp. 212–215.

[16] Pinon, C., "Système de mesure et de commande de type Bus géré par micro-ordinateur," thesis, Ecole Polytechnique, Université de Montréal, Montréal, Canada, 1987.

[18] Mansfeld, F., "Electrochemical Methods for Atmospheric Corrosion Studies," *Atmospheric Corrosion,* W. H. Ailor, Ed., Wiley, New York, 1982, pp. 139–160.

Section IV: Laboratory Tests

Gardner Haynes[1]

Review of Laboratory Corrosion Tests and Standards

REFERENCE: Haynes, G., **"Review of Laboratory Corrosion Tests and Standards,"** *Corrosion Testing and Evaluation: Silver Anniversary Volume, ASTM STP 1000,* R. Baboian and S. W. Dean, Eds., American Society for Testing and Materials, Philadelphia, 1990, pp. 281–288.

ABSTRACT: ASTM Subcommittee G01.05 on Laboratory Corrosion Tests currently has nine task groups working on the development of new standards and revisions of its existing 13 standards. Revisions to existing test methods and practices often have been overlooked, resulting in confusion regarding compliance with the standards. This paper highlights the changes that have been made in existing standards over the last ten years. Problems and misconceptions associated with existing standards such as the salt spray test are discussed.

Particular attention is paid to corrosion testing of electronic materials and modified salt spray testing. The former is the topic of a draft proposal in ISO, while standardization of the latter has been fragmented. The need for a coherent approach to standardization of salt spray tests is discussed. Round-robin data showing the interlaboratory reproducibility of the salt spray test are presented.

KEY WORDS: laboratory corrosion tests, corrosion standards, accelerated corrosion tests, salt spray test, cyclic salt spray test, electronics corrosion

The object of an accelerated test is to cause degradation or failure in a shorter time period than under natural conditions without changing the failure mechanisms. This can be accomplished using electrochemical techniques, simple immersion tests, cabinet tests, simulated service tests (for example, automotive test tracks), accelerated coastal exposure, and in situ field service tests. In general, the ability of the test to predict actual service performance increases with the length and complexity of the test. The most reliable predictor of performance is, of course, service experience.

The job of the investigator is to choose or develop a laboratory corrosion test that will predict service performance and distinguish materials. The importance of correlating service performance with accelerated test results cannot be overemphasized. For example, the introduction of latex paints was delayed for many years due to poor performance (50 h to failure) in the salt spray test when compared to oil-alkyds (1000 h to failure) until it was found that the service performance of the latex was comparable or superior to that of the oil-alkyds [*1*]. The cause of the misleading accelerated test results was a change in the failure mechanisms. Another important aspect of accelerated testing is the acceleration factor. Proving ground tests have shown an acceleration factor of between 1.7:1 and 26:1 for the same test duration depending on the mechanism of degradation [*2*]. In order to establish a meaningful accelerated test it is necessary to correlate service performance with test results

---

[1] Member, group technical staff, Electrochemical and Corrosion Laboratory, Mail Station 10–13, Texas Instruments Inc., Attleboro, MA 02703.

for the material of interest and establish an approximate acceleration factor that ensures that the mechanisms of degradation are not changed. Recent ASTM STPs have been published on laboratory corrosion tests and synthetic environments for corrosion testing which offer some guidance on selection and development of tests [*3,4*].

Technical societies (ASTM, NACE, ISO, etc.), government bodies (DOD), industry groups (MTI), and individual companies (GM, Ford, etc.) have developed standards on laboratory corrosion tests. Many of these tests are similar; however, conformance with a standard issued by one group does not necessarily ensure conformance with the same standard issued by another group. For example, the concentration of salt solution as well as solution collection rates in the salt spray test are specified differently by ASTM, military standards, and federal test methods [*5*]. A methodology for locating and identifying standards has been published recently which should be useful for minimizing some of this confusion [*6*].

Although ASTM Committee G-1 on Corrosion of Metals was established in 1964 to consolidate standardization of corrosion tests, many other ASTM committees have jurisdiction over corrosion standards which relate specifically to their area of interest, and some continue to develop new standards. As a result, corrosion testing standards are scattered throughout many volumes of the *Annual Book of ASTM*. The recent decision by ASTM to publish a compendium of corrosion standards not contained in the volume on *Metal Corrosion* (Vol. 03.02) will aid users in locating corrosion standards.

ASTM Subcommittee G01.05 on Laboratory Corrosion Tests has responsibility within Committee G-1 for developing new standards and for reviewing and revising existing standards on laboratory corrosion tests. ASTM requires that all existing standards be reviewed and revised or reapproved every five years. Changes in the rules and regulations governing ASTM standards has resulted in many modifications to existing standards [*7*]. Often standards users are not aware of these changes and, in some cases, may no longer be in compliance with the current revision of a standard. The purpose of this paper is to highlight significant changes that have been made to ASTM standards on laboratory corrosion tests during the last ten years. Problems and misconceptions associated with existing standards such as the salt spray test are discussed.

Laboratory Corrosion Tests

The fixed designations (for example, B 117) of the standards on laboratory tests, their places in the *Annual Book of ASTM Standards*, and their titles are listed in Table 1. The number immediately following the designation (for example, -85) indicates the year of original adoption or the year of the last revision. The number in parentheses indicates the last year of reapproval. These standards can be divided into the following categories: (1) general corrosion practices; (2) specific immersion tests; and (3) cabinet tests.

General Corrosion Practices

These practices given general guidance on conducting and evaluating laboratory corrosion tests. An extensive reorganization and revision of the ASTM Practice for Preparing, Cleaning, and Evaluating Corrosion Test Specimens (G 1-88) was completed in 1988. The list of chemical and electrolytic cleaning methods was greatly expanded based on a Draft International Standard [*8*]. These cleaning methods have been gleaned from ASTM, NACE, literature, and individual experiences. Other significant changes to ASTM G 1-88 include improvement of the section on marking specimens, inclusion of a discussion on corrosion product analysis, and the addition of a section on precision and bias.

TABLE 1—*Standards under jurisdiction of subcommittee G01.05.*

Designation	Volume in the *Annual Book of ASTM Standards*	Title
B 117–85	02.05,03.02,06.01	Method of Salt Spray (Fog) Testing
B 287–74(1980)	02.05,03.02,06.01	Method of Acetic Acid-Salt Spray (Fog) Testing
G 1–88	03.02	Practice for Preparing, Cleaning, and Evaluating Corrosion Test Specimens
G 16–88	03.02	Guide for Applying Statistics to Analysis of Corrosion Data
G 28–85	03.02	Method for Detecting Susceptibility to Intergranular Attack in Wrought Nickel-Rich, Chromium-Bearing Alloys
G 31–72(1985)	03.02	Practice for Laboratory Immersion Corrosion Testing of Metals
G 34–86	03.02	Test Method for Exfoliation Corrosion Susceptibility in 2XXX and 7XXX Series Aluminum Alloys (EXCO Test)
G 43–75(1980)	02.05,03.02	Method of Acidified Synthetic Sea Water (Fog) Testing
G 46–76(1986)	03.02	Practice for Examination and Evaluation of Pitting Corrosion
G 48–76(1980)	03.02	Test Method for Pitting and Crevice Corrosion Resistance of Stainless Steels and Related Alloys by the Use of Ferric Chloride Solution
G 60–86	03.02	Method for Conducting Cyclic Humidity Tests
G 66–86	03.02	Method for Visual Assessment of Exfoliation Corrosion Susceptibility of 5XXX Series Aluminum Alloys (Asset Test)
G 67–86	03.02	Test Method for Determining the Susceptibility to Intergranular Corrosion of 5XXX Series Aluminum Alloys by Mass Loss after Exposure to Nitric Acid (NAMLT Test)
G 85–85	03.02	Practice for Modified Salt Spray (Fog) Testing
G 87–84	03.02	Practice for Conducting Moist SO_2 Tests

The ASTM Guide for Applying Statistics to Analysis of Corrosion Product Data (G 16–88) has been completely reorganized and revised for a more consistent presentation of statistical methods. The intent of this revision was to make the document more concise and of practical value. An active task group in Subcommittee G01.05 is still in the process of revising the examples in the appendixes.

The ASTM Practice for Laboratory Immersion Corrosion Testing of Metals (G 31–72), and the ASTM Practice for Examination and Evaluation of Pitting Corrosion (G 46–76) have not been revised since they were originally adopted and have had only a few minor editorial changes.

Specific Immersion Tests

These test methods have been developed to determine the susceptibility of particular alloys to specific forms of corrosion. They are predictors of actual service performance because results have been correlated with the occurrence of that form of corrosion in actual environments. Although they produce quantitative or semiquantitative results, there are no performance specifications within the standards as Committee G-1 is not a balanced committee and does not write specifications. Often, however, these standards are used by other committees for specification purposes. The ASTM Method of Detecting Susceptibility to Intergranular Attack in Wrought Nickel-Rich, Chromium-Bearing Alloys (G 28–85) was originally published in 1971 and consisted of a boiling ferric sulfate-sulfuric acid test for specific alloys [*9*]. It was revised in 1985 to include an alternative test solution for another specific alloy [*10*]. At that time, as required by ASTM, sections on precision and bias were included, and the references were updated. Data from a round-robin study conducted in 1985 addressing the precision and bias of this method are available from ASTM as Research Report RR:G01-1002.

There have been some problems and confusion with the ASTM Test Method for Exfoliation Corrosion Susceptibility in 2XXX and 7XXX Series Aluminum Alloys (EXCO Test) (G 34–86). When originally published in 1972, this standard was intended for research purposes. Subsequently it was approved for use by DOD, and lot acceptance criteria in some specifications were based on the photographic classifications of exfoliation susceptibility in this test method. In a 1979 revision the photographs were changed and cleaning of the specimens before rating was required. This revision made the standard unsuitable for lot acceptance purposes and for several years, ASTM G 34–79 was the latest revision, while ASTM G 34–72 was published in the gray pages of the *Annual Book of ASTM Standards* for specification purposes. In 1986 ASTM G 34 was revised to satisfy the needs of the existing specifications, and cleaning of the specimens before rating was made optimal. At that time the significance and use statement was modified to emphasize the use of the method for research and development and "not as the optimum method for quality acceptance." Despite these efforts to clarify the purpose of the method, dissatisfaction about its use for lot acceptance continued. A task group in Subcommittee G01.05 continues to address this problem and currently is balloting a revision which specifically states that ASTM G 34 "should not be construed as a method for quality acceptance."

The Materials Technology Institute (MTI) has test procedures for determination of critical pitting temperatures and critical crevice corrosion temperatures, which are often confused with the ASTM Test Method for Pitting and Crevice Corrosion Resistance of Stainless Steels and Related Alloys by the Use of Ferric Chloride Solution (ASTM G 48–76). ASTM G 48 specifies fixed test temperatures of 22 or 50°C, while the MTI procedures have temperature as the test result. Often results obtained using the MTI procedures are reported as having been obtained using the ASTM procedure. A task group in Subcommittee G01.05 currently is conducting round-robin tests in order to develop a unified test procedure for testing in ferric chloride solution.

The last two specific immersion tests (Table 1) were developed to detect susceptibility to exfoliation (ASTM G 66–86) and intergranular (ASTM G 67–86) corrosion of 5XXX series aluminum alloys. These methods were originally adopted in 1980. The last revision in 1986 incorporated new precision and bias sections in both documents.

Cabinet Tests

The ASTM Method for Conducting Cyclic Humidity Tests (G 60–86) describes procedures for conducting cyclic humidity tests with a corrosive dip. Originally developed for the automotive industry [*12*], it is used to rank steels under conditions which retard the formation of a protective type of rust and should not be used for simulating atmospheric exposure of weathering steels. Adopted in 1979, it was revised in 1986 to include statements on precision and bias.

The ASTM Practice for Conducting Moist SO_2 Tests (G 87–84) is useful for detecting pores or other sources of weakness in protective coatings and deficiencies in corrosion resistance associated with unsuitable alloy compositions or treatments. Based on the German

Kesternich test (DIN 50018), it consists of exposure to condensing humidity containing either 0.2 or 2 L of sulfur dioxide in a 300-L cabinet. This test is considered quite severe, and, although useful for comparative testing, its relevance to performance in specific environments must be considered carefully. Although it is similar to the sulfur dioxide test in ASTM B 605, it should not be confused with this test.

The oldest and most widely used standardized laboratory corrosion test is the ASTM Method of Salt Spray (Fog) Testing (B 117–85), which was originally approved in the early 1900s. A history of ASTM activity on salt spray testing was first published by McMaster [*13*] and later updated by Ketcham [*14*]. Over the years the concentration of the salt solution has ranged from 3.5 to 20%. The present 5% concentration was established in 1954. Although used extensively for specification purposes, results from salt spray tests seldom correlate with service performance [*15,16*]. The use of the salt spray test in research is adequately described in Appendix X2 of ASTM B 117–85. In the 1985 revision of B 117 the scope was modified to state specifically: "It should be noted that there is seldom a direct relation between salt (fog) resistance and resistance to corrosion in other media, because the chemistry of the reactions, including the formation of films and their protective value, frequently varies greatly with the precise conditions encountered [*11*]." The water for the salt solution was also changed to Type IV water described in the ASTM Specification for Reagent Water (D 1193). Despite these revisions, some users continue to assume that there is a direct correlation with service performance.

The salt spray test is useful for comparing the relative corrosion resistance of closely related materials and has been used successfully for many years for specification purposes. The task group on the Salt Spray Test within Subcommittee G01.05 has moved cautiously on revising the test due to its widespread use. A round-robin study for establishing a standard panel for assessing comparative corrosivity of chambers was completed in 1987. The participants in the round-robin are listed in Table 2. It is interesting to note that three of the thirteen laboratories in the round-robin had to be eliminated since they had incorrect collection rates at the end of the test. The round-robin consisted of exposure of cold-rolled carbon sheet steel (76 by 127 by 0.8 mm) in the chamber for 48, 96, and 168 h. Mass loss measurements were made on the exposed panels. The mean mass loss and ±2 standard deviations are plotted in Fig. 1. The rate of mass loss was 1.66 ± 0.42 $g/m^2/h$, which is comparable to the rate specified in a draft ISO standard [*17*].

The mass loss of steel in a chamber run according to ASTM B 117–85 should fall within the ±2 standard deviations since this includes 95% of all data, provided random variations

TABLE 2—*List of participants in salt spray round-robin.*

Contact	Company
M. J. Klimowski	Meta Coatings Int., Inc.
T. Wollan	Underwriters Laboratories Inc.
T. J. Summerson	Kaiser Aluminum & Chemical Corp.
V. Agarwala	Naval Air Development Center
D. Courtright	Naval WPNSTA
F. Lutze	ACT Testing Laboratories
R. Baboian	Texas Instruments Inc.
H. Anderson	Pacific Gas and Electric
...	National Steel Corp.
H. Lawson	ARMCO Inc.
D. Snyder	Harshaw/Filtrol
N. Tipton	Singleton Corp.
T. A. DeBold	Carpenter Technology Corp.

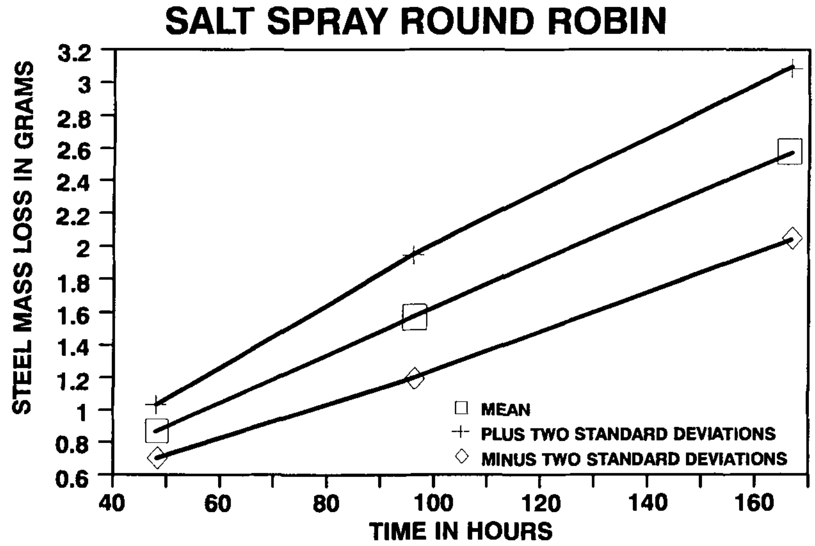

FIG. 1—*Mass loss of cold-rolled carbon sheet steel in ASTM B 117.*

are the only source of error. Although the ultimate goal is to include a standard panel in ASTM B 117–85 for evaluating the corrosivity of a cabinet, the task group is initially balloting an appendix to ASTM B 117–85, which gives a procedure for determining the mass loss of steel without setting limits. The appendix does state that the mass loss would not vary 20% from test to test. A second round-robin involving many more laboratories is currently in progress so that specific limits can be incorporated into ASTM B 117–85.

A number of variations of the salt spray test have been standardized for specific purposes. These include the ASTM Method of Acetic Acid-Salt (Fog) Testing (B 287), which was developed for research studies on decorative chromium plating on steel or zinc die-cast base, the ASTM Method for Copper-Accelerated Acetic Acid-Salt Spray (Fog) Testing (CASS Test) (B 368), which was developed for production control and acceptance purposes for decorative chromium plating, and the ASTM Method of Acidified Synthetic Sea Water (Fog) Testing (G 43), which was particularly applicable for exfoliation testing of aluminum alloys. In 1985, in order to minimize proliferation of salt spray tests and avoid confusion, the ASTM Practice for Modified Salt Spray (Fog) Testing (G 85–85) was adopted. This standard included ASTM B 287, ASTM G 43, and a salt/SO_2 test which was useful for simulating aircraft carrier exposure [*18*] in a single standard and was constructed such that additional methods involving the salt spray test could be added. Subsequently ASTM B 287 and ASTM G 43 were discontinued in 1988 and no longer appear in the *Annual Book of ASTM Standards*. Since ASTM B 368 is not under the jurisdiction of Committee G–1, it was not included in this consolidation; however, a similar consolidated salt spray standard under development by ISO does include the CASS test [*17*]. Recently there has been activity in Subcommittee D01.27 to develop a standard on cyclic salt spray testing. It would be helpful to standards users to incorporate ASTM B 368 and any future modified salt spray tests into ASTM G 85 so that all variations of the salt spray test are in a single standard.

A cabinet test that has received much attention in the area of standardization is the flowing mixed gas test for corrosion of electronic and magnetic materials. This test consists of exposure of specimens in a stream of air containing very small concentrations (parts per billion) of pollutants such as chlorine, nitrogen dioxide, hydrogen sulfide, or sulfur dioxide under controlled humidity conditions. Results from this test have been reported to correlate with field experience in a number of electronics environments [*19–21*]. Presently most specifications for these tests exist within individual companies; however, ISO is already working on a draft proposal for mixed gas testing. Other national or international committees interested in these tests include IEEE TC-1, IEC TC-50, and ASTM Committees B–4 and G–1. The goals of the task group on corrosion of electronic and magnetic materials within Subcommittee G01.05 include establishment of a standard multigas corrosion chamber, establishment of standard methods for measuring and reporting atmosphere corrosion of electronics, and establishment of standards for various levels of corrosive environments.

Summary

The purpose of the ASTM regulation that all standards be reapproved or revised every five years is to ensure quality and timeliness. At the discretion of the appropriate committee, standards may be revised more often. Revisions follow the normal balloting sequence, and those interested in the standards should participate in the process. Failure to do so can result in the type of problems and confusion encountered with specifications when ASTM G 34 was revised in 1979.

The focus of this paper has been to highlight significant changes in ASTM standards for laboratory corrosion tests over the last ten years. ASTM standards which have been revised extensively include G 1, G 16, G 28, G 34, G 85, and B 117. It is important for those who use these standards to ensure that they have a copy of the latest revision. Those using standards on laboratory corrosion tests for specification purposes should also be aware of the latest revision as well as the discontinuance of ASTM B 287 and ASTM G 43.

Current activities that will result in revision of existing standards or new standards on laboratory corrosion tests have also been described in this paper. The goal of developing a standard panel for salt spray chambers appears to be attainable. The development of a standard for mixed gas testing for electronics corrosion currently is underway. The development of a unified test method for ferric chloride testing (ASTM G 48) also will alleviate a great deal of existing confusion. It is strongly recommended that the work initiated in Subcommittee G01.05 to unify salt spray testing procedures into one standard be continued.

References

[*1*] Appleman, B. R. and Campbell, P. G. "Salt Spray Testing for Short Term Evaluation of Coatings," *Journal of Coatings Technology,* Vol. 54, No. 686, March, 1982.

[*2*] Hook, G., "The Historical Development of a Proving Ground Accelerated Corrosion Test," *Automotive Corrosion by Deicing Salts,* R. Baboian, Ed., National Association of Corrosion Engineers, Houston, TX, 1981.

[*3*] *Laboratory Corrosion Tests and Standards, ASTM STP 866,* G. S. Haynes and R. Baboian, Eds., American Society for Testing and Materials, Philadelphia, 1985.

[*4*] *The Use of Synthetic Environments for Corrosion Testing, ASTM STP 970,* P. E. Francis and T. S. Lee, Eds., American Society for Testing and Materials, Philadelphia, 1988.

[*5*] Altmayer, F., "Critical Aspects of the Salt Spray Test," *Plating and Surface Finishing,* AES, Orlando, September 1985.

[*6*] Musser, L. R., "Identifying Standards," *ASTM Standardization News,* April 1989.

[*7*] *Form and Style for ASTM Standards,* American Society for Testing and Materials, Philadelphia.

[*8*] Metal and Alloys—Procedures for Removal of Corrosion Products from Corrosion Test Specimens, Draft International Standard ISO/DIS 8407.3, International Standards Organization, Switzerland.

[*9*] Streicher, M. A., *Corrosion,* Vol. 19, 1963, pp. 272t–284t.

[*10*] Manning, P. E., "An Improved Intergranular Corrosion Test for Hastealloy Alloy C-276," *Laboratory Corrosion Tests and Standards, ASTM STP 866,* G. S. Haynes and R. Baboian, Eds., American Society for Testing and Materials, Philadelphia, 1985, pp. 437–454.

[*11*] Renner, M., Heubner, U., Rockel, M. B., and Wallis, E., "Temperature as a Pitting and Crevice Corrosion Criterion in the $FeCl_3$ Test," *Werstoffe und Korrosion,* Vol. 37, 1986, p. 183.

[*12*] Opinsky, A. J., Thomson, R. F., and Boegehold, A. L., "A Cyclic Humidity Accelerated Corrosion Test for Sheet Steel," *ASTM Bulletin,* January 1953.

[*13*] McMaster, W. D., "A History of the Salt Spray Tests," General Motors Research Pub. GMR-497, available from American Society for Testing and Materials, Philadelphia, as RR: G01-1003.

[*14*] Ketcham, S. J., "History of ASTM B 117 Salt Spray Test," available from American Society for Testing and Materials, Philadelphia, as RR: G01-1003.

[*15*] Doppke, T. S. and Bryant, A. W. "The Salt Spray Test-Past, Present, and Future," *Proceedings,* Second Automotive Corrosion Prevention Conference, Society of Automotive Engineers, Warrendale, PA, December 1983, pp. 57-72.

[*16*] Money, K. L. and Kain, R. M. "Synthetic Versus Natural Marine Environments for Corrosion Testing," *The Use of Synthetic Environments for Corrosion Testing, ASTM STP 970,* P. E. Francis and T. S. Lee, Eds., American Society for Testing and Materials, Philadelphia, 1988, pp. 205-216.

[*17*] Corrosion Tests in Artificial Atmosphere—Salt Spray Tests; Draft International Standard ISO/DIS 9227, International Standards Organization, Switzerland.

[*18*] Ketcham, S. J. and Jankowsky, E. J. "Developing an Accelerated Test: Problems and Pitfalls," *Laboratory Corrosion Tests and Standards, ASTM STP 866,* G. S. Haynes and R. Baboian, Eds., American Society for Testing and Materials, Philadelphia, 1985, pp. 14-23.

[*19*] Rice, D. W., Peterson, P., Rigby, E. B., Phipps, P. B., Cappell, R. J., and Tremoureux, R., "Atmospheric Corrosion of Copper and Silver," *JES,* Vol. 128, No. 2, Feb., 1981.

[*20*] Abbott, W. H., "Field vs Laboratory Experience in the Evaluation of Electronic Components and Materials," *Materials Performance,* August 1985.

[*21*] Abbott, W. H., "Corrosion Still Plagues Electronic Packaging," *Electronic Packaging and Production,* August 1989.

Russell D. Kane,[1] *S. Mark Wilhelm,*[1] *and Dale R. McIntyre*[2]

Application of the Critical Pitting Temperature Test to the Evaluation of Duplex Stainless Steel

---

REFERENCE: Kane, R. D., Wilhelm, S. M., and McIntyre, D. R., "**Application of the Critical Pitting Temperature Test to the Evaluation of Duplex Stainless Steel,**" *Corrosion Testing and Evaluation: Silver Anniversary Volume, ASTM STP 1000,* R. Baboian and S. W. Dean, Eds., American Society for Testing and Materials, Philadelphia, 1990, pp. 289–302.

ABSTRACT: This paper presents the results of a laboratory testing program whose objective was to evaluate the localized corrosion resistance of duplex stainless steel weldments and to validate screening test methods for this task. The results of sodium chloride (NaCl) critical pitting temperature (CPT) tests, ferric chloride tests, electrochemical polarization (pitting) scans, and simulated service environment tests are presented. These studies revealed that the sodium chloride CPT screening test provided the best correlation with long-term simulated service environment tests in terms of rank ordering resistance to pitting and in the morphology of attack. In terms of pitting resistance of duplex stainless steel weldments, it was found that pitting susceptibility could be related to both ferrite content and pitting index (PI) of the weld metal. At equivalent values of PI and ferrite content, the weld metal had higher resistance to pitting than the base metal.

KEY WORDS: corrosion testing, localized corrosion, pitting, duplex stainless steel, welding, critical pitting temperature, microstructure, electrochemistry

In recent years, there has been increasing interest in the use of corrosion resistant alloys (CRAs) for use in the production of oil and gas. Their inherent resistance to corrosion offers attractive engineering alternatives to conventional inhibitors and steel for many applications. The use of CRAs is of particular importance to off-shore development where hydrogen sulfide, carbon dioxide, and brine are produced. In these systems, the use of duplex stainless steels for pipelines is being developed as a means to reduce overall maintenance cost and extend the period of reliable field operations.

A number of problems, however, have been encountered in the application of duplex stainless steels for off-shore pipelines. A major hurdle for the widespread use of these materials is the low productivity resulting from the conventional field welding processes needed for these materials versus the high-rate welding that can be utilized in carbon steels. Alternate welding techniques are available for duplex stainless steels. Nevertheless, there is difficulty with the use of rapid welding techniques in that they produce welds with potentially inferior mechanical and corrosion properties.

The present study was conducted as part of a major multiclient-sponsored research program to explore alternate techniques and consumables for rapid field welding of duplex stainless steels. One of the facets of this program was the evaluation of welding techniques

---

[1] Cortest Laboratories, Inc., 11115 Mills Rd., Suite 102, Cypress, TX 77429.

[2] Currently with ARAMCO, Dhahran, Saudi Arabia.

which would preserve adequate corrosion performance in these materials. Therefore, a significant effort was directed at studying the applicability of various screening tests used for evaluation of the corrosion of duplex stainless steel weldments.

Background

Duplex stainless steels exhibit optimum corrosion and stress corrosion cracking performance when the ratio of ferrite to austenite in their structure is near 50:50 (see Fig. 1) [*1,2*]. In homogeneous wrought materials, this can be easily attained by a combination of compositional balance of ferrite and austenite forming elements, followed by annealing at a suitable temperature. During welding the ferrite and austenite balance also is dependent on the cooling rate, which, in turn, determines the time spent in the temperature range from 425 to 650°C [*3*].

When weld deposition rate is high, heat input is typically low, which ultimately results in high cooling rates. Consequently, in welded duplex stainless steels, high welding speed will result in a nonoptimum balance of ferrite and austenite. Under these conditions, the ferrite content of the weld metal and particularly, the heat-affected zone (HAZ) can increase. Weld metal ferrite content, however, can also be controlled by varying the composition of the filler wire used in the welding processes. In production welds, ferrite content is usually maintained in the range from 40 to 60%, with higher ferrite contents associated with unacceptable corrosion and mechanical performance.

Another related problem is that there has been little success with conventional screening tests for ranking the relative susceptibility to localized corrosion of duplex stainless steels. The experience with the ferric chloride test per the ASTM Test Method for Pitting and Crevice Corrosion Resistance of Stainless Steels and Related Alloys by the Use of Ferric Chloride Solution (G 48) has been that it is generally too severe for duplex stainless steels, and the results have not correlated with service experience [*4*].

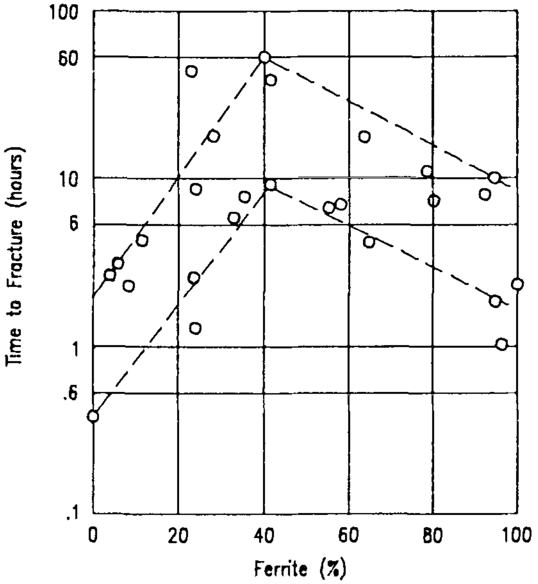

FIG. 1—*Effect of ferrite content of duplex stainless steels on SCC resistance in* $MgCl_2$.

Experimental Procedure

Materials

The present study was conducted on commercially available duplex stainless steel pipe with a nominal composition of 22% chromium, 5.5% nickel, 3% molybdenum, and 0.14% nitrogen made in accordance with the ASTM Specification for Seamless and Welded Ferritic/Austenitic Stainless Steel Tubing for General Service (A 789/A 789M). The composition, austenite/ferrite, percentages, and pitting index (PI = Cr + 3.3 Mo + 13 N) values are given in Table 1.

To make welds of varying properties, different filler wires of various compositions, diameters, and sources were used. The weld wires ranged in PI values from 29.5 to 37.1. All welds in the duplex stainless steels were made with the pulsed gas metal arc welding (PGMAW) method using a cover gas of 95% argon/5% carbon dioxide.

A total of eight welds made with different weld wires and cooling rates were utilized in the corrosion study. The composition of the welds were determined at both root and midfill locations. Weld metal compositions are given in Table 2. Table 3 presents the ferrite percent and PI for the various weld metals sampled.

Corrosion Testing

Four types of corrosion tests were conducted:

1. Critical pitting temperature (CPT) tests.
2. Electrochemical polarization curves per the ASTM Test Method for Conducting Cyclic Potentiodynamic Polarization Measurements for Localized Corrosion Susceptibility of Iron, Nickel, or Cobalt-Based Alloys (G 61).
3. Ferric chloride (CPT) tests per a modified ASTM G 48 procedure.
4. Simulated service environment tests in high-pressure autoclaves.

Sodium Chloride Critical Pitting Temperature (CPT) Tests

The CPT tests were used to screen all welds for susceptibility to localized corrosion. The method utilized was adapted from previous studies [5] used for evaluating stainless steels for seawater service.

The current CPT experiments were conducted in a 2% sodium chloride (NaCl) solution, acidified to a pH of 4.5 with glacial acetic acid. This solution was used to simulate corrosive gas-gathering service, including the effects of chlorides from produced fluids along with the pH depression that occurs from relatively high partial pressures of carbon dioxide in the produced hydrocarbon gas.

TABLE 1—*Chemical composition of pipe.*

Identification: Duplex P-2
Diameter (mm): 324
Wall thickness (mm): 17.5
Composition, weight percent:
0.017 C; 1.73 Mn; 0.41 Si; 0.019 P; 0.016 S; 23.1 Cr, 6.1 Ni; 3.1 Mo, 0.09 V, 0.165 N; 0.05 Cu; 0.014 W; 0.01 Al
Austenite/ferrite, vol. percent: 52.2/47
PI: 35.4

TABLE 2—*Duplex weld metal chemical analyses, weight percent.*

Weld Number	Location	Element											
		C	Mn	Si	P	S	Cr	Ni	Mo	V	N	O	PI[a]
43–1	Root	0.035	1.16	0.69	0.02	0.01	22.9	7.9	2.9	0.05	0.212	0.036	35.2
43–1	Midfill	0.035	1.56	0.47	0.20	0.01	23.1	7.8	2.9	0.01	0.156	0.043	
45–2	Root	0.025	1.15	0.41	0.02	0.01	23.8	7.9	3.2	0.04	0.152	0.036	36.3
45–2	Midfill	0.029	1.50	0.26	0.02	0.01	23.2	8.6	3.0	0.12	0.105	0.068	
47–5	Root	0.039	1.72	0.83	0.02	0.01	21.7	9.5	3.2	0.10	0.071	0.022	33.2
47–5	Midfill	0.028	1.54	0.28	0.02	0.01	23.2	8.7	3.0	0.13	0.095	0.054	
49–7	Root	0.024	1.61	0.45	0.02	0.01	23.4	7.6	3.0	0.06	0.152	0.161	35.3
	Midfill	0.027	1.57	0.47	0.02	0.01	23.3	7.8	2.9	0.05	0.030	0.039	
51–8	Root	0.030	1.22	0.70	0.02	0.01	23.7	8.10	3.1	0.07	0.180	0.036	36.3
51–8	Midfill	0.028	1.52	0.48	0.02	0.01	23.2	7.8	2.9	0.05	0.161	0.036	
54–9	Root	0.027	1.15	0.42	0.02	0.01	24.6	8.2	3.4	0.04	0.149	0.037	37.8
54–9	Midfill	0.027	1.53	0.46	0.02	0.01	23.3	7.7	3.0	0.05	0.161	0.042	
58–12	Root	0.039	1.75	0.84	0.02	0.01	22.0	9.8	3.0	0.09	0.074	0.024	32.9
58–12	Midfill	0.028	1.58	0.48	0.02	0.01	23.1	8.0	3.0	0.05	0.138	0.037	
60–14	Root	0.023	1.57	0.44	0.02	0.01	23.1	7.6	2.9	0.06	0.153	0.028	34.7
60–14	Midfill	0.029	1.56	0.45	0.02	0.01	23.2	7.8	2.9	0.05	0.155	0.042	

[a] PI = Pitting index (Cr + 3.3 Mo + 13 N) for root pass weld metal composition only.

TABLE 3—*Percent ferrite and pitting index in duplex welds.*

			Ferrite, %			
			Root			
Weld Number	Filler Wire	Cooling Time, t 1200/800 s	HAZ	Weld	PI[a]	Midfill Weld
43–1	W-1	4.66	68.0	42.5	35.2	39.0
45–2	W-2	4.66	65.0	51.5	36.3	43.0
53–3	W-5	4.66	62.0	24.0	...	42.0
46–4	W-6	4.66	67.0	21.0	...	43.0
47–5	W-7	4.66	67.0	44.0	33.2	39.0
48–6	W-8	4.66	67.0	18.5	...	38.0
49–7	W-10	4.66	58.0	48.0	35.3	43.0
51–8	W-1	6.47	55.0	33.5	36.3	40.0
54–9	W-2	6.47	64.0	40.0	37.8	37.0
57–11	W-6	6.47	59.0	7.0	...	35.5
58–12	W-7	6.47	63.0	25.0	32.9	36.5
60–14	W-10	6.47	59.0	44.0	34.7	38.0

[a] Weld metal pitting index (PI = Cr + 3.3 Mo + 13 N) values for root pass only.

The specimens were sections from weldments and therefore contained parent metal, weld metal, and HAZ. They were machined into 35-mm-long by 6.4-mm-diameter rods with the weldment located 9.5 mm from the bottom of the specimen. After machining, the specimens were cleaned and degreased.

The test solution was mixed, then deaerated by nitrogen purging and heated to 40°C. Once at temperature, the specimens were placed into the solution and held there for a period of 10 min under continuous nitrogen purging and stirring. During this time, the corrosion potential was monitored. The specimens then were polarized to 300 mV anodic to the corrosion potential for a period of 10 min. All potentials were measured relative to a saturated calomel electrode (SCE). Nitrogen purging, stirring, and specimen polarization were maintained during the entire experiment.

The test sequence was to increase the solution temperature by 5°C over a 5-min period, followed by a hold for an additional 10-min period. This procedure was repeated until pitting was detected. The specimen was monitored for pitting by both visual and electrochemical means. Pitting was detected by the increased current necessary to polarize the specimen. Typically, pitting could be observed visually at ×20 when approximately an order of magnitude current increase was detected.

Electrochemical Polarization Pitting Scans

A series of pitting scans were conducted on selected duplex stainless steel weldments. They were performed in a deaerated solution of 2% sodium chloride at a pH of 4.5 obtained by additions of glacial acetic acid. The solution temperature for these tests was 55°C. Forward/reverse anodic polarization scans per ASTM G 61 were conducted whereby both the forward and reverse scans were made at a rate of 0.5 mV/s. From these tests, three parameters were measured: (1) E_{corr}, corrosion potential; (2) E_p, pitting potential; and (3) E_r, repassivation potential.

Ferric Chloride CPT Tests

A series of tests were conducted using a 10% ferric chloride solution. The test was modified from that given in ASTM G 48. It utilized a special specimen holder which exposed just the root pass of the weld area on the internal pipe surface to the ferric chloride solution. The specimens were exposed for 23-h periods starting at 20°C. After each exposure period, the specimen was rinsed, weighed, and examined for pitting. It was then put into a fresh solution, the temperature was raised 2°C, and the exposure was repeated until localized corrosion was observed. In this manner, a ferric chloride CPT value was determined for the various weldments.

Simulated Service Environment Tests

High-pressure autoclave tests were conducted in which the gas-gathering line environment was simulated. The objectives of these tests were: (1) to develop a better understanding of the corrosion behavior of duplex stainless steels and their weldments; and (2) to better correlate the results of the laboratory screening tests to service conditions.

The autoclave test utilized specimens of both base metal and the various weldments. They included unstressed corrosion coupons taken from the inside diameter of the pipe containing the root pass, HAZ, and base metal.

The autoclave environment consisted of a deaerated 5% sodium chloride solution saturated with a test gas of 800 psia carbon dioxide and 1 psia hydrogen sulfide. The tests were conducted at 93°C for a period of 30 days. The gas composition in the autoclave was monitored weekly and replenished as necessary to maintain the gas composition to ±20% of the desired hydrogen sulfide level.

At the completion of the autoclave test, the gas pressure was released and the specimens removed from the autoclave. The specimens were then rinsed, reweighed, and observed for localized corrosion. Pit depths were measured on all specimens on only the side corresponding to the pipe inside diameter surface.

Results and Discussion

Sodium Chloride CPT Tests

The results of the CPT tests are given in Table 4. They indicate a range of CPT values from less than 40 to 60°C for the various duplex stainless steel weldments. Also shown in

TABLE 4—*Results of sodium chloride critical pitting temperature tests.*

Weld Number	Filler Wire	PI[a]	Ferrite, %			CPT, °C	Failure Location
			HAZ	Weld	PI[a]		
43-1	W-1	33.8	68.0	42.50	35.2	58	Parent and weld
45-2	W-2	37.1	67.8	51.5	36.3	60	Parent and weld
53-3	W-5	35.7	61.5	24.0	...	48	Weld
46-4	W-6	29.5	7.0	21.0	...	53	Weld
47-5	W-7	31.0	67.3	38.7	33.2	57.5	Parent and weld
48-6	W-8	24.9	67.0	18.5	...	<40	Weld
49-7	W-10	58.5	58.5	48.0	35.3	60	Parent and weld
51-8	W-1	33.8	52.0	33.5	36.3	58	Parent and weld
P-2[c]						57	

[a] Pitting index of filler wire.
[b] Pitting index of weld metal root pass.
[c] Parent metal (pipe) only.

this table are the percent ferrite in the root pass HAZ and weldment, along with the PI for the weldment. The percentage of ferrite varied from 7.0 to 68.0% in the HAZ and from 18.5 to 51.5% in the weld metal.

In Fig. 2*a–c*, the CPT results presented in Table 4 are plotted as functions of the following: (1) weld metal ferrite percentage; (2) weld metal PI; and (3) filler metal PI. From this presentation of the data, it can be seen that the CPT value is dependent on both composition, as evident in the PI, and on the ferrite content. Typically, pitting resistance, as measured by CPT, increased with increasing PI of either the weld metal or filler metal. Furthermore, pitting resistance increased with weld metal ferrite content over the range 18.5 to 51.5%. Pitting resistance did not correlate to HAZ ferrite content in this study.

The visual observations of the CPT specimens following the test revealed that, in all cases, the location of pitting failure was in either the parent metal or weld metal or both. The HAZ did not play a significant role in determining the corrosion performance of the weldment, even though in some cases the ferrite content was significantly above 60% and below 40%. The lack of any correlation between CPT values and HAZ ferrite percentage support this conclusion.

In terms of absolute resistance to pitting corrosion, it appears that many of the weldments made in this study have resistance greater than or equal to that of the parent metal. As shown in Fig. 2, the CPT values of the parent metal were consistently less than those exhibited by the weld metal at an equivalent ferrite content and PI value. An explanation for this behavior was found in subsequent metallurgical analysis of the materials. Scanning electron microscopy (SEM) and EDAX analysis of the austenite and ferrite in the weld and parent metal revealed that significantly less alloy partitioning (variation in composition between ferrite and austenite phase) took place in the weld metal than in the parent metal. This is probably the result of the limited diffusion taking place in the weld metal due to its rapid cooling rate versus the long period of time the parent metal spends at elevated temperatures during processing.

Based on the outcome of the CPT tests, in all but one case welds of varying ferrite content and PI values could be separated using this test method. These test results indicate that the localized corrosion resistance of the duplex stainless steel weldments made with rapid welding techniques was determined by ferrite content and composition in weld and parent metal, not the HAZ.

Ferric Chloride CPT Tests

The results of the ferric chloride CPT tests are given in Table 5. They show CPT values ranging from 26 to 34°C. In most of the ferric chloride CPT specimens, pitting was initiated in the HAZ. This result is substantially different than that found for the CPT tests conducted in the 2% sodium chloride solution at pH 4.5. In the case of the sodium chloride CPT tests, pitting was commonly observed in either the parent or weld metal with the HAZ not significantly contributing to the overall corrosion performance of the weldment.

As shown in Fig. 3*a–c*, the ferric chloride CPT varied with the PI values determined from the weld metal and filler metal compositions. Generally, ferric chloride CPT increased with increasing PI value. However, the degree of scatter in the test data is much greater for the ferric chloride CPT than in the sodium chloride CPT data presented previously. By comparison, the sodium chloride CPT increased with the PI of the filler metal and was found to be relatively insensitive to the PI of the weld metal root pass over the range of values examined.

The most interesting aspect of the ferric chloride tests is that most of the failures were produced in the HAZ. Therefore, it would be expected that a relationship should exist between the ferric chloride CPT and the condition of the HAZ. Figure 3*c* shows ferric

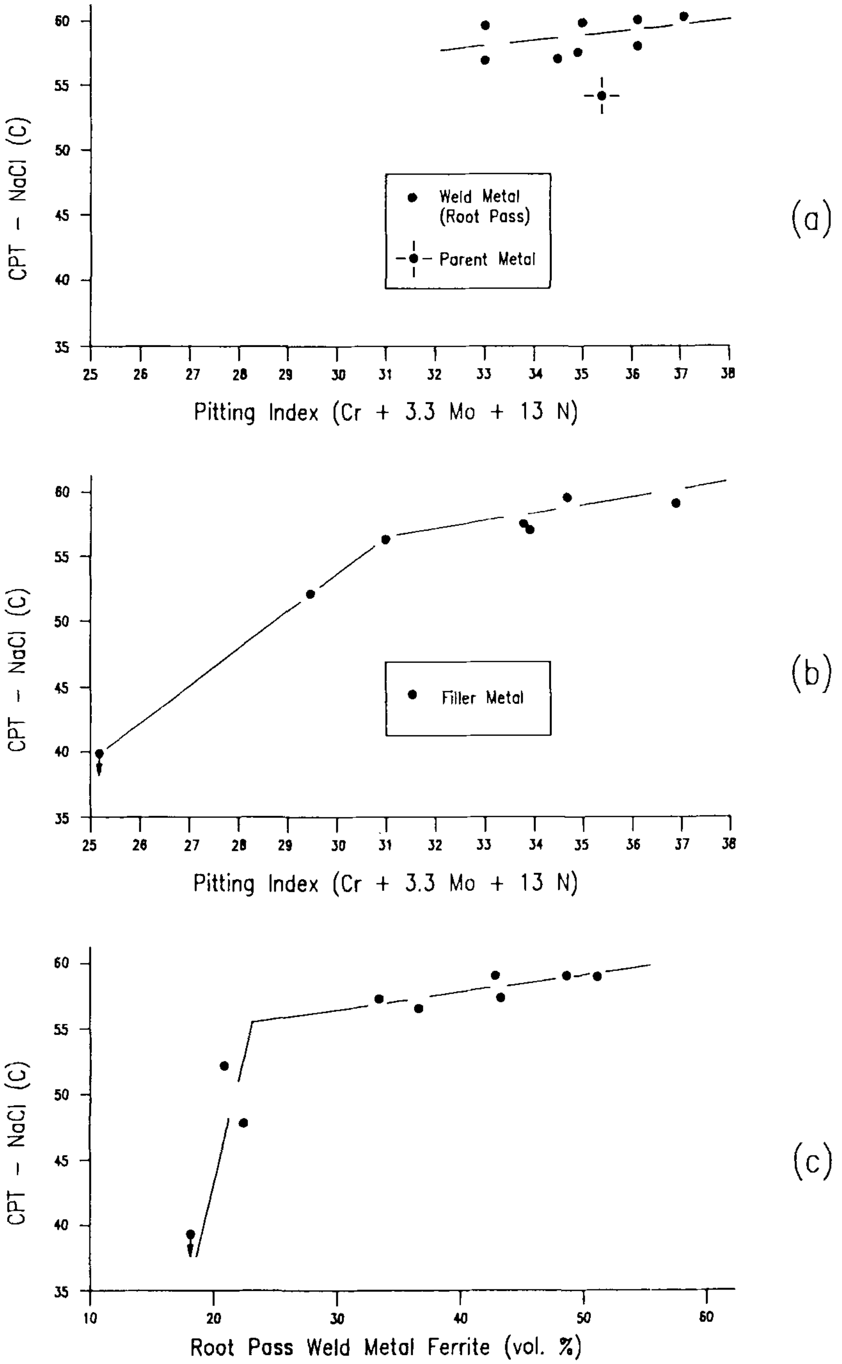

FIG. 2—*Effects of pitting index and ferrite content on resistance to pitting using the NaCl CPT test.*

TABLE 5—*Corrosion testing summary, duplex.*

Weld Number	Filler Wire	PI[a]	Cooling Rate, *T* 1200/800, (s)	Ferrite, % HAZ	Ferrite, % Root	PI[b]	$FeCL_3$ Pitting Temperature, °C	$FeCL_3$ Pitting Failure Location
P-2[c]						35.5	34	Parent
43-1	W-1	33.8	4.66	68	42.5	35.2	26	HAZ
45-2	W-2	37.1	4.66	65	51.5	36.3	30	HAZ
47-5	W-7	31.0	4.66	67	39.2	33.2	33	Weld
49-7	W-10	34.6	4.66	68	48.0	35.3	32	HAZ-Weld
51-8	W-1	33.8	6.47	55	33.5	36.3	34	HAZ
54-9	W-2	37.1	6.47	64	40.0	37.8	32	HAZ-Weld
58-12	W-7	31.0	6.47	63	25.5	32.9	20	Weld
60-14	W-10	34.6	6.47	59	44.0	34.7	26	HAZ
52-15	W-1	33.8	10.94	57	35.2	...	34	HAZ

[a] Pitting index of filler wire.
[b] Pitting index of weld metal root pass or parent metal.
[c] Parent metal only.

chloride CPT plotted versus the ferrite content of the HAZ and the weld metal root pass. As can be seen in this figure, no clear relationship exists.

By comparison, the sodium chloride CPT data show pitting in the weld metal and parent metal. The sodium chloride CPT increased with the ferrite content of the root pass of the weld metal. These results are in direct contrast of the ferric chloride CPT tests.

Electrochemical Polarization Tests

The results of the forward/reverse scan electrochemical polarization tests are given in Table 6. This table shows the various electrochemical parameters (E_{corr}, E_p, and E_r) for selected weldments and parent metal conducted in the sodium chloride test solution. For comparison, the results of the sodium chloride and ferric chloride CPT tests are also given.

In these tests, there appears to be significant scatter in the E_{corr} values for the various materials. It is not expected that this variation resulted from electrochemical differences in the weldments but rather from variations in the initial conditions during the start-up transient period of the test. This scatter could probably have been reduced by increasing the initial exposure period prior to the measurement of E_{corr}.

The values of E_p and E_r are generally more consistent and appear to give better indications of the actual corrosion behavior of the materials. The values of E_p ranged from +50 to +600 mV. Rank ordering the weldments from the highest E_p to the lowest (relating to highest resistance to pitting initiation to lowest) gives the same ranking of pitting performance as found in the sodium chloride CPT test. However, based on limited ferric chloride CPT test data, a similar correlation is not possible. In terms of E_r, the electrochemical pitting scan measurements show a different ranking with values of E_r ranging from +0 to −150 mV, with higher values of E_r relating to better repassivation performance. This ranking does not directly correspond to that found in the sodium chloride CPT test. The E_r results correspond much better to the limited ferric chloride CPT. This may indicate that good ferric chloride test results are derived from the ability of the material to repassivate in the aggressive solution. More data over a wider range of welding conditions is necessary, however, before a definite relationship can be made with the results of the ferric chloride CPT tests.

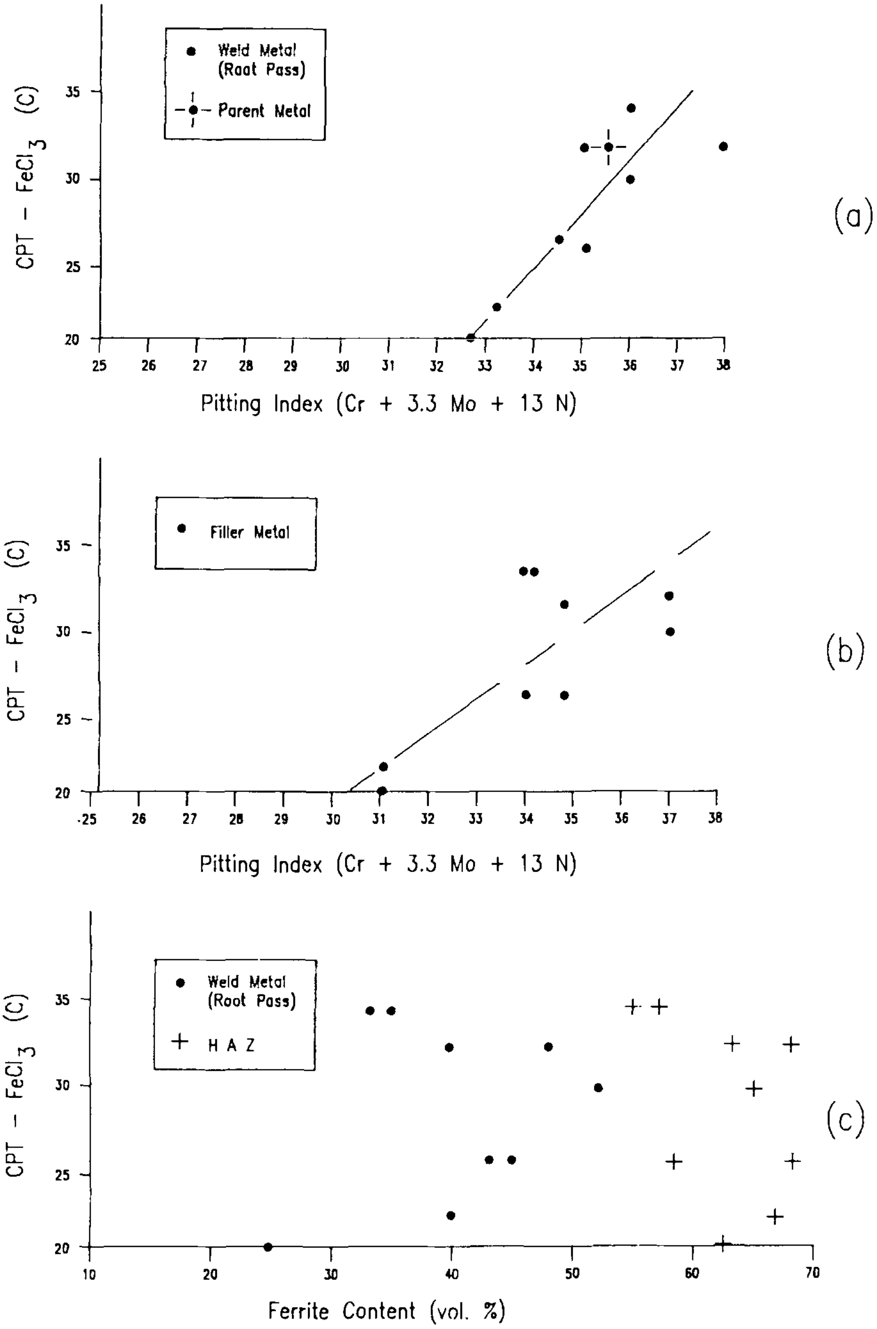

FIG. 3—*Effects of pitting index and ferrite content on resistance to pitting using the FeCl$_3$ CPT test.*

TABLE 6—*Electrochemical pitting-scan test results.*[a]

Weld Number	Filler Wire	E_{corr}, mV, SCE	E_p, mV, SCE	E_r, mV, SCE	Failure Location
P-2	Base pipe	−138	+350	+ 0	Parent
P-2	Base pipe	−396	+300	+ 0	Parent
45-2	W-2	−244	+350	− 50	Parent/weld
45-2	W-2	−422	+600	− 50	Parent/weld
46-4	W-6	−462	+250	− 50	Root weld
46-4	W-6	−490	+300	− 50	Root weld
48-6	W-8	−454	+250	−150	Root weld
48-6	W-8	−499	+ 50	−100	Root weld
51-8	W-1	−452	+350	+ 0	Parent/weld
51-8	W-1	−152	+350	+ 0	Parent/weld

[a] All tests were conducted per ASTM G 61 at 55°C in a deaerated solution of two% sodium chloride in distilled water, acidified with glacial acetic acid to a pH of 4.5.

In general, the E_p values determined from the electrochemical pitting scan tests correlate very well with those of the sodium chloride CPT tests. This may be fortuitous, since both tests determine resistance to pit initiation. However, the true significance of any results from the results of the CPT tests and pitting scan tests must be based primarily on the correlation to simulated service environment tests and their ability to predict service behavior of the various weldments.

Simulated Environment Autoclave Test

The results of the simulated service environment autoclave test are given in Table 7. The results are presented in terms of maximum pitting rate (mm/month) measured on the welded coupons. As can be seen in this table, the results of the sodium chloride CPT tests indicate that all of the duplex stainless steel test welds evaluated should have generally comparable susceptibility to pitting, whereas the ferric chloride CPT tests show significant variation in the pitting resistance.

TABLE 7—*Summary of simulated environment autoclave test data.*

			Ferrite Content			CPT(C)			
Weld	Wire	PI[a]	HAZ	Root	PI[b]	NaCl	$FeCl_3$	Pitting, mm/month	Maximum Pitting, mm/month
51-8	W-1	38.8	55	33.5	36.3	60	30	0.053 0.610 0.028	0.061
54-9	W-2	37.1	64	40.0	37.8	58	34	0.071 0.043 0.028	0.071
58-12	W-7	31.0	63	25.0	32.9	60	22	0.084 0.018	0.084
P-2[c]	...		...	47.0	35.4	35	34	0.071 0.043 0.061	0.071

[a] Pitting index of filler wire.
[b] Pitting index of weld metal root pass.
[c] Parent metal only.

The autoclave tests indicate that the welds have a comparable resistance to pitting, having maximum pitting rates in the range of 0.061 to 0.084 mm/month. The total variation in pitting rates observed on the coupons in the autoclave test was 0.018 to 0.084 mm/month.

Most importantly, it was noted that the nature of the pitting attack on the specimens in the autoclave test was similar to that found in the sodium chloride CPT test and not at all like that in the ferric chloride test. The pits in the coupons exposed in the autoclave test were distributed in both the parent metal, weld metal, and HAZ with no preference to any particular location. Preferential attack of the HAZ in the duplex stainless steel weldments did not occur in the simulated service environment as would have been predicted by the results of the ferric chloride test.

Figure 4*a–c* shows the results presented in Table 7 plotted versus CPT, PI value, and ferrite content. Figure 4*a* indicates that based on the sodium chloride CPT data all weld and parent metal specimens should exhibit pitting tendencies of similar magnitude by virtue of the fact that all materials had sodium chloride CPT values between 55 and 60°C. The ferric chloride CPT values show a substantial range of values from 20 to 34°C. In fact, the specimens from the autoclave test had similar pitting behavior.

As shown in Fig. 4*a–c*, there were no observable trends in the autoclave pitting data based on PI value or ferrite content. This indicates that, over the limited range of PI (33 to 38) and a wide range of ferrite contents (25 to 64%), these parameters were not significant in determining pitting performance under the simulated service environment evaluated. Based on the results of the sodium chloride CPT tests in Fig. 2*a–c*, it is seen that over the range of PI and ferrite content evaluated in the autoclave tests, CPT did not vary considerably until the PI was less than 30 and the ferrite content was less than 25. In this regard, the short-term sodium chloride CPT screening test provided remarkable correlation with the results of the long-term simulated service environment test.

As a final statement, the results of the simulated service environment tests have been corroborated through a full-scale simulated environment test conducted on the same material. In this test, pit depths were found to be in the range of 0.010 to 0.065 mm, which is very consistent with the results of the laboratory autoclave test presented in this study.

Conclusions

Based on the experimental study on the pitting behavior of duplex stainless steels in acidic chloride solutions described herein, the following conclusions were made:

1. The sodium chloride CPT test was found to have very good correlation with the results of long-term simulated environment tests. They showed the relationships between pitting susceptibility and various parameters such as pitting index (PI) and ferrite content.
2. The sodium chloride CPT test provided better correlation than that found for ferric chloride CPT tests based on the actual pitting morphology and behavior as observed in a simulated service environment.
3. The results of electrochemical polarization curve (pitting) scans gave the same ranking of materials as obtained through the use of the sodium chloride CPT test based on comparison of the E_p and CPT.
4. The localized corrosion resistance of duplex stainless steel weldments made with rapid welding techniques such as PGMAW appears to be equivalent or better than that of the parent metal for many combination of filler wires. When compared at equivalent PI or ferrite content, the weld metal often exhibits higher sodium chloride CPT values.

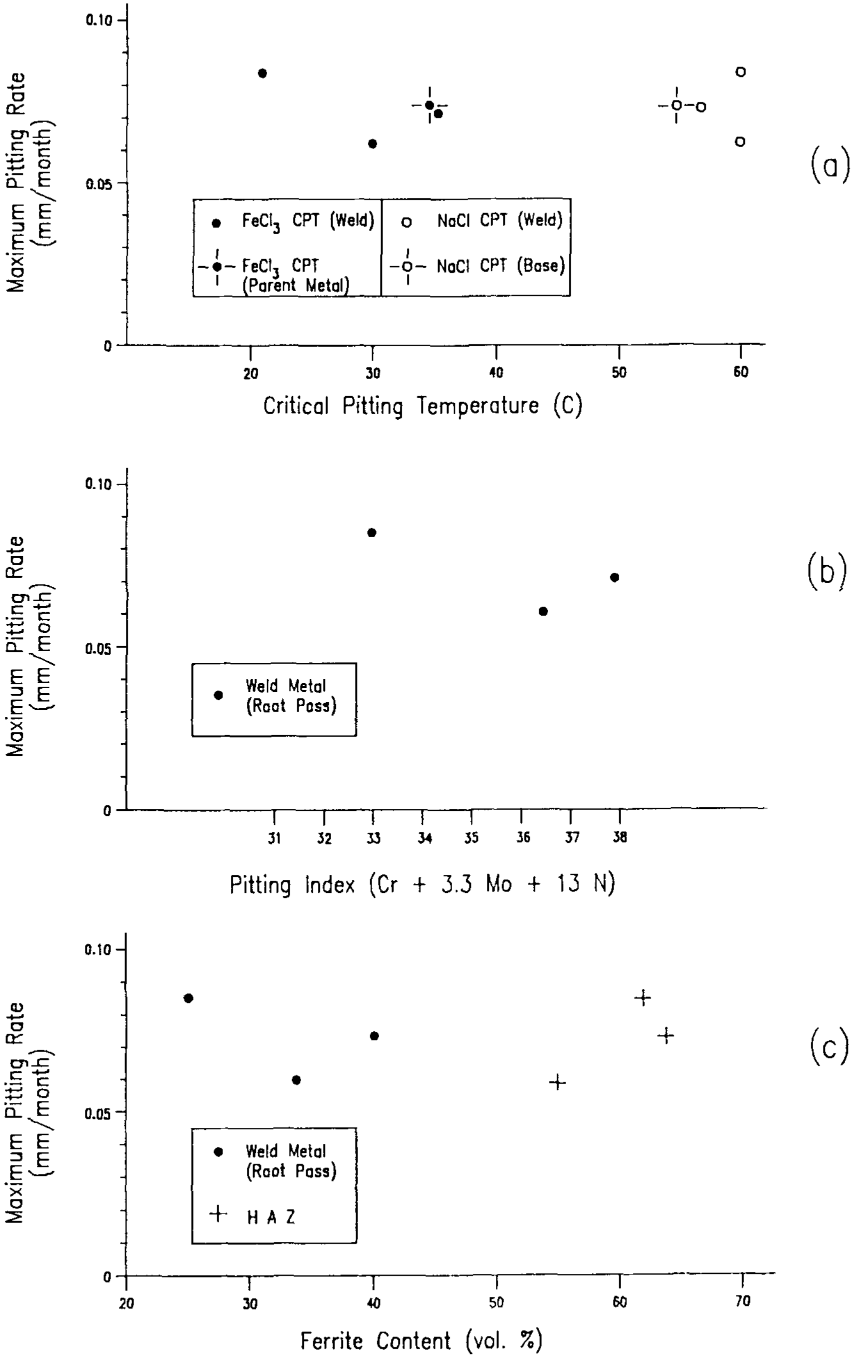

FIG. 4—*Effects of CPT, pitting index, and ferrite content on pitting resistance in* CO_2/H_2S *autoclave test.*

Acknowledgments

The authors of this paper would like to thank all of the corporate members of the multiclient-sponsored research program entitled "Development of Techniques for High Production Rate, Mechanized Field Girth Welding of Selected, High Alloy Corrosion Resistant Pipeline Materials." Furthermore, acknowledgment should be given to the organizers of this program. They are CRC-Evans Automatic Welding, Cortest Laboratories, Inc., J. P. Kenny and Microalloying International, Inc., and Curt Christensen of Korrosioncentralen for the successful completion of the full-scale tests. The authors would also like to thank Scott Gordon and other members of the Cortest Laboratories technical staff for their assistance on this research effort.

References

[*1*] Suzucki, et al., *Nippon Kinzoku Gakaishi,* Vol. 32, 1968, p. 1171.
[*2*] Heritier, B., et al., *NACE Corrosion/86,* Paper No. 158, NACE, Houston, TX, March 1986.
[*3*] Honeycombe, J. and Gooch, T. G., Welding Institute, Research Report No. 286/1985, September, 1985.
[*4*] Sridhar, N., et al., *Materials Performance,* Vol. 23, No. 12, 1984, p. 52.
[*5*] Bernhardsson, S., et al., *NACE/Corrosion/80,* Paper No. 85, NACE, Houston, TX, March, 1980.

Te-Lin Yau,[1] *Jeff A. Andrews,*[1] *H. Rob Henson,*[1] *and Derrill R. Holmes*[1]

Practice for Conducting Corrosion Coupon Tests on Zirconium and Its Alloys

---

REFERENCE: Yau, T.-L., Andrews, J. A., Henson, H. R., and Holmes, D. R., **"Practice for Conducting Corrosion Coupon Tests on Zirconium and Its Alloys,"** *Corrosion Testing and Evaluation: Silver Anniversary Volume, ASTM STP 1000,* R. Baboian and S. W. Dean, Eds., American Society for Testing and Materials, Philadelphia, 1990, pp. 303–311.

ABSTRACT: Zirconium and its alloys resist attack by most strong acids and alkalies. These alloys are often considered for highly corrosive applications. Conducting corrosion coupon tests for candidate materials under simulated or actual service conditions is popular in the process of materials selection. However, certain procedures in existing ASTM and NACE standards, i.e., ASTM Standards G 4 and ASTM G 31 and NACE Standard TM-01-69, are not applicable to zirconium and its alloys. A tailored practice for conducting corrosion coupon tests on zirconium and its alloys in chemical environments has been prepared. Emphasis is placed on coupon quality and preparation, galvanic corrosion, test duration, contamination resulting from the corrosion of other metals, and handling of corroded coupons. This practice should be used with applicable ASTM and NACE standards.

KEY WORDS: zirconium, zirconium alloys, corrosion coupon tests, coupon quality, cleaning, pickling, oxide formation, pyrophoric film

In recent years, the chemical process industry (CPI) has undergone some dramatic changes. There is a pronounced emphasis on process efficiency, product quality, plant safety and reliability, and waste minimization. Consequently, the use of metals and alloys that have high corrosion resistance is on the rise. These metals are necessary for new and advanced processes that take place in harsh corrosives at elevated temperatures and pressures. In 1983, the use of highly corrosion-resistant metals in the CPI was conservatively estimated to be increasing by 2.8% per year for the next five years [*1*].

Zirconium and its alloys are among the most corrosion-resistant metals. They resist attack by strong acids and alkalies. They are being used in the CPI at an increasing rate. Reasons for this increase include:

1. A better understanding of the corrosion properties of zirconium and its alloys has been achieved.
2. The CPI, equipment designers, and fabricators have become more knowledgeable about the properties of zirconium and its alloys.
3. The price of zirconium and its alloys has been stable during the past decade. On the other hand, prices for alternate high-performance alloys have been increasing and fluc-

---

[1] Head and corrosion specialists, respectively, Corrosion Group, Research and Development Division, Teledyne Wah Chang Albany, Albany, OR.

tuating. Zirconium and its alloys are often found to be the most economical solution to many corrosion problems [*2*].

The CPI presents a complex set of materials selection challenges. Conducting corrosion coupon tests for candidate materials under simulated or actual service conditions is popular in the process of materials selection. The ASTM Guide for Conducting Corrosion Coupon Tests in Plant Equipment (G 4) and the ASTM Recommended Practice for Laboratory Immersion Corrosion Testing of Metals (G 31) and the NACE Standard for Laboratory Corrosion Testing of Metal for the Process Industries (TM–01–69) are the general guides for immersion testing. This practice is very useful in making a preliminary list of the best candidate materials. However, these standards are most suited for the more common metals and alloys such as steels, aluminum alloys, and copper alloys. Certain procedures, e.g., cleaning methods, in these standards are not applicable to zirconium and its alloys. Although the ASTM Practice for Aqueous Corrosion Testing of Samples of Zirconium and Zirconium Alloys (G 2) was prepared specifically for zirconium and its alloys, it was designed for nuclear applications. Therefore, a tailored practice for conducting corrosion coupon tests on zirconium and its alloys in chemical environments is needed. Without such procedures, tests results may be invalid or flawed.

For example, field tests were conducted on zirconium and other metals and alloys in acetic acid environments [*3*]. Zirconium was the only metal tested to exhibit excellent corrosion resistance under most conditions. It suffered, however, severe general corrosion and pitting in acetic acid when the acid was contaminated with both acetic anhydride and copper ions. The presence of copper ions was the result of the corrosion of copper coupons which were tested at the same time. In fact, zirconium resists attack by a wide range of acetic acid and anhydride environments when such contamination is not a factor. Zirconium is an important structural material in the production of acetic acid and anhydride [*4*].

The corrosion group at Teledyne Wah Chang Albany (TWCA) has been actively testing zirconium and its alloys during the past decade. The group is often asked to examine the results, particularly unusual ones, of corrosion tests conducted by chemical companies. This experience is the basis for the following recommended procedures for conducting laboratory or field tests on zirconium and its alloys. Emphasis is placed on coupon quality and preparation, galvanic corrosion, test duration, contamination resulting from the corrosion of other metals, and handling of corroded coupons. The procedures recommended herein should be used in conjunction with applicable ASTM and NACE standards.

Coupon Identity

Zirconium ores generally contain a few percent of hafnium. Zirconium and hafnium are similar chemically and metallurgically, but differ markedly in their nuclear properties. Zirconium is almost transparent to thermal neutrons, and hafnium is highly opaque to thermal neutrons. As a result, there are nuclear and nonnuclear grades of zirconium and its alloys. The nuclear grades are essentially hafnium-free, and the nonnuclear grades may contain up to 4.5% hafnium. The alloy names Zircaloy, Zr-2.5Nb, and Zr1Nb apply to nuclear grade materials. Zircaloy is the general term for a series of zirconium-tin alloys containing minor amounts of iron, chromium, and nickel that were developed by the US Navy Nuclear Propulsion Program. Only Zircaloy-2 and Zircaloy-4 are still in common usage. For commercial applications, ASTM specifications list three grades, namely UNS R60702 (Grade 702), UNS R60704 (Grade 704), and UNS R60705 (Grade 705). Grade 702 is commercially pure zirconium, and Grades 704 and 705 are correspondingly close to Zircaloy-4 and Zr-2.5Nb, respectively. Commercial grades of zirconium and its alloys produced by TWCA are given a trade name, that is, ZIRCADYNE 702, 704, and 705. There are many other less common zirconium alloys and names.

The first step in corrosion testing is to correctly identify corrosion coupons. One common mistake is to use the name Zircaloy for other alloys, such as Zircaloy 705. The reason for this mistake is probably because of the familiarity and spelling of Zircaloy. When corrosion coupons need an identifying mark, a vibrating tool can be used. Record the alloy grade and coupon number.

Coupon Quality

It is impossible to determine if coupons are of good quality without chemical or metallurgical examination. Nevertheless, each coupon should be examined visually for irregularities such as stains, scratches, foreign particles, etc. Unusual features should be recorded. Surface condition is very important in corrosion resistance.

Zirconium coupons, sent to TWCA for examinations, were sometimes found to be of poor quality. They were supplied by various sources. One of the major problems is cross-contamination resulting from coupon fabrication. Examples of contaminated areas of several coupons are given in Table 1. Obviously, test results are invalid when these coupons are used. It is important to obtain corrosion coupons from reliable sources.

Precautions

Hazardous chemicals are used frequently in corrosion coupon preparation and testing. This is particularly true for zirconium and its alloys. First, zirconium and its alloys are covered with a hard and tightly bonded oxide that defies removal by ordinary chemical or mechanical means. Second, zirconium and its alloys are often evaluated for highly corrosive applications. Detailed information on safe handling of involved chemicals and zirconium should be obtained from competent sources.

TABLE 1—*Results of EDX analyses of contaminated areas of untested coupons from various sources.*

	Composition, wt %									
Element	1	2	3	4	5	6	7	8	9	10
Zr	83.08	97.83	16.15	99.11	83.56	43.35	91.71	38.35	61.24	79.55
Ti	...	...	1.27	...	0.60	...	...	...	0.37	...
Fe	...	2.17	4.05	...	...	1.79	...	15.22	8.54	13.59
Cr	...	...	...	...	...	...	...	3.65	...	...
Cu	...	...	...	...	...	...	...	...	3.01	1.40
Cd	...	...	...	...	...	...	...	7.63	...	...
Al	...	...	1.59	0.89	...	7.70	...	...	...	1.21
Si	14.25	...	34.48	...	7.90	15.27	8.29	24.98	2.67	4.26
Na	...	...	...	...	...	7.60	...	...	7.01	...
Mg	...	...	13.50	...	...	...	...	...	...	...
Cl	...	...	5.14	...	4.87	9.56	...	7.79	0.62	...
S	...	...	8.98	...	...	...	...	...	...	...
K	...	...	1.53	...	3.07	4.75	...	1.47	...	...
Ca	2.67	...	12.46	...	...	6.37	...	0.91	0.16	...
Zn	...	...	...	...	...	3.61	...	...	16.37	...

Preparation of Corrosion Coupons

Corrosion Coupons

The size and shape of corrosion coupons is affected by several factors and cannot be rigidly defined. Convenient standard coupons for laboratory and field tests are 25 by 50 by 1.6 mm (1 by 2 by 0.062 in.) and 50 by 50 by 1.6 mm (2 by 2 by 0.062 in.). A round coupon 38 by 1.6 mm (1.5 by 0.062 in.) or 50 by 1.6 mm (2 by 0.062 in.) is sometimes employed.

The edges of corrosion coupons should be machined or ground in order to eliminate cold-worked metal unless the effects of cold working are being studied.

Cleaning

Usually corrosion coupons with as-manufactured surfaces are tested without further surface treatment other than cleaning. Corrosion coupons can be cleaned in a cleaner such as Cole-Parmer's MICRO cleaner or in 5 to 10% aqueous ammonia. An ultrasonic device can be used if available. Use a nylon brush or other nonmetallic brush if required. Rinse cleaned coupons in running cold water for 5 min. Then coupons may be air-dried, wiped dry with a clean, lint-free cloth, or blown with clean, dry air. Handle cleaned coupons only with clean, lint-free gloves or forceps. When not being processed, enclose the coupons in a clean container or wrap in cloth, plastic, or clean heavy paper that will not affect weight or appearance.

Pickling

Pickling is necessary if one of the following situations exists:

1. The surface condition of coupons is poor.
2. The effects of pickling are being studied.
3. Coupons will be subsequently treated to form thick oxide films.

For unalloyed zirconium and the zirconium-tin alloys, the volumetric bath composition for pickling is 3.0 ± 0.5% of hydrofluoric acid (52%), 39 ± 10% of nitric acid (sp gr 1.42), and the remainder distilled water. The pickling bath temperature should not exceed 50°C, preferably maintained at 35°C.

For zirconium-niobium alloys, the volumetric bath composition for pickling is 9 ± 1% of hydrofluoric acid (52%), 30 ± 5% of nitric acid (specific grade 1.42), 30 ± 5% of sulfuric acid (sp gr 1.84), and the remainder distilled water. The pickling bath temperature should be controlled to 55 ± 5°C.

Corrosion coupons should be completely immersed in the bath. If a large number of coupons is pickled, the bath should be vigorously agitated. It takes about 30 to 60 s to get a good, smooth surface finish. However, the required pickling time is a function of temperature, acid concentration, and surface condition. Visual inspection can be exercised to determine the required time.

Pickled coupons should be transferred from the pickling bath to the first rinse tank as rapidly as possible. If any acid product remains on the surface or is allowed to dry on the surface, the coupons will not rinse clean and must be repickled. The first rinse tank contains cool flowing water. Coupons should be completely immersed for at least 5 min. The final rinse is in distilled water. It may be performed in either a dynamic or a static system. Rinsed coupons may be air-dried, wiped dry with a clean, lint-free cloth, or blown with dry air. They should be handled only with clean, lint-free gloves.

Detailed procedures for pickling are given in ASTM Standard G 2-88.

Methods of Oxide Formation

The corrosion resistance of zirconium and its alloys is due to a stable, protective, and strongly cohesive oxide film. This film forms spontaneously when a fresh surface is exposed to an oxygen-containing environment. It may be invisibly thin, but gives excellent corrosion resistance in many corrosives. In order to take full advantage of the unique properties of this protective zirconium oxide, several methods of oxide formation are possible. Thick oxide-coated metal has superb friction resistance, corrosion resistance, and electrical insulation. Normal methods include:

1. Autoclaving in high-temperature water or steam.
2. Formation in air at high temperatures.
3. Formation in a molten salt.

Autoclave film formation is common in the nuclear industry. In this process, a uniform film of high integrity can be formed in pressurized water at 360°C for 14 days or in high purity steam at 400°C for 1 to 3 days.

The most common film used in the CPI is that formed in air. Coupons are heated in a clean furnace at 550°C for 30 min to 6 h. This film varies in color from a straw yellow through an iridescent blue or purple, to a powdery tan or light grey.

The thickness of the oxide film formed in air, water, or steam ranges from less than one to several micrometers. This oxide film enhances corrosion resistance and serves as an excellent bearing surface for sliding contacts. It can be damaged by a striking action. Attempts to form a much thicker layer of oxide film with excellent properties in air, water, or steam have not been successful. Zirconium and its alloys undergo breakaway oxidation when the conditions are excessive.

However, a thick, protective, strongly cohesive oxide film can be formed on zirconium and its alloys by a patented process developed at TWCA [5]. In this process, coupons are treated in fused sodium cyanide containing 1 to 3% sodium carbonate, or in an eutectic mixture of sodium and potassium chlorides to which 5% sodium carbonate is added. Treatment is carried out at temperatures from 600 to 800°C for up to 50 h. A treatment time of several hours typically is used. The thickness of oxide film formed in the fused salt bath ranges from 20 to 30 μm. This oxide film has greatly improved resistance to abrasion and galling over thick oxides grown by other means.

Dimensions, Weight, and Inspection

Measure and weigh each clean, dry coupon. Dimensions determined to the third significant figure and mass determined to an accuracy of 0.1 mg are suggested. Do not weigh coupons until they are thoroughly dry and at the same temperature as the balance. Examine each coupon for folds, cracks, blisters, foreign material, luster, brown acid stain, etc. Reject any bad coupon or record any significant findings.

Corrosion Testing

Installation of Corrosion Coupons

In laboratory testing, zirconium coupons should not be placed in the same container with coupons of other metals. The supporting device and container should also not cause contamination of the test solution.

In field testing, zirconium coupons should be placed nearest the inlet of the process solution when other metals are also being tested. It is desirable to have the coupon or test rack securely fixed in place. Eliminate the possibility of galvanic effects resulting from metal-to-metal contact by using an insulating material.

Polytetrafluoroethylene tape, tube, and washers can be used to prevent the galvanic coupling. Properly oxidized Zircaloy materials can also be used for this purpose. Zirconium oxide is an excellent insulating material. Zircaloy-2 or Zircaloy-4 is preferred here since its resistance to breakaway oxidation is much better than that of unalloyed zirconium.

A note should be made about the location and position of test coupons in the testing unit. Preferably, corrosion coupons should be placed so that any flow of liquid will be against the edges of the coupons. The same condition of agitation of the liquid should then be encountered by all coupons.

Test Solutions

Test solutions should be prepared accurately from chemicals conforming to the specifications of the Committee on Analytical Reagents of the American Chemical Society and distilled water unless they are naturally occurring solutions or plant solutions. The pH and specific gravity of fresh and tested solutions should be measured and recorded. Minor constituents should not be overlooked because they often affect corrosion rates. If there is any doubt, the composition of the test solutions should be checked by analysis. In corrosion testing, one should always expect the unexpected. For example, significant amounts of chloride and fluoride have been found in reagent grade nitric and sulfuric acids [*6*].

The composition of the test solutions should be controlled to the fullest extent possible. Change in composition can occur, for example, resulting from evaporation or depletion. Evaporation losses may be controlled by a constant level device or by frequent addition of appropriate solution to maintain the original volume within ±1%. The use of a reflux condenser ordinarily precludes the need to add solution.

In some cases the composition of the test solutions may change as a result of catalytic decomposition or by reaction with the test coupons. These changes should be determined, if possible. Where required, the exhausted constituents should be replenished or a fresh solution provided during the course of the test.

Temperature of Solution

Temperature of the test solutions should be controlled within 2°C, and the temperature must be reported with the test results.

Aeration of Solution

Unless specified, the test solutions should not be aerated. Most tests related to process equipment should be run with the natural atmosphere inherent in the process, such as the vapors of the test solutions.

If aeration is required, test coupons should not be located in the direct oxygen or air stream from the sparger. Unrelated effects can be encountered if the gas stream impinges on the coupons.

If exclusion of dissolved oxygen is necessary, specific techniques are required, such as prior heating of the test solutions and sparging with an inert gas (usually nitrogen). A liquid atmospheric seal is required on the test vessel to prevent further contamination.

Solution Velocity

Effects of velocity are not usually determined in most laboratory tests, although specific tests have been designed for this purpose. In field testing, the velocity of the test solution should be measured and recorded.

Tests at the boiling point should be conducted with the minimum possible heat input, and boiling chips should be used to avoid excessive turbulence and bubble impingement. Cleaning may be needed to remove trace amounts of impurities in boiling chips before their usage. For example, amphoteric alundum granules, which may have some fluoride contamination, should be cleaned in boiling 20% sulfuric acid (H_2SO_4) for 24 h, rinsed in water, cleaned in boiling 40% nitric acid (HNO_3) for 24 h, rinsed in water, and dried.

In test solutions of high viscosity, supplemental controlled stirring with a magnetic stirrer is recommended.

Volume of Test Solution

The volume of the test solution should be large enough to avoid any appreciable change in its corrosivity during the test, either through exhaustion of corrosive constituents or by accumulation of corrosion products that might affect further corrosion. A minimum solution volume-to-coupon area ratio of 20 mL/cm^2 (125 $mL/in.^2$) is recommended.

Duration of Test

Zirconium and its alloys are normally either reactive or highly corrosion resistant when they are tested in a corrosive. In an incompatible environment, corrosion can show up within a short period of time, that is, a few hours to a few days. On the other hand, in a compatible environment, coupon weight can show little change (gain or loss) for years. Consequently, the commonly suggested test duration in hours, which is 50 divided by the corrosion rate in millimetres per year (mm/y) or 2000 divided by the corrosion rate in mils per year (mpy), may be excessive and impractical. For example, if the corrosion rate is 0.0025 mm/y (0.1 mpy), the suggested test duration would be 20 000 h!

An often-used test schedule at TWCA is the 2–4–2 day cycle. This schedule gives some indication about the time effect on the corrosivity of the test solution and the corrodibility of the test coupon.

Nevertheless, the duration of any test should be determined by the nature and purpose of the test. In studying the effects of a minor impurity, the duration of test can be 1 h or shorter, depending on the time required to measure an effect. In a confirmation test, the duration of the test can be 14 days to a year.

During the test, frequent checks should be made, if possible, at the test vessel for changes in solution color, temperature, pressure, bubbling, etc.

Removal of Coupons from Test

The condition and appearance of the holder and coupons after removal from the test should be noted and recorded. It may be desirable to photograph the holder and coupons. Coupons should then be rinsed in water and dried. They can be cleaned with a nylon brush or other nonmetallic brush if required. In removing the coupons, care should be taken to keep them in proper order relative to each other so that any coupon may be identified from the original record of its position on the holder. This is important if corrosion has been so severe that identification marks have been removed. Corroded coupons should be handled by forceps.

Coupons of zirconium and its alloys can be covered with a layer of pyrophoric film when they are tested under certain specific conditions, for example, a stagnant solution of 77.5% sulfuric acid and 200 ppm ferric ion at 80°C for ten days [7]. Treating in hot air or steam can eliminate this pyrophoric tendency. This takes 20 to 30 min at 250°C. It should be noted that most corroded coupons do not have a pyrophoric layer. The formation of pyrophoric films is possible but not guaranteed when *both* the following conditions exist:

1. The test solution is stagnant or there are stagnant areas (e.g., under a gasket) on the test coupons.
2. The test solution can cause localized corrosion on a macroscale.

To clean exposed coupons, a nonmetallic brush or rubber stopper can be used if necessary. There is not an applicable chemical or electrolytic cleaning method for zirconium and its alloys since zirconium oxide and most corrosion products on zirconium alloys are very inert.

Interpretation and Calculation of Results

After exposed coupons have been cleaned, they should be reweighed with an accuracy corresponding to that of the original weighing. The mass change during the test period can be the principal measure of corrosion.

The pH and specific gravity of spent solutions should be measured and recorded. Spent solutions should be saved for a reasonable period of time. They should be analyzed if test results are unexplainable.

Each tested coupon should be examined carefully for the presence of any pits or unusual marks. If there are any pits, the average and maximum depths of pits are determined with a pit gage or a calibrated microscope.

If tested coupons are suspected of being subject to intergranular attack, a cross section of the coupons should be examined microscopically for evidence of such attack.

Tested coupons may be subjected to simple bending tests to determine whether any embrittlement has occurred. Metallographic examination should be carried out on coupons if hydrogen embrittlement is a concern.

The corrosion rate of each coupon should be calculated as follows

$$\text{Corrosion rate, mm/y} = 87.6 \frac{\Delta W}{D \times A \times t}$$

$$\text{Corrosion rate, mpy} = 534 \frac{\Delta W}{D \times A \times t}$$

where

ΔW = weight loss, mg,
D = density (6.50 for Grades 702 and 704 and 6.53 for Grade 705), g/cm^3,
A = area of coupon, cm^2 (top equation), or in.^{2} (bottom equation), and
t = time, h.

Report

It is important to report all data as completely as possible. Expansion of the testing program in the future or correlating the results with other test results will be possible only if all pertinent information is properly recorded. The following checklist is a guideline.

1. Names of personnel and laboratory involved.
2. Date.
3. Identification of coupon material and number.
4. Form and metallurgical conditions of coupons.
5. Treatment used to prepare coupons.
6. Weights and dimensions of coupons before and after the corrosion testing.
7. Composition of the test solution.
8. Volume of test solution.
9. The pH and specific gravity of the test solution before and after the corrosion testing.
10. Type of vessel used for test.
11. Test temperature, pressure, aeration.
12. Agitation.
13. Duration of each test.
14. Visual appearance remarks of each coupon before and after the corrosion testing.
15. Evaluation of attack if other than general.
16. Cleaning method.
17. Corrosion rate.
18. Minor occurrences or deviations from the proposed test program should be reported if known.

References

[*1*] *Anti-corrosion Methods and Materials,* Vol. 30, No. 8, 1983, p. 3.
[*2*] Webster, R. T., "Zirconium Cost Effective Uses in Corrosive Applications," Paper No. 459, *Corrosion/87,* NACE, Houston, TX, 1987.
[*3*] Takaaki, S., Takamura, A., and Segawa, S., *Boshoku Gijutsu,* Vol. 15, No. 2, 1966, pp. 49–55.
[*4*] "Zirconium Heat Exchangers Resist Corrosion in the Production of Acetic Acid and Anhydride," *Outlook,* Vol. 4, No. 2, 1983, p. 1, Teledyne Wah Chang Albany, Albany, OR.
[*5*] Haygarth, J. and Fenwick, L., "Improved Wear Resistance of Zirconium by Enhanced Oxide Films," *Thin Solid Films,* Vol. 118, 1984, pp. 351–362.
[*6*] Yau, T. L., "Chemical Impurities Create New Challenges in Material Selection," *Outlook,* Vol. 9, No. 4, 1988, p. 4, Teledyne Wah Chang Albany, Albany, OR.
[*7*] Yau, T. L., "Methods to Treat Pyrophoric Film on Zirconium," *Industrial Applications of Titanium and Zirconium: Third Conference, ASTM STP 830,* ASTM, Philadelphia, PA, 1984, pp. 124–129.

Richard S. Treseder[1]

A Comparison of Sulfide Stress Cracking Tests

REFERENCE: Treseder, R. S., "**A Comparison of Sulfide Stress Cracking Tests,**" *Corrosion Testing and Evaluation: Silver Anniversary Volume, ASTM STP 1000,* R. Baboian and S. W. Dean, Eds., American Society for Testing and Materials, Philadelphia, 1990, pp. 312–318.

ABSTRACT: Sulfide stress cracking, a form of hydrogen embrittlement, first became a serious problem in the oil industry in 1951. Subsequent improvements in the metallurgy of steels for high-pressure gas and oil wells and improved selection methods for high-strength alloys have been based on laboratory test methods. Of the large number of test methods that have been used, five have survived: the Shell bent beam test, the uniaxial load tension test, the double-cantilever-beam test, the C-ring test, and the slow strain rate test. Major features of these tests are compared in terms of their applicability to specific sulfide stress cracking problems. In addition, a general comparison is made of the testing requirements for the sulfide stress cracking system and for anodic stress corrosion cracking systems involving hydrogen sulfide. These comparisons illustrate the need to design environmental cracking tests which reflect both corrosion mechanism factors and application requirements.

KEY WORDS: review, sulfide stress cracking (SSC), oil industry, laboratory tests, tension test, bent beam test, double-cantilever-beam test (DCB), C-ring test, slow strain rate test, hydrogen sulfide, low alloy steels, corrosion resistant alloys (CRAs)

The first major equipment failures that were identified as sulfide stress cracking (SSC) failures were reported in 1951 and 1952 and involved relatively high-strength steel tubing and casing in sour gas wells in the US and Canada. These were followed shortly by the catastrophic failure of drill pipe and casing in the Lacq field in France. As a result of these failures early industry practice was to select steels for sour service on the basis of hardness. A maximum of 20 HRC was commonly used. Some operators restricted tubular goods to a minimum yield strength of 380 MPa (55 ksi) and a maximum yield strength of 550 MPa (80 ksi). With greater understanding of the sulfide stress cracking effect, new SSC-resistant tubular steels were developed. Currently, steels with a specified minimum yield strength of 620 MPa (90 ksi), a maximum yield strength of 720 MPa (105 ksi), and a maximum hardness of 26 HRC are being used with the prospect of raising this strength level in the near future. This increase in strength of tubular steels acceptable for sour service has permitted development of sour gas reservoirs with depths of 6000 m (20 000 ft) as contrasted to the 3000-m (10 000-ft) limit existing in 1951 [*1*].

These developments were made possible by the existence of reliable laboratory tests for evaluating SSC resistance. Since 1951 a large number of test methods have been used, included the following:

1. U-bend.
2. Ductility test after exposure.

---

[1] Consulting corrosion engineer, Oakland, CA 94611.

3. Two-point beam.
4. Three-point beam.
5. Four-point beam.
6. Cantilever beam.
7. Tuning fork.
8. C-ring.
9. Direct tension.
10. Double cantilever beam.
11. Slow strain rate.

The methods were patterned after commonly used stress corrosion cracking methods [2]. Specimens were either smooth or with a stress raiser such as a notch and with either a fixed load or fixed deformation. In each case there have been variations of the test environment and means of evaluation. Of these many tests five have found general acceptance in the oil industry. One of these has been standardized by NACE [NACE Standard for Testing of Metals for Resistance to Sulfide Stress Cracking at Ambient Temperatures (TM0177–86)]. The other four tests are in the final stages of standardization by NACE Committee T–1F. This paper is a review of the characteristics of these five test methods, with emphasis on the roles of engineering requirements and cracking mechanism in the selection of specimen features and test procedures. Since many of the latter are common to well-known environmental cracking test methods, this discussion will concentrate on features that are specific to the sulfide stress cracking problem.

Test Factors

Specimen Size

The engineering products of main concern are tubular goods, primarily tubing and casing, and these have dictated the specimen size requirements. A typical tubing size is 73 mm (2.875 in.) outside diameter and 5.5 mm (0.217 in.) wall thickness. Most early failures were observed transverse to the tubing axis, indicating axial tensile stress to be the dominant stress factor. This supported the concept of tension or beam-type specimens with relatively narrow widths and with the long direction of the specimen parallel to the axis of the tubing.

Tensile Load

Although the design load in axial tension for tubing and casing is significantly below the specified minimum yield strength, the presence of stress raisers plus bending and tonging effects could be expected to result in local stresses exceeding the yield strength. Therefore, some of the tests have incorporated plastic deformation as a test factor.

Environment

In 1951 and 1952 there was no agreement as to the mechanism of the observed failures. Some thought it was a form of hydrogen embrittlement and others considered it to be a form of stress corrosion cracking. The currently accepted explanation is that the failures of low-alloy steels result from hydrogen stress cracking, with the hydrogen being provided by corrosion by hydrogen sulfide in the presence of water (NACE TM0177–86). This conclusion has simplified the test procedure since it can be argued that a single test environment should suffice, providing the amount of hydrogen entering the steel corresponds to that which could enter under the most severe well conditions.

Hydrogen entry was shown to be increased by lowering the pH and was not affected significantly by increasing hydrogen sulfide concentration beyond a relatively low value. This resulted in the acceptance of a low-pH test solution in equilibrium with hydrogen sulfide gas at 1 atm. A pH value of 3 was chosen. This corresponds to the pH resulting from the high combined pressure of hydrogen sulfide and carbon dioxide found in deep gas wells. To avoid use of pressure equipment, 0.5% acetic acid was added to provide the required pH. The acetic acid addition was rationalized from the known presence of aliphatic acids in some natural gas reservoirs. Chloride ion, in the form of sodium chloride, was added to the test solution to simulate the high salt content of some well fluids and to provide a more severe environment, particularly for alloys. The concentration chosen was 5%. This hydrogen sulfide-saturated, 0.5% acetic acid, 5% sodium chloride solution is commonly known as the "NACE solution" because of its use in NACE TM0177–86.

Temperature

Since hydrogen effects in steels have been found to decrease with increasing temperatures above ambient temperature, selection of 20 to 25°C as a test temperature was both convenient and mechanistically acceptable [*3*].

Duration

Time to failure was found to be quite fast for susceptible steels, failures being observed in a few hours under severe constant load or constant deformation conditions. To be conservative, test durations of 21 to 30 days commonly have been used.

Corrosion-Resistant Alloys

In oil and gas wells general corrosion is controlled either by using carbon and low-alloy steels plus inhibition or by using corrosion-resistant alloys (CRAs). CRAs include stainless steels (austenitic, ferritic, martensitic, and duplex), nickel-base alloys, cobalt-base alloys, titanium alloys, and zirconium alloys. For CRAs exposed to sour gas systems, the amount of hydrogen required to initiate sulfide stress cracking failure may not result from normal corrosion, but could occur under conditions of galvanic contact with a less noble metal (such as carbon steel) or under conditions of cathodic protection. This factor has been introduced into some sulfide stress cracking tests by coupling the test specimen to carbon steel or by an applied potential.

Acceptance Criteria

In early laboratory tests it was demonstrated that all steels would fail by cracking in a severe test environment if strained to a sufficient degree [*4*]. However, field experience had shown that only high-strength steels above about 550-MPa (80-ksi) yield strength were subject to failure. From this fact it was concluded that normal field conditions were such that severe straining did not occur, and that susceptibility of steels to cracking was related to the strain required for failure. Thus it became a matter of correlating field experience with laboratory test results to define an acceptability criterion as described below for the bent beam test.

Test Methods

Bent Beam Test

This three-point loaded bent beam test is based on the Shell Sc test developed between 1952 and 1958 [*4,5*]. It was used extensively by Shell and others in the early development of SSC-resistant steels. It is of interest that this relatively simple, empirical test method has survived despite subsequent development of more sophisticated test methods. For example, it was one of the tests used recently in research aimed at developing SSC-resistant steels with specified minimum yield strengths of the order of 700 MPa (100 ksi) [*6*].

The Sc test makes use of a small beam [4.6 by 1.5 by 67 mm (0.18 by 0.06 by 2.65 in.)] with stress raisers in the form of two small drilled holes, 0.7 mm (0.028 in.) diameter, in the center of the beam. The beam is loaded with a screw at the center point and is supported at each end. The test solution is a 0.5% acetic acid solution saturated with hydrogen sulfide at atmospheric pressure. Tests are made at 20 to 25°C. Multiple tests are made with measured variations in the beam deflection. A statistical determination is made of the beam deflection required for a 50% probability of failure in 21 days. The deflection value is converted to a nominal maximum stress value in ksi, which is divided by ten to give the Sc value. The Sc value becomes a number for rank ordering the sulfide stress cracking resistance of the steel being tested. Typically, susceptible steels such as API Grade P–110 steel would have Sc values in the range from 2 to 5, whereas resistant steels like API Grade J–55 steel would range from 15 to 20. Correlation with field experience led to critical acceptance Sc values in the range from 10 to 12 [7]. Use of a unique number rather than a stress or strain value was intentional to discourage engineers from assuming that a critical stress or strain value obtained in such an arbitrary test could be used as a design parameter.

The 50% probability of failure concept follows the practice used in other failure/no failure systems such as toxicity studies. The advantage of this approach as compared to the threshold stress approach is that it is less subject to influence by an erratic test result.

Advantages of the Sc test are:

1. The spread of results that are obtained on both sides of the acceptability criterion provides a good tool for research on improved steels since one has a measure of the nearness to the desired goal.
2. The test evaluates the effect of plastic strain, thus simulating a common field condition.
3. The small area of maximum strain allows evaluating SSC susceptibility of localized areas and minimizes inclusion-related hydrogen effects (see below).
4. The test can be used to evaluate environmental factors such as temperature, pH, and hydrogen sulfide concentration.

A limitation of the Sc test is the constant deformation aspect, which deemphasizes crack growth factors.

Tension Test

It was not until 1977 that industry agreed on a standard test method (NACE TM0177). This method uses a smooth, tension bar specimen as described in the ASTM Standard Practice for Preparation and Use of Direct Tension Stress Corrosion Test Specimens (G 49). The specimen is exposed under constant load or sustained load to a solution of 0.5% acetic acid plus 5% sodium chloride saturated with hydrogen sulfide at 1 atm. The test results in an apparent threshold stress for failure in 30 days (expressed as percent of yield strength). API Specification 5CT for Casing and Tubing requires the minimum threshold stress to be 80% of the specified minimum yield strength for Grade C90 products.

One of the stated advantages of this test is that it uses a specimen with a well-defined stress state. One drawback of NACE TM0177 is that the presence of nonmetallic inclusions may lead to hydrogen-induced cracking (HIC) related failures in lower strength steels at lower threshold stress values than normally expected for such steels [*8*]. By comparison, the probability of such a failure in a single Shell Sc test is very much lower than in a NACE TM0177 test since the probability of a significant inclusion existing in the small volume of metal under maximum strain in the Sc test is very low.

Double-Cantilever-Beam Test

The double-cantilever-beam (DCB) test uses fracture mechanics techniques in the evaluation of the SSC resistance of tubular steels [*9*]. Typically it employs a 9.5 by 25 by 100 mm (0.375 by 1.0 by 4.0 in.) specimen with side grooves and loaded with a double taper wedge. In some cases a precracked specimen is used. A typical test duration is 14 days.

The DCB test has the major advantage of providing a numerical result, critical stress intensity, that has general engineering acceptance. In contrast to the Sc test, it emphasizes crack growth factors rather than crack initiation factors. The fact that the DCB test provides a rank-ordering number rather than a failure/no failure result makes it useful in the development of improved steels and alloys. One disadvantage is the specimen size, which limits its application, although a subsize specimen, 4.8 mm (0.188 in.) thick, is considered acceptable in some cases.

C-Ring Test

This test utilizes an unnotched C-ring type specimen machined from tubing or bar stock as described in the ASTM Standard Practices for Making and Using C-Ring Stress Corrosion Test Specimen (G 38). Load is applied by a conventional bolt assembly. Test duration is 30 days. Specimens are exposed at varying levels of outer fiber stress, and an apparent threshold stress for failure is determined. The advantage of this test is that it evaluates the effect of circumferential stress and thus serves as an adjunct to the NACE TM0177 tension test when testing tubular goods.

Slow-Strain-Rate Test

The slow-strain-rate test has seen only limited use in sulfide stress cracking testing aimed at finding improved steels. One reason may be the difficulty of establishing a criterion for failure in borderline cases. However, it has been very useful in evaluating the stress corrosion cracking susceptibility of CRAs as a function of environmental factors such as gas composition, gas pressure, temperature, chloride ion concentration, and free sulfur concentration [*10*].

The test details follow those of conventional methods for slow-strain-rate testing. Dimensions of the test section of the uniaxial tension specimen are commonly 3.8 mm (0.150 in.) diameter by 25 mm (1.0 in.) long, with an overall diameter of about 6 mm (0.25 in.). A typical extension rate for such a specimen is 1×10^{-4} mm/s (4×10^{-6} in./s). Tests commonly are made at temperatures in the range from 90 to 230°C (200 to 450°F) in the presence of H_2S and CO_2 at pressures as high as 35 MPa (5000 psi).

Other Failure Mechanisms

Stress Corrosion Cracking

The mechanistic differences between sulfide stress cracking and stress corrosion cracking (anodic type) are significant and influence the test methods used. Stated simply, the critical variable in SSC of carbon and low-alloy steels is the strain required to initiate failure in an arbitrarily selected severe environment. In stress corrosion cracking the critical variables are the electrochemical polarization characteristics of the metal/environment system, which control the anodic processes involved in crack initiation and growth. Therefore, the comparison of stress corrosion cracking susceptibility of different alloys is done by determining the critical environmental factors (temperature, chloride concentration, etc.) required to cause failure of a severely stressed specimen.

For many alloys in sour gas systems there is the possibility of failure occurring from either sulfide stress cracking or stress corrosion cracking. Obviously this complicates the testing program by requiring evaluation by two different testing procedures.

Hydrogen-Induced Cracking

Hydrogen-induced cracking (HIC) is also called step-wise cracking and hydrogen blistering. It differs from sulfide stress cracking in that it is associated with inclusions in the steel and is observed with lower strength steels. Crack initiation results from formation of molecular hydrogen at inclusions and discontinuities in the steels, and crack growth results from the applied and residual stresses aided by the embrittling effect of hydrogen. HIC is prevented by controlling the number, size, and shape of inclusions, particularly sulfide inclusions. Evaluation is via tests which measure the number and size of subsurface cracks following exposure to a standard hydrogen sulfide solution, which may be similar to that used for SSC testing. As noted above, this type of failure may complicate the evaluation of the SSC susceptibility of some carbon steels when certain test methods are used.

Conclusions

The complex nature of the sulfide stress cracking testing problem results from: (1) existence of three possible failure mechanisms (sulfide stress cracking, stress corrosion cracking, and hydrogen-induced cracking), which can occur with steels exposed to sour well environments; and (2) the wide range of equipment types and well environments that exist in sour well operations.

Each of the five tests discussed has been shown to have a unique property that has resulted in its survival as a test for evaluating sulfide stress cracking of materials for the oil and gas industry.

The Shell bent beam test has been used because: (1) it emphasizes the effect of localized plastic strain on crack initiation, an important aspect of SSC of steels; and (2) the test evaluation technique gives a rank ordering number useful in research aimed at improved steels and in evaluating critical environmental factors such as temperature and hydrogen sulfide concentration.

The tension test (NACE TM 0177–86) has been used primarily as an acceptability test because of its simplicity and its versatility for a wide range of materials.

The DCB test has been used because it emphasizes factors controlling crack growth rate and provides a rank ordering number of engineering significance (critical stress intensity) useful both as an acceptability criterion and as an evaluation tool in research aimed at improved steels.

The C-ring test has been useful in evaluating anisotropic properties of tubular steels that could be factors in hoop stress-induced failures and thus provides a useful acceptability test.

The slow-strain-rate test has been useful in evaluating environmental effects, particularly those involving the stress corrosion cracking susceptibility of CRAs.

References

[1] Treseder, R. S. and Tuttle, R. N., "Historical Review of the Sulfide Stress Cracking Problem in Oil and Gas Production," *Proceedings*, Sixth Asian-Pacific Corrosion Control Conference, Singapore, 1989, Asian-Pacific Materials & Corrosion Assn., Sydney, Australia.
[2] *Metals Handbook*, 9th ed., Vol. 13, American Society of Metals International, Metals Park, OH, 1987, pp. 245–282.
[3] *Stress Corrosion Cracking and Hydrogen Embrittlement of Iron Base Alloys*, National Association of Corrosion Engineers, Houston, TX, 1977, pp. 147–161.
[4] Fraser, J. P. and Treseder, R. S., *Corrosion*, Vol. 8, No. 10, 1952, p. 342.
[5] Fraser, J. P., Eldredge, G. G., and Treseder, R. S., *Corrosion*, Vol. 14, No. 11, 1958, p. 37.
[6] Kaneko, T., Okada, Y., and Ikeda, A., *Corrosion*, Vol. 45, No. 1, 1989, p. 2.
[7] Treseder, R. S. and Swanson, T. M., *Corrosion*, Vol. 24, No. 2, 1968, p. 31.
[8] Greer, J. B., *Materials Performance*, Vol. 16, No. 9, 1977, p. 9.
[9] Heady, R. B., *Corrosion*, Vol. 33, No. 3, 1977, p. 98.
[10] McIntyre, D. R., Kane, R. D., and Wilhelm, S. M., "Slow Strain Rate Testing for Materials Evaluation in High Temperature H_2S Environments," *Corrosion/86*, paper No. 149, National Association of Corrosion Engineers, Houston, TX, 1986.

Leah G. Everhart[1] *and Christopher E. Price*[2]

Stress Corrosion Cracking in Alloy 400 (UNS NO4400) at Room Temperature

---

REFERENCE: Everhart, L. G. and Price, C. E., "**Stress Corrosion Cracking in Alloy 400 (UNS N04400) at Room Temperature,**" *Corrosion Testing and Evaluation: Silver Anniversary Volume, ASTM STP 1000,* R. Baboian and S. W. Dean, Eds., American Society for Testing and Materials, Philadelphia, 1990, pp. 319–334.

ABSTRACT: Selective pitting studies were used to determine environments likely to cause stress corrosion cracking (SCC) in Alloy 400. Slow strain rate tests were performed on waisted specimens, with solution composition and concentration, strain rate, grain size, and prior cold work as variables. It was found that environments which caused pitting also caused SCC; examples include ammonium hydroxide, ammonium persulfate, and hydrofluoric acid in the presence of an oxidizer.

As in the case of both hydrogen and liquid metal embrittlement of Alloy 400 and other nickel-base alloys, the SCC at low strain levels was intergranular with a transition to transgranular at higher strains. The fractography of the SCC resembled that of the other embrittling environments.

KEY WORDS: corrosion, stress corrosion cracking, pitting, Alloy 400, intergranular cracking, transgranular cracking

The efficiency of detecting general corrosion has been improving rapidly, resulting in new specialized alloys that resist general corrosion. This allows materials to be used in more aggressive environments, with increased severity of the operating stresses, temperatures, and concentrations. Consequently, localized corrosion is on the rise, leading to a great increase in the frequency of failures due to environmental-assisted cracking (EAC). EAC introduces a high potential for catastrophic failure. This disaster potential is often compensated for by the use of overly conservative design. With the increasing cost of materials and the severity of many common environments, overdesigning is an insufficient answer.

One of the most important material systems utilized in industries for general corrosion resistance is stainless steel. Stainless steels, however, are often subject to EAC. As the corrosion resistance of stainless steel is often improved by increasing the molybdenum content, it is distressing that the presence of molybdenum has been shown to have a detrimental effect on the stress corrosion cracking (SCC) resistance in some environments [*1,2*]. The nickel-base alloys generally are used to combat SCC where austenitic stainless steels have failed. However, two events have occurred that necessitate an increased knowledge of SCC resistance [*3,4*]. First, there is now an almost continuous range of alloy content from stainless steels to nickel-base alloys. Second, the nickel-base alloys are now being used under more severe conditions.

---

[1] Research engineer, The Johns Hopkins University, Applied Physics Laboratory, Baltimore, MD 20707; formerly a graduate student at Oklahoma State University.

[2] Professor, School of Mechanical and Aerospace Engineering, Oklahoma State University, Stillwater, OK 74078.

Due to their use in extreme environments, the tendencies of nickel-base alloys towards EAC must be understood and the susceptibility anticipated. It has been determined, for example, that many nickel-base alloys can experience hydrogen embrittlement (HE) at room temperature [*5–10*]. Additionally, nickel-base alloys are susceptible to liquid metal embrittlement (LME), at least by mercury [*11*]. In some instances, alloys that were found to be resistant to LME in slow strain rate tests (SSTs), such as Alloys 800 and 825, were severely embrittled under cyclic loading [*12*]. Nickel-base alloys have generally been considered to be resistant to SCC [*4*]. However, the similarities of susceptibility to cracking in stainless steels and nickel-base alloys, as noted by Jones [*13*], imply that SCC could become a major problem. Kolts [*4*] goes as far as to state that virtually every nickel-base alloy is susceptible to SCC in chloride solutions if the proper conditions exist.

Several cases of SCC in nickel-base alloys at elevated temperatures have been cited in recent years, often associated with the segregation of damaging elements to the grain boundaries [*14–24*]. In particular, a problem has arisen with Alloys 600 and ×750 in nuclear power plants [*21–24*]. This is a theme of a recent international symposium on environmental degradation of materials in nuclear power systems [*25*]. Further, since diverse nickel-base alloys suffer HE and LME at room temperature, it is likely that there are many environments that can cause SCC at room temperature. This has been demonstrated for Alloy 600 in tetrathionate and thiosulfate solutions [*26*].

SCC is caused by localized corrosion, as is pitting; the two often occur together, with the attack of both austenitic stainless steels and aluminum alloys in chlorides being the most obvious examples. A material's susceptibility to pitting at room temperature is easy to establish. Since SCC cracks often initiate at pits, pitting studies may provide a guide to SCC susceptibility. For this reason, preliminary observations of the pitting characteristics of several nickel-base alloys in an oxidizing environment were used as a prelude to a more detailed study upon Alloy 400, involving both pitting experiments and SSTs.

The scope of this study has four main objectives:

1. To illustrate that pitting can occur in different nickel-base alloys at room temperature.
2. To discover environments that cause pitting in Alloy 400, in addition to aerated HF (see later).
3. To seek a correlation between pitting and SCC in Alloy 400.
4. To compare the cracking characteristics obtained with Alloy 400 suffering SCC with those obtained after HE and LME.

Alloy 400 (UNS N04000)

The emphasis placed on Alloy 400 stems from the observation that it is the nickel alloy system most susceptible to EAC [*10–12*]. Alloy 400 is a two-to-one nickel-copper solid solution alloy that is also available in an age-hardening version Alloy K500 (NO5500). It has comparatively poor mechanical properties in many service situations. For example, the fatigue limits of copper and nickel in air are above their yield strength, but with Alloy 400, it is less than half the yield strength [*12*]. EAC failures of Alloy 400 in hydrogen or mercury may occur at only 5% elongation [*27,28*]. Service failures of Alloys 400 and K500 in the oil industry, due to HE, have been reported recently [*29,30*]. Fatigue in mercury may decrease the lifetime of Alloy 400 by more than a hundredfold [*12*]. Much of the EAC damage is caused by ready intergranular (IG) cracking. It is not clear why this occurs, but phosphorous segregation can sometimes be a factor [*27*].

Caustics are known to cause SCC in Alloy 400 at elevated temperatures [*31*]. At room temperature, the only deleterious service environment recorded is hydrofluoric acid vapor;

immersion in the liquid is harmless [*32–34*]. Several failures in this environment, mostly involving sheet specimens, have been reported. Both IG and transgranular (TG) fractures, as well as longitudinal splits on cold worked material, have occurred. The isocorrosion chart for Alloy 400 in hydrofluoric acid indicates only slight attack at room temperature and is insensitive to HF concentration above 20%; the rates given are <1 mils/year (air free), <10 mils/year (aerated) [*31*]. Graf and Wittich [*35*] conducted laboratory experiments on 0.3-mm-thick sheet specimens of different nickel-copper alloys. The study involved the influence of temperature and concentration of copper fluoride (CuF_2) additions to the hydrofluoric acid. They determined that the time to fracture decreased with increasing temperature, over the range from 12 to 63°C, generally independent of the HF and CuF_2 concentrations. It was also noted that alloys in the Alloy 400 range of approximately 30% copper performed the worst. This may be expected since the composition of Alloy 400 corresponds to the highest general corrosion resistance in the nickel-copper system [*31*]. It would imply a heightened sensitivity to localized corrosion.

Experimental Procedure

Materials

The alloys studied are 400 (N04400) and K500 (N05500), to a lesser extent, supplied as 12.7-mm-diameter rod. Some preliminary pitting tests utilized 12.7-mm-diameter hot-rolled rods of other nickel-base alloys. Additional pitting studies were conducted with 1.5-mm-thick coupons, approximately 25 by 12 mm, of Alloy K500 sheet specimens in the solution heat-treated condition.

The SST specimens of Alloy 400 were annealed in a mild vacuum, 15 Pa pressure, at temperatures of 750 to 1050°C for periods of up to 12 h to give grain sizes of 35 to 350 μm. This was followed by furnace cooling under vacuum.

Surface Preparation

A 600-grit finish was used for immersion tests on the nickel-base alloys. The Alloy K500 coupons were sanded through 600 grit, mechanically polished through 0.05-μm alumina, using flooded wheels at low speeds, then chemically polished at 90°C in mixed acids [*36*].

For SSTs, the specimens were mechanically polished through a 600-grit finish, cleaned, and lightly etched by immersion in a 50/50 solution of nitric and acetic acids for 45 s. Finally, they were rinsed in water, flooded with methanol, and blow-dried with warm air.

Immersion Tests

For exploratory pitting tests on nickel-base alloys, the specimens were placed in covered petri dishes containing solutions of hydrofluoric acid with copper chloride. The specimens were observed in place for up to 26 days; upon removal, they were examined before and after rinsing and drying.

The pitting studies on Alloy K500 coupons utilized twelve different solutions. The coupons were immersed in covered 50-mL containers containing 30 mL of prepared solutions. The temperature was 23°C; the solutions were not agitated and not aerated specifically, but the environment above the solutions was air. Alloys K500 and 400 have similar chemical properties and essentially identical chemical behavior [*37*]. Therefore, the solutions were selected based upon the anticipation of slight attack, in the range from 0.25 to 1.25 mm per year, of the appropriate order for pitting, largely using data from Hoyt [*38*]. Environments were selected to encompass a wide range of pH, confined to comparatively common systems for Alloy 400, while emphasizing short time tests, to correlate with subsequent SSTs. Accordingly, the coupons were removed for study within the first hour and then hourly for periods of up to 30 h. Upon final removal from solution, each coupon was rinsed with water, sprayed with methanol, and blow-dried with warm air.

Slow Strain Rate Tests

The SSTs used waisted specimens of a 6.35-mm minimum diameter that gradually increased to 12.7 mm at the shoulders at the end of the gage length, 44 mm. An advantage of this geometry is the strain gradient, hence a damage gradient, along the gage length, which maximizes the information obtained from each test. The SSTs were conducted at room temperature on an MTS machine under displacement control. The ram speeds were between 3.6×10^4 and 1.8×10^6 s for a 76-mm displacement, giving initial strain rates at the gage length center of 3×10^{-5} to 6×10^{-7} s^{-1} approximately. These strain rates were based on prior measurements with small strain gages [*12*]. Time constraints did not allow the use of strain rates of the order of 10^{-8} s^{-1}, which are sometimes optimum for SCC experiments.

Preliminary tests were conducted in air to permit the direct measurement of the strain at any location at any given time. For subsequent tests, the appropriate selected liquids were contained in a poly(methyl methacrylate) (PMMA) container that surrounded the specimen. The container had a neoprene O-ring to ensure a tight seal at the bottom of the test section; the container lid had a 12.7-mm-diameter opening at its center. The top of the chamber rested just below the upper shoulder of the specimen, leaving a gap sufficient for the addition of fluid, for bubbling air through, or to allow a vapor zone. Several tests were conducted with the chamber filled to just above the waist.

Observations

Surfaces of all specimens were observed under a stereoscopic zoom microscope (SZM) at up to ×70 magnification. Pertinent samples were prepared for view under a metallograph. Additionally, selected specimens were studied in a scanning electron microscope (SEM).

Results

Immersion Tests on Nickel-Base Alloys

After the immersion of nine different nickel-base alloys in a 0.5 *M* $CuCl_2$, 1.0 *M* HF acid solution for 26 days, three alloys showed gross general attack and five showed pitting. One alloy was unaffected, as viewed under a SZM (Table 1). The pitting that occurred ranged from several large pits, over 1 mm in depth and breadth, in the Alloys 825, 800 and ×750, to occasional small but deep pits in Alloy 600, to numerous shallow pits in Alloy 718. The alloy that seemed to be unaffected by this solution was 625. However, small pits were detected in the SEM as well as preferential grain boundary attack (Fig. 1). The very different nature of the pitting in Alloys 600 and ×750 is shown for comparison in Fig. 2. Within the pits of Alloy ×750, the corrosion was TG, with individual grain facets distinct.

Immersion Tests on Alloy K500

The observations from the immersion of the coupons in twelve different solutions are summarized in Table 2. A wide variation in corrosion behavior occurred, with appreciable

TABLE 1—*Appearance of nickel alloy coupons after a 26-day immersion in a 0.5* M $CuCl_2$, *1.0* M *HF solution. The last column ranks the alloys (1 is most) in terms of total corrosion, based on appearance.*

Alloy	UNS Number	Top Surface	Bottom Surface	Rank
200	N02200	C	C	3
400	N04400	C	C	1
K500	N05500	C	C	1
600	N06600	B-C	B	7
625	N06625	A	A	9
718	N07718	B	A	8
×750	N07750	B-C	B	6
800	N08800	B-C	B	5
825	N08825	B-C	B	4

NOTE: A = no change, B = pitting, C = general attack, with deposits.

differences from the behavior anticipated from the data of Hoyt [*38*]. However, these tests were for screening purposes only and longer time tests may have given a better correlation. From these observations, solutions based on ammonium hydroxide, ammonium persulfate, and lead chromate, as well as HF-based solutions, were considered to be appropriate for SSTs. Lead chromate was later deleted from this list because of possible complications due to sediments.

The pitting in ammonium persulfate solutions was explored further as a function of solution concentration, time, and grain size and condition. The time factor was considered to be critical because a typical SST lasted about 12 h. The extent of the pitting was found to increase as the solution concentration rose from 0.0125 to 0.4 *M*. General corrosion became

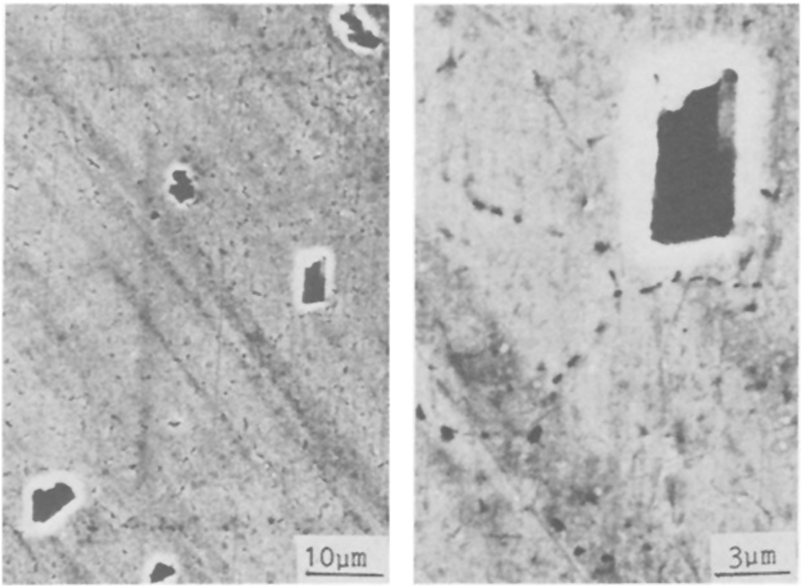

FIG. 1—*Small isolated pits in Alloy 625, with grain boundary attack visible at a higher magnification, after a 26-day immersion in a 0.5* M $CuCl_2$, *1.0* M *HF solution.*

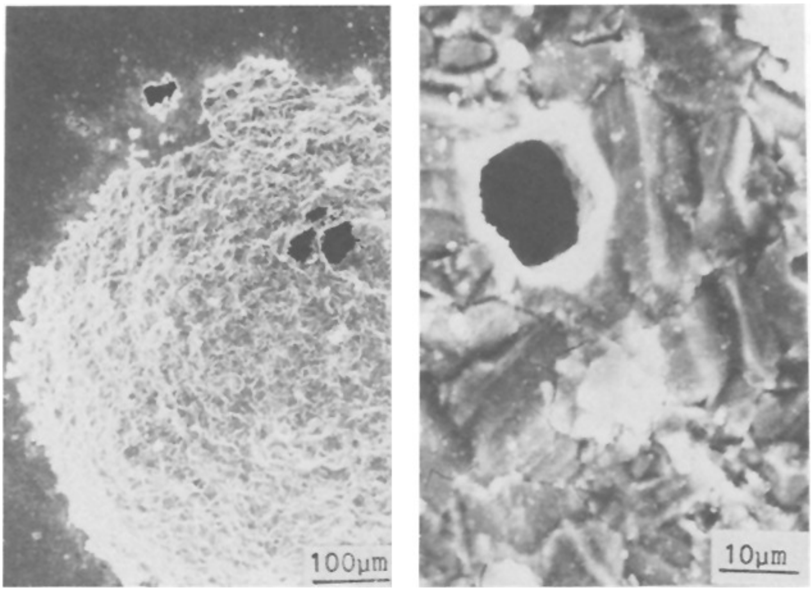

FIG. 2—*A contrast in pit formation in Alloy* ×*750 (left) and Alloy 600, after a 26-day immersion in a 0.5* M *$CuCl_2$, 1.0* M *HF solution.*

extensive at solution concentrations of 0.2 *M* and above. The extent of pitting increased continually with time; Fig. 3 shows the appearance in the SEM of specimens immersed for 2 and 16 h in a 0.05 *M* solution. In the former situation, remains of the 600 grit finish and grain boundary etching are discernable; in the latter, there is no evidence of preferential grain boundary attack. Neither grain size (25 to 500 μm) nor prior cold work (HRB 55 to 97) made discernable differences in the degree of pitting.

Slow Strain Rate Tests

The initial tests involved an Alloy 400 with a grain size of 35 μm and a strain rate of 1.2×10^{-6} s^{-1}. These conditions were used as a basis for any comparisons. Tests in air

TABLE 2—*The results of immersion tests on Alloy K500.*

Solution	Concentration	Corrosion Rate, mm/year,		Observations
		Hoyt [*38*]	Measured	
Ammonium hydroxide	29%	1	24	B to C
Ammonium persulfate	0.175 *M*	72	109	B to C
Hydrogen peroxide	10%	...	3	A
Hydrofluoric acid	26%	1	52	B to C
Hydrobromic acid	12%	...	30	A
Ferric chloride	0.125 *M*	80	32	C
Nitric acid	28%	...	3000	C
Hydrochloric acid	19%	1	15	C
Acetic acid	10%	<1	3	A
Potassium chromate	0.15 *M*	...	6	C
Lead chromate	0.1 *M*	...	30	B to C
Lactic acid	10%	1	1	A

NOTE: A = thin film formation or polishing, B = pitting, C = general corrosion.

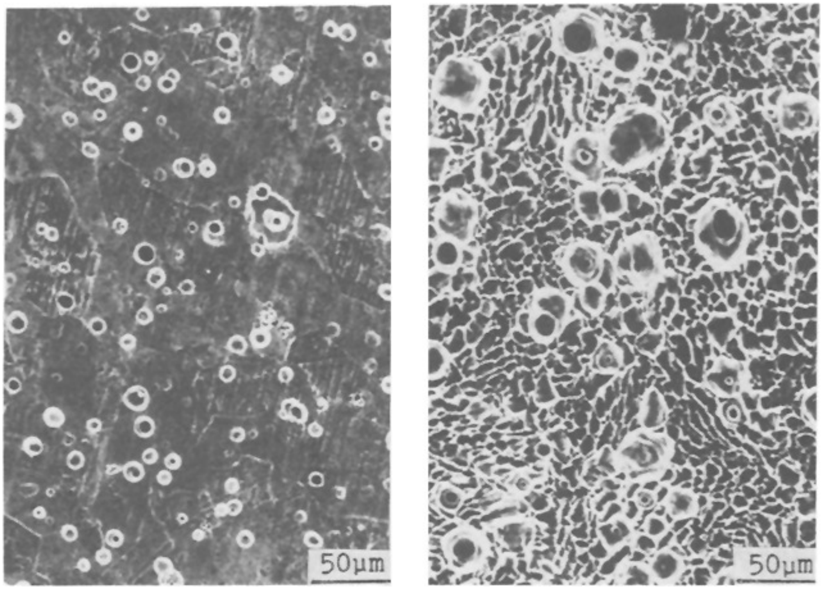

FIG. 3—*Pitting in Alloy 400 after a 2-h (left) and a 16-h immersion in a 0.05* M *ammonium persulfate solution.*

lasted approximately 12 h and gave cup and cone fractures. The tensile strength in air was approximately 630 MPa, the yield strength was 220 MPa, and the reduction in area was about 72%. All tests in environments causing SCC gave cup and cone fractures, too, with no change in the tensile strength. When SCC occurred, the surface cracks were up to 3 grains deep. Representative examples of the SCC are shown in Fig. 4.

Inactive Environments

Fused sodium hydroxide has been noted to cause SCC in Alloy 400 at elevated tempertures [*31*]. For elimination purposes, one specimen was tested at room temperature, in an aqueous solution of sodium hydroxide (0.25 *M*). As expected, no indications of corrosion or cracking occurred.

It was presumed that a hydrofluoric acid solution (26%) would also not cause cracking. This was confirmed, even though a coarse grain size of 350 µm was used to amplify any tendency towards cracking. Some minor pitting, however, did occur. Also, localized IG cracking was detected in the vapor region, near the top shoulder.

Active Environments

All tests in solutions of ammonium hydroxide (15%), ammonium persulfate (0.175 *M*), and various hydrofluoric acid solutions containing an oxidizer caused cracking. In each instance, the cracking was IG near the shoulders in regions of low strain, with a transition to TG nearer the waist. The TG cracking often occurred along slip bands or at tranverse grinding grooves.

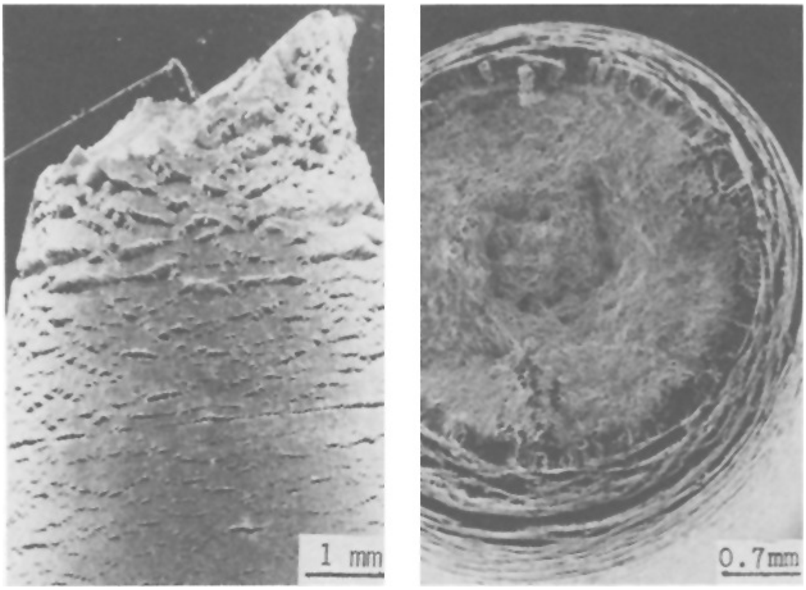

FIG. 4—*Side and fracture surface views of an Alloy 400 specimen after a SST in a 0.063* M *CuF_2, 0.38* M *HF solution. Extensive transverse cracking is seen, with gaping in the fracture vicinity. Except where associated with machining grooves, the cracks are short and wavy.*

Effect of Grain Size

An increase in the grain size, within the range investigated, 35 μm to 350 μm, led to more extensive cracking. This was also the situation for the SSTs of Alloy 400 in liquid mercury [*28*]. The coarse grain size facilitated the SEM observations because the slip bands were more distinct and the increased plastic deformation led to gaping of the cracks, permitting views into the cracks. Consequently, many subsequent tests utilized a coarse grain size.

Effect of Concentration

The immersion tests on ammonium hydroxide solutions showed slight pitting. In accord, the SCC that occurred during SSTs increased as the solution concentration increased from 15 to 29%. The IG and TG cracking was shallow and the original 600-grit surface finish appeared unaffected.

Consistent with the immersion tests, showing extensive general and pitting attack at all concentrations studied, the SSTs with ammonium persulfate solutions illustrated that the SCC decreased with an increase in solution concentration. Both the IG and TG cracking were more severe than for ammonium hydroxide, and the original 600-grit finish was eliminated. Figure 5 shows the appearance ~5 and ~10 mm from the fracture, after a SST in a 0.10 *M* solution. Both views reveal gaping IG cracks. A difference is that the grain attack is more uniform in the more highly strained zone nearer to the fracture. Away from the fracture, the grain attack becomes more localized, and individual pits are discernable. After a SST in a 0.175 *M* solution, the appearance away from the fracture zone is shown in Fig. 6. General grain pitting can be seen with a pit-free zone adjacent to the grain boundary, with a renewal of pitting at the grain boundary leading to cracks.

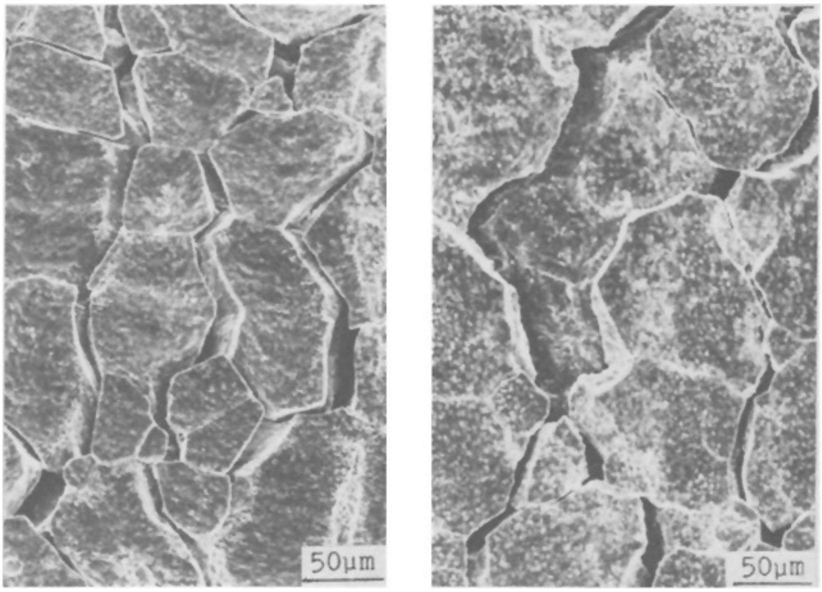

FIG. 5—*Gaping IG cracking, ~5 mm (left) and ~10 mm from the fracture point, after a SST in a 0.10* M *ammonium persulfate solution. General grain attack is more evident nearer the fracture.*

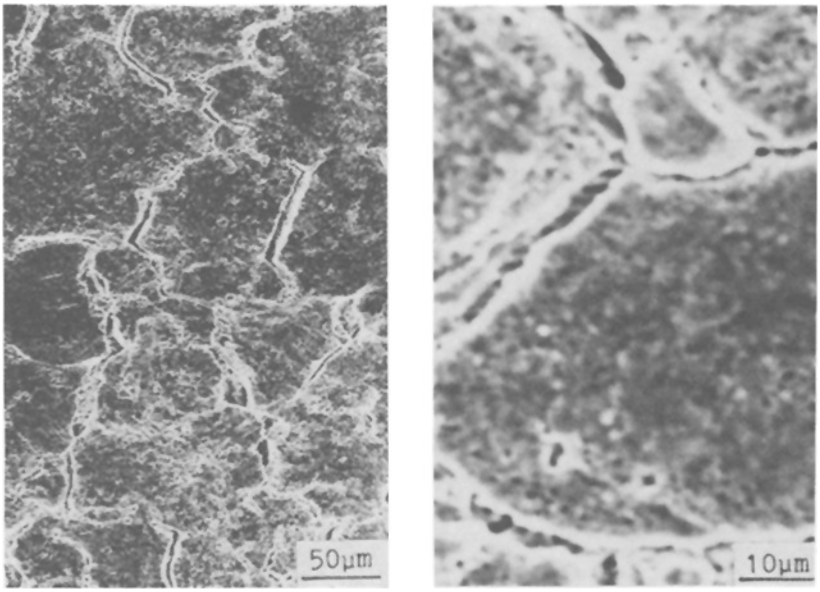

FIG. 6—*Pitting and IG cracking away from the fracture location, after a SST in a 0.175* M *ammonium persulfate solution. There is a pit-free zone adjacent to the grain boundary, with a renewal of pitting at the grain boundary.*

SCC was always obtained in solutions of hydrofluoric acid and an oxidizer. The HF concentration was varied from 0.38 to 18 *M*; the oxidizers used were $CuCl_2$ (0.125 to 0.5 *M*), CuF_2 (0.063 to 0.125 *M*), and air bubbled through the HF solution. Increasing the concentration always increased the general corrosion and the deposits of corrosion byproducts. For example, a solution of 0.25 *M* $CuCl_2$, 0.5 *M* HF led to an encrusted salt deposit for ~6.5 mm below the fracture point. The scale was loosely adherent; where the scale was broken away, pitting was seen. IG cracking was most conspicuous near the top shoulder above the liquid level. A specimen of grain size ~350 μm subjected to aerated 26% HF had gaping TG cracks to a depth of ~1 mm, containing corrosion byproducts. A specimen immersed in a 0.063 *M* CuF_2, 0.38 *M* HF solution to just above the waist had a dark scale and copper oxide in the immersed portion and a blue salt with metallic copper in the upper levels. This occurrence of copper and copper oxide was noted previously by both Copson and Cheng [*32*] and Graf and Wittich [*35*]. Both halves contained a multitude of blunted cracks; both halves exhibited IG and TG cracking. The cracking characteristics in this solution are shown in Figs. 7 to 10 for a specimen of ~350-μm grain size. In Fig. 7, taken ~3 mm from the fracture, extensive TG cracking can be seen, along with plastic deformation; a more localized view shows the stepped nature of an inner crack surface. General and detailed views of mixed mode cracking occurring further from the fracture are seen in Fig. 8. The higher magnification reveals mild IG cracking with much more prominent TG cracking adjacent. Near to the shoulder, the TG cracking is less prominent (Fig. 9). Neither the TG nor the IG cracking demonstrated by this specimen are associated with pitting. The contrast with the behavior in ammonium persulfate solutions can be seen from a comparison of Figs. 6 and 9. The appearance of the TG cracking at the fracture location is illustrated in Fig. 10. There is a strong resemblance to the TG cracking resulting from both HE and LME [*28*].

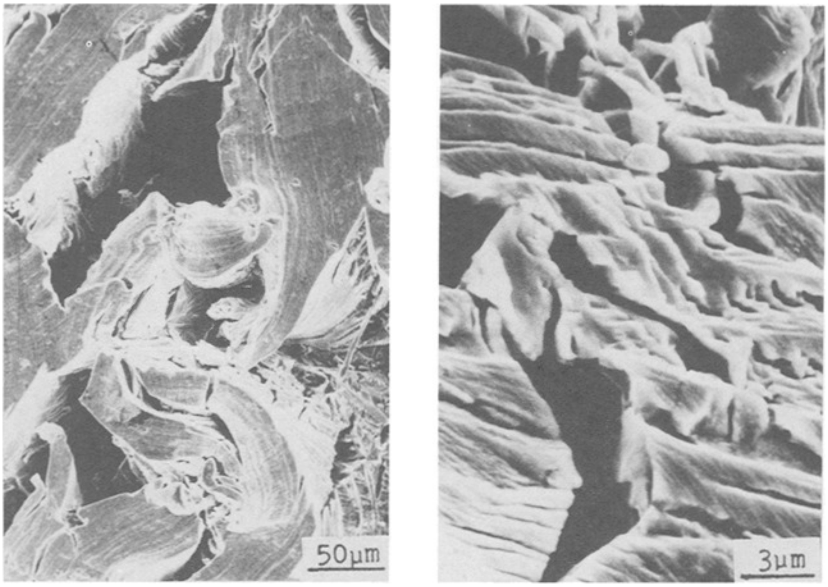

FIG. 7—*Plastic deformation and gaping TG cracks (left), with a view into one crack. The SST was in a 0.063* M *CuF_2, 0.38* M *HF solution.*

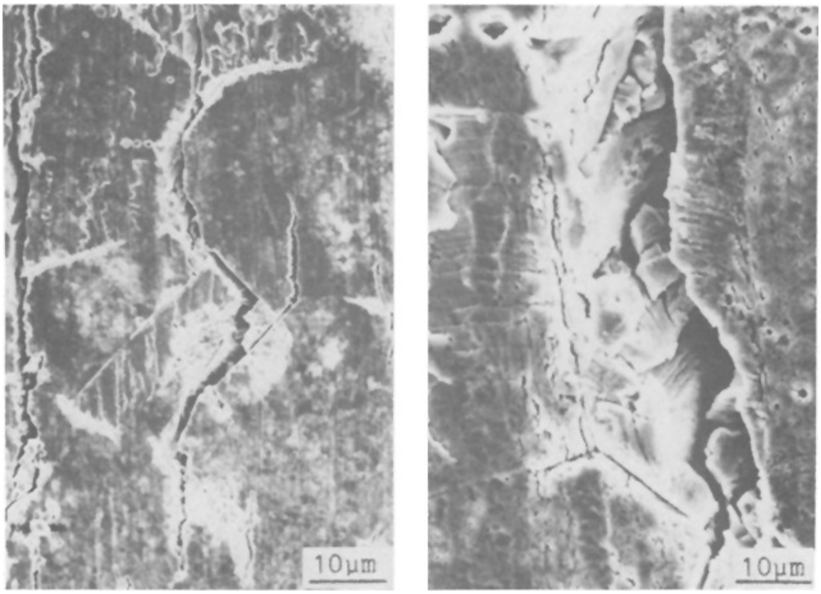

FIG. 8—*Mixed mode cracking on the same specimen as Fig. 7, occurring further from the fracture. The detailed view (right) shows pitting, slip bands, and many small cracks. At this magnification, the most prominent crack is seen to be TG, adjacent to a mildly cracked grain boundary.*

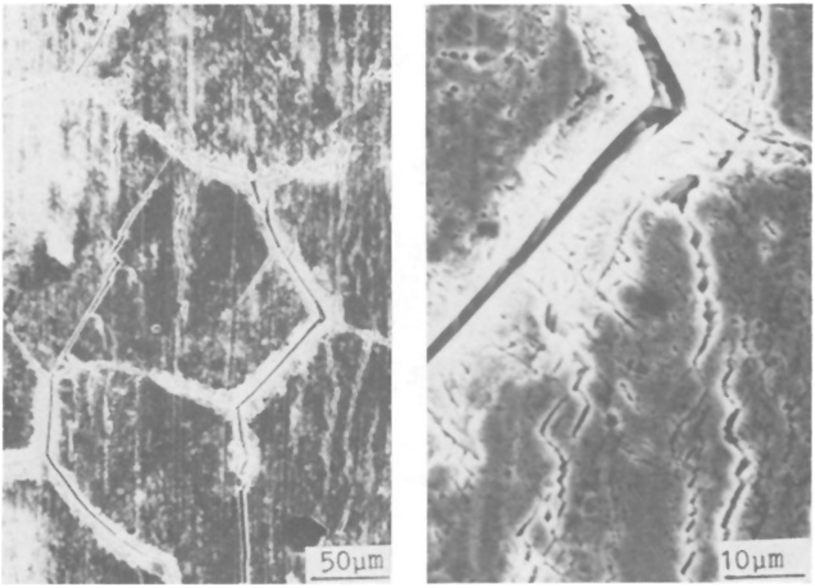

FIG. 9—*The surface appearance towards the shoulder on the same specimen as Figs. 7 and 8. The TG cracking persists but is on a finer scale; the IG cracking is not obviously associated with pitting.*

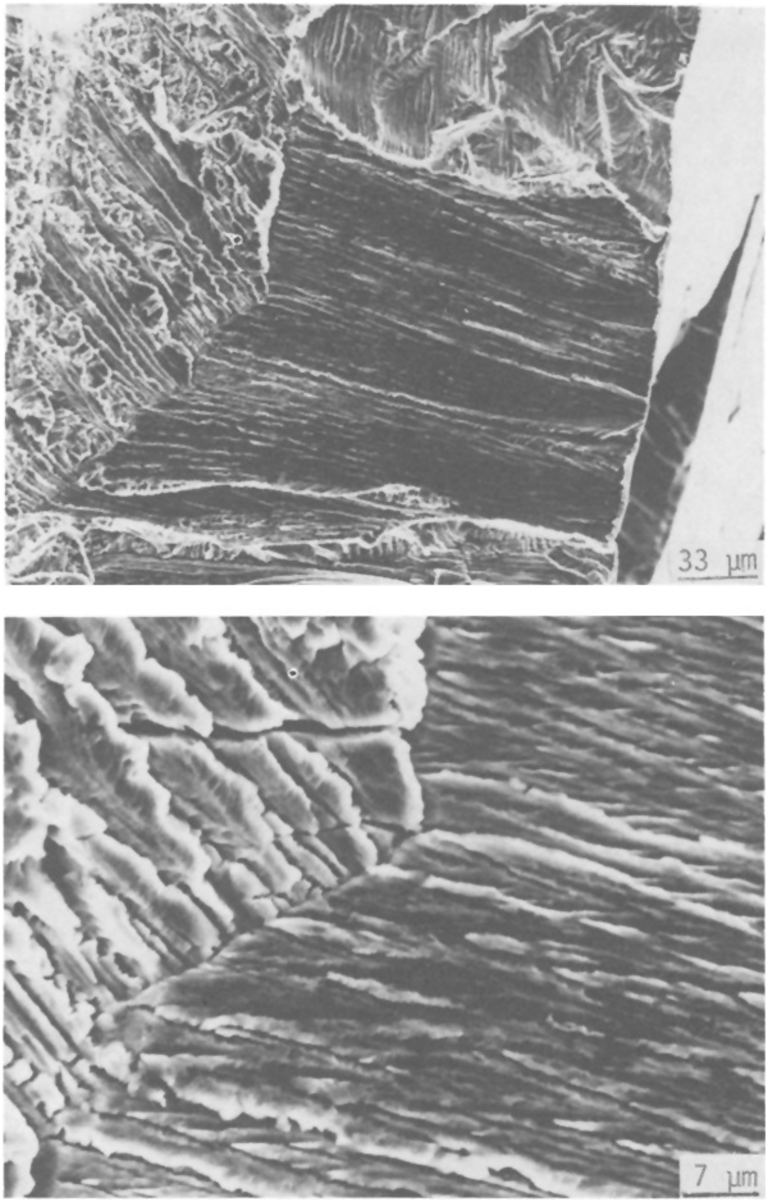

FIG. 10—*The fracture surface appearance of the specimen of Figs. 7 to 9. The TG zone ends gradually, about two grains deep. The higher magnification view shows the variation in surface detail across a grain boundary.*

Effect of Strain Rate

The effect of strain rate was explored in two solutions, ammonium hydroxide (15%) and a CuF_2 (0.063 *M*), HF (0.38 *M*) solution. Increasing the strain rate, as may be anticipated, decreased the attack. At a strain rate of 30 × 10^{-6} (30 min to failure), no attack occurred in the former solution, but TG cracking still occurred in the latter solution to a distance of ~6 mm from the fracture location; there was no IG cracking. By contrast, at the strain rate of 1.2 × 10^{-6} s^{-1} the TG cracks extended for ~18 mm from the waist, with IG cracks beginning at ~12 mm. The gradation in cracking is illustrated in Fig. 11.

Effect of Cold Work

The as-received Alloy 400 rod was in the cold-worked condition with a hardness of ~97 HRB, at a grain size of ~25 μm. Specimens tested without heat treatment showed, without exception, less cracking. The TG cracking extended to ~8 mm from the waist, and no IG cracking was detected. The cracks were shallow, closed, and not visible in the SZM. An annealed specimen, prestrained in air, behaved similarly. The active solutions investigated were ammonium persulfate (0.175 *M*), ammonium hydroxide (29%), aerated hydrofluoric acid (29%), and a CuF_2 (0.063 *M*), HF (0.38 *M*) solution.

Alloy K500

Alloy K500 samples were tested in a 0.063 *M* CuF_2, 0.38 *M* HF solution for both the as-received and annealed conditions. The as-received condition was supposedly age-hardened but only had a hardness of ~23 HRC, compared to handbook values of 32 HRC, so was not fully hard [37]. The observed cracking was similar to that described previously for Alloy 400.

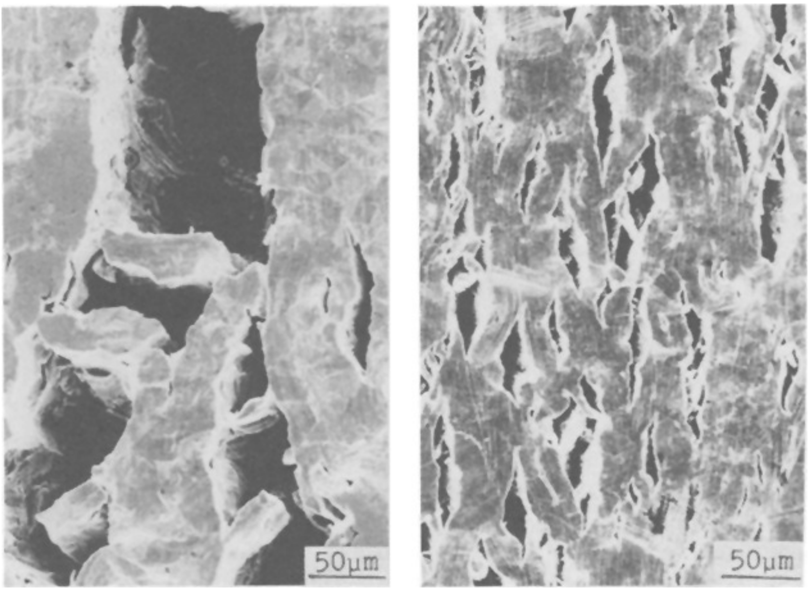

FIG. 11—*Gaping cracks (left) near the fracture zone of the specimen of Fig. 4. A specimen tested a tenfold higher strain rate (right) shows extensive side cracking, but the cracks are smaller.*

Discussion

This study has demonstrated the occurrence of SCC in Alloy 400 at room temperature in several environments, all of which also caused pitting attack. Thus, pitting corrosion is a guide to SCC susceptibility. It is probable that many other environments can be found that will cause both pitting and SCC. Furthermore, the demonstration of pitting in other nickel-base alloys is suggestive that room temperature SCC can occur in those alloys. It is important to note that SCC does not have to be associated with the precipitation of a damaging species at the grain boundary, and that both IG and TG cracking occur on the same specimen.

SCC has been demonstrated over a wide range of concentrations of both ammonium persulfate and active hydrofluoric acid solutions. In the former, the SCC increased with a decrease in concentration because of less general corrosion. However, even in the most dilute solution studied, 0.01 *M*, the general corrosion was still greater than in any HF base solution tested, as witnessed by the disappearance of the original grinding marks. The greater attack in ammonium persulfate accounts for the differences in appearance of the IG attack in the two solutions, as well as the intensity of pitting in ammonium persulfate. In retrospect, tests in a diluter solution of ammonium persulfate would have been of value. Another contrast, illustrated by Figs. 3 and 6, demonstrates that pitting attack alone does not outline the grain boundaries. The presence of a stress is required and results in the grain boundary becoming anodic with respect to the adjacent zones, which will then show a marked decrease in the pitting attack.

A significant observation is the prevalence of IG cracking in the lower stress regions near the shoulders, with a transition to TG cracking near the waist. The same situation has been observed in HE and LME of Alloy 400 [*28*], as well as with nickel [*39*], and Alloys 600 and 800 [*10,40*]. In Alloy 400, the IG cracking occurred at about the yield stress for both HE and LME, as it did here for SCC. Near the shoulder, the cross-section area is three to four times that at the waist, and the yield strength of the Alloy 400 is of the order of a third of the tensile strength. With yielding, the high-energy sites are the grain boundaries and IG attack ensues, with maybe some additional attack at points of stress concentration, such as grinding grooves (Fig. 4). With continued plastic deformation, the slip bands become the higher energy sites and a transition to TG cracking occurs. For EAC resistance, the heavily cold-worked state is to be preferred because of general, rather than localized, high-energy locations. The observations of this study are in accord.

The previous paragraph has pointed out the transition from IG to TG cracking that occurs with HE, LME, and SCC. The fractography of the embrittlement is also indistinguishable. Features found in SCC, as demonstrated in Figs. 7 and 10, can also be found in both HE and LME. For example, there is a strong resemblance between Fig. 7 and the Fig. 11*b* of Ref *28*. Differences between the HE, LME, and SCC of Alloy 400 may be in degree only. It is apparent that SCC tests at slower rates could give fractures with very low elongations. Alloy 400, therefore, is an appropriate system to explore the extent of the commonality of the cracking mechanisms.

Conclusions

SCC can be obtained in Alloy 400 at room temperature in diverse oxidizing environments. The occurrence of pitting is an indication of a susceptibility to SCC. It is anticipated that the demonstrated occurrence of pitting in other nickel-base alloys indicates the potential for SCC in those alloys. The SCC cracking mode is intergranular at low strain levels with a transition to transgranular at higher strain levels. In the cold-worked state the susceptibility is reduced and the cracking is transgranular. Intergranular cracking begins at the yield stress.

The cracking sequence and the fractography are indistinguishable from those observed during the hydrogen embrittlement or liquid metal embrittlement of Alloy 400.

References

[1] Bernhardsson, S., Norberg, P., Eriksson, H., and Forssell, O., *Anti-Corrosion,* Vol. 33, No. 1, 1986, pp. 14–17.
[2] Craig, B., in *Metals Handbook,* 9th Ed., Vol. 13 (*Corrosion*), American Society for Metals International, Metals Park, OH, 1987, pp. 145–189.
[3] Barteri, M., Marcia, F., Tamba, A., and Bruno, R., *Corrosion,* Vol. 43, 1987, pp. 518–524.
[4] Kolts, J., in *Metals Handbook,* 9th Ed., Vol. 13 (*Corrosion*), American Society for Metals International, Metals Park, OH, 1987, pp. 647–652.
[5] Berkowitz, B. J. and Kane, R. D., *Corrosion,* Vol. 36, 1980, pp. 24–28.
[6] Kane, R. D. and Berkowitz, B. J., *Corrosion,* Vol. 36, 1980, pp. 29–36.
[7] Coyle, R. J., Kargol, J. A., and Fiore, N. F., *Metallurgical Transactions,* Vol. 12A, 1981, pp. 653–658.
[8] Caskey, G. R., *Microstructural Science,* Vol. 9, 1981, pp. 413–419.
[9] Cornet, M., Bertrand, C., and Da Cunha Belo, D., *Metallurgical Transactions,* Vol. 13A, 1982, pp. 141–144.
[10] Price, C. E. and Morris, J. A., *Corrosion of Nickel Base Alloys,* American Society for Metals, Metals Park, OH, 1986, pp. 69–78.
[11] Price, C. E. and Good, J. K., *Journal of Engineering Materials and Technology, ASME Transactions,* Vol. 106(H), 1984, pp. 184–190.
[12] Price, C. E. and Good, J. K., *Journal of Engineering Materials and Technology, ASME Transactions,* Vol. 106(H), 1984, pp. 178–183.
[13] Jones, R. H., *Journal of Metals,* Vol. 39, No. 12, 1987, pp. 32–39.
[14] Ugiansky, G. M. and Johnson, C. E., in *Stress Corrosion Cracking: The Slow Strain Rate Technique, ASTM STP 665,* American Society for Testing and Materials, Philadelphia, 1979, pp. 113–131.
[15] Asphanani, A. I., in *Stress Corrosion Cracking: The Slow Strain Rate Technique, ASTM STP 665,* American Society for Testing and Materials, Philadelphia, 1979, pp. 279–293.
[16] Wilson, I. L. W. and Mager, T. R., *Corrosion,* Vol. 42, 1986, pp. 352–361.
[17] Latanision, R. M., *Journal of Materials Engineering,* Vol. 10, 1988, pp. 143–162.
[18] Caramihas, C. A. and Taylor, D. F., *Corrosion,* Vol. 40, 1984, pp. 382–385.
[19] Bandy, R., Roberge, R., and van Rooyen, D., *Corrosion,* Vol. 41, 1985, pp. 142–150.
[20] Bandy, R. and van Rooyen, D., *Corrosion,* Vol. 40, 1984, pp. 281–289.
[21] Crum, J. R., *Corrosion,* Vol. 42, 1986, pp. 368–372.
[22] Briant, C. L., O'Toole, C. S., and Hall, E. L., *Corrosion,* Vol. 42, 1986, pp. 15–27.
[23] Kekkonen, T. and Hannen, H., *Corrosion Science,* Vol. 25, 1985, pp. 789–803.
[24] Bandy, R. and van Rooyen, D., *Corrosion of Nickel Base Alloys,* American Society for Metals, Metals Park, OH, 1986, pp. 117–126.
[25] Proceedings, Fourth International Symposium on Environmental Degradation of Materials in Nuclear Power Systems-Water Reactors, Jekyll Island, Georgia; sponsored by NACE, ANS, and TMS, Aug. 6–10, 1989.
[26] Bandy, R., Roberge, R., and Newman, R. C., *Corrosion,* Vol. 39, 1983, pp. 391–398.
[27] Funkenbusch, A. W., Heldt, L. D., and Stein, D. F., *Metallurgical Transactions,* Vol. 13A, 1982, pp. 611–618.
[28] Price, C. E. and Fredell, R. S., *Metallurgical Transactions,* Vol. 17A, 1986, pp. 889–898.
[29] Efird, K. D., *Materials Performance,* Vol. 24, No. 4, 1985, pp. 37–40.
[30] Erlings, J. G., deGroot, H. W., and van Roy, J. F. M., *Materials Performance,* Vol. 25, No. 10, 1986, pp. 28–34.
[31] Comley, M A. and Evans, T. E., in *Corrosion of Metals and Alloys,* Vol. 1, L. L. Sheir, Ed., Wiley, New York, 1963, pp. 103–125.
[32] Copson, H. R. and Cheng, C. F., *Corrosion,* Vol. 12, No. 12, 1956, pp. 71–77.
[33] Degnan, T. F., in *Metals Handbook,* 9th ed., Vol. 13 (*Corrosion*), American Society for Metals International, Metals Park, OH, 1987, pp. 1166–1184.
[34] McGuire, G. E., *Oil and Gas Journal,* Vol. 84, No. 23, 1986, pp. 48–52.
[35] Graf, L. and Wittich, W., *Werkstoffe und Korrosion,* Vol. 5, 1966, pp. 385–405.
[36] Tegart, W. J. M., *The Electrolytic and Chemical Polishing of Metals,* 2nd Ed., Pergamon Press, Oxford, England, 1959, p. 102.

[37] *Handbook of Huntington Alloys,* 4th Ed., The International Nickel Co. Inc., Huntington, WV, 1968.
[38] Hoyt, S. L., *Metal Data,* Battelle Memorial Institute, Reinhold Publishing Corp., New York, 1952.
[39] Price, C. E. and Traylor, L. B., *Corrosion,* Vol. 43, 1987, pp. 229–238.
[40] Price, C. E. and Good, J. K., *Journal of Materials Engineering,* Vol. 9, 1987, pp. 283–291.

DISCUSSION

W. R. Waike[1] (*written discussion*)—Would the authors expect the same results for K500?

L. G. Everhart and C. E. Price (*author's closure*)—Yes, similar behavior was noted when Alloy K500 was examined. Tests were conducted on Alloy K500 in both the annealed and the as-received conditions using 0.38 M HF and 0.063 M CuF_2, at a strain rate of 1.2 (10^{-6}) s^{-1}.

The annealed sample displayed a 16-mm side cracking zone with widely gaping TG cracks near the fracture and IG cracks in the lower strain regions. The sample closely resembled the annealed Alloy 400 samples.

The hardness of the as-received sample was only slightly higher than the cold-worked Alloy 400. Alloy K500 exhibited a 10-mm side cracking zone near the fracture. There was a distinct TG cracking border of ~0.3 mm deep. The side cracking was similar to that of the annealed sample but less severe. Also, the as-received sample did not show any IG cracking.

---

[1] Amoco Corp., P.O. Box 3011, Naperville, IL 60566.

Richard A. Corbett[1]

Using Multisample Test Apparatus for the ASTM A 262, Practice C Nitric Acid Corrosion Testing of Types 304 and 304L Stainless Steels

---

REFERENCE: Corbett, R. A., **"Using Multisample Test Apparatus for the ASTM A 262, Practice C Nitric Acid Corrosion Testing of Types 304 and 304L Stainless Steels,"** *Corrosion Testing and Evaluation: Silver Anniversary Volume, ASTM STP 1000,* R. Baboian and S. W. Dean, Eds., American Society for Testing and Materials, Philadelphia, 1990, pp. 335–347.

ABSTRACT: The single-sample, single-flask method generally is used by testing laboratories when industry and government agencies specify corrosion evaluation of Types 304 and 304L stainless steels to ASTM A 262, Practice C. Information presented confirms that multisample test equipment in use for many years has permitted major savings in chemicals, labor, laboratory space, and equipment and at the same time has successfully avoided problems associated with the detrimental buildup of hexavalent chromium ions. A new multisample tester design is also discussed. This new design avoids the problems of weight, bulk, and expense associated with early multisample testers and yields results of the same accuracy and reproducibility as both the single-sample, single-flask method and earlier multisample testers.

KEY WORDS: nitric acid testing, Huey test, multisample testing, corrosion evaluation, acceptance test

To ensure optimum intergranular corrosion resistance of critical stainless steel process equipment in severe environments, Types 304 and 304L stainless steels have been nitric acid acceptance tested for many years. In some process exposures, the corrosion resistance of these alloys may vary greatly depending on their composition and heat treatment. Therefore, it is important to know in advance that the chemistry and metallurgical condition of the alloys are capable of withstanding the various heating operations encountered during fabrication, field installation, and repair and will still possess the expected corrosion resistance. Over the years, some companies as well as many government agencies have required that samples taken from heats and lots of stainless steels intended for fabrication into critical equipment for use in certain corrosive environments pass a nitric acid acceptance test.

The conventional boiling 65% nitric acid acceptance test is found in Practice C of the ASTM Practices for Detecting Susceptibility to Intergranular Attack in Austenitic Stainless Steels (A 262). In this test, a single stainless steel sample is exposed to boiling 65% nitric acid in a 1-L flask on an electrically heated hot plate for a total exposure time of 240 h. The acid is replaced every 48 h. Experience has shown, and it has been widely reported in the literature [*1–5*], that if more than one sample is exposed in the same flask, the buildup of hexavalent chromium ion corrosion product may cause the corrosion rate of all samples

---

[1] President, Corrosion Testing Laboratories, Inc., Wilmington, DE 19804.

to accelerate exponentially [1]. (How hexavalent chromium is formed, why and how it affects the corrosion of stainless steel, and the role different condensers play in this process have been thoroughly reviewed and discussed by Streicher [6].) However, it is possible to expose more than one sample simultaneously in the same flask if the accumulated hexavalent chromium ion concentration does not exceed approximately 30 ppm [2,3]. The problem with the flask method is that, with multiple samples, the sample surface-area-to-acid-volume ratio allows only very low corrosion rates before the critical 30-ppm chromium concentration is exceeded. If a single sample fails with a high corrosion rate, the chromium concentration may become high enough that corrosion is severe on all, including acceptable samples. If more than one sample fails, all samples must then be retested individually. Even if all samples in the same flask have acceptable rates, the rates usually will be higher than with single sample exposure because of the increasing accumulation of chromium ion. Since retesting can be both costly and time consuming, there is great reluctance to test more than one sample in the same flask.

Nitric Acid Testing

There are two major objections to performing the nitric acid acceptance tests on austenitic stainless steels. The first is the time and cost. The test requires 240 h of test exposure, plus the time needed for acid change-outs (approximately 12 to 14 days). Little can be done about shortening the time for the test exposure. From a cost standpoint, the acid needed to test a single sample is about 3 L and currently costs about $11. Disposal and handling this amount of strongly oxidizing concentrated nitric acid may add substantially to the cost of testing each sample.

The second objection is concern for the possible detrimental accumulation of hexavalent chromium ion in some tests, even for single samples during a 48-h exposure. Some alloys with high but marginally acceptable test rates may fail the test because the accumulation of chromium ion in the nitric acid during the individual test periods increased the overall corrosion rate beyond the acceptable limit.

Space and equipment are also considerations. On any major construction project where much critical equipment requires the nitric acid acceptance testing of many heats, forms, and shapes of Types 304 and 304L stainless steels, hundreds of flasks and thousands of litres of nitric acid, not to mention considerable laboratory space, may be required at any given time.

Multisample Testing Apparatus

The first multisample testing apparatus (MSTA) appeared in the late 1940s [1] and different types of MSTA have been described by various authors [2,3,5,7,8]. While they all successfully addressed the problems of acid consumption and chromium ion buildup, most had other limitations such as cost, complex construction, limited sample capacity, size or large space requirements. The earliest successful MSTA was developed by DeLong in 1948, when the need for testing many thousands of samples each year required large amounts of laboratory space, took many skilled technicians away from other important tasks, and was very costly. The DeLong apparatus was constructed of high-silicon cast iron and heated by steam. Its successful operation eliminated 4 fume hoods, 44 hot plates, and 350 flasks for an annual saving of $12 000 (1948 dollars).[2] This basic DeLong apparatus was used for nitric acid acceptance testing by DuPont for over 40 years. Recently, DuPont replaced the silicon cast-iron pot with the glass pot described in this paper.

---

[2] W. B. DeLong, private communication, 1986.

While the DeLong equipment performed satisfactorily and served well for many years, it also had several drawbacks. The silicon cast-iron pot was fragile, subject to thermal shock, difficult to repair, as well as being heavy, awkward, and expensive to operate and replace. Because of these limitations, the author developed a MSTA, based on the DeLong apparatus, which was lightweight, small in size, comparatively inexpensive, and capable of testing from 1 to 100 samples simultaneously without any acid changes during the 240-h test.

This new appratus is illustrated in Fig. 1 (schematic depicted in Fig. 2). It consists of an 8-L glass pot, similar to the conventional resin kettle, as the outer chamber. A 2.5-L glass test cup is supported inside the glass pot. The samples rest on one of four Teflon trays held in place by a glass funnel device. The trays are specially machined so that the tray surface area in contact with the samples is minimized and each sample receives a maximum amount of acid circulation. A glass cold-finger condenser fits snugly in the top of the glass pot and is similar to Fig. 9 in ASTM A 262. The glass pot is insulated and heated by a jacketed heating mantle controlled by a variable voltage regulator. Chilled cooling water to the cold-finger condenser is recirculated to a refrigerator constant temperature bath. In the event of a failure in the cooling water system, a thermometer and temperature sensing device controls the power to the heating mantle.

This glass MSTA requires only 4 L of nitric acid to charge both the inner and outer chambers. Since the apparatus is well-insulated, less than 1000 W of power are required to maintain the acid at boiling. It can be plugged into any standard 120-V a-c outlet. When

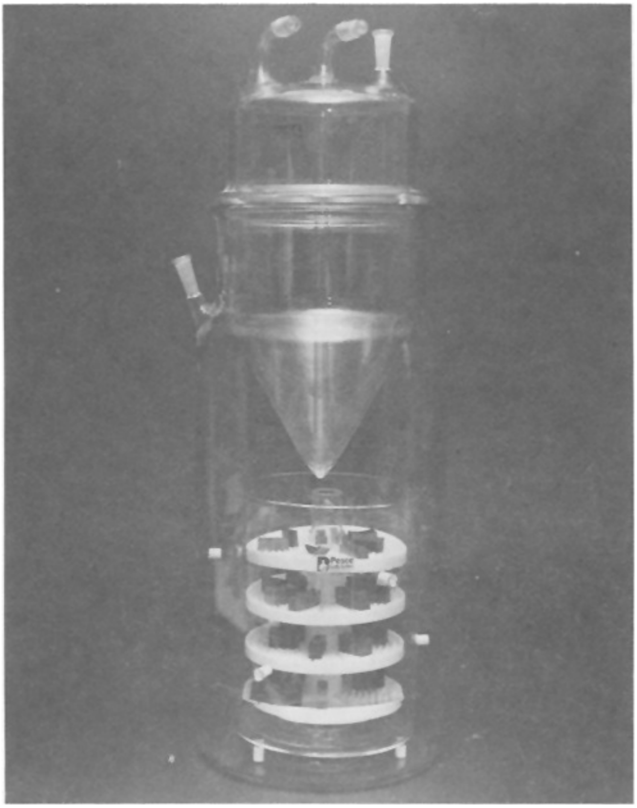

FIG. 1—*Glass multisample testing (GMST) apparatus.*

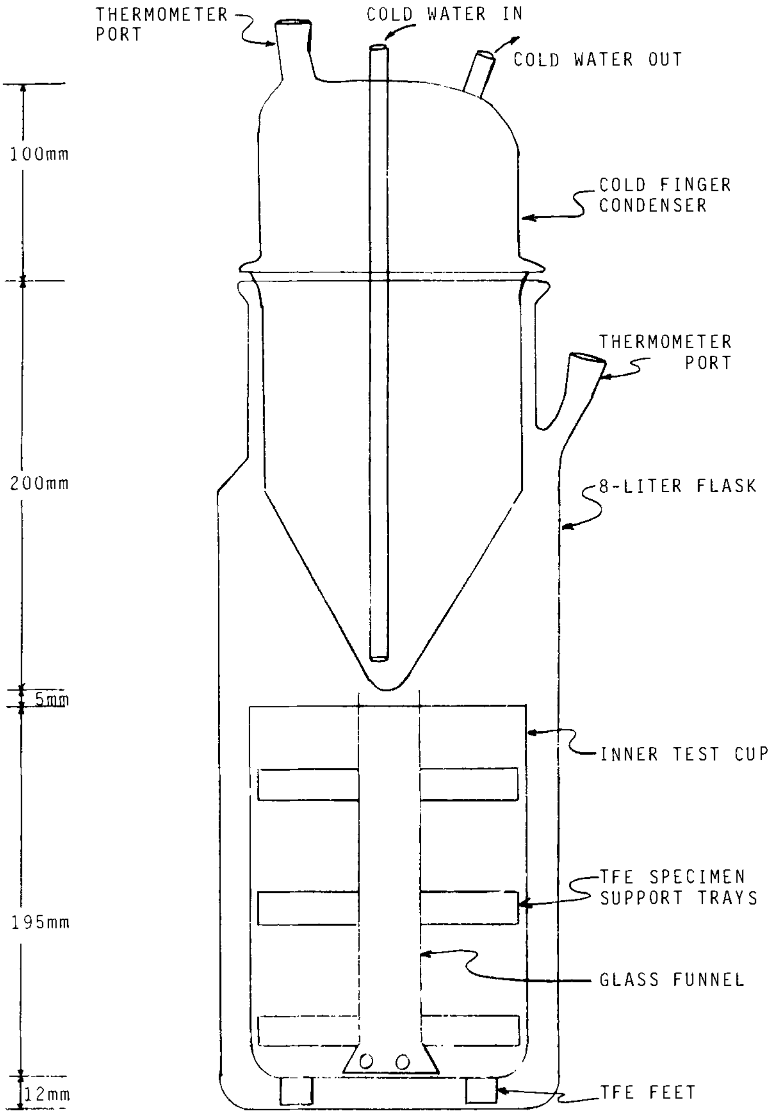

FIG. 2—*Schematic of GMST apparatus.*

empty, the glass pot and mantle weigh less than 20 lb. The entire apparatus, including refrigerated bath, occupies approximately 4 ft^2 and is easily accommodated on the top of a laboratory bench or in a standard fume hood. (*Safety Note:* Any hot, fuming acid should be handled under an exhaust hood or vent.) As many as 100 samples can be tested simultaneously.

Evaluating the Glass Multisample Testing Apparatus

The DuPont Co. has more than satisfied itself that the DeLong MSTA provided accurate and reliable nitric acid acceptance test information. Recently, DuPont has been able to demonstrate that the glass multisample testing apparatus designed by Corrosion Testing Laboratories, Inc. (CTL) and described herein not only provides the same accuracy and reliability, but also is more economical to operate than the original DeLong MSTA. Industry in general, however, still appears to have questions and perhaps, doubts regarding the use of glass MSTA. Actually, many of the questions about the glass apparatus are the same as they would be for the high-silicon cast-iron DeLong equipment and come down to questions more about use of multisample testing versus single-sample, single-flask testing in general.

During many years of close association and involvement with corrosion acceptance testing in general and ASTM A 262, Practice C nitric acid testing in particular, the author has had many opportunities to compare and review different nitric acid acceptance testing procedures, equipment and techniques, and their results. From this long association, and much experience in explaining the sampling, testing procedures, and interpretation of results to government agencies, industrial users, alloy suppliers, and fabricators, the following five questions are typical of those frequently asked:

1. When the same sample is tested in a single-sample flask and in a multisample tester, what differences in corrosion rates can be expected?
2. What are the advantages of a continuous 240-h exposure versus an exposure where four acid changes are required?
3. If a highly sensitized sample is added to the array of test samples in a multisample tester, will the corrosion rates of the other samples be adversely affected?
4. What is the measured acid exchange rate in the test cup of a multisample tester?
5. What is the cost advantage of using the multisample tester over the individual sample flask method?

Since these five questions keep recurring and the answers are important in making a choice between using the single sample flask technique or the multisample apparatus, they will be discussed and answered here.

Corrosion Rate Comparison—Single Sample Flask versus MSTA

To better compare the corrosion rates for the same sample using the two different types of test apparatus (flask with cold finger versus MSTA), some background should be reviewed first. In 1984, ASTM Subcommittee A01.17 on Flat Stainless Steel Products solicited twelve different laboratories to participate in a round-robin test of ASTM A 262, Practice C, on Type 304 strip material containing various levels of residuals and with different analytical tolerances. Ten samples were submitted to each laboratory to be tested in accordance with the practice. The twelve laboratories were to use the single-flask method according to ASTM A 262, Practice C. A summary of the results is presented in Table 1. There is considerable variation, even though none of these samples had any susceptibility to intergranular attack. If test results from Laboratories 4 and 5 are eliminated because of the unusually low values, the deviation is about ±25% from the average result.

At a later date, the author chose to run the same test samples in a CTL glass pot apparatus without any acid change. The results (Table 1, GMST) deviated less than 10% from the round-robin average rate and indicated that the use of the glass pot did indeed produce acceptable results. The results of this round-robin test also provided an idea of the variation that can be expected in laboratories that are supposedly experienced and following the same specification.

In another test, a variety of sample forms and types were selected for direct comparison between the single flask method and the glass pot using the same specification. The sample

TABLE 1—*ASTM A 262, Practice C Round-robin test results for Type 304 stainless steel with varying Cr, Ni, Cu, Mo levels. Corrosion rates are in in./month.*[a]

	Sample Number									
LAB	1	2	3	4	5	6	7	8	9	10
1	0.0009	0.0009	0.0009	0.0010	0.0008	0.0008	0.0009	0.0009	0.0008	0.0008
2	0.0009	0.0009	0.0010	0.0010	0.0008	0.0007	0.0010	0.0009	0.0009	0.0008
3	0.0009	0.0009	0.0010	0.0009	0.0008	0.0008	0.0009	0.0010	0.0009	0.0008
4	0.0004	0.0004	0.0005	0.0004	0.0005	0.0004	0.0005	0.0005	0.0004	0.0004
5	0.0001	0.0001	0.0002	0.0002	0.0001	0.0001	0.0002	0.0002	0.0001	0.0001
6	0.0010	0.0010	0.0011	0.0012	0.0009	0.0009	0.0012	0.0012	0.0010	0.0010
7	0.0009	0.0009	0.0009	0.0010	0.0008	0.0008	0.0010	0.0010	0.0009	0.0008
8	0.0008	0.0009	0.0008	0.0009	0.0007	0.0008	0.0010	0.0010	0.0007	0.0007
9	0.0010	0.0010	0.0011	0.0012	0.0009	0.0009	0.0011	0.0011	0.0010	0.0010
10	0.0009	0.0009	0.0009	0.0010	0.0006	0.0008	0.0009	0.0009	0.0008	0.0008
11	0.0013	0.0013	0.0013	0.0014	0.0011	0.0011	0.0013	0.0013	0.0013	0.0013
12	0.0009	0.0009	0.0010	0.0010	0.0008	0.0008	0.0011	0.0010	0.0009	0.0008
GMST[b]	0.0008	0.0009	0.0008	0.0011	0.0008	0.0008	0.0010	0.0008	0.0010	0.0010
$\bar{v}$[c]	0.0010	0.0010	0.0010	0.0011	0.0008	0.0008	0.0010	0.0010	0.0009	0.0009
±[d]	−2/+3	−1/+3	−2/+3	−2/+3	−2/+3	−1/+3	−1/+3	−1/+3	−2/+4	−2/+4

[a] To convert from in./month to mm/month, multiply by 25.4.

[b] Glass multisample test results, not part of the round robin.

[c] Averaged rate of Labs 1–3 and 6–12; Labs 4 and 5 were omitted due to extremely low rates.

[d] Spread in rates ($\times s10^{-3}$) between labs and the averaged value $\bar{v}$.

forms and types included bar, castings, tube, sheet, pipe, weldments, and plate. For the test using the glass pot, all samples were run together simultaneously and continuously without an acid change for 240 h. In the comparison test, each sample was placed individually in a single flask for a total exposure of 240 h, but with acid changes at 48-h intervals.

Table 2 indicates the results of this comparison test on the various shapes and forms. While variation is expected, out of the 78 pairs of numbers, 83% were within ±0.0003 and 91% were within ±0.0005. In these comparison tests, it was generally observed that if the sample passed the acceptance criteria [*9*], it passed in both tests, and if it failed, it failed both tests, even if the numerical results for the corrosion rates were not the same. In this particular series of tests, the glass pot accepted two samples that were rejected by the single-flask method and rejected one sample that passed in the flask method. In these cases, it has been suggested that scale on the two samples involved in the flask method test may not have been completely removed after the sensitizing heat treatment [*10*]. However, it is more likely that there actually will be certain cases near the acceptance rate [*9*] of 0.0020 in./month (0.05 mm/month or 0.61 mm/year) where the flask test will fail a sample which passes in the pot test and visa versa.

TABLE 2—*ASTM A 262, Practice C Type 304L stainless steel, sensitized 1 h at 1250°F (676.6°C); individual flask method versus glass multisample tester. (Corrosion rates are in inches per month.*[a]*)*

Form	Sample	Flask Corrosion Rates, in./month[b]	Glass Pot Corrosion Rates, in./month[c]
Bar	1	0.0016	0.0019
	2	0.0007	0.0007
Casting	3	0.0005	0.0005
	4	0.0007	0.0007
	5	0.0007	0.0009
	6	0.0005	0.0005
	7	0.0006	0.0006
	8	0.0006	0.0006
	9	0.0011	0.0016
	10	0.0006	0.0007
	11	0.0006	0.0007
	12	0.0006	0.0006
	13	0.0007	0.0008
	14	0.0004	0.0005
	15	0.0004	0.0005
	16	0.0005	0.0005
	17	0.0006	0.0008
	18	0.0007	0.0007
	19	0.0011	0.0008
	20	0.0004	0.0005
	21	0.0008	0.0007
Seamless tube	22	0.0011	0.0007
	23	0.0009	0.0011
Sheet	24	0.0011	0.0008
Seamless pipe	25	0.0007	0.0006
	26	0.0007	0.0008
	27	0.0008	0.0015
	28	0.0009	0.0011
	29	0.0007	0.0006
	30	0.0051	0.0030

TABLE 2—*Continued.*

Form	Sample	Flask Corrosion Rates, in./month[b]	Glass Pot Corrosion Rates, in./month[c]
	31	0.0008	0.0007
	32	0.0008	0.0007
	33	0.0019	0.0011
	34	0.0006	0.0007
	35	0.0006	0.0009
	36	0.0007	0.0009
	37	0.0005	0.0006
	38	0.0009	0.0007
	39	0.0009	0.0007
Welded pipe	40	0.0008	0.0009
	41	0.0012	0.0015
	42	0.0011	0.0012
	43	0.0009	0.0011
	44	0.0013	0.0013
	45	0.0009	0.0009
	46	0.0008	0.0010
	47	0.0010	0.0012
	48	0.0013	0.0014
	49	0.0007	0.0008
	50	0.0016	0.0011
	51	0.0008	0.0010
	52	0.0007	0.0007
	53	0.0008	0.0008
	54	0.0019	0.0023
	55	0.0011	0.0015
	56	0.0010	0.0010
	57	0.0010	0.0008
	58	0.0011	0.0008
	59	0.0027	0.0015
	60	0.0010	0.0008
	61	0.0010	0.0008
	62	0.0011	0.0008
	63	0.0042	0.0027
	64	0.0009	0.0008
	65	0.0008	0.0010
	66	0.0006	0.0007
	67	0.0007	0.0008
	68	0.0007	0.0008
	69	0.0007	0.0009
Plate	70	0.0008	0.0009
	71	0.0012	0.0009
	72	0.0009	0.0010
	73	0.0024	0.0032
	74	0.0007	0.0008
	75	0.0007	0.0008
	76	0.0043	0.0025
	77	0.0031	0.0018
	78	0.0009	0.0007

NOTE: The typical industrial criteria for acceptable material has been reported [*8,9*]. For Type 304L stainless steel, the passing criterion, after a sensitization heat treatment, is a corrosion rate of no more than 0.0020 in./month.

[a] To convert from in./month to mm/month, multiply by 25.4.

[b] Five 48-h periods, acid changed after each period.

[c] One 240-h exposure, no acid change.

Continuous 240-h Exposure

The need for frequent nitric acid changes has been discussed and detailed extensively in earlier publications [*1,3,5,12*]. These earlier works have confirmed, without doubt, that buildup of hexavalent chromium ion in 65% nitric acid greatly accelerates the corrosive attack on stainless steel. This increase in the corrosion rate is most dramatic above the concentration of only 30 ppm of the chromium ion. It has also been demonstrated and confirmed that changing the acid every 48 h will minimize this buildup, even when severely sensitized samples are tested. However, the hexavalent chromium ion must be kept to a minimum during the entire exposure period.

The CTL glass pot design discussed herein continuously replenishes the test cup with redistilled acid. All the condensed acid from the boiling liquid is returned to the test cup, and it has been determined that this amounts to more than 9 L (about four test cup changes) of redistilled acid per hour. This continuous acid replenishment flushes corrosion products, particularly the chromium ion, from the test cup into the outer pot where it accumulates and remains during the testing cycle.

Effect on Other Samples While Exposing a Heavily Sensitized Sample

As has been discussed before, there is good reproducibility of test results when mildly sensitized samples of the same lot of material are exposed in the MSTA. To explore the effect that one highly sensitized sample would have on other less-sensitized samples in the same MSTA, the following two tests were performed:

1. One heavily sensitized stainless steel sample was tested along with five mildly sensitized samples.
2. One mildly sensitized stainless steel sample was tested along with five heavily sensitized samples.

The results of these two tests are presented in Table 3. Neither the single highly sensitized sample nor the five highly sensitized samples appeared to have a significant effect on the corrosion rate of the other samples in the test. This indicated that there was no significant buildup of the hexavalent chromium ion in the test cup after 240 h exposure in the same acid charge.

Acid Exchange Rate in the MSTA

Using a MSTA of a largely different design, another laboratory [2] evaluated the rate at which the test cup was flushed of corrosion products during normal operation. In their test, they added a chromium ion solution (100 ppm Cr^{+6}) directly to the test cup and, with the acid boiling, analyzed the acid in the test cup for chromium at frequent intervals for 2 h. The results of their tests indicated that half of the chromium was flushed from the cup in about 40 min, and that 90% was removed after 2 h. Since the MSTA used in that test was different from the glass pot currently being discussed, the test was repeated using the equipment of this current design. For this retest, 200 ppm of Cr^{+6} ion was added to the acid in the test cup and the solution in the apparatus brought to a normal boil. Acid samples were taken from the test cup every 5 min for 2 h and the chromium content determined by the atomic absorption method. The results of this test are shown in Fig. 3. The Cr^{+6} concentration was reduced by half in less than 30 min, and 90% of the Cr^{+6} ion was removed in less than 2 h.

TABLE 3—*Effects of heavily sensitized samples[a] on corrosion rates; a comparison between the flask method and the glass pot.*

Sample	Corrosion Rate, in./month[b]
Flask method, single sample	
Type 304	0.0148
Type 304L	0.0008
Glass pot, five Type 304L mildly sensitized samples plus one Type 304 heavily sensitized sample:	
304L-1	0.0008
304L-2	0.0009
304L-3	0.0008
304L-4	0.0010
304L-5	0.0011
304S-1	0.0121
Glass pot, five Type 304 heavily sensitized samples plus one Type 304L mildly sensitized sample:	
304S-6	0.0132
304S-7	0.0135
304S-8	0.0145
304S-9	0.0128
304S-10	0.0139
304L-6	0.0012

[a] Sensitized 1 h at 1250° F.

[b] To convert from in./month to mm/month, multiply by 25.4.

In another test, in the glass pot containing nitric acid, 200 ppm of Cr^{+6} ion was added to the test cup. The system was boiled for 1 h. Three samples representing three different heats of stainless steel were placed in the test cup and exposed for a single 240-h period. Three duplicate samples were also tested by the single-flask method for 240 h with acid changes at the end of the usual 48-h periods. The results are presented in Table 4. The rates on all samples from both tests were within an acceptable variation. These results agree with those of Alger et al. [2] and indicate once more that the undesirable hexavalent chromium ion is being removed constantly from the presence of the stainless steel samples in the test cup. The results also indicate that use of the glass pot, with a single nitric acid exposure of 240 h, provides accurate results equal to the single-flask method.

In an evaluation test exposing 102 samples of sensitized Type 304L in the glass pot for a continuous 240 h, metal ion concentrations were measured after testing. The maximum corrosion rate for any of these samples was 0.0022 in./month. Analysis of the acid in the outer chamber was 68 ppm Ni, 142 ppm Cr, and 620 ppm Fe; the inner test cup analysis was 26 ppm Ni, 21 ppm Cr, 120 ppm Fe. The concentration of deleterious chromium ion was below the critical level of 30 ppm and again emphasized the acceptability of using a continuous 240-h exposure.

Cost Advantages of the Glass MSTA

While the CTL glass pot costs more than the flask apparatus for testing a single sample, the glass pot has clear cost advantages when numerous samples are tested on a frequent basis. For ten or less samples the individual flasks may be less expensive, but for more than ten samples, and as the number increases, the glass pot becomes more and more the economic choice. A cost comparison is made in Table 5.

As mentioned earlier, a significant amount of concentrated nitric acid is used in acceptance testing. To perform the test in individual flasks, the acid must be changed at 48-h intervals. The total 240-h exposure will require approximately 3 L of acid for each flask. With a single sample of each flask, the acid will cost over $11 per sample at current prices. With no acid changes during the 240-h exposure, and up to 100 samples per 4-L acid charge, the acid savings alone with the glass pot are obvious.

In addition to the savings in acid consumption, some other areas where the 240-h glass pot may result in substantial savings are:

1. Less laboratory bench and fume hood space used.
2. Less waste acid for disposal.
3. Less cooling water and power used during testing.

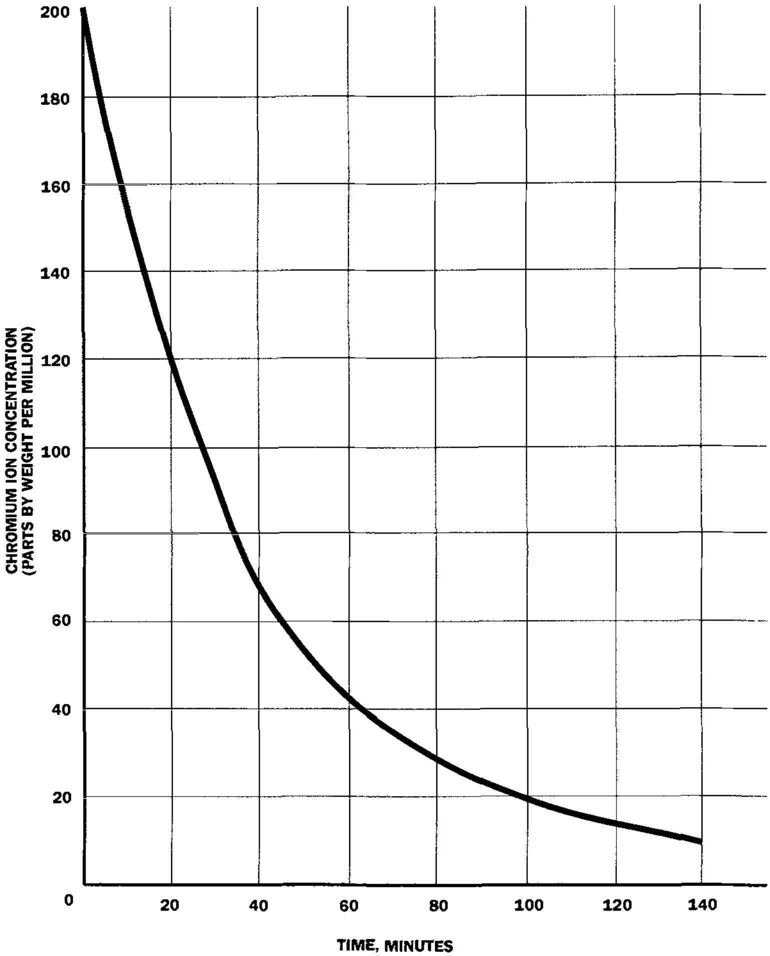

FIG. 3—*Chromium concentration versus time for normal boiling of inner test cup.*

TABLE 4—*Type 304L corrosion rate comparisons, flask versus glass pot.*[a]

Heat	Carbon, %	Sample	Flask,[b] in./month[d]	Glass Pot,[c] in./month[d]
A	0.010	1	0.0008	0.0009
		2	0.0009	0.0010
		3	0.0009	0.0009
B	0.028	1	0.0048	0.0045
		2	0.0040	0.0040
		3	0.0046	0.0038
C	0.026	1	0.0010	0.0011
		2	0.0013	0.0009
		3	0.0011	0.0012

[a] 200-ppm Cr^{+6} ion added to boiling acid in glass pot test cup 1 h prior to adding samples.

[b] Five 48-h periods, acid changed after each period.

[c] One 240-h exposure, no acid change.

[d] To convert from in./month to mm/month, multiply by 25.4.

4. Less technician attention and flask manipulation (a serious safety consideration) during testing.

Summary

The procedure usually used for ASTM A 262, Practice C nitric acid corrosion acceptance testing of stainless steels, involves a single sample in a single flask with an acid change every 48 h to prevent accumulation of undesired hexavalent chromium ion during the 240-h test period. A glass multisample testing apparatus can accommodate up to 100 samples simultaneously and uses only 4 L of nitric acid. Its unique design recycles freshly distilled acid over the samples and flushes away the products of corrosion. The test results compare

TABLE 5—*Cost comparison between flask method and glass pot method (1989 dollars).*[a]

	Each	10	50
Flask method equipment:			
Flasks	$ 5.60	$ 34.00	$ 230.00
Condensers	$ 50.50	$ 455.00	$2275.00
Hot plates	$ 210.00	$1020.00	$5100.00
Tubing	$ 5.00	$ 20.00	$ 100.00
Cradles	$ 8.30	$ 83.00	$ 830.00
Total	$ 279.40	$1612.00	$8535.00
Glass pot equipment:			
Glass pot	$ 610.00		
Teflon support rings	$ 475.00		
Heating mantle	$ 150.00		
Voltage regulator	$ 116.00		
Tubing	$ 15.00		
Total	$1366.00		

[a] Accessory equipment which can be added to either system:

Refrigerated recirculating water cooler for condensers $1200.00

Temperature controller to override power to heaters in event of cooling water failure $ 600.000

favorably with those obtained when the same samples are exposed in individual flasks with periodic acid changes.

For the testing laboratory performing a significant number of the nitric acid acceptance tests on a regular basis, there is the potential for major economic savings in acid consumption, manpower, and use of laboratory space.

Additional work is needed before the pot method should be applied to Types 316, 316L, and other stainless steels. Hopefully the author will be able to report on this work in the future.

Acknowledgments

The author wishes to express his gratitude to W. S. Morrison, S. V. Fox, and J. D. Demo for their technical assistance. The efforts of the staff of Pesce Lab Sales in producing the custom glassware used for this project are gratefully acknowledged.

References

[*1*] DeLong, W. B., *Evaluation Tests for Stainless Steels, ASTM STP 93,* American Society for Testing and Materials, Philadelphia, 1949, pp. 211–214.

[*2*] Alger, J. V., Roberts, E. C., Lent, R. P., and Anderton, G. W., *Bulletin,* No. 214, May 1956, American Society for Testing and Materials, Philadelphia, pp. 57–60.

[*3*] Truman, J. E., *Journal of Applied Chemistry,* Vol. 4, May 1954, pp. 273–283.

[*4*] Henthorne, M., *Localized Corrosion—Cause of Metal Failure, ASTM STP 516,* American Society for Testing and Materials, Philadelphia, 1972, pp. 66–119.

[*5*] Streicher, M. A., *Journal of the Electrochemical Society,* Vol. 106, March 1959, pp. 161–180.

[*6*] Streicher, M. A., *Corrosion/80,* Paper 87, National Association of Corrosion Engineers, Houston, March 1980.

[*7*] Tisinai, G. F. and Samans, C. H., *Bulletin,* Vol. 4, May 1959, American Society for Testing and Materials, Philadelphia, p. 64.

[*8*] Atkinson, J. T. N. and VanDroffelaar, H., *Corrosion and Its Control, An Introduction to the Subject,* National Association of Corrosion Engineers, Houston, 1982, pp. xv–xxi.

[*9*] Corbett, R. A. and Saldanha, B. J., *Metals Handbook, Volume 13 Corrosion,* American Society of Metals International, Metals Park, Ohio, 1987, pp. 239–241.

[*10*] Schluter, J. M. and Chivinsky, J. A., *Laboratory Corrosion Tests and Standards, ASTM STP 866,* American Society for Testing and Materials, Philadelphia, 1985, pp. 455–464.

[*11*] Huey, W. R., *Transactions,* American Society for Steel Treating, ASM, Metals Park, OH, Vol. 18, 1930, pp. 1126–1143.

Section V: Electrochemical Tests

John R. Scully[1]

Electrochemical Methods for Laboratory Corrosion Testing

REFERENCE: Scully, J. R., **"Electrochemical Methods for Laboratory Corrosion Testing,"** *Corrosion Testing and Evaluation: Silver Anniversary Volume, ASTM STP 1000,* R. Baboian and S. W. Dean, Eds., American Society for Testing and Materials, Philadelphia, 1990, pp. 351–378.

ABSTRACT: Electrochemical methods are extremely useful for the study of aqueous corrosion phenomena, particularly when utilized in conjunction with other techniques. Basic electrochemical principles are reviewed and examples given of application of a variety of electrochemical techniques to corrosion. Standards of ASTM Subcommittee G1.11 on Electrochemical Measurements in Corrosion Testing describe some useful experimental guidelines for the application of many of the techniques discussed.

KEY WORDS: anode, anodic polarization, auxiliary electrode, breakdown potential, cathode, cathodic polarization, corrosion, corrosion potential, corrosion rate, current density, diffusion limited current density, electrode, electrode potential, electrochemical cell, equilibrium cell, exchange current density, galvanic current, galvanic couple, galvanic current density, galvanostatic, impedance, intergranular corrosion, localized corrosion, mixed potential, open circuit potential, overvoltage, oxidation, passivation, passive, pitting, polarization, polarization resistance, potentiodynamic, potentiostat, reduction, stress corrosion cracking, Tafel slope, uniform corrosion, working electrode

Metallic corrosion is usually an electrochemical process. Electrochemical processes require anodes and cathodes in electrical contact and an ionic conduction path through an electrolyte. The electrochemical process includes electron flow between the anodic and cathodic areas, which quantify the rates of the oxidation and reduction reactions that occur at the surfaces. Monitoring this electron flow provides the capability of assessing the kinetics of the corrosion process, not simply the thermodynamic tendencies for corrosion nor only the metal loss registered after the test. Several textbooks cover many of the major aspects associated with the application of electrochemical methods in corrosion [*1–8*]. Electrochemical techniques for studying corrosion phenomena have been the subject of several symposia [*9–14*].

Most forms of metallic corrosion, including uniform, localized, galvanic, dealloying, stress corrosion, and hydrogen-induced failure, can be studied with electrochemical techniques. Passivation, anodization, cathodic and anodic protection, and performance of barrier and sacrificial coatings on metals can be investigated with electrochemical techniques. Electrochemical techniques for studying hydrodynamic (mass transport controlled) corrosion processes [*15*] as well as transient electrochemical methods [*16*] designed to avoid mass transport control are also available. Electrochemical techniques have been applied to high-temperature, high-pressure aqueous applications as well as to the study of corrosion processes in

---

[1] Formerly, Metallurgy Dept., Sandia National Laboratories, Albuquerque, NM, 87185. Presently, Center for Electrochemical Sciences and Engineering, Department of Materials Science, University of Virginia, Charlottesville, VA 22901.

nonaqueous environments and aqueous environments of low conductivity. Here we present specific examples of various electrochemical methods to study corrosion.

Conducting an Electrochemical Polarization Experiment

According to mixed-potential theory, any electrochemical reaction can be algebraically divided into separate oxidation and reduction reactions, and there can be no net electrical charge accumulation [17]. For corrosion in the absence of externally applied potential, the oxidation of the metal and the reduction of some species in solution occur simultaneously at the metal/electrolyte interface. Under these circumstances the net measurable current is zero. However, a finite rate of corrosion (metal oxidation) occurs at local anodic sites on the metal surface. Such a current-potential relationship is shown schematically in Fig. 1.

When the corrosion potential, E_{corr}, is located at a potential that is distinctly different from the reversible electrode potentials (redox potential, or E_{redox}) of either the corroding metal or the species in solution that are cathodically reduced, the oxidation of the cathodic species or the reduction of any metallic ions in solution becomes negligible. E_{corr} indicates the potential at which the metal oxidation rate equals the reduction rate, and the net current measured externally is zero

$$i_{app} = i_{ox} - i_{red} \tag{1}$$

Because the metal oxidation current present at the corrosion potential is the quantity of interest in the corroding system, this parameter must be determined independently of the reaction rates of other adsorbed or dissolved reactants. Electrochemical polarization techniques can be utilized to determine the corrosion rate. Figures 2 and 3 illustrate a typical experimental arrangement and electrochemical cell, respectively. The potential can be applied in a ramp fashion, stepped as a function of time (sometimes called potentiostaircase), or held at a fixed potential as in the potentiostatic method and the change in current measured [18]. Conversely, the current can be applied in a continuous galvanostatic or stepped galvanostaircase manner and the change in potential monitored. Several American Society for Testing and Materials (ASTM) standards discuss methods for performing these experiments [19,20].

Measurement of I_{ox} at the potential of interest, where $I_{ox} = i_{ox} \times$ Area, over a known period of time leads to direct determination of the weight loss

$$W = (I \times t \times M/nF) \tag{2}$$

where

W = the weight loss, g
$I \times t$ = the product of current and time, C,
n = the number of electrons involved in the electrochemical reaction,
F = Faraday's constant, 96 487 C/g-equivalent, and
M = the molecular weight of the electroactive species.

This relation is known as Faraday's law. Rearrangement of Eq 2 leads to a straightforward determination of the penetration rate (applicable only when I_{ox} is uniformly distributed over the entire wetted surface area or where the localized actively corroding area, A, is known), as follows:

$$CR = 3.27 \times 10^{-3} \times i_{ox} \times EW/\rho \tag{3}$$

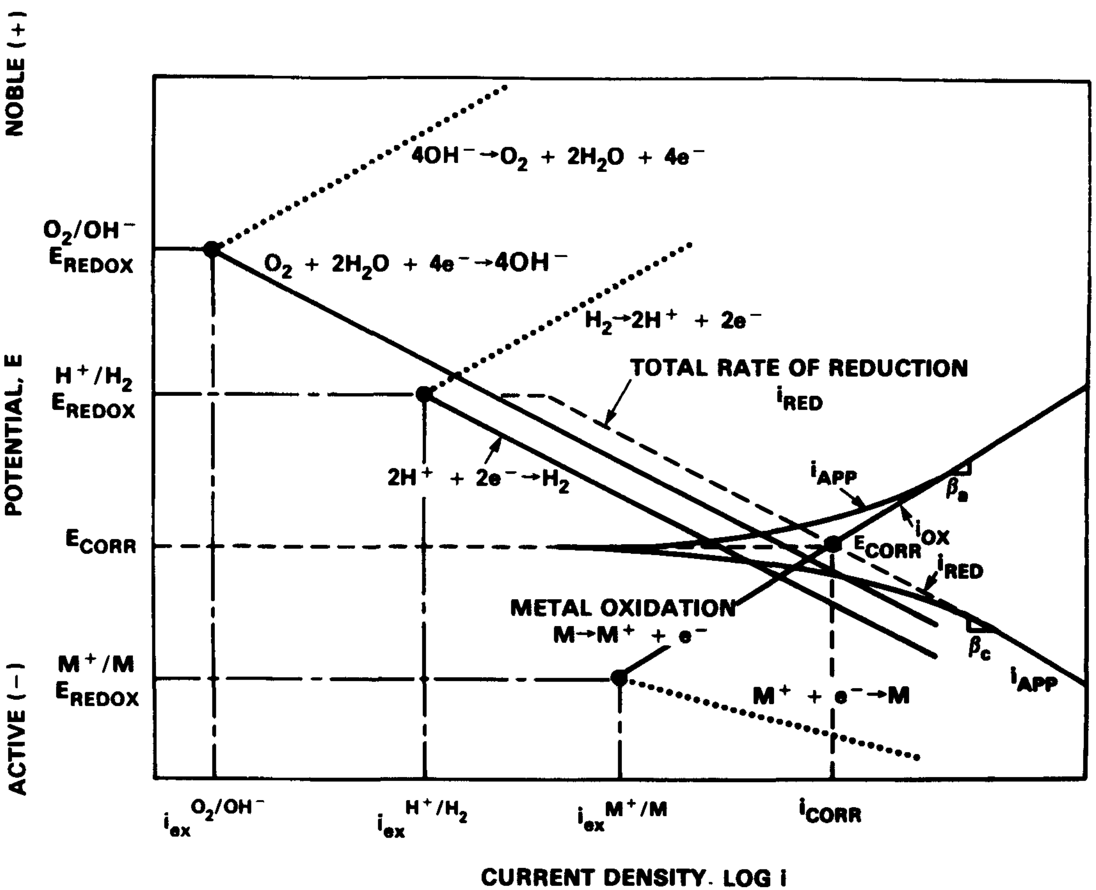

FIG. 1—*Schematic electrochemical potential-current relationship for a corroding system consisting of two cathodic reactions and one anodic electrochemical reaction.*

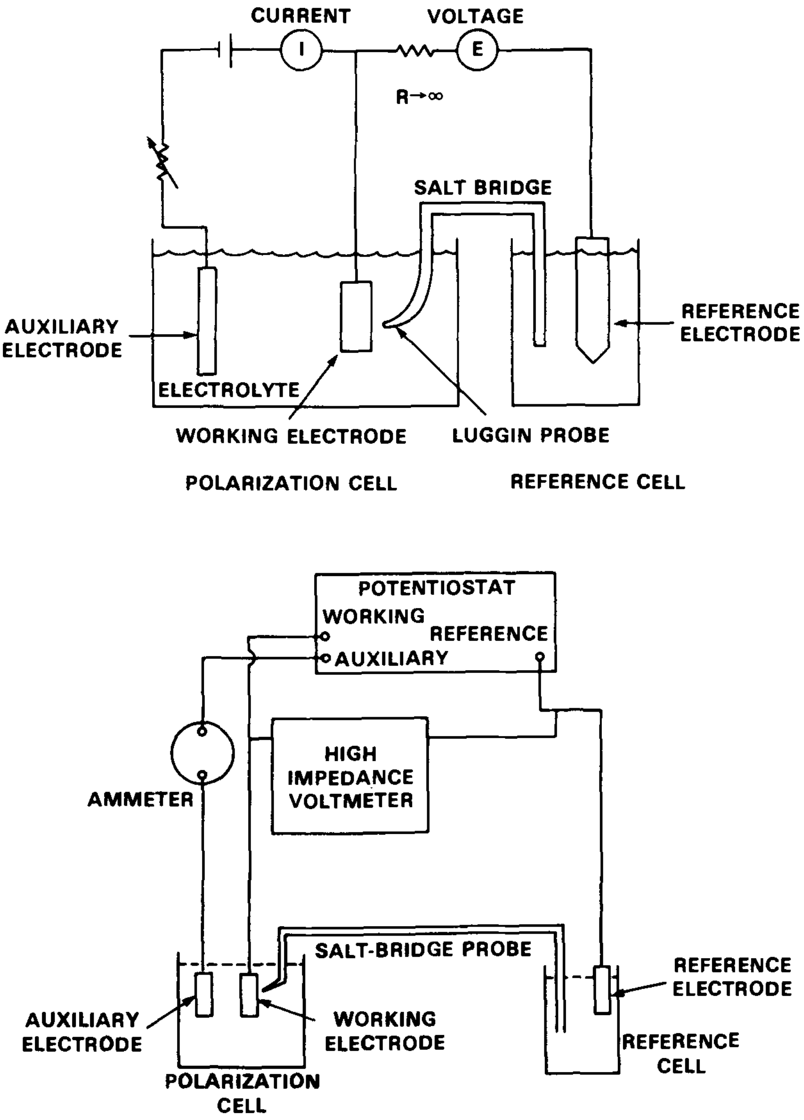

FIG. 2—*Instrumentation setup for electrochemical polarization cell.*

where

CR = the corrosion rate, mm/years,
EW = the equivalent weight, g,
ρ = the metal or alloy density g/cm^3, and
i_{ox} = the corrosion current density, μA/cm^2.

For alloys, the equivalent weight, EW, should be calculated using the atomic fractions of each alloying element

$$EW = \Sigma f_i / \Sigma (f_i \times n_i / AW_i) \tag{4}$$

where

f_i = the atomic fraction of the ith component of the alloy,
AW_i = the atomic weight of the ith component element,
n_i = the electron loss required to oxidize the ith component element under the conditions of the corrosion process [n is usually equal to the stable valence of the elements oxidized or must be determined from either a Pourbaix (potential-pH) diagram or experimentally from an analysis of the corroding solution], and
i = the number of component elements in the alloy.

This expression assumes that all the component elements oxidize when the alloy corrodes and that they are all oxidizing at essentially a uniform rate. In some situations, these assumptions are not valid; in these cases, the calculated corrosion rate will be in error. For example, if an alloy is composed of two or more phases and one phase preferentially oxidizes, the calculation must take this into consideration.

Electrochemical Methods for the Study of Uniform Corrosion: Polarization Methods

The following relationship observed between applied current and potential provides the basis for the electrochemical polarization technique [*1,2,21*]:

$$i_{\text{app}} = i_{\text{corr}}\{\exp[2.3\,(E - E_{\text{corr}})/\beta_a] - \exp[-2.3\,(E - E_{\text{corr}})/\beta_c]\} + C(dE/dt) \qquad (5)$$

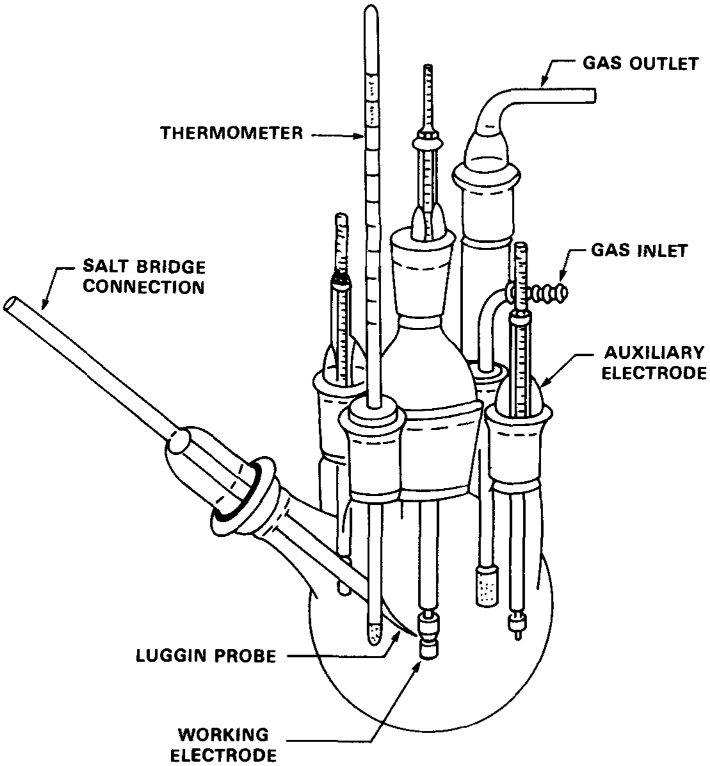

FIG. 3—*Typical electrochemical polarization cell illustrating locations for working and auxiliary electrodes and associated cell components.*

where

i_{app} = the applied current density based on the electrochemical surface area,
i_{corr} = the corrosion current density,
E = the applied voltage,
E_{corr} = the open-circuit or freely corroding potential,
C = the interfacial capacitance associated with the electrochemical doublelayer [1,2],
β_a = the anodic Tafel coefficient related to the slope of the polarization curve in the anodic regime,
β_c = the cathodic Tafel coefficient related to the slope of the polarization curve in the cathodic regime, and
dE/dt = the time rate of change in applied potential, or voltage, scan rate.

Ideally, the second term of the expression $C \times dE/dt$ approaches 0 at low potential scan rates. Note that i_{app} becomes approximately equal to either i_{ox} or i_{red} at large overpotentials, η. At very large anodic or cathodic overpotentials, Eq 5 can be rearranged in a more simplistic form [1–3,5,7]

$$\eta_a = \beta_a \log(i_{\mathrm{app}}/i_{\mathrm{corr}}) \tag{6}$$

$$\eta_c = -\beta_c \log(i_{\mathrm{app}}/i_{\mathrm{corr}}) \tag{7}$$

where

$\eta = E - E_{\mathrm{corr}}$,
η_a = the anodic overpotential, and
η_c = the cathodic overpotential.

The reader should note that these equations are only valid for one anodic and one cathodic reaction.

Tafel Extrapolation

By plotting η versus $\log(i_{\mathrm{app}})$, a linear relationship between current density and potential is obtained [1,5,7,21]. i_{corr} is determined from extrapolation of applied current from either the anodic or the cathodic Tafel region to the open-circuit potential (zero overpotential). Figure 4 illustrates this method.

Complications with the Polarization Method Involving Solution Resistance

Polarization techniques can be complicated by several factors. One such factor arises from the resistivity of the solution, the cell geometry, the location of the reference electrode, and the magnitude of applied current [2,6]. Placement of the reference electrode near the working electrode is facilitated with a Luggin-Haber capillary. This arrangement is used to minimize the solution resistance error, which can be estimated from the product of the applied current density, the solution resistivity, and the distance from the Luggin probe to the specimen surface. The error contributes to the measured overpotential in the following manner

$$\eta_{\mathrm{app}} = \eta_{\mathrm{true}} + IR \tag{8}$$

where

IR = equal to $I_{\mathrm{app}} \times R_{\mathrm{sol}}$.

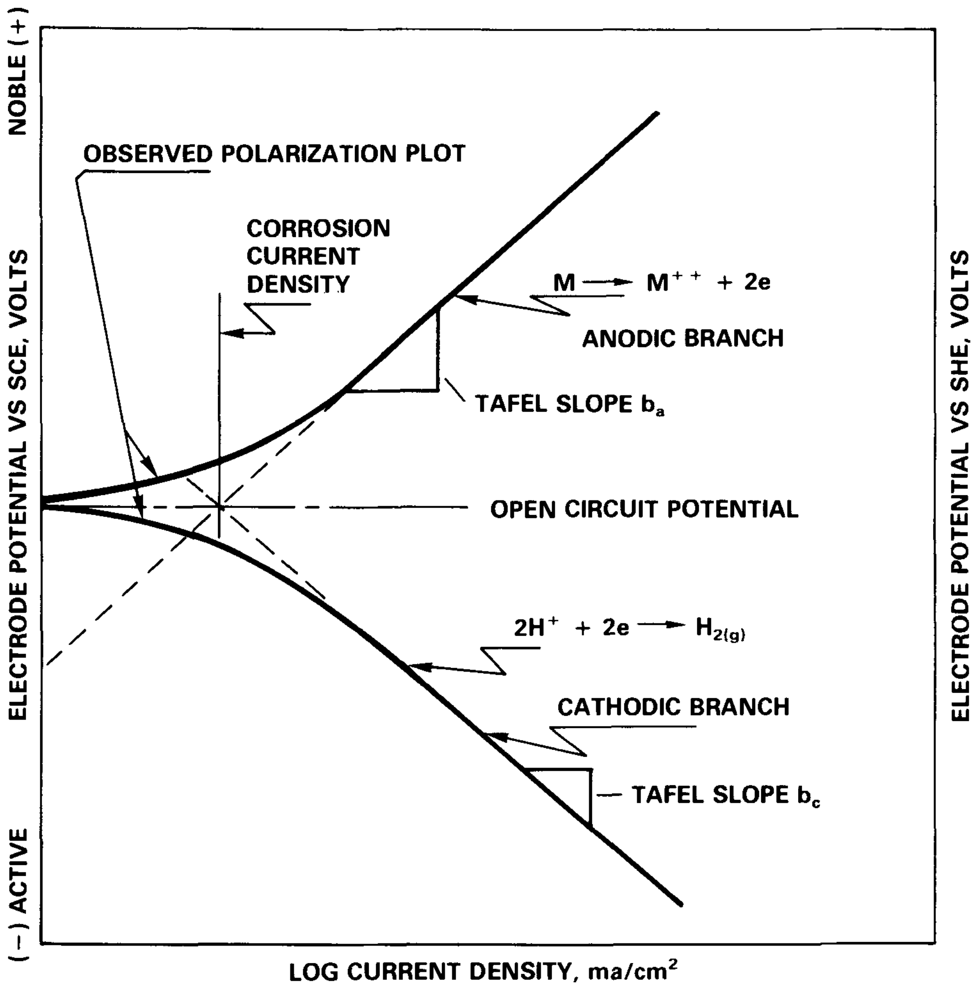

FIG. 4—*Experimentally measured Tafel polarization plot.*

R_{sol} is the uncompensated component of solution resistance between the working and reference electrodes. Thus, the true overpotential is overestimated at each applied current density, and the Tafel slope becomes inaccurate. The true scan rate in the potentiodynamic technique may also be altered. Several excellent reviews are available on the subject of the voltage error introduced from solution resistance [*23–26*].

Complications Involving Concentration Polarization Effects

The Tafel relationship established above is dependent on pure activation control, or charge transfer control. An additional consideration involves the concept of concentration polarization. In this case, the reaction rate is large enough that the electroactive species is depleted or concentrated at the reacting surface. In order to maintain the reaction rate, diffusion becomes the kinetic limitation, and the reaction becomes diffusion controlled at the limiting current density, i_L. The deviation from activation control is described by [5]

$$\eta = 2.3RT/nF \log(1 - i_{app}/i_L) \qquad (9)$$

where

R = the gas constant, and
T = the absolute temperature.

As i_{app} approaches i_L, the overpotential,η, becomes very large. Many corroding systems are under mixed activation and mass transport control [5]. This behavior can be described mathematically by the algebraic combination of Eqs 5 and 9. To increase the reaction rate and thus minimize the contribution of Eq 9 to the overpotential, the diffusional boundary layer thickness is decreased by solution stirring or by the use of a rotating cylinder or disk electrode [15].

Other Issues Concerning Tafel Extrapolation

Experimentally, there are several problems with the Tafel extrapolation method. Large applied current densities may not be representative of the true corrosion situation occurring at open circuit. This is particularly true in the case of anodic polarization, in which the surface is changing because of corrosion and/or passivation of the metal. In the cathodic case, an excess of adsorbed hydrogen or a buildup of hydroxyl ions in solution at the metal surface may result in alterations of surface chemistry not representative of the freely corroding case. In addition, concentration polarization may eliminate the Tafel region entirely.

Polarization Resistance Methods

For anodic and cathodic polarization within 10 mV of the corrosion potential, it is often observed that the applied current density is approximately linear with potential [1]. This behavior is shown in Fig. 5 for 430 stainless steel in sulfuric acid (H_2SO_4). The slope of this plot is determined at the corrosion potential, as shown in Fig. 5 [27,28]. This slope has units of resistance-area and is the polarization resistance. Stern and Geary simplified the Butler-Volmer equations describing charge transfer controlled reaction kinetics (Eq 5) for the case of small overpotential perturbations at the corrosion potential [29,30]. This simplified relationship has this form if $C \times dE/dt$ is negligible

$$i_{corr} = (\Delta i_{app}/2.3A\Delta E)(\beta_a\ \beta_c/\beta_a + \beta_c) \tag{10}$$

$$i_{corr} = (1/2.3R_p)(\beta_a\ \beta_c/\beta_a + \beta_c) \tag{11}$$

where

R_p = the polarization resistance,
β_a = the anodic Tafel slope, and
β_c = the cathodic Tafel slope.

The value R_p is determined from the slope of the potential-current density plot. The surface area of the working electrode must be known. Knowledge of R_p and Tafel slope values permit direct determination of the corrosion rate at any instant in time [28–31]. The ASTM standards G-59 [20] and D-2776 [32] describe procedures for conducting polarization resistance measurements. These standards do not address all possible complications.

Complications with Polarization Resistance Measurements

The literature reports several complications and possible alternative methods in the use of the polarization resistance method [33–38]. Three of the most obvious errors that are

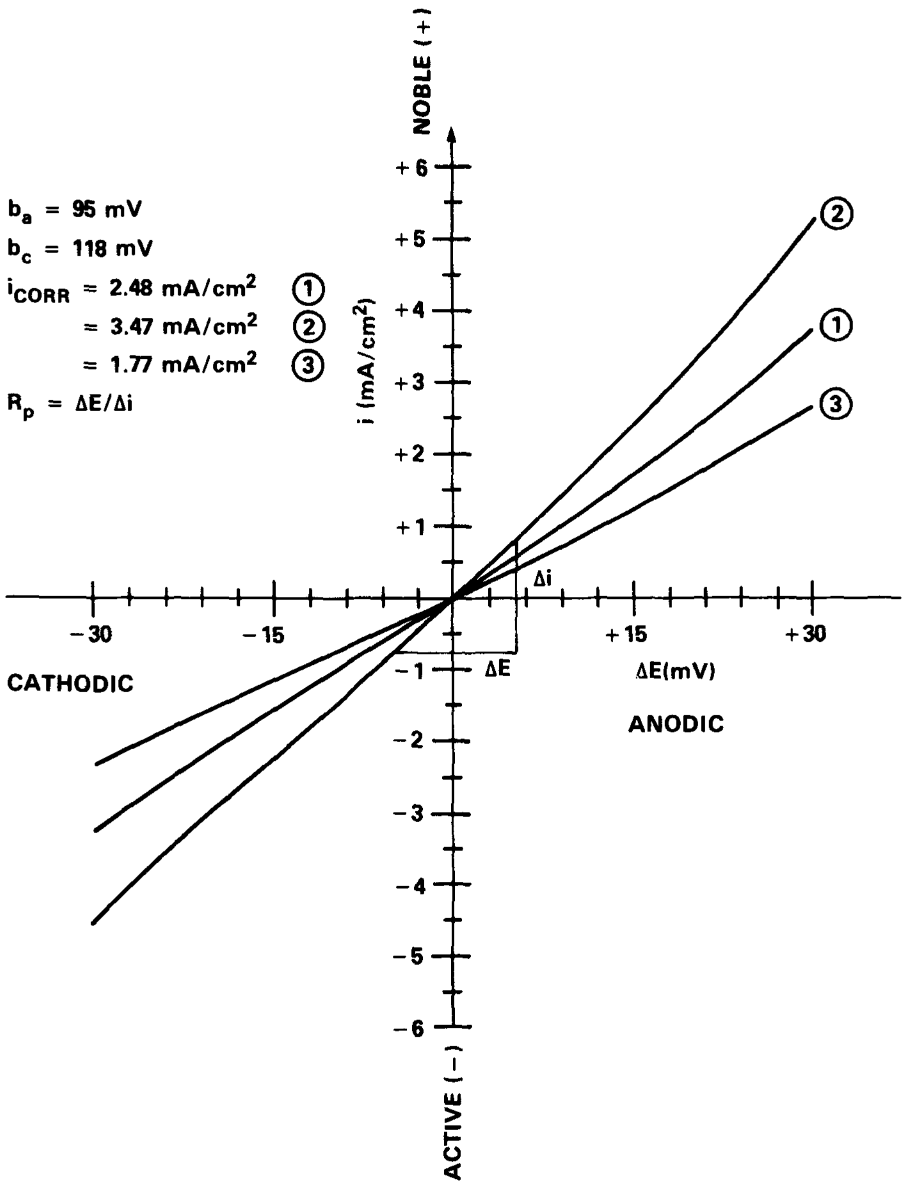

FIG. 5—*Polarization curves for polarization resistance measurements based on the results from eight independent laboratories for type 430 stainless steel in 1* N *H_2SO_4. Curve 1 is the mean result, with curves 2 and 3 showing ±2 standard deviations* [20].

possible when using these methods involve invalidation of the results through oxidation of some other electroactive species besides the corroding metal in question, a change in the open-circuit or corrosion potential during the time taken to perform the measurement, and the application of a large applied potential resulting in inadvertent departure from linear current density versus potential behavior. Several techniques actually take advantage of the departure from nonlinearity in order to calculate the anodic and cathodic Tafel slopes at a low overpotential and thus avoid some of the problems associated with large polarization [*38*].

Another source of error involves cases in which both the anodic and cathodic reactions are not charge transfer controlled processes, as required for the derivation of Eq 10. Corrections to Eq 10 exist for cases in which pure activation control is not maintained, such as in the case of partial diffusion control or passivation [*39*]. Other researchers have attempted to calibrate their results through gravimetric determination of mass loss [*40*]. In fact, in one case, polarization resistance data for a number of alloy-electrolyte systems were compared to the observed corrosion currents determined from weight change [*31*]. A linear correspondence was obtained over six orders of magnitude in corrosion rates.

Two other frequently encountered complications are the need to correct for the electrolyte (solution) resistance, R_{sol}, and the effects of capacitive hysteresis, $C \times dE/dt$, occurring as a function of the voltage scan rate [*2*]. Hysteresis in the current density-potential plot is observable when the time rate of change, dE/dt, of the applied potential is large or the interfacial capacitance and polarization resistance are large. The effect can be minimized by performing the polarization resistance test at a lower scan rate or by taking two or more d-c current density-potential measurements instead of continuously varying the potential. The solution, or ohmic resistance, on the other hand, still complicates the measurement because the algebraic sum of the polarization resistance and the solution resistance is measured in a d-c measurement.

Many treatments of this subject have used an electrical equivalent circuit model to simulate the corroding metal/electrolyte interface [*41,42*]. The simplest form of such a model, the Randles circuit, is shown in Fig. 6. The three parameters discussed above (R_p, R_{sol}, and C) are shown in the relationship to one another that best approximates a corroding electrochemical interface of a metal. The sum of the polarization resistance and the uncompensated solution resistance is measured when a d-c measurement is performed because the capacitive reactance approaches infinity. Thus, the true corrosion rate will be underestimated when R_{sol} is appreciable. Conversely, any experiment conducted at a fast voltage scan rate causes the algebraic sum of the ohmic resistance and the resultant parallel impedance of the parallel resistive-capacitive network to be measured. This value will be lower than the sum of R_p and R_{sol} determined at an infinitely slow scan rate. This will usually result in an overestimation

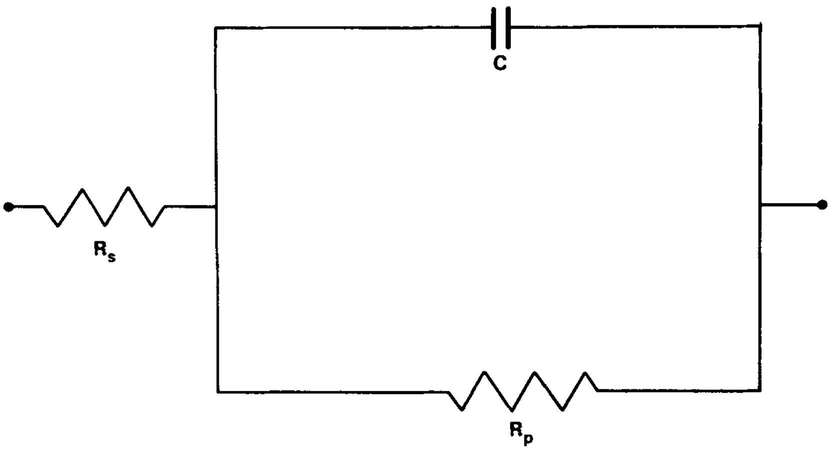

FIG. 6—*Electrical equivalent circuit model simulating a simple corroding metal/electrolyte interface (see also Fig. 7).*

of the true corrosion rate. These complications can be overcome by using the electrochemical impedance method.

Electrochemical Impedance Methods

One approach for determining the corrosion rate of a metal involves the electrochemical impedance (sometimes known as a-c impedance) method [*41–45*]. In this technique, a small-amplitude sinusoidal potential perturbation is applied to the working electrode at a number of discrete frequencies. At each one of these frequencies, the resulting current waveform will exhibit a sinusoidal response that is out of phase with the applied potential signal by a certain amount. The electrochemical impedance is a frequency-dependent proportionality factor that acts as a transfer function by establishing a relationship between the excitation voltage signal and the current response of the system. As such, an electrochemical impedance is a fundamental characteristic of the electrochemical system it describes. A knowledge of the frequency dependence of impedance for a corroding system allows a determination of an appropriate equivalent electrical circuit describing that system. Figure 6 illustrates in the most simple case the equivalent electrical circuit model for an actively corroding metal. The following expression describes the impedance for that system

$$Z = R_{sol} + R_p/(1 + \omega^2 R_p^2 C^2) - j\omega C R_p^2/(1 + \omega^2 R_p^2 C^2) \tag{12}$$

where

Z = the impedance magnitude,
ω = $2\pi f$ is the frequency of the applied signal, rad/s,
C = the interfacial capacitance, and
$j^2 = -1$.

Experimentally, it can be easily seen from Fig. 7 that, at very low frequencies

$$Z_{min} = R_{sol} + R_p \tag{13}$$

while at very large frequencies

$$Z_{max} = R_{sol} \tag{14}$$

A calculation of the polarization resistance is possible in media of high resistivity because R_p can be mathematically separated from R_{sol} by measuring Z at high and low frequencies and subtracting the two ($R_p = Z_{min} - Z_{max}$). Determination of the corrosion rate also requires accurate values for the anodic and cathodic Tafel slopes β_a and β_c, as shown in Eq 11. The minimum frequency required to obtain $R_{sol} + R_p$ is estimated by

$$f_{min} < f_{bp} = [2\pi C(R_s + R_p)]^{-1} \tag{15}$$

where

f_{bp} = the breakpoint frequency, and
f_{min} = the minimum test frequency required.

Since C, R_{sol}, and R_p are not known explicitly a priori, prudence dictates that f_{min} equal 0.1 to 0.5 of the estimated f_{bp}. Thus, large values of C, R_{sol}, or R_p mean that a lower frequency is required to accurately obtain Z_{min}. A frequency minimum of 1 mHz is typically chosen,

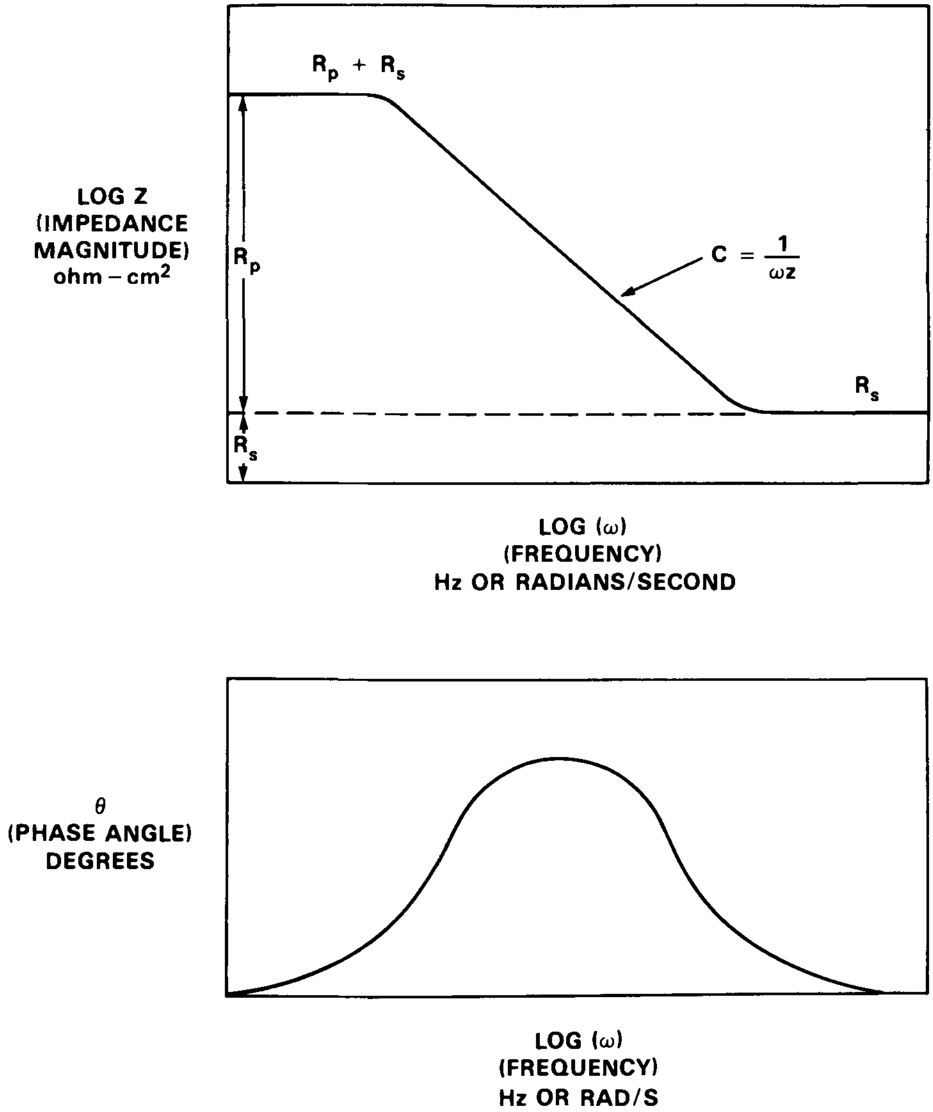

FIG. 7—*Bode phase in magnitude plots demonstrating the frequency dependence of electrochemical impedance for the circuit model shown in Fig. 6.*

but it is obvious from Eq 15 that either lower or higher frequencies are acceptable under the given circumstances. This issue equally plagues time domain and frequency domain measurements of R_p since in the time domain measurement the triangle waveform is simply the Fourier synthesis of a series of sinusoidal functions.

Other information determined from this technique includes the value of C, the capacitance. In the simple case of active corrosion, C may be found to scale linearly with the true electrochemical surface area from the relationship $C = c \times A$, where c is a specific capacitance per unit area, and A is the true electrochemical surface area [*46*].

Electrochemical Methods for the Study of Galvanic Corrosion

Methods Based on Mixed-Potential Theory

Galvanic corrosion can be explained by mixed-potential theory as schematically illustrated in Fig. 8. In the case of bimetal or multimetal galvanic attack in which two or more metals are electrically in contact with one another, there is in theory a minimum of two cathodic and two anodic reactions. One of each of these reactions is occurring on each metal. In this case, the more noble of the two metals is cathodically polarized and its anodic reaction rate will thus be suppressed. Conversely, the less noble or anodic material is anodically polarized and the anodic reaction rate is accelerated. The mixed potential (the galvanic couple potential, E_{couple}) of the galvanic couple and the resulting galvanic current can be uniquely determined from the sums of all of the individual anodic and cathodic currents obtained for each material at each potential when the following condition is met

$$\Sigma\, i_a \times A_a = \Sigma\, i_c \times A_c \qquad (16)$$

where

$\Sigma\, i_a \times A_a$ = the sum of the anodic currents (current density multiplied by area), and
$\Sigma\, i_c \times A_c$ = the sum of the cathodic currents for all of the metals coupled.

This relationship will be uniquely satisfied at one value of the applied potential and can be determined if: (1) potential versus anodic and cathodic current density data are available for each material in the galvanic couple; (2) the area of each metal is known; and (3) the current distribution is uniform. Thus this mixed potential will depend strongly on kinetic considerations as well as thermodynamic considerations. In simple bimetal cases, direct superposition of polarization data (corrected for wetted surface) yield the same result [*47*]. This technique is schematically illustrated in Fig. 8. However, because applied currents, not anodic or cathodic currents, are measured in the polarization experiment, the technique will introduce the least error when the cathodic reduction reaction rate on the anode material is negligible and the anodic oxidation reaction rate on the cathode material is negligible at the galvanic couple potential. Obviously when the open-circuit potentials of the anode and cathode material are similar, this complication is more likely to arise but, in this case, galvanic corrosion may be less significant. In addition, special care must be taken in the procedures used to develop the polarization data [*47*], especially if time effects are to be taken into consideration when evaluating long-term galvanic corrosion behavior.

Direct Measurement of Galvanic-Corrosion Rates

A more straightforward procedure involves immersing the two dissimilar metals in an electrolyte and electrically connecting the materials together using a zero-resistance ammeter to measure current [*9,48,49*]. In this method, the galvanic current is directly determined as a function of time. A reference electrode is used to determine the galvanic couple potential.

Electrochemical Methods for the Study of Passivity and Localized Corrosion

Pitting and crevice corrosion are associated with the breakdown of passivity [*50*]. The anodic electrochemical behavior of a passive alloy in deaerated acid is shown schematically in Fig. 9. Changes in the characteristics of this diagram with the addition of halides or other species which promote pitting aid in determining the resistance of an alloy to localized attack. Electrochemical tests for evaluating the susceptibility of a material to pitting and

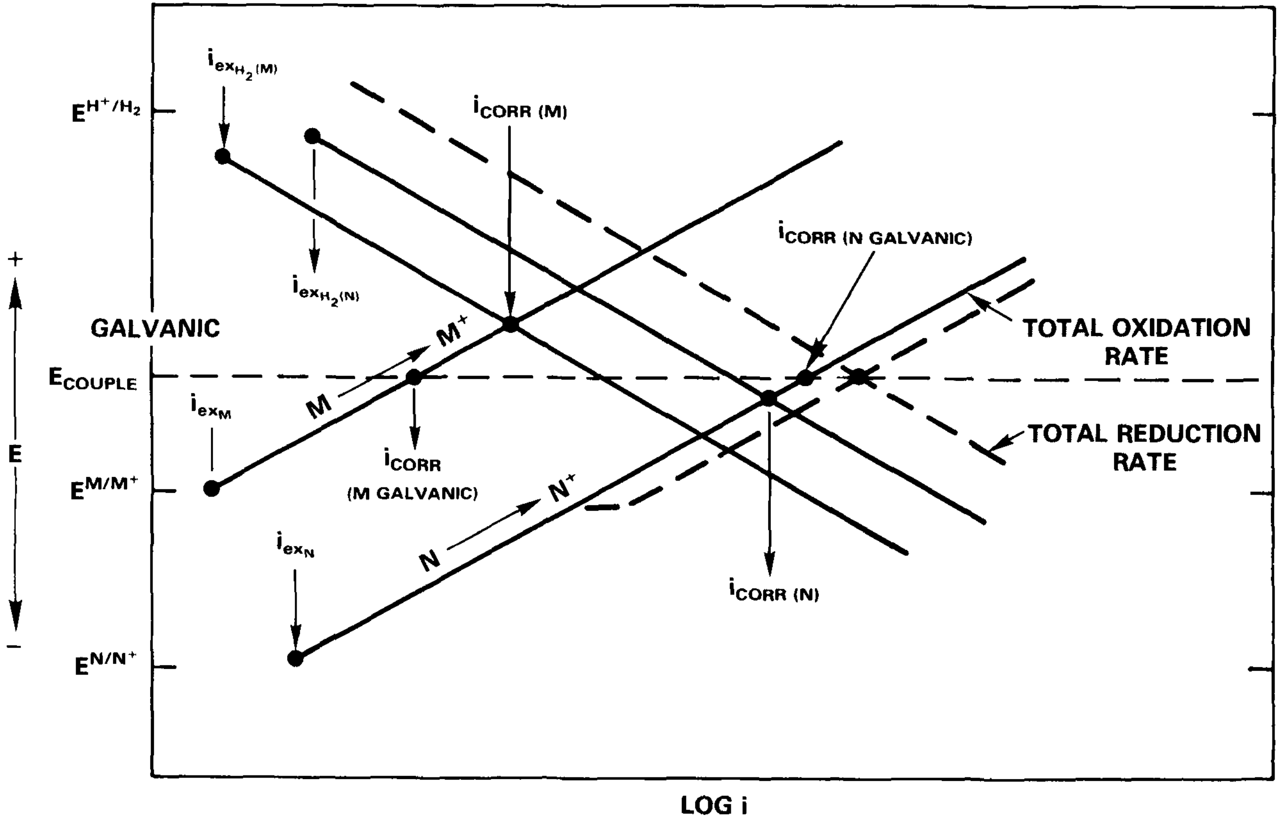

FIG. 8—*Potential-current relationships for the case of a galvanic couple between two corroding metals. M is the more nobel metal, N is less noble* [5].

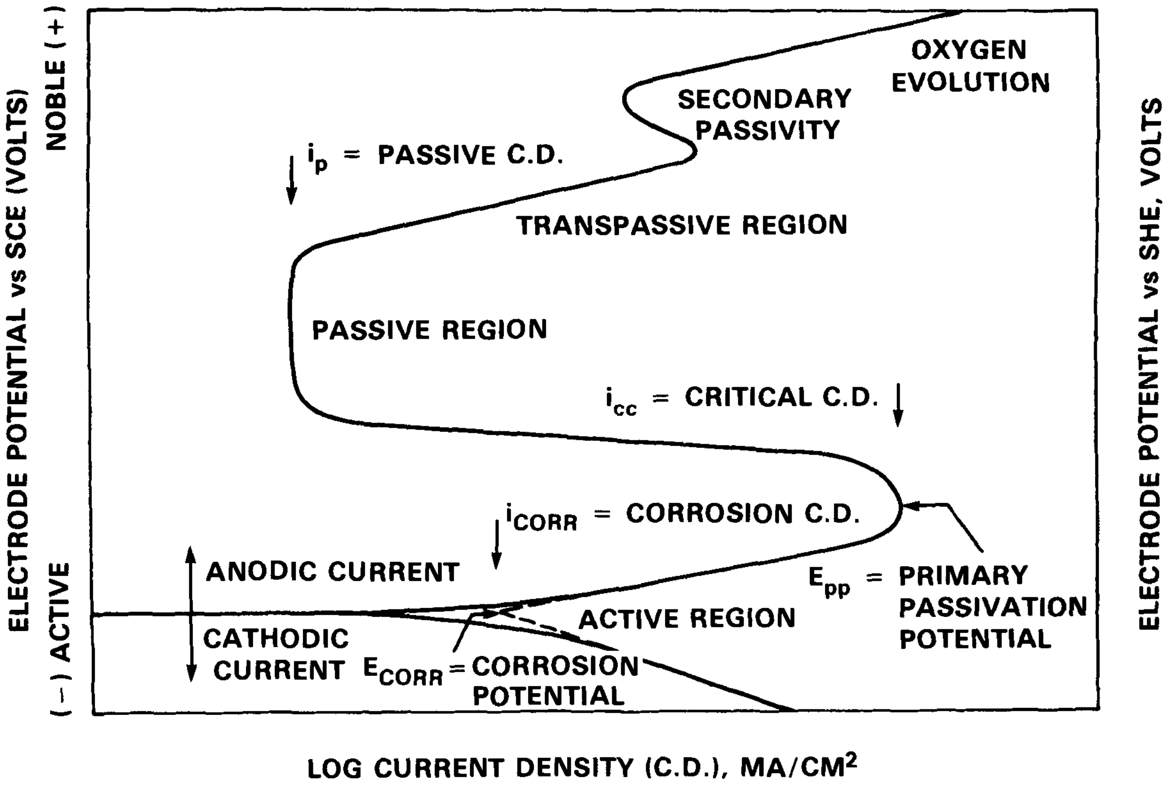

FIG. 9—*Hypothetical anodic and cathodic polarization behavior for a material exhibiting passive anodic behavior* [22].

crevice corrosion include potentiodynamic, potentiostatic, scratch potentiostatic, tribo-ellipsometric methods, pit-propagation rate curves, galvanostatic, and electrochemical noise measurements [*50–52*].

Cyclic Potentiodynamic Polarization Methods

The ASTM Test Method for Conducting Cyclic Potentiodynamic Polarization Measurements for Localized Corrosion Susceptibility of Iron-, Nickel-, or Cobalt-Based Alloys (G 61) describes a procedure for conducting cyclic potentiodynamic polarization measurements to determine relative susceptibility to localized corrosion [*53*]. The test method is designed for use with iron- or nickel-based alloys in chloride environments. In this test, a cyclic anodic polarization scan is performed at a fixed voltage scan rate. Particular attention is focused on two features of cyclic polarization behavior. The first is the potential at which the anodic current increases significantly with applied potential (the breakdown potential). In general, the more noble this potential, obtained at a fixed scan rate in this test, the less susceptible the alloy is to the initiation of localized attack. The second feature of great interest is the potential at which the hysteresis loop is completed upon reverse polarization scan. In general, once initiated, localized corrosion can propagate only at some potential more positive than the potential at which the hysteresis loop is completed (when determined at a fixed scan rate). In other words repassivation will occur at more negative potentials even after localized corrosion initiation. Therefore, the more positive the potential at which the hysteresis loop is completed, the less likely that localized corrosion will propagate. This potential is known as the protection potential. Figure 10 illustrates cyclic polarization behavior for Hastelloy C-276 and 304 stainless steel in 3.5% sodium chloride solution. Based on this criterion, it is evident that Hastelloy C-276 is more resistant to localized corrosion in this environment.

Complications With Cyclic Potentiodynamic Polarization Methods

Although the cyclic method is a reasonable method for screening variations in alloy composition and environments, the cyclic potentiodynamic polarization method has been found to have a number of shortcomings [*52–56*]. One major problem concerns the effect of the potential scan rate. The values of both the protection potential and the breakdown potential are a strong function of the manner in which the tests are performed, particularly the potential scan rate employed. This problem is related predominantly to the induction time required for pitting, the repassivation rates, and complications arising from allowing too much pitting propagation to occur before reversing the scan direction. This alters the localized chemistry in pits and subsequently affects the polarization behavior after the reversal in the direction of scanning.

Potentiostatic and Galvanostatic Methods for Localized Corrosion

The shortcomings of the cyclic potentiodynamic polarization method have become the basis for several other electrochemical techniques. Other methods are illustrated schematically in Fig. 11. Potentiostatic methods can be used to overcome the inherent problems involving scan rate. Figure 11*a* shows a schematic of the cyclic potentiodynamic method. A refinement to the breakdown potentials shown can be obtained by polarizing individual samples for long periods of time at potentials above and below the E_{prot} and E_{bd} previously determined from the potentiodynamic method. Eventual initiation is indicated by a current increase. A new value for E_{prot} can be determined. In the second method (Fig. 11*b* and *c*), initiation of pits is intentionally induced by applying a potential above the breakdown

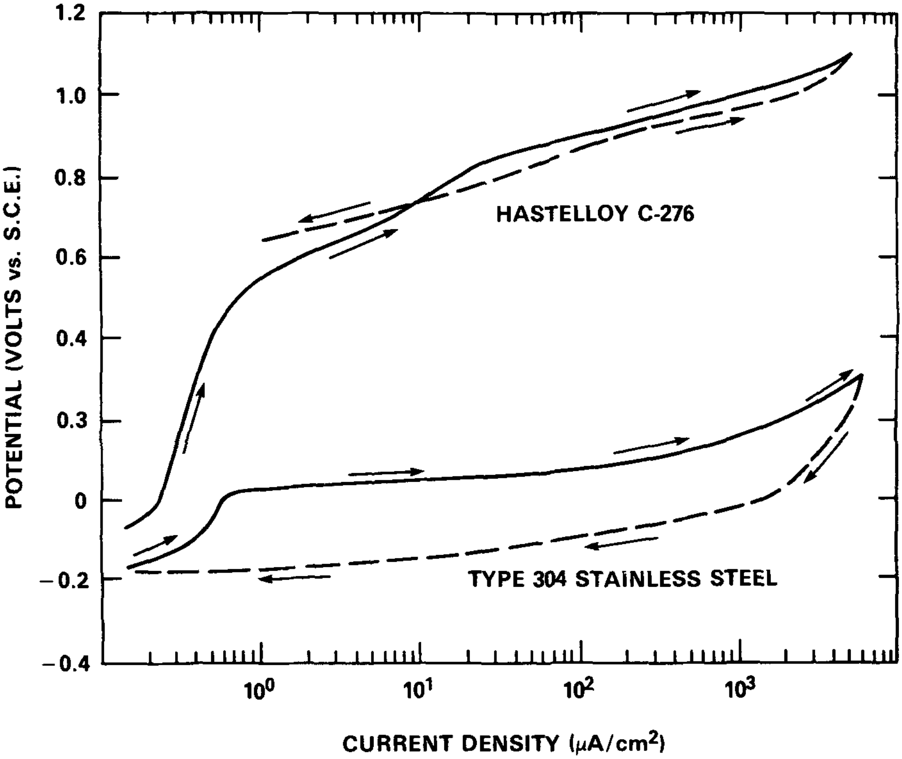

FIG. 10—*Cyclic potentiodynamic polarization curves for Hastelloy C-276 and Type 304 stainless steel in 3.56 wt. % NaCl solution* [53].

potential and then quickly shifting to a potential below that value. If this second applied potential is above the protection potential, propagation of the existing pits will continue and the current will increase. However, at potentials less than E_{prot} the pits will eventually repassivate and the current will subsequently decrease with time. In the galvanostatic or galvanostaircase technique (Fig. 11*d*), potential is measured versus time at various constant applied currents that are increased incrementally in steps, then reversed and decreased. Potential measurements are made until the time rate of change in potential approaches zero. This forward and reverse potential-current density data is extrapolated to the zero current density to obtain E_{bd} and E_{prot}. The technique is described by ASTM G 100 as a test method for aluminum alloys [57].

The Scratch-Repassivation Method for Localized Corrosion

One additional technique to be mentioned in the area of localized corrosion involves the scratch method [58]. In this method, the alloy surface is scratched at a constant potential and the current is measured as a function of time. The potential dependencies of the induction time and the repassivation time are determined by monitoring the current change over a range of different potentials. This is illustrated in Fig. 12. From this information the critical pitting potential, thought to be less than the breakdown potential, can be determined. Other methods of studying localized corrosion are also available [*19*].

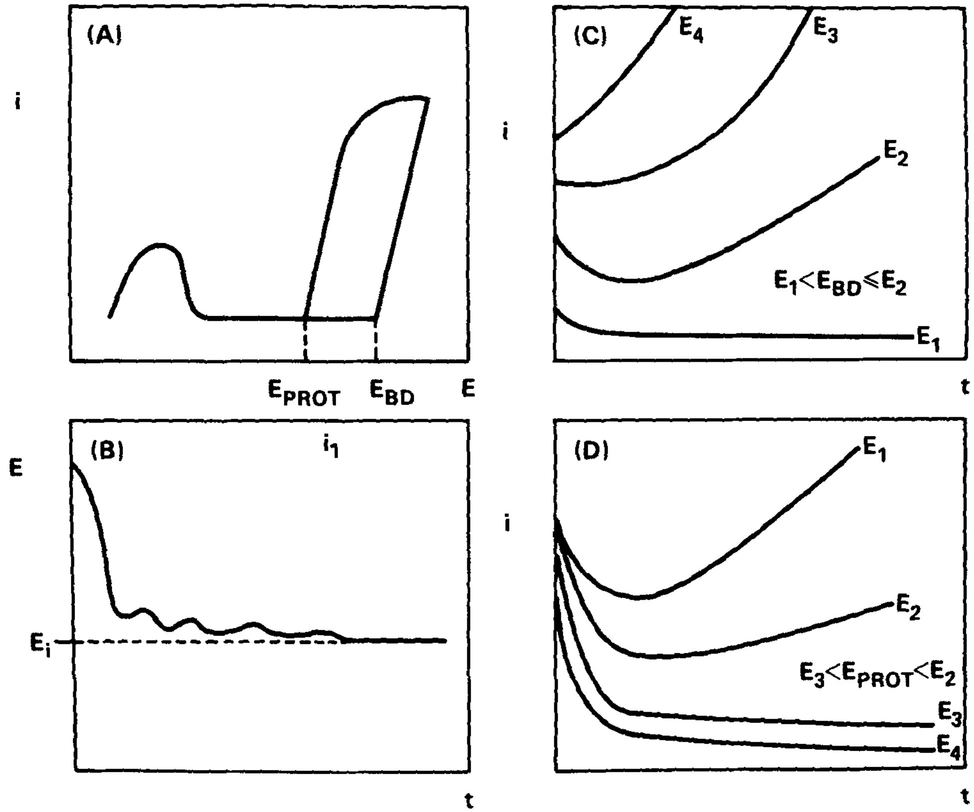

FIG. 11—*Schematic representations for* (a) *a cyclic potentiodynamic polarization curve,* (b) *potentiostatic current-time curves with a passivated surface,* (c) *potentiostatic current-time curves for an activated surface, and* (d) *a galvanostatic potential-time curve* [50].

Environmental Cracking

There are several electrochemical techniques for assessing susceptibility to environmental cracking. One of the techniques is for alloys that undergo slip-induced passive film rupture and anodic dissolution. The scratch-repassivation technique discussed above may be more useful to study stress corrosion cracking (SCC) than pitting [59]. This is because natural pitting is often initiated at defect sites in the passive film that are electronic or chemical in nature and not necessarily mechanical. Mechanical defects induced by scratching synthetically simulate SCC where mechanical film rupture processes are operative. The tribo-ellipsometric method is an advancement to the scratch method and has been used to distinguish between the case where an alloy is susceptible to localized corrosion, such as pitting or SCC. In general, once the passive film is disturbed mechanically at some potential, an electrochemical current can be measured that will decay back to a low level when repassivation has occurred. The total anodic current will consist of the sum of the repassivation current and the current corresponding to dissolution of the exposed bare metal without film formation. The electrochemical current measurement is conducted in conjunction with the optical ellipsometric method to measure the rate of film thickening. This combination offers a method of separating the two currents (dissolution-repassivation) from one another because it is a means of studying the kinetics of the film thickening associated with repassivation

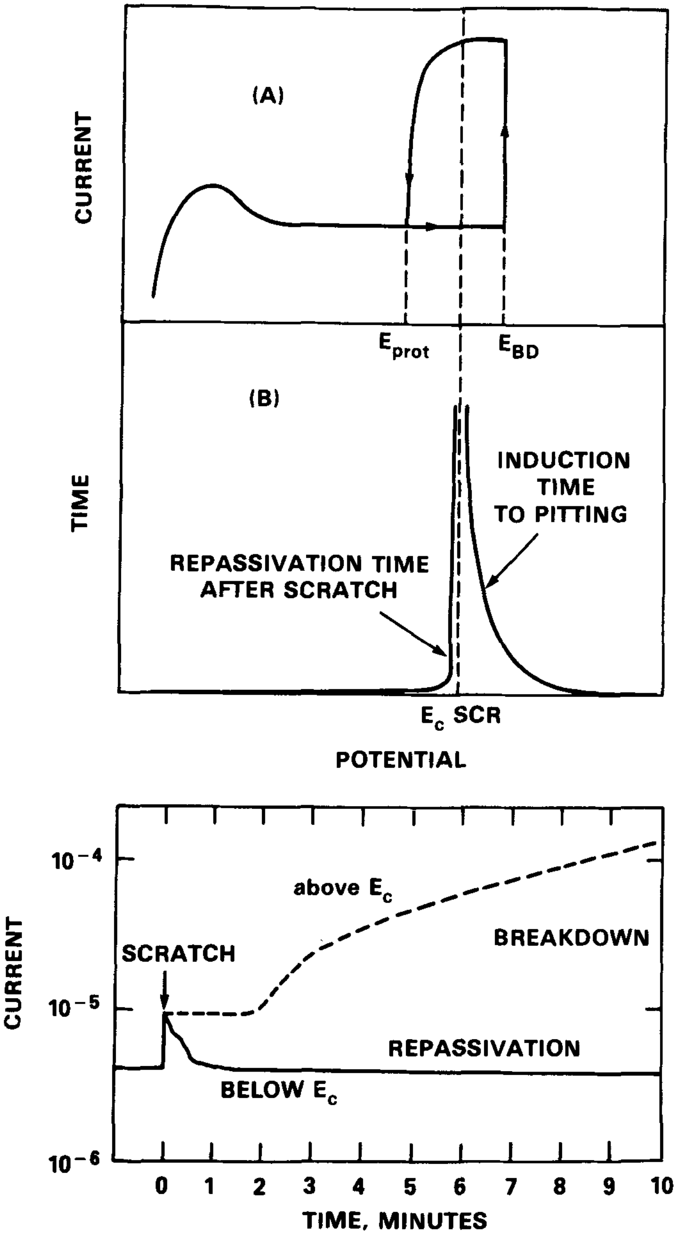

FIG. 12—*Potential versus time plot of scratch test illustrating the critical potential,* Ec, (a) *as it relates to the induction time, and* (b) *the repassivation time* [50].

(assuming that the oxidized species and density of the film are known so that charge can be determined from thickness). Based on the ratio of the charge involved in dissolution and the charge associated with repassivation, a criteria for stress corrosion is established

$$R_{scc} = 1 + Q_d/Q_r \tag{17}$$

where

Q_d = the charge involved in dissolution, and
Q_r = the charge associated with repassivation.

For example, a low-carbon steel was not found to be susceptible to SCC in a solution in which R_{scc} was 2.8. The steel was found to be susceptible when the ratio was 26, and it was not susceptible again in a solution in which R_{scc} was 75 [*59*]. In the latter case, widespread pitting occurred instead.

Evaluation of Alloy Sensitization

Measurement of the quantity of coulombs generated during the electrochemical polarization of a material from the passive range to the active corrosion potential can be used to detect the susceptibility to intergranular attack associated with the precipitation of chromium carbides and chromium nitrides at grain boundaries [*60–62*]. A modification of this procedure, called the double loop electrokinetic repassivation test [*63,64*], involves polarizing the metal surface initially from the open-circuit potential in the active region to a potential in the passive range. This is followed by reverse polarization in the opposite direction back to the open-circuit potential. Both variations of the method are illustrated in Fig. 13. In the latter method, the degree of sensitization is determined by taking the ratio of the maximum current generated in the reactivation or reverse scan to that generated in the initial anodic scan (I_r/I_a). The rationale for this procedure is contingent on the presence of anodic current upon the reactivation scan that results mainly from incomplete passivation of the region adjacent to the grain boundaries because of chromium depletion at grain boundaries. For nonsensitized material, the passive film essentially remains intact during the reverse scan, and the size of the reactivation polarization peak remains small. As a result the charge Q (obtained from integration of current versus potential for a known voltage scan rate) in the single loop is small. As a refinement to the method the charge is normalized by the grain-boundary area (GBA) because this is the area from which most of the current arises in the single reactivation scan [*62*].

$$P,\ \mathrm{C/cm^2} = Q/\mathrm{GBA} \tag{18}$$

$$\mathrm{GBA} = A_S\,[5.0954 \times 10^{-3} \times \exp(0.34696 \times GS)] \tag{19}$$

where

P = the reaction charge density associated with the sensitized area,
A_S = the specimen surface area, and
GS = the ASTM grain size.

The same procedure was used for the ratio I_r/I_a [*64*]. The current peak, I_r, for the reactivation scan was normalized for the grain boundary area while the initial anodic current peak was normalized to the wetted surface area, A_s.

$$i_r/i_a = I_r/I_a\,[5.0954 \times 10^{-3} \times \exp(0.34696 \times GS)] \tag{20}$$

A number of investigators have correlated this electrochemically derived ratio with optical metallographic evaluations of the degree of material sensitization such as those outlined in ASTM A 262 [*65*]. This has been accomplished for several different iron-nickel-chromium alloys [*66–68*]. The technique is nondestructive and can be applied in the field.

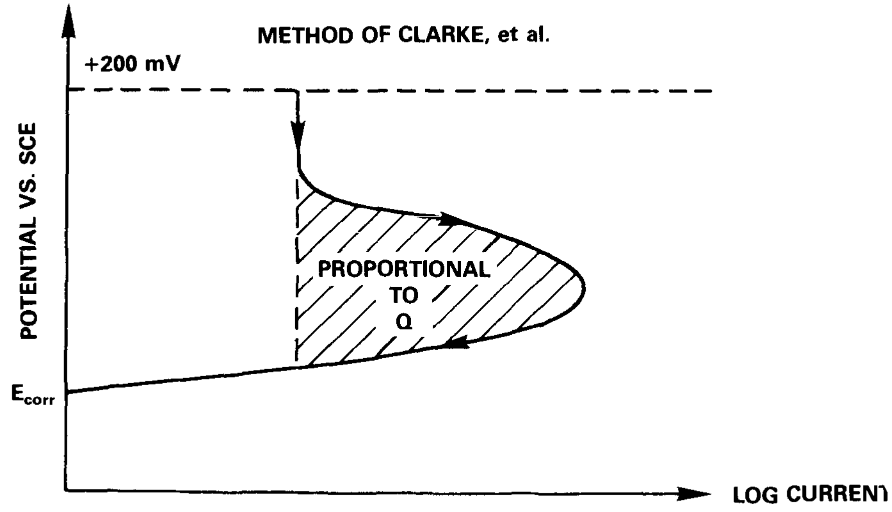

(a)

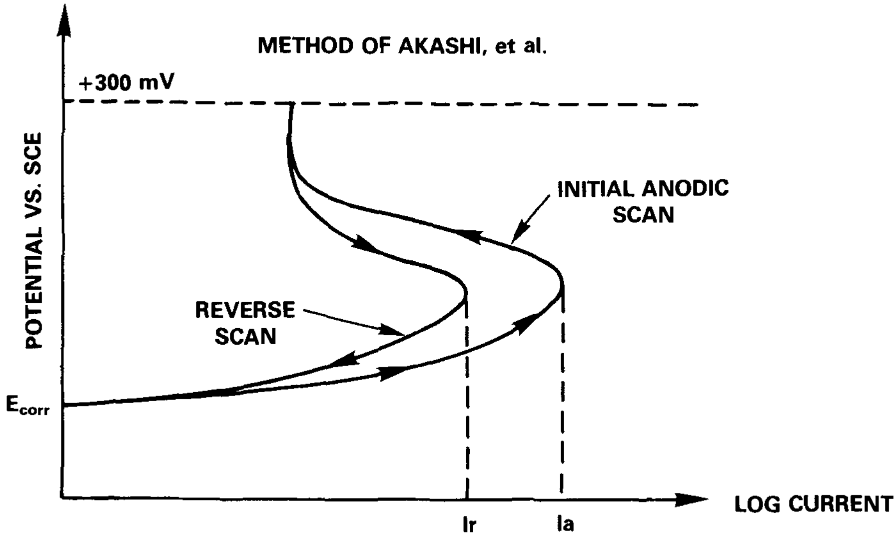

(b)

FIG. 13—*Schematics of two procedures for anodic reactivation polarization testing:* (a) *Clarke method* [61,62]; (b) *Akashi method* [63,64].

Electrochemical Evaluation of Protective Coatings and Films

Numerous a-c and d-c electrochemical methods have been used to study the performance and the quality of protective coatings, including passive films on metallic substrates and evaluation of the effectiveness of various surface pretreatments. Several are discussed below.

Anodized Aluminum Corrosion Test

The Ford anodized-aluminum corrosion test (FACT) [*69,70*] involves the cathodic polarization of the anodized aluminum surface by using a small cylindrical glass clamp-on cell and a special 5% sodium chloride (NaCl) solution containing cupric chloride ($CuCl_2$) acidified with acetic acid. A large voltage is applied across the cell by using a platinum auxiliary electrode. The alkaline conditions created by the cathodic polarization promote dissolution at small defects in the anodized aluminum. The coating resistance is decreased, more current begins to flow, and the voltage decreases. The cell voltage (auxiliary electrode to specimen voltage) is monitored for 3 min, and the cell voltage multiplied by time is recorded. ASTM B 538 describes the method in greater detail [*69*]. A similar test, known as the cathodic breakdown test, involves cathodic polarization to −1.6 V versus saturated calomel electrode (SCE) for a period of 3 min in acidified NaCl. Again, the test was designed for anodized aluminum alloys because the alkali created at the large applied currents will promote the formation of corrosion spots at defects in the anodized film.

The Electrolytic Corrosion Test

This test was designed for electrodeposits of nickel and chromium on less noble metals, such as zinc or steel [*71–73*]. Special solutions are used, and the metal is polarized to +0.3 V versus the standard calomel electrode. The metal is taken through cycles of 1 min anodically polarized and 2 min unpolarized. An indicator solution is then used to detect the presence of pits that penetrate to the substrate. Each exposure cycle attempts to simulate one year of exposure under atmospheric-corrosion conditions. ASTM B 627 describes the method in greater detail [*74*].

The Paint Adhesion on a Scribed Surface Test

This involves the cathodic polarization of a small portion of painted metal. The area exposed contains a scribed line that exposes a line of underlying bare metal. The sample is polarized cathodically for 15 min in 5% NaCl. At the end of this period the amount of delaminated coating is determined from an adhesive tape pulling procedure.

The Impedance Test for Anodized Aluminum

The method described by ASTM B 457 is used to study the seal performance of anodized aluminum [*75–77*]. In this sense, the test is similar to the FACT test except that this method uses a 1-V root-mean-square 1-kHz signal source from an impedance bridge to determine the sealed anodized aluminum impedance. The test area again is defined with a portable cell and a platinum or stainless steel auxiliary electrode typically is used. The sample is immersed in 3.5% NaCl [*75*].

Electrochemical Impedance Spectroscopy

The electrochemical impedance technique offers an advanced method of evaluating the performance of metallic coatings (passive film forming or otherwise) and organic barrier coatings [*75–86*]. The method does not accelerate the corrosion reaction and is nondestructive. The technique is quite sensitive to changes in the resistive-capacitive nature of coatings as well as the electrochemical interface as shown in Fig. 14. It is also possible to monitor the corrosion rate with this technique. In this respect, the electrochemical impedance technique offers several advantages over d-c electrochemical techniques in that resistances related

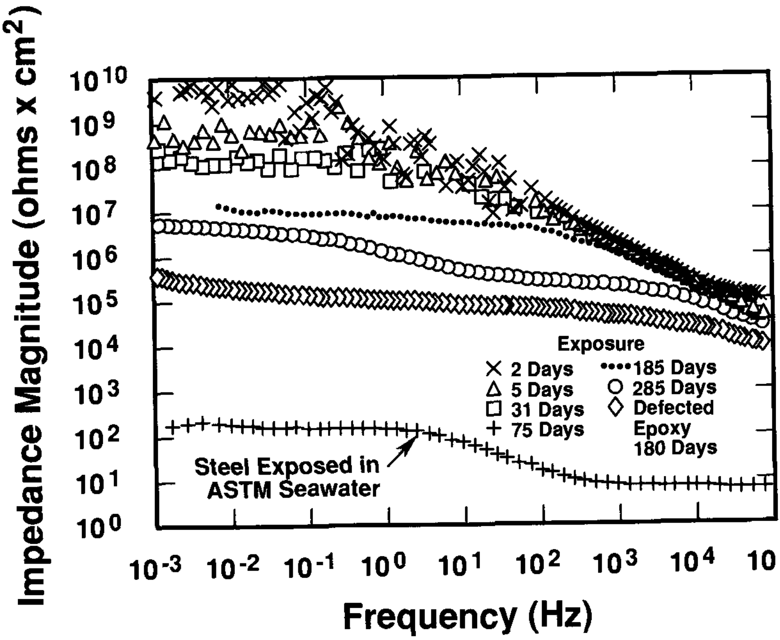

FIG. 14—*Bode magnitude response of initially defect free coated steel in ASTM artificial ocean water from 2 to 285 days* [85].

to the corrosion rate can be separated from the high d-c resistance of the dielectric coating. This is not possible with the d-c methods. Because a large frequency bandwidth is utilized for the applied signal (usually from the mHz range to the kHz range), the electrochemical impedance technique is "spectroscopic" and surpasses the capabilities of single-frequency impedance methods. The reason for this lies in the capability of the electrochemical impedance technique to discriminate between the resistive properties of the coating or passive film because of its ionic and or electronic conductance and the capacitive nature of the passive film or coating due to its dielectric constant, area, and thickness. Although impedance circuit models for coatings (Fig. 15) are complex compared to the model shown in Fig. 6, frequency regimes in which impedance information primarily is due to the coating capacitance or coating resistance can be separated from one another and analyzed independently by using a broad frequency bandwidth. If the coating or passive film capacitance can be determined and if the dielectric constant is known, then the film thickness can be estimated for a given exposed area

$$C = \epsilon\epsilon_o A/d \tag{21}$$

where

A = the surface area,
d = the dielectric thickness,
ϵ_o = the electric permittivity of free space (8.854×10^{-12} F/m), and
ϵ = the dielectric constant for the passive film or coating.

In addition to this correlation, the uptake of water in an organic coating can be monitored because the dielectric constant for water is over an order of magnitude greater than the

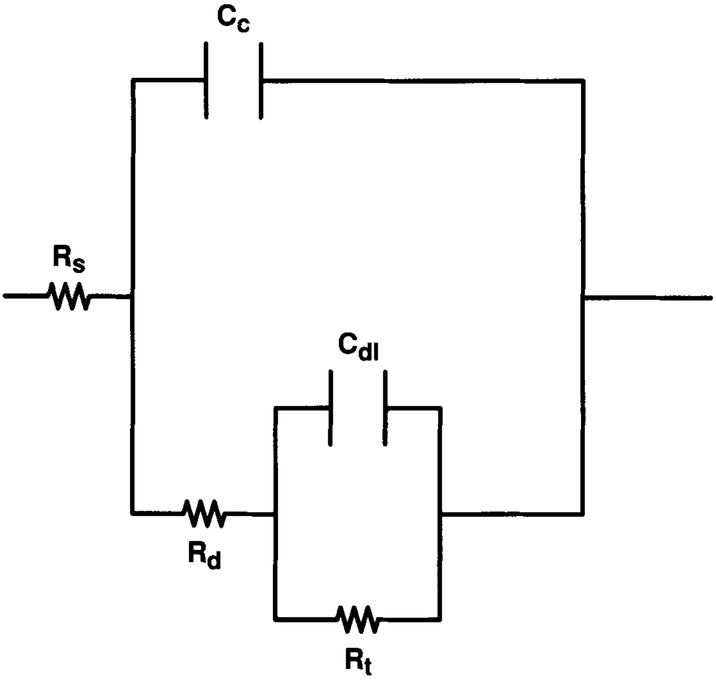

FIG. 15—*Simplified electrical equivalent circuit to simulate a coated steel panel with a defect* [86].

dielectric constant for the dry organic coating. The quantity of water absorbed in the organic coating is estimated as follows [*82*].

$$\text{H}_2\text{O, vol\%} = 100 \log(C_t/C_0)/\log(79) \tag{22}$$

where

C_t = the coating capacitance after some exposure time, and
C_0 = time zero when the exposure begins.

The coating resistance can also be monitored as a function of exposure time. Large decreases signify permeation of ionic species through the coating or the presence of defects in the coating [*85,86*]. The high-frequency breakpoint frequency is a useful method for determining the area fraction of physical defects in an organic coating [*84–86*]. The following expression describes the dependency between breakpoint frequency and defect area

$$f_{bpt} = A_d/(2\pi\epsilon\epsilon_0\rho A) \tag{23}$$

where

A_d = the defect area,
A = the total area, and
ρ = the resistivity of the coating at the defect.

Increases in the specimen breakpoint frequency often occur mainly as a function of the increases in the defective area. The relationship between f_{bpt} and the defect area is shown in Fig. 16.

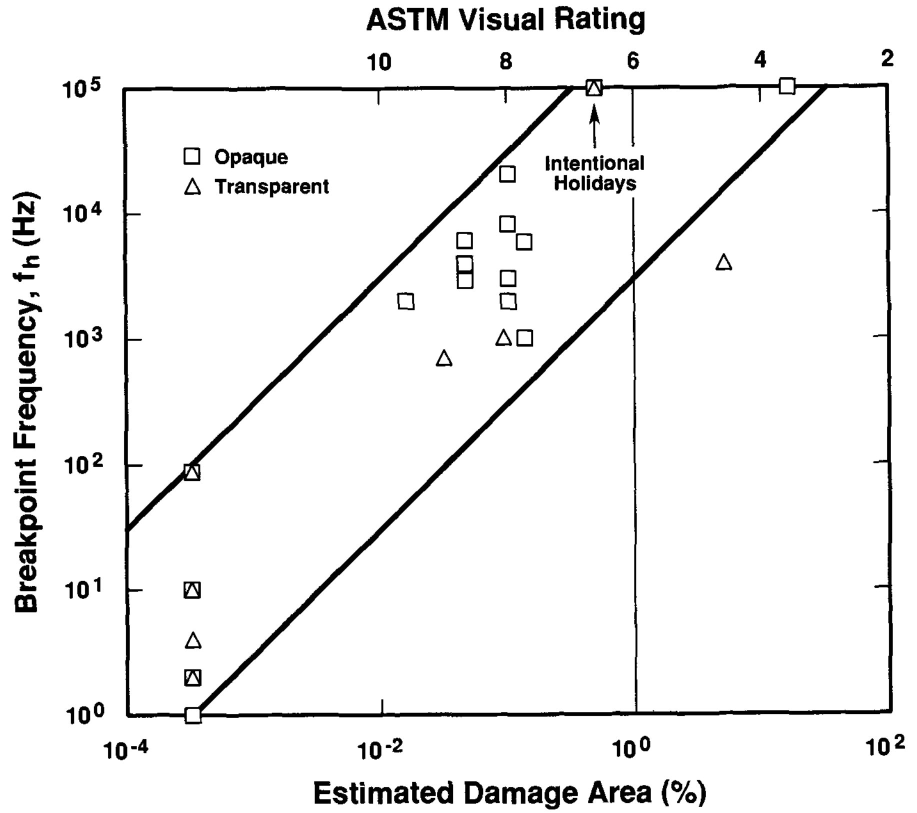

FIG. 16—*Relationship between breakpoint frequency and estimated electrochemically active area for opaque and transparent epoxy coatings on steel. Solid lines are added to indicate the expected relationship between breakpoint frequency and defect area according to Eq 23* [85,86].

Examples of metallic corrosion testing with a-c and d-c electrochemical methods have been described. Despite the long list of applications, electrochemical techniques are not always successful and it is instructive to identify some of the more general reasons for this situation. First and most obvious is the requirement that the metallic corrosion process be an electrochemical phenomena. Three more specific keys to successful application of these techniques include the implementation of relevant environment, relevant alloy and surface preparation, and relevant mechanical perturbations. Without these essentials even the most sophisticated electrochemical test will be destined for failure. More subtle but equally important is the necessity that any electrochemical acceleration of the corrosion act only upon the prevailing mechanism of corrosion under normal nonaccelerated conditions. Finally, careful application of electrochemical methods in conjunction with other methods can be a tremendous aid in solving corrosion problems.

Acknowledgement

This work was performed at Sandia National Laboratories supported by the US Department of Energy under contract number DE-AC04-76DP00789.

References

[*1*] Bockris, J. O'M. and Reddy, A. K. N., *Modern Electrochemistry,* Vol. 2, Plenum Press, New York, 1970.

[*2*] Gileadi, E., Kirowa-Eisner, E., and Penciner, J., *Interfacial Electrochemistry, An Experimental Approach,* Addison-Wesley, Reading, PA, 1975.

[*3*] Tomashov, N. D., *Theory of Corrosion and Protection of Metals,* Macmillan, New York, 1966.

[*4*] Scully, J. C., *The Fundamentals of Corrosion,* Pergamon Press, New York, 1975.

[*5*] Fontana, M. G. and Greene, N. D., *Corrosion Engineering,* McGraw-Hill, New York, 1978.

[*6*] Newman, J., *Electrochemical Systems,* Prentice-Hall, Englewood Cliffs, NJ, 1973.

[*7*] Uhlig, H. H. and Revie, R. W. *Corrosion and Corrosion Control,* John Wiley & Sons, New York, 1985.

[*8*] Bockris, J. O'M., Conway, B. E., Yeager, E., and White, R. E., Eds., *Electrochemical Materials Science, Vol. 4, Comprehensive Treatise of Electrochemistry,* Plenum Press, New York, 1981.

[*9*] Baboian, R., Ed., *Electrochemical Techniques for Corrosion,* National Association of Corrosion Engineers, Houston, TX, 1977.

[*10*] Bertocci, U. and Mansfeld, F., Eds., *Electrochemical Corrosion Testing, ASTM STP 727,* American Society for Testing and Materials, Philadelphia, 1981.

[*11*] Haynes, G. and Baboian, R., Eds., *Laboratory Corrosion Tests and Standards, ASTM STP 866,* American Society for Testing and Materials, Philadelphia, 1985.

[*12*] Moran, G. C. and Labine, P., Eds., *Corrosion Monitoring in Industrial Plants Using Nondestructive Testing and Electrochemical Methods, ASTM STP 908,* American Society for Testing and Materials, Philadelphia, 1986.

[*13*] Baboian, R., Ed., *Electrochemical Techniques for Corrosion Engineers,* National Association of Corrosion Engineers, Houston, TX, 1986.

[*14*] Baboian, R., France, W. D., Jr., Rowe, L. C., and Rynewicz, J. F., Eds., *Galvanic and Pitting Corrosion—Field and Laboratory Studies, ASTM STP 576,* American Society for Testing and Materials, Philadelphia, 1974.

[*15*] Riddiford, A. C., *Advanced Electrochemical Engineering,* Vol. 4, 1966, p. 47.

[*16*] MacDonald, D. D., *Transient Techniques in Electrochemistry,* Plenum Press, New York, 1977.

[*17*] Wagner, C. and Traud, W., *Z Electrochemistry,* Vol. 44, 1938, p. 391.

[*18*] France, W. D., Jr., "Controlled Potential Corrosion Tests. Their Application and Limitations," *Material Research Standardization,* Vol. 9, No. 8, 1969, p. 21.

[*19*] "Standard Reference Test Method for Making Potentiostatic and Potentiodynamic Anodic Polarization Measurements," ASTM G 5, *Annual Book of ASTM Standards, Vol. 03.02,* American Society for Testing and Materials, Philadelphia.

[*20*] "Standard Practice for Conducting Potentiodynamic Polarization Resistance Measurements," ASTM G 59, *Annual Book of ASTM Standards, Vol. 03.02,* American Society for Testing and Materials, Philadelphia.

[*21*] Tafel, Z., *Physik. Chem.,* Vol. 50, 1905, p. 641.

[*22*] "Standard Practice for Conventions Applicable to Electrochemical Measurements in Corrosion Testing," ASTM G 3, *Annual Book of ASTM Standards, Vol. 03.02,* American Society for Testing and Materials, Philadelphia.

[*23*] Britz, D., *Journal of Electroanalytical Chemistry,* Vol. 88, 1978, p. 309.

[*24*] Hayes, M. and Kuhn, J., *Journal of Power Sources,* Vol. 2, 1977–1978, p. 121.

[*25*] Mansfeld, F., *Corrosion,* Vol. 38, No. 10, 1982, p. 556.

[*26*] Scribner, L. L. and Taylor, S. R., Eds., *The Measurement and Correction of Electrolyte Resistance in Electrochemical Tests, ASTM STP 1056,* American Society for Testing and Materials, Philadelphia, 1990.

[*27*] Stern, M. and Roth, R. M., *Journal of the Electrochemical Society,* Vol. 104, 1957, p. 390.

[*28*] Stern, M. and Geary, A. L., *Journal of the Electrochemical Society,* Vol. 105, 1958, p. 638.

[*29*] Stern, M. and Geary, A. L., *Journal of the Electrochemical Society,* Vol. 104, 1957, p. 56.

[*30*] Evans, S. and Koehler, E. L., *Journal of the Electrochemical Society,* Vol. 108, 1961, p. 509.

[*31*] Stern, M. and Weisert, E. D., "Experimental Observations on the Relation Between Polarization Resistance and Corrosion Rate," *Proceedings,* Vol. 59, American Society for Testing and Materials, Philadelphia, 1959, p. 1280.

[*32*] "Test Methods for Corrosivity of Water in the Absence of Heat Transfer (Electrical Methods)," ASTM D 2776, *Annual Book of ASTM Standards, Vol. 03.02,* American Society for Testing and Materials, Philadelphia.

[*33*] Mansfeld, F. and Kendig, M., *Corrosion,* Vol. 37, No. 9, 1981, p. 556.

[*34*] Leroy, R. L., *Corrosion,* Vol. 29, 1913, p. 272.

[35] Bandy, R. and Jones, D. A., *Corrosion*, Vol. 32, 1976, p. 126.
[36] Danielson, M. J., *Corrosion*, Vol. 36, No. 4, 1980, p. 174.
[37] Reeve, J. C. and Bech-Nielsen, G., *Corrosion Science*, Vol. 13, 1973, p. 351.
[38] Oldham, K. B. and Mansfeld, F., *Corrosion Science*, Vol. 13, 1973, p. 813.
[39] Epelboin, I., Gabrielli, C., Keddam, M., and Takenouti, H., in *Electrochemical Corrosion Testing, ASTM STP 727*, F. Mansfeld and U. Bertocci, Eds., American Society for Testing and Materials, Philadelphia, 1981, p. 150.
[40] Makrides, A. C., *Corrosion*, Vol. 29, No. 9, 1973, p. 148.
[41] MacDonald, D. D. and McKubre, M. C. H., in *Electrochemical Corrosion Testing, ASTM STP 727*, F. Mansfeld and U. Bertocci, Eds., American Society for Testing and Materials, Philadelphia, 1981, p. 110.
[42] Bard, A. J. and Faulkner, L. R., *Electrochemical Methods: Fundamentals and Applications*, John Wiley & Sons, New York, 1980.
[43] Mansfeld, F., *Corrosion*, Vol. 36, No. 5, 1981, p. 301.
[44] Mansfeld, F., Kendig, M. W., and Tsai, S., *Corrosion*, Vol. 38, 1982, p. 570.
[45] "Practice for Verification of Algorithm and Equipment for Electrochemical Impedance Measurements," *Annual Book of ASTM Standards, Vol. 03.02*, American Society for Testing and Materials, Philadelphia.
[46] Murray, J. N., Moran, P. J., and Gileadi, E., *Corrosion*, Vol. 44, No. 8, 1988, p. 533.
[47] Hack, H. and Scully, J. R., *Corrosion*, Vol. 42, No. 2, 1986, p. 79.
[48] Baboian, R., in *Galvanic and Pitting Corrosion—Field and Laboratory Studies, ASTM STP 576*, R. Baboian et al., Eds., American Society for Testing and Materials, Philadelphia, 1974, p. 5.
[49] Mansfeld, F. and Kenkel, J. V., in *Galvanic and Pitting Corrosion—Field and Laboratory Studies, ASTM STP 576*, R. Baboian et al., Eds., American Society for Testing and Materials, Philadelphia, 1974, p. 20.
[50] Kruger, J., in *Passivity and Its Breakdown on Iron and Iron Based Alloys*, R. W. Staehle and H. Okada, Eds., National Association of Corrosion Engineers, Houston, 1976.
[51] Sato, N. and Okamoto, G., in *Electrochemical Materials Science, Vol. 4, Comprehensive Treatise of Electrochemistry*, J. O'M. Bockris, B. E. Conway, E. Yeager, and R. E. White, Eds., Plenum Press, New York, 1981, p. 193.
[52] Wilde, B. E., *Corrosion*, Vol. 28, 1972, p. 283.
[53] "Standard Test Method for Conducting Cyclic Potentiodynamic Polarization Measurements for Localized Corrosion Susceptibility of Iron-, Nickel-, or Cobalt-Based Alloys," ASTM G 61, *Annual Book of ASTM Standards, Vol. 03.02*, American Society for Testing and Materials, Philadelphia.
[54] Syrett, B. C., *Corrosion*, Vol. 33, 1977, p. 221.
[55] Pessall, N. and Liu, C., *Electrochimica Acta*, Vol. 16, 1971, p. 1987.
[56] Wilde, B. E. and Williams, E., *Journal of the Electrochemical Society*, Vol. 118, 1971, p. 1057.
[57] "Standard Test Method for Conducting Cyclic Galvanostaircase Polarization," ASTM G 100, *Annual Book of ASTM Standards, Vol. 03.02*, American Society for Testing and Materials, Philadelphia.
[58] Ambrose, J. R. and Kruger, J., *Journal of the Electrochemical Society*, Vol. 121, 1974, p. 599.
[59] Ambrose, J. R. and Kruger, J., in *Proceedings*, Fifth International Congress on Metallic Corrosion, National Association of Corrosion Engineers, Houston, 1974, p. 406.
[60] Novak, P., Stefec, R., and Franz, F., *Corrosion*, Vol. 31, No. 10, 1975, p. 344.
[61] Clarke, W. L., Romero, V. M., and Danko, J. C., Paper No. 180, *Corrosion/77*, National Association of Corrosion Engineers, Houston, 1977.
[62] Clarke, W. L., Cowan, R. L., and Walker, W. L., in *Intergranular Corrosion of Stainless Alloys, ASTM STP 656*, R. F. Steigerwald, Ed., American Society for Testing and Materials, Philadelphia, 1978, p. 99.
[63] Akashi, M., Kawamoto, T., and Umemura, F., *Corrosion Engineering*, Vol. 29, 1980, p. 163.
[64] Majidi, A. P. and Streicher, M. A., *Corrosion*, Vol. 40, No. 11, 1984, p. 584.
[65] "Standard Practices for Detecting Susceptibility to Intergranular Attack in Austenitic Stainless Steels," A 262/A 262M, *Annual Book of ASTM Standards, Vol. 03.02*, American Society for Testing and Materials, Philadelphia.
[66] Lee, J. B., *Corrosion*, Vol. 42, No. 2, 1986, pp. 67–69.
[67] Roelandt, A. and Vereecken, J., *Corrosion*, Vol. 42, No. 5, 1986, p. 289.
[68] Scully, J. R. and Kelly, R., *Corrosion*, Vol. 42, No. 9, 1986, p. 537.
[69] "Standard Method of Testing FACT (Ford Anodized Aluminum Corrosion Test) Testing," ASTM B 538, *Annual Book of ASTM Standards, Vol. 02.05*, American Society for Testing and Materials, Philadelphia.
[70] Stone, J., Tuttle, H. A., and Bogart, H. N., *Plating*, Vol. 43, 1965, p. 877.

[*71*] Saur, R. L. and Basco, R. P., *Plating,* Vol. 53, 1966, p. 33.
[*72*] Saur, R. L. and Basco, R. P., *Plating,* Vol. 53, 1966, p. 981.
[*73*] Saur, R. L. and Basco, R. P., *Plating,* Vol. 53, 1966, p. 320.
[*74*] "Standard Method of Electrolytic Corrosion Testing (EC Test)," ASTM B 627, *Annual Book of ASTM Standards, Vol. 02.05,* American Society for Testing and Materials, Philadelphia.
[*75*] "Standard Method for Measurement of Impedance of Anodic Coatings on Aluminum," ASTM B 457, *Annual Book of ASTM Standards, Vol. 02.05,* American Society for Testing and Materials, Philadelphia.
[*76*] Englehart, E. T. and Sowinski, G., Jr., *SAE Journal,* Vol. 72, 1974, p. 51.
[*77*] Englehart, E. T. and George, D. J., *Materials Protection,* Vol. 3, 1964, p. 25.
[*78*] Scantlebury, J. D., Ho, K. N., and Eden, D. A., in *Electrochemical Corrosion Testing, ASTM STP 727,* F. Mansfeld and U. Bertocci, Eds., American Society for Testing and Materials, Philadelphia, 1981, p. 187.
[*79*] Narian, S., Bonanos, N., and Hocking, M. G., *Journal of the Oil Colour Chemical Association,* Vol. 66, No. 2, 1983, p. 48.
[*80*] Strivens, T. A. and Taylor, C. C., *Materials Chemistry,* Vol. 7, 1982, p. 199.
[*81*] Mansfeld, F., Kendig, M. W., and Tsao, S., *Corrosion,* Vol. 38, No. 9, 1982, p. 478.
[*82*] Kendig, M., Mansfeld, F., and Tsao, S., *Corrosion Science,* Vol. 23, No. 4, 1983, p. 317.
[*83*] Touhasaent, R. and Liedheiser, H., *Corrosion,* Vol. 28, No. 12, 1982, p. 435.
[*84*] Haruyama, S., Asari, M., Tsuru, T., in *Corrosion Protection by Organic Coatings,* M. Kendig and H. Liedheiser, Jr., Eds., The Electrochemical Society Softbound Proceedings Series, Pennington, 1980, p. 197.
[*85*] Scully, J. R., *Journal of the Electrochemical Society,* Vol. 136, No. 4, 1989, p. 979.
[*86*] Kendig, M. W. and Scully, J. R., *Corrosion,* Vol. 46, No. 1, 1990, p. 22.

David C. Silverman[1]

Simple Models/Practical Answers Using the Electrochemical Impedance Technique

---

REFERENCE: Silverman, D. C., "**Simple Models/Practical Answers Using the Electrochemical Impedance Technique,**" *Corrosion Testing and Evaluation: Silver Anniversary Volume, ASTM STP 1000,* R. Baboian and S. W. Dean, Eds., American Society for Testing and Materials, Philadelphia, 1990, pp. 379–396.

ABSTRACT: One practical use of the electrochemical impedance technique is rapid screening of either alloy corrosion resistance or process corrosivity as a function of process conditions. Curve-fitting of the impedance spectra using simple circuit analogue models can allow polarization or charge transfer resistances to be extracted even when there is limited understanding or characterization of the system under study. Practical corrosion predictions can be made from these results. Some successes and shortcomings in the technology are explored using corrosion of steel and 304SS in several environments. The results show that corrosion rates between 2.5 × 10^{-4} and 250 mm/year can be estimated and predictions made even when only limited information on the solution chemistry and corrosion mechanism is available. Some discussion is presented on how one can gain confidence that the model circuit elements are providing reliable information.

KEY WORDS: electrochemical impedance technique, electrochemical impedance spectroscopy, steel, 304SS, corrosion prediction, corrosion modeling, polarization resistance, electrochemistry

The electrochemical impedance technique or Electrochemical Impedance Spectroscopy has been gaining more popularity as a tool for corrosion measurement and prediction. Recent articles show that a variety of corrosion phenomena can be studied and corrosion rates estimated [*1–5*]. Among the areas demonstrated in these published articles are rapid estimation of corrosion rates, estimation of low corrosion rates, assessment and ranking of corrosion inhibitors, corrosion rate estimation in low conductivity media, and evaluation of organic and inorganic coatings.

The popularity of this technology can be attributed to the present ease of generating the results. There are a plethora of methods available [*6*]. Commercial instrumentation is available from several manufacturers. Though care must be taken in setting up the experiment, for example overall cell design or the positioning of the reference electrode sensing point, most problems can be overcome and data acquisition has become fairly routine.

Generation of the "raw" impedance spectra only provides one part of the required information. The data must still be interpreted to provide both information on the corrosion process and estimates of the corrosion rate. At present, difficulties in data interpretation remain an obstacle to making practical, routine use of this technology. This interpretation includes both modeling of the frequency response and determining that the model is valid and represents the corrosion process.

---

[1] Monsanto Co., St. Louis, MO 63167.

Though much literature discusses use of frequency response analysis to try to understand corrosion mechanisms, this type of information may be of only secondary importance to the corrosion practitioner. Faced with the decision of what material of construction to use, the practitioner needs a rapid survey of potential candidates followed by a more detailed analysis of only those candidates that seem to be promising. Faced with a process change, the practitioner must often quickly estimate how that process change will affect corrosion of a given alloy. Faced with the increasing need for product purity, the practitioner must quickly estimate if the containment vessel can contaminate the product. Vessel failure is not always the concern. Time and funding are often inadequate to allow detailed mechanistic conclusions to be made.

The information available from the electrochemical impedance technique can fulfill these needs since the technique has the potential for being used to make rapid estimates of corrosion rates from 2.5×10^{-4} to 250 mm/year [*5*]. The ability to use this technology to estimate such low corrosion rates has been demonstrated by several workers [*5,7*]. Practical and routine use is now mostly limited to situations in which corrosion can be classified as general corrosion. This usage includes corrosion under coatings [*8*].

Making predictions requires some way of deconvoluting the impedance spectra to extract those corrosion-related parameters that can be used to predict the corrosion rate or mechanism. Two general philosophies have arisen for modeling the data and, from the resulting model, for obtaining quantitative estimates of important corrosion characteristics. The first and more prevalent method is modeling by use of circuit analogues and making predictions from the magnitudes of the elements. An analogous electrical circuit composed of resistors, capacitors, and inductors is constructed for modeling the data. These circuit analogues allow the corrosion practitioner to bridge the gaps in knowledge so that corrosion rates might be estimated, corrosion mechanisms hypothesized, and materials selections made in these poorly characterized systems. Certain elements of the circuit are said to model such electrochemical parameters as the polarization resistance and the double-layer capacitance [*1,2*]. For example, fairly good agreement has been achieved between corrosion rates estimated by using the polarization resistance and as estimated directly by mass loss or solution analyses [*5,9,10*].

This type of data analysis has sometimes required the introduction of certain empirical factors such as the angle of depression below the real axis being expressed as an exponent on the frequency which has a value lying between 0 and 1 [*5,10–12*]. This depression (constant phase element) is created by a kind of dispersion of the capacitive time constant around a central value. The cause may not be understood (e.g., transmission line effects, inadequate placement of reference electrode, etc.), but to properly fit the data by circuit analogues this parameter often must be included.

Corrosion is both a physical and a chemical process governed by laws of thermodynamics and kinetics which might be difficult to understand in poorly characterized, real-life systems. Circuit analogues are only simplified models. Agreement with the model does not always mean agreement with the physics that the model is thought to represent. This shortcoming has led some workers to attempt to adopt a second philosophy and develop kinetic and diffusion equations to describe the frequency response and then show that the physical constants so derived are reasonable. If successful, this type of approach should eliminate some of the empiricisms mentioned above. An example of this approach is the model of three-dimensional, inhomogeneous surfaces [*13,14*]. This model has been able to predict the impedance spectra for several systems from consideration of only diffusion and chemical reactions. The results strongly suggest that this type of approach to data analysis may ultimately provide a way to obtain both mechanistic and rate information from first principles.

However, information required for such a fundamental approach is often not readily available in the complex environments that may be encountered in everyday corrosion testing. Often, the solutions are not well characterized. Not only might the components not be known, but determining them might be impossible. These shortcomings in knowledge usually mean that less fundamental, more phenomenological models such as circuit analogues may be the only approach to characterizing the corrosion process to obtain corrosion rates. Use of circuit analogues has been the approach used in this study to obtain rapid estimates of corrosion rates from simple models so that practical predictions can be made when knowledge is incomplete.

The objective of this paper is to provide a practitioner's view of the strengths and limitations of the electrochemical impedance technique for rapidly estimating corrosion rates so as to make practical predictions quickly and efficiently. The paper uses several examples to show how different circuit analogues can be used to classify corrosion in order to make rapid, practical predictions when knowledge, funding, and time are limited. The examples are rapid estimation of low corrosion rates and rapid estimation of corrosion rates in complex, poorly characterized systems. Corrosion of steel and 304 Stainless Steel (304SS) in DEQUEST® (registered trademark of Monsanto Company) 2016 product (the salt of 1-hydroxy ethylidene-1,1 diphosphonic acid) and steel in a waste stream are the examples used. In both cases, the goal is to make rapid estimates of corrosion in a minimum amount of time and with limited funding.

Circuit Analogue Models

Four simple circuits were constructed. These circuits are expected to model empirically four distinct types of corrosion phenomena [*5*]. These models are shown in detail in Fig. 1. They represent a single relaxation time constant, two relaxation time constants, extended diffusion analysis of John and Dawson [*15*], and pseudoinductance analysis similar to that of Epelboin and Keddam [*12*]. These circuits were chosen to model a single charge transfer reaction, a partially coated electrode as might be found with an inhibitor, diffusion through a finite boundary layer, and an adsorbed intermediate that might cause pseudoinductance. All models allow for dispersion of the time constant (depression below the real axis in Nyquist format). The maximum number of adjustable parameters was kept to a minimum so that agreement between the calculated and actual frequency response hopefully would reflect the adequacy of the model. This approach was taken to circumvent the problem of having so many adjustable parameters that one model fits any response. These four circuit analogues have been found to cover a large percentage of the situations analyzed at Monsanto.

Experimental

The experimental arrangement has been discussed in detail previously [*5*] and is shown in Fig. 2. A Hewlett-Packard 9816S microcomputer guides the experiment by controlling the flow of commands. The frequency response is measured by a Solartron 1250A Frequency Response Analyzer and a Princeton Applied Research 173D potentiostat with a 276 programmable interface. The algorithm for the experiment first optimizes the gain of the potentiostat every half decade of frequency by finding the maximum gain that does not cause a current overload. This gain is implemented at each half decade of frequency during generation of the spectrum. The minimum gain (1 Ω) is used between 10 000 and 1000 Hz or 100 Hz. The choice depends on the amount of instrument-induced phase angle shift that is observed at high frequency. Also, the potentiostat low-pass filter is turned on below 0.5

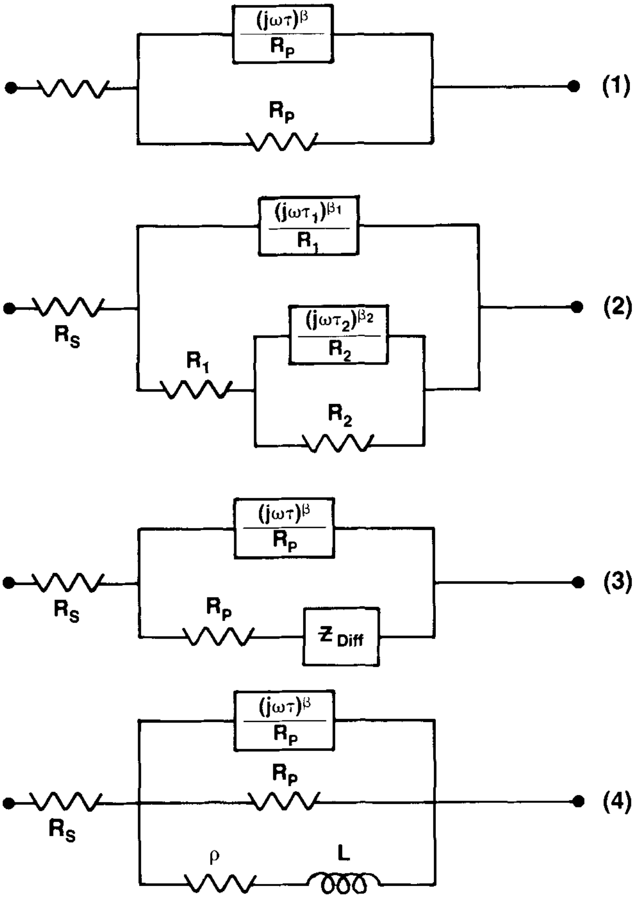

FIG. 1—*Circuits used to analyze the electrochemical impedance results:* (*1*) *one relaxation time constant;* (*2*) *two relaxation time constants;* (*3*) *one relaxation time constant with extended diffusion analysis;* (*4*) *one relaxation time constant with pseudoinductance* [5].

Hz so that only one sine wave is needed at each frequency below that point. The excitation amplitude for these studies was 2, 5, or 10 mV depending on the situation. If nonlinearity between input and response was suspected, all three amplitudes were used to verify that no such nonlinearities existed.

The data are uploaded to an IBM mainframe computer for analysis in terms of the circuit analogues mentioned before and shown in Fig. 1. The subroutine used to estimate the circuit elements performs a nonlinear regression of the data against the equations for the impedance which represent the circuits. The sum of the squares of the residuals between the calculated and actual spectra in real and imaginary coordinates is minimized automatically.

Two different experimental setups were used depending on experiment, a static cell or the rotating cylinder electrode described in detail elsewhere [*16*]. Both electrochemical cells were fitted with ports for the Luggin-Haber capillary, counterelectrode feed-through, thermocouple or thermometer, and gas sparger. the rotating cylinder electrode was operated at 200 rpm in the experiments reported here. There were brief excursions to 1000 rpm to examine the sensitivity of corrosion to fluid velocity.

Two different solutions were used. The first is DEQUEST 2016 product. This product is the sodium salt of 1-hydroxy-ethylidene-1,1 diphosphonic acid, a sequestrant. The product is a concentrated solution of the salt, about 50 wt% in water. The pH of this product ranges from 10 to 12. The goal is to determine if steel or 304SS might be used for storage under ambient conditions. Therefore, the temperature used was 50°C (323 K), the expected maximum temperature of the product when contained in a tank exposed to direct sunlight. The static electrode was used since a sensitivity of corrosion to fluid velocity was not expected. The frequency responses were generated at various times over 48 h for steel and 72 h for 304SS. Mass losses were obtained. In the case of 304SS, the solutions were analyzed as well by inductively coupled plasma (ICP) for iron, nickel, and chromium.

The second solution is the combined waste stream described previously [*10,17*]. It was made by combining waste solution samples in proportion to the amounts expected in the plant. Water was the predominant component. The exact composition is not known and could not be determined. However, the mixed solution tested is known to have small amounts of iminodiacetic acid, nitrilotriacetic acid, low molecular weight organic acids, and ammonium sulfate. The conductivity was not measured. The presence of salts at the several weight percent levels coupled with the small uncompensated resistance indicated by the intersection of the high-frequency portion of the spectrum with the real axis (Nyquist format) shown here and elsewhere [*10,17*] suggest that low solution conductivity would not be a problem with the measurements. The goal of the portion of the study discussed here is a quick assessment of the effect of excursions of pH from that pH range in which corrosion seems to be minimized.

The inhibitor normally used in the plant was added at the beginning of the experiment in the appropriate level of 40 ppm. The inhibitor is a sulfite-containing solution. It is supplied

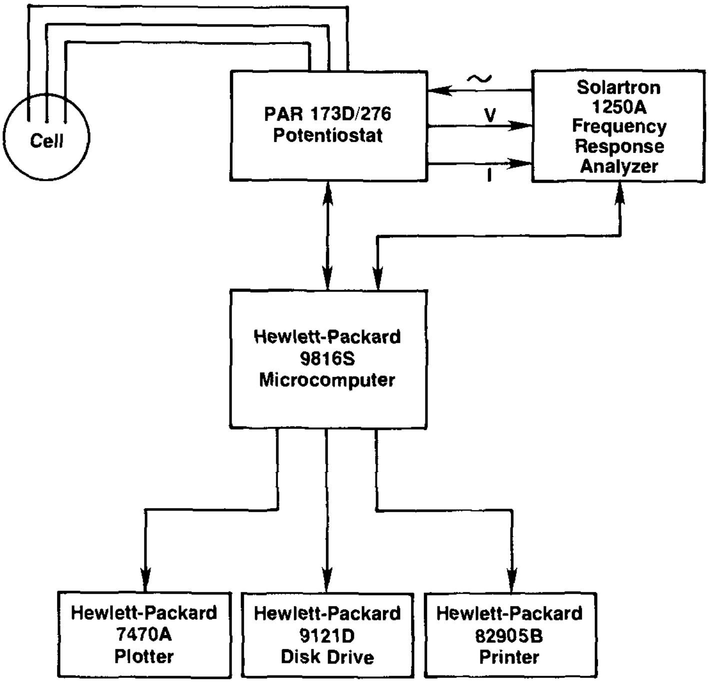

FIG. 2—*Diagram of the experimental arrangement* [5].

to Monsanto. Its composition was not divulged so it is one of the unknown components. However, since it was added at the same concentration in all of the experiments, it is a constant unknown. The pH was adjusted to 9.0 using reagent grade ammonium hydroxide and from 9.0 to 7.5 using reagent grade sulfuric acid. The latter addition is not expected to introduce new components because the waste already contained sulfate ions. The temperature was 49°C (322 K), the highest expected temperature. Impedance spectra were generated periodically over a period of five to seven days. A ntirogen blanket was maintained at all times. The nitrogen was taken directly from a cylinder. A small, e.g. ppm, level of oxygen might have been present though no attempt was made to measure it.

Results

Corrosion in DEQUEST 2016

Figures 3 and 4 show the impedance spectra in Nyquist and Bode formats for steel in DEQUEST 2016 product after 24 h. Figures 5 and 6 show the impedance spectra in both formats for 304SS in DEQUEST 2016 product after 48 h. The calculated curve in Figs. 3 and 4 corresponds to Circuit 2 in Fig. 1. The calculated curve for Figs. 5 and 6 corresponds to Circuit 1 in Fig. 1. These models provided the best fit and did not change with exposure time.

Tables 1 and 2 show the estimated polarization resistances and corrosion rates for steel and 304SS, respectively. The resistances that correspond to each of the two time constants for steel are listed in Table 1. The polarization resistance for the steel is hypothesized to be R_2, the low frequency resistance, in Circuit 2 in Fig. 1. The proportionality factor between

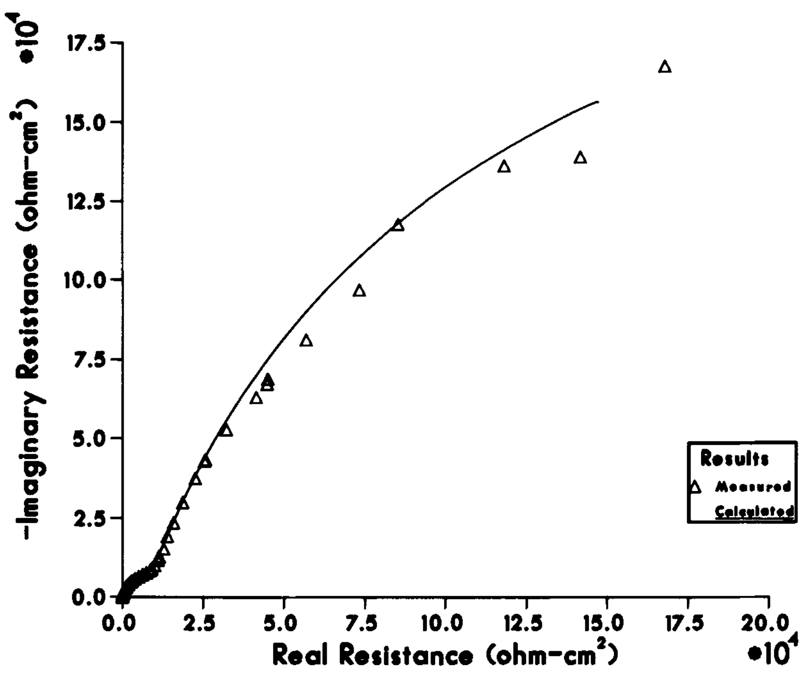

FIG. 3—*Impedance spectrum in Nyquist format of carbon steel in DEQUEST 2016 product at 50°C (323 K), 24 h exposure.*

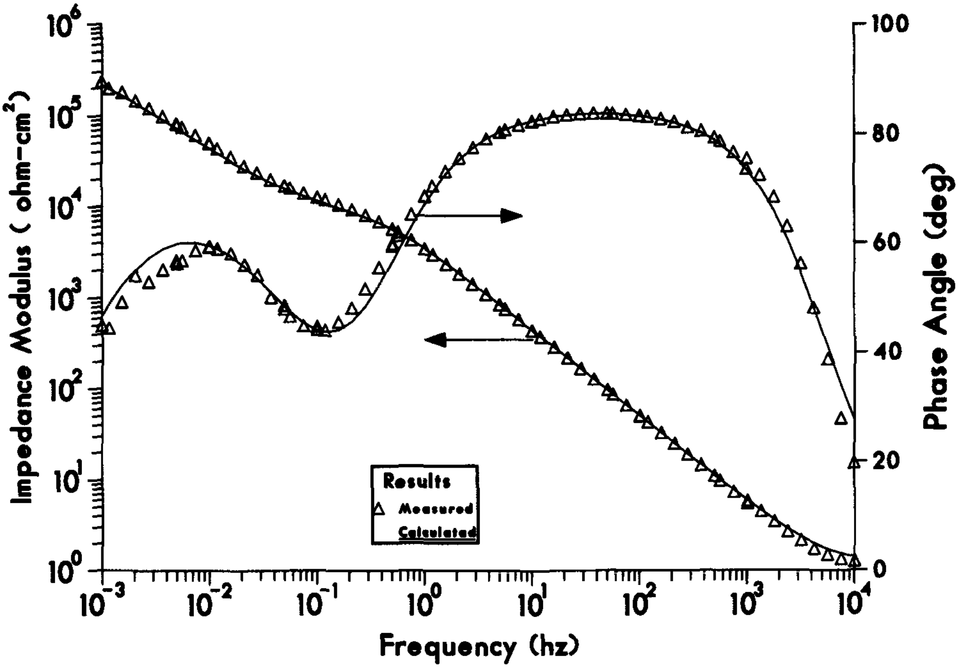

FIG. 4—*Impedance spectrum in Bode format of carbon steel in DEQUEST 2016 product at 50°C (323 K), 24 h exposure.*

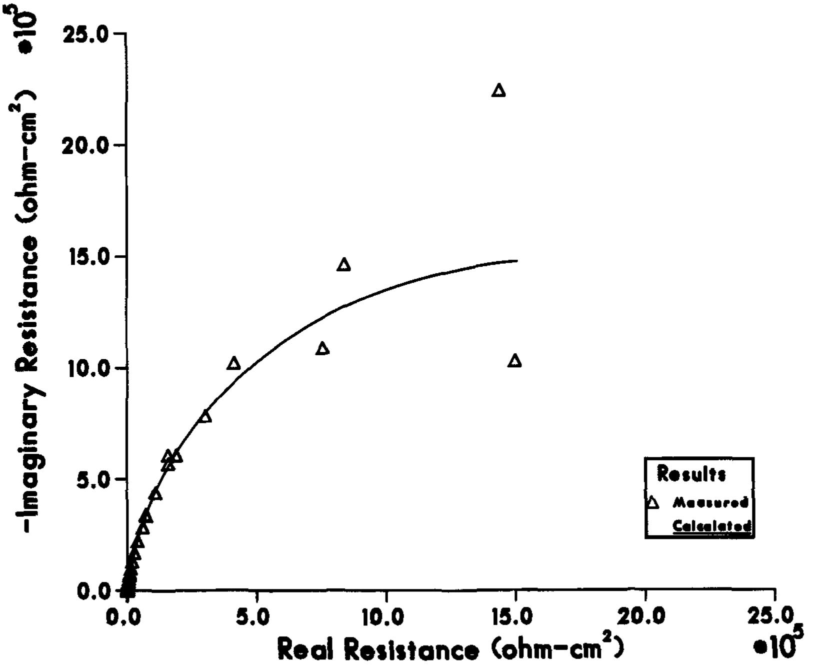

FIG. 5—*Impedance spectrum in Nyquist format of 304SS in DEQUEST 2016 product at 50°C (323 K), 24 h exposure.*

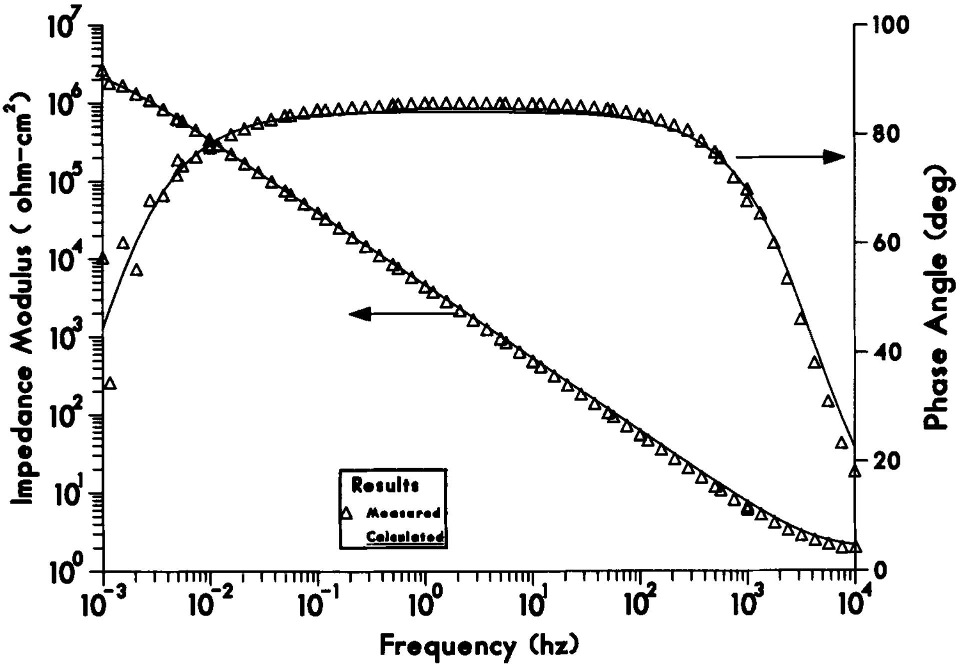

FIG. 6—*Impedance spectrum in Bode format of 304SS in DEQUEST 2016 product at 50°C (323 K), 24 h exposure.*

the polarization resistance and the corrosion rate was assumed to be 0.05 V. This value should provide an overestimate since the value is normally expected to lie in the range of 0.025 V, especially for steel in aqueous solutions [*18*]. This factor could not be derived from a curve-fit of d-c type of results assuming one anodic and one cathodic reaction [*5*]. There are two reasons. First, the currents measured during generation of the small amplitude d-c curves to 0.02 V (cathodic and anodic to the corrosion potential) were near the noise threshold of the potentiostat. Second, and more importantly, the corrosion mechanism is unknown. Therefore, how the proportionality factor is related to the Tafel slopes and the appropriate form of the equations relating corrosion current to potential are unclear. For example, if the corrosion potential is within 0.025 V or so of the reversible potential of one of the reactants, then both the forward and reverse reactions involving that species would have to be included [*19*]. Determination of the reaction steps involved and development of the appropriate form for the current versus potential function were beyond the scope of this effort.

TABLE 1—*Corrosion rate estimate for steel in DEQUEST 2016.*

Time, h	High Frequency Resistance, Ω-cm^2	Low Frequency Resistance, Ω-cm^2	Corrosion Rate,	
			mm/year	mpy
1	1.29×10^4	8.15×10^4	6×10^{-3}	3×10^{-1}
5	1.17×10^4	6.19×10^5	1×10^{-3}	3×10^{-2}
24	1.39×10^4	5.68×10^5	1×10^{-3}	4×10^{-2}
48	1.09×10^4	4.71×10^5	1×10^{-3}	5×10^{-2}
72	1.21×10^4	1.08×10^6	5×10^{-4}	2×10^{-2}

TABLE 2—*Corrosion rate estimate for 304SS in DEQUEST 2016.*

Time, h	Resistance, Ω-cm²	Corrosion Rate, mm/year	Corrosion Rate, mpy
1	1.63×10^5	3×10^{-3}	1×10^{-1}
5	5.44×10^5	1×10^{-3}	4×10^{-2}
24	3.20×10^6	2×10^{-4}	6×10^{-3}
48	3.46×10^6	2×10^{-4}	5×10^{-3}

Metal ion accumulation in the solution in which 304SS corrosion was estimated are shown in Table 3. Inductively coupled plasma (ICP) was used to analyze the concentrations in duplicate solution samples. This analysis was not done for the solution in which steel corrosion was estimated.

The results show that there was no increase in concentration from 304SS within the accuracy of the analysis (about 1 ppm or so). The solution volume for the corrosion study was 500 cm.[3] A 1 ppm increase would correspond to a corrosion rate of under 10^{-3} mm/year. This finding is in approximate agreement with the low corrosion rates estimated from the electrochemical impedance spectra of 10^{-4} to 10^{-3} mm/year. In addition, mass loss of the electrodes was within the accuracy of the analytical balance, less than 5×10^{-4} g. This result would be expected for the low corrosion rates estimated in Tables 1 and 2. This agreement is a necessary but not a sufficient condition to corroborate the impedance results.

Corrosion in Plant Waste

The goal of this study was to assess steel corrosion in a combined waste stream from a chemical plant as a function of pH, velocity, and inhibitor level. Previous results have shown that in the presence of the inhibitor the optimum pH lies between about 8 and 9 [*17*]. The problem was that excursions can occur in process conditions. The question was, "Can those excursions accelerate corrosion to undesirable rates which can affect equipment integrity?"

The most common excursion was expected to be a decrease in pH. Previous results had shown that lower pH values could increase the corrosion rate, possibly to undesirable levels. The electrochemical impedance technique was used to rapidly assess the effect of such an excursion. The experiment was first to expose the steel to the waste at a pH of 9. Then the pH of the solution was dropped to a value of 7.5 with sulfuric acid. The impedance spectra and parameters estimated from them after the drop in pH were compared to those for exposure to a pH of 7.5 only to determine if some protection might remain from the higher pH exposure. Results reported here are for a rotation rate of 200 rpm in the rotating cylinder electrode apparatus.

TABLE 3—*ICP analysis of metal contamination in DEQUEST 2016 By 304SS.*

Solution	Metal Ion Contamination, ppm by weight: Iron	Nickel	Chromium
As received	5.4	0.0[a]	2.5
	5.7	0.5	2.9
After 24 h	4.0	0.0[a]	2.1
of immersion	4.0	0.4	2.3
After 48 hr	4.7	0.0[a]	2.6
of immersion	5.4	0.0[a]	2.8

[a] Some metal was detected but was below the threshold of being quantitative.

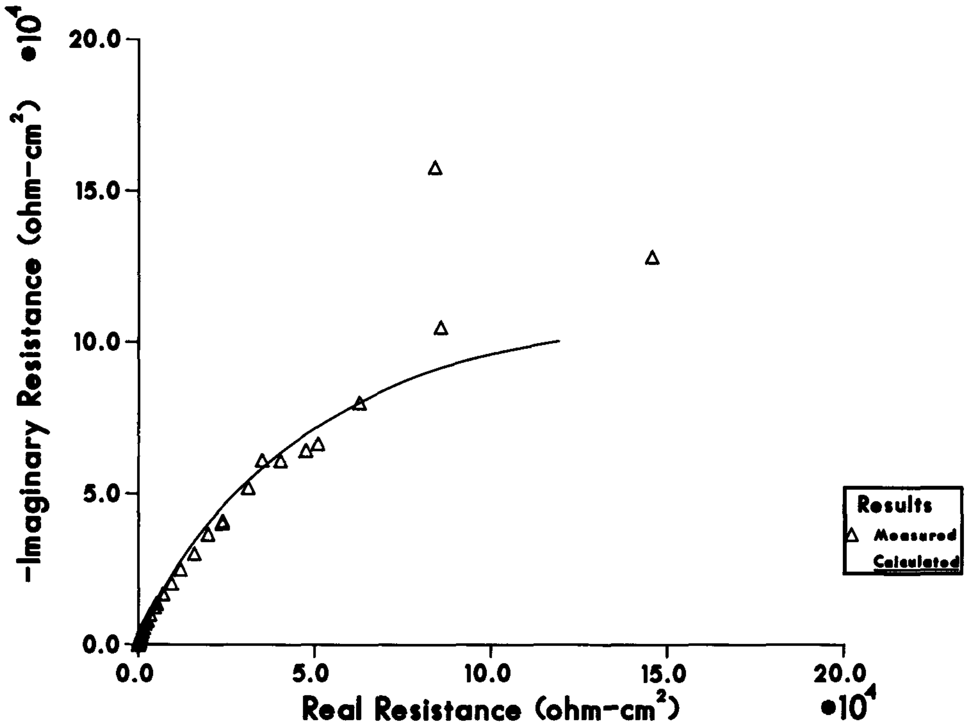

FIG. 7—*Impedance spectrum in Nyquist format of carbon steel in waste at 49°C (322 K), pH = 9.0, 200 rpm, 45 h exposure* [17].

Figures 7, 8, 9, and 10 show the impedance spectra at a pH of 9 just before adjustment to a pH of 7.5 (24 h after passivation occurred at the pH of 9) and 24 h after lowering the pH. The corrosion potential had reached approximate steady state for a number of hours prior to the generation of each spectrum. Both plots could be modeled by two relaxation time constants. In both cases, the resistance associated with the high frequency time constant was of the order of 1000 Ω-cm^2 (900 and 1500 Ω-cm^2). Also, this model fit the data for an exposure to a pH of 9 only for about one week as reported elsewhere [*17*]. However, the resistance associated with the low frequency relaxation time constant changed from about 2.8×10^5 Ω-cm^2 at a pH of 9 to the range of 1×10^4 to 1.5×10^4 Ω-cm^2 at a pH of 7.5. Note that about 20 h were required for the steel to passivate at a pH of 9.

Figures 11 and 12 show the results generated after about 119 h of exposure to the waste at a pH of 7.5 without preexposure to a pH of 9. This response was modeled by one relaxation time constant, Circuit 1 of Fig. 1. This model applied throughout that exposure.

Table 4 shows the exposure time, resistances, and estimated corrosion rates for exposure to a pH of 7.5 after exposure to the pH of 9. Included are the ranges of the polarization resistances measured for the exposures to a pH of 7.5 and a pH of 9 only. Corrosion rates were estimated from the polarization resistances by using a proportionality constant, *B*, of 0.025 V in lieu of actual values. This approach was followed because of the complexity of the corrosion process as evidenced by the complexity of the structure of the impotance spectra. This complexity suggests that use of one anodic and one cathodic charge transfer process might not be appropriate to model the current versus voltage response. The iminodiacetic acid or nitrilotriacetic acid in the solutions could be complexing with iron and affecting the corrosion rate [*20*]. The two time-constant response could either be caused by diffusion of some species, possibly oxygen, through the removable crust on the electrode surface that seemed to form under basic conditions or by some type of adsorbed intermediate suggested to occur in this environment [*20*]. As discussed later, use of 0.025 V yields reasonable agreement between the average corrosion rates estimated from the impedance results and the time-averaged corrosion rate estimated from the mass loss. This assumed value of the constant is not unreasonable for this screening since, as shown in Table 4, the effect of pH on corrosion is so large that even if the value is off by 50% the conclusion of the effect of preexposure to a pH of 9 would not change.

Discussion

As mentioned previously, simple models might allow practical answers to be obtained and practical predictions to be made from the electrochemical impedance results. This paper has shown how this procedure might work in practice. The major difficulty with using such models is proving that the corrosion rates estimated do predict those in the actual system. This proof is important because often there is a paucity of information on the solution chemistry and answers must be provided before a definitive study of the corrosion mechanism can be completed or even undertaken. The less that is known about the solution chemistry or corrosion mechanism, the more imperative is the need for such corroboration. The following discussion shows how and from what results one might obtain the information necessary to provide confidence in the corrosion rate estimate. The discussion is meant to give a flavor for the approach.

When corrosion rates are to be estimated, the best corroboration is an alternative estimate

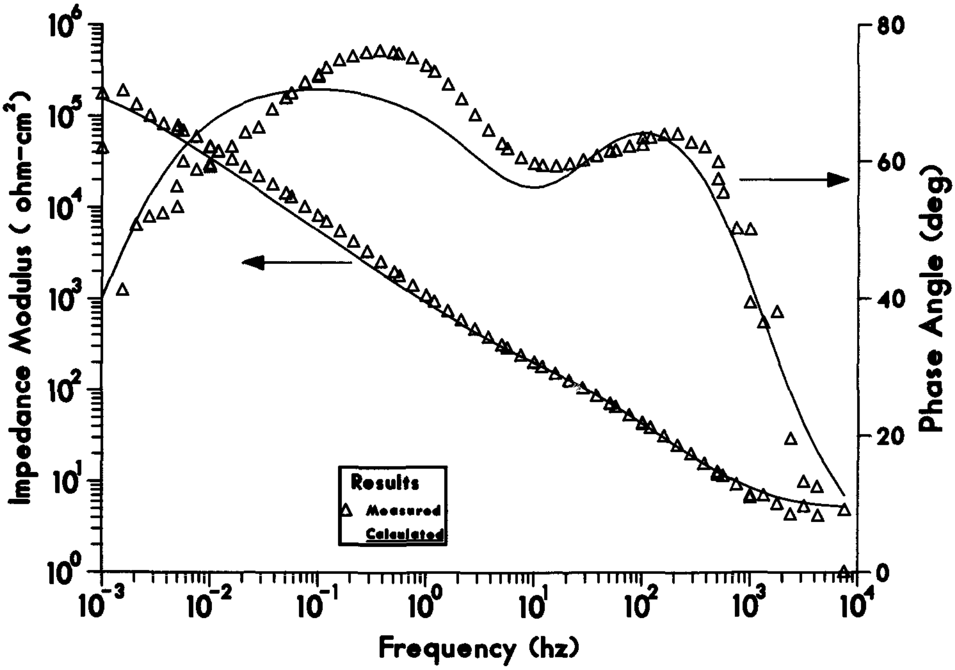

FIG. 8—*Impedance spectrum in Bode format of carbon steel in waste at 49°C (322 K), pH = 9.0, 200 rpm, 45 h exposure* [17].

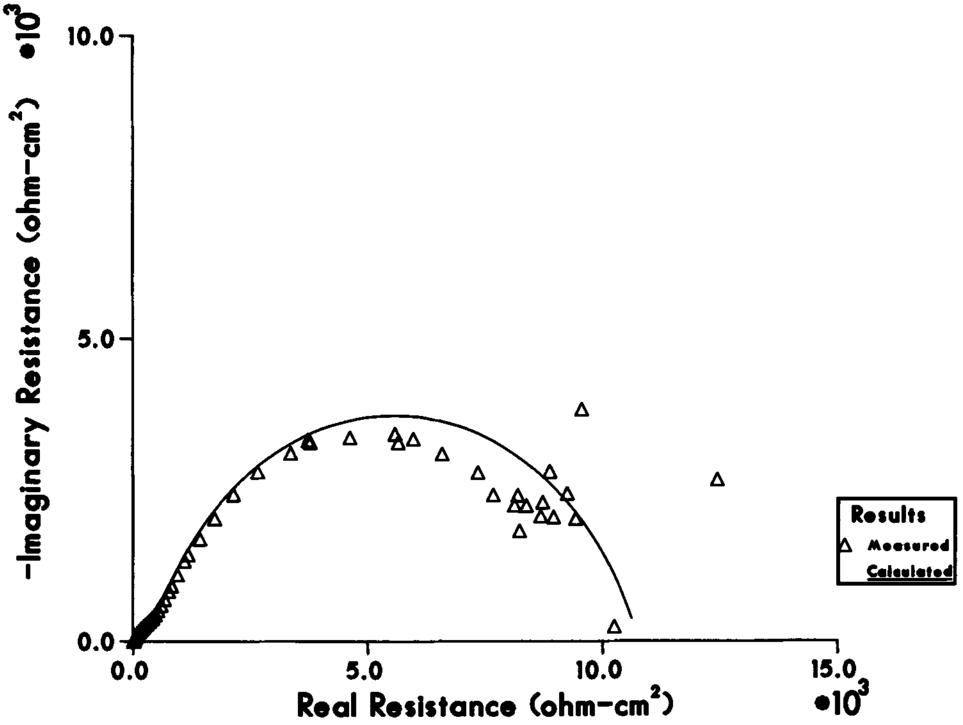

FIG. 9—*Impedance spectrum in Nyquist format of carbon steel in waste at 49°C (322 K), pH = 7.5, 200 rpm, 73 h exposure. pH changed from 9.0 to 7.5 after 53 h* [17].

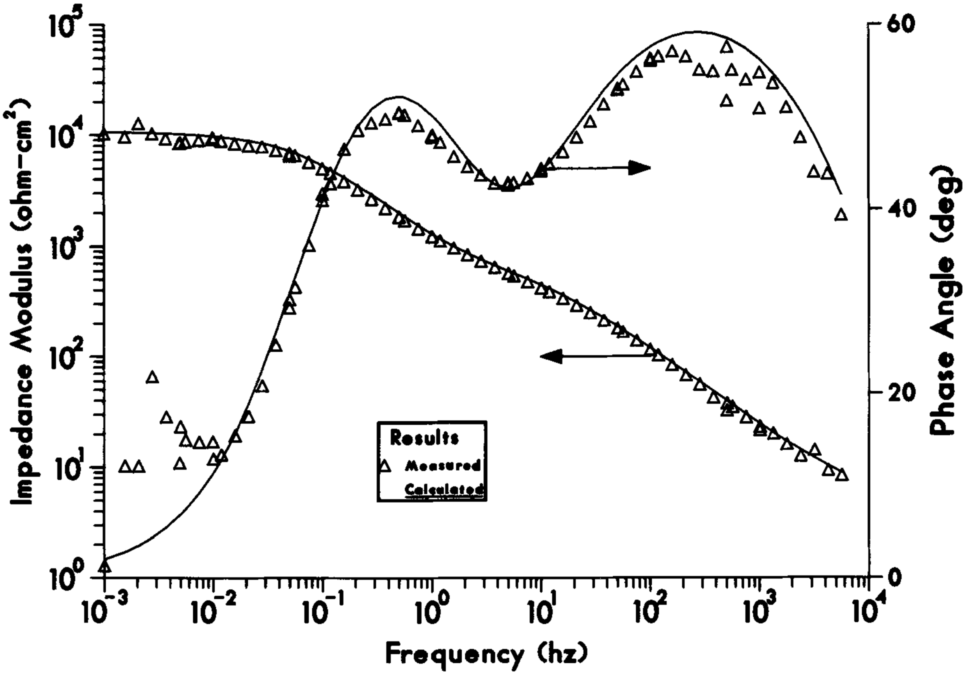

FIG. 10—*Impedance spectrum in Bode format of carbon steel in waste at 49°C (322 K), pH = 7.5, 200 rpm, 73 h exposure. pH changed from 9.0 to 7.5 after 53 h* [17].

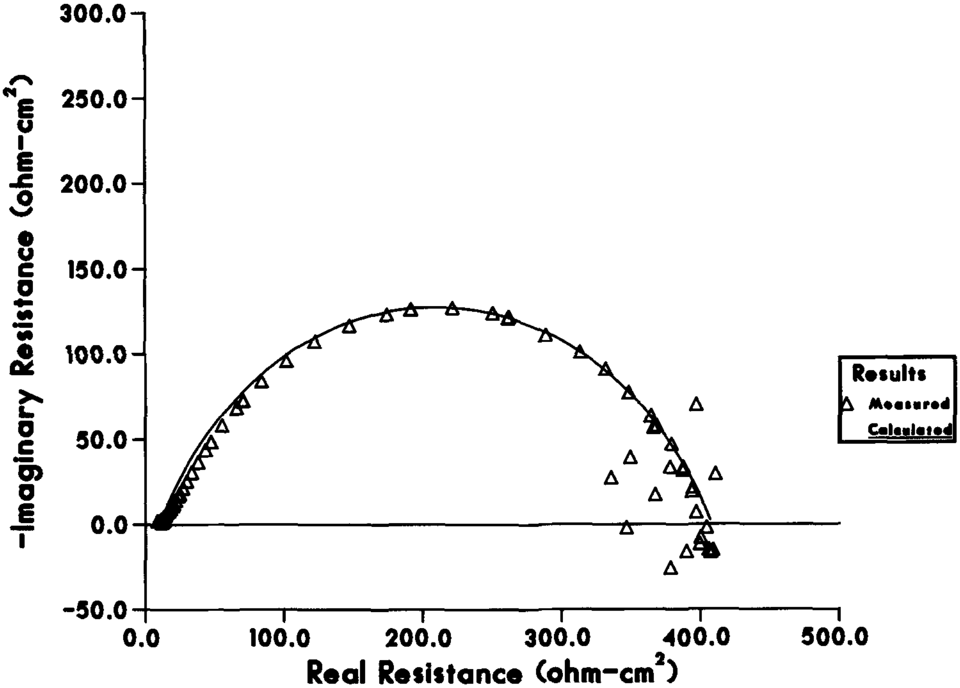

FIG. 11—*Impedance spectrum in Nyquist format of carbon steel in waste at 49°C (322 K), pH = 7.5, 200 rpm, 119 h exposure* [17].

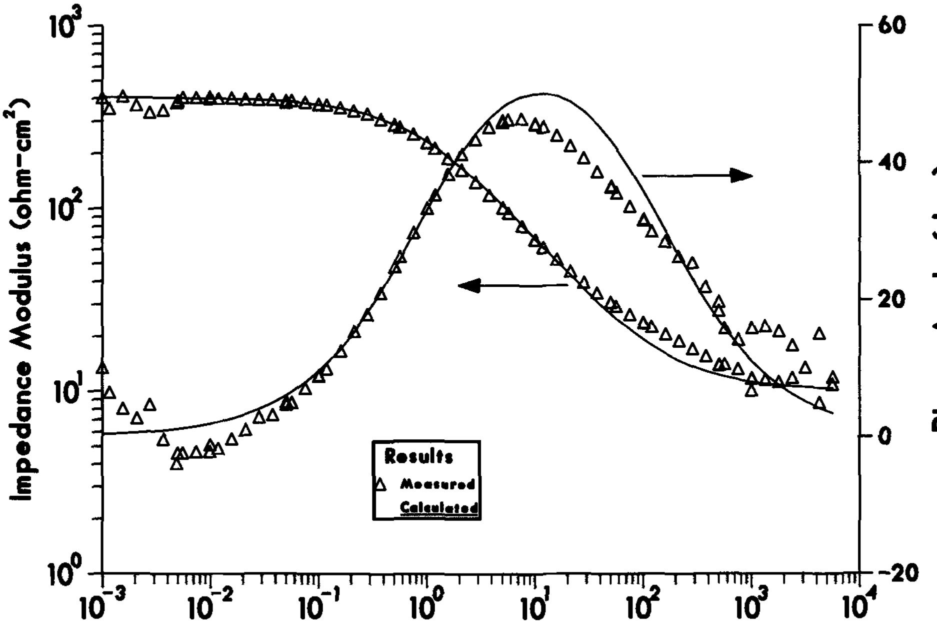

FIG. 12—*Impedance spectrum in Bode format of carbon steel in waste at 49°C (322 K), pH = 7.5, 200 rpm, 119 h exposure* [17].

TABLE 4—*Corrosion rate as a function of time.*

Time, h	Resistance,[a] Ω-cm^2	pH[b]	Corrosion Rate, mm/year	Corrosion Rate, mpy
1	1.50×10^3	9	2×10^{-1}	8
4	1.40×10^3	9	2×10^{-1}	8
21[c]	8.00×10^2	9	4×10^{-1}	2×10
45	2.76×10^5	9	1×10^{-3}	4×10^{-2}
71	9.90×10^3	7.5	3×10^{-2}	1
73	9.80×10^3	7.5	3×10^{-2}	1
106	1.19×10^4	7.5	3×10^{-2}	1
170	1.50×10^4	7.5	2×10^{-2}	8×10^{-1}

[a] For exposure to pH of 9 only, the low-frequency resistance ranged from 5×10^4 to 7×10^4 Ω-cm^2. For exposure to pH of 7.5 only, the polarization resistance ranged from 300 to 600 Ω-cm^2.

[b] pH changed to 7.5 after 53 h.

[c] There was a large decrease in corrosion rate after 21 h of exposure accompanied by a several hundred millivolt shift in corrosion potential in the anodic direction.

of the corrosion rate in the same solution and under the same exposure conditions. Mass loss and solution analysis are the two most practical methods. However, they are only useful when the corrosion rate is large enough or the exposure long enough so that mass or ion changes are measurable.

In the case of the waste stream study, such corroboration was possible because the mass loss of the steel electrode was measurable. For example, the average corrosion rate from mass loss at pH values of 7.5, 8.0, and 9.0 are 0.56, 0.12, and 0.05 mm/year [*17*]. Those derived from the impedance results are 0.47, 0.15, and 0.034 mm/year for the same values of pH [*17*]. In addition, the experimental results listed in Table 4 yield an average corrosion rate from mass loss of 0.57 mm/year. That from the impedence results using the Tafel slope-related parameter equal to 0.025 V is 0.64 mm/year. The 10^{-3} mm/year corrosion rate suggesting a passivation of the surface was assumed to last for 24 h. The others were averaged together over the times consistent with the appropriate pH of the solution. This agreement strongly suggests that use of the models in Fig. 1 in conjunction with the estimated Tafel parameter results in acceptable predictions of corrosion even though the solution, chemistry, and corrosion mechanism are not clearly understood.

This type of corroboration may not always be possible. Under these circumstances, corrosion rates predicted from the impedance spectra must stand alone for corrosion prediction. The results for steel and 304SS in DEQUEST 2016 product are examples. For this study, the problem addressed is contamination and not system integrity. As shown in Tables 1

TABLE 5—*Time constants and pseudocapacitance for corrosion of steel in DEQUEST 2016.*

Time, h	High Frequency: Time Constant, s	High Frequency: Pseudo-capacitance, μF/cm^2	Low Frequency: Time Constant, s	Low Frequency: Pseudo-capacitance, μF/cm^2
1	1.1	8.2×10^1	3.9×10^1	4.7×10^2
5	4.7×10^{-1}	4.0×10^1	1.9×10^2	2.7×10^2
24	3.3×10^{-1}	2.4×10^1	1.5×10^2	2.6×10^2
48	4.7×10^{-1}	4.3×10^1	2.9×10^2	6.1×10^2
72	4.4×10^{-1}	3.6×10^1	5.6×10^2	5.2×10^2

TABLE 6—*Time constants and pseudo-capacitance for corrosion of 304SS in DEQUEST 2016.*

Time, h	Relaxation Time Constant, s	Pseudo-capacitance, μF/cm^2
1	2.7×10^1	1.7×10^2
5	3.6×10^1	6.6×10^1
24	1.7×10^2	5.3×10^1
48	1.6×10^2	4.5×10^1

through 3, the corrosion rates are about 1×10^{-4} to 1×10^{-3} mm/year. As shown by Williams and Asher, corrosion rates as small as several tens of microns (10^{-3} mm/year) per year may be estimated by the electrochemical impedance technique [7]. Thus, the rates shown are not really beyond the possible range of this technology. The problem is to verify the validity of the estimates.

The question addressed is the amount of metal ion contamination that might be present after storage. The moderately alkaline pH range of 10 to 12 and the near-ambient conditions suggest that the actual corrosion rate of steel would not be very large. Both alloys would not be expected to pose risks of catastrophic failure. Corrosion rates less than 2.5×10^{-3} mm/year (0.1 mpy) might be expected for 304SS. Using the rule of thumb that test time in days equals 2000/mpy would suggest a required immersion test of 2×10^4 h to minimize errors on an analytical balance. Such immersion times were beyond the project time constraints. Solution analyses by the ICP technique might shorten the required time but would increase the expense.

The fact that the mass change of the electrode is in the range of the accuracy of the analytical balance is a necessary condition for this corroboration, not a sufficient condition. Since the electrode areas were about 5 cm^2, a corrosion rate of 10^{-3} mm/year would have resulted in a mass loss of about 3×10^{-5} g over 48 to 72 h, below the threshold of the analytical balance. The ionic concentration would have been less than 0.1 ppm, again below the detectable limit of the ICP analysis. The reported corrosion rates being so low support the idea of using the electrochemical impedance technique for predicting long-term metal ion contamination.

Other corroborating evidence is provided by the analysis of the time constants. The relaxation time constant in the first circuit and the high-frequency relaxation time constant in the second circuit of Fig. 1 might be hypothesized to represent the double layer capacitance. The value would be expected to be in the range of 20 μF/cm^2 [*21*], especially if the electrode is not corroding. Tables 5 and 6 show the values of the pseudocapacitances associated with the various relaxation time constants. Except for the results after very short exposure times, the capacitances estimated from the high frequency relaxation time constant for steel and the relaxation time constant for 304SS approach this 20 μF/cm^2 value. This finding suggests that these time constants represent the double layer at the electrode-solution interface. More importantly, the resistances associated with the low-frequency relaxation time constant for steel and the relaxation time constant for 304SS might be hypothesized to be caused by the charge transfer reactions. Without more information on the mechanism, this conclusion remains a strong hypothesis. Nevertheless, these resistances were used to estimate the corrosion rates shown in Tables 1 and 2.

Unfortunately, the Kramers-Kronig transforms cannot be used to assess the reliability of many of these results. The reason is that the impedance spectra at the lowest measured frequency must be close or equal to its limit at zero frequency. As shown in Figs. 3 to 6, even at 0.001 Hz there remains a large capacitive contribution. This result is often found when measuring low corrosion rates because the D-C limit is not reached. Thus, the Kramers-

Kronig transformations would not be useful for assessing if the impedance spectra are correct transforms for most of the studies reported here. This discussion agrees with that of Shih and Mansfeld who discuss this shortcoming when trying to use the Kramers-Kronig transformations as a general, practical criterion against which to test correctness of the impedance spectra [*22*]. Care is required when using the Kramers-Kronig transforms.

One last point must be discussed further. As mentioned before, the parameter derived from the Tafel slopes must be used to relate the polarization resistance to the corrosion rate. Estimating this parameter is difficult for the two studies discussed here. In the case of the waste streams, the complex, poorly characterized chemistry and the possibility that some of the components might complex with steel strongly suggest that an assumption of one controlling anodic reaction and one controlling cathodic reaction may be in error. The procedure of using nonlinear regression to fit a Wagner-Traud type of relationship with one anodic and one cathodic reaction [*5*] is not necessarily correct in this case. However, though the Tafel slopes might not be obtained by regression of the voltage-current date generated during small amplitude d-c polarization [*5*], the internal agreement with the mass loss results strongly suggests that the 0.025 V assumed for the constant is reasonable. This value may be used for the purpose of screening of steel in this system.

However, in the case of corrosion in DEQUEST 2016, not only is the interaction between the alloys and the solution not understood, but the currents generated during a small amplitude d-c polarization are close to the noise level of the potentiostat. Both observations again strongly suggest that estimating the Tafel slopes for this situation would be difficult. Unfortunately, corroboration of the estimated corrosion rate by other techniques is not easily done. Therefore, one practical alternative is to chose a proportionality factor that is expected to be larger than the actual value. Then if the calculated rate is acceptable, the real rate should be acceptable. The hypothesis is that a value of 0.05 V or even 0.1 V fulfills this need. A value of 0.05 V was used in this portion of the study. Obviously more work is required to define an appropriate value of the Tafel-related parameter or a procedure for estimating it. This need is very apparent when trying to use the electrochemical impedance technique for estimating very low corrosion (contamination) rates.

Acknowledgment

The author would like to thank J. E. Carrico, who performed all of the experiments.

References

[*1*] Gabrielli, C., *Identification of Electrochemical Processes by Frequency Response Analysis,* Solartron Instrumentation Group, 1980.

[*2*] Mansfeld, F., "Evaluation of Corrosion Protection With Electrochemical Impedance Spectroscopy," Paper 481, *Corrosion/87,* National Association of Corrosion Engineers, Houston, 1987.

[*3*] Gabrielli, C., Keddam, M., and Takenouti, H., "The Use of A-C Impedance Techniques in the Study of Corrosion and Passivity," *Treatise in Materials Science and Technology,* H. Herman, Ed., Vol. 23, Academic Press, San Diego, 1983, p. 395.

[*4*] Macdonald, D. D., "Theoretical Analysis of Electrochemical Impedance," Paper 479, *Corrosion/87,* National Association of Corrosion Engineers, Houston, 1987.

[*5*] Silverman, D. C. and Carrico, J. E., *Corrosion,* Vol. 44, No. 5, 1988, p. 280.

[*6*] McKubre, M. C. H., "Techniques for A-C Impedance Measurements in Corrosion Systems," paper 480, *Corrosion 87,* National Association of Corrosion Engineers, Houston, 1987.

[*7*] Williams, D. E. and Asher, J., *Corrosion Science,* Vol. 24, No. 1, 1984, p. 185.

[*8*] Scully, J. R., "Electrochemical Impedance Spectroscopy for Evaluation of Organic Coating Deterioration and Under-Film Corrosion—A State of the Art Technical Review," *Report SME-86-006,* David W. Taylor Naval Ship and Development Center, Bethesda, MD, September 1986.

[*9*] Lorenz, J. W. and Mansfeld, F., *Corrosion Science,* Vol. 21, 1981, p. 647

[*10*] Silverman, D. C., *Corrosion,* Vol. 45, No. 10, 1989, p. 824.

[11] Kendig, M. W., Meyer, E. M., Lindbergh, G., and Mansfeld, F., *Corrosion Science*, Vol. 23, 1983, p. 1007.
[12] Epelboin, I. and Keddam, M., *Journal of the Electrochemical Society*, Vol. 117, 1970, p. 1052.
[13] Juttner, K., Lorenz, W. J., Kendig, M. W., and Mansfeld, F., *Journal of the Electrochemical Society*, Vol. 135, No. 2, 1988, p. 332.
[14] Mitzloff, M., Hoffmann, H. N., Juttner, K., and Lorenz, W. J., *Berichte Bunsengesellschaft Physikalische Chemie*, Vol. 92, No. 11, 1988, p. 1234.
[15] Dawson, J. L. and John, D. G., *Journal of Electroanalytical Chemistry*, Vol. 110, 1980, p. 37.
[16] Silverman, D. C., *Corrosion*, Vol. 40, No. 5, 1984, p. 220.
[17] Silverman, D. C., "Rapid Corrosion Screening in Poorly Defined Systems by Electrochemical Impedance Technique," *Corrosion/90*, National Association of Corrosion Engineers, Houston, 1990, accepted by *Corrosion Journal* (publication expected August 1990).
[18] Mansfeld, F., "The Polarization Resistance Technique for Measuring Corrosion Currents," *Advances in Corrosion Science and Technology*, M. G. Fontana and R. W. Staehle, Eds., Vol. 6, Ch. 3, Plenum Press, New York, 1976.
[19] Mansfeld, F. and Oldham, K. B., *Corrosion Science*, Vol. 11, 1971, p. 787.
[20] Silverman, D. C., *Corrosion*, Vol. 44, No. 9, 1988, p. 606.
[21] Kaesche, H., *Metallic Corrosion*, translation by R. A. Rapp, National Association of Corrosion Engineers, Houston, TX, 1985.
[22] Mansfeld, F. and Shih, H., *Corrosion Science*, Vol. 28, No. 9, 1988, p. 933.

DISCUSSION

A. VanOrden[1] (*written discussion*)—What techniques can you recommend for validation for the electrochemical impedance techniques since you suggested it is important to use several different techniques rather than relying only on electrochemical impedance measurements?

D. C. Silverman (*author's closure*)—Your question is important because good experimental procedure should include two independent measures of the same phenomenon. Additional independent measures of the corrosion rate which could be used to corroborate the estimate from impedance spectra are mass loss of the electrode itself and analysis of the metal ion content of the solution. There are limitations to both in terms of the change being large enough to be measured or, in the case of metal ion content, having a solution which is conducive to such measurement. Polarization resistances estimated from impedance spectra should agree with those measured by d-c polarization resistance techniques. Lastly, if an actual process is being simulated, the results must be consistent with those in the actual process.

N. Berke[2] (*written discussion*)—Did you get the chance to run longer-term experiments to verify that the early results were correct? How do the predictions compare to field experience?

D. C. Silverman (*author's closure*)—Unfortunately, long-term experiments could not be run before the predictions from the impedance spectra had to be translated into recommendations. However, as far as the plant waste study, tighter control of pH has been implemented. At this point, corrosion seems to have been decreased by making this change.

S. T. Hirozawa[3] (*written discussion*)—When a metal/alloy is immersed in an inhibiting medium, the corrosion rate is high initially and decreases with time. The corrosion inhibition

---

[1] AS&M, NASA, Langley Research Center, Hampton, VA 23665.
[2] W. R. Grace, Cambridge, MA.
[3] BASF Corp., 1419 Biddle Ave., Wyandotte, MI 48192.

process takes about 24 h or longer. It is common practice to immerse a specimen about 20 to 24 h before running the corrosion test. However, the corrosion rates in the first 2 h, when there is a rapid drop in the rate and a rapid drift in the open circuit potential, are very desirable because these data are related to the kinetics of the passiviation process. The passivation kinetics may decide whether an alloy can withstand depassivation processes such as cavitation erosion, sand abrasion, and hot surface corrosion which are found in the automobile cooling system. We have developed a potentiostaircase polarization resistance method which can determine corrosion rates in very unstable systems.

Is it possible to run EIS in such unstable systems, perhaps by using alternating current instead of the usual alternating voltage?

D. C. Silverman (*author's closure*)—Your question amplifies a critical need in corrosion science and engineering, an ability to measure transient phenomena on a routine and reliable basis. A paper has recently appeared [*1*] in which the authors claim to have developed a procedure for using impedance techniques for examining nonstationary systems. Special mathematical procedures (spline under tension functions) had to be used to implement this technology. The procedure is definitely experimental at this point.

The more traditional methodology of using electrochemical impedance spectroscopy will only be partially successful. Stability is one of the criteria that must be fulfilled for the Laplace transform of the ratio of the voltage to the current or the current to the voltage to be an impedance. Stability means that the system must return to its original state after the perturbation is removed. A transient system will not be at the same state at the beginning and end of each perturbation, whether the perturbation is voltage or current. The only hope is that the degree of stray is small enough that nonlinearities are not introduced. As discussed in a recent paper [*2*], one way to estimate the system drift is to monitor the corrosion potential. One could, in principle, measure the impedance spectrum up to that time at which the system has not strayed far from its initial state and then use circuit analogues to extrapolate to low frequency. The assumption would be that no additional time constants arise. If this procedure is followed, then an independent measure of corrosion should be made to insure that the assumptions are correct. For example, the time-averaged corrosion rate from the impedance spectra could be compared to the time-averaged corrosion rate from mass loss.

[*1*] Berthier, F. Diard, J.-P., Jussiaume, A., and Rameau, J.-J., *Corrosion Science*, Vol. 30, Nos. 2/3, 1990, p. 239.

[*2*] Silverman, D. C., "Rapid Corrosion Screening in Poorly Defined Systems by Electrochemical Impedance Technique," accepted for publication by *Corrosion Journal*, 1990.

Theresa C. Simpson,[1] *Patrick J. Moran,*[1] *Howard Hampel,*[1]
Guy D. Davis,[2] *Barbara A. Shaw,*[2] *Chike O. Arah,*[2]
Tammy L. Fritz,[2] *and Kenneth L. Zankel*[3]

Electrochemical Impedance Measurements for Evaluating and Predicting the Performance of Organic Coatings for Atmospheric Exposure

---

REFERENCE: Simpson, T. C., Moran, P. J., Hampel, H., Davis, G. D., Shaw, B. A., Arah, C. O., Fritz, T. L., and Zankel, K. L., **"Electrochemical Impedance Measurements for Evaluating and Predicting the Performance of Organic Coatings for Atmospheric Exposure,"** *Corrosion Testing and Evaluation: Silver Anniversary Volume, ASTM STP 1000,* R. Baboian and S. W. Dean, Eds., American Society for Testing and Materials, Philadelphia, 1990, pp. 397–412.

ABSTRACT: This paper focuses on the use of electrochemical impedance spectroscopy (EIS) as a predictive tool in assessing organic coating deterioration. EIS has been used by a number of investigators in recent years to assess coating deterioration. Good correlations between EIS data in immersion environments and other deterioration parameters exist (primarily evaluated visually). The potential use of EIS for sensing coating degradation in atmospheric exposure has not been fully evaluated. We have recently developed an atmospheric electrochemical monitor (ATMEIS) designed to assess degradation of painted metal substrates during atmospheric exposure using EIS. The monitor consists of a painted steel coupon upon which a gold electrode was electron-beam deposited to serve as a reference/counter electrode. EIS measurements are made between the underlying steel substrate and the gold reference/counter electrode residing on the coating surface. The ATMEIS has been tested both in immersion exposure and in an atmospheric exposure chamber and has been found to generate EIS data consistent with those predicted for a painted metal coupon in an aggressive environment. This paper reports the details of recent studies by other investigators in immersion environments using EIS to sense coating deterioration and discusses the design and testing of our ATMEIS monitor for atmospheric EIS.

KEY WORDS: acidic deposition, atmospheric, coating, corrosion, electrochemistry, steel

Electrochemical impedance spectroscopy (EIS) is a sensitive, essentially nondestructive technique that is ideally suited for detection and monitoring of the deterioration of organic coatings on metallic substrates. EIS has been used by a number of investigators in immersion environments to detect coating degradation [*1–14*]. This paper will include a brief review of some of the most recent studies, particularly those which report correlations with visual or other degradation parameters. Recently, Scully [*1*] has reported a good correlation between

---

[1] Dept. of Materials Science and Engineering, The Johns Hopkins University, Baltimore, MD 21218.
[2] Martin-Marietta Laboratories, 1450 S. Rolling Rd., Baltimore MD 21227.
[3] Versar, Inc., 9200 Rumsey Rd., Columbia, MD 21045.

early EIS data and long-term coating performance in immersion in seawater. Epoxy-coated steel specimens were immersed in ASTM artificial seawater for 550 days, and EIS data were collected throughout the exposure period. The goal of the study was to determine which, if any, EIS parameters could best be used to predict long-term coating deterioration and to establish the earliest time when such information could be obtained from EIS data. Coating capacitance, coating resistance, near d-c impedance, and the break point frequency [frequency (in high frequency range) at which a 45° phase angle shift occurs] were the parameters investigated. The EIS parameters which correlated most closely with actual performance were near d-c impedance and the break point frequency. Ten-day EIS data were favorably correlated with performance for 550 days of seawater immersion.

Similarly, Tait [*2*] has used EIS to examine corrosion behavior of coated aerosol containers and steel drums. Three types of EIS data were observed for exposure periods of approximately 100 days which correlated well with service data for these coatings. Coated metal samples that exhibited purely capacitive behavior throughout the exposure time had service lives in excess of two years. Those that showed resistive/capacitive behavior typical of a coated metal containing defects failed in service at a rate which was proportional to the rate of decrease of the polarization resistance. Some specimens exhibited low-frequency data consistent with a Warburg model. These coatings did not fail due to underfilm corrosion, but rather due to electrolyte-induced delamination at the coating/metal interface. In these specimens, the rate of coating capacitance changes correlated well with the extent of coating delamination.

Skerry et al. [*3*] have used EIS to characterize degradation of vinyl chloride and alkyd paints on mild steel substrates in seawater. Decreases in polarization resistance (as determined using EIS) correlated well with extent of blistering and rusting evaluated visually. In addition, EIS data was clearly distinct for the two coatings, indicating the sensitivity of the impedance method to differences in coating properties. At early exposure times, EIS data for vinyl chloride specimens are purely capacitive, consistent with an intact coating in the absence of defects. After 2000 h of exposure, evidence for significant defects becomes apparent. In contrast, the alkyd coating shows evidence of porosity or defects within the first 24 h after immersion.

Fastrup and Saarnak [*4*] evaluated alkyd, acrylate, and vinyl chloride paints on cold-rolled steel which were exposed to a simulated acidic deposition environment. Exposure conditions consisted of spraying the specimens with acidic solutions at regular intervals and allowing intermittent drying. EIS data were collected after exposure (specimens were immersed in the same acidic solution as the spray during EIS data collection). The EIS data were compared to visual performance of these specimens after three months' exposure. The performance of these coatings was generally quite good, which limited the extent of comparison possible. The only parameter for which a good correlation was established for these systems was coating capacitance. In general, large changes in coating capacitance corresponded to poor coating performance. Minimal changes occurred for good coatings. No low-frequency correlation was established between impedance data and coating performance.

Wang and Radovic [*5*] evaluated two automotive paint coating systems applied to cold-rolled or galvanized steel in sodium chloride immersion. Some specimens were defected intentionally by drilling small holes in the coating to expose the underlying substrate. After EIS data were collected, specimens were removed from exposure, cross-sectioned, and examined by optical microscopy. Changes in EIS data correlated well with visual corrosion. All of the coatings that did not have intentional defects showed capacitive EIS data, with near d-c impedance values of $\sim 10^9$ ohm-cm^2 throughout the 500-h test. Rust was not observed on these panels after cross sectioning. Samples containing intentional defects showed EIS behavior consistent with that predicted for a coated specimen containing defects; near d-c impedance values were three to five orders of magnitude lower than those for the intact films. Further, the polarization resistance decreased as a function of exposure time, indicating increased degradation of the metal substrate. Examination of the cross sections confirmed this increase in corroded area.

Hirst et al. [*6*] evaluated three coating systems applied on various pretreated surfaces of four types of aluminum. The specimens/coatings were designed for aerospace applications. EIS, the ASTM Method for Measuring Adhesion by Tape Test (D 3359, Method A), the ASTM Test Methods for Adhesion of Organic Coatings by Scrape Adhesion Tester (D 2197, Method A), and flexibility were used to evaluate coating performance. Specimens were exposed in a variety of ways: (1) immersion in lubricating oil, hydraulic fluid, a hydrocarbon solvent, or water; (2) low temperature exposure (−51°C); (3) corrosion resistance to salt spray, 2000 h [ASTM Method of Salt Spray (Fog) Testing (B 117)] or SO_2/salt spray, 500 h [ASTM Practice for Modified Salt Spray (Fog) Testing (G 85)]. EIS data were collected for specimens immersed in slightly acidic solution for exposure periods up to 1200 h. Coatings that performed well under the accelerated exposure conditions exhibited high impedances and essentially capacitive behavior throughout the exposure time. Similarly, the types of paint panels that performed poorly in mechanical and other tests showed impedance data for nominally identical specimens, consistent with defected paint films.

To date, however, EIS has not been adequately applied to coatings during exposure to atmospheric or vapor phase conditions. The correlations which exist between EIS data and visual or other degradation parameters for immersion exposure, however, provide encouragement that similar success could be achieved for EIS monitoring in atmosphere. We have recently reported the design and preliminary testing of an atmospheric electrochemical monitor (ATMEIS) used to generate EIS data during atmospheric exposure [*15*]. The ATMEIS monitor consists of a painted steel coupon upon which a gold electrode (covering less than 10% of the front surface of the sample coupon) is electron-beam deposited. The impedance of the substrate/coating system is determined in a two-electrode measurement using the steel substrate and the electron beam-deposited electrode. The monitor can be used, therefore, in the absence of a remote reference or counter electrode. The monitor was developed to assess the degradation of organic coatings in atmospheric exposures simulating acid deposition.

The monitor relies on the assumption that the impedance of the interface of the deposited electrode lying on the surface of the coating is low relative to the impedance of the coating and the steel-coating interface, which has been verified and will be demonstrated later in this text [*15*]. This enables a two-electrode measurement rather than a conventional three-electrode measurement to be completed. The two-electrode approach is valid because placement of the deposited electrode at the surface of the coating enables its entire interface with the coating to be wetted and utilized, resulting in a low interfacial impedance relative to the coating or the steel-coating interface. The primary value of this monitor is that it has the potential of being used for completely in-situ monitoring of atmospheric or vapor phase coating deterioration on a real-time basis and/or on real structures. Such a method is currently unavailable. The method is clearly distinct from coated atmospheric corrosion monitors (ACM) developed by Mansfeld and others that are primarily designed to monitor time of wetness [*17–18*]. These monitors have been used to collect EIS data to characterize coated metal systems, but must employ remote reference and counter electrodes in immersion environments to enable this [*17–18*]. The method is also distinct from the curing/temperature monitors developed by Senturia et al. which measure changes in dielectric properties to evaluate extent of cure [*19–20*].

The objectives of the work reported in this paper were: (1) to design and test the monitor in immersion environments in order to determine whether the EIS data are consistent with predicted behavior; (2) to determine whether the deposited gold electrode interfered with the normal degradation of the coating in a sulfuric acid environment; (3) to demonstrate the feasibility of the use of the ATMEIS monitor in atmospheric chamber studies; and (4) to correlate changes in EIS data with mechanical degradation parameters.

Experimental

Preparation of Samples

All sample coupons [25.4 by 25.4 by 1.6 mm (1 by 1 by 1/16 in.)] were prepared from low-carbon steel [ASTM Specification for Steel, Carbon, (0.15 Maximum, Percent), Hot-Rolled Sheet and Strip, Commercial Quality (A 569 CQ)] and were painted with the oil/alkyd system, Dupont Dulux (681-FD-704) primer and Dulux (96-Y-67632) topcoat, which is typically used for maintenance painting of steel structures. Prior to painting, coupons were solvent-degreased with methyl ethyl ketone and grit-blasted to a white metal finish. The alkyd paint system was then spray-applied to the specimens. The front side of the coupons was coated with a layer of primer, followed by a single or double layer of topcoat. The back side of the coupons was coated with one layer of primer and two layers of topcoat. The edges were coated with primer and brush-coated twice with topcoat. Specimens had total dry film thicknesses of 100 to 150 μm. All the coupons were oven-cured in air at 100°C for 1 h, with a gradual heat-up rate (taking approximately 70 min) from room temperature to 100°C. This accelerated cure process was adopted to decrease the time necessary between sample preparation and use. The acceleration of cure was required to ensure that significant additional cure would not take place during exposure studies which could obscure results. The temperature and time selected for accelerated cure were recommended by the coating manufacturer.

ATMEIS specimens were prepared by using electron beam evaporation to deposit a layer of gold (0.2 μm thick) onto the surface of the coated steel specimens. A photoresist was then spun down on the surface and cured at 80°C for 25 min. The photoresist was then exposed to UV (320 nm, 20 s) through a mask (18 mW/cm^2, positive) containing the desired electrode pattern. The remaining gold, not covered by the photoresist, was then etched with potassium iodide/iodine (KI/I_2) (30 s). An oxygen plasma was used to strip the photoresist, resulting in the final coupon. Figure 1 shows a picture of the ATMEIS monitor mounted for chamber exposure. The grid consists of a series of lines of gold which are 0.48 mm wide separated by 1.82 mm. The outer dimensions of the central grid (excluding bonding pads) are 13 by 13 mm. The bonding pads are 1.5 by 1.5 mm and are attached to the central grid by 0.48 by 5 mm lines of gold. Electrical lead wires were attached to the bonding pads on the gold electrode using silver paint.

Experimental Apparatus and Methods

All EIS data was collected using an EG&G PAR 273 potentiostat equipped with a 5208EC lock-in amplifier which was computer-controlled. EIS measurements were collected over a frequency range from 100 kHz to 5 mHz, applying a sinusoidal voltage signal of 10 mV, peak-to-peak. Low-frequency data (below 5 Hz) were collected using a Fast-Fourier trans-

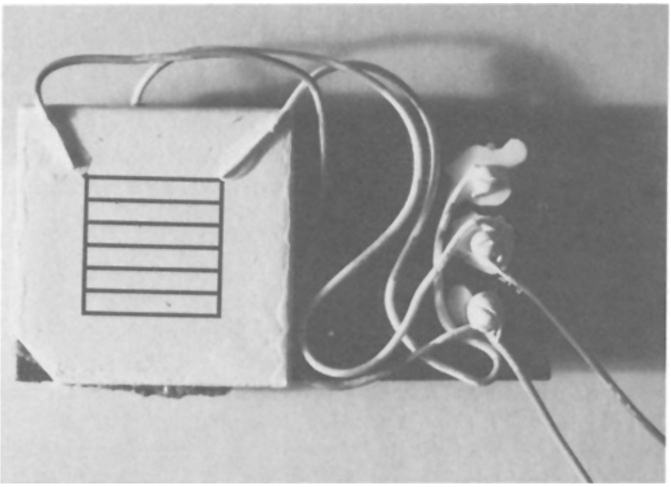

FIG. 1—*Picture of the ATMEIS monitor, mounted for chamber exposure. In immersion exposures only the central portion of the 2.54 by 2.54-cm coupon (portion which contains the gold grid electrode) would be exposed.*

form (FFT) method to apply the voltage signal and collect the data. All experiments employed the M378 software commercially available from PAR.

Immersion exposures were conducted in a custom-designed cell, which exposes only the front central portion (2.5 cm^2) of the specimen to solution and excludes the edges and back of the specimen from direct contact with the solution. Commercially available SCE reference electrodes and graphite counter electrodes were used when remote electrodes were employed. All immersion exposures were conducted in aerated, pH 3, sulfuric acid. EIS data were collected daily to weekly depending on the specific exposure experiment.

Chamber exposures were completed in a custom-designed environmental exposure chamber capable of controlled introduction of pollutant gases and regulation of conditions of temperature and relative humidity. The chamber was composed of a 4-in.-diameter, 2-ft-long sample chamber that can accommodate up to 78 1 by 1 by 1/16 in. coupons mounted flush with the chamber wall. The inside walls were quartz, and the rest of the system exposed to the gas was Teflon. A computer collected the data required to maintain and monitor chamber conditions and controlled the 60 L/min mass flow controllers (wet stream) and the sample heater/chiller unit, which regulated sample temperature. All chamber specimens discussed in this manuscript were exposed to 1 ppm sulfur dioxide, 95% relative humidity, and either constant temperature or thermal cycling (12 h dew cycle followed by a 12-h dry cycle) for exposure periods of one to two months. Control samples were also run under the same conditions, but in the absence of sulfur dioxide. Data for ATMEIS monitor specimens were collected at the beginning of the dry cycle at daily-to-weekly time intervals. Four ATMEIS monitor specimens (two control, two sulfur dioxide) were evaluated in chamber exposure and are discussed in this paper.

Tensile adhesion testing of conventionally prepared specimens was completed using a SEMicro pneumatic-adhesion tensile testing instrument after removal of specimens from the atmospheric exposure chamber. The test required bonding of a 1.25-cm-diameter aluminum stud to the paint surface with a two-part epoxy resin shortly after removal from the chamber. The epoxy was cured for 48 h. The tensile test consisted of applying increasing force to the aluminum stud until separation of the stud from the coupon occurred. The locus of failure (evaluated visually) and strength of failure then were determined. Adhesion testing was conducted on specimens after 0, 5, and 28 days of chamber exposure. All results of adhesion testing on chamber-exposed specimens are presented as averages of at least three specimens. Tension adhesion testing on immersion exposed specimens were conducted using the same basic method, except that bonding occurred 24 h after removal of specimens from exposure.

Results and Discussion

Validation of the two-electrode approach was reported in the preliminary testing of this monitor, which demonstrated that EIS data collected in immersion with the ATMEIS were equivalent regardless of whether: (1) remote reference and counter electrodes are used; (2) the gold electrode is used as the reference/counter combination and the sample is in aqueous acid electrolyte; or (3) the gold electrode is used as the reference/counter combination and the sample is in air [*15*]. Figure 2 contains EIS data for the ATMEIS after one day and two weeks immersion in pH 3 sulfuric acid monitored using remote electrodes (SCE, graphite counter). In addition, EIS data collected for this same sample using the gold electrode as a reference/counter combination with the aqueous electrolyte removed, that is, in air, is shown in Fig. 2. It has further been verified that EIS data for a specimen with significant defects are essentially equivalent regardless of whether the gold electrode is used as a reference/counter combination or whether remote electrodes are used. This confirms that the gold/coating impedance is small relative to the overall impedance and validates the two-electrode method. It should also be noted that EIS data were collected for a specimen with gross defects (coating and gold electrode were visually damaged), and, in all cases, the deviation in EIS data collected using the gold electrode and using remote electrodes was less than a factor of two. Based on these data, the ATMEIS is appropriate for use in the evaluation of coating degradation. In each case, data are consistent with our model of a coated metal containing little or no, minor, or significant defects. The equivalent circuit that applies to our system is shown in Fig. 3.

Comparison of Monitor to Conventionally Prepared Specimens

It was necessary to evaluate the effect of the gold electrode residing on the surface of the coating on the normal degradation of the coating during exposure to ensure that either the preparation or physical presence of the gold would not significantly alter normal degradation processes. To evaluate the extent of this effect, degradation of samples containing the ATMEIS was compared with samples that were otherwise identical, but did not contain the monitor. Figure 4 presents a comparison of the EIS behavior of an ATMEIS to that of a conventionally coated sample after ten weeks of exposure of pH 3 sulfuric acid. Nearly identical EIS behavior was seen for these two samples throughout the exposure period. These data were the first monitor to nonmonitor comparison and were extremely encouraging. The effect of sample-to-sample variation was also evaluated and has been previously reported in detail [*16*]. It should be noted that the preparation methods used in these studies did not involve precision industrial spray equipment and are expected to result in some sample-to-sample variation. It was necessary to evaluate whether the ATMEIS monitor specimens would perform significantly differently from nonmonitor specimens given the sample preparation constraints. It was expected that a spread in impedance data would

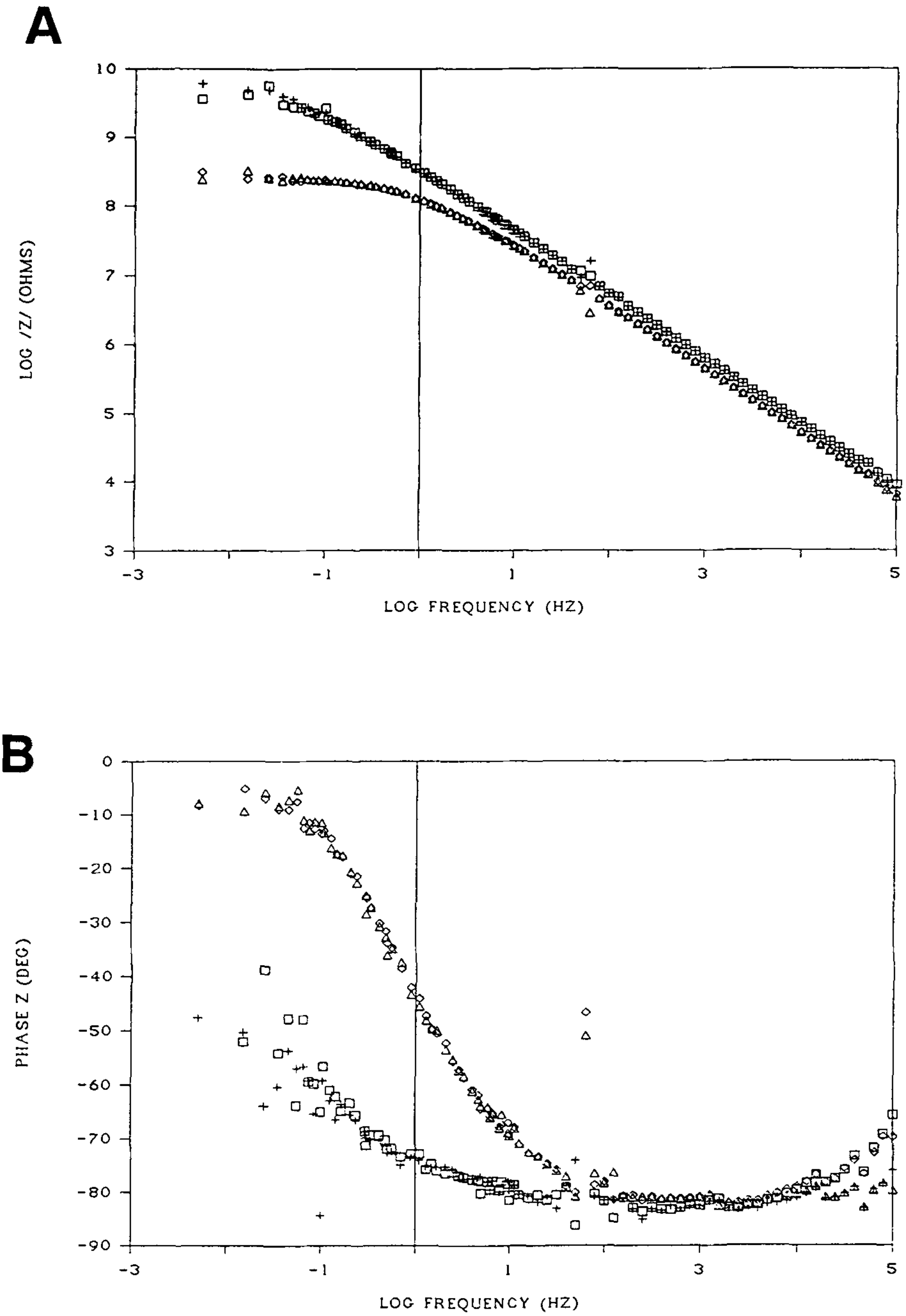

FIG. 2—*Bode magnitude (A) and phase (B) plots of EIS data for the ATMEIS monitor collected using remote reference/counter electrodes* (+,△) *or the gold electrode as reference/counter with the aqueous electrolyte removed* (□, ◇) *after one day, two weeks' exposure to aerated pH 3* H_2SO_4.

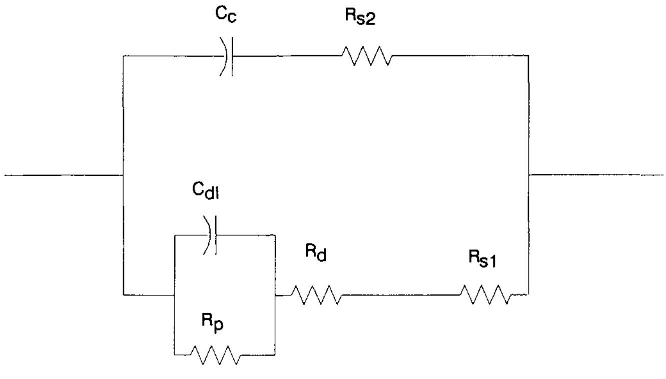

R_p = Polarization Resistance
C_c = Coating Capacitance
C_{dl} = Double Layer Capacitance
R_d = Defect or Pore Resistance
R_{s1} = Solution Resistance (return from defect)
R_{s2} = Solution Resistance (return from coating)

FIG. 3—*Equivalent circuit model for a painted steel coupon in an aggressive environment (containing defects or pores).*

exist, and that this could be attributed to sample-to-sample variations and would not reflect the validity of the method. Evaluation of this effect consisted of exposure of six nominally identical samples, three containing the ATMEIS monitor, and three without, to aerated, pH 3 sulfuric acid (in the cell described above) and the collection of EIS data as a function of time. Figure 5 is a plot of near d-c impedance (5 to 20 mHz), as a function of exposure time for the three ATMEIS samples with extrema lines overlayed for the three nonmonitor samples. One nonmonitor sample had significantly lower impedance values at earlier times than did either of the others, and the dotted line corresponds to exclusion of data for this sample from the data set. The comparison of data for monitor-to-nonmonitor specimens is quite good, particularly when excluding the one sample from Fig. 5 which had unusually low impedance values at early times. Thus, the presence of the gold electrode on the sample surface does not appear to effect the normal chemistry/degradation process of this coating system in sulfuric acid.

Chamber Exposure of ATMEIS Monitor

Figure 6 presents EIS data for a sample containing the ATMEIS monitor as a function of exposure time in the atmospheric chamber to 1 ppm sulfur dioxide, 95% relative humidity, with thermal cycling. The quality of the EIS data, as well as the expected decrease in low frequency impedance with exposure time, demonstrates the feasibility of the monitor for studying and evaluating coating degradation in atmospheric exposures. Figure 7 compares near d-c impedance values as a function of exposure time for ATMEIS specimens during the sulfur dioxide experiment with tensile adhesion strength measurements for a series of conventional specimens (samples which do not contain the ATMEIS monitor, but are otherwise nominally identical) exposed during the same chamber run. Decreases in near d-c

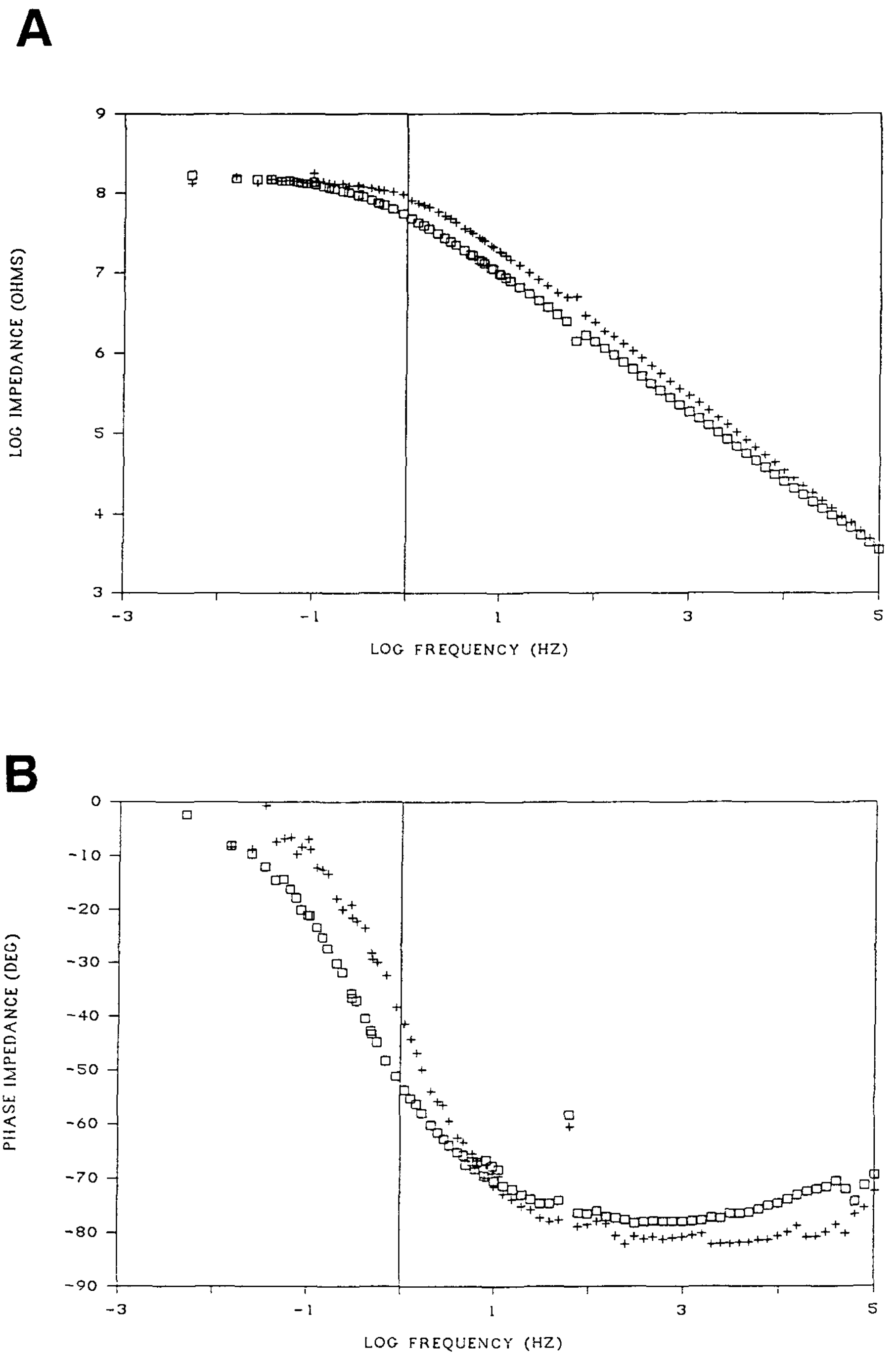

FIG. 4—*Bode magnitude* (A) *and phase* (B) *plots comparing EIS data for a conventional specimen* (+) *to EIS data for an ATMEIS monitor specimen* (□) *after ten weeks' immersion exposure to aerated pH 3* H_2SO_4.

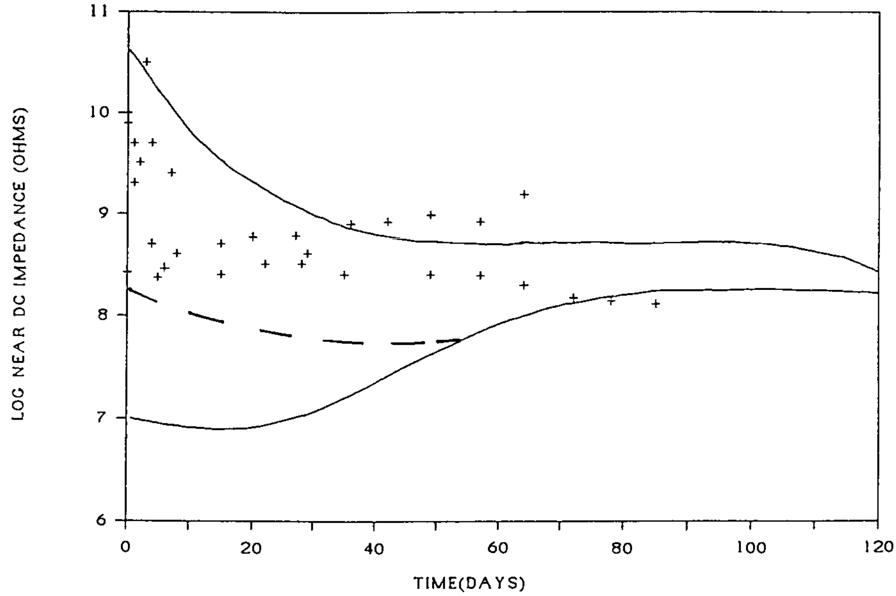

FIG. 5—*Near d-c impedance values (~5 to 20 mHz) as a function of exposure time for three specimens containing the ATMEIS monitor which were immersed in aerated pH 3* H_2SO_4. *Extrema lines for three conventional specimens exposed under the same conditions are drawn in. Dotted line indicates exclusion of one conventional specimen which had particularly low early impedance values.*

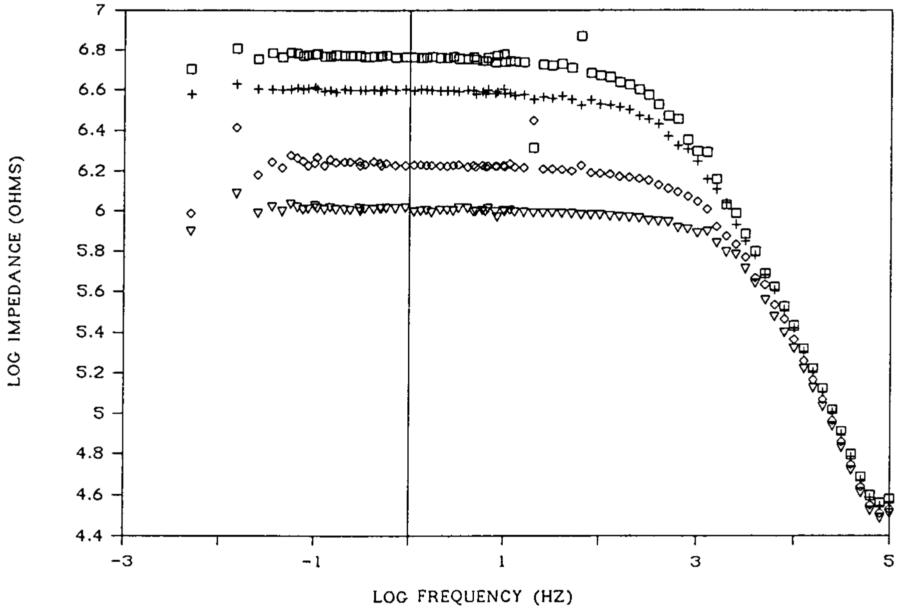

FIG. 6—*EIS data, plotted in the Bode magnitude format, for an ATMEIS monitor after 2* (□), *5* (+), *7* (◇), *and 19* (▽) *days' exposure in the atmospheric exposure chamber to 1 ppm* SO_2, *95% RH.*

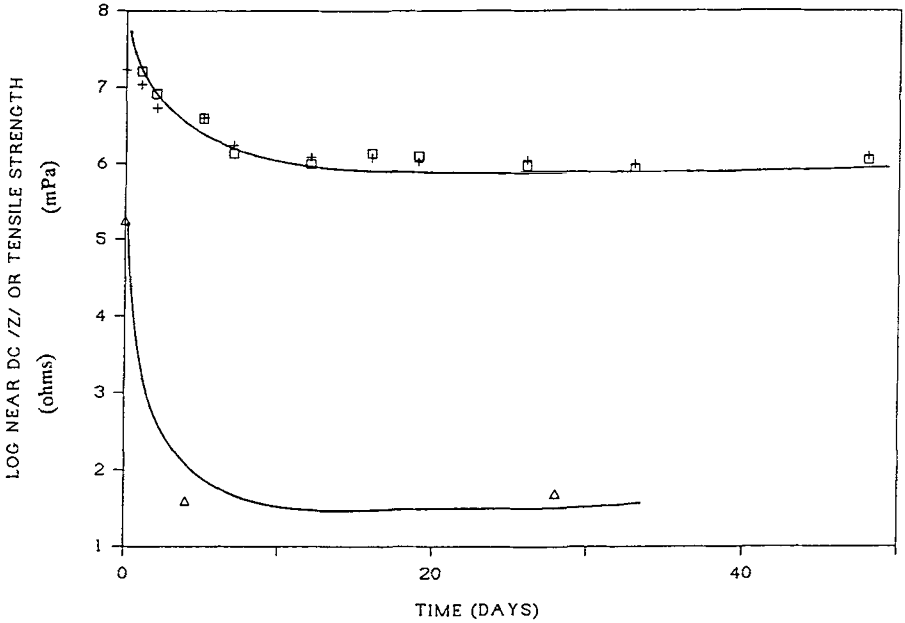

FIG. 7—*Comparison of near d-c impedance values (~5 to 20 mHz) for two ATMEIS monitor specimens (+,□) to average tensile adhesion strength values for conventional specimens (△) as a function of exposure time in the atmospheric exposure chamber to 1 ppm SO_2, 95% RH.*

impedance correspond well to changes in the mechanical properties. ATMEIS data are given for two different samples and tensile adhesion values are averages of at least three specimens. Locus of failure in the tensile specimens occurs initially within the paint system, but shifts to the metal primer interface at later exposure times. Visual examination of the failure surface indicates that this failure is associated with corrosion at the metal/primer interface. Thus, EIS is detecting corrosion at the interface.

Figure 8 compares EIS data for the ATMEIS during exposure to sulfur dioxide, 95% relative humidity to data for exposure in the atmospheric exposure chamber under the same conditions, but in the absence of sulfur dioxide. Although these data only represents a comparison of two chamber runs, the data are suggestive of enhanced degradation of the coating in the presence of sulfur dioxide. It further indicates the sensitivity of the monitor in indicating degradation. Confirmation of these data is underway. Nevertheless, the changes detected during the chamber run clearly demonstrate the feasibility of the ATMEIS monitor for atmospheric monitoring. Further, these changes are consistent with the changes in the mechanical integrity of the coating system.

One unexpected observation was the magnitude of the low-frequency impedance data at early exposure times for the chamber exposed ATMEIS. Initial low-frequency values for specimens with the ATMEIS ranged from 10^{11} to 10^{9} ohms in immersion exposure. Initial low-frequency values for specimens with the ATMEIS in chamber exposure ranged from 10^{8} to 10^{7} ohms. This behavior is likely due to the existence of defects at the sample edges which would not be exposed in the immersion exposures used to preliminarily evaluate these samples as validated in a previous report [*16*]. The fact that the monitor is sensitive to such defects indicates that the monitor can detect defects in areas other than those immediately adjacent to the gold electrode. To further evaluate this effect, an ATMEIS specimen, exposed

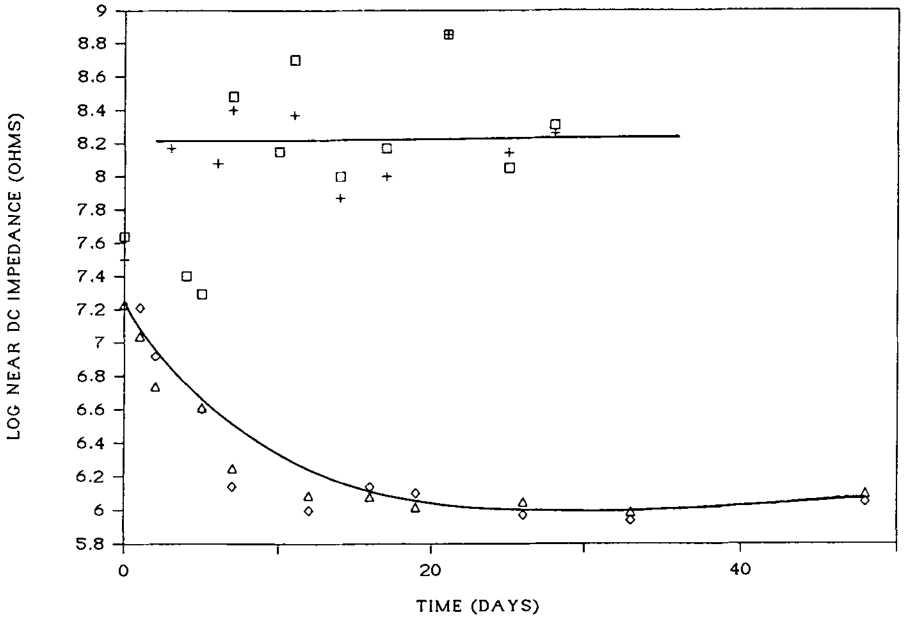

FIG. 8—*Comparison of near d-c impedance values (~5 to 20 mHz) for two ATMEIS monitor specimens (◇,△) exposed to 1 ppm SO_2, 95% RH to near d-c impedance values for two ATMEIS monitor specimens (□,+) exposed to 95% RH as a function of exposure time in the atmospheric exposure chamber.*

via immersion, was intentionally defected to expose ~1.2 mm^2 of the underlying steel substrate between the gold grid lines. EIS data were collected prior to and after the imposition of this intentional defect and are shown in Fig. 9. A change in the near d-c impedance behavior of several orders of magnitude was witnessed, clearly demonstrating the ability of the monitor to detect defects in areas adjacent to the gold electrode. The remote sensing ability of the monitor is likely due to conductivity through the moisture film present on, or within, the coating surface.

Correlation of EIS Data with Tensile Adhesion Data

The relationship between EIS data obtained with the ATMEIS monitor and tensile adhesion strength for samples exposed to the same environment provides encouragement that EIS data may be used as an indicator of mechanical properties and the changes in these properties due to degradation. Although one other study reports similar effects [*6*], we are not aware of any studies that have evaluated the extent of this correlation for the same samples. To fully evaluate this effect specimens were immersed in pH 3 sulfuric acid for exposure times ranging from 1 h to several weeks, and EIS data were collected throughout this exposure time. One day after specimens were removed from exposure, tensile adhesion testing was completed according to the procedure described in the experimental section. The correlation between tensile adhesion data and near d-c impedance measured just prior to removal from exposure is shown in Fig. 10. Data points are averages of 3 to 20 specimens at each exposure time. Although this data is for a limited number of samples, the correlation is quite good. It should be noted that the one high point (10^{11} ohms, 900 psi) represents the average value for several (10 to 20) unexposed samples. Figure 11 shows the correlation

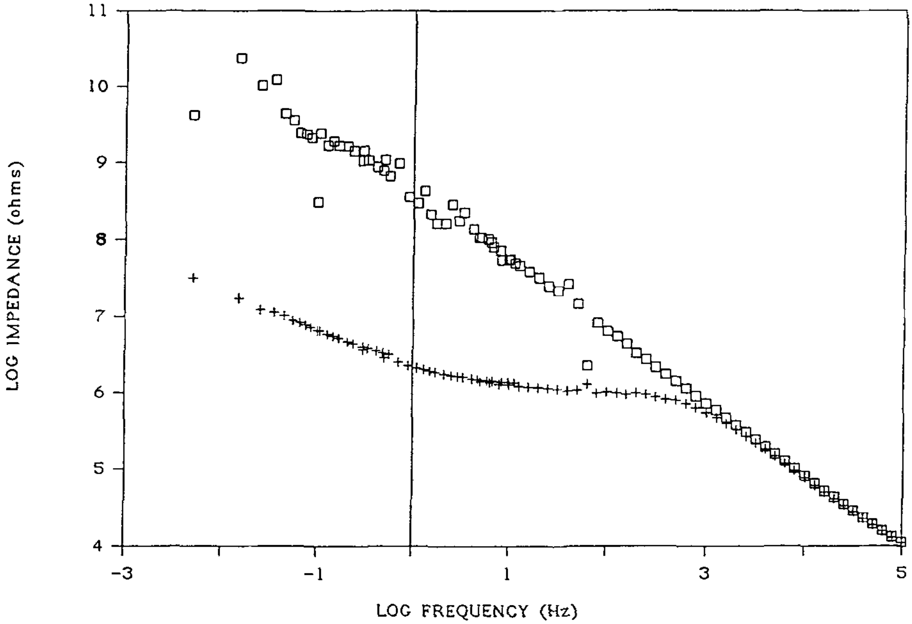

FIG. 9—*EIS data, plotted in the Bode magnitude format, for an ATMEIS monitor specimen prior to* (□) *and after* (+) *the imposition of an intentional defect.*

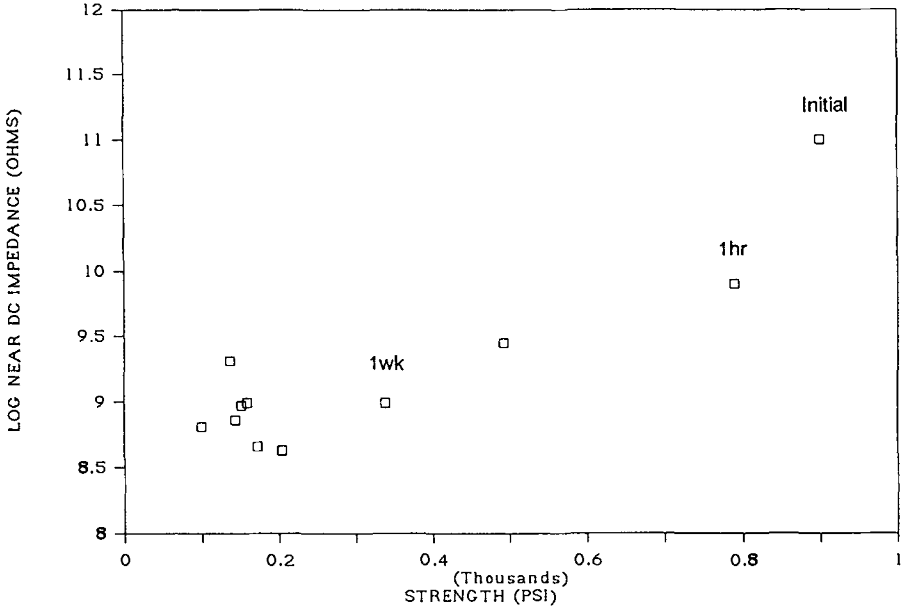

FIG. 10—*Plot of average near d-c impedance values as a function of average tensile adhesion strength for specimens which were immersion exposed in aerated pH 3* H_2SO_4. *EIS data were collected just prior to removal from exposure; tensile adhesion strength was measured on the same samples after removal from exposure. Averages are computed at each exposure time (1 h to several weeks).*

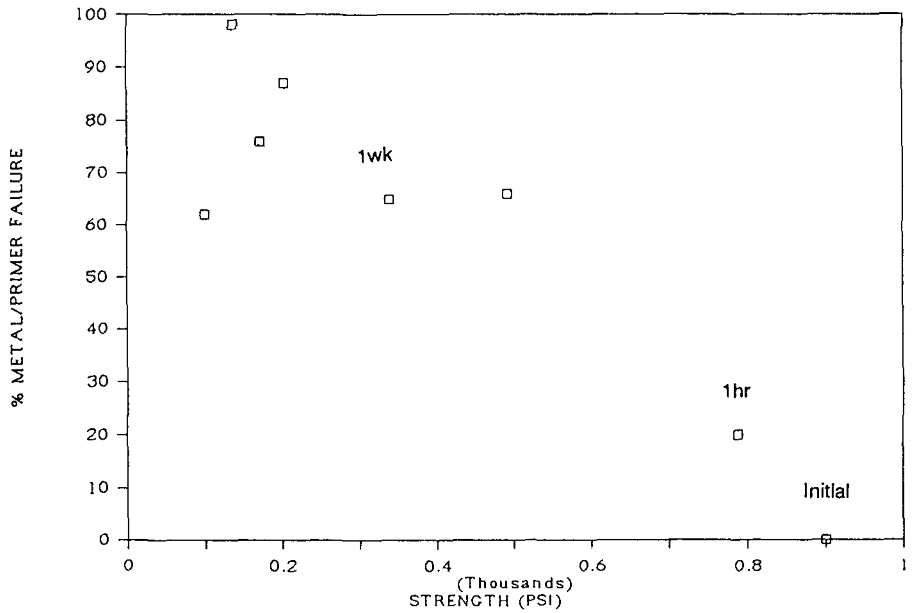

FIG. 11—*Plot of average tensile adhesion strength as a function of average percent metal/primer failure for specimens which were immersion exposed in aerated pH 3* H_2SO_4*. Percent metal/primer failure was evaluated visually. Averages are computed at each exposure time (1 h to several weeks).*

of tensile adhesion strength for these specimens to percent metal/primer failure. This correlation is also quite good. As was previously mentioned, the locus of failure in unexposed specimens or after very short exposure times generally is cohesive in the paint system, that is, occurring within the layers of the paint system. After longer exposure times, this failure shifts to the metal/primer interface and has been visually associated with corrosion of the interface [*21*]. Thus, the facts that strength measurements correlate well with percent metal/primer failure and that EIS data correlate well with strength indicates that EIS may be used as a nondestructive means of assessing changes in mechanical properties and extent of corrosion at the metal/primer interface. This report is the first which presents a direct comparison of EIS data to mechanical properties for the same samples.

Conclusions

An atmospheric electrochemical monitor capable of sensing coating degradation during atmospheric exposure has been designed and tested. This monitor has been used to generate EIS data equivalent to those collected using remote reference and counter electrodes for immersion exposures. The monitor has also been used to generate EIS data upon removal from immersion and during exposure in an atmospheric exposure chamber that are consistent with those expected for a coated metal in an aggressive environment. The effect of this monitor in influencing normal sample degradation/chemistry has also been evaluated. For the system studied, in sulfuric acid environments, the extent or mechanism of degradation of samples containing this monitor is not significantly different from that of conventionally prepared samples which do not contain the ATMEIS monitor. EIS data for the chamber-exposed ATMEIS monitor are consistent with tensile adhesion strength data collected for conventional samples exposed to the same environment for equivalent exposure times. In addition, preliminary EIS data indicate a good correlation between near d-c impedance and tensile adhesion strength. Such changes in tensile data have been correlated to corrosion at the interface, indicating the possible predictive capabilities of the impedance method. Chamber-exposed ATMEIS monitors have initial low-frequency impedance values that are a few orders of magnitude lower than immersion-exposed monitors, presumably due to low impedance pathways at the edges of the specimens which would not be exposed in the immersion exposures. This monitor and its potential applicability for nondestructive, real-time monitoring of coating degradation represents a necessary addition to field of coatings research. Further design and testing of this monitor is anticipated to provide considerable information regarding coating degradation in aggressive environments.

Disclaimer

Although this research was funded in part by the US Environmental Protection Agency, it does not represent official US EPA policy and any mention of trade names or commercial products does not constitute endorsement or recommendation for use.

Acknowledgment

The authors wish to acknowledge the US EPA and John Spence (project officer) for financial support of this research under cooperative agreements CR 814347-01-0 and CR 814347-01-1.

References

[*1*] Scully, J. R., "Electrochemical Impedance of Organic Coated Steel: Correlation of Impedance Parameters with Long Term Coating Deterioration," *Journal of the Electrochemical Society,* Vol. 136, No. 4, 1989, p. 979.
[*2*] Tait, W. C., *Journal of Coatings Technology,* Vol. 61, No. 768, 1989, p. 57.
[*3*] Skerry, B. S., Alavi, A., and Lindgren, K. I., *Journal of Coatings Technology,* Vol. 60, No. 765, 1988, p. 97.
[*4*] Fastrup, B. and Saarnak, A., *Progress in Organic Coatings,* Vol. 16, 1988, p. 277.
[*5*] Wang, Y. M. and Radovic, D., *Plating and Surface Finishing,* Vol. 76, No. 2, 1989, p. 52.
[*6*] Hirst, D. J., Hegedus, C. R., Spadafora, S. J., and Eng, A. T., "Primerless Finishing Systems For the Corrosion Protection of Aluminum," Final Report for Project RS34A52, Report NA2A, Naval Air Development Center, Warminster, PA, September, 1988.
[*7*] Leidheiser, H., Jr., *Progress in Organic Coatings,* Vol. 7, 1979, p. 79.
[*8*] Standish, J. V. and Leidheiser, H., Jr., *Corrosion Control by Organic Coatings,* H. Leidheiser, Jr., Ed., National Association of Corrosion Engineers, Houston, TX, 1981, p. 38.
[*9*] Walter, G. W., *Journal of Electroanalytical Chemistry and Interfacial Electrochemistry,* Vol. 118, 1981, p. 259.
[*10*] Hepburn, B. J., Callow, L. M., and Scantlebury, J. D., *Journal of the Oil and Colour Chemists Association,* Vol. 66, 1983, p. 93.
[*11*] "Evaluation of Organic Coatings by Electrochemical Impedance Measurements," Application Note AC-2, available upon request from EG&G Princeton Applied Research, Electrochemical Instruments Division, Princeton, NJ,
[*12*] Hubrecht, J. and Vereecken, J., *Journal of the Electrochemical Society,* Vol. 132, 1985, p. 2886.
[*13*] Mansfeld, F. and Kendig, M. W., "*Electrochemical Methods in Corrosion Research,*" M. Duprat, Ed., *Materials Science Forum,* Vol. 8, 1986, p. 337.
[*14*] Mansfeld, F. and Kendig, M., *Organic Coatings Science and Technology,* Marcel Dekker, New York, Vol. 8, 1986, p. 513.
[*15*] Simpson, T. C., Moran, P. J., Moshier, W. C., Davis, G. D., Shaw, B. A., Arah, C. O., and Zankel, K. L., "An Electrochemical Monitor for the Detection of Coating Degradation in Atmosphere," *Journal of the Electrochemical Society,* Vol. 136, No. 9, 1989, p. 2961.

[16] Simpson, T. C., Moran, P. J., Hampel, H., Davis, G. D., Shaw, B. A., Arah, C. O., Fritz, T. L., and Zankel, K. L., "Electrochemical Monitoring of Organic Coating Degradation During Atmospheric of Vapor Phase Exposure," *Corrosion*, Vol. 46, No. 4, pp. 331–336.

[17] Mansfeld, F., Jeanjaquet, S. L., and Kendig, M. W., *Corrosion Science*, Vol. 26, No. 9, 1986, p. 735.

[18] Haagenrud, S., Kucera, V., and Gullman, J., *Atmospheric Corrosion*, W. H. Ailor, Ed., John Wiley and Sons, New York, 1982.

[19] Senturia, S. D., Sheppard, N. F. Jr., Lee, H. L., and Day, D. R., *Journal of Adhesion*, Vol. 15, 1982, p. 69.

[20] Senturia, S. D., Sheppard, N. F. Jr., Lee, H. L., and Marshall, S. B., "Cure Monitoring and Control with Combined Dielectric/Temperature Probes," NTIS AD-A123512, National Technical Information Series, 1983.

[21] Davis, G. D., Shaw, B. A., Arah, C. O., Fritz, T. L., Moshier, W. C., Simpson, T. C., Moran, P. J., and Zankel, K. L., "Effects of SO_2 Deposition on Painted Steel Substrates," *Surface and Interface Analysis*, Vol. 15, 1990, pp. 107–112.

DISCUSSION

N. Berke[4] (*written discussion*)—The Bode plots look like they could be fit by a simple Randle's circuit. This indicates that the coating failure is not necessarily related to pores forming. What is your view of the failure mechanism?

T. C. Simpson et al. (*authors' closure*)—We agree with the comment that the Bode plots look like those that would result in a system with a single time constant. However, they are also consistent with the expected behavior for a coated metal system when initial defects form. Such behavior has been well documented in the literature.

C. Sauseirio[5] (*written discussion*)—Was polyurethane (arc coatings) tested?

T. C. Simpson et al. (*author's closure*)—No.

L. Zook[6] (*written discussion*)—When performing the coating tensile adhesion evaluations, was the coating cut to the substrate around the anvil in order to obtain the actual adhesion of the coating to the substrate, as opposed to obtaining the tensile strength of the coating and substrate?

T. C. Simpson et al. (*authors' closure*)—No, the coating was not intentionally cut to the substrate around the anvil prior to tensile adhesion testing. It should be noted, however, that prior to completion of the adhesion test method a steel "cut-off" ring replaces the Teflon ring and some severing of the coating likely occurs. In any case, the tensile strength (≃20 psi) of the coating is at least an order of magnitude less than typical tensile adhesion strengths. It is expected that the effect of this variable on our measurements is negligible.

[4] W. R. Grace, Cambridge, MA.

[5] St. Louis, MO.

[6] USBI, Inc., P.O. Box 21212, Kennedy Space Center, FL 32815.

Stanley T. Hirozawa[1] *and Daniel E. Coker*[1]

Electrochemical Screening of Synergism of Surfactants in the Inhibition of Corrosion of Aluminum by Silicate

---

REFERENCE: Hirozawa, S. T. and Coker, D. E., "**Electrochemical Screening of Synergism of Surfactants in the Inhibition of Corrosion of Aluminum by Silicate,**" *Corrosion Testing and Evaluation: Silver Anniversary Volume, ASTM STP 1000,* R. Baboian and S. W. Dean, Eds., American Society for Testing and Materials, Philadelphia, 1990, pp. 413–424.

ABSTRACT: The passivation current obtained from galvanostaircase polarization curves indicates whether aluminum can be passivated in a given environment. The change in passivation current with increased passivation of aluminum is much more sensitive than changes in breakdown or corrosion potentials. This great sensitivity of passivation current was used to develop a rapid screening method to determine whether a surfactant was synergistic or antisynergistic with the inhibition of aluminum by silicate at elevated temperature. The passivation current was also used to screen surfactants for inhibition of aluminum corrosion in the absence of silicate.

KEY WORDS: electrochemical, synergism, surfactants, corrosion inhibition, aluminum, passivation current, screening, galvanostaircase

Chemistry of Aluminum

Aluminum is a base metal with a standard reference potential of 1.66 V versus the standard hydrogen electrode. It should evolve hydrogen from water, but it is quite stable in air as well as in nonaggressive aqueous systems because of a stable aluminum oxide layer. In neutral medium, the oxide layer is 25 to 50 A thick, and the hydroxide layer can be 2000 to 5000 A thick. The general corrosion rate of aluminum is related to the rate of hydrolysis of the oxide to yield the hydroxide [*1*].

$$Al_2O_3 + 3H_2O \longrightarrow 2Al(OH)_3 \tag{1}$$

Aluminum hydroxide is amphoteric, that is, it can behave as an acid or base.

$$Al(OH)_3 + 3OH^- \longrightarrow Al(OH)_6^{-3} \tag{2}$$

$$Al(OH)_3 + 3H^+ \longrightarrow Al^{+3} + 3H_2O \tag{3}$$

Equations 2 and 3 show that the protective film formed in Eq 1 is unstable at high and low

---

[1] Senior research associate and applications technical specialist, respectively, BASF Corp., Wyandotte, MI 48192.

pH. The region of passivity in mildly acidic to mildly basic media can be extended by certain inhibitors.

Electrochemistry of Aluminum

When aluminum is polarized galvanostatically in slightly basic borate buffer, the voltage rises to 400 V with no sign of breakdown [*2*]. Because of this very strong tendency to passivate, it is virtually impossible to carry out d-c electrochemistry without first overcoming this strong passivity. Some ions that were found capable of overcoming this passivity are chloride, nitrate, chlorate, bromate, and perchlorate [*3*]. It is a common practice to add 100 ppm of sodium chloride (NaCl) to all test solutions. But, even in the presence of chloride, the difficulty in breaking through the protective layer formed by certain inhibitors creates a severe inductive effect with a large shift of the breakdown potential, E_b, in the noble direction during potential, E^-, controlled polarization [*4–6*]. The positively biased protection potential, E_{prot}, and E_b data did not correlate with other laboratory test results and field results [*5,6*].

To overcome the inductive effect discussed above, a galvanostaircase polarization (GSCP) technique was developed [*5,7,8*]. GSCP involves the application of a current staircase signal to a metal electrode and recording of the voltage response as shown by the schematics in Fig. 1 (taken from the ASTM Test Method for Conducting Cyclic Galvanostaircase Polarization [G100-89]) [*7*]. In practice, the data presentation is simplified by making the horizontal axis the current, which allows elimination of the current information in the bottom curve in Fig. 1; also, the downstep portion of the curve is reversed to show the separation between E_b and E_{prot}, if any, as shown in Fig. 2. The points at the end of each step are used to determine E_b and E_{prot}. E_b is determined by extrapolating the up-step points to zero current, while E_{prot} is determined by extrapolating the down-step points to zero current.

Passivation Current

The great sensitivity of $i_{pass'n}$ to changes in susceptibility to corrosion of aluminum was discovered when we were studying temperature effects on the GSCP curves of experimental and commercial coolants [*8*]. Figure 3 gives the GSCP curves of aluminum at three concentrations of a commercial antifreeze at room temperature. Note that both E_b and E_{prot} are lowered by dilution. This antifreeze is adequate at all concentrations at room temperature. However, at elevated temperature, it becomes totally inadequate, as shown in Fig. 4. $i_{pass'n}$ is determined by extrapolation of the steepest part of the curve to the corrosion potential, E_{corr}. $i_{pass'n}$ may be thought of as the rate of generation of Al^{+++} ions that is required to initiate the passivation process. The 15% antifreeze gives no sign of passivation while at 25 and 45% levels, 900 and 320 $\mu A/cm^2$, respectively, are required to initiate passivation.

Figure 5 shows the effect of pH on the GSCP curves of aluminum in 25% ethylene glycol containing 1% sodium nitrate and 1% borax. $i_{pass'n}$ is determined by the extrapolation of the steepest part of the forward scan to E_{corr}, while the depassivation current, i_{depass}, is determined by the extrapolation of the steepest part of the reverse scan to the plateau preceding the drop in current (see the pH 11 curve). $i_{pass'n}$ and i_{depass} determined in Fig. 5 are plotted in Fig. 6. These i-pH curves are similar to the Pourbaix diagrams, indicating the regions of passivity and the regions of vulnerability. We have applied only $i_{pass'n}$ to our studies because: (1) it shows better correlation with other test results and field results [*8*]; (2) extrapolations are sharper; and (3) test duration is shorter.

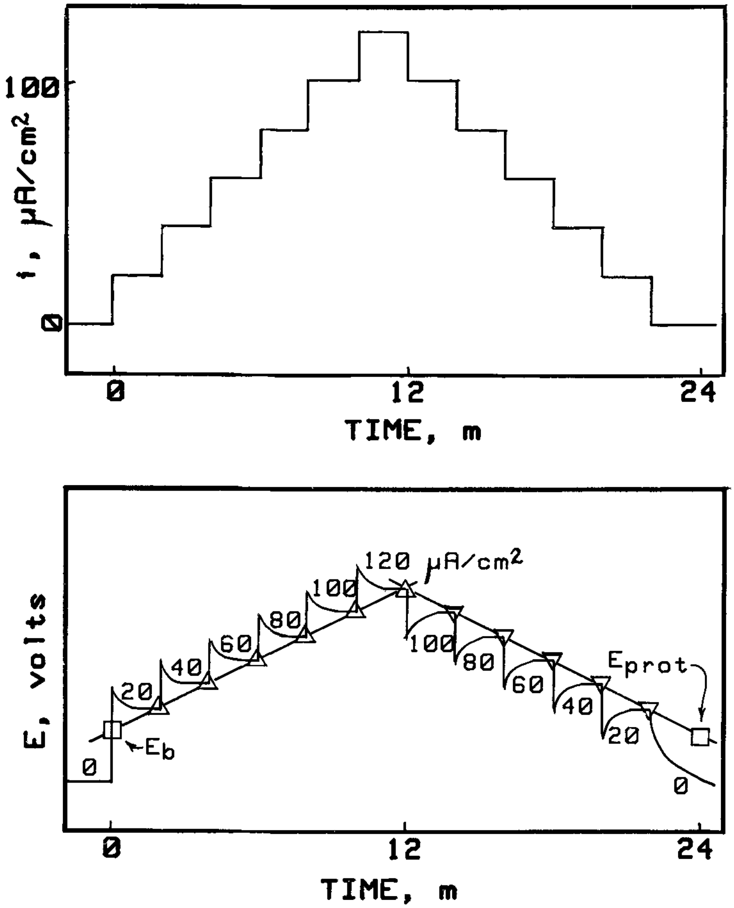

FIG. 1—*Schematic of current staircase signal and GSCP curve.*

Experimental

The apparatus consisted of the Solartron 1286 potentiostat and the Hewlett Packard 300 series computer using the Solartron 1091A software. The electrochemical cell and preparation of the aluminum specimens and the test media were the same as described earlier [3] and more recently in ASTM G100-89 except that the samples were polished with 600 grit paper just prior to the test.

Results and Interpretation

The Critical pH of a Coolant

In Fig. 6, the $i_{\text{pass'n}}$ versus the pH curve of aluminum shows a sharp rise in the current at pH 8. That point of the sharp break is defined as the critical pH of the system. The aluminum will be vulnerable at pH greater than eight in that medium. Some of the failures of commercial antifreeze coolants were traced to operating pHs that were greater than its critical pH. The

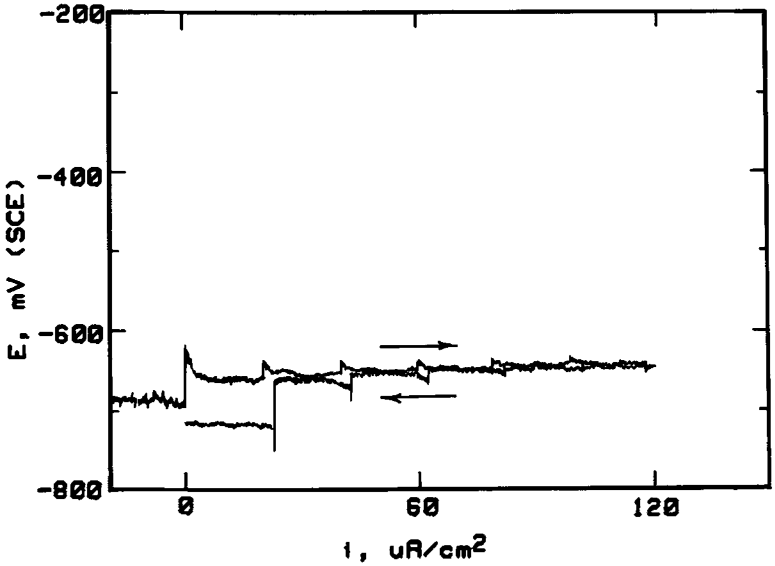

FIG. 2—*GSCP curve for Al in 3000-ppm NaCl.*

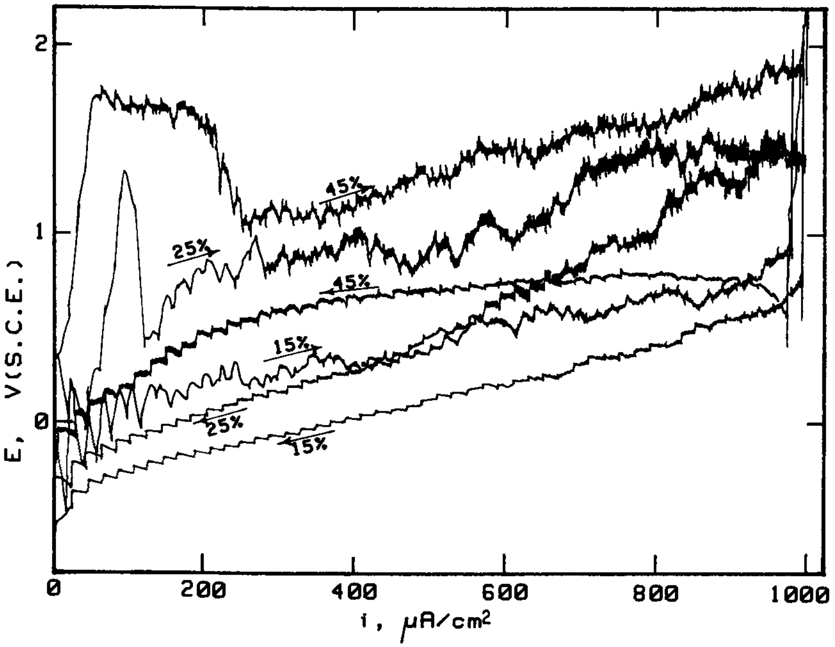

FIG. 3—*GSCP curves of 45, 25, and 15% commercial antifreeze at room temperature.*

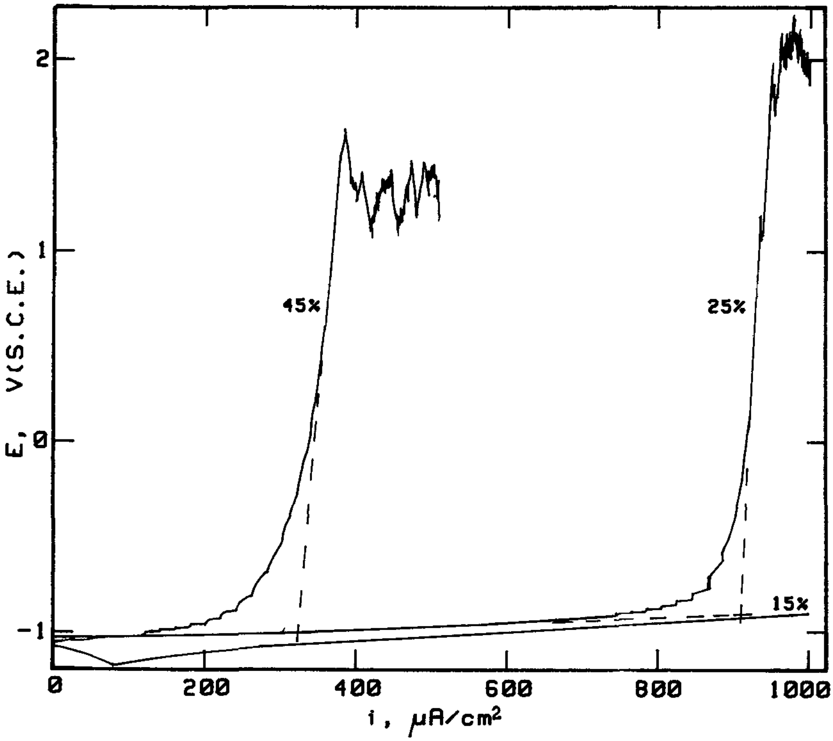

FIG. 4—*Same as Fig. 3 but at 180 °F (82 °C).*

critical pH of commercial coolants vary widely (pH 7 to 12) and sometimes they are very sensitive to temperature, for example, compare Figs. 3 and 4.

Synergism between Silicate and Surfactants

Figure 7 shows the effect of silicate level on $i_{\mathrm{pass'n}}$ as well as E_b and E_{prot} as a function of silicate concentration. There is no significant change in E_b, while E_{prot} and especially $i_{\mathrm{pass'n}}$ yield sharp breaks which corroborate each other.

The sharp-breaking region in the $i_{\mathrm{pass'n}}$ curve in Fig. 7 was used to screen various surfactants for synergism with silicate in the protection of aluminum from corrosion under depassivation. Two solutions, X and Y, were prepared. X contained 2% borax · $5H_2O$, 0.263% nitric acid, 0.1% sodium nitrite, and 0.1% tolyltriazole. Y contained the same level of ingredients as X, but in addition contained 0.0625% silica (as stabilized sodium silicate). The reference test solution was prepared by mixing 65 parts of Y with 35 parts of X, yielding a silica concentration of 0.0406%. This reference test solution yielded a $i_{\mathrm{pass'n}}$ that fell in the middle of the sharp break. The reference test solution was spiked with a surfactant, and $i_{\mathrm{pass'n}}$ was determined. The results are given in Table 1. The first column gives the surfactants; the concentration is 0.5% unless given otherwise. The second column gives the $i_{\mathrm{pass'n}}$ in the spiked reference test solution; results at lower concentrations are given in parentheses. The third column gives $i_{\mathrm{pass'n}}$ in the reference solution minus the silicate; these results tell you whether the surfactants themselves inhibit the corrosion of aluminum. The reference test solution

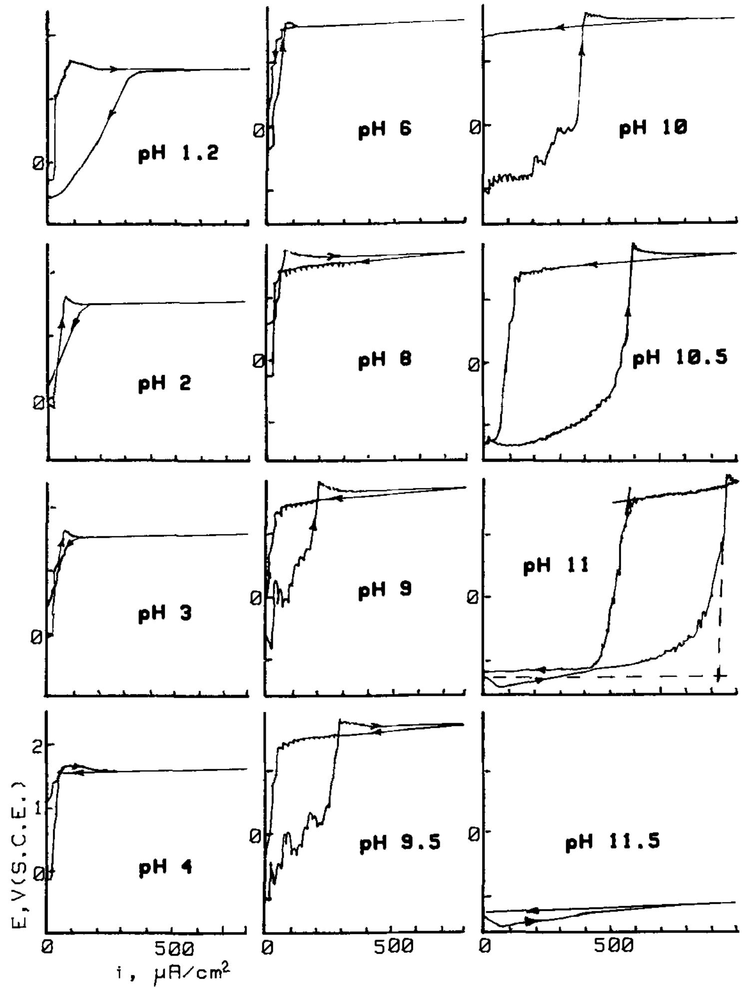

FIG. 5—*pH effect on the GSCP curves of Al.*

had a $i_{pass'n}$ of 387 $\mu A/cm^2$. The surfactants are arranged according to increasing synergism based on their 0.5% solutions. Surfactants above the reference are synergistic while those below the reference are antisynergistic.

The seven surfactants with asterisks are synergistic, but they are too insoluble and some separate as an oily phase during normal operation at elevated temperature. PLURAFAC RA-30 surfactant is synergistic, but the cloud point is 35°C, which may cause the surfactant to separate under very warm storage. PLURAFAC C-17 surfactant is quite synergistic and looks promising. The most promising appeared to be TETRONIC 1304 and TETRONIC 1104 surfactants; however, they were slightly too foamy under normal operation. TETRONIC 1302 and TETRONIC 1102 surfactants yield virtually no foam, but they are insoluble. The most appropriate surfactants would be TETRONIC 1303 and TETRONIC

1103, but they are not found on the grid (Fig. 8), which meant that they are not manufactured; therefore, they were specially synthesized. At 0.5% concentration, TETRONIC 1103 surfactant behaves like the reference and TETRONIC 1303 surfactant is slightly antisynergistic. However, the results at the lower concentrations show that there is maximum synergism at around 0.1% for both surfactants. This concentration of maximum synergism is believed to be related to the critical micelle concentration, *cmc,* of the system. At the *cmc,* the coverage of the metal surface with the surfactants molecules should be just completed.

When an alkoxylated alcohol is phosphorylated to yield KLEARFAC AA270 surfactant, the result is high antisynergism. It appears that AA270 is interfering with the formation of the protective aluminum silicate film.

Inhibition by Surfactants

In the absence of silicate (results in third column), any $i_{\text{pass'n}}$ value below 800 indicates some inhibition. The nonionic surfactants do not adequately inhibit aluminum corrosion at the selected pH. The only anionic surfactant investigated, KLEARFAC AA270, appears to be a good inhibitor, and it improves as the concentration is lowered.

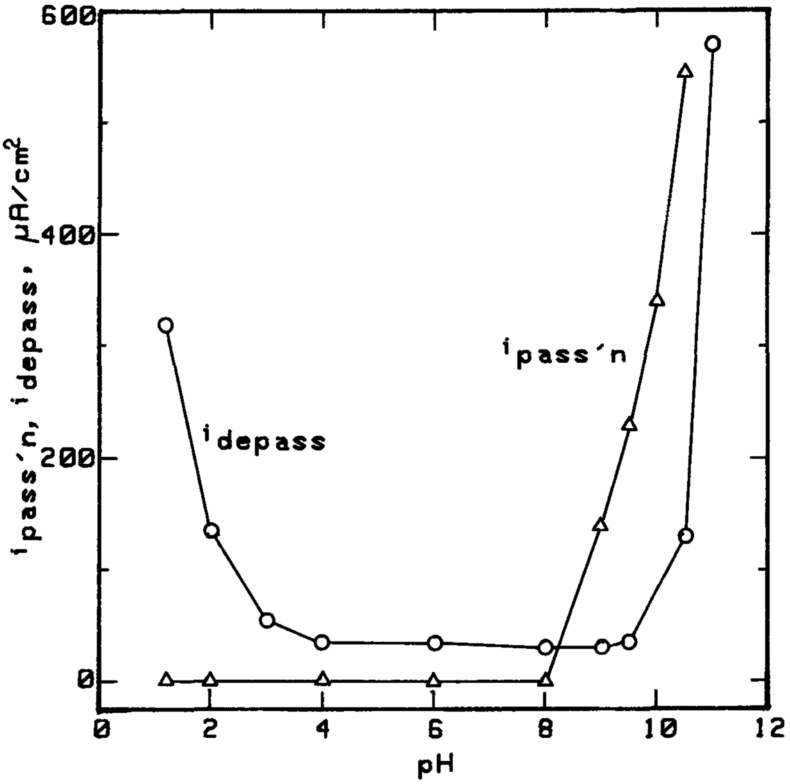

FIG. 6—*Current-pH curves derived from data in Fig. 5.*

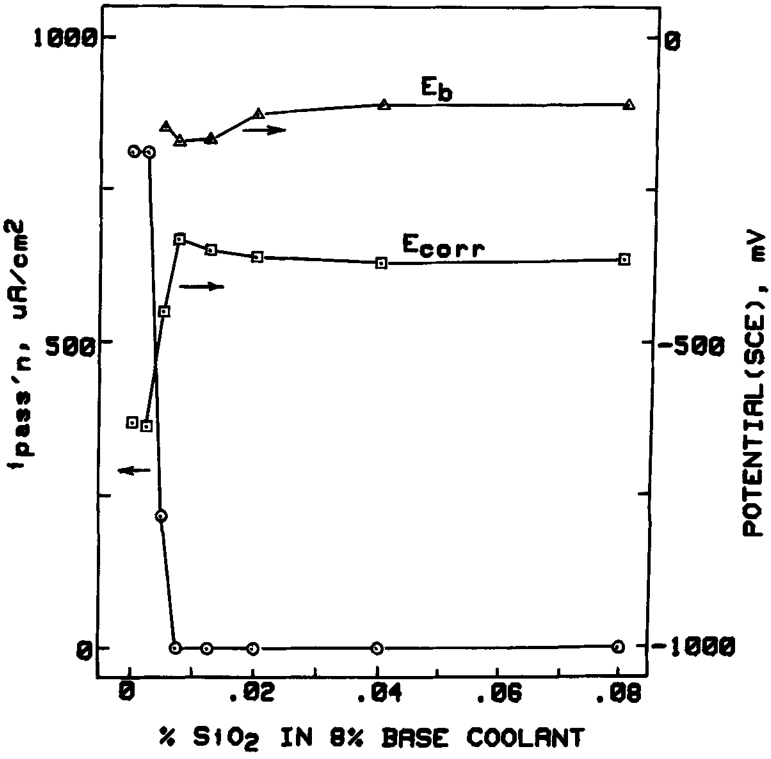

FIG. 7—*Effect of silicate level on* $i_{pass'n}$, E_{corr}, *and* E_b.

Discussion

Structure of Surfactants

Figure 9 lists the structures of the surfactants covered in this study. The PLURONIC surfactant has a polyoxypropylene block in the middle and two polyoxyethylene blocks at the ends. In the reverse PLURONIC, the positions of the oxyethylene (EO) and oxypropylene (PO) blocks are reversed. In the TETRONIC surfactants, four PO blocks are added to ethylene diamine, and four EO blocks are placed on the ends. In the TETRONIC R surfactants the positions of the PO and EO blocks are reversed. PLURAFAC surfactants involve the oxyalkylation of an alkyl alcohol. KLEARFAC surfactants are obtained by the phosphorylation of an alkoxylated alcohol. The ICONOL surfactants are alkanol and alkylphenol ethoxylates.

TETRONIC Grid

The grid system is a very efficient way to display all of the members of a class of surfactants. The TETRONIC grid is shown in Fig. 8. The physical properties vary smoothly horizontally and vertically so that the surfactant with the desired properties can be selected or designed.

TABLE 1—*Synergism of surfactants with inhibition of Al by silicate.*

	$i_{pass'n}$, μA/cm²		
Surfactants	*w* SiO_2	*wo* SiO_2	MW[a]
PLURONIC L64,[b]	132		2 900
PLURONIC L64,0.1%	318[c]	>800	2 900
PLURAFAC RA-40[b]	138		821
PLURAFAC RA-30	139		625
TETRAONIC 1304	152	360	10 500
TETRONIC 1304,0.16%	202[c]		10 500
ICONOL DA-6[b]	173		
ICONOL TDA-8[b]	218		
TETRONIC 1104	220	362	8 300
PLURAFAC C-17	223	575	820
TETRONIC 504	227	>680	3 400
PLURONIC L44,[b]	225		2 200
PLURONIC L44,0.1%	228[c]	>800	2 200
ICONOL DA-9	230	650	
PLURAFAC RA20	260		791
C12E8[d]	268		522
TETRONIC 904	286		6 700
PLURAFAC D25	298		932
PLURONIC L62,[b]	310		2 360
PLURONIC L62,0.1%	454[c]	636	2 360
ICONOL OP-10[b]	310		
PLURAFAC B-26	316	592	1 030
PLURONIC 25R2	320	530	3 100
C12E2[d]	356		250
TETRONIC 1504	381		12 000
REFERENCE	387	>800	
TETRONIC 1103,	388	>800	7 000
TETRONIC 1103,0.2%	252[c]		7 000
TETRONIC 1103,0.1%	148[c]		7 000
TETRONIC 1103,0.05%	415[c]		7 000
PLURONIC 103	410	>800	4 950
TETRONIC 50R8	500	>800	10 200
TETRONIC 1303,	508	>800	8 860
TETRONIC 1303,0.2%	325[c]		8 860
TETRONIC 1303,0.1%	52[c]		8 860
TETRONIC 1303,0.05%	388[c]		8 860
TETRONIC 90R4	667	650	7 240
KLEARFAC AA270,	>800	118	902
KLEARFAC AA270,0.2%	518[c]	58[c]	902
KLEARFAC AA270,0.1%	>800[c]	25[c]	902
KLEARFAC AA270,0.05%		>800[c]	902
KLEARFAC 870	>800		

[a] See section on TETRONIC grid under Discussion for the estimation of the molecular weights.

[b] Incompletely soluble, therefore not run in the absence of silicate.

[c] Surfactant concentrations <0.5%.

[d] Ethylene oxide adducts of dodecyl alcohol.

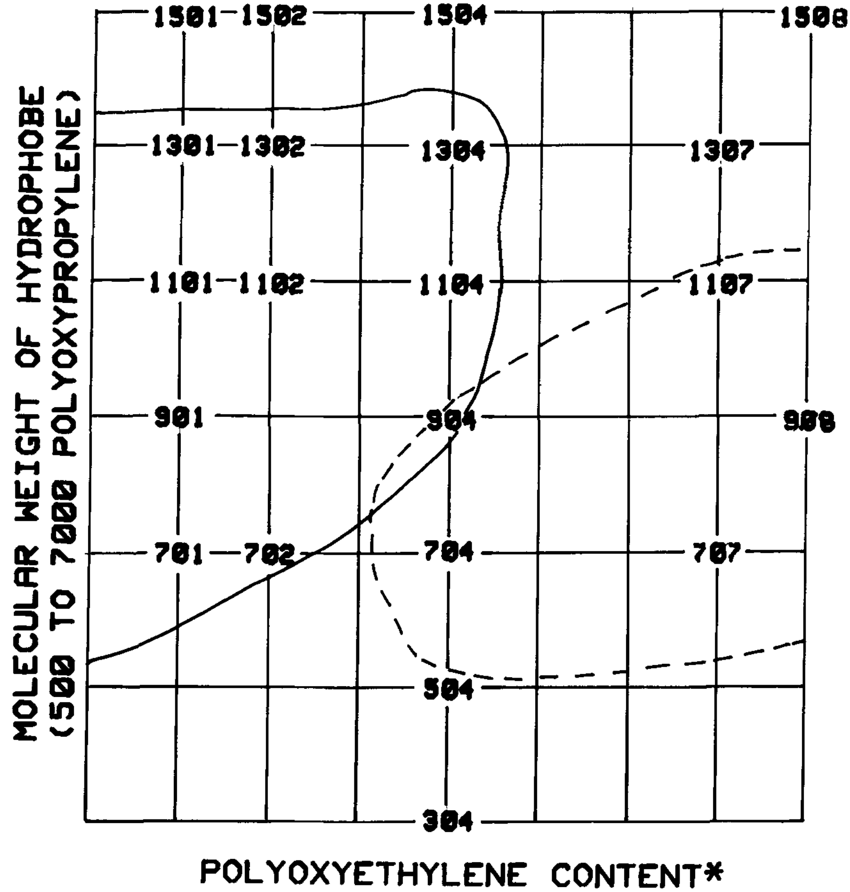

FIG. 8—*TETRONIC surfactants grid. Please refer to the TETRONIC grid section for the meaning of the numerals in the grid as well as the solid and broken lines.*

The numerals preceding the last digit, that is, 30 to 150, give the vertical position on the grid, which is related to the molecular weight of the PO blocks. The last digit multiplied by ten gives the percent of the EO blocks. For example, the molecular weight of TETRONIC 1504 = 7000 + 0.4/0.6(7000) = 11 667 ~ 12 000.

In Fig. 8, the area bounded by the solid line gives the best wetting surfactants, while the area bounded by the broken line gives the surfactants with high foaming tendencies. TETRONIC 1304 and 1104 surfactants were selected initially for their wetting ability plus the fact that they were out of the foaming region. However, they were still found to be too foamy. Moving left on the grid, 1303 and 1103 cut down the foaming but the solubility was not reduced sufficiently to give problems. Had the solubility been reduced too much, the EO content could have been increased to 35%, in which case the name of the surfactants would have been TETRONIC 1303.5 and 1103.5 surfactants. This ability to fine tune the physical properties of a surfactant is the advantage of the grid system. The example given here is also applicable to PLURONIC, PLURONIC R, and TETRONIC R surfactants.

KLEARFAC AA270 Surfactant

The biggest surprises in this study were the strong antisynergism between AA270 and silicate in the inhibition of aluminum corrosion and the strong inhibition of aluminum corrosion by AA270 at elevated temperature in the absence of silicate.

Conclusion

The extremely high sensitivity of the passivation current to the passivation of aluminum by silicate was used for the rapid screening for synergism by surfactants. The passivation currents were obtained from galvanostaircase polarization curves.

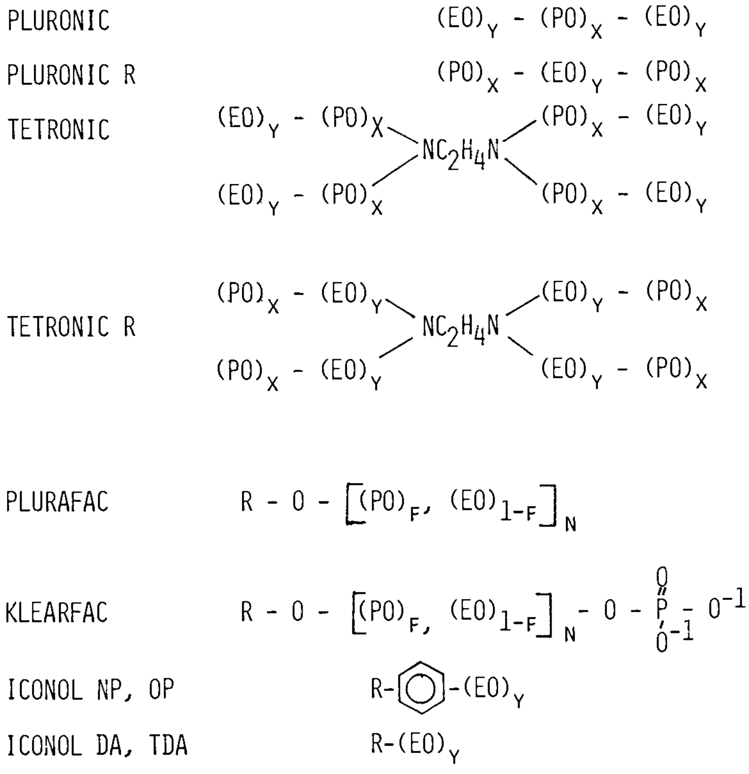

WHERE:
PO = OXYPROPYLENE
EO = OXYETHYLENE
R = LINEAR ALKYL
F = FRACTION 1
NP = NONYL PHENOL
OP = OCTYL PHENOL
DA = DECYL ALCOHOL
TDA = TRIDECANE ALCOHOL

FIG. 9—*Surfactant types.*

The two most synergistic surfactants were TETRONIC 1303 and 1103 surfactants. TETRONIC 1304 and 1104 surfactants were also synergistic, but they were too foamy. PLURAFAC C-17 surfactant was synergistic. KLEARFAC AA270 was very antisynergistic, while in the absence of silicate it showed great promise for inhibiting the corrosion of aluminum under depassivating conditions. This was confirmed when the ASTM Test Method for Cavitation Erosion-Corrosion Characteristics of Aluminum Pumps with Engine Coolants (D 2809) aluminum pump cavitation test was passed in the absence of silicate and carboxylates, which are well known for their effectiveness against cavitation erosion.

References

[*1*] Videm, K., "The Electrochemistry of Uniform and Pitting Corrosion of Aluminum," Kjeller report, Institute of Atomenergi, Norway, 1974.

[*2*] Takashi, H. and Nagayama, M., *Corrosion Science,* Vol. 18, 1978, p. 911.

[*3*] Hirozawa, S. T., "Mechanism for the Inhibition of Localized Corrosion of Aluminum in Antifreeze Coolants," Paper No. 263, *CORROSION/82,* National Association of Corrosion Engineers, Houston, 1982.

[*4*] Rudd, W. J. and Scully, J. C., *Corrosion Science,* Vol. 20, 1980, p. 611.

[*5*] Hirozawa, S. T., *Journal of the Electrochemical Society,* Vol. 130, 1983, p. 1718.

[*6*] Hirozawa, S. T., "Study of the Mechanism for the Inhibition Localized Corrosion of Aluminum by Galvanostaircase Polarization," *Corrosion Inhibition—Theory and Practice,* R. Hausler, Ed., National Association of Corrosion Engineers, Houston, 1988, p. 105.

[*7*] Hirozawa, S. T., "Review of the Use of Galvanostaircase and Potentiostaircase Polarization in the Study of Corrosion Inhibition in Antifreeze Coolants," Paper No. 453, *CORROSION/89,* National Association of Corrosion Engineers, Houston, 1989.

[*8*] Hirozawa, S. T., "Corrosion Monitoring by Galvanostaircase Polarization," *Electrochemical Techniques for Corrosion Engineering,* R. Baboian, Ed., National Association of Corrosion Engineers, Houston, 1986, p. 321.

Neal S. Berke[1] *and Maria C. Hicks*[1]

Electrochemical Methods of Determining the Corrosivity of Steel in Concrete

REFERENCE: Berke, N. S. and Hicks, M. C., **"Electrochemical Methods of Determining the Corrosivity of Steel in Concrete,"** *Corrosion Testing and Evaluation: Silver Anniversary Volume, ASTM STP 1000,* R. Baboian and S. W. Dean, Eds., American Society for Testing and Materials, Philadelphia, 1990, pp. 425–440.

ABSTRACT: Steel-reinforced concrete is used throughout the world in the construction of bridges, marine structures, parking garages, and buildings. The alkaline environment of the concrete protects the steel from corrosion; however, this protective environment can be disrupted due to the migration of chloride ions to the steel and/or to carbonation of the concrete. In this paper several electrochemical techniques that can be used to determine and predict the corrosion of steel in concrete are described. Further, it is shown how these techniques can be used to show the effectiveness of corrosion inhibitors and other modifications to the concrete mixture on corrosion control.

Solution testing in calcium hydroxide and in sodium/potassium hydroxide pore water solutions can be used to determine corrosion mechanisms and the effectiveness of inhibitors when chloride is present. The use of cyclic polarization in these solutions to determine the effects of chloride and calcium nitrite is discussed.

Corrosion testing of steel in concrete provides more direct evidence of the effect of the concrete mix design on corrosion performance. Three techniques are quite common in this laboratory and in others. They are polarization resistance, electrochemical impedance, and the measurement of the macrocell corrosion between two layers of bars. The use of these techniques is discussed, and several examples of their use and comparison to visual attack of the steel are given. The techniques, as used, correlate very well with the observed corrosion damage on the embedded steel.

Because polarization resistance and electrochemical impedance are nondestructive, they can be used to monitor the corrosion rates of steel in concrete, whereas mass loss or visual observation require destruction of the concrete to observe the bar. The use of these techniques to monitor the long-term behavior of steel in concrete is demonstrated.

KEY WORDS: concrete, corrosion, corrosion testing, electrochemical techniques, polarization resistance, electrochemical impedance spectroscopy, cyclic polarization, macrocell, pore water

Steel-reinforced concrete is a widely used and durable construction material. Usually, the steel is as durable as the concrete because it is protected from corrosion by a passivating layer of iron oxide which forms in the alkaline conditions prevailing in the concrete. Unfortunately, concrete is permeable, and, if exposed to corrosive agents, these may be able to penetrate through the concrete and reach the reinforcing steel (rebars). In some cases, this may result in a rapid deterioration in the strength and the integrity of the concrete structure.

Bridges, parking garage, and marine structures are particularly vulnerable as they are exposed to deicing agents. The chlorides in these agents are able to break down the passive

---

[1] W. R. Grace & Co., Conn. Construction Products Div., Cambridge, MA 02140.

film on the rebars and promote corrosion of the depassivated steel. The rate of attack is determined by the concentration of the chlorides, the nature of the exposure (continuous or intermittent), the pH in the pores, the presence of oxygen, and the ambient temperature. Because the corrosion products have a larger volume than the reactants, the concrete is subjected to tensile forces that cause cracking and spalling, which leads to a reduction in its strength and ultimately to failure of the structure.

The time to corrosion initiation can be reduced by decreasing the permeability of the concrete by the addition of pozzolans such as microsilica and/or by the addition of corrosion inhibitors which enhance the stability of the passivating film on the rebars. Rebars coated with organic films are also widely used, but their efficacy against localized attack at flaws is questionable [*1*]. The additives ideally are added at the time of mixing the concrete. However, techniques are being developed for protecting and rehabilitating existing structures by exposing them to corrosion inhibitors and by overlaying them with concrete containing pozzolans (expecially microsilica) or latex.

The importance of these developments can be gaged by estimates of the Strategic Highway Research Program that $450 to $550 million per year can be saved by correcting corrosion problems in existing bridges [*2*]. Consequently, it has become imperative to have reliable methods for accurately measuring the rate of corrosion in structures and for comparing the corrosion protection afforded by various inhibitors and pozzolans. Ideally these tests should be rapid and nondestructive. Electrochemical techniques are now being widely used for this purpose. Long-term exposure studies and visual inspection are still necessary, however, as a means of confirming the results of electrochemical measurements.

The traditional electrochemical method of measuring the corrosion potential, the ASTM Test Method for Half-Cell Potentials of Uncoated Reinforcing Steel in Concrete (C 876), may be misleading as it does not provide complete information on corrosion rate effects [*3*]. Other electrochemical methods, specifically certain polarization techniques and electrochemical impedance spectroscopy (EIS), provide a more reliable indication of corrosion in concrete. The cyclic polarization technique is a useful tool in assessing the pitting tendency of a metal in a particular environment. The macrocell corrosion testing method is a simple procedure that does not require the use of sophisticated electronic equipment.

In this paper, we will describe several electrochemical techniques appropriate to rebar testing and present data obtained in our laboratories using polarization resistance, EIS, cyclic polarization, and macrocell procedures. In addition, the protection offered by a calcium nitrite corrosion inhibitor will be discussed.

Electrochemical Methods

Because corrosion is essentially an electrochemical process in which the rate of corrosion is determined by the current flowing between anodic and cathodic sites on the metal surface, the basis of many electrochemical techniques is to measure this current. The value of the corrosion current may then be used to calculate a rate of metal loss according to Faraday's law. Because in the metal's natural state the corrosion current flowing from anode to cathode is exactly balanced by a current flowing from cathode to anode, it is necessary to displace the metal from its equilibrium potential to obtain an estimate of the corrosion current.

Many polarization methods for estimating the corrosion current have been devised [*4–10*], each providing specific information and having characteristic advantages and disadvantages. Apart from the reliability of the method, the time needed to complete a test, the cost of the equipment required, the degree of training required for the operators, and the difficulty in interpreting the data are important considerations when selecting a test method.

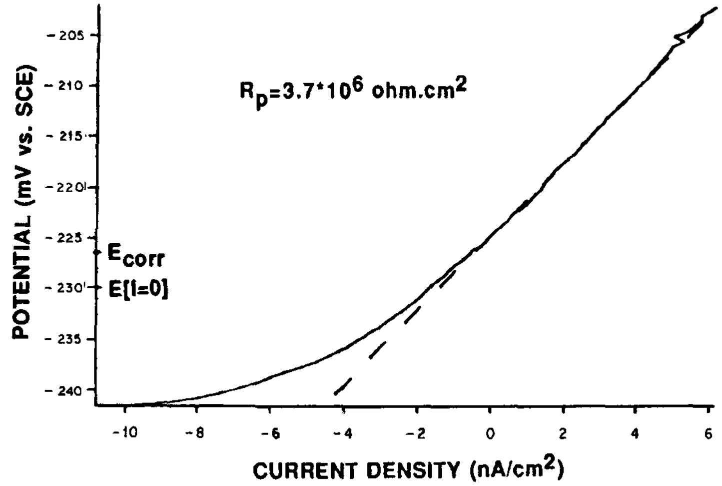

FIG. 1—*Example of a polarization curve for determining* R_p.

Two methods that have proved useful for evaluating the corrosion resistance of rebars in concrete are polarization resistance and electrochemical impedance spectroscopy (EIS). These methods are nondestructive and require the use of a potentiostat, and EIS additionally requires the use of a transfer function analyzer. Data obtained with the EIS technique are also more difficult to interpret.

Polarization Resistance

The polarization resistance essentially quantifies the degree to which the system resists corrosive attack by the environment. This measurement technique, which is described in the ASTM Practice for Conducting Potentiodynamic Polarization Resistance Measurements (G 59), requires a minimum of equipment and is relatively low cost as well as easy to learn and use. A potentiostat is used to displace the equilibrium of the metal by about 10 to 20 mV as measured relative to a reference electrode, and the current flowing between the metal (rebar) and a counter electrode is measured.

In practice, the potential is applied to a value of about 20 mV below the equilibrium value and then swept at a low scan rate of about 0.1 mV/s to a potential of about 20 mV above the equilibrium value. The current response is recorded.

As shown in Fig. 1, the current-voltage relationship is linear around the zero-current portion of the curve, and the polarization resistance, R_p, is obtained from the slope

$$R_p,\ \Omega\text{-cm}^2 = E/i$$

where

E = the potential, and
i = the current density.

Values of less than 50 kΩ·cm^2 usually indicate the onset of corrosion of rebars in concrete. Values below 20 kΩ·cm^2 are associated with severe corrosion [*11*].

The corrosion current at equilibrium can be calculated from the relationship developed

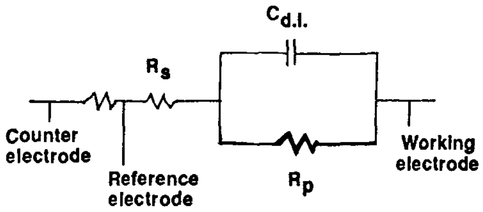

FIG. 2—*Equivalent circuits for rebars corroding in concrete, uncoated.*

by Stern and Geary [*12*], of which the following is a simplification

$$i_{\text{corr}} = B/R_p \tag{1}$$

where B is a constant for a given system. A typical value for concrete is $B = 26$ mV [*12*].

One problem that arises when applying this method to reinforcing steel in concrete is that the resistance of the concrete material between the reference electrode and the rebar, R_s in Fig. 2, can be several kΩ·cm², and may be comparable to the value of the polarization resistance of the rebar, particularly when the latter is in the corrosion regime. The resistance of the concrete must be known to calculate the true polarization resistance

$$R_p = R_{p\text{.measured}} - R_{\text{concrete}}$$

Electronic techniques involving an IR adjustment or current interrupt procedure may be used to correct for this error. In the current interrupt method [*6,13,14*], the value of the uncompensated resistance is sampled regularly and the ohmic drop is subtracted from the measured potential. As suggested by the name, the current flowing through the cell is stopped for some 200 μs at fixed time intervals. Because the only potential in the circuit at zero current is that due to the electrical double layer on the rebar, the potential drop due to the resistance of the concrete can be estimated. The current interrupt technique has been found to compensate accurately for the resistance of the concrete as determined by EIS techniques [*14*].

Electrochemical Impedance Spectroscopy (EIS)

By applying an alternating current over a range of frequencies, more mechanistic information on the corrosion process can be obtained than when using a direct current. This is because the electrochemical circuit is in fact a network of capacitances and resistances (Fig. 2), and the measured impedance can be related to various elements of the circuit, depending on the frequency. Based on the equivalent circuit for a rebar in concrete (Fig. 3), at high frequencies the impedance is due to the ohmic or uncompensated resistance, and at low frequencies it is due to the sum of this and the polarization resistance, now called the charge transfer resistance. The impedance may be represented by [*15*]

$$\overline{Z} = R_s + R_p(1 - j\omega CR_p)/[1 + (\omega CR_p)^2]$$

where

$\overline{Z}$ = the total impedance measured at frequency f, Hz,
$\omega = 2\pi f$ rads/s, and
$j = \sqrt{-1}$.

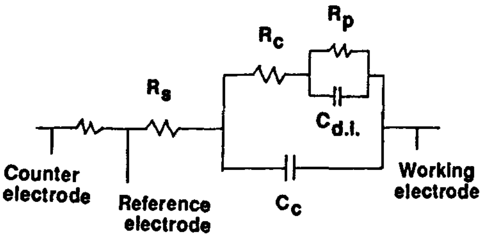

FIG. 3—*Equivalent circuits for rebars corroding in concrete, coated or passivated rebars.*

The equivalent circuit shown in Fig. 3 has been found to model the effect of protective coatings or films on the rebar; different circuits have been proposed to allow for other surface treatments and effects within the concrete itself. Such effects may be important in the presence of passivating inhibitors or if diffusion through the concrete matrix is rate controlling.

EIS requires special purpose equipment including computer control, and sophisticated software is used for analyzing the data obtained. In general, it is slower than the polarization resistance method, requires more expensive equipment, better trained operators, and careful interpretation of the results.

The experimental data are commonly displayed using Nyquist or Bode plots (Fig. 4), although other representations may be used to highlight specific phenomena. The method of obtaining the value of R_p from the data is illustrated in Fig. 4 for the circuit shown in Fig. 3. Once R_p is known, the corrosion current is determined as before, using Eq 1.

Special-Purpose Methods

The polarization resistance and EIS methods provide an average corrosion current and do not give an indication of the susceptibility of the rebar to pitting or other localized attack. Rebars exposed to chloride environments are particularly susceptible to pitting attack, so it is important that the corrosion engineer have a means of assessing the likelihood of attack by this mechanism. By applying the polarization potential in a cyclic manner, it is possible to learn something of the tendency to pit.

On the other hand, if the objective is simply to compare the efficacy of different corrosion protection systems, it is not necessary to use the sophisticated equipment needed for polarization measurements. In this case, sufficient information can usually be obtained by measuring the current flowing in a macrocell.

Cyclic Polarization

Cyclic polarization testing provides a useful method of gaining information on the pitting tendency of a metal in a particular environment. This is achieved by shifting the applied potential from the cathodic zone toward the anodic region at a rate slow enough to allow for the formation of a protective film, followed by a scan in the reverse direction. This latter scan is done quickly so as to minimize the amount of time that the specimen is subjected to high current. In ASTM G 61 (Test Method for Conducting Cyclic Potentiodynamic Polarization Measurements for Localized Corrosion, Susceptibility of Iron-, Nickel-, or Cobalt-Based Alloys), both forward and reverse scan rates are kept constant at 0.17 mV/s. Because the applied potential brings the sample potential into regions far removed from the corrosion potential (500 mV or more), this technique is destructive. Under actual field conditions, such high values are not encountered unless large, stray voltages are present.

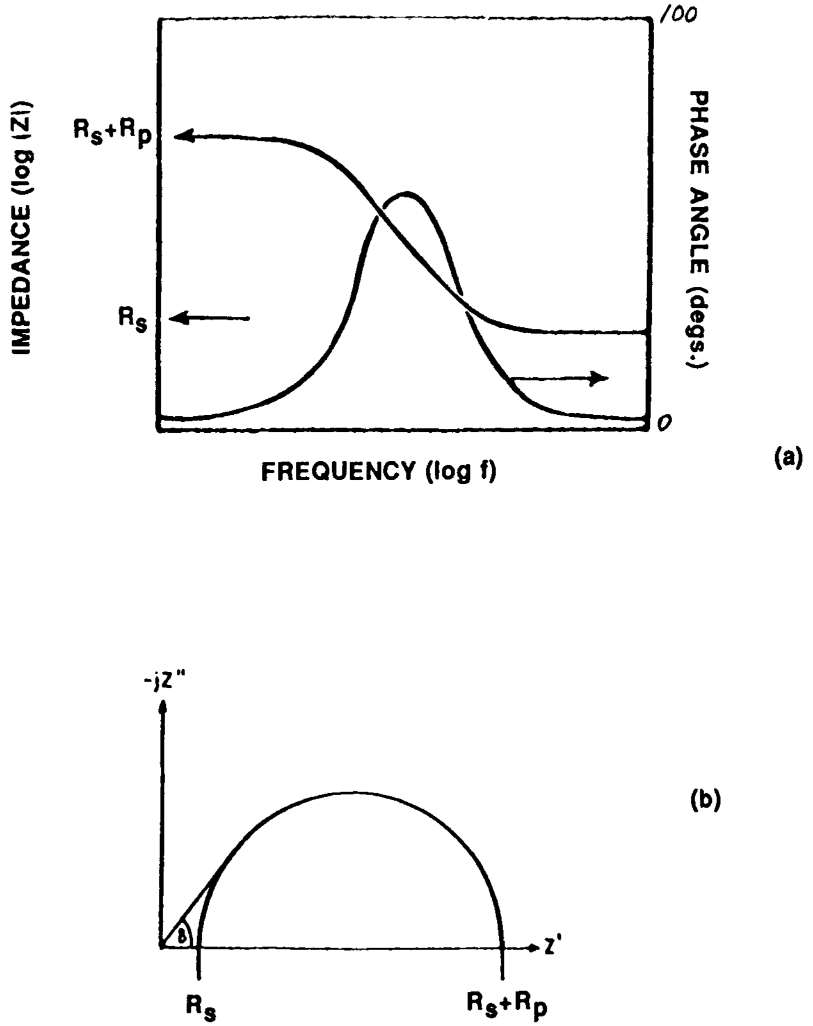

FIG. 4—*Idealized impedance behavior for the equivalent circuits of Fig. 3,* (a) *Bode plot;* (b) *Nyquist plot.*

Because it is destructive, the method cannot be applied to concrete structures in the field, nor is it a monitoring technique. Its use is restricted to the examination of test specimens in the laboratory. To avoid errors caused by the large potential (IR) drop in the concrete, the tests may be carried out in a solution that simulates the concrete environment. Based on the initial findings of Page and Treadaway [*16*] that polarization results in saturated calcium hydroxide are similar to those obtained in cement pastes, Berke [*17*] further showed that this method is applicable to solutions containing inhibitors in addition to corrosive agents such as chlorides.

Solutions commonly used are saturated calcium hydroxide solutions and calcium hydroxide–saturated pore water solutions (0.3 *M* NaOH + 0.6 *M* KOH) with sodium chloride. A typical cyclic polarization curve for mild steel in saturated calcium hydroxide solution (pH between 12 and 13) might be run from −800 mV (versus SCE) in the noble direction to +800 mV (or until the current reaches a preselected value) and then reversing the scan to −700 mV.

Two potentials, namely the pitting potential, E_p, and the nucleation or breakdown potential, E_b, are of interest in examining pitting (Fig. 5). E_p is the potential below which pitting cannot occur and is taken to be the potential at which the forward scan intersects the reverse scan. E_b is the potential at which a pit first nucleates and occurs when the forward scan breaks away from a curve in which there is no pitting. If pitting is not present, there is no hysteresis in the forward and reverse scans (dotted line in Fig. 5). The area between the forward and reverse scans can be taken as a measure of the potential for crevice corrosion.

Macrocell Corrosion Technique

A macrocell is formed by the working electrode and a counter electrode connected by a resistance of known value, 100 Ω, for example. The working electrode is a rebar in concrete which is in contact with the corrosive environment, whereas the rebar serving as the counter electrode is not exposed to the corrosive agent, but should have good access to oxygen (Fig. 6). The current flowing in the resistance can be obtained by measuring the potential drop across the resistance.

Although this simple method is acceptable for comparing different corrosion inhibitors in otherwise similar systems, it should not be used to obtain an indication of the absolute corrosion rate. The macrocell technique tends to underestimate absolute corrosion rates. For example, a zero macrocell current may be recorded, even in the presence of localized corrosion [*18*].

Experimental

Polarization Resistance

Specimens described in this paper consisted of No. 3 steel bars (19 mm diameter), cleaned with sulfuric acid and then wire-brushed and embedded in concrete cylinders 7.5 cm in diameter by 15 cm long (3 by 6 in.). The protruding length of rebar, as well as a short length of embedded rebar, was covered with electroplater's tape, leaving 26 cm^2 of exposed rebar embedded within the concrete. Various concrete mixture designs were tested and are given

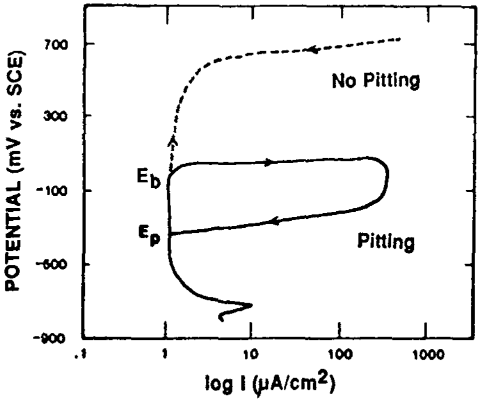

FIG. 5—*Idealized cyclic polarization curve for steel in an alkaline environment.*

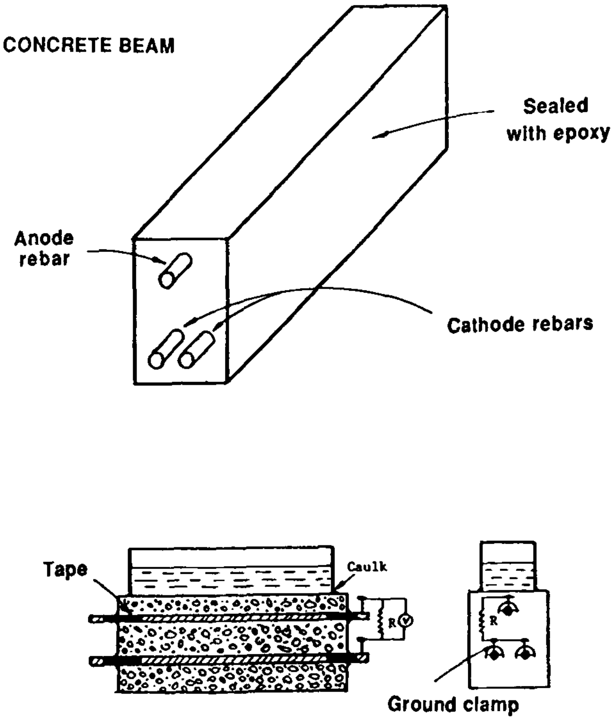

FIG. 6—*Minibeam for macrocell corrosion testing. The voltmeter* V *is connected only when taking a measurement.*

when the results are discussed. In particular, the effects of the water to cement ratio (*W/C*), inhibitors, and/or microsilica additions are of interest. The bars used in one set of specimens consisted of commercial-coated fusion-bonded epoxy that was not cleaned as above, but just rinsed in distilled water and dried.

After 28 days of curing in a fog room at 22°C, the specimens were submerged to half their height in a 3% sodium chloride/tap water solution. The solution was changed monthly.

The polarization resistance was measured using a PAR Model 351 System consisting of a computer-controlled potentiostat and associated software. The applied potential was increased at a rate of 0.1 mV/s from 20 mV below the equilibrium or corrosion potential to a final potential of 20 mV above the corrosion potential. To eliminate errors due to the large concrete resistance, the current-interrupt feature of the system was enabled in obtaining the data.

In addition, tests were conducted with rebars immersed in pore-water solutions (0.3 *M* NaOH + 0.6 *M* KOH) saturated with calcium hydroxide and containing 1 *M* sodium chloride.

EIS

Concrete specimens used here were the same as described for the polarization resistance tests. As before, steel rebars with and without epoxy coating were tested in pore-water solution to determine whether these data are representative of the concrete system. The bars were 19 mm diameter by 17.5 cm long, and only 15 cm^2 were immersed in the solution.

The PAR Model 368-1 AC Impedance System consisting of a Model 173 Potentiostat/Galvanostat combined with the Model 276 Interface Plug-In, the Model 5206 Computer-Controlled Lock-In System, and the Apple IIe microcomputer with peripherals, and the Model 368 AC Impedance Software System was used. A Fast-Fourier technique was applied over the range of 0.002 to 1 Hz, using seed frequencies of 0.002, 0.01, and 0.1 Hz. The voltage amplitude was $<\pm 10$ mV versus E_{corr}. The impedance at 20 kHz was used as an approximation of the concrete and solution resistivity, R_s. The sum of the charge transfer resistance, R_p, and the concrete and solution resistivities is equal to the measured impedance at low frequencies, which is when the phase-angle shift first approaches zero and where the Bode plot for impedance becomes horizontal.

Cyclic Polarization

As mentioned, these tests were carried out by immersing the rebars in solutions that simulate the concrete environment [*16,17*]. In the present tests, the rebar specimens were machined into cylinders (1.25 by 1.25 cm) to fit an EG & G Princeton Applied Research cylindrical specimen holder [*19*]. The cylinders were degreased with acetone prior to testing. Solutions used were saturated calcium hydroxide with 0.5 *M* sodium chloride and pore water (0.3 *M* NaOH + 0.6 *M* KOH) saturated with calcium hydroxide and with 1 *M* sodium chloride. In addition, these solutions with 0.33 *M* calcium nitrite were used to demonstrate the effectiveness of this additive as a corrosion inhibitor.

Various scan rates were examined to determine whether a single, fast scan rate can provide a valid indication of pitting conditions. This would have the advantage of considerably reducing the time required for a measurement, and in addition would reduce the length of time the metal is exposed to high potentials, thus reducing the amount of destruction. The best scan rate was determined by comparing the cyclic polarization curves at a range of scan rates with the curve obtained at the prescribed slow/fast scan.

Macrocell Corrosion

Concrete specimens were made using the following mix design:

Cement type—ASTM C 150 Type 1,2.
Coarse aggregate—Trap rock, 1.3 cm (1/2 in), 1067 kg/m^3 (1800 lb/yd^3).
Fine aggregate—Sand, 719 kg/m^3 (1212 lb/yd^3).
Cement factor—356 kg/m^3 (600 lb/yd^3).
W/C—0.5.
Air—6%.

Beams 30 by 11.5 by 15 cm (11 by 4.5 by 6 in.) were made which contained one top bar and two bottom reinforcing bars (No. 4, 1.3 cm diameter) made of black steel. The top bar was placed at 19 or 25 mm (3/4 or 1 in.) from the top of the surface. The bottom bars were 25 mm from the bottom. Control beams as well as minibeams containing 20 L/m^3 (4 gal/yd^3) of 30% calcium nitrite solution or 2% solids on solids (s/s) calcium chloride were made for assessment of the corrosion-inhibiting properties of calcium nitrite. The reinforcing bars were taped with electroplater's tape to expose 17.8 cm (7 in.) of rebar. After a curing period in the fog room at 22°C, a 7.6-cm (3-in.)-high plastic dam with inside dimensions of 15.2 by 7.6 cm (6 by 3 in.) was caulked to the top. The four sides of the sample and top surface outside the dam were coated with a concrete epoxy. Ground clamps were used to attach a

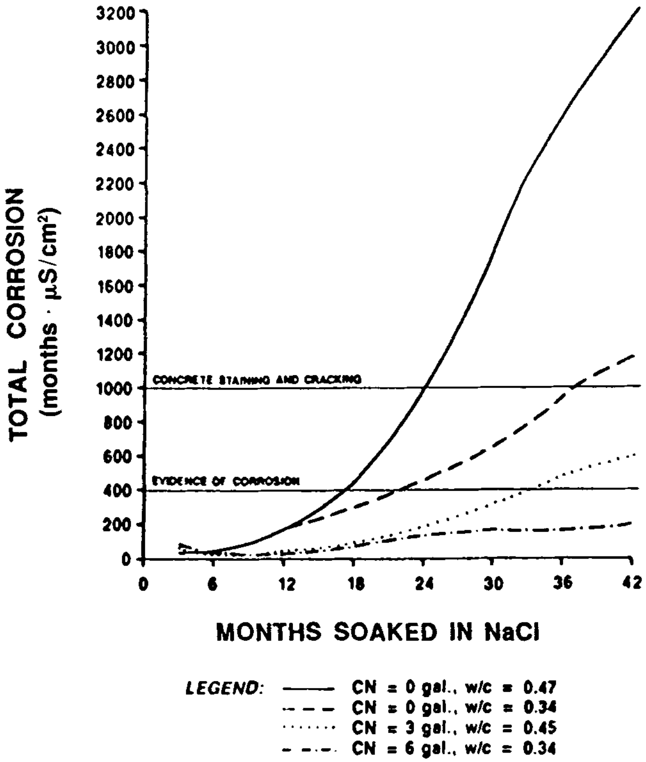

FIG. 7—*Effect of calcium nitrite addition and W/C on the corrosion of steel in concrete.*

100-Ω resistor between the top and one of the bottom rebars. The two bottom rebars also were electrically connected. The minibeams were cyclically ponded with 3% sodium chloride solution on a two-week wet, two-week dry cycle. The voltage drop across the 100-Ω resistor was measured at monthly intervals.

Results and Discussion

Polarization Resistance

The polarization resistance technique has been used effectively to show the improvement in corrosion resistance of steel in concrete by reducing the water-to-cement ratio and by adding inhibitors such as calcium nitrite. Figure 7 [*20*] clearly shows this effect by integrating $1/R_p$ over time. Later work has also demonstrated the effectiveness of microsilica addition [*21*]. Good correlations to visual appearance of the steel and related chloride contents in the concrete were demonstrated.

In a series of tests conducted with specimens with a cement factor of 344 kg/m³, $W/C = 0.49$, the value of the resistance integrated over the time of exposure (three years) was compared with the degree of corrosion as determined by visually inspecting the rebars at the conclusion of the tests. As can be seen from Fig. 8, the measured data are in excellent agreement with the observed corrosion. Note that increasing the inhibitor reduced the overall corrosion and increased corrosion initiation times.

EIS

Past studies showed that the EIS technique was in remarkably good agreement with the polarization resistance technique [*11,14,20*]. Bode plots for the black-steel and the epoxy-coated rebars are shown in Fig. 9 for concrete specimens. The concrete used in making these specimens was made with Type 1,2 cement, W/C = 0.4 and a cement factor of 390 kg/m^3 (658 lb/yd^3). The associated polarization resistance values are included in Table 1 for both concrete and pore water tests.

In general, the EIS and d-c techniques show good agreement between the calculated values of the polarization resistance for both the pore-water solution and the concrete specimens. Corrosion rates ($1/R_p$) in pore water are higher due to the fact that chloride is in the vicinity of the bar. Corrosion rates in the concrete are, for all practical purposes, negligible for both the epoxy and the black steel.

As stated, the advantage of EIS is that more information on the system is obtained. For example, the value of the resistance of the concrete, R_s, is obtained from the high frequency end of the Bode plot. It can be observed that this value for the epoxy case (68 kΩ·cm^2) is some five times higher than that for the uncoated rebar (13 kΩ·cm^2). This difference is either attributed to the fact that the exposed area was assumed to be the same (26 cm^2) in both cases and the effective exposed area of the epoxy-coated bar is about one-fifth that area, or that the model given in Fig. 3 is more correct and the resistance of the coating is added to the R_s value.

Also of interest is the fact that, in chloride pore-water solutions, even though the epoxy bar showed a high negative corrosion potential (−507 mV versus SCE), the corrosion rate as measured by polarization resistance and EIS was extremely low. This points to the fallacy of using ASTM C 876 to estimate corrosion rates. We are not sure at this point if the low potential is due to a lack of oxygen reaching the bar because of the coating or to pitting occurring over a small area of the bar. Further work to resolve these questions is planned.

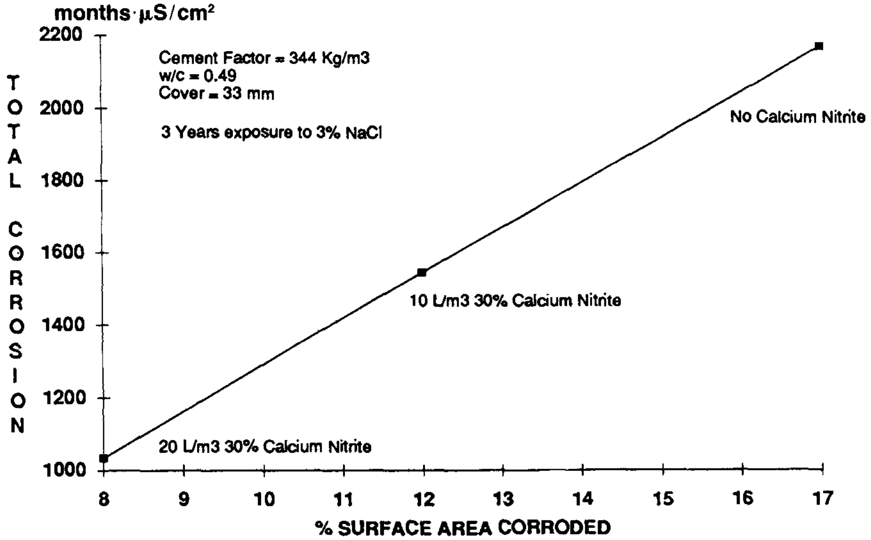

FIG. 8—*Comparison of the total corrosion as measured by polarization resistance techniques and observed values.*

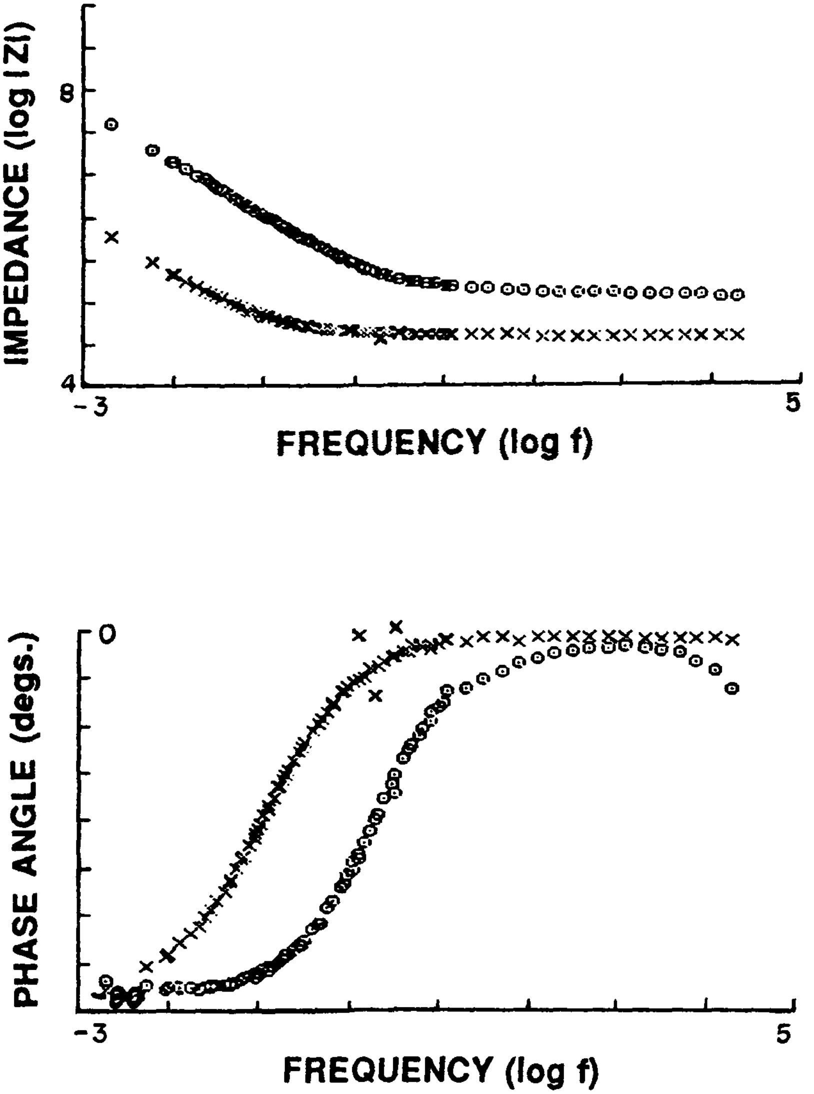

FIG. 9—*Measured Bode plots for rebars in concrete, X = black steel, O = epoxy-coated.*

TABLE 1—*Polarization resistance of black steel and epoxy-coated rebars, KΩ · cm²*.

	In Concrete				In Pore-Water Solution + 1 *M* NaCl			
			EIS[b]				EIS[b]	
	E_{corr}, mV SCE	PR[a]	R_s	R_p	E_{corr}, mV SCE	PR[a]	R_s	R_p
Black steel	−15	433	14	> 570	−260	17	5E-3	4
Epoxy coated	−40	77E3	68	>35E3	−507	280	200E-3	300

[a] Using dc with IR compensation.

[b] Measured by electrochemical impedance spectroscopy.

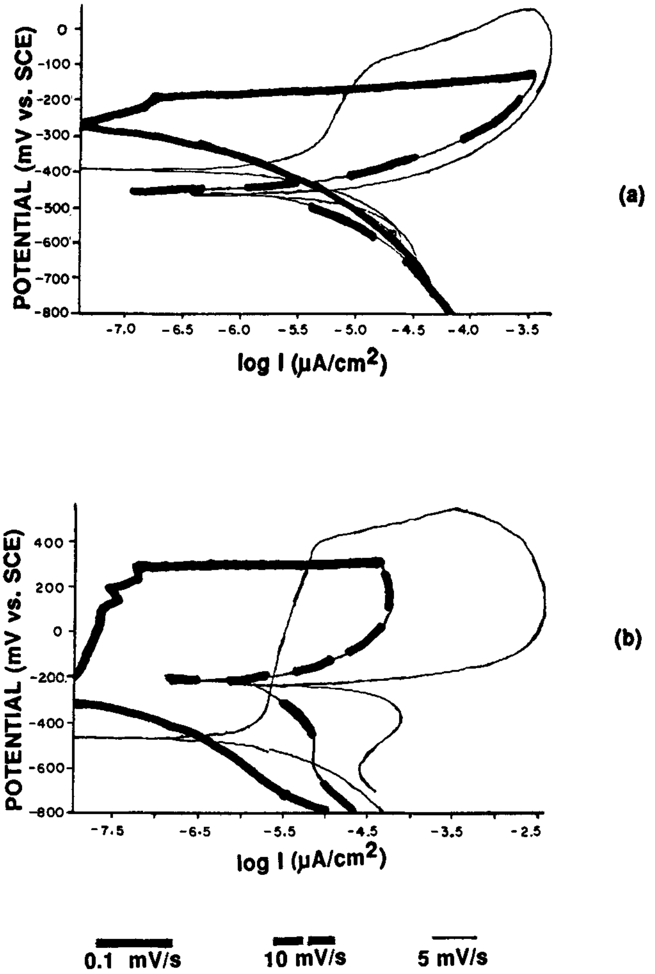

FIG. 10—*Cyclic polarization curves for rebars in pore water:* (a) *saturated calcium hydroxide plus 0.5* M *sodium chloride;* (b) *pore water plus 1* M *sodium chloride plus 0.33* M *calcium nitrite plus saturated calcium hydroxide.*

Cyclic Polarization

The value of the pitting potential, E_p, approached that of the base curve as the scan rate was increased from 0.1 to 10 mV/s, with the best match being obtained at a scan rate of 5 mV/s. As shown in Fig. 10, the value for E_p obtained at 5 mV/s is in good agreement with the base values both in the presence and absence of calcium nitrite.

It takes three hours to conduct a test at a forward scan rate of 0.1 mV/s and a reverse scan rate of 10 mV/s for a typical sweep of 1200 mV in each direction. By using a scan rate of 5 mV/s, the test time can be reduced to about 10 min.

The cyclic polarization curves of Fig. 10 clearly illustrate that pitting is an important consideration in chloride environments. The effectiveness of calcium nitrite in controlling pitting attack is also illustrated in Fig. 10. As can be seen, calcium nitrite shifts the pitting potential, E_p, to more noble values (by 200 to 300 mV), making it less likely that pitting will occur.

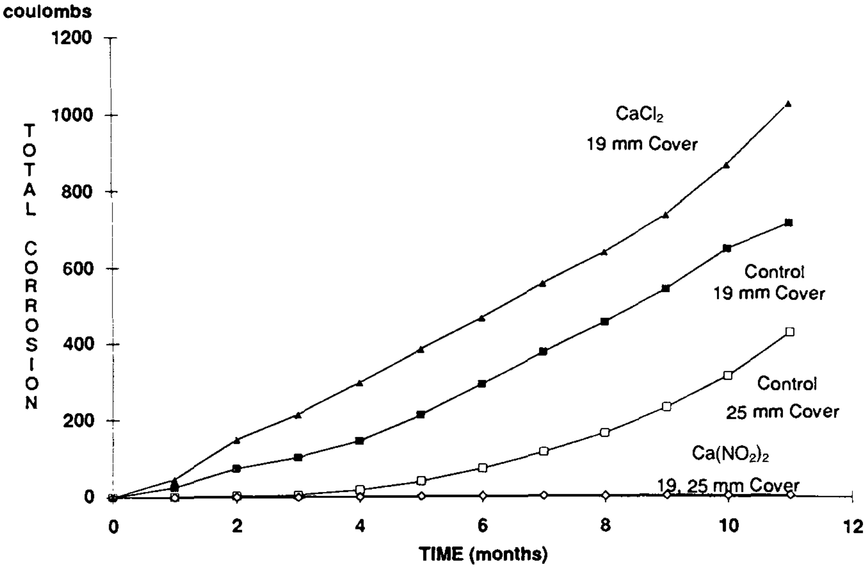

FIG. 11—*Corrosion rates in chloride environments as determined by the macrocell technique.*

Macrocell

The total corrosion (current × time) values obtained over a period of eleven months with the minibeams made for the macrocell corrosion testing are represented in Fig. 11. The control beams with 19 mm cover as well as the beams with calcium chloride show the greatest amount of corrosion. The beams containing the calcium nitrite corrosion inhibitor showed virtually no corrosion, even after eleven months' exposure, again illustrating the effectiveness of this additive.

Some of the beams were broken open to compare the amount of corroded surface with the measured values. As can be seen from Table 2, the measured and observed corrosion are in good agreement. In addition, deep pitting was observed in several bars. However, as anticipated from the cyclic polarization tests, pitting did not occur in the presence of calcium nitrite.

TABLE 2—*Visual inspection of rebars after eleven months of testing.*

	Corroded Area, %			
Test ID	Top Bar	Bottom Bars		Coulombs
21	17.8[a]	0.2	0.6	830
75	56.4	0	0	869
84	42.2	0.3	0.3	777
115	0	0	0.2	4
136	0.3	0	0	5
158	0	0	0	5
181	18.8[a]	2.2	7.4	1153
194	34.4[a]	3.7	2.2	912

[a] Deep pitting was observed on these bars.

Conclusions

1. The EIS and polarization resistance techniques yield comparable values for R_p. These methods provide a measure of the actual corrosion rate at the time of the tests.
2. An indication of the integrity of the coating on a rebar can be determined from the value of R_s as measured by EIS at high frequencies.
3. Values of the pitting potential can be determined with adequate accuracy and considerable time savings by conducting cyclic polarization tests at a fixed scan rate of 5 mV/s.
4. Calcium nitrite reduces the rate of pitting that occurs in chloride environments by shifting the pitting potential to more noble values.
5. The low-cost macrocell technique provides a good indication of the relative degree of corrosion that occurs with various mix designs.
6. Long-term monitoring of corrosion rates can be achieved using polarization resistance, EIS, or macrocell techniques.

References

[*1*] Zayed, A. M., Sagues, A. A., and Powers, R. G., "Corrosion of Epoxy Coated Reinforcing Steel," *NACE Corrosion 89*, Paper 379, National Association of Corrosion Engineers, Houston, TX, 1989.

[*2*] "Strategic Highway Research Program Research Plans. Final Report," TRA-4-1, Transportation Research Administration, Washington, DC, May 1986.

[*3*] Berke, N. S., "Corrosion Rates of Steel in Concrete," *ASTM Standardization News*, March 1986.

[*4*] Gonzales, J. A., Algaba, S., and Andrade, C., *British Corrosion Journal*, Vol. 15, 1980, p. 135.

[*5*] Dean, S. W. Jr., "Electrochemical Tests for Corrosion Testing," *Electrochemical Techniques for Corrosion*, R. Boboian, Ed., National Association of Corrosion Engineers, Houston, TX, 1977.

[*6*] Mansfield, F. "Don't be Afraid of Electrochemical Techniques—But Use Them with Care," *Corrosion*, Vol. 44, No. 12, 1988, pp. 856–868.

[*7*] Gonzales, J. A., Molina, A., Esadero, M., and Andrade, M. C., "A Comparison of Linear Polarization and A. C. Impedance in the Determination of Corrosion Rates of Reinforcements Embedded in Concrete," *NACE Corrosion 85*, Paper 257, National Association of Corrosion Engineers, Houston, TX, 1985.

[*8*] Dawson, J. L., Callow, L. W., Hardky, K., and Richardson, J. A., "Electrochemical Impedance Measurements Applied to the Corrosion of Reinforcing Steel in Concrete," *NACE Corrosion 78*, Paper 125, National Association of Corrosion Engineers, Houston, TX, 1978.

[*9*] Sagues, A. A., "Evaluation of Corrosion Rate by Electrochemical Impedance in a System with Multiple Polarization Effects," *NACE Corrosion 89*, Paper 25, National Association of Corrosion Engineers, Houston, TX, 1989.

[*10*] Dawson, J. L., "Corrosion Monitoring of Steel in Concrete," *Corrosion of Reinforcement in Concrete Construction*, A. P. Crane, Ed., Ellis Horwood Ltd., London, England, 1983, pp. 175.

[*11*] Berke, N. S., "The Effects of Calcium Nitrite and Mix Design on the Corrosion Resistance of Steel in Concrete (Part 1)," *NACE Corrosion 85*, Paper 273, National Association of Corrosion Engineers, Houston, TX, 1985.

[*12*] Stern, M. S. and Geary, A. J., *Journal of the Electrochemical Society*, Vol. 105, No. 638, 1958.

[*13*] Mansfield, F., Chin, Y. C., and Shih, H., "Determination and Elimination of the Uncompensated Resistance in Low Conductivity Media," *Electrochemical Techniques for Corrosion*, R. Baboian, Ed., National Association of Corrosion Engineers, Houston, TX, 1977.

[*14*] Berke, N. S., Shen, D. F., and Sundberg, K. M., "Comparison of Current Interruption and Electrochemical Impedance Techniques in the Determination of the Corrosion Rates of Steel in Concrete," *The Measurement and Correction of Electrolyte Resistance in Electrochemical Tests, ASTM STP 1056*, American Society for Testing and Materials, Philadelphia, 1989.

[*15*] Mansfield, F., "Recording and Analysis of AC Impedance Data for Corrosion Studies," *Corrosion*, Vol. 37, No. 5, 1981, pp. 301–307.

[*16*] Page, C. L. and Treadaway, K. W. T., *Nature*, Vol. 297, No. 109, 1982.

[*17*] Berke, N. S., "The Use of Anodic Polarization to Determine the Effectiveness of Calcium Nitrite as an Anodic Inhibitor," *Corrosion Effects of Stray Currents and the Technique for Evaluating Corrosion of Rebars in Concrete, ASTM STP 906*, V. Chaker, Ed., American Society for Testing and Materials, Philadelphia, 1986, pp. 78–91.

[*18*] Berke, N. S., Shen, D. F., and Sundberg, K. M., "Comparison of the Polarization Resistance Technique to the Macrocell Corrosion Technique," *The Measurement and Correction of Electrolyte Resistance in Electrochemical Tests, ASTM STP 1056,* American Society for Testing and Materials, Philadelphia, 1989.

[*19*] *Model 350A Corrosion Measurements System Operating and Service Manual,* EG & G Princeton Applied Research, Princeton, NJ 1980 pp. III-2 to III-4.

[*20*] Berke, N. S., "The Effects of Calcium Nitrite and Mix Design on the Corrosion Resistance of Steel in Concrete (Part 2, Long-Term Results), *NACE Corrosion 87,* Paper 132, National Association of Corrosion Engineers, Houston, TX, 1987.

[*21*] Berke, N. S., Pfeifer, D. W., and Weil, T. G., "Protection Against Chloride-Induced Corrosion," *Concrete International,* December 1988.

DISCUSSION

George Nekoksa (*written discussion*)—Would increasing the tensile strength of concrete above the pressure of corrosion products control the corrosion of rebar? Would use of fibers in concrete help?

N. S. Berke and H. C. Hicks (*author's closure*)—Increasing the tensile strength of concrete above the pressure exerted by the corrosion products would be beneficial. However, since tensile forces exerted could exceed 10 000 psi, a concrete compressive strength of about 100 000 psi would be needed. Currently, commercially produced concrete is approaching 20 000 psi in limited markets where good quality aggregates are available, with the use of high-range water reducers, superplasticizers, and pozzolans—especially microsilica. Thus, in the foreseeable future, it is unlikely that concrete tensile strengths can be improved to the point of restricting cracking due to corrosion products. Fibers could potentially be helpful if they could prevent spalling and be noncorrosive. Replacement of the reinforcing bars and/or prestressing wires with fibers providing equivalent structural performance is expensive and not always possible. The current solution utilizing good quality concrete, corrosion inhibitors, and/or other protection systems provides a cost-effective means of enabling a concrete-reinforced structure to reach its design life.

Author Index

Subject Index

ISBN 0-8031-1406-0